Appendix A

Ruben Reininger’s report for the optical design of SST

Ruben Reininger, Ph.D.
77 Constantine Way
Mt. Sinai, NY 11766, USA
Voice & Fax (631) 403 4954
ruben@sas-rr.com
www.sas-rr.com

Revised optical design of the NIST soft and tender x-ray beamline complex at NSLS II

Ruben Reininger
(Dated: May 5, 2012)

We describe the modified optical design of the NIST beamline complex at NSLS-II required due to the change in undulator positions in the NSLS-II storage ring straight section. The multi station beamline complex is based on two canted undulators, one for soft x-rays and one for tender x-rays. The beamlines will have a total of 6 experimental stations, three will be served by the soft x-ray undulator and three by the tender x-ray undulator, thus a variety of soft and tender spectroscopy experiments can be accomplished simultaneously in this beamline complex. Two of the experimental endstations (HAXPES/NEXAFS and the μXPS nanoscope) can utilize the soft and tender X-ray undulators (sequentially or even simultaneously) enabling a continuous selection of X-rays from 100 eV to 7.5 keV. The spot size at each one of the experimental stations as well as the higher order contamination are presented.

I. INTRODUCTION

New assumptions on the maximum allowed deviation of the electron beam inside the straight section (SS) of the storage ring both in angle and divergence put severe limitations on the low energy operation of an elliptical polarized undulator (EPU) in circular and linear vertical polarizations. The solution to this new restriction is to change the positions of the insertion devices (ID) such that the high energy ID is located upstream and the EPU is downstream. Evidently, this change requires a complete redesign of the optical arrangement described in our previous report [1].

The advanced in ion figuring and optical metrology made possible the manufacturing of better ellipsoidal mirrors with RMS meridional and sagittal slope errors better than 1 μrad and 10 μrad, respectively. This development allows us to simplify the optical arrangement, making all the deflections leading to the μXPS microscope to be in the horizontal plane. Another big advantage in using ellipsoidal mirrors is the fact that a small change in yaw allows to increase the spot size significantly, replacing the fast dithering assumed in our previous report as the basis for enlarging the spot size in the μXPS station. The modification requires to have a stigmatic image at the exit slits. Therefore, the exit slits need to be water cooled.

The new optical design and the expected spot sizes at the different experimental stations are described below. **It should be noted that we assumed that both IDs are 2 m long and that their centers are at 1.25 m from the center of the SS. These numbers will have to be approved (or changed) by the NLSL II accelerator group. The exact parameters of the optics and their positions will have to be revised once the final ID lengths and their positions are determined.**

The flux expected at the different experimental stations was not explicitly calculated but should be similar to that reported in Ref. [1].

The distance between M4B and the μEXAFS station was increased relative to our report dated 4/29 from 3 m to 3.2 m to provide more distance between the HAXPES/NEXAFS station and L3. Therefore, the illumination of L3 is slightly larger than described below and the soft x-ray spot at the μEXAFS station is slightly larger than in Fig. 9

II. OPTICAL LAYOUT

The optical layout is designed to accommodate a total of six experimental stations (see Table I). Two of the stations can be illuminated with soft and tender x-rays, three only with soft x-rays, and one only with tender x-rays. The two common stations could be illuminated with both IDs at the same time if an experiment requires two different photon energies. Table I also lists the expected size of the beam at each one of the experimental stations.

The PDF file ("Multistation 2 mrad .pdf') showing the position of the optical elements and experimental stations as well as the names used in this report are sent with this report. For completeness, we present in Fig. 1 a copy of the PDF file fitting in the page. One should note that we have assumed the beamline complex is located in a straight section with a "long" experimental floor. The position of the optical elements and of the end stations relative to the center of the straight section are given in Table II. The table also lists the deflection angles of the mirrors and the function of the different components. A more detailed description of the opti-

TABLE I. Experimental stations, their sources, and expected spot sizes including slope errors on the optical elements. The spot sizes are calculated assuming the soft ID is tuned to 200 eV with the medium energy grating and a 20μm exit slit, and the tender ID is tuned to 1.5 keV.

Experimental Station	Source	Spot Size (FWHM) (h.×v.) (mm×mm)	
HP NEXAFS	Tender	0.8×0.6[a]	3.3×2.5[b]
HAXPES/NEXAFS	Tender	0.1×0.016[a]	4.0×3.0[b]
	Soft	0.064×0.031	0.45×0.43[c]
μXPS Microscope	Tender	0.015×0.002	
	Soft	0.014×0.005	
HP NEXAFS/FY	Soft	2.1×2.2	
NEXAFS/XPS	Soft	0.032×0.044	0.032×5[d]
μNEXAFS Imaging	Soft	1.1×1.2	20×20[e]

[a] L2A (toroid)
[b] L2B (plane)
[c] 0.1°yaw on M4A
[d] Dithering M5C
[e] Dithering M3C and M4D

cal components, their sizes calculated as 4 times the root mean square (RMS) beam footprint at 200 eV (soft x-ray mirrors) and 1500 eV (tender x-ray mirrors), and their function is given in the next subsections.

A. L1

The first optical element of the tender branch is a plane mirror deflecting the beam in the horizontal plane (by 1.2°). This mirror will be water cooled and will absorb the power emitted by the insertion device at photon energies beyond the energy range covered by the tender x-ray branch. Beam footprint on mirror: 305×2.4 mm^2. This mirror is inside the first optical enclosure (FOE).

B. L2A and L2B

This is a pair of interchangeable mirrors that deflect the tender beam in the horizontal plane (by 1.2°). L2A is a toroidal mirror which focuses the radiation onto the sample position of the HAXPES/NEXAFS station with a demagnification ≈1.2:1. L2B is a plane mirror deflecting the radiation towards the μXPS common station. Both mirrors are side cooled. Either of these mirrors can be used at the high pressure (HP) NEXAFS station. Beam footprint on mirrors: 350×2.7 mm^2. This mirror is located inside the FOE.

C. Tender x-ray monochromator

The crystals in the double crystal monochromator (DCM) diffract in the vertical direction. The DCM will be illuminated by a converging beam when L2A is used and by a divergent one when L2B is used. The beam divergence for photon energies higher than 1.5 keV with either mirror is less than 0.1 mrad. The monochromator changes the beam height by 15 mm. The first crystal of the monochromator requires liquid nitrogen cooling.

D. L3

L3 is a plane mirror used to guide the tender beam to the sample position of the μXPS station. L3 deflects the photon beam in the horizontal plane by 1.2°. Since L3 and L4 are placed after the crystal monochromator, they do not require cooling. Beam footprint on mirror: 660×5.5 mm^2.

E. L4

L4 is an ellipsoidal mirror that focuses the undulator radiation onto the sample position of the μXPS station. L4 deflects the photon beam in the horizontal plane by 1.2°. It images the source with a demagnification ≈23:1. Beam footprint on mirror: 720×5.7 mm^2.

F. M1

The first optical element of the soft branch is a plane mirror deflecting the beam in the horizontal plane (by 3.0°). This mirror will be water cooled and will absorb the power emitted by the insertion device at photon energies beyond the range covered by the soft x-ray branch. This is the only element of the soft branch inside the FOE. Beam footprint on mirror: 183×4.3 mm^2.

G. Soft x-ray VLS PGM monochromator

The basic principles of the monochromator have been described in detail in reference [2]. The major difference here is that the beam incident on M2 along the vertical direction is diverging and not vertically collimated as in the CSX beamline [2] planned for NSLS-II. The plane mirror (M2) in front of the gratings needs to be internally water-cooled and the gratings need to be side cooled to avoid performance impairment due to the absorbed power density. The chosen gratings have line densities of 250 (LEG), 600 (MEG), and 1200 (HEG) lines/mm at their centers and are operated with c values (=cos β/cosα, where α is the angle of normal incidence and β is the diffraction angle) of 1.5, 1.5 and 2.0, respectively. The expected resolution with an exit slit width of 20 μm and taking into account state of the art slope errors on the optical elements is given in Fig. 2. Reducing the exit slit to 10 μm improves the energy resolution by a factor between 1.3 and 1.8 in all gratings. The variation of

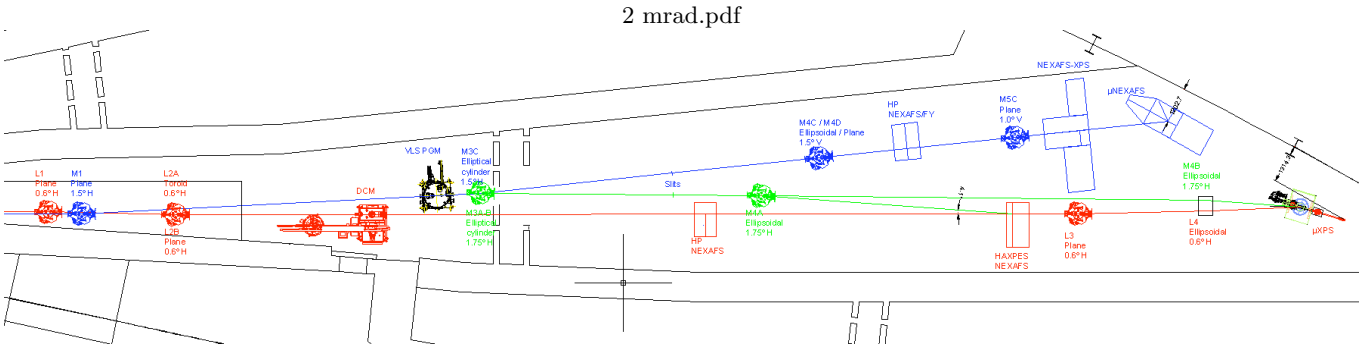

FIG. 1. ACAD drawing showing the optical elements and the experimental stations. Lines in blue and green represent the soft x-ray beams while those in red the tender x-ray beams.

TABLE II. Optical elements, figures, positions relative to the center of the straight section (at beam height), deflection and deflection angles, and their function. A horizontal (vertical) arrow represents a horizontal (vertical) deflection before the current element. The orthogonal coordinate system is: y is along and downstream the straight section, x points towards the storage ring, and z is along the vertical direction.

Label	Mirror Figure	Position (x,y,z) (mm, mm, mm)	Deflection & angle	Function
High energy ID		(0, -1250, 0)	hor. 1 mrad	
L1	Plane	(-29, 27450, 0)	hor. -1.2°	Heat sink
←L2A	Toroid	(57, 31756, 0)	hor. 1.2°	Focus at HAXPES/NEXAFS
←L2B	Plane	(57, 31756, 0)	hor. 1.2°	Deflects beam
←→Tender x-ray Mono		(51, 38394, 0)		Double crystal monochromator
←→↑↓ HP NEXAFS		(39, 49642, 15)		Using L2A or L2B
←→↑↓ HAXPES/NEXAFS		(29, 60039, 15)		Using L2A
←→↑↓ L3	Plane	(27, 62258, 15)	hor. 1.2°	Horizontal deflection
←→↑↓ → L4	Ellipsoidal	(-72, 66766,15)	hor. 1.2°	2D focusing at μXPS
←→↑↓ → → μXPS		(-201, 69763, 15)		
Low energy ID		(0, 1250, 0)	hor. -1 mrad	
M1	Plane	(27, 28580, 0)	hor. 3.0°	Heat sink
→ Soft x-ray Mono (M2 + grating)		(-589, 40564, 0)		Focuses vertically at exit slit.
→↑↓ M3AB	Elliptical Cyl.	(-666, 42062, 15)	hor. -3.5°	Focuses horizontally at AB exit slit.
→↑↓ M3C	Elliptical Cyl.	(-666, 42062, 15)	hor. 3.0°	Focuses horizontally at C exit slit.
→↑↓ ← Slit AB		(-603, 48562, 15)		Slit for AB stations. Requires cooling
→↑↓ ← M4A	Ellipsoidal	(-573, 51548, 15)	hor. -3.5°	Focuses vertically at HAXPES/NEXAFS.
→↑↓ ← ← HAXPES/NEXAFS		(29, 60039, 15)		
→↑↓ ← M4B	Ellipsoidal	(-427, 66571, 15)	hor. -3.5°	Focuses at μXPS
→↑↓ ← ← μXPS		(-201, 69763, 15)		
→↑↓ → Slit C		(-1339, 48527, 15.)		Slit forC stations. Requires cooling
→↑↓ → M4C	Ellipsoidal	(-1856, 53500, 15)	ver. 3.0°	Focuses vertically at NEXAFS/XPS
→↑↓ → M4CP	Plane	(-1856, 53500, 15)	ver. 3.0°	Used to dither for μNEXAFS
→↑↓ → ↑ HP NEXAFS/FY		(-2167, 56480, 172)		
→↑↓ → ↑ μNEXAFS Imaging		(-3063, 65093, 626)		
→↑↓ → ↑ M5C	Plane	(-2546, 60122, 364)	ver. -2.0°	Beam back to horizontal
→↑↓ → ↑↓ NEXAFS/XPS		(-2753, 62116, 399)		

TABLE III. Grating parameters. The grove density variation is given by $k(w) = k_0(1+2b_2w+3b_3w^2+...)$ w is positive towards the exit slit.

Grating	c	k_0 mm^{-1}	b_2 10^{-4}mm^{-1}	b_3 10^{-8}mm^{-2}	Coating	Blaze or trapezoidal angle	Groove depth nm	Groove width μm
LEG	1.5	250	2.451	2.75	Au	28°	20	2.4
MEG	1.5	600	2.450	2.75	Au	28°	8	1.0
HEG	2.0	1200	1.749	2.06	Au	0.9°		

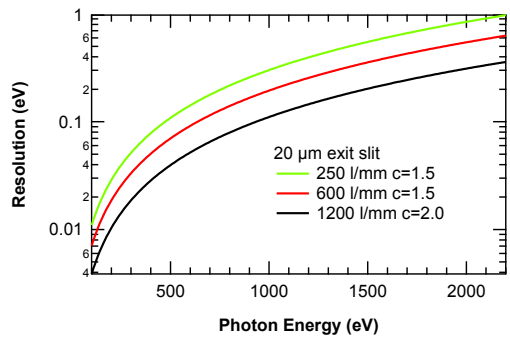

FIG. 2. Expected resolution with the three gratings assuming an exit slit width of 20μm..

the line densities and the grove parameters are listed in Table III.

H. M3AB and M3C

Both mirrors are elliptical cylinders focusing the beam along the horizontal direction at the corresponding exit slit. The demagnification of both mirrors is the same, 4.3:1. Evidently, only one of the mirrors will intercept the beam at any given time. M3AB deflects the beam horizontally by 3.5°whereas M3C deflects the beam, also horizontally, by 3.0°. Beam footprint on M3A is 234×8 mm^2 and on M3C is 273×8 mm^2. M3C is being used to make a 20 mm wide spot at the μNEXAFS station by dithering ±0.22 mrad.

I. M4A

M4A is an ellipsoidal deflecting the beam horizontally by 3.5°. It magnifies the beam at exit slit by onto the sample position of the HAXPES/NEXAFS station by ≈1:2.9. Beam footprint on mirror: 108×3.5 mm^2.

J. M4B

M4B is an ellipsoidal that images the exit slit onto the sample position of the μXPS station with a demagnification of 5.6:1. M4B deflects the beam by 3.5°along the horizontal direction. Beam footprint on mirror: 650×21 mm^2.

K. M4C

M4C is an ellipsoidal that images the exit slit onto the sample position of the NEXAFS/XPS station with a 1:1.7 magnification. The mirror deflects the beam by 3.0°in the vertical plane. Beam footprint on mirror: 225×5.5 mm^2. This mirror is interchangeable with M4D.

L. M4D

M4D is a plane mirror used to generate a large vertical spot at the μNEXAFS station. Beam footprint on mirror when M3C is being dithered to obtain a 20 mm spot at the μNEXAFS station: 225×20 mm^2. This mirror should be capable of dithering ±0.43 mrad to obtain a 20 mm tall spot at the μNEXAFS station.

M. M5C

M5C is a plane mirror that deflects the beam to the NEXAFS/XPS station sample position. Its position and angle were determined by the need to "recycle" the present experimental station. Taking this mirror out of the beam allows to get the radiation onto the μNEXAFS station. Beam footprint on mirror: 78×1.3mm^2. This mirror needs to be dithered by ±0.62 mrad to obtain a 5 mm vertical stripe at the sample of the NEXAFS/XPS station.

III. RAY TRACINGS

We performed ray tracings (using the SHADOW code [3]) to determine the spot size at each one of the experimental stations. We assumed slope errors on all the optical elements. The RMS meridional slope errors assumed for the most critical mirrors are "state of the art" values: for the plane mirrors 0.2 μrad, for the elliptical cylinders focusing the beam onto the exit slits (M3AB and M3C) we also assumed 0.2 μrad. For the ellipsoidal mirrors (M4A, M4B, M4C, and L4) and the toroidal mirror (L2A) we assumed RMS meridional (sagittal) slope errors equal to 1 (10) μrad.

For the soft x-ray branch the ray tracings were performed at a photon energy of 200 eV using the medium energy grating (MEG) assuming an exit slit of 20μm. The ray tracings at the exit slit plane (without a slit) showing the stigmatic focus are displayed in Fig. 3. The expected RMS size along the vertical direction without slope error is 3.9 μm, smaller than the value in the figure. Along the horizontal direction, the contribution due to the slope errors assumed on M1 and the elliptical cylinder are negligible. We note that the horizontal slit size should be $>$ 6 mm to allow for the enlarged horizontal beam when dithering the M3C mirror.

The tender ray tracings were done at 1.5 keV and did not include the crystal monochromator. The resulting FWHMs of the spots at the different stations are summarized in Table I.

A. HP NEXAFS station

The spot pattern of the tender beam at the HP NEXAFS station when using the toroidal mirror (L2A, used

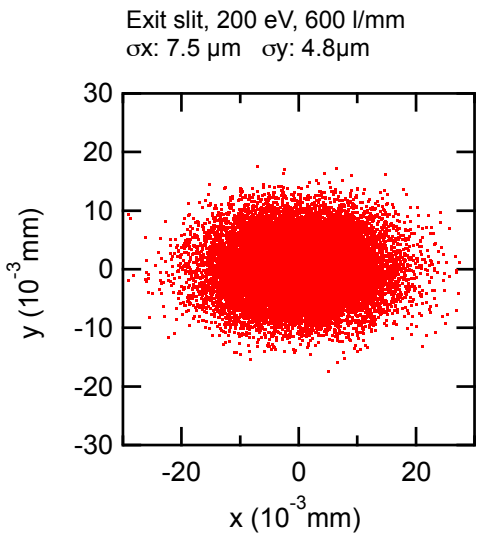

FIG. 3. Spot pattern of 200 eV at the exit slit planes of the soft x-ray branches. The caption above the figure gives the horizontal and vertical RMS values.

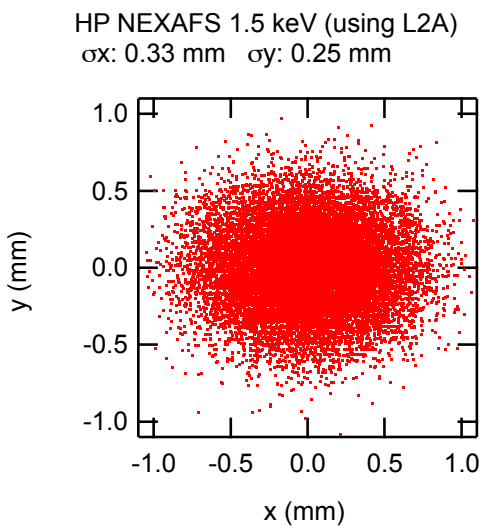

FIG. 4. Spot pattern of 1500 eV at the HP NEXAFS station when the toroid L2A is inserted in the beam. Caption as in Fig. 3.

to focus onto the HAXPES/NEXAFS station) is shown in Fig. 4. If a larger spot size is required (see Fig. 5) one could use instead the plane mirror L2B used by the μXPS station.

B. HAXPES/NEXAFS

This station accepts both the soft and tender x-rays. The tender beam spot at the sample position of this station is presented in Fig. 6. The focusing of the tender radiation at this station is done with a single toroid, L2A. This leads to significantly different beam sizes along the

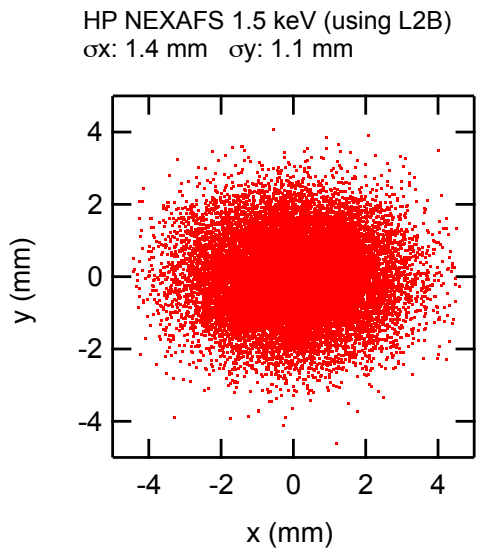

FIG. 5. Spot pattern of 1500 eV at the HP NEXAFS station when the plane L2B is inserted in the beam. Caption as in Fig. 3.

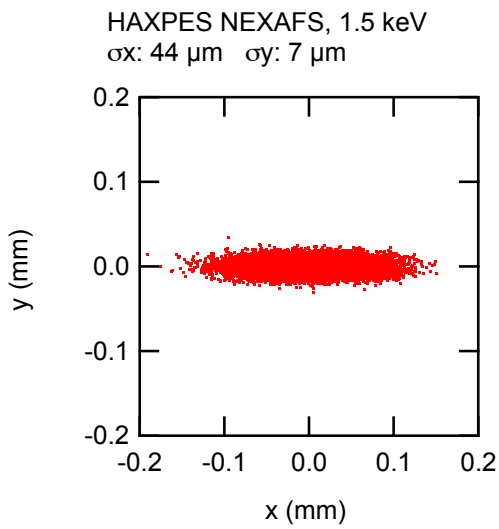

FIG. 6. Spot pattern of 1500 eV at the HAXPES/NEXAFS station. Caption as in Fig. 3.

horizontal and vertical directions, as it is in the source. If a much larger spot size is required, one could use the plane mirror L2B instead of the toroid. In this case the expected RMS beam values are 1.7 mm and 1.2 mm along the horizontal and vertical directions, respectively.

Fig. 7 shows the spot pattern at this station for 200 eV. The spot size is slightly larger along the horizontal direction than that given by the magnification of the slit due to the meridional slope errors on the M4A ellipsoidal.

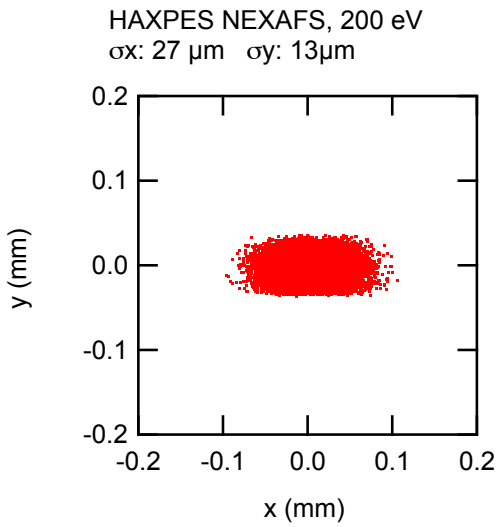

FIG. 7. Spot pattern of 200 eV at the HAXPES/NEXAFS station. Caption as in Fig. 3.

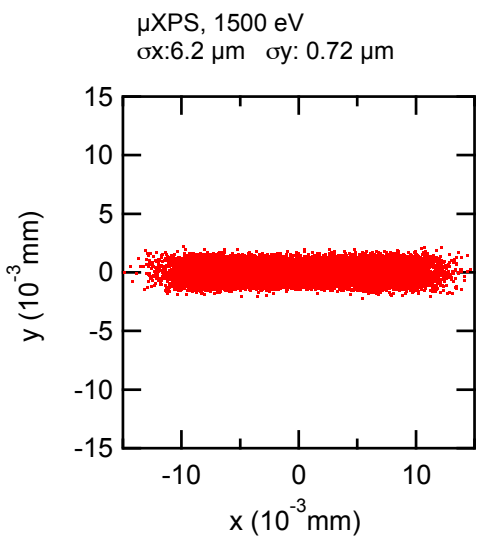

FIG. 8. Spot pattern of 1500 eV at the μXPS station. Caption as in Fig. 4

C. XPS Microscope

This station can also be illuminated by the tender and the soft x-ray beams. The focusing of each beam onto this experimental station is done with an ellipsoidal mirror to avoid the vertical deviations and the geometrical constrains due to the different angles of incidence on the soft and tender mirrors. The ellipsoidal mirrors are located at the same distance from the μXPS station, 3 m, and should share the same mirror tank. In the tender line there is no focusing upstream of L4 whereas in the soft branch the ellipsoidal mirror demagnifies the exit slit. Fig. 8 and Fig. 9 show the spot patterns at this station for 1500 and 200 eV, respectively. The RMS values of the beams are very similar along the horizontal direction but along the vertical the low energy spot is less that three times larger than the tender. In fact, in both directions the spot sizes have contributions due to the slope errors on the optics. A significant advantage on using ellipsoidals for the focusing is the fact the beam can be easily zoomed out by a small yaw rotation. As seen in Fig. 10, yaw angles of a few hundreds of a degree can increase the beam in both direction to be > 0.1 mm diameter.

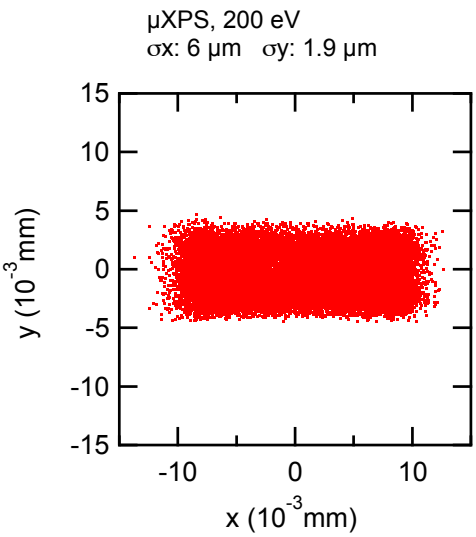

FIG. 9. Spot pattern of 200 eV at the μXPS station. Caption as in Fig. 4

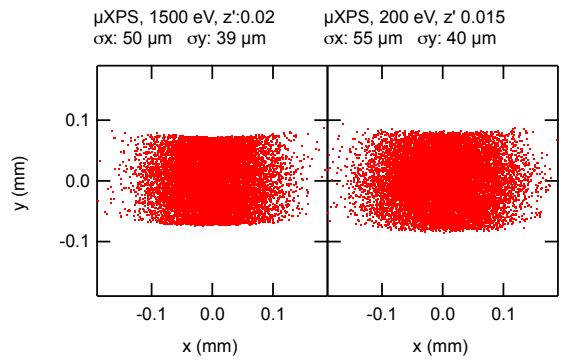

FIG. 10. Spot patterns at the μXPS station with a yaw rotation of 0.02°on L4 (left panel) and 0.015°on M4B (right panel). Caption as in Fig. 4

D. HP NEXAFS/FY

The spot at this station (see Fig. 11) is due to the converging beam towards the NEXAFS/XPS station. The horizontal size could be up to 13 mm horizontally by dithering M3C ± 0.22 mrad and 5 mm vertically by dithering M4D ± 0.43 mrad (the values required to get a

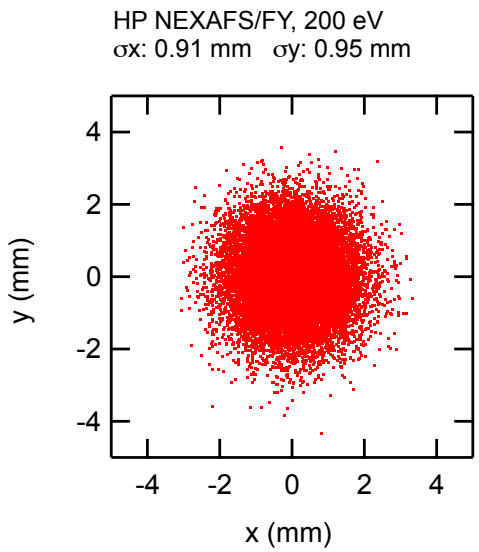

FIG. 11. Spot pattern of 200 eV at the HP NEXAFS/FY station. Caption as in Fig. 4

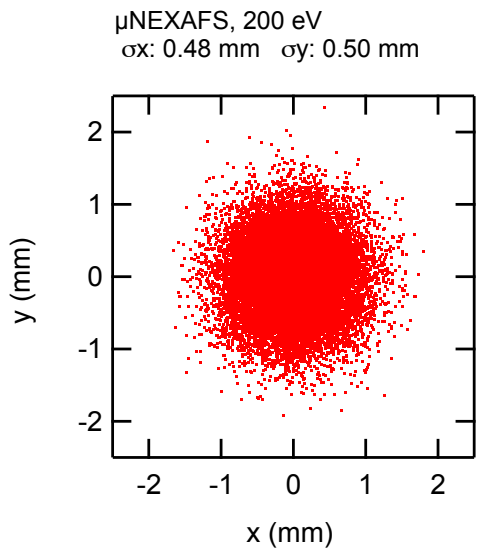

FIG. 13. Spot pattern of 200 eV at the μNEXAFS station using the M4C mirror. Caption as in Fig. 4

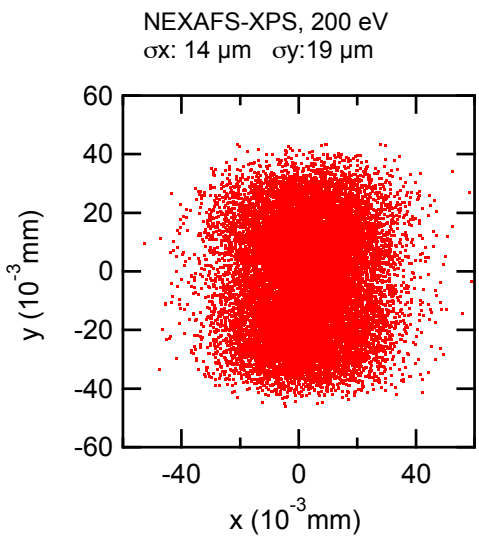

FIG. 12. Spot pattern of 200 eV at the NEXAFS/XPS station. Caption as in Fig. 4

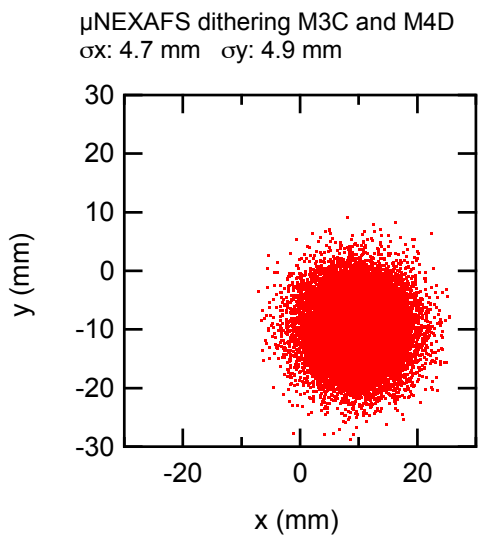

FIG. 14. Spot pattern of 200 eV at the μNEXAFS station when the pitch angles of M3C and M4C are changed by 0.2 mrad and 0.43 mrad, respectively. Caption as in Fig. 4

20 mm wide beam on sensitive samples at the μNEXAFS station).

E. NEXAFS/XPS

The spot at the NEXAFS/XPS station is displayed in Fig. 12. The dithering M4C by of ± 0.14 mrad will allow to increase the vertical spot size to 5 mm when performing NEXAFS on radiation sensitive samples.

F. μNEXAFS

The spot at this station (see Fig. 13) can be due to the beam diverging from the NEXAFS/XPS station when using M4C or that reflected by M4D. The former case is shown Fig. 13. When using M4D the beam RMS size at this station is <5 mm diameter. By dithering M3C by ± 0.22 mrad and M4D by ± 0.43 mrad will yield a 20×20 mm^2 spot at this station. Fig. 14 shows that by changing the pitch angles of M3C by 0.22 mrad and M4D by 0.43 mrad the illumination of the sample is centered at (-10mm ,-10mm) and the spot size of the beam is

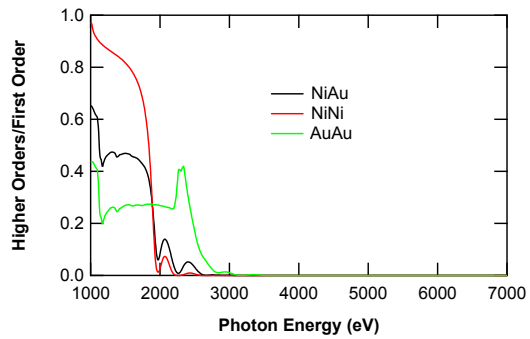

FIG. 15. Ratio of higher orders to first order from the reflectivities of L1 and L2

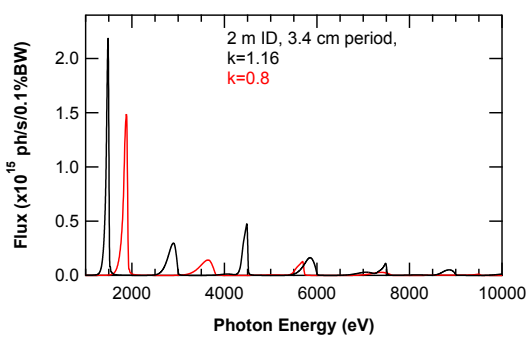

FIG. 16. Undulator flux from a 2 m device with 3.4 cm period though an aperture of $106\times72\mu\text{rad}^2$ (aperture equal to 4 times the central cone at 1.5 keV) when tuned to emit 1.5 keV (black trace) and 1.88 keV (red trace).

unchanged.

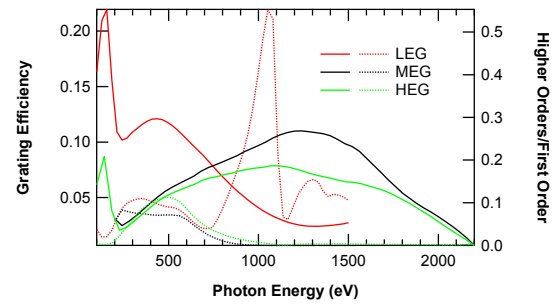

FIG. 17. Combined M2 and grating efficiencies (solid lines) and higher orders to first order ratio (dotted lines) when the monochomator is operated with the LEG (red), MEG (black) and HEG (green)

IV. HIGHER ORDERS

A. Tender branch

The ratio of higher orders to first order given by the reflectivity of the L1 and L2 mirrors when using the different optical coatings configurations is shown in Fig. 15. As seen in the figure, the contribution of higher orders is less than 13% for photon energies higher than 1.9 keV when one of the coatings is Ni. For lower energies the undulator itself will also provide suppression of higher orders. An example of the higher order contributions at 1.5 and 1.88 keV is seen in Fig. 16. From the figure, which shows the flux of the undulator as a function of the photon energy for two different k values, one obtains that the higher order contamination at 1.5 keV is 34 % and at 1.88 keV is 14 %.

B. Soft branch

We have designed the grove profile of the three gratings such as to obtain good efficiency for the combined M2 and grating operation as well as good higher order suppression. The parameters of the three gratings, calculated using Neviere's code [4], are listed in Table III. The three gratings are coated with Au and we have assumed Au for the coating of the M2 mirror. The LEG and the MEG groove profile are trapezoidal (the angle given in the table is a typical angle and will not change dramatically the results) and were selected to minimize the higher order contamination. The HEG, which is to be used for the higher energies, can be blazed providing higher efficiency than a trapezoidal. As seen in Fig. 17 the LEG provides less than 11% of higher order contribution between 100 and 828 eV. The higher order contamination of the MEG and HEG is less than 5% above 688 eV. The choice between them being dictated b the required energy resolution which is summarized in Fig 2.

[1] R. Reininger, *Optical design of the NIST soft and tender x-ray beamline complex at NSLS II (100 eV to 7.5 keV) for spectroscopy at the nanoscale*, Tech. Rep. (REPORT,

2010).
[2] R. Reininger, K. Kriesel, S. L. Hulbert, C. Sánchez-Hanke, and D. A. Arena, Rev. Sci. Instrum. **79**, 033108 (2008).
[3] C. Welnak, G. Chen, and F. Cerrina, Nucl. Instr. and Meth. A **347**, 344 (1994).
[4] M. Neviere, P. Vincent, and R. Petit, Nouv. Rev. Optique **5**, 65 (1974).

Appendix B

FMB Table of optics (location/specs)

APPENDIX B OPTICAL COMPONENT COORDINATES

Revised geometry with L2, M4A & HAXPES/NEXAFS moved downstream - this sheet takes into account the revised source location i.e. it incorporates both the undulators at 1.0 mrad.

	Component Coordinates			Distance from previous optical element			Total (vector) distance from previous optical element	Horizontal Turning Angle (degrees)	Resultant angle of beam (degrees)	Resultant angle of beam (mRad)	Vertical Turning Angle (degrees)	Resultant angle of beam (degrees)	Resultant angle of beam (mRad)	Agrees with cad model?	Component Coordinates from revised optical design report			Difference between revised component coordinates and optical design		
Optical Component	Z	X (Calculated)	Y	ΔZ	ΔX	ΔY									Z	X	Y	Z diff	X diff	Y diff
High energy insertion device	-1250	1.02	0					0.05729578	0.05729578	1.00	0	0	0	y	-1250	0	0	0	1	0
L1 (PLANE)	27450	29.72	0	28700.0	28.7	0.0	28700.0	-1.15	-1.0927042	-19.07	0	0	0	y	27450	29	0	0	1	0
L2A (TOROID)/L2B (PLANE)	34500	-104.75	0	7050.0	-134.5	0.0	7051.3	1.225675938	0.13297172	2.32	0	0	0	y	31756	-57	0	2744	-48	0
TENDER X-RAY MONO IN	46700.5	-76.43	0	12200.5	28.3	0.0	12200.5	0	0.13297172	2.32	0	0	0	y						
TENDER X-RAY MONO OUT	47590	-74.37	15	889.5	2.1	15.0	889.6	0	0.13297172	2.32	0	0	0	y						
HP NEXAFS	49642	-69.61	15	2052.0	4.8	0.0	2052.0	0	0.13297172	2.32	0	0	0	y	49642	-39	15	0	-31	0
HAXPES/NEXAFS	60347.6	-44.76	15	10705.6	24.8	0.0	10705.6	0	0.13297172	2.32	0	0	0	y	60039	-29	15	309	-16	0
L3 (PLANE)	62258	-40.33	15	1910.4	4.4	0.0	1910.4	1.225675938	1.35864766	23.71	0	0	0	y	62258	-27	15	0	-13	0
L4 (ELLIPSOID)	66766	66.59	15	4508.0	106.9	0.0	4509.3	1.225675938	2.58432359	45.10	0	0	0	y	66766	72	15	0	-5	0
µXPS	69763	201.86	15	2997.0	135.3	0.0	3000.1	0	2.58432359	45.10	0	0	0	y	69763	201	15	0	1	0

Figure 11. Co-ordinates of optical components on the 'L Branch'

Optical Component	Component Coordinates			Distance from previous optical element			Total (vector) distance from previous optical element	Horizontal Turning Angle (degrees)	Resultant angle of beam (degrees)	Resultant angle of beam (mRad)	Vertical Turning Angle (degrees)	Resultant angle of beam (degrees)	Resultant angle of beam (mRad)	Agrees with cad model?	Component Coordinates from revised optical design report			Difference between revised component coordinates and optical design		
	Z	X (Calculated)	Y	ΔZ	ΔX	ΔY									Z	X	Y	Z diff	X diff	Y diff
Low energy insertion device	1250	1.02	0					-0.05729578	-0.0572958	-1.00	0	0	0	y	1250	0	0	0	1	0
M1 (PLANE)	28580	-26.31	0	27330.0	-27.3	0.0	27330.0	3	2.94270422	51.36	0	0	0	y	28580	-27	0	0	1	0
SOFT X-RAY MONO IN	40080	564.85	0	11500.0	591.2	0.0	11515.2	0	2.94270422	51.36	0	0	0	y						
SOFT X-RAY MONO OUT	41173	621.03	15	1093.0	56.2	15.0	1094.5	0	2.94270422	51.36	0	0	0	y						
M3C (TANG ELLIPSE)	42062	666.73	15	889.0	45.7	0.0	890.2	3	5.94270422	103.72	0	0	0	y	42062	666	15	0	1	0
M3AB (TANG ELLIPSE)	42062	666.73	15	889.0	45.7	0.0	890.2	-3.5	-0.5572958	-9.73	0	0	0	y	42062	666	15	0	1	0
SLIT AB	48562	603.51	15	6500.0	-63.2	0.0	6500.3	0	-0.5572958	-9.73	0	0	0	y	48562	603	15	0	1	0
M4A (ELLIPSOID)	51628.77	573.68	15	3066.8	-29.8	0.0	3066.9	-3.5	-4.0572958	-70.81	0	0	0	y	51548	573	15	81	1	0
HAXPES/NEXAFS	60347.6	-44.76	15	8718.8	-618.4	0.0	8740.7	0	-4.0572958	-70.81	0	0	0	y	60039	-29	15	309	-16	0
M4B (ELLIPSOID)	66570.0	428.35	15	18008.0	-175.2	0.0	18008.9	-3.5	-4.0572958	-70.81	0	0	0	y	66571	427	15	-1	1	0
µXPS	69763	201.86	15	3193.0	-226.5	0.0	3201.0	0	-4.0572958	-70.81	0	0	0	y	69763	201	15	0	1	0
SLIT C	48527	1339.70	15	6465.0	673.0	0.0	6499.9	0	5.94270422	103.72	0	0	0	y	48527	1339	15	0	1	0
M4C (ELLIPSOID)	53500	1857.35	15	4973.0	517.7	0.0	4999.9	0	5.94270422	103.72	3	3	52.3598776	y	53500	1856	15	0	1	0
M4D (PLANE)	53500	1857.35	15	4973.0	517.7	0.0	4999.9	0	5.94270422	103.72	3	3	52.3598776	y	53500	1856	15	0	1	0
HP NEXAFS/FY	56480	2167.55	172	7918.0	1564.0	157.0	8072.5	0	5.94270422	103.72	0	3	52.3598776	y	56480	2167	172	0	1	0
M5C (PLANE)	60122	2546.66	364	6622.0	689.3	348.9	6666.9	0	5.94270422	103.72	-2	1	17.4532925	y	60122	2546	364	0	1	0
NEXAFS/XPS	62116	2754.22	399	1994.0	207.6	35.0	2005.1	0	5.94270422	103.72	0	1	17.4532925	y	62116	2753	399	0	1	0
µNEXAFS IMAGING	65093	3064.11	626	11593.0	1206.8	610.8	11671.6	0	5.94270422	103.72	0	1	17.4532925	y	65093	3063	626	0	1	0

Figure 12. Co-ordinates of the optical components in the 'M Branch' and transfer branches

Appendix C

FMB PDR documents and review reports

150506 SST PDR

Wednesday, May 06, 2015
9:01 AM

Present: Andrew Ackerman, Zhong Zhong, Bruce Ravel, Dan Fischer, Rob Todd, John Fabijanic, Joe Woicik, Mary Carlucci-Dayton, Steve O'Hara, Lori Stiegler, Amy Xia (at BNL), Mike Gaffney. Scott Mowat, Andrew Broadbent (in Oxford).

General overview of the beamline.

- Cryocooler rack interferes with a pylon - minor problem, will be optimized. Needs care with the egress aisle space.
- Viewports should be covered with Lexan.

Vacuum considerations

- AF provided a guided tour of the vacuum sections - all seems sensible.
- Question about whether VS18 could be split into 2 sections - action Dan to decide (would need some extra vacuum hardware).
- Concern about Kapton (from AML) in white beam sections. Options include alternative radiation hard cable (including different Kapton, eg from Allectra), or shielding of cables.
- Bakeout heaters and controllers to be provided by BNL.
- Rob Todd asked about water cooled pumps - outside the scope of this review (this is NIST supplied items).
- Rob asked about cables. Doug Smith will calculate the cable lengths and may ask BNL to procure this for NIST.
- FOE WB and PB valves can be retrofitted with additional switches for interface to the EPS. Action BNL/NIST.
- Relief of overpressure conditions: burst discs on all WB/PB mirrors, monos, plus M3, not (cooled) slits or any of the (uncooled) mono beam components.
- Calculation required at FDR of sizing of LN2 to GN2 relief in the DCM.
- Cryocooler: standard product. At FDR details on line support (extremes of rotation), fatigue - show model with carriage in max/min positions.

Lifting

- Lifting diagrams for all large items
- Jackable casters bolt on - as for CSX.
- Approved rigging accessories only.
- Cryocooler lifting frame - same as CSX/HXN. Nothing special required.
- Mike Question about use of the frame for maintenance - BSA employees? Who does maintenance.

PPS

- Need to schedule the IWG for this beamline (not relevant to this beamline)
- Need to order the vacuum switches. These can be fitted to "T-pieces" on gauge ports.

Safety

Safety overview of installation and commissioning - taken from HXN. No Be hazards. No questions or concerns. Lori had left, but Andrew Ackerman was present.

Radiation safety

- Exposed lead to be painted red.
- Secondary BS shields don't want to be too close to the wall.
- The soft x-ray beam pipe, first section after hutch may require shielding. Amy will advise later whether this is required, followed her calculations.
- Beam stops to be in separate vessels
- Dan needs to check PGM viewport locations - same window materials as CSX - should be ok.
- DCM D/S viewport - NIST to decide how to deal with this - Lead glass or camera inside a restricted enclosure.

Other
Some stands still required to be added to the model.

150505 PDR discussion

Tuesday, May 05, 2015
6:19 AM

General layout:

1. egress aisles. Ideas for new locations;

- Upstream egress aisle - upstream of DCM, downstream of M3
- Downstream egress aisle - upstream of M4A and downstream of HP NEXAFS end station. Need to check this is a useful location with respect to the QAS end station or equipment.
- Add gate valves downstream of precision slits. Need roughing port. Dan to ask Klaus to contribute to the cost of the gate valves.

2. Diagnostics

- Soft x-ray BPMs defined by Ruben.
  - Dan is interested in the inclusion of an evaporation system for all diagnostic modules. May need an extra port on the side. **Talk about this off-line**.
  - Need diagnostic modules upstream of microNEXAFS, including slits, as other modules, etc.
  - Single pair of diagnostic modules needed upstream of microNEXAFS - support on the same stable stand. Can slits also be fitted in this location? Action FMB-O.
- Tender:
  - Kapton foil can be very thin (down to 7.5 microns) Scott sent note to Dan about this. NIST want thinnest possible foils and have nanoBPM retractable, and place for nanoBPM just at "nanoBPM position 2".
  - After DCM, PBS in separate vessel, 4 jaw slits, diagnostic module (YAG screen, Ni mesh intensity monitor and photodiode intensity monitor), ie as standard but with Ni not Au on the mesh.
  - Just before the HAXPES chamber use the NanoBPM. Additional diagnostic not needed since this is available after the DCM (see above).

- An additional NanoBPM could included, initially be located at DM1 just downstream of DCM - then moved downstream to final location downstream of HAXPES.
- Support stand (for dual diagnostic module comprising, for each beamline: two intensity monitors (Au/Ni mesh for Soft/Tender branches respectively), photodiode and YAG screen module), and slits (if possible) to be added when the microXPS interfaces are defined. (Action NIST).

- AF has a layout drawing - useful to go through.

4. Model

- Was up to date except: pumps - FMB-O to add pumps under the fluorescent screens in the FOE.
- Needs some other changes now (diagnostics, see below)

- Hexapods
- Move after power failure?
- Range of angular motion? L3 - range specified is less than the standard motions (question from Joe). The "real" specs are in the HFS documents and may be less due to bellows or other constraints.

- Andrew has sent the Parasolid , split up as requested, some updates to be made. Will send an update mid-next week.

7. Software changes

- FMB-B will quote. The will quote too low.
- CosyLab will charge for all aspects of each change.
- Basic functionality for each component.
- Scott doesn't know the scope of the PGM
- Dithering interface not included
- NIST went out to bid for the software, CosyLab rang up and were given the impression that there was a preferred bidder.

- Shutters - AF can show layout with shutters. Seems ok.

9. Radiation shielding

- Shielding of the pink beam scattered from DCM. Use a flange after the DCM before the gate valve with a small hole in order to stop scattered beam. ***Later thoughts in discussion with Andrew Fairley: this is not needed, see Amy's calculations: basic vessel and transport pipes are fine to shield the incoming pink beam, therefore scattered pink beam from first crystal should be no problem***.
- Leave the PBS inside the DCM, as manufactured, but this is part of the EPS, not PPS - this helps to protect the gate valve from pink beam damage. New PBS in diagnostics module is the PPS device.

- Utilities - looked at the drawings from Brian. Caution: secondary Bremsstrahlung shields go close to wall.
- Get an example cable study for Doug Smith
- Make sure the first pair of cable trays

Reference Documents:

Reference Number	Date/ Issue	Title
SB1341-14-CN-0042-PART I	19/09/14	NIST Contract
	05/05/12	Revised optical design of the NIST soft and tender x-ray beamline complex at NSLS-II (Ruben Reninger).
E3160	April 2014	NIST NSLS-II SST and BMM Beamline Backbones, Volume 2A, SST Technical Proposal
S3160	Nov 2014/REV 01	NIST SST BEAMLINE S3160 QUALITY PLAN
LT-C-XFD-STD-BL-COORD-001	May 2011	Beamline Coordinate System Standards
SR-DG-LAY-3007	19/12/2014	DIAGNOSTICS LAYOUT NIST SST1-SST2, C07-S1
FOR FULL LIST OF REFERENCE DOCUMENTS, SEE APPENDIX A		

FMB Oxford
Units 1-3 Ferry Mills,
Osney Mead,
Oxford, OX2 0ES,
UK,

Contact: Andrew Fairley
Telephone: +44 (0)1865 320 313
Fax: +44 (0)1865 320 301
E-mail: andrew.fairley@fmb-oxford.com

Change log:

Revision	Date	Summary of Change	Approval
1.0	20/03/15	First Issue	SM
2.0	23/03/15	Component Corrections around L4/M4B.	
3.0			
4.0			
5.0			

TABLE OF CONTENTS **1**
1. *INTRODUCTION* **3**
1.1 CO-ORDINATE SYSTEM 3
2. *SPECIFICATIONS* **4**
2.1 BEAMLINE SOURCE 4
2.2 BEAMLINE MODES 4
2.3 BEAMLINE COMPONENTS 6
2.3.1 Tender beamline "L" branch *6*
2.3.2 Soft beamline "M" branch *8*
2.3.3 Transfer Branch to HAXPES/NEXAFS *11*
2.3.4 Transfer Branch to μXPS *13*
2.4 VACUUM DESIGN 14
2.5 UTILITIES 14
3. BEAM CONDITIONING ELEMENTS **15**
3.1 DIAGNOSTICS 15
3.2 FLUORESCENT SCREENS 16
3.3 BEAM SHUTTERS 18
4. SHIELDED PINK BEAM TRANSPORT TO DCM **19**
4.1 PUMP BOX AND SUPPORTS 21
4.2 BELLOWS 22
4.3 SHIELDED PIPE CONSTRUCTION METHOD 22
5. *SCOPE OF SUPPLY* **23**
APPENDIX A – REFERENCE DOCUMENTS **24**
APPENDIX B OPTICAL COMPONENT COORDINATES **25**
APPENDIX C SOURCE REFERENCE DRAWING **27**

1. *INTRODUCTION*

This document describes the optical layout and operation modes of the NIST SST beamline at NSLS-II. Detailed specifications for the individual beamline components (fixed cooled mask, mirror systems, diagnostic modules, precision slits, DCM) and beamline controls can be found in separate documents – see Appendix A for the full list of reference documents.

1.1 CO-ORDINATE SYSTEM

Figure 1 below shows the beamline coordinate system. At the source height (1400 mm above the experimental hall floor y=0. The origin (in terms of x and z) is located at the centre of the straight section – see NSLS-II drawing SR-DG-LAY-3007 (Appendix C)

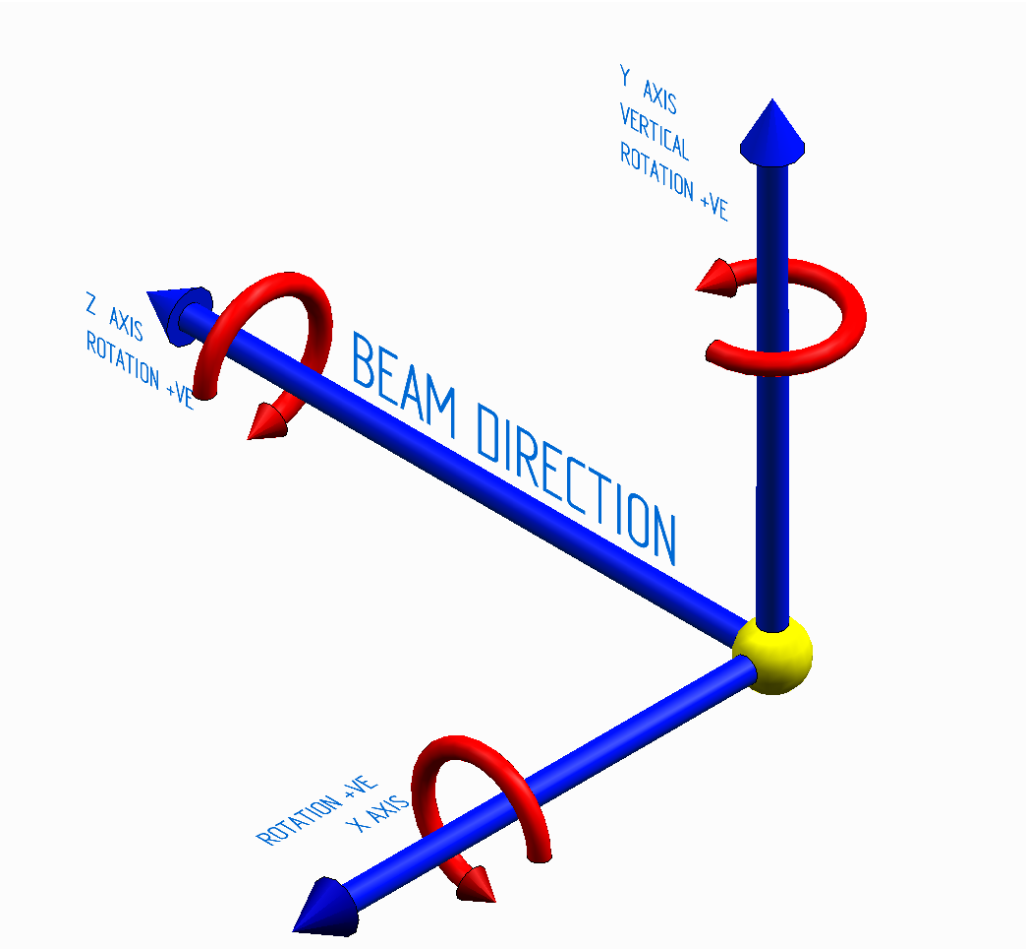

Figure 1. NSLS-II Coordinate System

The co-ordinate system employed complies with NSLS-II document:

Beamline Co-ordinate System Standards LT-C-XFD-STD-BL-COORD-001.

2. *SPECIFICATIONS*

2.1 BEAMLINE SOURCE

The source for the SST beamlines is a pair of undulators, canted at 2mrad to each other (see Figure 2). The source parameters can be found in the document "RSI for the Sources and Front-Ends for the SST1&2 and BMM Beamlines (NIST)".

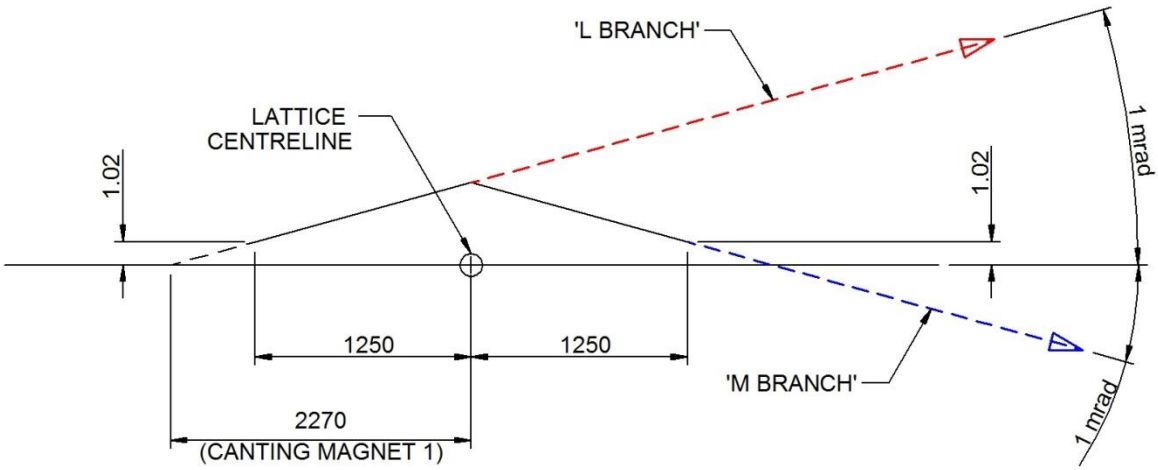

Figure 2. Canted Undulator Source Geometry

2.2 BEAMLINE MODES

The optical layout is designed to accommodate a total of six experimental end stations. Two of the end stations can be illuminated by soft and tender x-rays (HAXPES NEXAFS and µXPS), three only with soft x-rays (HP NEXAFS FY, NEXAFS XPS and µNEXAFS) and one only with tender x-rays (HP NEXAFS).

There are 13 mirror optics in the SST beamline (excluding the optic located in the PGM – M2). The optics are located in ten hexapods, with the L2, M3AB/M3C and M4C/M4D mirror systems holding two optics each.

All of the optics are side bounce except for M4C (bounce up), M4D (bounce up) and M5C (bounce down). There are four cooled optics located in the white beam section hutch/first optical enclosure (FOE) – L1, M1, L2A and L2B. The first optical elements in the soft and tender beamlines (L1 and M1) are internally cooled. The second optics in the 'L' branch (L2A and L2B) are side cooled. M3AB and M3C are both temperature stabilised using water cooling. All of the other optics are located outside the hutch and are uncooled.

Table 2. End Station Details

End Station	Optical path to end station	Energy	Comments
HP NEXAFS	U42-L1-L2A-DCM **or** U42-L1-L2B-DCM for larger spot size.	Tender	L1 and L2B are planar optics. L2A is a toroid designed to focus at HAXPES/NEXAFS.
HAXPES / NEXAFS	U42-L1-L2A-DCM **or** U42-L1-L2B-DCM for larger spot size.	Tender	The focus of the toroidal optic L2A is at this end station i.e. the meridional and sagittal radii are specified for focus at this end station.
	EPU-M1-PGM-M3AB-V.SLIT AB-M4A	Soft	M3AB is a horizontally focussing tangential ellipse. It's focus is on the precision vertical slit AB. The vertical slit forms a secondary source which is refocused horizontally and vertically (at HAXPES/NEXAFS) using ellipsoidal optic M4A.
µXPS	U42-L1-L2B-DCM-L3-L4	Tender	L4 is the first focussing optic in the optical path to this end station. It is an ellipsoidal optic which focusses horizontally and vertically. It can be yawed to produce a larger spot size.
	EPU-M1-PGM-M3AB-V.SLIT AB-M4B	Soft	As with the HAXPES/NEXAFS endstation, slit AB forms a secondary source. Ellipsoidal optic M4B refocuses horizontally and vertically at the end station.
HP NEXAFS/FY	EPU-M1-PGM-M3C-V.SLIT C-M4D	Soft	Takes the converging beam which is focused at NEXAFS/XPS. M3C and M4D can be dithered to increase the spot size in width and height (respectively).
NEXAFS/XPS	EPU-M1-PGM-M3C-V.SLIT C-M4C-M5C	Soft	Bounce-up ellipsoidal optic M4C images the secondary source of precision vertical slit C at this end station. Bounce down plane optic M5C is dithered about a horizontal axis to increase the vertical size of the spot at this end station.
µNEXAFS	EPU-M1-PGM-M3C-V.SLIT C-M4D **or** EPU-M1-PGM-M3C-V.SLIT C-M4C	Soft	Tangential ellipse optic M3C can be rotated about a vertical axis (dithered) to increase the horizontal size of the spot at the end station. Planar optic M4D can be dithered about a horizontal axis to increase the vertical size of the spot at the end station. Alternatively, the spot at this end station can be due to the diverging beam from M4C (whose focus is at NEXAFS/XPS)

2.3 BEAMLINE COMPONENTS

2.3.1 Tender beamline "L" branch

Item	Description	Vacuum Section
1	*Gate Valve 0 (DN150). Not in scope*	1
2	Bellows DN150 (Hydroformed)	1
3	Ion pump, 300l on pumping tee with vac gauges	1
4	Fixed cooled mask	1
5	Ion pump 150l on pumping tee	1
6	Bellows DN100	1
7	**L1 (includes vacuum gauges)**	1
8	Gate Valve 1 (DN100)	2
9	Bellows with spool piece DN100	2
10	**M1 (includes vacuum gauges)**	2
11	Gate Valve 2 (DN100)	3
12	Bellows DN100	3
13	Diagnostics module with cooled slits, cooled white beam stop (FS1), ion pumps (75l and 300l) and vacuum gauges	3
14	Gate valve 3 (DN63)	4
15	Flight tube (Location of in-air secondary Bremsstrahlung collimator).	4
16	Bellows DN63	4
17	Zero length adapter	4
18	Pump Stand with DE Ion pump, 300l	4
19	Bellows DN150	4
20	**L2A/L2B (includes vacuum gauges)**	4
21	Bellows DN150	4
22	Stand with short tube (This holds the in-air tungsten Bremsstrahlung block. Space will be required for an in-vacuum bremsstrahlung block)	4
23	Bellows DN40	4

24	Flight tube with cooled CVD diamond fluorescent screen added (FS2)	4
25	Bellows	4
26	FOE Shutter 1 (NSLS-II standard – NIST supply)	4
27	Gate Valve 5 (DN63) – located inside the hutch	5
28	Shielded Pink Beam Flight Tube (DN100) through hutch wall/guillotine	5
29	Bellows, DN100 hydroformed.	5
30	DE Ion pump 150l	5
31	Bellows, DN100 hydroformed.	5
32	Shielded Pink Beam Flight Tube (DN100)	5
33	Bellows DN100	5
34	**DCM (including Gate Valve 6 to isolate the turbo pump)**	5
35	Gate Valve 7 (DN100)	6
36	Bellows DN100	5
38	**Diagnostic module 1** with pink beam stop (transferred from DCM), Fluorescent screen (FS3), slits and vacuum gauges	6
39	Bellows DN63	6
40	Flight tube. Removeable – may be replaced with beam shutter	6
41	Gate valve 8 (DN63)	7
42	**HP NEXAFS End Station**	7
43	Gate valve 9 (DN63)	8
44	Bellows DN63	8
45	Beam Shutter 2 (NSLS-II standard – NIST supply)	8
46	Bellows DN63	8
47	Flight tube	8
48	DE Ion pump 150l	8
49	Flight tube with vacuum gauges and RA valve	8
50	DE Ion pump150l	8
51	Flight tube with **uncooled fluorescent screen (FS4)**	8

52	Bellows DN63	8
53	Gate valve 10 (DN63)	9
54	**HAXPES/NEXAFS endstation**	9
55	Gate valve 11	10
56	Bellows DN63	10
57	Flight tube	10
58	Bellows DN63	10
59	**L3**	10
60	Bellows	10
61	Flight tube with uncooled fluorescent screen (FS5). Manual actuator.	10
62	Bellows DN63	10
63	Beam Shutter 3 (NSLS-II standard – NIST supply)	10
64	Bellows DN63	10
65	DE Ion pump 150l	10
66	Bellows	10
67	Flight tube	10
68	Bellows DN63	10
69	Gate valve 12 (DN63)	11
70	**L4/M4B**	11
71	Gate Valve 13	12
72	Bellows DN63	12
73	Flight tube with **uncooled fluorescent screen (FS6)**	12
74	**µXPS endstation**	12

2.3.2 Soft beamline "M" branch

Item	Description	Vacuum Section

1	***M1***	*2*
2	*Gate Valve DN100*	*3*
3	*Bellows DN100*	*3*
4	*Diagnostics module with cooled slits, cooled white beam stop, ion pumps (75l and 300l) and vacuum gauges - this unit is item 13 in the 'L' branch above.*	*3*
5	Gate valve 4 (DN63)	13
6	Flight tube (location for in-air secondary Bremsstrahlung collimator)	13
7	Bellows DN63	13
8	Zero length adapter	13
9	DE Ion pump, 150l	13
10	Zero length adapter	13
11	Bellows	13
12	Tube with flange to accommodate in-flange Bremsstrahlung collimator	13
13	Flight tube with vac gauges and cooled CVD diamond fluorescent screen added (FS7).	13
14	FOE Shutter 4 (NSLS-II standard – NIST supply)	13
15	Short flight tube through hutch wall	13
16	Gate valve 4	14
17	Flight Tube	14
18	Bellows	14
19	DE Ion pump 150l	14
20	Flight Tube	14
21	Bellows DN100	14
22	Plane Grating Monochromator. Vacuum gauges included.	14
23	Bellows with spool piece	14
24	Gate valve 15	15
25	M3 (M3C)	15
26	Bellows DN100	15
27	Vessel with coated beam stop (FS8)	15

28	Flight tube	15
29	Gate valve 23	21
30	Bellows DN63	21
31	Beam Shutter 7 (NSLS-II standard – NIST supply)	21
32	Bellows	21
33	Flight tube	21
34	**Diagnostic Module 5** with Fluorescent screen (FS13), Gold mesh intensity monitor, diode intensity monitor, slits and vacuum gauges.	21
35	Flight tube	21
36	Bellows	21
37	DE Ion pump 150l	21
38	Bellows	21
39	Flight tube	21
40	Bellows DN40	21
41	**Precision cooled vertical slit C**	21
42	Bellows DN40	21
45	Flight tube	21
46	DE Ion pump 150l	21
47	Flight tube	21
48	Gate valve 24 (DN63)	21
49	Bellows DN100	22
50	**M4C/M4D**	22
51	Bellows DN100	22
52	Flight tube	22
53	Bellows	22
54	**Diagnostic Module 6** with Fluorescent screen (FS14), Gold mesh intensity monitor, diode intensity monitor and slits.	22
55	Bellows	22
56	Gate valve 25 (DN63)	23
57	**HP NEXAFS/FY**	23

58	Gate valve 26 (DN63)	24
59	Bellows	24
60	Flight tube	24
61	Bellows	24
62	DE Ion pump, 150l	24
63	Bellows	24
64	Flight tube	24
65	Bellows DN63	24
66	Beam Shutter 8 (NSLS-II standard – NIST supply)	24
67	Bellows DN63	24
68	**M5C**	24
69	Bellows	24
70	Flight tube with **uncooled fluorescent screen (FS15)**	24
71	Gate valve 27	25
72	Bellows	25
73	**NEXAFS/XPS µNEXAFS endstation**	25
74	Beam Shutter 9 (NSLS-II standard – NIST supply)	25
75	**µNEXAFS endstation**	25

2.3.3 Transfer Branch to HAXPES/NEXAFS

Item	Description	Vacuum Section
1	M3 (M3AB)	15
2	Bellows	15
3	Flight tube with uncooled fluorescent screen	15
4	Gate valve 16 (DN63)	16
5	Bellows	16
6	Flight Tube	16
7	**Diagnostic Module 2** with Fluorescent screen (FS9), Gold mesh	16

	intensity monitor, diode intensity monitor, slits and vacuum gauges.	
8	Flight tube	16
9	Bellows	16
10	DE Ion pump 150l	16
11	Bellows	16
12	Flight Tube	16
13	**Precision cooled vertical slit AB**	16
14	Bellows	16
15	Flight tube	16
16	Bellows	16
17	Gate valve 17	17
18	**M4A**	17
19	Gate valve 18	18
20	Bellows	18
21	Flight tube in splitter vessel	18
22	DE Ion Pump 300l	18
23	Flight Tube	18
24	Bellows	18
25	Flight Tube	18
26	Beam Shutter 5 (NSLS-II standard – NIST supply)	18
27	Bellows	18
28	Flight tube	18
29	**Diagnostic Module 3** with Fluorescent screen (FS10), Gold mesh intensity monitor, diode intensity monitor, slits and vacuum gauges.	18
30	Gate valve 19	9
31	Bellows	9
32	Flight tube with vac gauges and RA valve	9
33	**HAXPES/NEXAFS Endstation**	9

2.3.4 Transfer Branch to µXPS

Item	Description	Vacuum Section
1	**M4A**	18
2	Gate valve 18	18
3	Bellows	18
4	Flight Tube in splitter vessel	18
5	DE Ion Pump 300l	18
6	Flight Tube	18
7	Bellows	18
8	Flight Tube	18
9	DE Ion pump 150l	18
10	Bellows	18
11	Flight tube	18
12	*Beam Shutter 6 (NSLS-II standard – NIST supply)*	18
13	Bellows	18
14	**Diagnostic Module 4** with Fluorescent screen (FS11), Gold mesh intensity monitor, diode intensity monitor and slits.	18
15	Bellows	18
16	Gate valve 20	19
17	Flight tube with vacuum gauges and RA valve	19
18	DE Ion pump 150l	19
19	Bellows	19
20	Flight tube	19
21	Bellows DN63	19
22	Gate valve 21 DN63	20
23	**L4/M4B (includes vacuum gauges)**	20
24	Gate valve 22 DN63	12
25	Bellows	20
26	*Flight tube with* ***uncooled fluorescent screen (FS12)***	12

27	**µXPS Endstation**	12

2.4 VACUUM DESIGN

Vacuum	UHV compatible (< 5 x10^{-10} mbar). Masses >38 AMU shall have total pressure <10^{-11} Torr (1.33 x 10^{-11} mbar).
Helium leak rate	< 1 x 10 $^{-10}$ mbar l/sec
Vacuum gauges	One pirani gauge (MKS type 317) and one cold cathode gauge (MKS type 422) located in each vacuum section.
Vacuum gauge controllers	MKS 937B
Ion Pumps	Each vacuum section will be fitted with one or more Gamma Vacuum ion pumps
Ion Pump Controllers	Gamma MPC controller
Gate Valves	VAT Valve Series 108 with position switches. Gate valves must be connected to the reticulated air supply by NIST/BNL
Right Angle Valves	Each vacuum section to be fitted with DN40 CF VAT Valve Series 54.

2.5 UTILITIES

Utilities requirements are described on the top level drawing for the beamline (ABM0042).

3. BEAM CONDITIONING ELEMENTS

3.1 DIAGNOSTICS

The six diagnostic modules are located as follows (see Figures 3 and 4):

1. DM1 - Downstream of the DCM in the tender 'L' beamline – between the DCM and the HP NEXAFS end station. Located at 48241 mm from the middle of the straight section.

2. DM2 - Between mirror system M3AB/M3C and the precision vertical slit 'AB' on the soft x ray transfer branch. Located at 45362 mm from the middle of the straight section.

3. DM3 - Downstream of the M4A mirror system in the HAXPES/NEXAFS branch of the 'M' soft x ray beamline. Located at 56593 mm from the middle of the straight section.

4. DM4 - Downstream of the M4A mirror system in the μXPS branch of the 'M' soft beamline, allowing monitoring with optic in beam and out of beam (i.e. directly from the precision slit). Located at 57825 mm from the middle of the straight section.

5. DM5 - Between mirror system M3AB/M3C and the precision vertical slit 'C' on the soft x ray beamline ('M' branch). Located at 46784 mm from the middle of the straight section.

6. DM6 - Immediately downstream of the M4C/M4D mirror system. This enables monitoring of the beam with the optics in or out of beam. Located at 54326 mm from the middle of the straight section.

3.2 FLUORESCENT SCREENS

There are 15 fluorescent screens in the NIST SST beamlines. All six of the fluorescent screens located in the diagnostic modules use YAG crystals (Yttrium Aluminium Garnet) as the fluorescent material.

The fluorescent screens used on the diagnostic modules are motorised and mounted on a DN63/CF114 conflat. A Prosilica CCD mono camera and 18mm lens are used to view the screen.

The details of the fluorescent screens are as follows:

Fluorescent Screen	Location	Notes
FS1	White beam stop	Beam stop is P43 coated, camera is shielded.
FS2	L branch exiting first optical enclosure	Cooled CVD diamond
FS3	In diagnostic module 1	YAG
FS4	On the L branch, entering HAXPES/NEXAFS - TBC	YAG
FS5*	At exit of mirror L3	
FS6	At the exit of mirror L4	
FS7	M branch exiting first optical enclosure	Cooled CVD diamond
FS8*	Imaging beam stop at exit of PGM	Beam stop/FS is P43 coated.
FS9	Exiting M3AB in Diagnostic Module 2	YAG
FS10	Imaging precision slit AB in Diagnostic Module 3	YAG
FS11	Exiting M4A in Diagnostic Module 4	YAG
FS12*	At exit of mirror M4B	
FS13	Exiting M3C in Diagnostic Module 5	YAG
FS14	Exiting M4CD in Diagnostic Module 6	YAG, also images directly precision slit AB
FS15	Exiting M5C	YAG

*Indicates a fluorescent screen that has been added since the tender.

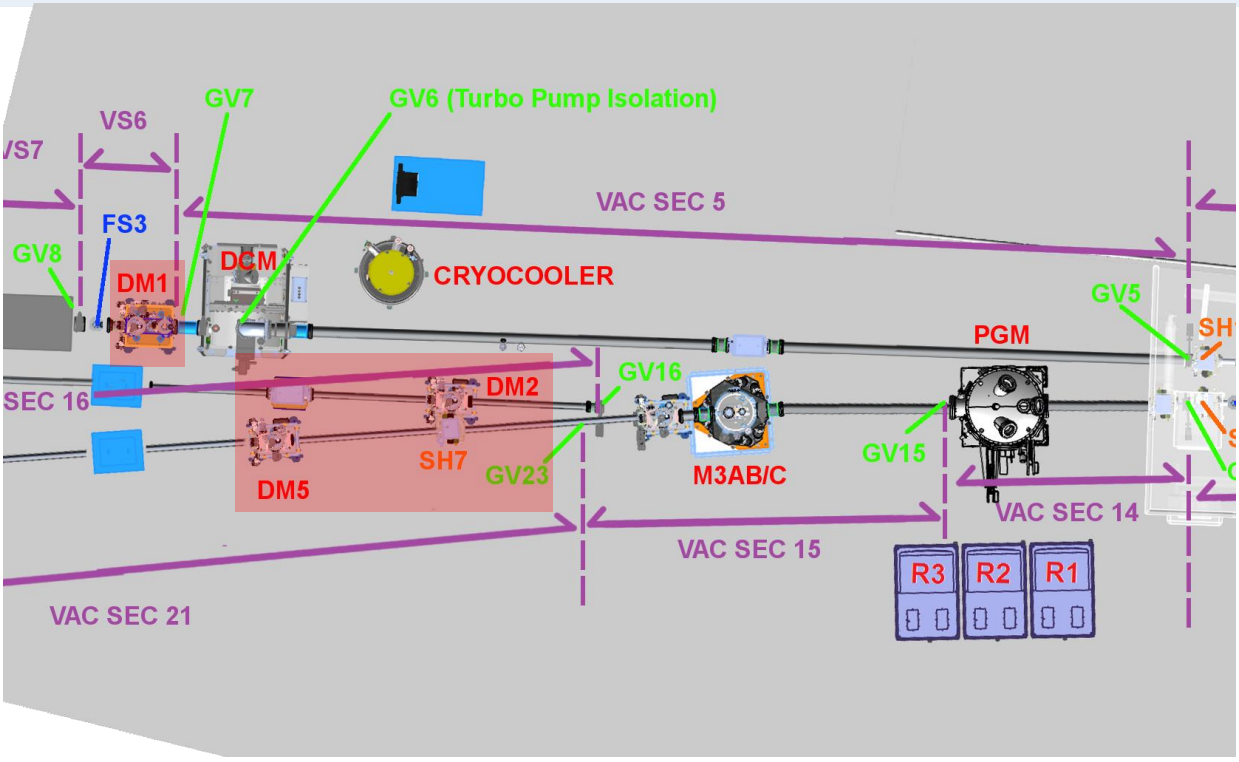

Figure 3. Diagnostic modules DM1, DM2 and DM5.

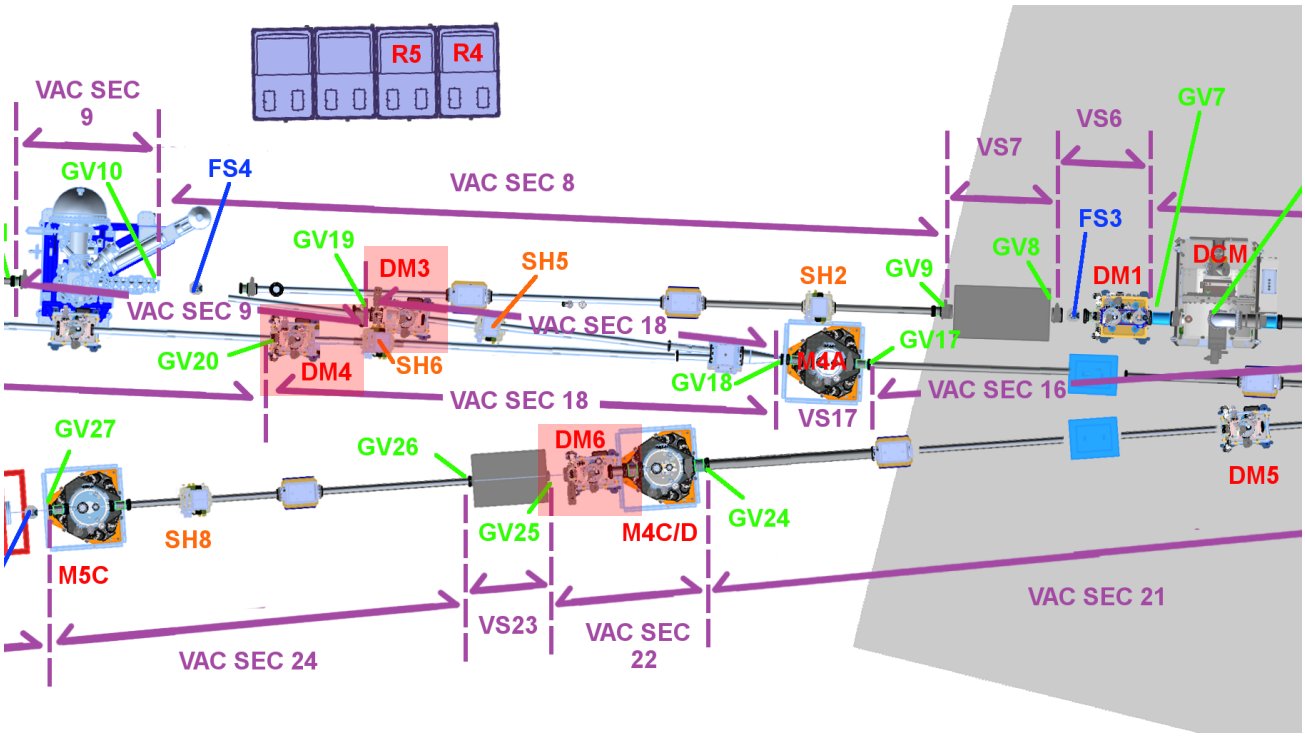

Figure 4. Diagnostic modules DM3, DM4 and DM6.

3.3 BEAM SHUTTERS

It is assumed that BNL will integrate beam shutters into the SST beamline. They are positioned in the following locations:

1. At the end of the white beam section in the 'L' branch, before the hutch wall (SH1)
2. Downstream of the HP NEXAFS end station (SH2)
3. Downstream of the mirror system L3, on the 'L' branch (SH3)
4. At the end of the white beam section in the 'M' branch, before the hutch wall (SH4)
5. Upstream of the HAXPES/NEXAFS end station, on the transfer branch from M4A (SH5)
6. Downstream of the M4A mirror system, on the transfer to μXPS end station (SH6)
7. Downstream of the M3AB/C mirror system, on the 'M' branch (SH7)
8. Upstream of the M5C mirror system (SH8)
9. Between the NEXAFS XPS end station and the μNEXAFS end station (SH9)

The selection of standard NSLS II beam shutters in these locations will facilitate the safety approval process and allow rapid connection into the facility EPS/PSS.

NIST will therefore deliver, align and install the nine off standard NSLS II beam shutters complete with vacuum vessels and stands, into position at a time agreed with all parties.

Note that shutters 8 and 9 need to substantially taller than the other 7 shutters to suit the inclined (3°) beam pipes situated downstream of the M4C/M4D mirror system.

4. SHIELDED PINK BEAM TRANSPORT TO DCM

Figure 5. Shielded Vacuum Tube on XPD Beamline at NSLS II

The shielded vacuum tubes have radiation shielding that conforms to existing equivalent radiation standards. FMBO have elected to work with INNOSPEC with whom we have delivered shielded vacuum sections into the Australian Synchrotron and NSLS II.

The pink beam shielded pipe section includes 2 support posts in addition to a double support post which supports the lead box which encloses the pump and bellows in the middle of the section.

Parameter	**Value**
Shielding Material	Pb (EN12588)
Vacuum Tube Pb Thickness	7 mm
Pump box Pb Thickness	8 mm
Wall Collar	8 mm
Cover Material	Stainless Steel
Vacuum Tube thickness	2 mm
Flange box thickness	2 mm

The steel stands, parts will be painted RAL5007 (FMBO Oxford Standard), as per other stands on the SST beamline.

Any exposed lead will be painted Flame Red RAL 3000 as per BSA's specs.

All pipes will have non-rotatable Conflat flanges on the upstream end and rotatable Conflat flanges on the downstream end.

Lead collars will be supplied for installation at the exit of the optics hutch. All guillotines will be supplied by BSA/NIST. The lead shielded pipe exceeds 5.5 m in length from the external wall of the hutch. The lead shielded pipe will include a pump stand and two pipe stands.

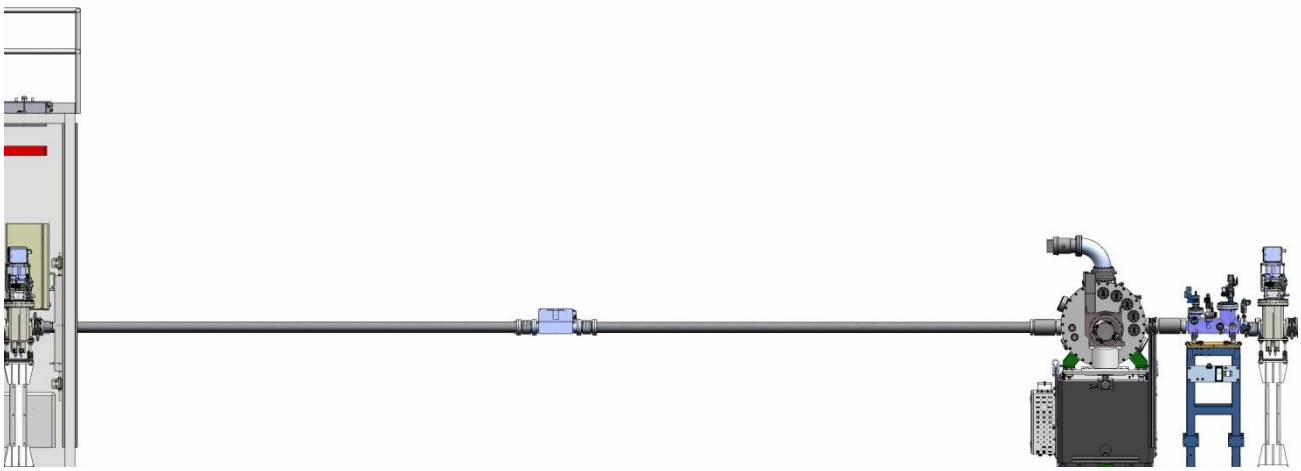

Figure 6. Shielded Pink Beam Tube

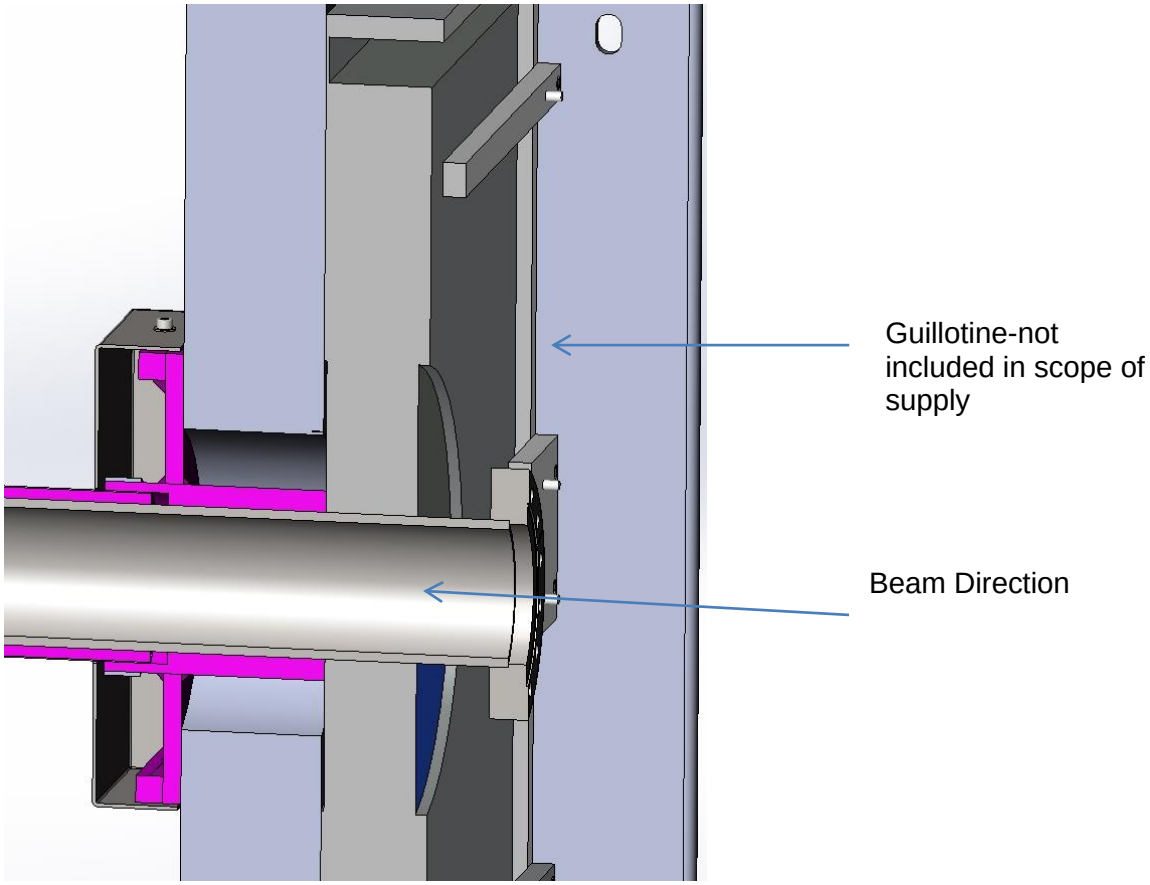

Figure 7. Image showing the lead collar between the shielded beamtube and the hutch wall

4.1 PUMP BOX AND SUPPORTS

The lead box includes tube collars on either end to ensure sufficient lead coverage as shown in the image below. The stands will provide an adjustment of ±30mm.

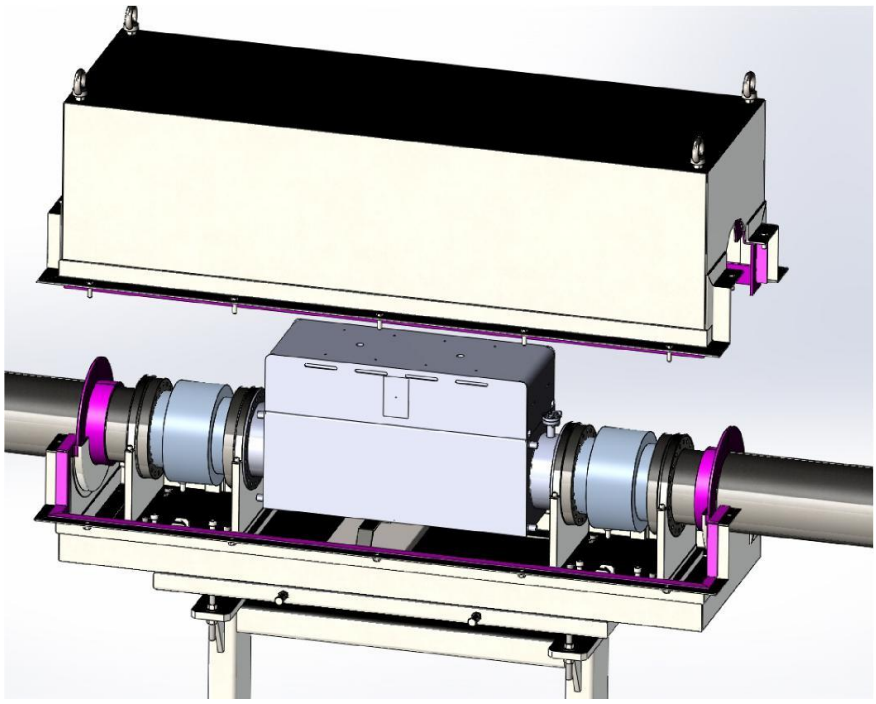

Figure 8. Pump Box and bellows

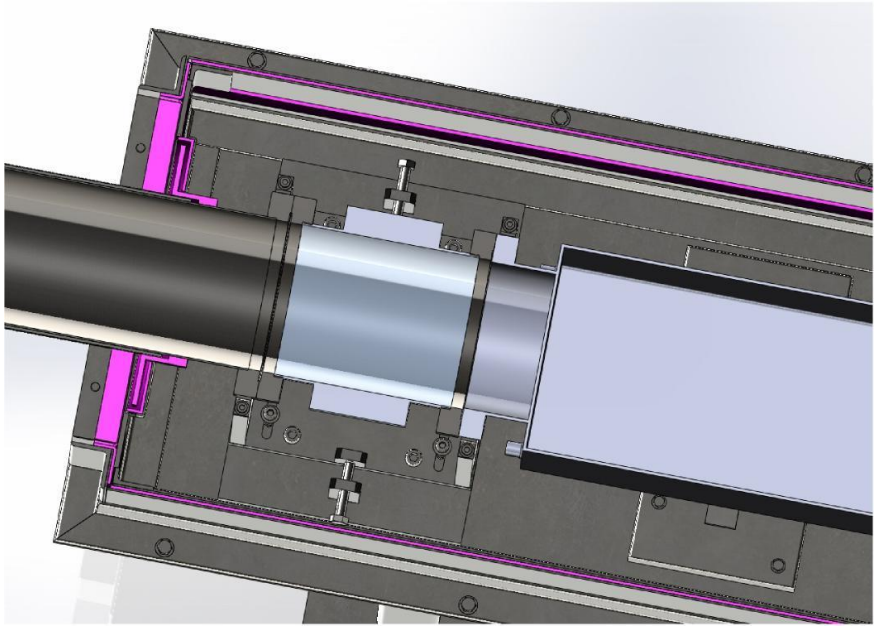

Figure 9. Pump Box

4.2 BELLOWS

Bellows connecting the shielded tube sections are:
200 mm long Stainless Steel Hydroformed Bellows
Axial and Lateral compliance ±5mm
DN100/CF150 (6” OD) Fixed at upstream end
DN100CF150 (6” OD) Rotatable at downstream end

4.3 SHIELDED PIPE CONSTRUCTION METHOD

The lead shielded tubes will be manufactured by Innospec. They will be pre-baked in the FMBO factory and sealed, to maintain cleanliness. They will then be delivered to Innospec for lead shielding. The lead shielding is done by forming a shell which fits around the tube and is then welded. A pair of thin stainless steel shells are then fitted to cover the lead.

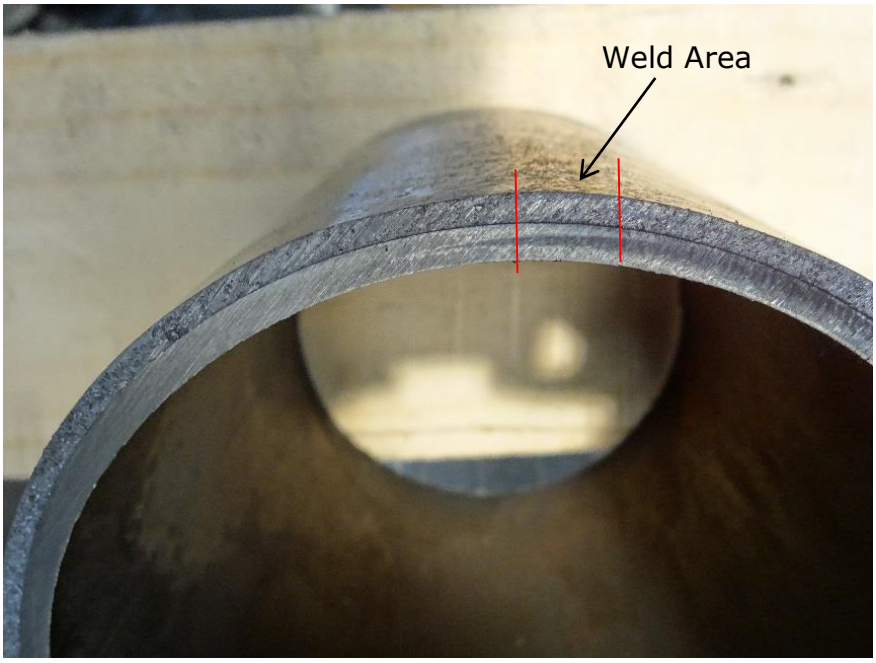

No visible inhomogeneous areas in the surrounding of the seam. Lead is closely attached to the tube.

Figure 10. Cross section through lead clad tube

5. *SCOPE OF SUPPLY*

The scope of supply includes the following items which are based upon FMB Oxford's understanding of the Technical Requirements:

- Project Management
- Customer Documentation: User manuals, test procedures, project plan, quality plan, factory test reports, build logs and a set of top level drawings
- Beamline Components – supplied by FMB Oxford (excluding the safety shutters)
- Factory Acceptance Testing of Beamline Components at FMB Oxford
- VAT Gate Valves for each vacuum section
- Packing Shipping, Insurance, Duties and Taxes paid
- On-site installation and commissioning
- Warranty is 24 months from delivery or 18 months from acceptance, whichever comes first.

The scope of supply does not include the following items, which are supplied by NIST:

- Floor Drilling according to a template available 3 months before installation
- All Equipment Protection elements
- Water supply connection, conditioning, distribution, monitoring and alarms
- Pneumatic supplies and controls for relevant components
- Position sensing cabling and controls for gate valves
- Heater Controllers (for Vacuum Bakeout heaters)
- Cable management – cable trays, supports, etc.
- Install nine off standard NSLS II beam shutters complete with vacuum vessels and stands, into position at a time agreed with all parties.

APPENDIX A – REFERENCE DOCUMENTS

Reference Number	Date/ Issue	Title
SB1341-14-CN-0042-PART I	19/09/14	NIST Contract
	05/05/12	Revised optical design of the NIST soft and tender x-ray beamline complex at NSLS-II (Ruben Reninger).
E3160	April 2014	NIST NSLS-II SST and BMM Beamline Backbones, Volume 2A, SST Technical Proposal
S3160	Nov 2014	NIST SST BEAMLINE S3160 QUALITY PLAN
SR-DG-LAY-3007	19/12/2014	DIAGNOSTICS LAYOUT NIST SST1-SST2, C07-S1
PS-C-XFD-RSI-SST-BMM-001	12/02/15	RSI for the Sources and Front-Ends for the SST1&2 and BMM Beamlines (NIST)
	16/01/15, Rev 05	Functional Specification - White Beam Section Optics for NIST at BNL S2263B
	11/12/12, Rev 03	Functional Specification - White Beam Section Functional Specification S2263C
	06/03/15	S3160 NIST SST Beamline Control and Software Functional Specification Rev 01
	27/02/15	S3160 NIST SST Mirror System L3 Functional Specification Rev 02
	27/02/15	S3160 NIST SST Mirror System L4 Functional Specification Rev 02
	27/02/15	S3160 NIST SST Mirror System M3 Functional Specification Rev 02
	27/02/15	S3160 NIST SST Mirror System M4A Functional Specification Rev 02
	27/02/15	S3160 NIST SST Mirror System M4B Functional Specification Rev 02
	27/02/15	S3160 NIST SST Mirror System M4C M4D Functional Specification Rev 02
	27/02/15	S3160 NIST SST Mirror System M5C Functional Specification Rev 02
	25/02/15	S3160 NIST SST Dignostic Modules Rev 01
ABM0042		Floor drilling, Local power outlets, Utilities Schedule Document - on beamline top level drawing
	Feb 2015	NIST SST Beamline Control & Software Functional Specification

APPENDIX B OPTICAL COMPONENT COORDINATES

Revised geometry with L2, M4A & HAXPES/NEXAFS moved downstream - this sheet takes into account the revised source location i.e. it incorporates both the undulators at 1.0 mrad.

	Component Coordinates			Distance from previous optical element			Total (vector) distance from previous optical element	Horizontal Turning Angle (degrees)	Resultant angle of beam (degrees)	Resultant angle of beam (mRad)	Vertical Turning Angle (degrees)	Resultant angle of beam (degrees)	Resultant angle of beam (mRad)	Agrees with cad model?	Component Coordinates from revised optical design report			Difference between revised component coordinates and optical design		
Optical Component	Z	X (Calculated)	Y	ΔZ	ΔX	ΔY									Z	X	Y	Z diff	X diff	Y diff
High energy insertion device	-1250	1.02	0					0.05729578	0.05729578	1.00	0	0	0	y	-1250	0	0	0	1	0
L1 (PLANE)	27450	29.72	0	28700.0	28.7	0.0	28700.0	-1.15	-1.0927042	-19.07	0	0	0	y	27450	29	0	0	1	0
L2A (TOROID)/L2B (PLANE)	34500	-104.75	0	7050.0	-134.5	0.0	7051.3	1.225675938	0.13297172	2.32	0	0	0	y	31756	-57	0	2744	-48	0
TENDER X-RAY MONO IN	46700.5	-76.43	0	12200.5	28.3	0.0	12200.5	0	0.13297172	2.32	0	0	0	y						
TENDER X-RAY MONO OUT	47590	-74.37	15	889.5	2.1	15.0	889.6	0	0.13297172	2.32	0	0	0	y						
HP NEXAFS	49642	-69.61	15	2052.0	4.8	0.0	2052.0	0	0.13297172	2.32	0	0	0	y	49642	-39	15	0	-31	0
HAXPES/NEXAFS	60347.6	-44.76	15	10705.6	24.8	0.0	10705.6	0	0.13297172	2.32	0	0	0	y	60039	-29	15	309	-16	0
L3 (PLANE)	62258	-40.33	15	1910.4	4.4	0.0	1910.4	1.225675938	1.35864766	23.71	0	0	0	y	62258	-27	15	0	-13	0
L4 (ELLIPSOID)	66766	66.59	15	4508.0	106.9	0.0	4509.3	1.225675938	2.58432359	45.10	0	0	0	y	66766	72	15	0	-5	0
µXPS	69763	201.86	15	2997.0	135.3	0.0	3000.1	0	2.58432359	45.10	0	0	0	y	69763	201	15	0	1	0

Figure 11. Co-ordinates of optical components on the 'L Branch'

Optical Component	Component Coordinates			Distance from previous optical element			Total (vector) distance from previous optical element	Horizontal Turning Angle (degrees)	Resultant angle of beam (degrees)	Resultant angle of beam (mRad)	Vertical Turning Angle (degrees)	Resultant angle of beam (degrees)	Resultant angle of beam (mRad)	Agrees with cad model?	Component Coordinates from revised optical design report			Difference between revised component coordinates and optical design		
	Z	X (Calculated)	Y	ΔZ	ΔX	ΔY									Z	X	Y	Z diff	X diff	Y diff
Low energy insertion device	1250	1.02	0					-0.05729578	-0.0572958	-1.00	0	0	0	y	1250	0	0	0	1	0
M1 (PLANE)	28580	-26.31	0	27330.0	-27.3	0.0	27330.0	3	2.94270422	51.36	0	0	0	y	28580	-27	0	0	1	0
SOFT X-RAY MONO IN	40080	564.85	0	11500.0	591.2	0.0	11515.2	0	2.94270422	51.36	0	0	0	y						
SOFT X-RAY MONO OUT	41173	621.03	15	1093.0	56.2	15.0	1094.5	0	2.94270422	51.36	0	0	0	y						
M3C (TANG ELLIPSE)	42062	666.73	15	889.0	45.7	0.0	890.2	3	5.94270422	103.72	0	0	0	y	42062	666	15	0	1	0
M3AB (TANG ELLIPSE)	42062	666.73	15	889.0	45.7	0.0	890.2	-3.5	-0.5572958	-9.73	0	0	0	y	42062	666	15	0	1	0
SLIT AB	48562	603.51	15	6500.0	-63.2	0.0	6500.3	0	-0.5572958	-9.73	0	0	0	y	48562	603	15	0	1	0
M4A (ELLIPSOID)	51628.77	573.68	15	3066.8	-29.8	0.0	3066.9	-3.5	-4.0572958	-70.81	0	0	0	y	51548	573	15	81	1	0
HAXPES/NEXAFS	60347.6	-44.76	15	8718.8	-618.4	0.0	8740.7	0	-4.0572958	-70.81	0	0	0	y	60039	-29	15	309	-16	0
M4B (ELLIPSOID)	66570.0	428.35	15	18008.0	-175.2	0.0	18008.9	-3.5	-4.0572958	-70.81	0	0	0	y	66571	427	15	-1	1	0
µXPS	69763	201.86	15	3193.0	-226.5	0.0	3201.0	0	-4.0572958	-70.81	0	0	0	y	69763	201	15	0	1	0
SLIT C	48527	1339.70	15	6465.0	673.0	0.0	6499.9	0	5.94270422	103.72	0	0	0	y	48527	1339	15	0	1	0
M4C (ELLIPSOID)	53500	1857.35	15	4973.0	517.7	0.0	4999.9	0	5.94270422	103.72	3	3	52.3598776	y	53500	1856	15	0	1	0
M4D (PLANE)	53500	1857.35	15	4973.0	517.7	0.0	4999.9	0	5.94270422	103.72	3	3	52.3598776	y	53500	1856	15	0	1	0
HP NEXAFS/FY	56480	2167.55	172	7918.0	1564.0	157.0	8072.5	0	5.94270422	103.72	0	3	52.3598776	y	56480	2167	172	0	1	0
M5C (PLANE)	60122	2546.66	364	6622.0	689.3	348.9	6666.9	0	5.94270422	103.72	-2	1	17.4532925	y	60122	2546	364	0	1	0
NEXAFS/XPS	62116	2754.22	399	1994.0	207.6	35.0	2005.1	0	5.94270422	103.72	0	1	17.4532925	y	62116	2753	399	0	1	0
µNEXAFS IMAGING	65093	3064.11	626	11593.0	1206.8	610.8	11671.6	0	5.94270422	103.72	0	1	17.4532925	y	65093	3063	626	0	1	0

Figure 12. Co-ordinates of the optical components in the 'M Branch' and transfer branches

APPENDIX C SOURCE REFERENCE DRAWING

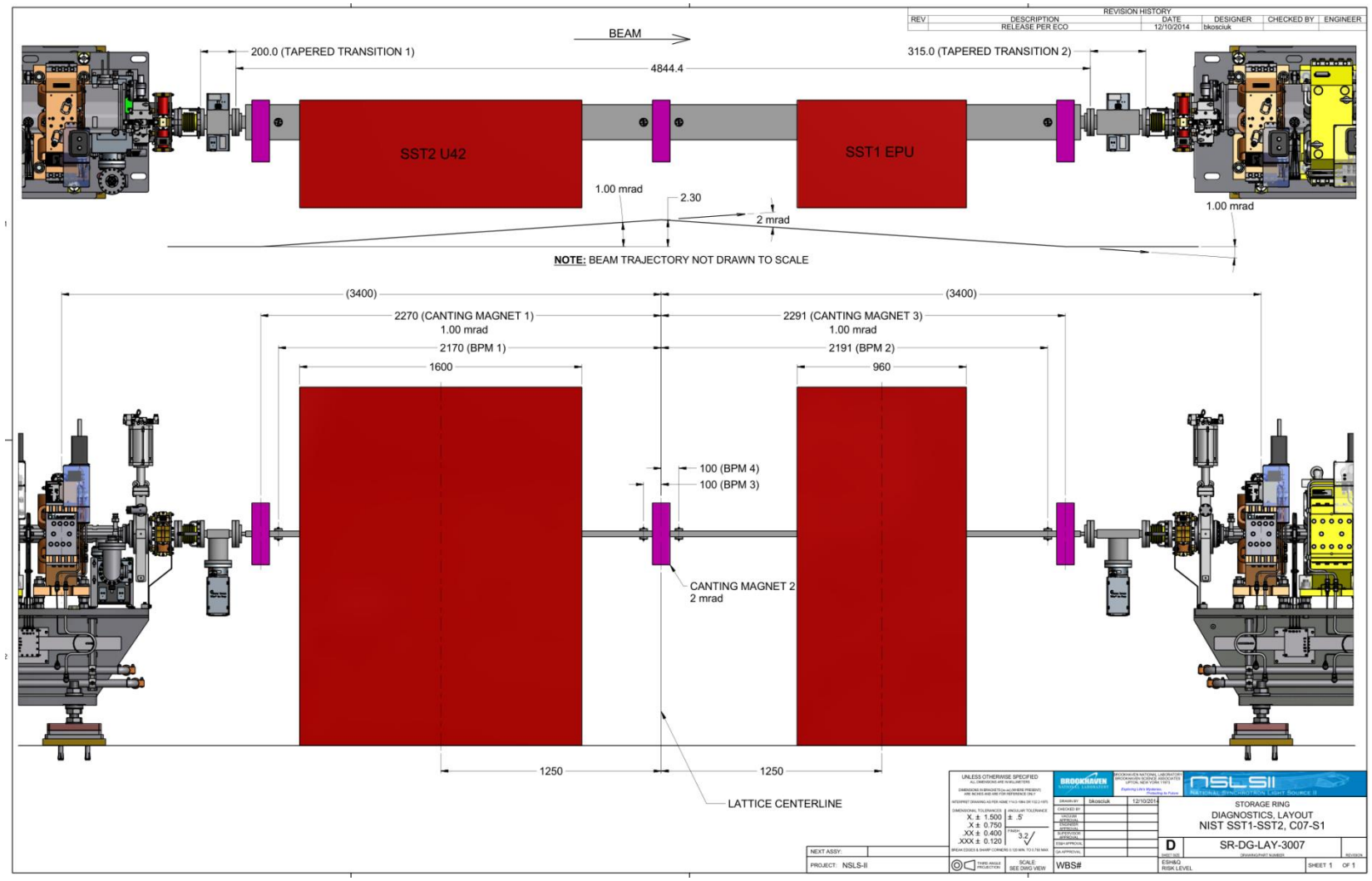

Reference Documents:

Reference Number	Date/ Issue	Title
SB1341-14-CN-0042	19/09/14	NIST Contract
	April 2014	NIST NSLS-II SST and BMM Beamline Backbones, Volume 2A, SST Technical Proposal
S3160	Nov 2014/REV 01	NIST SST BEAMLINE S3160 QUALITY PLAN
DOCM0110	June 2014	I400 4-Channel Digital Electrometer User Manual
-	Feb 2015, rev 03	Nano Beam Positioning Monitor User Manual
LT-C-XFD-STD-BL-COORD-001	May 2011	Beamline Coordinate System Standards
-	-	S3160 NIST SST Beamline Functional Specification
-	-	S3160 NIST SST Beamline Control and Software

FMB Oxford
Osney Mead
Oxford OX2 0ES
UK

Contact: Andrew Fairley
Telephone: +44 (0)1865 320 313
Fax: +44 (0)1865 320 301
E-mail: andrew.fairley@fmb-oxford.com

Change log:

Revision	Date	Summary of Change	Approval
1.0	23/03/15	First Issue	RG
2.0	02/04/15	Photodiode intensity monitor to place photodiode directly into beam. Scattering foil removed. NanoBPM removed from DM1.	
3.0			
4.0			
5.0			

TABLE OF CONTENTS 1

1. *INTRODUCTION* **3**

1.1 AXIS 3

2. *SPECIFICATIONS* **4**

2.1 DIAGNOSTIC MODULE LOCATIONS 4

3. DIAGNOSTIC MODULE COMPONENTS **9**

3.1 4 BLADE IN-FLANGE SLITS 9

3.1.1 JAW SLITS PERFORMANCE PARAMETERS *10*

3.2 FLUORESCENT SCREEN 11

3.3 PINK BEAM STOP (DIAGNOSTIC MODULE 1 ONLY) 11

3.4 INTENSITY MONITORS 13

3.4.1 SOFT X-RAY MESH INTENSITY MONITOR (GOLD MESH) *13*

3.4.2 PHOTODIODE INTENSITY MONITOR *14*

3.4.3 Intensity Monitor/ Fluorescent Screen Actuator Motions *14*

3.4.4 Intensity Monitor Linear Actuator *14*

3.4.5 Intensity Monitor Encoder Data *14*

4. VACUUM SYSTEM **16**

4.1 VACUUM SPECIFICATION 16

4.2 VACUUM VESSEL PORTS 16

4.2.1 Diagnostic module 1 ..... *16*

4.2.2 Diagnostic module 2-6 ..... *17*

5. DIAGNOSTIC MODULE STAND **18**

5.1 LIFTING POINTS 18

5.2 ALIGNMENT FEATURES 18

6. INTERFACE PANEL **19**

6.1 DIAGNOSTIC MODULE 1 19

6.2 DIAGNOSTIC MODULE 2-6 19

7. FACTORY TESTING **20**

8. INSTALLATION AND UNIT ACCEPTANCE **21**

9. SCOPE OF SUPPLY **22**

1. *INTRODUCTION*

The NIST SST beamline includes six diagnostic modules. These include four-jaw uncooled slits for beam conditioning, in addition to diagnostics - fluorescent screen, intensity monitors (gold mesh and photodiode). Diagnostic module 1 differs from the other diagnostic modules in that a pink beam stop is installed and the intensity monitors are replaced by a NanoBPM.

1.1 AXIS

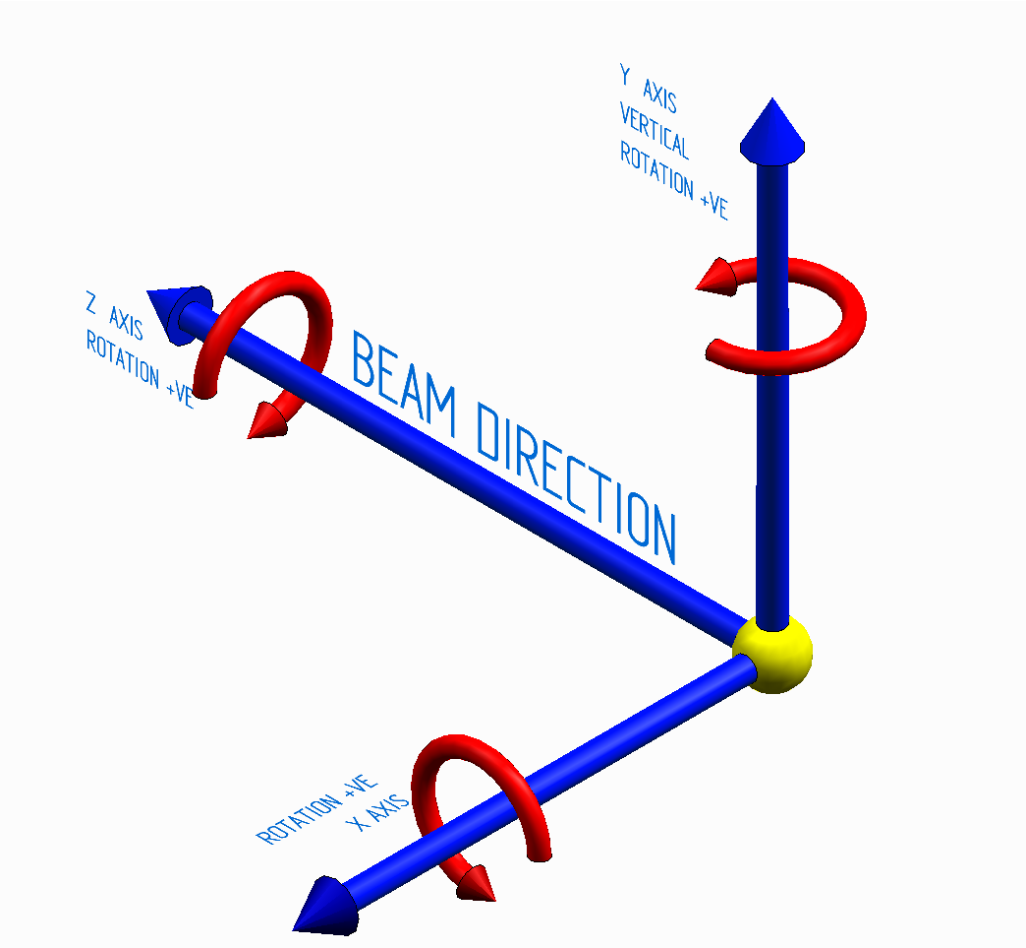

Figure 1. NSLS-II Coordinate System

The coordinate system employed complies with NSLS-II document:

Beamline Coordinate System Standards LT-C-XFD-STD-BL-COORD-001.

2. *SPECIFICATIONS*

2.1 DIAGNOSTIC MODULE LOCATIONS

The six diagnostic modules are located as follows (see Figures 2 and 3):

1. DM1 - Downstream of the DCM in the tender 'L' beamline – between the DCM and the HP NEXAFS end station. Beam-in located at 47939 mm and beam-out located at 48544 mm from the middle of the straight section.

2. DM2 - Between mirror system M3AB/M3C and the precision vertical slit 'AB' on the soft x ray transfer branch. Beam-in located at 45187 mm and beam-out located at 45538 mm from the middle of the straight section.

3. DM3 - Downstream of the M4A mirror system in the HAXPES/NEXAFS branch of the 'M' soft x ray beamline. Beam-in located at 56331 mm and beam-out located at 56856 mm from the middle of the straight section.

4. DM4 - Downstream of the M4A mirror system in the μXPS branch of the 'M' soft beamline, allowing monitoring with optic in beam and out of beam (i.e. directly from the precision slit). Beam-in located at 57608 mm and beam-out located at 58042 mm from the middle of the straight section.

5. DM5 - Between mirror system M3AB/M3C and the precision vertical slit 'C' on the soft x ray beamline ('M' branch). Beam-in located at 46571 mm and beam-out located at 46998 mm from the middle of the straight section.

6. DM6 - Immediately downstream of the M4C/M4D mirror system. This enables monitoring of the beam with the optics in or out of beam. Beam-in located at 54112 mm and beam-out located at 54540 mm from the middle of the straight section.

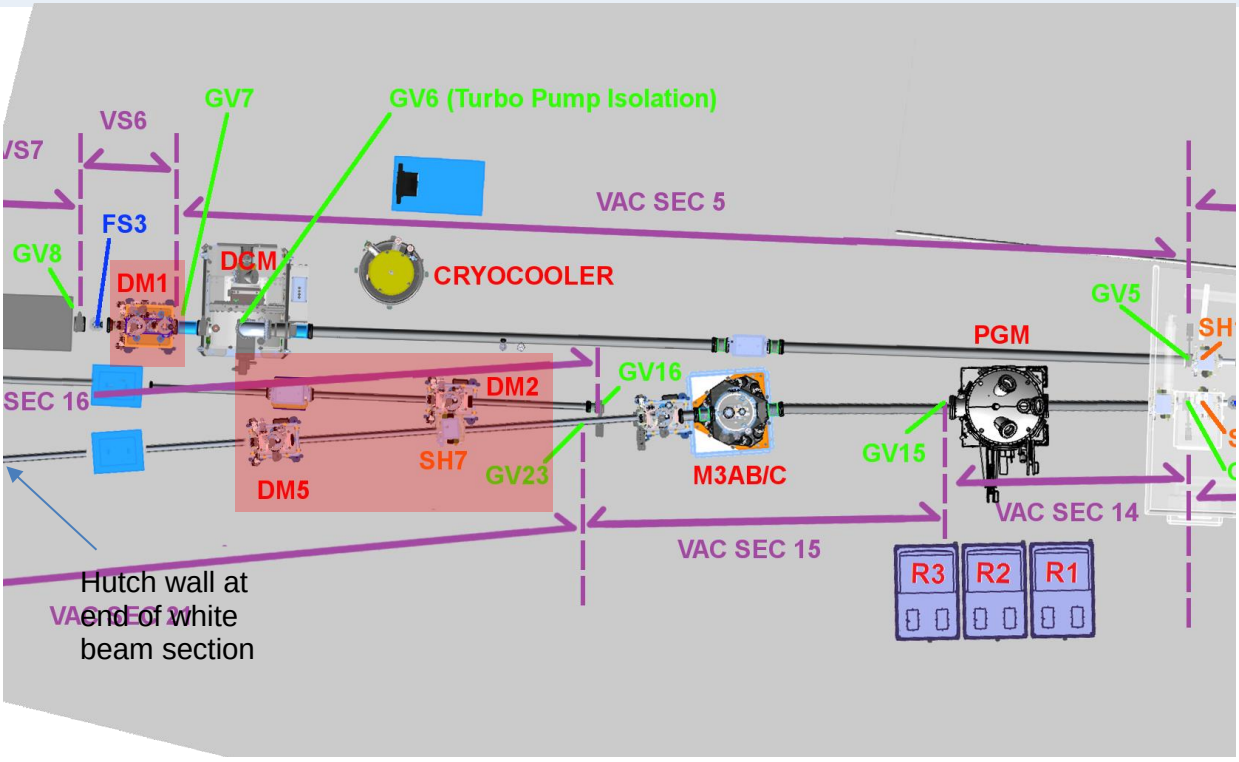

Figure 2. Location of Diagnostic modules DM1, DM2 and DM5.

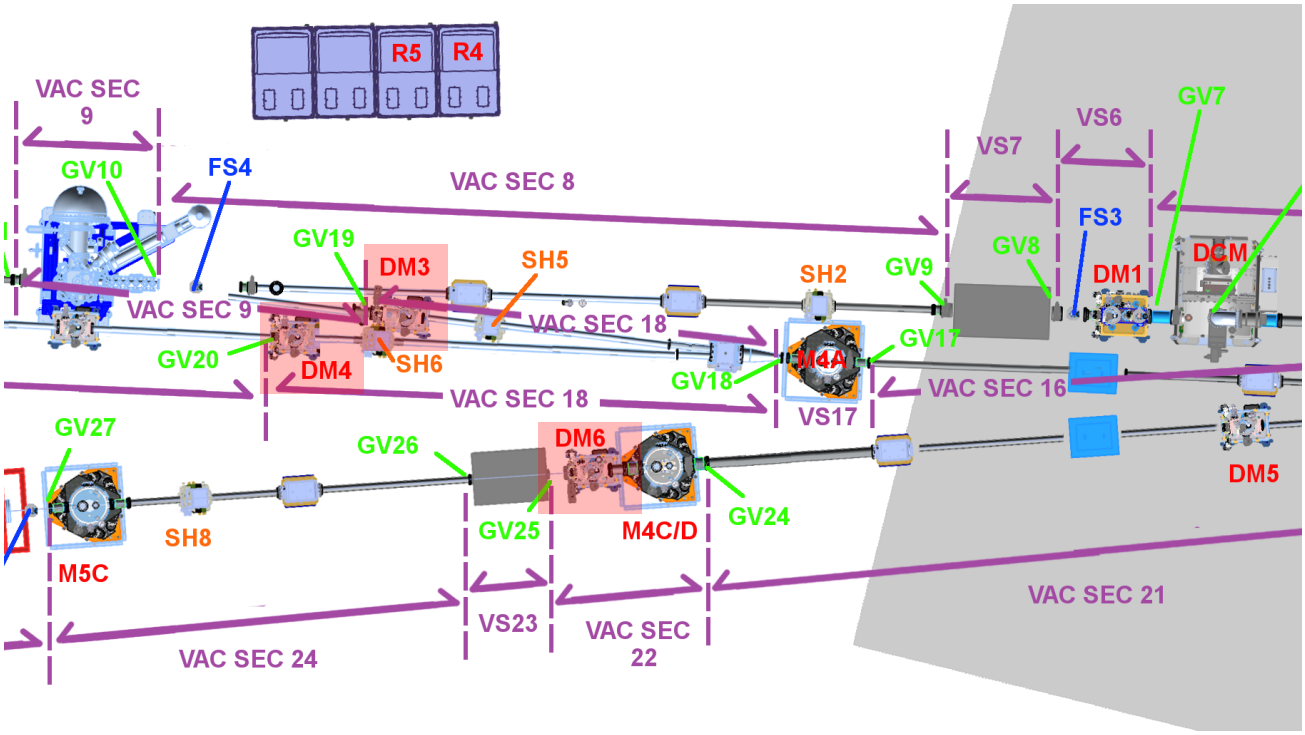

Figure 3. Location of diagnostic modules DM3, DM4 and DM6.

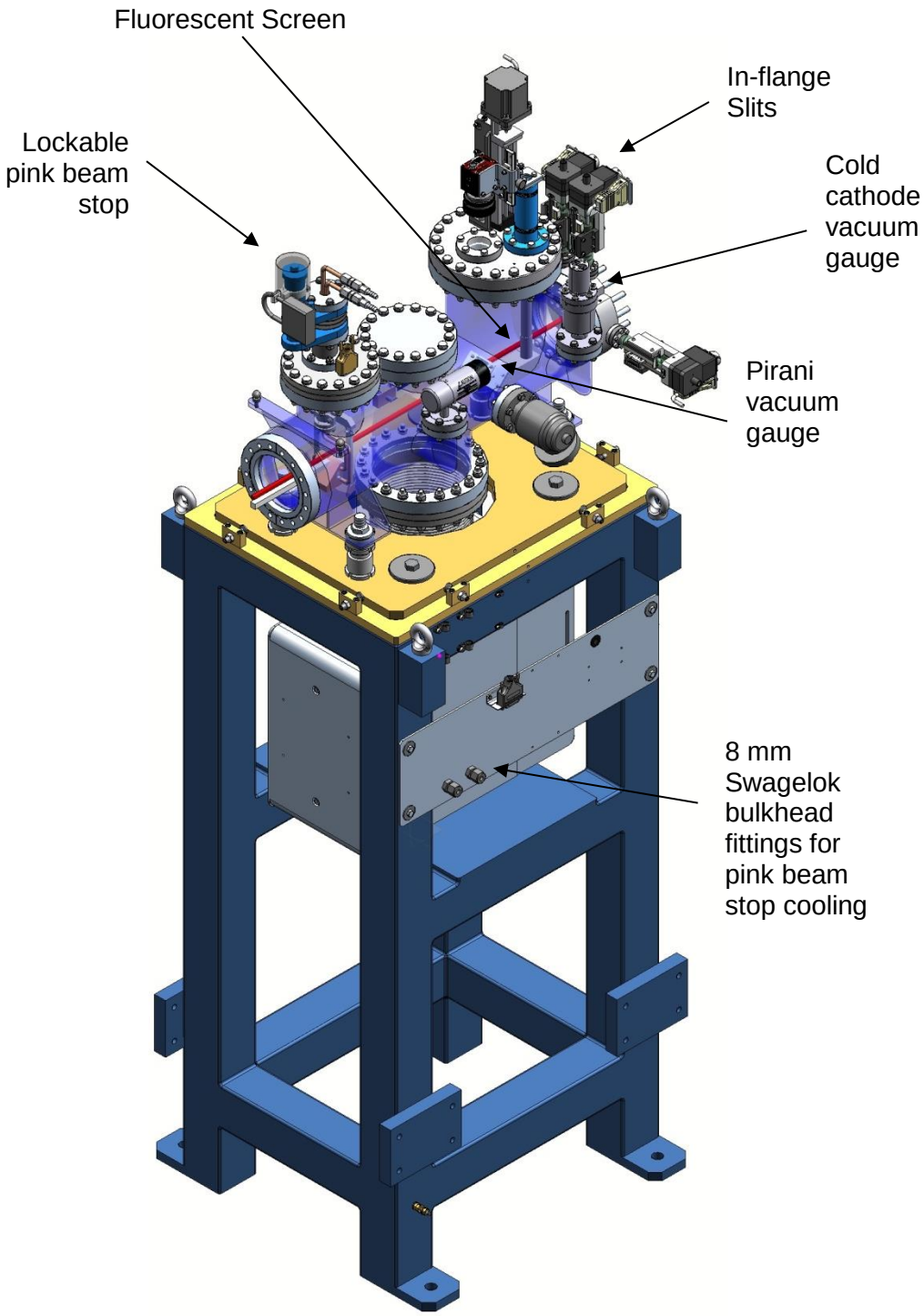

Figure 4. Diagnostic module 1

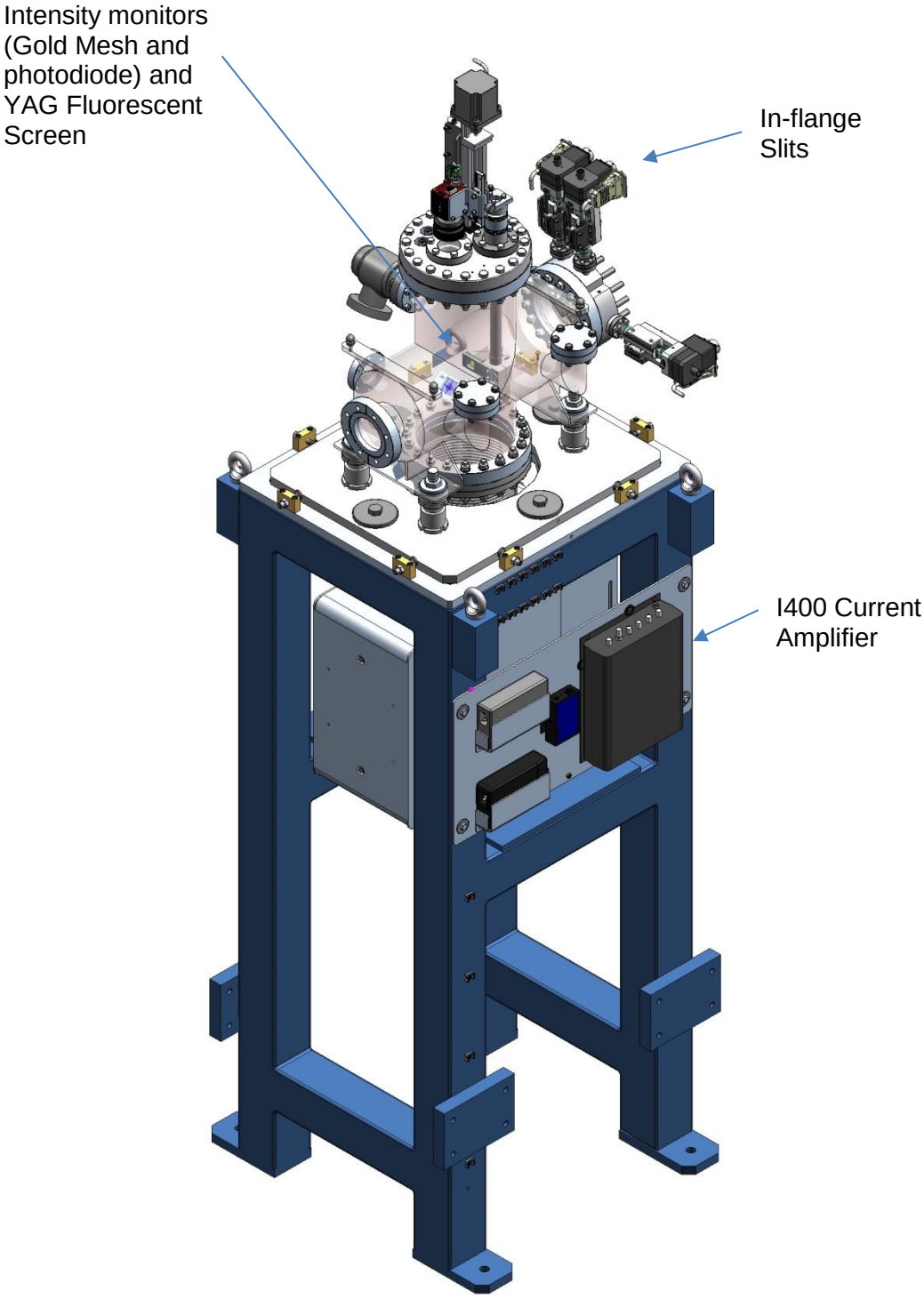

Figure 5. Diagnostic module 6

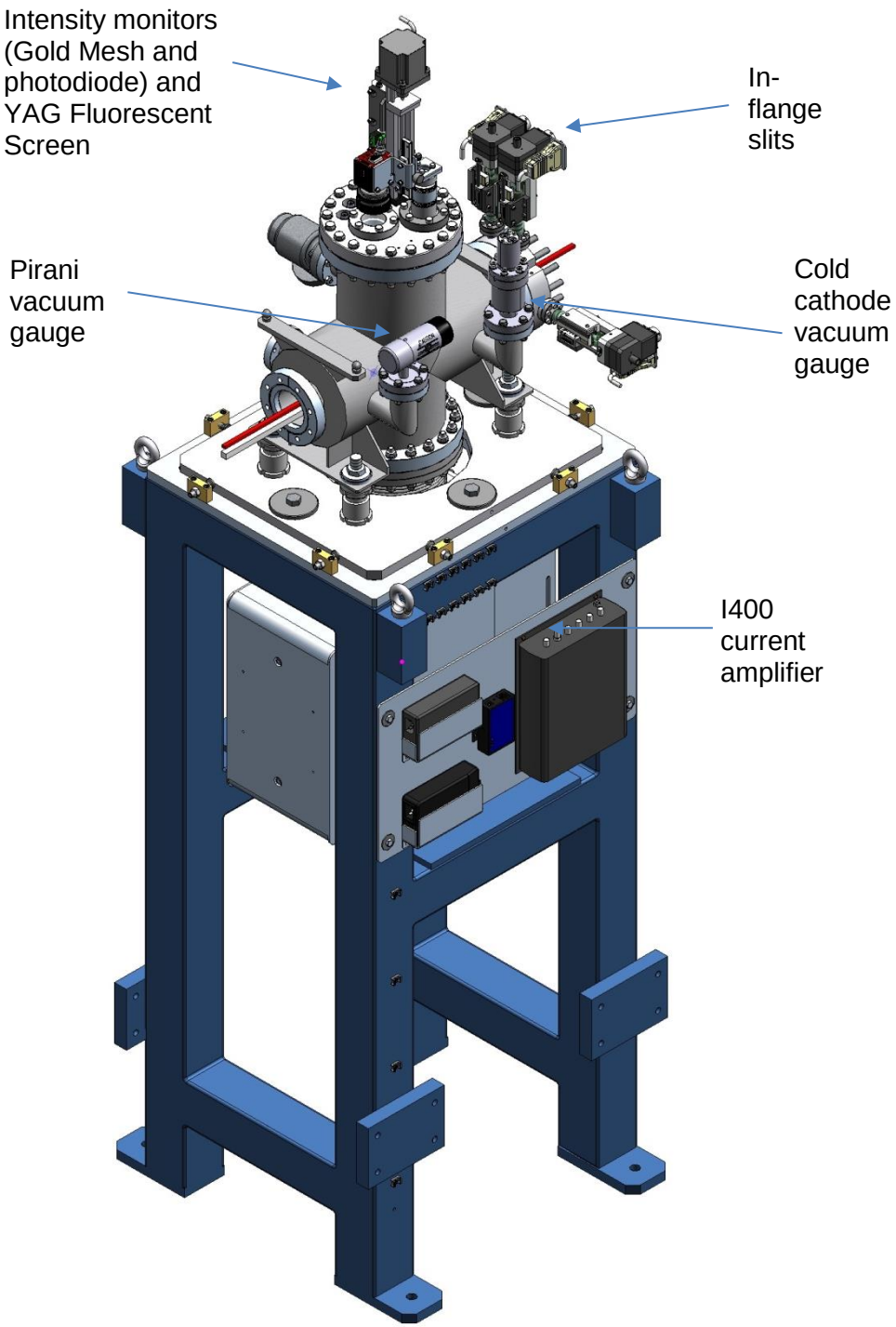

Figure 6. Diagnostic modules 2, 4 and 5

3. DIAGNOSTIC MODULE COMPONENTS

3.1 4 BLADE IN-FLANGE SLITS

The four blade in-flange slit unit consists of two blades to define the beam in the horizontal direction and two blades to defined the beam in the vertical direction. The slits are able to close fully in horizontal and vertical directions. The slit blades move along in-vacuum guides to ensure that they remain parallel to each other.

The slit blades will be manufactured from tungsten. Each slit blade is moved by a stepper motor via a lead screw. An incremental linear optical encoder provides continuous feedback of the actual slit position. Limit switches are fitted at each end of the actuator travel.

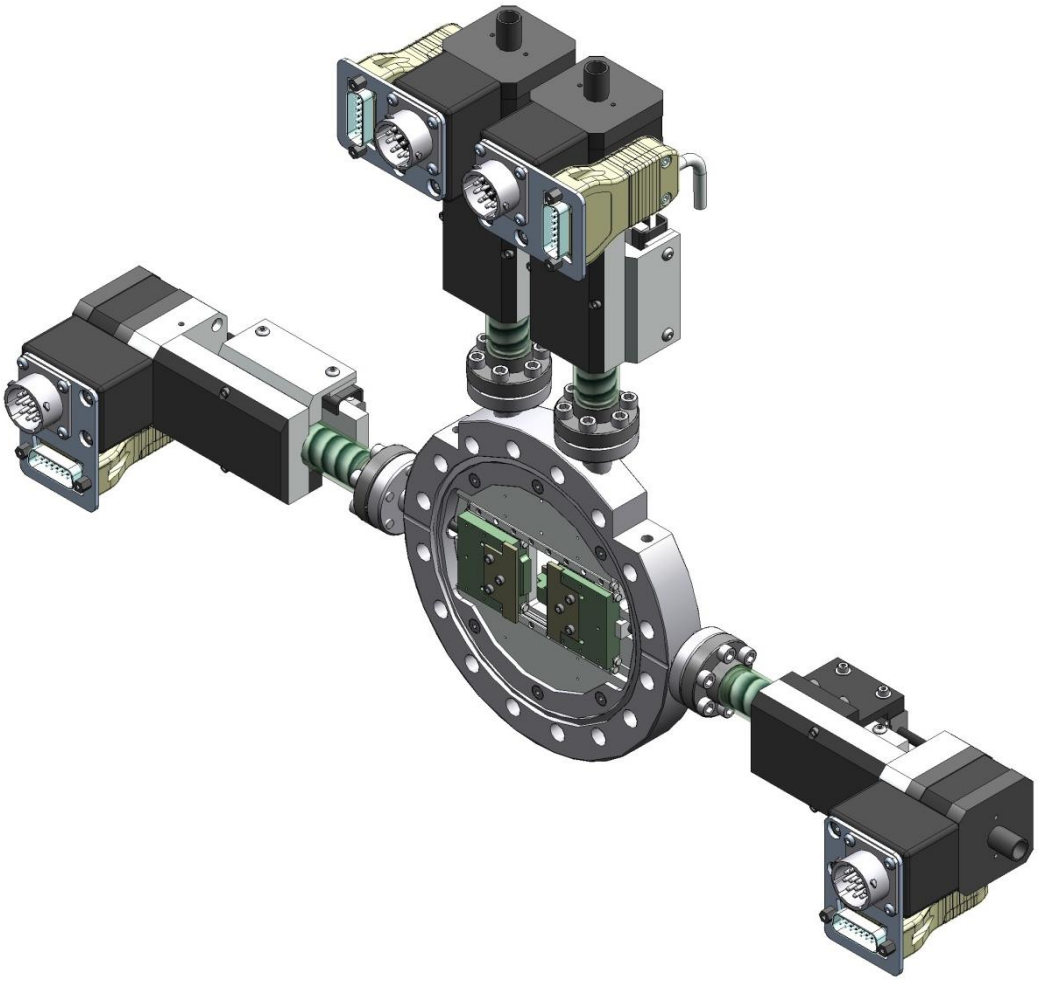

Figure 7. Four jaw in flange slits

3.1.1 JAW SLITS PERFORMANCE PARAMETERS

Slit Parameters

Maximum stroke available	15 mm
Maximum aperture	15 mm H x 15 mm V
Overlapping	Complete
Blade size	36 (W) mm x 20 mm (H) x 2 mm (T)
Blade Parallelism	10 μm
Blade defining edge radius	2 mm
Blade defining edge roughness	0.1 μm RMS
Blade defining edge straightness	< 5 μm
Resolution	< 0.5 μm
Repeatabillity	< 5 μm
Blade Material	Tungsten
End of travel limit switches	2, normally closed (one at each end of travel)
Mounting flange	DN100/CF150

Encoder details

Readhead type	Renishaw – Tonic T1000-05A
Interpolator type	Renishaw Ti0200E04A
Interpolator resolution	0.1 μm
Scale type	RGSZ20
Interpolator connector	15-Way sub D

Linear Actuator Parameters

Motor Type	Nanotec 2 phase, bi-polar, stepping linear actuator
Step angle (full step drive)	1.8° (200 steps/rev)
Driving current/Phase	1.4 A
Maximum velocity	20 mm/sec
Thread pitch	1 mm
Resolution per full step	5 µm
Maximum movement per actuator	20 mm
Maximum Overlap	5 mm
Maximum holding load (power off)	90 N
Motor connector	12 way Trim Trio

Limit switch parameters

Switch type	D2F Hinge lever
Max supply voltage	30 VDC
Max switching current	2A
Max temperature	65°C
Connector	12 way Trim Trio (with motor)

3.2 FLUORESCENT SCREEN

The fluorescent screen units located in the diagnostic modules use YAG crystals (Yttrium Aluminium Garnet) as the fluorescent material. The size of the crystal is 25 mm x 25 mm, with an aperture of 22 mm (H) x 15.5 mm (V).

The fluorescent screens used on the diagnostic modules are motorised and mounted on a DN150/CF200 conflat. The camera mount for the Prosilica GC1290 CCD camera is mounted on the same actuator to view the screen (see figure 5).

3.3 PINK BEAM STOP (DIAGNOSTIC MODULE 1 ONLY)

The pink beam stop has been transferred from the DCM and consists of a cooled copper block, which is fixed to a manually adjustable (lockable) vertical translation. The height of the block is 40mm and the inclined face height 29 mm. The range of the vertical translation is 25 mm (± 12.5 about the nominal position, with the beam incident on the top of the block - see Figure 6). The face of the block which sees the beam is inclined at 45 degrees to the beam axis. The stop is fitted with a thermocouple whose feedthrough is mounted on a separate port on the vacuum vessel.

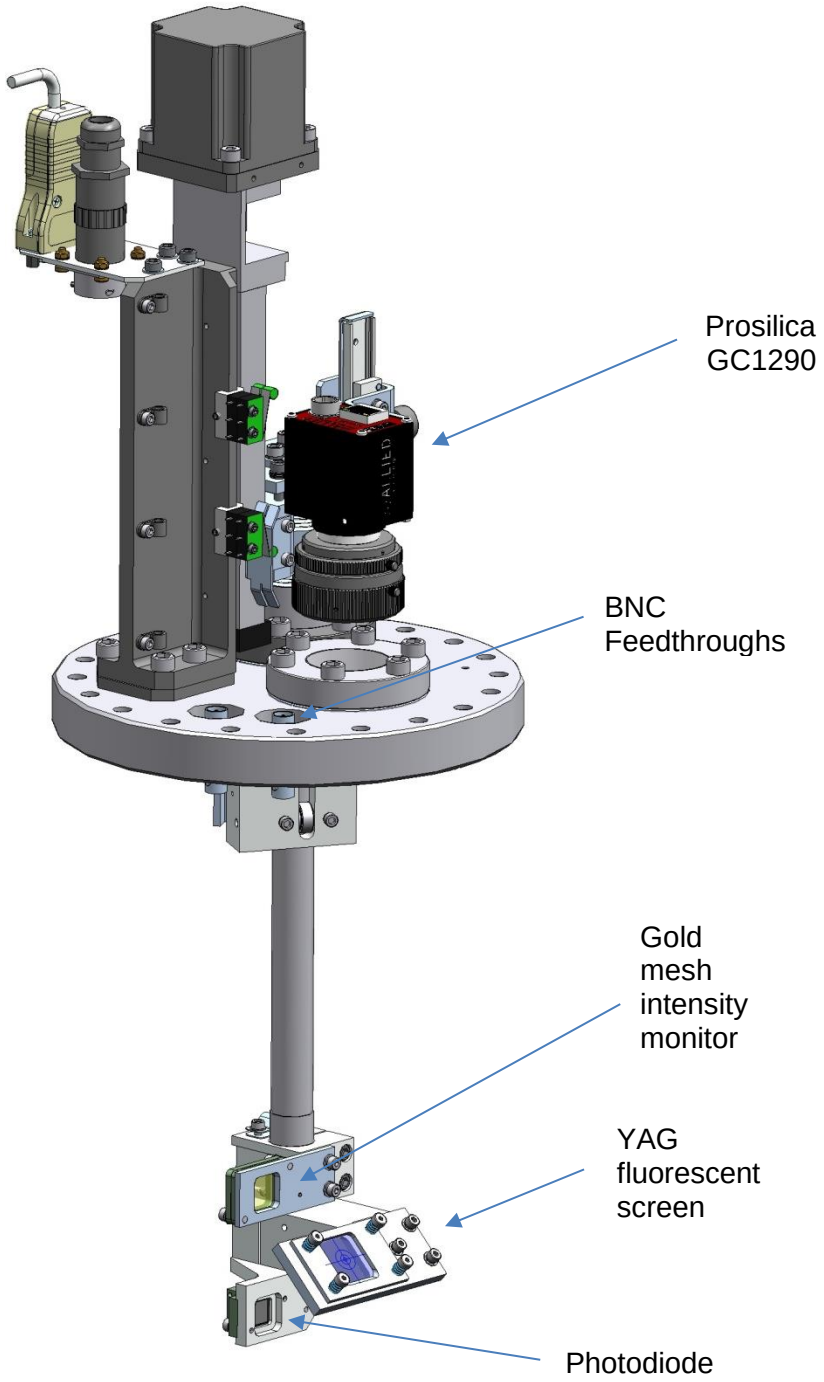

Figure 8. Fluorescent screen and intensity monitor actuator

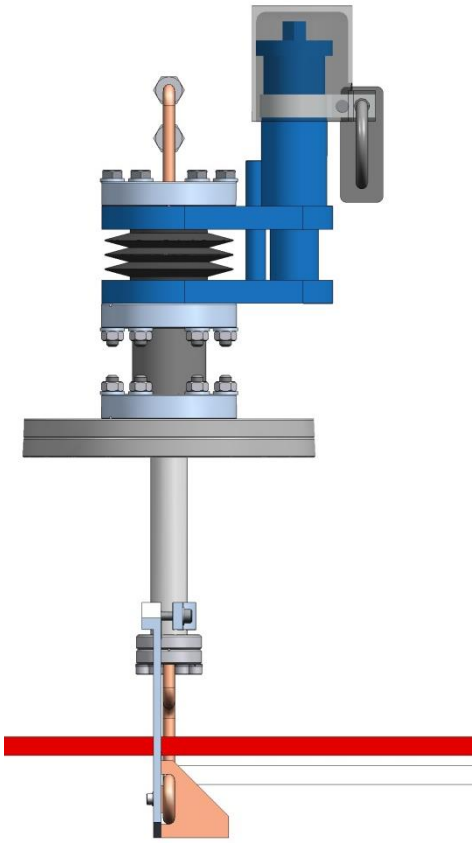

Figure 9. Cooled beam stop showing ‘pink’ and ‘mono’ beam at nominal position

3.4 INTENSITY MONITORS

Both intensity monitors are vertically stacked and mounted on the same stepper motor driven actuator.

3.4.1 SOFT X-RAY MESH INTENSITY MONITOR (GOLD MESH)

This diagnostic is used to measure the beam intensity by inserting an electrically isolated gold wire mesh into the beam and measuring the resultant photoionisation current using the I400 current amplifier. The photoionisation current is proportional to the beam intensity. Further details of the I400 are included in the supporting documents.

Gold Mesh Parameters

Size	16mm (H) x 12 mm (V)
Thickness	5 µm
Mesh pitch	100 lines per inch
Max transmission	Approx. 85%

3.4.2 PHOTODIODE INTENSITY MONITOR

The photodiode intensity monitor consists of mounted photodiode placed directly into the beam. The resultant output current from the photodiode is proportional to the beam intensity. This diagnostic interrupts the beam and therefore cannot be used for in-beam monitoring.

Photodiode parameters

Active Area	10 mm (H) x 10 (V) mm
Photodiode type	AXUV100G

3.4.3 Intensity Monitor/ Fluorescent Screen Actuator Motions

Linear actuator parameters

Motion	Parameter	Specification
Vertical (Y Direction)	Drive	Linear actuator, fitted with limit switches & encoder.
	Range	80 mm
	Repeatability	2 µm

3.4.4 Intensity Monitor Linear Actuator

Stepper motor and linear drive parameters

Motor Type	McLennan Type 23HSX-206, 2 phase, bi-polar stepper motor
Holding torque	98 Ncm
Step angle (full step drive)	1.8°/step or 200 steps/rev
Driving current	4.2 A
Thread pitch	2 mm
Resolution per half step	10 µm

3.4.5 Intensity Monitor Encoder Data

Stepper motor and linear drive parameters

Readhead type	Renishaw – Tonic T1001-05A
Readhead resolution	0.1 µm
Scale type	RGSZ20
Interpolator	Ti 0200 E 4 A
Connector	15-Way sub D

4. VACUUM SYSTEM

4.1 VACUUM SPECIFICATION

Maximum bakeout temperature – vessel and internal components	150-200 °C (110°C for diagnostic modules 2-6, limited by photodiode)
Vacuum	UHV compatible (< 5 x10^{-10} mbar).
Helium leak rate	< 1 x 10^{-10} mbar l/sec
Vacuum Pump	Vacuum pumps are not fitted to the diagnostic module, but are located adjacent in the same vacuum section.
Vacuum gauges	One pirani gauge (MKS type 317) and one cold cathode gauge(MKS type 422) located on the vacuum vessel
Right Angle Valve	VAT Valve type 54, DN40/CF70.

4.2 VACUUM VESSEL PORTS

4.2.1 Diagnostic module 1

Purpose	Location	Size	Qty
Beam In	Beam inlet port	DN100/CF150	1
Beam Out (in flange slits)	Beam outlet port	DN100/CF150 R	1
Roughing Port for RA valve	Inboard side of vessel	DN40/CF70	1
Vacuum Gauges	Inboard Side of vessel	DN40/CF70	2
Fluorescent screen and intensity monitor actuator	Top of vessel	DN160/CF200 R	1
NanoBPM port	Top of vessel	DN63/CF114 R	1
Pink beam stop port	Top of vessel	DN100/CF150 R	1
Feedthrough for pink beam stop thermocouple	Inboard side of vessel	DN40/CF70	1

4.2.2 Diagnostic module 2-6

Purpose	Location	Size	Qty
Beam In	Beam inlet port at end 1	DN63/CF114	1
Beam Out (in-flange slits)	Beam outlet port at end 2	DN100/CF150 R	1
Roughing Port for RA valve	Outboard side of vessel	DN40/CF70	1
Vacuum Gauges	Inboard side of vessel	DN40/CF70	2
Fluorescent screen and intensity monitor actuator	Top of vessel	DN160/CF200	1

5. DIAGNOSTIC MODULE STAND

The position of the diagnostic module components can be adjusted in x, y, and z relative to the support frame. There are two adjusters per side mounted on the frame, which can be used to adjust the lateral, longitudinal and angular (yaw) alignment of the vessel and components. In addition, the vessel is supported by adjustable feet (and spherical washers) which can be used to adjust the height, pitch and roll of the vessel.

Vessel Manual Adjustment (Lateral x & Longitudinal z)	±5 mm
Vessel Manual Adjustment (Vertical y)	±12.5 mm
Material	Mild Steel
Colour	RAL 5007 30% GLOSS

5.1 LIFTING POINTS

Diagnostic module weight 1: 200 kg approximately.

Diagnostic module 2-6 weight: 195 kg approximately.

The diagnostic module is provided with four M16 lifting points in the support frame.

A lifting diagram for the system will be included on the top level assembly drawing.

5.2 ALIGNMENT FEATURES

Fiducial mounts will be provided on the vacuum vessel. These will take the form of 0.25” reamed (H7) holes, suitable for 0.5” or 1.5” spheres.

6. INTERFACE PANEL

6.1 DIAGNOSTIC MODULE 1

The interface panel for diagnostic module 1 includes:

1. Bulkhead swagelok union fittings (8 mm) to connect to the pink beam stop cooling lines.
2. 15 way d-type connection to the pink beam stop thermocouple.

6.2 DIAGNOSTIC MODULE 2-6

The interface panel for diagnostic moduled 2-6 includes:

1. Mounting for the I400 and its power supply

7. FACTORY TESTING

Testing at FMB Oxford consists of Motion Testing, Vacuum Testing and Fiducialisation.

Full specifications and procedures covering all factory testing will be prepared in advance and these will be submitted to the customer prior to final design approval. Representatives from the customer are invited to witness these tests at FMB Oxford's works.

8. INSTALLATION AND UNIT ACCEPTANCE

The site acceptance testing, included in the installation option, will ensure that all components are carefully surveyed into position, all motors, actuators and sensors are functioning properly and the vacuum specifications are met. All motions will be tested and the correct functioning of all limit and datum switches checked. The complete set of detailed factory tests are not repeated on site.

There will be a full leak check of the installed vacuum sections. We expect that a turbo pump station, RGA rig, and He leak checker to be provided by the customer for our use while at the customer's site.

Final site acceptance will include:

- All factory test data, documentation and manuals
- Correct operation of all motions, limits and datum switches using FMB-O controls and cabling.
- Leak testing at the best achievable sensitivity after 24 hrs of pumping and prior to on site customer bakeout

9. SCOPE OF SUPPLY

- All modules:
  - 4 jaw in flange slits
  - Fluorescent screen (YAG)
- Module 1 only:
  - Cooled Pink beam stop
- Modules 2-6:
  - Gold mesh intensity monitor
  - Photodiode intensity monitor
  - I400 Current amplifier (for intensity monitors only).

S3160 BNL NSLS-II NIST SST BEAMLINE I/O LISTING

FMB Oxford

Prepared by:	D. Smith
Revision:	A (PDR issue)
Date:	22-Apr-15

Notes:
Shutters are handled by the PSS, shutters and PSS in NIST scope
Temperature and flow alarms must inhibit the beam
Vacuum alarms inhibit opening of the relevant gate valves and inhibits the beam
The beam must be inhibited when gate valves are not open

Note: The EPS PLC is in NIST scope, channels are for ref only
Note: GV0 is not in FMBO scope
Note: Flowmeters are not in the FMBO scope

Thermocouples

Channel	Part	Type	Device	Fault condition
TC01	Fixed Mask	PT100	Temp sensor Fixed mask	High temperature
TC02		PT100	Temp sensor Fixed mask	High temperature
TC03	L1	K Type	Thermocouple Mask	High temperature
TC04		K Type	Thermocouple Mirror	High temperature
TC05	M1	K Type	Thermocouple Mask	High temperature
TC06		K Type	Thermocouple Mirror	High temperature
TC07	WBS01	K Type	Thermocouple Inboard	High temperature
TC08		K Type	Thermocouple Outboard	High temperature
TC09		K Type	Thermocouple Mask plate	High temperature
TC10	SLW01	K Type	Thermocouple Slit 1 - 1	High temperature
TC11		K Type	Thermocouple Slit 1 - 2	High temperature
TC12		K Type	Thermocouple Slit 1 - 3	High temperature
TC13		K Type	Thermocouple Slit 1 - 4	High temperature
TC14	SLW02	K Type	Thermocouple Slit 2 - 1	High temperature
TC15		K Type	Thermocouple Slit 2 - 2	High temperature
TC16		K Type	Thermocouple Slit 2 - 3	High temperature
TC17		K Type	Thermocouple Slit 2 - 4	High temperature
TC18	L2	K Type	Thermocouple Mask Upper	High temperature
TC19		K Type	Thermocouple Mask Lower	High temperature
TC20		K Type	Thermocouple L2A	High temperature
TC21		K Type	Thermocouple L2B	High temperature
TC22	FS2	K Type	Thermocouple Screen	High temperature
TC23	FS7	K Type	Thermocouple Screen	High temperature
TC24	DCM	K Type	Thermocouple 1st Crystal - Si111	High temperature
TC25		K Type	Thermocouple 1st Crystal - Si220	High temperature
TC26		K Type	Thermocouple 1st Crystal - YB66	High temperature
TC27		K Type	Thermocouple 2nd Crystal - Si111	High temperature
TC28		K Type	Thermocouple 2nd Crystal - Si220	High temperature
TC29		K Type	Thermocouple 2nd Crystal - YB66	High temperature

Note: Thermocouples on motors are not monitored by EPS. They are sometimes monitored during the commissioning phase and if a fault is suspected.
Note: Temperatures from the cryocooler are not monitored by the EPS but by the cryocooler controls. A fault will generate an alarm from the cryocooler.

Analogue input

Channel	Part	Type	Device	Signal description	Tag Name

Digital input

Channel	Part	Type	Device	Signal description	Tag Name
DI00		PSS	FEO	Synchrotron beam not inhibited from PSS	BEAM
DI01		Relay N/O	Cryo1	Cryocooler healthy	Cryo1
DI02		Relay N/O	CC01	Vacuum gauge controller#1A Cold Cathode	Vac 1a
DI03		Relay N/O	CC02	Vacuum gauge controller#1B Cold Cathode	Vac 1b
DI04		Relay N/O	CC03	Vacuum gauge controller#2A Cold Cathode	Vac 2
DI05		Relay N/O	CC04	Vacuum gauge controller#2B Cold Cathode	Vac 3
DI06		Relay N/O	CC05	Vacuum gauge controller#3A Cold Cathode	Vac 4
DI07		Relay N/O	CC06	Vacuum gauge controller#4A Cold Cathode	Vac 5
DI08		Relay N/O	CC07	Vacuum gauge controller#6A Cold Cathode	Vac 6
DI09		Relay N/O	CC08	Vacuum gauge controller#7A Cold Cathode	Vac 8
DI10		Relay N/O	CC09	Vacuum gauge controller#9A Cold Cathode	Vac 9
DI11		Relay N/O	CC10	Vacuum gauge controller#10A Cold Cathode	Vac 10
DI12		Relay N/O	CC11	Vacuum gauge controller#11A Cold Cathode	Vac 11
DI13		Relay N/O	CC12	Vacuum gauge controller#3B Cold Cathode	Vac 13
DI14		Relay N/O	CC13	Vacuum gauge controller#5A Cold Cathode	Vac 15
DI15		Relay N/O	CC14	Vacuum gauge controller#6B Cold Cathode	Vac 16
DI16		Relay N/O	CC15	Vacuum gauge controller#7B Cold Cathode	Vac 17
DI17		Relay N/O	CC16	Vacuum gauge controller#8A Cold Cathode	Vac 18

DI18		Relay N/O	CC17	Vacuum gauge controller#9B Cold Cathode	Vac 19
DI19		Relay N/O	CC18	Vacuum gauge controller#11B Cold Cathode	Vac 20
DI20		Relay N/O	CC19	Vacuum gauge controller#5B Cold Cathode	Vac 21
DI21		Relay N/O	CC20	Vacuum gauge controller#8B Cold Cathode	Vac 22
DI22		Relay N/O	CC21	Vacuum gauge controller#10B Cold Cathode	Vac 24
DI23	FM / WBS01	Relay N/O	FLW01	Flowmeter Fixed mask & WBS	FM / WBS01
DI24	L1 / M1	Relay N/O	FLW02	Flowmeter L1 & M1	L1 / M1
DI27	SLW01	Relay N/O	FLW05	Flowmeter SLW01	SLW01
DI29	SLW02	Relay N/O	FLW07	Flowmeter SLW02	SLW02
DI31	L2	Relay N/O	FLW09	Flowmeter L2	L2
DI33	FS02 / 07	Relay N/O	FLW10	Flowmeter FS02 & FS07	FS02
DI35	DCM	Relay N/O	FLW12	Flowmeter DCM crystal cage	DCM
DI37	DM1	Relay N/O	FLW13	Flowmeter WBS	WBS
DI39	M3ABC	Relay N/O	FLW14	Flowmeter M3 mirrors	M3
DI41	PBS01	Relay N/O	FLW15	Flowmeter PB stop	PBS
DI43	SLVAB	Relay N/O	FLW16	Flowmeter slit blades	SLVAB
DI45	SLVC	Relay N/O	FLW17	Flowmeter slit blades	SLVC
DI47	GV00	Switch N/O	GV00O	Limit switch, gate valve V0 open	Pos GV0
DI49		Switch N/O	GV00C	Limit switch, gate valve V0 closed	
DI51	GV01	Switch N/O	GV01O	Limit switch, gate valve V1 open	Pos GV1
DI53		Switch N/O	GV01C	Limit switch, gate valve V1 closed	
DI55	GV02	Switch N/O	GV02O	Limit switch, gate valve V2 open	Pos GV2
DI57		Switch N/O	GV02C	Limit switch, gate valve V2 closed	
DI59	GV03	Switch N/O	GV03O	Limit switch, gate valve V3 open	Pos GV3
DI61		Switch N/O	GV03C	Limit switch, gate valve V3 closed	
DI63	GV04	Switch N/O	GV04O	Limit switch, gate valve V4 open	Pos GV4
DI65		Switch N/O	GV04C	Limit switch, gate valve V4 closed	
DI67	GV05	Switch N/O	GV05O	Limit switch, gate valve V5 open	Pos GV5
DI69		Switch N/O	GV05C	Limit switch, gate valve V5 closed	
DI71	GV06	Switch N/O	GV06O	Limit switch, gate valve V6 open	Pos GV6
DI73		Switch N/O	GV06C	Limit switch, gate valve V6 closed	
DI75	GV07	Switch N/O	GV07O	Limit switch, gate valve V7 open	Pos GV7
DI77		Switch N/O	GV07C	Limit switch, gate valve V7 closed	
DI79	GV08	Switch N/O	GV08O	Limit switch, gate valve V8 open	Pos GV8
DI81		Switch N/O	GV08C	Limit switch, gate valve V8 closed	
DI83	GV09	Switch N/O	GV09O	Limit switch, gate valve V9 open	Pos GV9
DI85		Switch N/O	GV09C	Limit switch, gate valve V9 closed	
DI87	GV10	Switch N/O	GV10O	Limit switch, gate valve V10 open	Pos GV10
DI89		Switch N/O	GV10C	Limit switch, gate valve V10 closed	
DI91	GV11	Switch N/O	GV11O	Limit switch, gate valve V11 open	Pos GV11
DI93		Switch N/O	GV11C	Limit switch, gate valve V11 closed	
DI95	GV12	Switch N/O	GV12O	Limit switch, gate valve V12 open	Pos GV12
DI97		Switch N/O	GV12C	Limit switch, gate valve V12 closed	
DI99	GV13	Switch N/O	GV13O	Limit switch, gate valve V13 open	Pos GV13
DI101		Switch N/O	GV13C	Limit switch, gate valve V13 closed	
DI103	GV14	Switch N/O	GV14O	Limit switch, gate valve V14 open	Pos GV14
DI105		Switch N/O	GV14C	Limit switch, gate valve V14 closed	
DI107	GV15	Switch N/O	GV15O	Limit switch, gate valve V15 open	Pos GV15
DI109		Switch N/O	GV15C	Limit switch, gate valve V15 closed	
DI111	GV16	Switch N/O	GV16O	Limit switch, gate valve V16 open	Pos GV16
DI113		Switch N/O	GV16C	Limit switch, gate valve V16 closed	
DI115	GV17	Switch N/O	GV17O	Limit switch, gate valve V17 open	Pos GV17
DI117		Switch N/O	GV17C	Limit switch, gate valve V17 closed	
DI119	GV18	Switch N/O	GV18O	Limit switch, gate valve V18 open	Pos GV18
DI121		Switch N/O	GV18C	Limit switch, gate valve V18 closed	
DI123	GV19	Switch N/O	GV19O	Limit switch, gate valve V19 open	Pos GV19
DI125		Switch N/O	GV19C	Limit switch, gate valve V19 closed	
DI127	GV20	Switch N/O	GV20O	Limit switch, gate valve V20 open	Pos GV20
DI129		Switch N/O	GV20C	Limit switch, gate valve V20 closed	
DI131	GV21	Switch N/O	GV21O	Limit switch, gate valve V21 open	Pos GV21
DI133		Switch N/O	GV21C	Limit switch, gate valve V21 closed	
DI135	GV22	Switch N/O	GV22O	Limit switch, gate valve V22 open	Pos GV22
DI137		Switch N/O	GV22C	Limit switch, gate valve V22 closed	
DI139	GV23	Switch N/O	GV23O	Limit switch, gate valve V23 open	Pos GV23
DI141		Switch N/O	GV23C	Limit switch, gate valve V23 closed	
DI143	GV24	Switch N/O	GV24O	Limit switch, gate valve V24 open	Pos GV24
DI145		Switch N/O	GV24C	Limit switch, gate valve V24 closed	
DI147	GV25	Switch N/O	GV25O	Limit switch, gate valve V25 open	Pos GV25
DI149		Switch N/O	GV25C	Limit switch, gate valve V25 closed	
DI151	GV26	Switch N/O	GV26O	Limit switch, gate valve V26 open	Pos GV26
DI153		Switch N/O	GV26C	Limit switch, gate valve V26 closed	
DI155	GV27	Switch N/O	GV27O	Limit switch, gate valve V27 open	Pos GV27
DI157		Switch N/O	GV27C	Limit switch, gate valve V27 closed	

Digital Output

Channel	Output	Tag	Signal description	Tag Name
DO00	24Vdc	SH00	Synchrotron beam not inhibited from EPS	Interlock
DO01	24Vdc	GV00	Allow Gate valve 0 to operate	Op GV0
DO02	24Vdc	GV01	Allow Gate valve 1 to operate	Op GV1
DO03	24Vdc	GV02	Allow Gate valve 2 to operate	Op GV2
DO04	24Vdc	GV03	Allow Gate valve 3 to operate	Op GV3
DO05	24Vdc	GV04	Allow Gate valve 4 to operate	Op GV4
DO06	24Vdc	GV05	Allow Gate valve 5 to operate	Op GV5
DO07	24Vdc	GV06	Allow Gate valve 6 to operate	Op GV6
DO08	24Vdc	GV07	Allow Gate valve 7 to operate	Op GV7
DO09	24Vdc	GV08	Allow Gate valve 8 to operate	Op GV8
DO10	24Vdc	GV09	Allow Gate valve 9 to operate	Op GV9
DO11	24Vdc	GV10	Allow Gate valve 10 to operate	Op GV10
DO12	24Vdc	GV11	Allow Gate valve 11 to operate	Op GV11
DO13	24Vdc	GV12	Allow Gate valve 12 to operate	Op GV12
DO14	24Vdc	GV13	Allow Gate valve 13 to operate	Op GV13
DO15	24Vdc	GV14	Allow Gate valve 14 to operate	Op GV14
DO16	24Vdc	GV15	Allow Gate valve 15 to operate	Op GV15
DO17	24Vdc	GV16	Allow Gate valve 16 to operate	Op GV16
DO18	24Vdc	GV17	Allow Gate valve 17 to operate	Op GV17
DO19	24Vdc	GV18	Allow Gate valve 18 to operate	Op GV18
DO20	24Vdc	GV19	Allow Gate valve 19 to operate	Op GV19
DO21	24Vdc	GV20	Allow Gate valve 20 to operate	Op GV20
DO22	24Vdc	GV21	Allow Gate valve 21 to operate	Op GV21
DO23	24Vdc	GV22	Allow Gate valve 22 to operate	Op GV22
DO24	24Vdc	GV23	Allow Gate valve 23 to operate	Op GV23
DO25	24Vdc	GV24	Allow Gate valve 24 to operate	Op GV24
DO26	24Vdc	GV25	Allow Gate valve 25 to operate	Op GV25
DO27	24Vdc	GV26	Allow Gate valve 26 to operate	Op GV26
DO28	24Vdc	GV27	Allow Gate valve 27 to operate	Op GV27

S3160 NIST SST MCS-8 Plus CONTROLLER AXIS DETAIL

CONTROL RACK 2

Status	#1	L1 Mirror, FLS09 & FLS13
ON SITE (S2263)	1	Hex leg 1
	2	Hex leg 2
	3	Hex leg 3
	4	Hex leg 4
	5	Hex leg 5
	6	Hex leg 6
	7	DM02-FLS09/BIM
	8	DM05-FLS13/BIM

Status	#2	M1 Mirror
ON SITE (S2263)	1	Hex leg 1
	2	Hex leg 2
	3	Hex leg 3
	4	Hex leg 4
	5	Hex leg 5
	6	Hex leg 6
	7	
	8	

Status	#3	WB Slits
ON SITE (S2263)	1	SLW01-VER-TOP
	2	SLW01-VER-BOT
	3	SLW01-HOR-OUT
	4	SLW01-HOR-IN
	5	SLW02-VER-TOP
	6	SLW02-VER-BOT
	7	SLW02-HOR-OUT
	8	SLW02-HOR-IN

Status	#4	L2 Mirror
ON SITE (S2263)	1	Hex leg 1
	2	Hex leg 2
	3	Hex leg 3
	4	Hex leg 4
	5	Hex leg 5
	6	Hex leg 6
	7	Wedge Jack
	8	

Status	#5	DM2 & DM5
In Design (SST S3160)	1	DM02-SLM02-VER-Top
	2	DM02-SLM02-VER-Bot
	3	DM02-SLM02-HOR-in
	4	DM02-SLM02-HOR-out
	5	DM05-SLM05-VER-Top
	6	DM05-SLM05-VER-Bot
	7	DM05-SLM05-HOR-in
	8	DM05-SLM05-HOR-out

CONTROL RACK 3

Status	#6	DCM
ON SITE (S2133)	1	Bragg
	2	Bragg enc
	3	1st Roll
	4	2nd Pitch
	5	2nd Roll
	6	2nd Perp
	7	2nd Parallel
	8	Lateral

Status	#7	M3AB/C Mirror
In Design (SST S3160)	1	Hex leg 1
	2	Hex leg 2
	3	Hex leg 3
	4	Hex leg 4
	5	Hex leg 5
	6	Hex leg 6
	7	
	8	

CONTROL RACK 4

Status	#8	M4A
In Design (SST S3160)	1	Hex leg 1
	2	Hex leg 2
	3	Hex leg 3
	4	Hex leg 4
	5	Hex leg 5
	6	Hex leg 6
	7	
	8	

Status	#9	M5C, FLS10 & FLS11
In Design (SST S3160)	1	Hex leg 1
	2	Hex leg 2
	3	Hex leg 3
	4	Hex leg 4
	5	Hex leg 5
	6	Hex leg 6
	7	DM03-FLS10/BIM
	8	DM04-FLS11/BIM

Status	#10	M4C/D Mirror & FLS14
In Design (SST S3160)	1	Hex leg 1
	2	Hex leg 2
	3	Hex leg 3
	4	Hex leg 4
	5	Hex leg 5
	6	Hex leg 6
	7	DM06-FLS14/BIM
	8	

Status	#11	DM01 & DM06
In Design (SST S3160)	1	
	2	DM01-FLS03
	3	DM01-SLM01-VER-Top
	4	DM01-SLM01-VER-Bot
	5	DM01-SLM01-HOR-IN
	6	DM01-SLM01-HOR-OUT
	7	DM06-SLM06-VER-Top
	8	DM06-SLM06-VER-Bot

Status	#12	DM03 & DM04
In Design (SST S3160)	1	DM03-SLM03-VER-Top
	2	DM03-SLM03-VER-Bot
	3	DM03-SLM03-HOR-IN
	4	DM03-SLM03-HOR-OUT
	5	DM04-SLM04-VER-Top
	6	DM04-SLM04-VER-Bot
	7	DM04-SLM04-HOR-IN
	8	DM04-SLM04-HOR-OUT

Status	#13	Pslit 01 & Pslit 02
In Design (SST S3160)	1	PSlit XY - SLV01
	2	PSlit XY stage Lat - LAT01
	3	Pslit XY stage Ver - VER01
	4	PSlit XY - SLV02
	5	PSlit XY stage Lat - LAT02
	6	Pslit XY stage Ver - VER02
	7	DM06-SLM06-HOR-IN
	8	DM06-SLM06-HOR-OUT

CONTROL RACK 6

Status	#14	L4 Mirror
In Design (SST S3160)	1	Hex leg 1
	2	Hex leg 2
	3	Hex leg 3
	4	Hex leg 4
	5	Hex leg 5
	6	Hex leg 6
	7	
	8	

Status	#15	M4B Mirror
In Design (SST S3160)	1	Hex leg 1
	2	Hex leg 2
	3	Hex leg 3
	4	Hex leg 4
	5	Hex leg 5
	6	Hex leg 6
	7	
	8	

Status	#16	L3 Mirror
In Design (SST S3160)	1	Hex leg 1
	2	Hex leg 2
	3	Hex leg 3
	4	Hex leg 4
	5	Hex leg 5
	6	Hex leg 6
	7	
	8	

Reference Documents:

Reference Number	Date/ Issue	Title
SB1341-14-CN-0042	19/09/14	NIST Contract
	April 2014	NIST NSLS-II SST and BMM Beamline Backbones, Volume 2A, SST Technical Proposal
S3160	Nov 2014/REV 01	NIST SST BEAMLINE S3160 QUALITY PLAN

FMB Oxford
Osney Mead
Oxford OX2 0ES
UK

Contact: Andrew Fairley
Telephone: +44 (0)1865 320 313
Fax: +44 (0)1865 320 301
E-mail: andrew.fairley@fmb-oxford.com

Change log:

Revision	Date	Summary of Change	Approval
1.0	06/01/15	First Issue	NJB
2.0	27/02/15	Platinum binder layer added for Gold coating. No binder layer permitted for Carbon coating.	
3.0			
4.0			
5.0			
6.0			

TABLE OF CONTENTS **1**

1. *INTRODUCTION* **3**

1.1 AXIS 3

2. *SPECIFICATIONS* **5**

2.1 MIRROR SYSTEM 5

2.1.1 L3 Mirror Optic *5*

2.2 MOTIONS 6

2.3 VACUUM SYSTEM 7

2.4 VACUUM VESSEL 8

2.5 ELECTRICAL DATA 9

2.5.1 Linear Actuators (Hexapod legs) *9*

2.5.2 Encoder Data *9*

2.6 LIFTING POINTS 9

2.7 ALIGNMENT FEATURES 9

3. FACTORY TESTING **10**

4. INSTALLATION AND UNIT ACCEPTANCE **11**

5. *SCOPE OF SUPPLY* **12**

1. *INTRODUCTION*

The L3 mirror system is located upstream of the μXPS endstation (and mirror system L4). The purpose the L3 mirror system is to guide the tender x rays towards L4 and the end station. The L3 optic is planar and uncooled. The optic is mounted to the base of the vacuum vessel and is manipulated using a hexapod, which gives six degrees of freedom.

1.1 AXIS

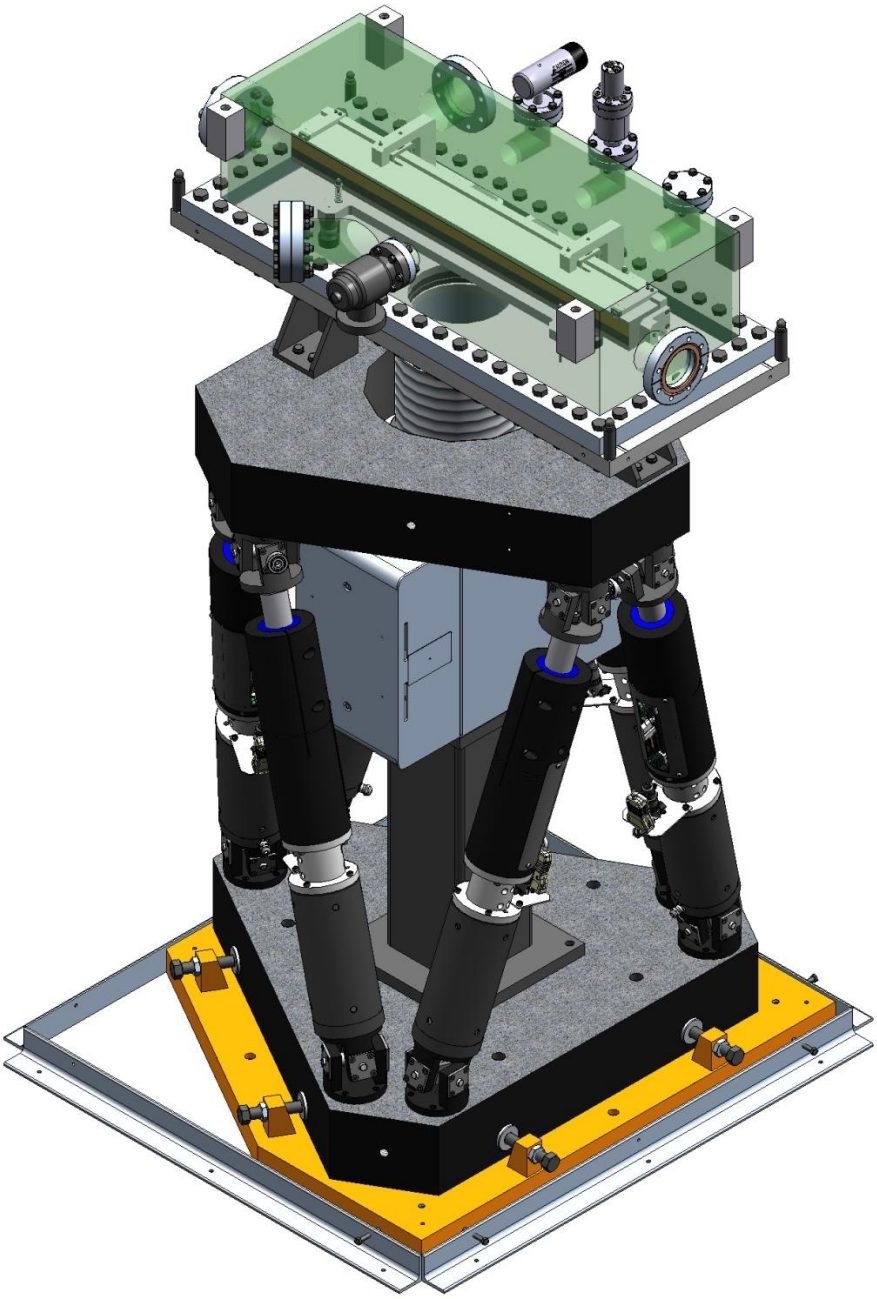

Figure 1. L3 mirror system

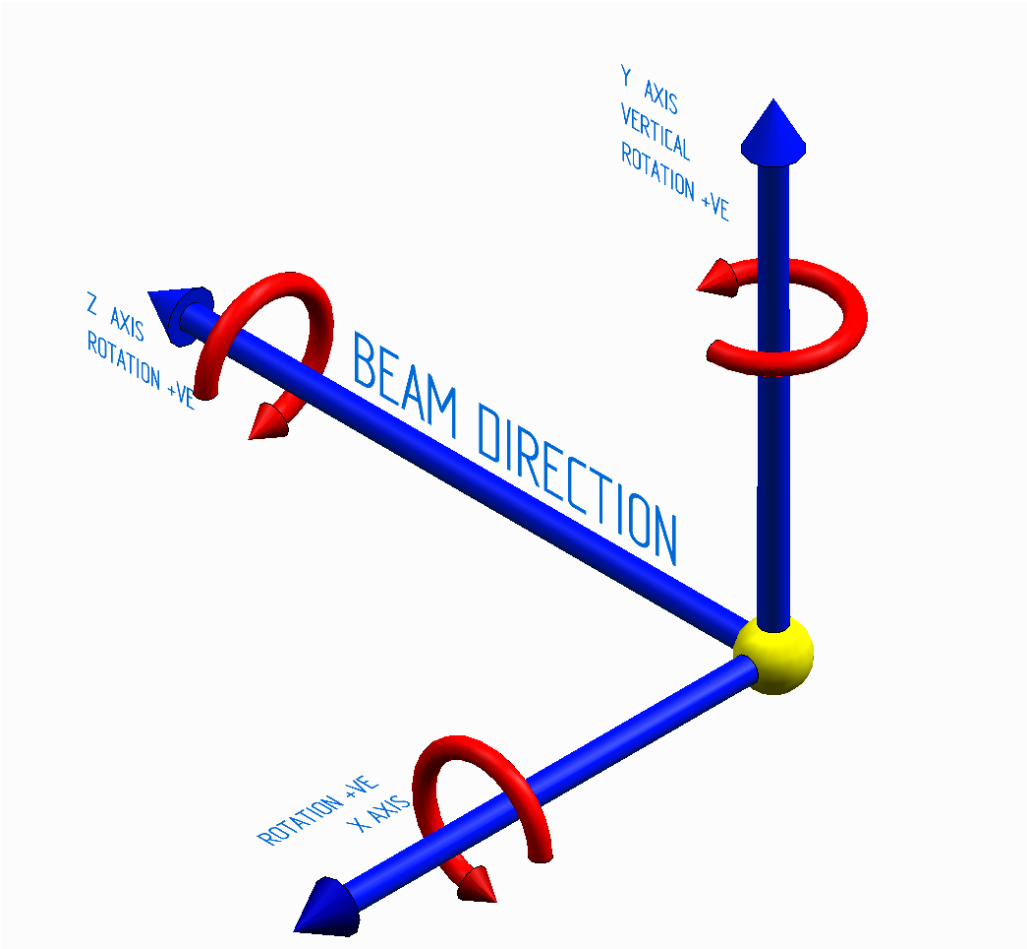

Figure 2. Beamline coordinate system

Inboard is defined as being in the negative x direction and outboard in the postive x direction.

The coordinate system employed complies with NSLS-II document:

Beamline Coordinate System Standards LT-C-XFD-STD-BL-COORD-001.

2. *SPECIFICATIONS*

2.1 MIRROR SYSTEM

Incoming Beam Height	1415 mm
Operating Position	Horizontally deflecting outboard
Manual Adjustments	± 10 mm in x and z (from grouted-in baseplate)
Optic location relative to centre of straight section (mm).	-40.33, 15, 62258 (x, y, z)

2.1.1 L3 Mirror Optic

Substrate material	Single crystal silicon
Substrate dimensions	670 mm L x 50 mm W x 60 mm D
Active Area (centred on substrate to within ± 0.5mm)	660 mm x 30 mm
Grazing incidence angle	0.61° [AF1]
Substrate Shape	Planar, Tangential Radius ≥20 km, Sagittal Radius ≥3 km
Tangential slope error	<0.25 µrad RMS over active length
Sagittal slope error	<5 µrad RMS over active length on prepared substrate
Coating	Au 300 Å ± 10% thick, 21 mm wide[AF2] over Pt 100 Å ± 10% thick binder layer C 300 Å ± 10% thick 21 mm wide. No binder layer permitted.
Surface Roughness	<3 Å RMS
Surface Quality	0.5 scratches or points per cm^2 over 99% of active optical area
Cooling	Uncooled

2.2 MOTIONS

Motion	Parameter	Specification
Pitch (Ry)	Drive	Linear actuators, fitted with limit switches & encoder.
	Range	Nominal position ± 10 mrad
	Resolution	< 1µrad
	Repeatability	< 5 µrad
Roll (Rz)	Drive	Linear actuators, fitted with limit switches & encoder.
	Range	± 10 mrad
	Resolution	< 5 µrad
	Repeatability	< 10 µrad
Yaw (Rx)	Drive	Linear actuators, fitted with limit switches & encoder.
	Range	± 10 mrad
	Resolution	< 5 µrad
	Repeatability	< 10 µrad
Vertical (Ty)	Drive	Linear actuators, fitted with limit switches & encoder.
	Range	± 20 mm
	Resolution	< 1 µm
	Repeatability	< 5 µm

Lateral (Tx)	Drive	Linear actuators, fitted with limit switches & encoder.
	Range	± 10 mm[AF3]
	Resolution	< 1 µm
	Repeatability	< 5 µm
Longitudinal (Tz)	Drive	Linear actuators, fitted with limit switches & encoder.
	Range	± 5 mm
	Resolution	< 2 µm
	Repeatability	< 10 µm

2.3 VACUUM SYSTEM

Maximum bakeout temperature – vessel and internal components	150-200 °C
Vacuum	UHV compatible (< 5 x10^{-10} mbar[AF4]). Masses > 38 AMU shall have total pressure < 10^{-11} Torr (1.33 x 10^{-11} mbar)
Helium leak rate	< 1 x 10 $^{-10}$ mbar l/sec
Vacuum Pump	Gamma vacuum 300T ion pump located beneath the vessel
Vacuum gauges	One pirani gauge (MKS type 317)and one cold cathode gauge(MKS type 422) located on the mirror vessel
Right Angle Valve	VAT Valve type 54, DN40/CF70.

2.4 VACUUM VESSEL

The vacuum vessel for the L3 mirror system is rectangular due to the length of the optic. The optic is mounted to the vessel, whose position is manipulated with the hexapod.

Purpose	Location	Size	Qty
Beam In	Beam inlet port at end 1	DN63/CF114	1
Beam Out	Beam outlet port at end 2	DN63/CF114R	1
Ion Pump	Mounted on the base granite of the hexapod.	DN150/CF200	1
Roughing Port for RA valve	Outboard side of vessel	DN40/CF70	1
Viewport	Outboard side of vessel	DN63/CF114	1
Viewport	Incoming wall of vessel angled to look at substrate surface	DN40/CF70	1
Vacuum Gauges	Side of vessel	DN40/CF70	2
Spare	Top of vessel	DN63/CF114	1
Spare	Top of vessel	DN40/CF70	1
Mirror Loading	Baseplate	Aluminium wire seal	1

2.5 ELECTRICAL DATA

2.5.1 Linear Actuators (Hexapod legs[AF5])

Motor Type	McLennan Type 23HS309 stepper motor
Holding torque	87 Ncm
Step angle (full step drive)	1.8°/ or 200 steps/rev
Driving current	2 A
Gear box ratio	25:1
Thread pitch	2 mm
Resolution per step	0.4 µm
Maximum movement per actuator	± 50 mm
Connector (Motor and limits)	12 way trim trio (UTO)

2.5.2 Encoder Data[AF6]

Readhead type	Renishaw Tonic T1000-05A
Readhead (interpolator) resolution	0.1 µm
Scale type	RGSZ20
Connector	15-Way sub D

2.6 LIFTING POINTS

L3 mirror system weight: 500 kg approximately.

The mirror system is provided with three M16 lifting points in the base of the hexapod, in addition to three in the upper platform.

A lifting diagram for the system will be provided.

2.7 ALIGNMENT FEATURES

Fiducial mounts will be provided on the baseplate and on the upper platform of the hexapod. These will take the form of 0.25” reamed (H7) holes, suitable for 0.5” or 1.5” spheres.

3. FACTORY TESTING

Testing at FMB Oxford consists of Motion Testing, Vacuum Testing and Fiducialisation.

Full specifications and procedures covering all factory testing will be prepared in advance and these will be submitted to the customer prior to final design approval. Representatives from the customer are invited to witness these TESTS at FMB Oxford's works.

4. INSTALLATION AND UNIT ACCEPTANCE

The site acceptance testing, included in the installation option, will ensure that all components are carefully surveyed into position, all motors, actuators and sensors are functioning properly and the vacuum specifications are met. All motions will be tested and the correct functioning of all limit and datum switches checked. The complete set of detailed factory tests are not repeated on site.

There will be a full leak check of the installed vacuum sections. We expect that a turbo pump station, RGA rig, and He leak checker to be provided by the customer for our use while at the customer's site.

Final site acceptance will include:

- All factory test data, documentation and manuals
- Correct operation of all motions, limits and datum switches using FMB-O controls and cabling.
- Leak testing at the best achievable sensitivity after 24 hrs of pumping and prior to on site customer bakeout

5. *SCOPE OF SUPPLY*

- L3 optic and mirror system
- 300 l/s ion pump & pump controller (Gamma)
- Right angle valve (Vat valve)
- Cold cathode (series 422) and pirani (series 317) gauges and gauge controller (MKS 937B)
- Motion controls as specified in the controls functional specification
- Field cables

Reference Documents:

Reference Number	Date/ Issue	Title
SB1341-14-CN-0042	19/09/14	NIST Contract
	April 2014	NIST NSLS-II SST and BMM Beamline Backbones, Volume 2A, SST Technical Proposal
S3160	Nov 2014/REV 01	NIST SST BEAMLINE S3160 QUALITY PLAN

FMB Oxford
Osney Mead
Oxford OX2 0ES
UK

Contact: Andrew Fairley
Telephone: +44 (0)1865 320 313
Fax: +44 (0)1865 320 301
E-mail: andrew.fairley@fmb-oxford.com

Change log:

Revision	Date	Summary of Change	Approval
1.0	06/01/15	First Issue	NJB
2.0	27/02/15	IC-101 replaced by I400. Port for drain current feedthrough added. Tangential slope error amended. L4/M4B functional specs combined	
3.0			
4.0			
5.0			
6.0			

TABLE OF CONTENTS **1**

1. *INTRODUCTION* **3**

1.1 AXIS 4

2. *SPECIFICATIONS* **5**

2.1 MIRROR SYSTEM L4/M4B 5

2.1.1 L4 Mirror Optic *5*

2.1.2 M4B Mirror Optic *6*

2.2 MOTIONS 7

2.3 VACUUM SYSTEM 8

2.4 VACUUM VESSELS 8

2.4.1 Vacuum Vessel L4 ..... *8*

2.4.2 Vacuum Vessel M4B *9*

2.5 MIRROR CURRENT TAKEOFFS 10

2.6 ELECTRICAL DATA 10

2.6.1 Linear Actuators (Hexapod legs) *10*

2.6.2 Encoder Data *10*

2.6.3 Electrical Interfacing *11*

2.7 LIFTING POINTS 11

2.8 ALIGNMENT FEATURES 11

3. FACTORY TESTING **12**

4. INSTALLATION AND UNIT ACCEPTANCE **13**

5. *SCOPE OF SUPPLY* **14**

1. *INTRODUCTION*

The L4/M4B mirror system is located directly upstream of the μXPS endstation. The purpose of both mirrors is to to focus the x rays at the μXPS end station. The M4B optic is ellipsoidal, uncooled and foucuses the soft x-rays from the transfer branch onto the end station. The L4 optic is also an uncooled, ellipsoidal optic which focuses the tender x-rays of the 'L branch' onto the end station. The optics are mounted to the bases of the vacuum vessels and are manipulated using a hexapod, which gives six degrees of freedom. The optics are fitted with drain current take offs.

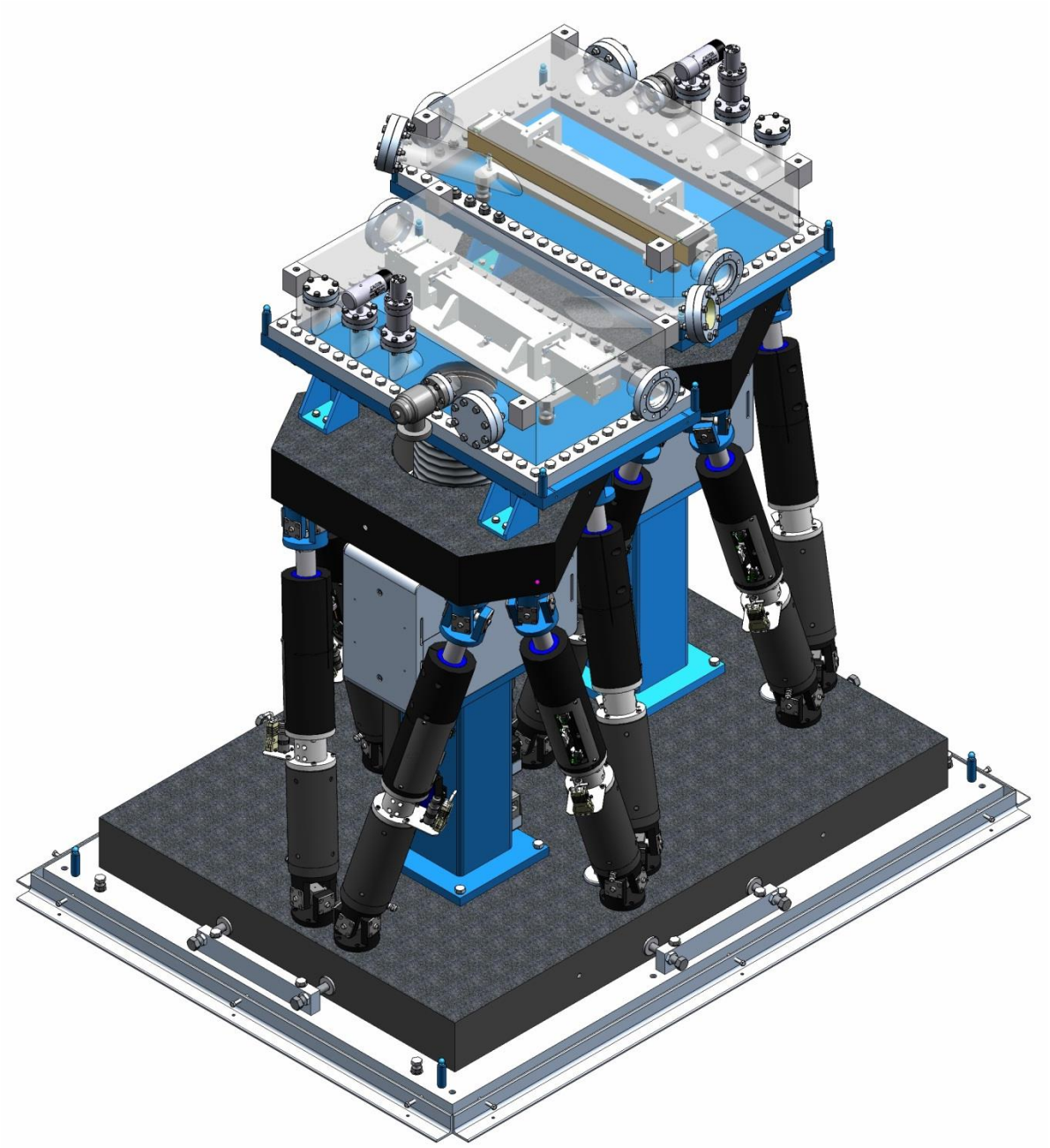

Figure 1. L4/M4B Mirror Sytem

1.1 AXIS

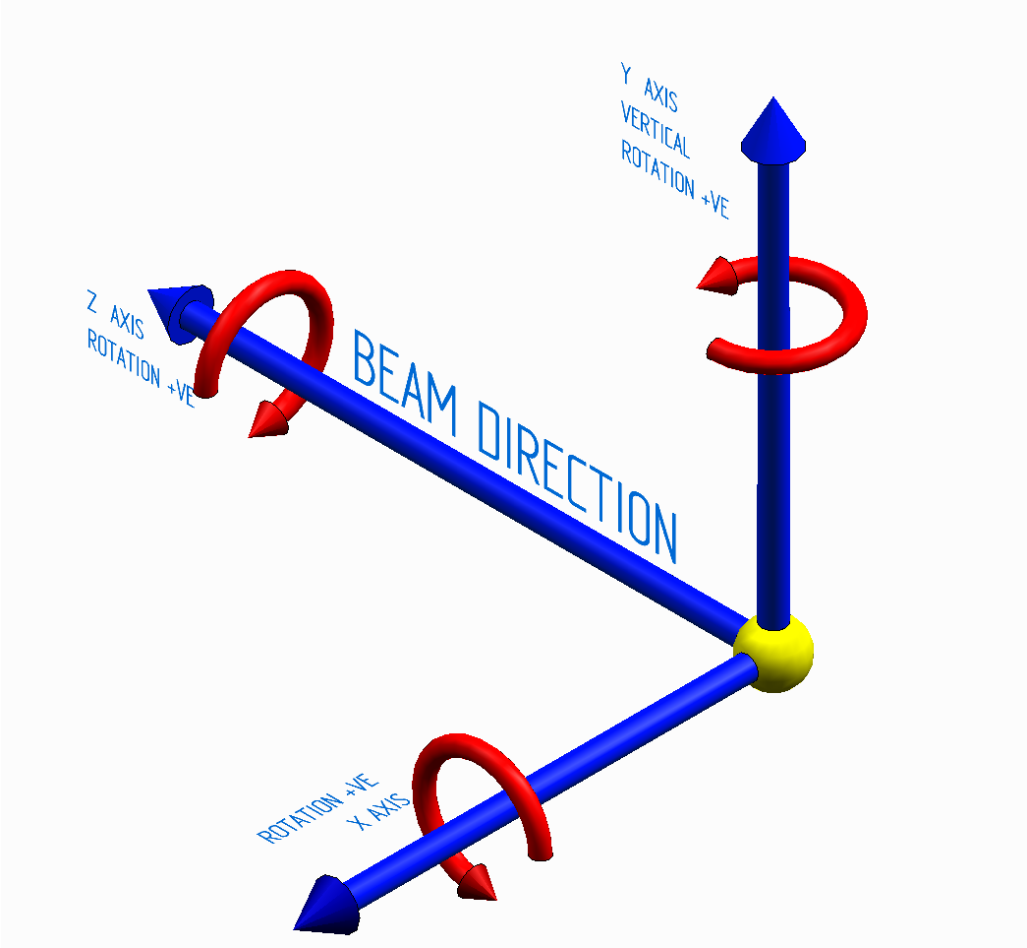

Figure 2. Beamline coordinate system

Inboard is defined as being in the negative x direction and outboard in the postive x direction.

The coordinate system employed complies with NSLS-II document:

Beamline Coordinate System Standards LT-C-XFD-STD-BL-COORD-001.

2. *SPECIFICATIONS*

2.1 MIRROR SYSTEM L4/M4B

Incoming Beam Height	1415 mm
Operating Position **(L4)**	Horizontally deflecting outboard, vertically and horizontally refocusing.
Operating Position **(M4B)**	Horizontally deflecting inboard, vertically and horizontally refocusing.
Manual Adjustments	± 10 mm in x and z (from grouted-in baseplate)
Optic location relative to centre of straight section (mm) – **(L4)**	66.59, 15, 66766 (x, y, z)
Optic location relative to centre of straight section (mm) – **M4B**	428.35, 15, 66570 (x, y, z)

2.1.1 L4 Mirror Optic

Substrate material	Fused silica
Substrate dimensions	600 mm L x 50 mm W x 60 mm D
Active Area (centred on substrate to within ± 0.5mm)	540 mm x 6 mm
Substrate Shape	Ellipsoidal. Major axis 35509.4 mm ± 1% Minor axis 152.8 mm ± 1%. Mirror pole X_0: 32509.7 mm (off axis) ± 1%. Mirror pole Y_0: 61.5 mm (off axis)
Grazing incidence angle	0.61°
Distance to source	68018.8 mm
Distance to image	3000.1 mm
Tangential slope error	<1.0 µrad RMS over active length

Sagittal slope error	<10 µrad RMS over active length on prepared substrate
Coating	Au 300 Á ± 10% thick 15 mm wide. No binder layer permitted.
Surface Roughness	<3 Å RMS
Surface Quality	0.5 scratches or points per cm^2 over 99% of active optical area
Cooling	Uncooled

2.1.2 M4B Mirror Optic

Substrate material	Fused silica
Substrate dimensions	600 mm L x 60 mm W x 60 mm D
Active Area (centred on substrate to within ± 0.5mm)	540 mm x 21 mm
Substrate Shape	Ellipsoidal. Major axis 10604.9 mm ± 1% Minor axis 231.9 mm ± 1%. Mirror pole X_0: 7405.7 mm (off axis) ± 1%.
Grazing incidence angle	1.75°
Distance to source	18008.9 mm
Distance to image	3201 mm
Tangential slope error	<1.0 µrad RMS over active length
Sagittal slope error	<10 µrad RMS over active length on prepared substrate
Coating	Au 300 Á ± 10% thick 30 mm wide No binder layers are permitted.
Surface Roughness	<3 Å RMS
Surface Quality	0.5 scratches or points per cm^2 over 99% of active optical area

Cooling	Uncooled

2.2 MOTIONS

Motion	Parameter	Specification
Pitch (Ry)	Drive	Linear actuators, fitted with limit switches & encoder.
	Range	Nominal position ± 10 mrad
	Resolution	< 1µrad
	Repeatability	< 5 µrad
Roll (Rz)	Drive	Linear actuators, fitted with limit switches & encoder.
	Range	± 10 mrad
	Resolution	< 5 µrad
	Repeatability	< 10 µrad
Yaw (Rx)	Drive	Linear actuators, fitted with limit switches & encoder.
	Range	± 10 mrad
	Resolution	< 5 µrad
	Repeatability	< 10 µrad
Vertical (Ty)	Drive	Linear actuators, fitted with limit switches & encoder.
	Range	± 20 mm
	Resolution	< 1 µm
	Repeatability	< 5 µm

Lateral (Tx)	Drive	Linear actuators, fitted with limit switches & encoder.
	Range	± 10 mm
	Resolution	< 1 µm
	Repeatability	< 5 µm
Longitudinal (Tz)	Drive	Linear actuators, fitted with limit switches & encoder.
	Range	± 5 mm
	Resolution	< 2 µm
	Repeatability	< 10 µm

2.3 VACUUM SYSTEM

Maximum bakeout temperature – vessel and internal components	150-200 °C
Vacuum	UHV compatible (< 5 x10^{-10} mbar). Masses > 38 AMU shall have total pressure < 10^{-11} Torr (1.33 x 10^{-11} mbar)
Helium leak rate	< 1 x 10 $^{-10}$ mbar l/sec
Vacuum Pump	Gamma vacuum 300T ion pump located beneath the vessel
Vacuum gauges	One pirani gauge (MKS type 317)and one cold cathode gauge(MKS type 422) located on the mirror vessel
Right Angle Valve	VAT Valve type 54, DN40/CF70.

2.4 VACUUM VESSELS

The vacuum vessels for both mirror systems are rectangular due to the lengths of the optics. The optics are mounted to the vessel, whose position is manipulated with the hexapod.

2.4.1 Vacuum Vessel L4

Purpose	Location	Size	Qty

Beam In	Beam inlet port at end 1	DN63/CF114	1
Beam Out	Beam outlet port at end 2	DN63/CF114R	1
Ion Pump	Mounted on the base granite of the hexapod.	DN150/CF200	1
Roughing Port for RA valve	Outboard side of vessel	DN40/CF70	1
Viewport	Outboard side of vessel	DN63/CF114	1
Viewport	Incoming wall of vessel angled to look at substrate surface	DN40/CF70	1
Vacuum Gauges	Side of vessel	DN40/CF70	2
Spare	Top of vessel	DN63/CF114	1
Spare	Top of vessel	DN40/CF70	1
Mirror Loading	Baseplate	Aluminium wire seal	1
Optic drain current feedthrough (2x BNC)	Baseplate	DN40/CF70	1

2.4.2 Vacuum Vessel M4B

Purpose	**Location**	**Size**	**Qty**
Beam In	Beam inlet port at end 1	DN63/CF114	1
Beam Out	Beam outlet port at end 2	DN63/CF114	1
Ion Pump	Mounted on the base granite of the hexapod.	DN150/CF200	1
Roughing Port for RA valve	Outboard side of vessel	DN40/CF70	1
Viewport	Outboard side of vessel	DN63/CF114	1
Viewport	Incoming wall of vessel angled to look at	DN40/CF70	1

	substrate surface		
Vacuum Gauges	Side of vessel	DN40/CF70	2
Spare	Top of vessel	DN63/CF114	1
Spare	Top of vessel	DN40/CF70	1
Mirror Loading	Baseplate	Aluminium wire seal	1
Drain current feedthrough	Baseplate	DN40/CF70	1

2.5 MIRROR CURRENT TAKEOFFS

Both mirrors are fitted with drain current takeoffs to monitor the beam intensity. Two physical takeoffs are fitted to the optic stripe to allow the continuity of the electrical connection to be checked. The drain current will be measured using an I400.

2.6 ELECTRICAL DATA

2.6.1 Linear Actuators (Hexapod legs)

Motor Type	McLennan Type 23HS309 stepper motor
Holding torque	87 Ncm
Step angle (full step drive)	1.8°/ or 200 steps/rev
Driving current	2 A
Gear box ratio	25:1
Thread pitch	2 mm
Resolution per step	0.4 μm
Maximum movement per actuator	± 50 mm
Connector (Motor and limits)	12 way trim trio (UTO)

2.6.2 Encoder Data

Readhead type	Renishaw Tonic T1000-05A
Readhead (interpolator) resolution	0.1 µm
Scale type	RGSZ20
Connector	15-Way sub D

2.6.3 Electrical Interfacing

All in air motors, limits and encoders are connected locally to the relevant drive.

2.7 LIFTING POINTS

Combined weight of L4/M4B: 1800 kg approximately.

The mirror system is provided with four M16 lifting points in the base of the hexapod, in addition to three in the upper platform.

A lifting diagram for the system will be provided.

2.8 ALIGNMENT FEATURES

Fiducial mounts will be provided on the baseplate and on the upper platform of the hexapod. These will take the form of 0.25” reamed (H7) holes, suitable for 0.5” or 1.5” spheres.

3. FACTORY TESTING

Testing at FMB Oxford consists of Motion Testing, Vacuum Testing and Fiducialisation.

Full specifications and procedures covering all factory testing will be prepared in advance and these will be submitted to the customer prior to final design approval. Representatives from the customer are invited to witness these tests at FMB Oxford's works.

4. INSTALLATION AND UNIT ACCEPTANCE

The site acceptance testing, included in the installation option, will ensure that all components are carefully surveyed into position, all motors, actuators and sensors are functioning properly and the vacuum specifications are met. All motions will be tested and the correct functioning of all limit and datum switches checked. The complete set of detailed factory tests are not repeated on site.

There will be a full leak check of the installed vacuum sections. We expect that a turbo pump station, RGA rig, and He leak checker to be provided by the customer for our use while at the customer's site.

Final site acceptance will include:

- All factory test data, documentation and manuals
- Correct operation of all motions, limits and datum switches using FMB-O controls and cabling.
- Leak testing at the best achievable sensitivity after 24 hrs of pumping and prior to on site customer bakeout

5. *SCOPE OF SUPPLY*

- L4 and M4B optics and mirror system
- I400 Current amplifier (optic drain current measurement)
- MOXA
- 300 l/s ion pump & pump controller (Gamma) for each mirror vessel
- Right angle valve (Vat valve) – one per mirror vessel
- Cold cathode (series 422) and pirani (series 317) gauges and gauge controller (MKS 937B) – one of each for each mirror vessel
- Motion controls as specified in the controls functional specification.
- Field cables

S3160 NIST SST – MIRROR SYSTEM M3

Reference Documents:

Reference Number	Date/ Issue	Title
SB1341-14-CN-0042	19/09/14	NIST Contract
	April 2014	NIST NSLS-II SST and BMM Beamline Backbones, Volume 2A, SST Technical Proposal
S3160	Nov 2014/REV 01	NIST SST BEAMLINE S3160 QUALITY PLAN

FMB Oxford
Osney Mead
Oxford OX2 0ES
UK

Contact: Andrew Fairley
Telephone: +44 (0)1865 320 313
Fax: +44 (0)1865 320 301
E-mail: andrew.fairley@fmb-oxford.com

Change log:

Revision	Date	Summary of Change	Approval
1.0	06/01/15	First Issue	NJB
2.0	27/02/15	Tangential slope error amended. Port added in baseplate for DPT feedthrough. No binder layers permitted.	AJF
3.0			
4.0			
5.0			
6.0			

TABLE OF CONTENTS **1**

1. *INTRODUCTION* **3**

1.1 AXIS 3

2. *SPECIFICATIONS* **4**

2.1 MIRROR SYSTEM 4

2.1.1 M3AB Mirror Optic *4*

2.1.2 M3C Mirror Optic *5*

2.2 MOTIONS 7

2.3 VACUUM SYSTEM 8

2.4 VACUUM VESSEL 9

2.5 DITHERING MECHANISM 9

2.6 THERMAL STABILISATION CIRCUIT 9

2.7 ELECTRICAL DATA 10

2.7.1 Linear Actuators (Hexapod legs) *10*

2.7.2 Dithering Mechanism *10*

2.7.3 Encoder Data *10*

2.8 LIFTING POINTS 10

2.9 ALIGNMENT FEATURES 11

3. FACTORY TESTING **12**

4. INSTALLATION AND UNIT ACCEPTANCE **13**

5. *SCOPE OF SUPPLY* **14**

1. *INTRODUCTION*

The M3 mirror system is located downstream of the plane grating monochromator, on the soft x-ray 'M' branch. The purpose the M3 mirror system is to direct the soft x rays either to the 'M' branch or to the transfer branches of the beamline. For this reason, the mirror system is equipped with two optics, both of which are tangential ellipses. The optics focus the x-rays horizontally at precision vertical slits – either one located in the transfer branch (slit AB) or one located in the 'M' branch (slit C).

The M3 optics (M3AB and M3C) are both uncooled. The optics are mounted to the base of the vacuum vessel and are manipulated with a hexapod, which provides six degrees of freedom.

The optics are arranged side by side, so the hexapod platform translates horizontally to switch between mirror M3AB (which directs beam down the transfer line) and mirror M3C (which directs beam down the 'M' branch).

The M3C optic is fitted with a flexure based dithering mechanism to increase the horizontal spot size at the μNEXAFS end station. The beam from M3C travels to M4D and then on to the μNEXAFS end station, or it goes on to M4C to M5C and then onwards to the NEXAFS/XPS end station. In addition, the M3 optics are fitted with a thermal stabilisation circuit.

1.1 AXIS

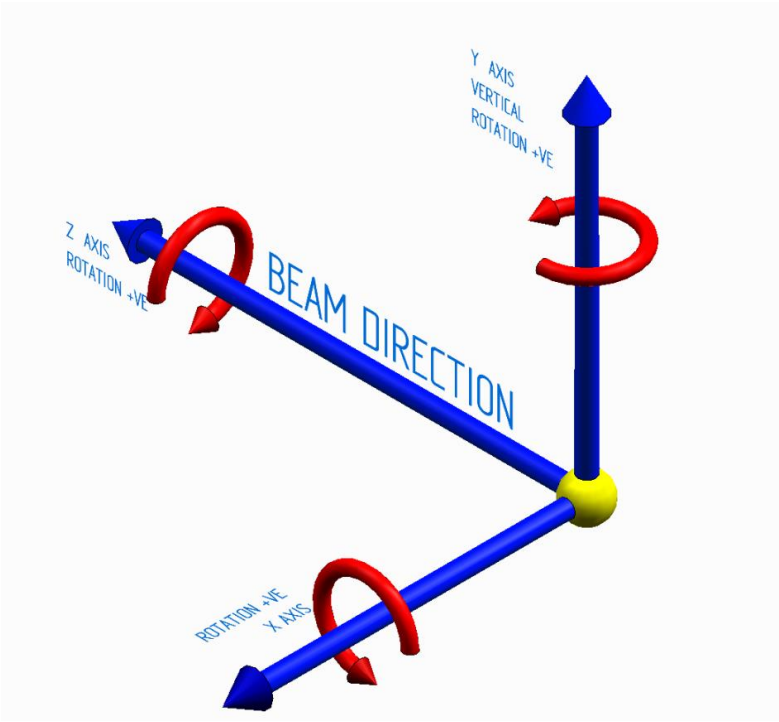

Figure 1. Beamline coordinate system

Inboard is defined as being in the negative x direction and outboard in the postive x direction.

The coordinate system employed complies with NSLS-II document:

Beamline Coordinate System Standards LT-C-XFD-STD-BL-COORD-001.

2. *SPECIFICATIONS*

2.1 MIRROR SYSTEM

Incoming Beam Height	1415 mm
Operating Position	Horizontally deflecting inboard, horizontally focusing (M3AB). Horizontally deflecting outboard, horizontally focusing (M3C).
Manual Adjustments	± 10 mm in x and z (from grouted-in baseplate)
Optic location relative to centre of straight section (mm)	666.7, 15, 42062 (x, y, z)

2.1.1 M3AB Mirror Optic

Substrate material	Fused silica
Substrate dimensions	280 mm L x 60 mm W x 40 mm D
Active Area (centred on substrate to within ± 0.5mm)	230 mm x 45 mm
Substrate Shape	Tangential Ellipse Major axis 23665.1 mm ± 1% Minor axis 497.5 mm ± 1% Mirror pole X_0: 17168.6 mm (off axis) ± 1%. *Sagittal Radius > 3km*
Grazing incidence angle	1.75° (deflecting beam inboard towards M4A & M4B)
Distance to source	40829.9 mm
Distance to image (precision vertical slit)	6500.3 mm
Tangential slope error	< 0.5 µrad RMS over active length
Sagittal slope error	< 10 µrad RMS over active length on prepared substrate

Coating	C 300 Ǻ ± 10% thick 13 mm wide Au 300 Ǻ ± 10% thick 13 mm wide Ni 300 Ǻ ± 10% thick 13 mm wide No binder layers are permitted.
Surface Roughness	<3 Å RMS
Surface Quality	0.5 scratches or points per cm^2 over 99% of active optical area
Cooling	Uncooled

2.1.2 M3C Mirror Optic

Substrate material	Fused silica
Substrate dimensions	310 mm L x 60 mm W x 40 mm D
Active Area (centred on substrate to within ± 0.5mm)	270 mm x 45 mm
Substrate Shape	Tangential Ellipse Major axis 23664.9 mm ± 1% Minor axis 426.4 ± 1% Mirror pole X_0 (off axis): 17167.8 mm ± 1%. *Sagittal Radius > 3km*
Grazing incidence angle	1.5° (deflecting outboard to M4C & M4D).
Distance to source	40829.9 mm
Distance to image (precision vertical slit)	6499.9 mm
Tangential slope error	<0.5 µrad RMS over active length
Sagittal slope error	< 10 µrad RMS over active length on prepared substrate

Coating	C 300 Ǻ ± 10% thick 13 mm wide Au 300 Ǻ ± 10% thick 13 mm wide Ni 300 Ǻ ± 10% thick 13 mm wide No binder layers are permitted
Surface Roughness	<3 Å RMS
Surface Quality	0.5 scratches or points per cm^2 over 99% of active optical area
Cooling	Uncooled

2.2 MOTIONS

Motion	Parameter	Specification
Pitch (Ry)	Drive	Linear actuators, fitted with limit switches & encoder.
	Range	Nominal position ± 10 mrad
	Resolution	< 1µrad
	Repeatability	< 5 µrad
Roll (Rz)	Drive	Linear actuators, fitted with limit switches & encoder.
	Range	± 10 mrad
	Resolution	< 5 µrad
	Repeatability	< 10 µrad
Yaw (Rx)	Drive	Linear actuators, fitted with limit switches & encoder.
	Range	± 10 mrad
	Resolution	< 5 µrad
	Repeatability	< 10 µrad
Vertical (Ty)	Drive	Linear actuators, fitted with limit switches & encoder.
	Range	± 20 mm
	Resolution	< 1 µm
	Repeatability	< 5 µm

Lateral (Tx)	Drive	Linear actuators, fitted with limit switches & encoder.
	Range	± 10 mm
	Resolution	< 1 µm
	Repeatability	< 5 µm
Longitudinal (Tz)	Drive	Linear actuators, fitted with limit switches & encoder.
	Range	± 5 mm
	Resolution	< 2 µm
	Repeatability	< 10 µm

2.3 VACUUM SYSTEM

Maximum bakeout temperature – vessel and internal components	150-200 °C
Vacuum	UHV compatible (< 5 x10^{-10} mbar). Masses > 38 AMU shall have total pressure < 10^{-11} Torr (1.33 x 10^{-11} mbar)
Helium leak rate	< 1 x 10^{-10} mbar l/sec
Vacuum Pump	Gamma vacuum 500T ion pump located on a stand adjacent to the mirror system
Vacuum gauges	One pirani gauge (MKS type 317)and one cold cathode gauge(MKS type 422) located on the mirror vessel
Right Angle Valve	VAT Valve type 54, DN40/CF70.

2.4 VACUUM VESSEL

The vacuum vessel for the M3 mirror system is rectangular.

Purpose	Location	Size	Qty
Beam In	Beam inlet port at end 1	DN63/CF114	1
Beam Out	Beam outlet port at end 2	DN63/CF114	1
Ion Pump	Mounted on the base granite of the hexapod.	DN150/CF200	1
Roughing Port for RA valve	Outboard side of vessel	DN40/CF70	1
Viewport	Outboard side of vessel	DN63/CF114	1
Viewport	Incoming wall of vessel angled to look at substrate surface	DN40/CF70	1
Vacuum Gauges	Side of vessel	DN40/CF70	2
Spare	Top of vessel	DN63/CF114	1
Spare	Top of vessel	DN40/CF70	1
Mirror Loading	Baseplate	Aluminium wire seal	1
DPT wiring feedthrough	Baseplate	DN40/CF70	1

2.5 DITHERING MECHANISM

The M3C mirror system is fitted with a piezo-driven flexure mechanism to dither the beam (increase the horizontal spot size) at µNEXAFS end station. The mirror needs to be dithered by approximately ±0.22 mrad to obtain a 20 mm horizontal stripe at the end station.

The M3C optic is used in combination with either the M4D optic (to the µNEXAFS end station) or the M4C and M5C optics (to the NEXAFS/XPS end station).

2.6 THERMAL STABILISATION CIRCUIT

Both optics are fitted with a side clamped copper block, which is attached to a cooled copper piece via flexible copper braids. The copper block is cooled by water provided by a chiller. There are no in vacuum water joints.

2.7 ELECTRICAL DATA

2.7.1 Linear Actuators (Hexapod legs)

Motor Type	McLennan Type 23HS309 stepper motor
Holding torque	87 Ncm
Step angle (full step drive)	1.8°/ or 200 steps/rev
Driving current	2 A
Gear box ratio	25:1
Thread pitch	2 mm
Resolution per step	0.4 µm
Maximum movement per actuator	± 50 mm
Connector (Motor and limits)	12 way trim trio (UTO)

2.7.2 Dithering Mechanism

Actuator type	Preloaded piezo stack driven flexure.
Range	±0.25 mrad

2.7.3 Encoder Data

Readhead type	Renishaw Tonic T1000-05A
Readhead (interpolator) resolution	0.1 µm
Scale type	RGSZ20
Connector	15-Way sub D

2.8 LIFTING POINTS

M3 mirror system weight: 500 kg approximately.

The mirror system is provided with three M16 lifting points in the base of the hexapod, in addition to three in the upper platform.

A lifting diagram for the system will be provided.

2.9 ALIGNMENT FEATURES

Fiducial mounts will be provided on the baseplate and on the upper platform of the hexapod. These will take the form of 0.25” reamed (H7) holes, suitable for 0.5” or 1.5” spheres.

3. FACTORY TESTING

Testing at FMB Oxford consists of Motion Testing, Vacuum Testing and Fiducialisation.

Full specifications and procedures covering all factory testing will be prepared in advance and these will be submitted to the customer prior to final design approval. Representatives from the customer are invited to witness these tests at FMB Oxford's works.

4. INSTALLATION AND UNIT ACCEPTANCE

The site acceptance testing, included in the installation option, will ensure that all components are carefully surveyed into position, all motors, actuators and sensors are functioning properly and the vacuum specifications are met. All motions will be tested and the correct functioning of all limit and datum switches checked. The complete set of detailed factory tests are not repeated on site.

There will be a full leak check of the installed vacuum sections. We expect that a turbo pump station, RGA rig, and He leak checker to be provided by the customer for our use while at the customer's site.

Final site acceptance will include:

- All factory test data, documentation and manuals
- Correct operation of all motions, limits and datum switches using FMB-O controls and cabling.
- Leak testing at the best achievable sensitivity after 24 hrs of pumping and prior to on site customer bakeout

5. *SCOPE OF SUPPLY*

- M3AB and M3C optics and mirror system
- DPT dithering and controls for M3C.
- 500 l/s ion pump & pump controller (Gamma)
- Right angle valve (Vat valve)
- Cold cathode (series 422) and pirani (series 317) gauges and gauge controller (MKS 937B)
- Motion Controls as specified in the controls functional specification.
- Field cables

Reference Documents:

Reference Number	Date/ Issue	Title
SB1341-14-CN-0042	19/09/14	NIST Contract
	April 2014	NIST NSLS-II SST and BMM Beamline Backbones, Volume 2A, SST Technical Proposal
S3160	Nov 2014/REV 01	NIST SST BEAMLINE S3160 QUALITY PLAN

FMB Oxford
Osney Mead
Oxford OX2 0ES
UK

Contact: Andrew Fairley
Telephone: +44 (0)1865 320 313
Fax: +44 (0)1865 320 301
E-mail: andrew.fairley@fmb-oxford.com

Change log:

Revision	Date	Summary of Change	Approval
1.0	06/01/15	First Issue	NJB
2.0	27/02/15	Port added for drain current feedthrough. No binder layers are permitted.	
3.0			
4.0			
5.0			
6.0			

TABLE OF CONTENTS **1**

1. *INTRODUCTION* **3**

1.1 AXIS 4

2. *SPECIFICATIONS* **5**

2.1 MIRROR SYSTEM 5

2.1.1 M4A Mirror Optic *5*

2.2 MOTIONS 6

2.3 VACUUM SYSTEM 7

2.4 VACUUM VESSEL 7

2.5 MIRROR CURRENT TAKEOFFS 8

2.6 ELECTRICAL DATA 9

2.6.1 Linear Actuators (Hexapod legs) *9*

2.6.2 Encoder Data *9*

2.7 LIFTING POINTS 9

2.8 ALIGNMENT FEATURES 9

3. FACTORY TESTING **10**

4. INSTALLATION AND UNIT ACCEPTANCE **11**

5. *SCOPE OF SUPPLY* **12**

1. *INTRODUCTION*

The M4A mirror system is located directly upstream of the HAXPES/NEXAFS endstation, on the soft x-ray transfer branch. The purpose the M4A mirror system is to focus the soft x rays at the HAXPES/NEXAFS end station. The M4A optic is ellipsoidal and uncooled. The optic is mounted to the base of the vacuum vessel and is manipulated using a hexapod, which gives six degrees of freedom. The optic is fitted with drain current take offs.

The M4A optic may also be moved out of beam to allow the soft x rays from optic M3AB to pass through to optic M4B, and from there be directed at end station μXPS.

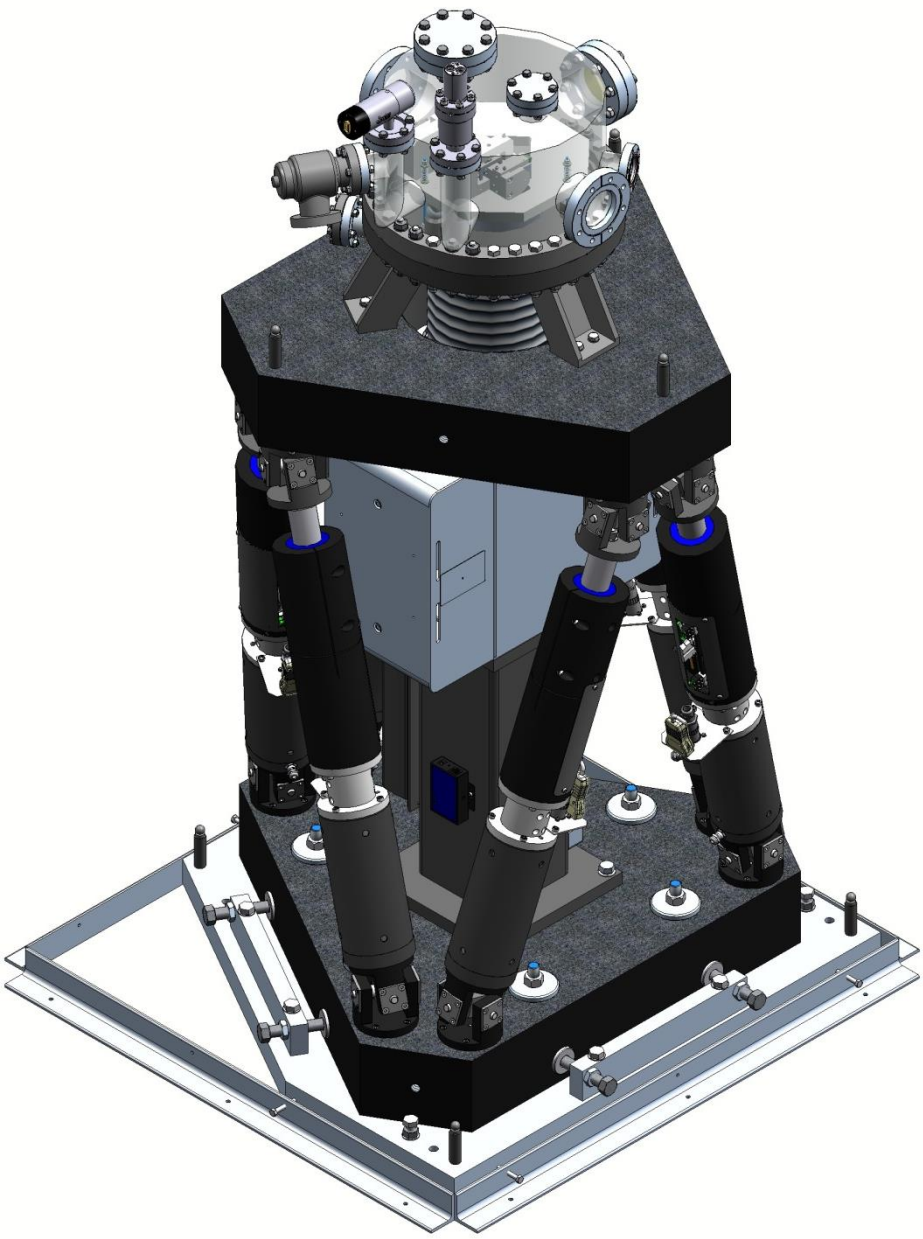

Figure 1. Mirror System M4A

1.1 AXIS

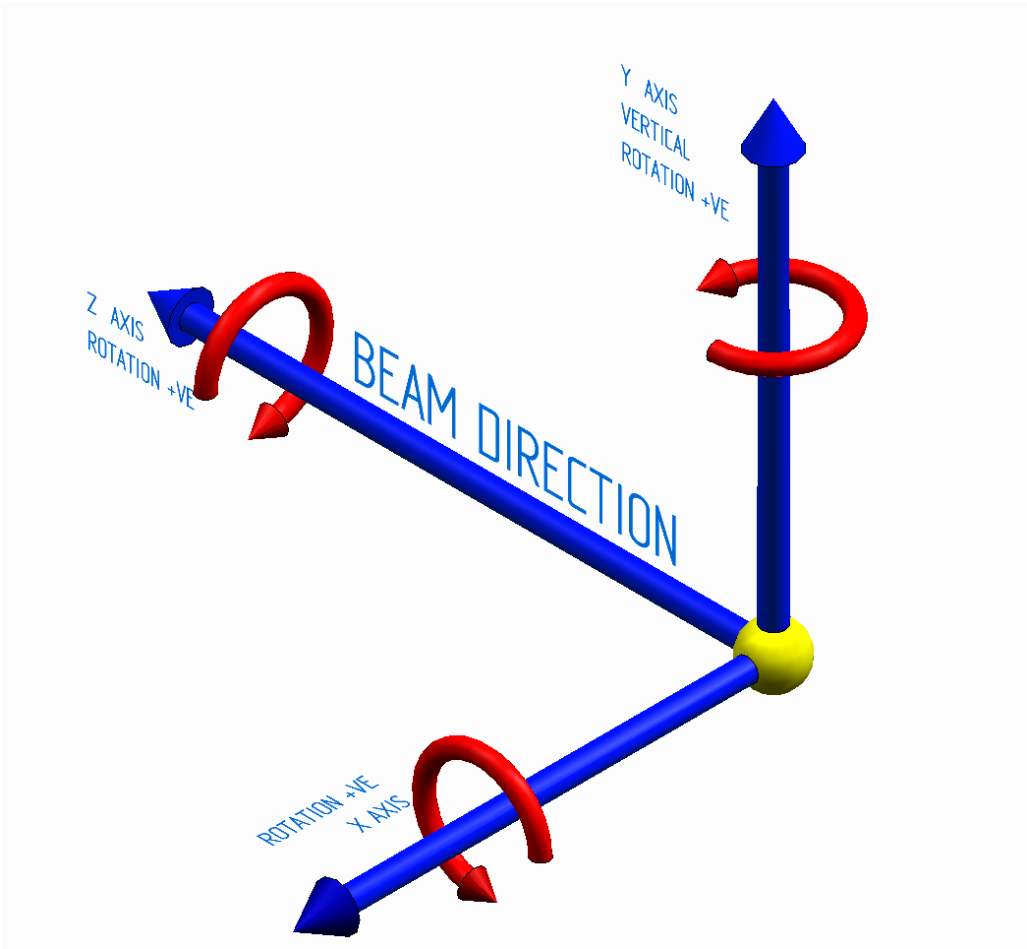

Figure 2. Beamline coordinate system

Inboard is defined as being in the negative x direction and outboard in the postive x direction.

The coordinate system employed complies with NSLS-II document:

Beamline Coordinate System Standards LT-C-XFD-STD-BL-COORD-001.

2. *SPECIFICATIONS*

2.1 MIRROR SYSTEM

Incoming Beam Height	1415 mm
Operating Position	Horizontally deflecting inboard, vertically and horizontally refocusing.
Manual Adjustments	± 10 mm in x and z (from grouted-in baseplate)
Optic location relative to centre of straight section (mm)	573.7, 15, 51628.8 (x, y, z)

2.1.1 M4A Mirror Optic

Substrate material	Fused Silica
Substrate dimensions	150 mm L x 25 mm W x 40 mm D
Active Area (centred on substrate to within ± 0.5mm)	110 mm x 10 mm
Substrate Shape	Ellipsoidal. Major axis 5903.8 ± 1% Minor axis 158.1 ± 1%. Mirror pole X_0 (off axis): 2837.9 mm ± 1%.
Grazing incidence angle	1.75°
Distance to source	3066.9 mm
Distance to image	8740.7 mm
Tangential slope error	<1.0 µrad RMS over active length
Sagittal slope error	<10 µrad RMS over active length on prepared substrate
Coating	Au 300 Å ± 10% thick 10 mm wide . No binder layers are permitted
Surface Roughness	<3 Å RMS

Surface Quality	0.5 scratches or points per cm^2 over 99% of active optical area
Cooling	Uncooled

2.2 MOTIONS

Motion	Parameter	Specification
Pitch (Ry)	Drive	Linear actuators, fitted with limit switches & encoder.
	Range	Nominal position ± 10 mrad
	Resolution	< 1µrad
	Repeatability	< 5 µrad
Roll (Rz)	Drive	Linear actuators, fitted with limit switches & encoder.
	Range	± 10 mrad
	Resolution	< 5 µrad
	Repeatability	< 10 µrad
Yaw (Rx)	Drive	Linear actuators, fitted with limit switches & encoder.
	Range	± 10 mrad
	Resolution	< 5 µrad
	Repeatability	< 10 µrad
Vertical (Ty)	Drive	Linear actuators, fitted with limit switches & encoder.
	Range	± 20 mm
	Resolution	< 1 µm
	Repeatability	< 5 µm

Lateral (Tx)	Drive	Linear actuators, fitted with limit switches & encoder.
	Range	± 10 mm
	Resolution	< 1 µm
	Repeatability	< 5 µm
Longitudinal (Tz)	Drive	Linear actuators, fitted with limit switches & encoder.
	Range	± 5 mm
	Resolution	< 2 µm
	Repeatability	< 10 µm

2.3 VACUUM SYSTEM

Maximum bakeout temperature – vessel and internal components	150-200 °C
Vacuum	UHV compatible (< 5 x10^{-10} mbar). Masses > 38 AMU shall have total pressure < 10^{-11} Torr (1.33 x 10^{-11} mbar)
Helium leak rate	< 1 x 10 $^{-10}$ mbar l/sec
Vacuum Pump	Gamma vacuum 300T ion pump located beneath the vessel
Vacuum gauges	One pirani gauge (MKS type 317)and one cold cathode gauge(MKS type 422) located on the mirror vessel
Right Angle Valve	VAT Valve type 54, DN40/CF70.

2.4 VACUUM VESSEL

The vacuum vessel for the M4A mirror system is cylindrical. The optic is mounted to the vessel, whose position is manipulated with the hexapod.

Purpose	Location	Size	Qty
Beam In	Beam inlet port at end 1	DN63/CF114	1

Beam Out	Beam outlet port at end 2	DN63/CF114	1
Ion Pump	Mounted on the base granite of the hexapod.	DN150/CF200	1
Roughing Port for RA valve	Outboard side of vessel	DN40/CF70	1
Viewport	Outboard side of vessel	DN63/CF114	1
Viewport	Incoming wall of vessel angled to look at substrate surface	DN40/CF70	1
Vacuum Gauges	Side of vessel	DN40/CF70	2
Spare	Top of vessel	DN63/CF114	1
Spare	Top of vessel	DN40/CF70	1
Mirror Loading	Baseplate	DN400/CF470	1
Drain current feedthrough (2 x BNC)	Baseplate	DN40/CF70	1

2.5 MIRROR CURRENT TAKEOFFS

The M4A mirror is fitted with drain current takeoffs to monitor the beam intensity. Two physical takeoffs are fitted to the optic stripe to allow the continuity of the electrical connection to be checked. The drain current will be measured using an I400.

2.6 ELECTRICAL DATA

2.6.1 Linear Actuators (Hexapod legs)

Motor Type	McLennan Type 23HS309 stepper motor
Holding torque	87 Ncm
Step angle (full step drive)	1.8°/ or 200 steps/rev
Driving current	2 A
Gear box ratio	25:1
Thread pitch	2 mm
Resolution per step	0.4 µm
Maximum movement per actuator	± 50 mm
Connector (Motor and limits)	12 way trim trio (UTO)

2.6.2 Encoder Data

Readhead type	Renishaw Tonic T1000-05A
Readhead (interpolator) resolution	0.1 µm
Scale type	RGSZ20
Connector	15-Way sub D

2.7 LIFTING POINTS

M4A mirror system weight: 500 kg approximately.

The mirror system is provided with three M16 lifting points in the base of the hexapod, in addition to three in the upper platform.

A lifting diagram for the system will be provided.

2.8 ALIGNMENT FEATURES

Fiducial mounts will be provided on the baseplate and on the upper platform of the hexapod. These will take the form of 0.25” reamed (H7) holes, suitable for 0.5” or 1.5” spheres.

3. FACTORY TESTING

Testing at FMB Oxford consists of Motion Testing, Vacuum Testing and Fiducialisation.

Full specifications and procedures covering all factory testing will be prepared in advance and these will be submitted to the customer prior to final design approval. Representatives from the customer are invited to witness these tests at FMB Oxford's works.

4. INSTALLATION AND UNIT ACCEPTANCE

The site acceptance testing, included in the installation option, will ensure that all components are carefully surveyed into position, all motors, actuators and sensors are functioning properly and the vacuum specifications are met. All motions will be tested and the correct functioning of all limit and datum switches checked. The complete set of detailed factory tests are not repeated on site.

There will be a full leak check of the installed vacuum sections. We expect that a turbo pump station, RGA rig, and He leak checker to be provided by the customer for our use while at the customer's site.

Final site acceptance will include:

- All factory test data, documentation and manuals
- Correct operation of all motions, limits and datum switches using FMB-O controls and cabling.
- Leak testing at the best achievable sensitivity after 24 hrs of pumping and prior to on site customer bakeout

5. *SCOPE OF SUPPLY*

- M4A optic and mirror system
- I400 Current amplifier (optic drain current measurement)
- MOXA
- 300 l/s ion pump & pump controller (Gamma)
- Right angle valve (Vat valve)
- Cold cathode (series 422) and pirani (series 317) gauges and gauge controller (MKS 937B)
- Motion controls as specified in the motion controls functional specification.
- Field cables

S3160 NIST SST – MIRROR SYSTEM M4C/M4D

Reference Documents:

Reference Number	Date/ Issue	Title
SB1341-14-CN-0042	19/09/14	NIST Contract
	April 2014	NIST NSLS-II SST and BMM Beamline Backbones, Volume 2A, SST Technical Proposal
S3160	Nov 2014/REV 01	NIST SST BEAMLINE S3160 QUALITY PLAN

FMB Oxford
Osney Mead
Oxford OX2 0ES
UK

Contact: Andrew Fairley
Telephone: +44 (0)1865 320 313
Fax: +44 (0)1865 320 301
E-mail: andrew.fairley@fmb-oxford.com

Change log:

Revision	Date	Summary of Change	Approval
1.0	06/01/15	First Issue	NJB
2.0	10/03/15	I200 replaced by I400. M4D binder layer removed. Ports added for feedthroughs. Tangential slope errors amended.Beam in and out ports size increased to DN100. Lateral range increased.	
3.0	25/03/15	Ion pump size reduced.	
4.0			
5.0			
6.0			

TABLE OF CONTENTS **1**

1. *INTRODUCTION* **3**

1.1 AXIS 4

2. *SPECIFICATIONS* **5**

2.1 MIRROR SYSTEM 5

2.1.1 M4C Mirror Optic *5*

2.1.2 M4D Mirror Optic *6*

2.2 MOTIONS 7

2.3 VACUUM SYSTEM 8

2.4 VACUUM VESSEL 8

2.5 MIRROR CURRENT TAKEOFFS 9

2.6 DITHERING MECHANISM 9

2.7 ELECTRICAL DATA 10

2.7.1 Linear Actuators (Hexapod legs) *10*

2.7.2 Encoder Data *10*

2.7.3 Dithering Mechanism *10*

2.8 LIFTING POINTS 10

2.9 ALIGNMENT FEATURES 11

3. FACTORY TESTING **12**

4. INSTALLATION AND UNIT ACCEPTANCE **13**

5. *SCOPE OF SUPPLY* **14**

1. *INTRODUCTION*

The M4 mirror system is located downstream of mirror system M3 and the precision vertical slit 'C', on the soft x-ray 'M' branch. The purpose of the M4 mirror system is to refocus and direct the soft x rays to the next (planar) mirror M5C (using optic M4C) and then on to the NEXAFS/XPS endstation or to guide and vertically dither the beam towards the last endstation on the 'M' branch (using optic M4D) - μNEXAFS.

The mirror system is equipped with two optics, an ellipsoid to refocus horizontally and vertically (M4C) and a plane optic (M4D) to provide vertical dithering (increased spot size).

The M4 optics (M4C and M4D) are both uncooled. Both optics are mounted to the vacuum vessel, which is manipulated with a hexapod.

The optics are arranged side by side, so the hexapod platform translates horizontally to switch between the optics.

The M4D optic is fitted with a flexure based dithering mechanism to increase the vertical spot size at the μNEXAFS end station. In addition, both optics are fitted with drain current takeoffs.

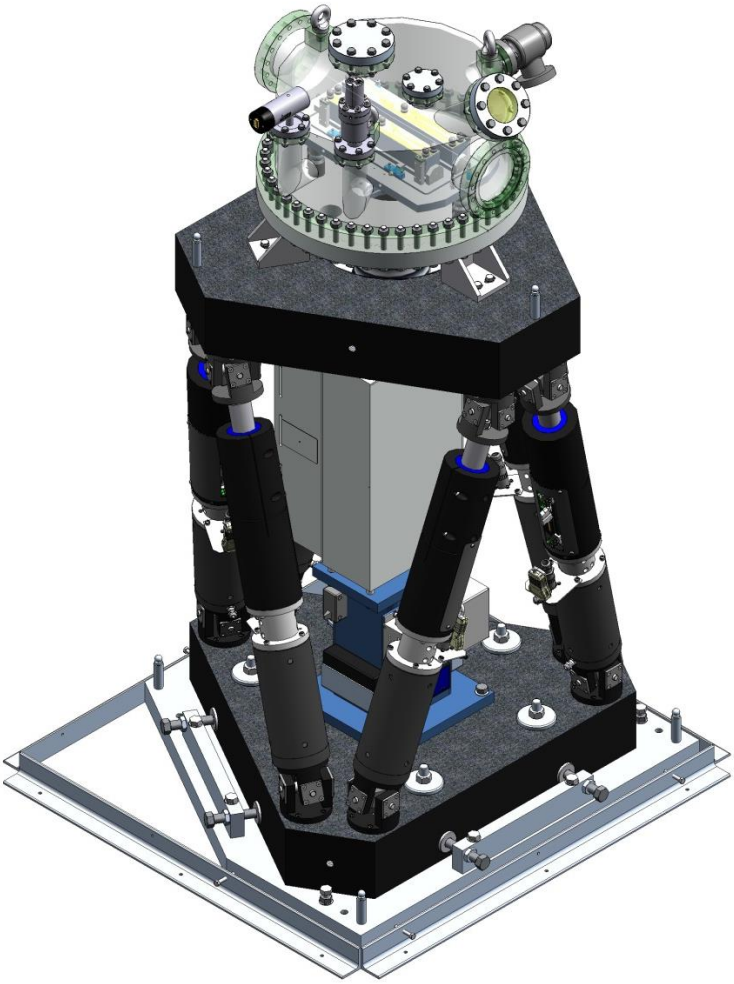

Figure 1. Mirror System M4C/D

1.1 AXIS

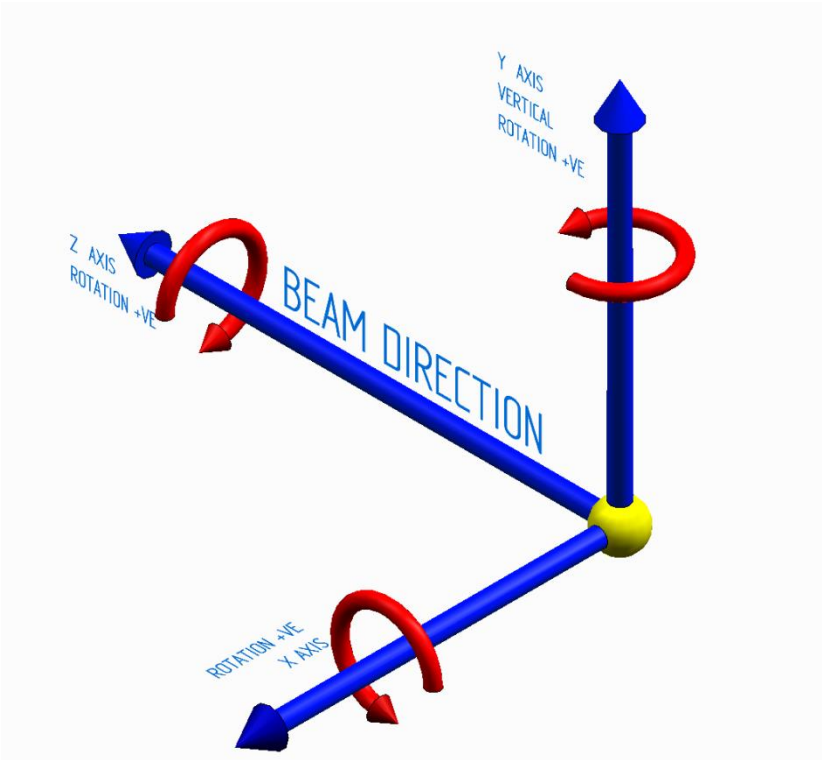

Figure 2. Beamline coordinate system

Inboard is defined as being in the negative x direction and outboard in the postive x direction.

The coordinate system employed complies with NSLS-II document:

Beamline Coordinate System Standards LT-C-XFD-STD-BL-COORD-001.

2. *SPECIFICATIONS*

2.1 MIRROR SYSTEM

Incoming Beam Height	1415 mm
Operating Position	Vertically deflecting upwards, horizontally and vertically refocusing (M4C). Vertically deflecting upwards (M4D).
Manual Adjustments	± 10 mm in x and z (from grouted-in baseplate)
Optic location relative to centre of straight section (mm).	1857.35, 15, 53500 (x, y, z)

2.1.1 M4C Mirror Optic

Substrate material	Fused Silica
Substrate dimensions	270 mm L x 35 mm W x 50 mm D
Active Area (centred on substrate to within ± 0.5mm)	230 mm x 15 mm
Substrate Shape	Ellipsoid Major axis 6835.9 mm ± 1% Minor axis 172.4 mm ± 1% Mirror pole X_0: 1836.6 mm (off axis) ± 1%. *Sagittal Radius > 3km*
Grazing incidence angle	1.5°
Distance to source	4999.9 mm
Distance to image	8672 mm
Tangential slope error	< 1.0 µrad RMS over active length
Sagittal slope error	< 10 µrad RMS over active length on prepared substrate
Coating	Au 300 Á ± 10% thick 15 mm wide No binder layers permitted

Surface Roughness	<3 Å RMS
Surface Quality	0.5 scratches or points per cm^2 over 99% of active optical area
Cooling	Uncooled

2.1.2 M4D Mirror Optic

Substrate material	Titania silicate low expansion glass
Substrate dimensions	250 mm L x 35 mm W x 50 mm D
Active Area (centred on substrate to within ± 0.5mm)	230 mm x 20 mm
Substrate Shape	Plane Tangential radius > 20 km Sagittal radius > 3km
Grazing incidence angle	1.5°
Distance to source	∞ m
Distance to image	∞ m
Tangential slope error	<0.25 µrad RMS over active length
Sagittal slope error	< 5 µrad RMS over active length
Coating	Au 300 Å ± 10% thick 15 mm wide over Pt 300 Å ± 10% binder layer
Surface Roughness	<3 Å RMS
Surface Quality	0.5 scratches or points per cm^2 over 99% of active optical area
Cooling	Uncooled

2.2 MOTIONS

Motion	Parameter	Specification
Pitch (Ry)	Drive	Linear actuators, fitted with limit switches & encoder.
	Range	Nominal position ± 10 mrad
	Resolution	< 1µrad
	Repeatability	< 5 µrad
Roll (Rz)	Drive	Linear actuators, fitted with limit switches & encoder.
	Range	± 10 mrad
	Resolution	< 5 µrad
	Repeatability	< 10 µrad
Yaw (Rx)	Drive	Linear actuators, fitted with limit switches & encoder.
	Range	± 10 mrad
	Resolution	< 5 µrad
	Repeatability	< 10 µrad
Vertical (Ty)	Drive	Linear actuators, fitted with limit switches & encoder.
	Range	± 10 mm
	Resolution	< 1 µm
	Repeatability	< 5 µm

Lateral (Tx)	Drive	Linear actuators, fitted with limit switches & encoder.
	Range	± 40 mm
	Resolution	< 1 µm
	Repeatability	< 5 µm
Longitudinal (Tz)	Drive	Linear actuators, fitted with limit switches & encoder.
	Range	± 5 mm
	Resolution	< 2 µm
	Repeatability	< 10 µm

2.3 VACUUM SYSTEM

Maximum bakeout temperature – vessel and internal components	150-200 °C
Vacuum	UHV compatible (< 5 x10^{-10} mbar). Masses > 38 AMU shall have total pressure < 10^{-11} Torr (1.33 x 10^{-11} mbar)
Helium leak rate	< 1 x 10 $^{-10}$ mbar l/sec
Vacuum Pump	Gamma vacuum 300T ion pump located beneath the vessel
Vacuum gauges	One pirani gauge (MKS type 317)and one cold cathode gauge(MKS type 422) located on the mirror vessel
Right Angle Valve	VAT Valve type 54, DN40/CF70.

2.4 VACUUM VESSEL

The vacuum vessel for the M4 mirror system is cylindrical.

Purpose	Location	Size	Qty
Beam In	Beam inlet port at end 1	DN100/CF150	1

Beam Out	Beam outlet port at end 2	DN100/CF150	1
Ion Pump	Mounted on the base granite of the hexapod.	DN100/CF150	1
Roughing Port for RA valve	Outboard side of vessel	DN40/CF70	1
Viewport	Incoming wall of vessel angled to look at substrate surface	DN63/CF114	1
Vacuum Gauges	Side of vessel	DN40/CF70	2
Spare	Top of vessel	DN63/CF114	1
Spare	Top of vessel	DN40/CF70	1
Mirror Loading	Baseplate	DN400/CF470	1
Double BNC feedthrough for optic drain currents	Baseplate	DN40/CF70	2
Feedthrough for dithering DPT (9 way d-type)	Baseplate	DN40/CF70	1

2.5 MIRROR CURRENT TAKEOFFS

The M4 optics are both fitted with drain current takeoffs to monitor the beam intensity. Two physical takeoffs are fitted to each optic stripe to allow the continuity of the electrical connection to be checked. The drain currents will be measured using an I400.

2.6 DITHERING MECHANISM

The M4D mirror system is fitted with a piezo-driven flexure mechanism to dither the beam (increase the vertical spot size) at the µNEXAFS end station. The mirror needs to be dithered by approximately ±0.43 mrad to obtain a 20 mm vertical stripe at the end station.

2.7 ELECTRICAL DATA

2.7.1 Linear Actuators (Hexapod legs)

Motor Type	McLennan Type 23HS309 stepper motor
Holding torque	87 Ncm
Step angle (full step drive)	1.8°/ or 200 steps/rev
Driving current	2 A
Gear box ratio	25:1
Thread pitch	2 mm
Resolution per step	0.4 µm
Maximum movement per actuator	± 50 mm
Connector (Motor and limits)	12 way trim trio (UTO)

2.7.2 Encoder Data

Readhead type	Renishaw Tonic T1000-05A
Readhead (interpolator) resolution	0.1 µm
Scale type	RGSZ20
Connector	15-Way sub D

2.7.3 Dithering Mechanism

Actuator type	Preloaded piezo stack driven flexure.
Range	±0.5 mrad

2.8 LIFTING POINTS

M4 mirror system weight: 500 kg approximately.

The mirror system is provided with three M16 lifting points in the base of the hexapod, in addition to three in the upper platform.

A lifting diagram for the system will be provided.

2.9 ALIGNMENT FEATURES

Fiducial mounts will be provided on the baseplate and on the upper platform of the hexapod. These will take the form of 0.25” reamed (H7) holes, suitable for 0.5” or 1.5” spheres.

3. FACTORY TESTING

Testing at FMB Oxford consists of Motion Testing, Vacuum Testing and Fiducialisation.

Full specifications and procedures covering all factory testing will be prepared in advance and these will be submitted to the customer prior to final design approval. Representatives from the customer are invited to witness these tests at FMB Oxford's works.

4. INSTALLATION AND UNIT ACCEPTANCE

The site acceptance testing, included in the installation option, will ensure that all components are carefully surveyed into position, all motors, actuators and sensors are functioning properly and the vacuum specifications are met. All motions will be tested and the correct functioning of all limit and datum switches checked. The complete set of detailed factory tests are not repeated on site.

There will be a full leak check of the installed vacuum sections. We expect that a turbo pump station, RGA rig, and He leak checker to be provided by the customer for our use while at the customer's site.

Final site acceptance will include:

- All factory test data, documentation and manuals
- Correct operation of all motions, limits and datum switches using FMB-O controls and cabling.
- Leak testing at the best achievable sensitivity after 24 hrs of pumping and prior to on site customer bakeout

5. *SCOPE OF SUPPLY*

- M4C and M4D optics and mirror system
- I400 Current amplifier (optic drain current measurement)
- DPT dithering and controls for M4D.
- 200 l/s ion pump & pump controller (Gamma)
- Right angle valve (Vat valve)
- Cold cathode (series 422) and pirani (series 317) gauges and gauge controller (MKS 937B)
- Motion controls as specified in the motion controls functional specification.
- Field cables

S3160 NIST SST – MIRROR SYSTEM M5C

Reference Documents:

Reference Number	Date/ Issue	Title
SB1341-14-CN-0042	19/09/14	NIST Contract
	April 2014	NIST NSLS-II SST and BMM Beamline Backbones, Volume 2A, SST Technical Proposal
S3160	Nov 2014/REV 01	NIST SST BEAMLINE S3160 QUALITY PLAN

FMB Oxford
Osney Mead
Oxford OX2 0ES
UK

Contact: Andrew Fairley
Telephone: +44 (0)1865 320 313
Fax: +44 (0)1865 320 301
E-mail: andrew.fairley@fmb-oxford.com

Change log:

Revision	Date	Summary of Change	Approval
1.0	06/01/15	First Issue	NJB
2.0	27/02/15	Ports added for dithering feedthrough and drain currents. Platinum binder layer added.	
3.0			
4.0			
5.0			
6.0			

TABLE OF CONTENTS **1**

1. *INTRODUCTION* **3**

1.1 AXIS 4

2. *SPECIFICATIONS* **5**

2.1 MIRROR SYSTEM 5

2.1.1 M5C Mirror Optic *5*

2.2 MOTIONS 6

2.3 VACUUM SYSTEM 7

2.4 VACUUM VESSEL 7

2.5 MIRROR CURRENT TAKEOFFS 8

2.6 DITHERING MECHANISM 8

2.7 ELECTRICAL DATA 9

2.7.1 Linear Actuators (Hexapod legs) *9*

2.7.2 Encoder Data *9*

2.7.3 Dithering Mechanism *9*

2.8 LIFTING POINTS 9

2.9 ALIGNMENT FEATURES 10

3. FACTORY TESTING **11**

4. INSTALLATION AND UNIT ACCEPTANCE **12**

5. *SCOPE OF SUPPLY* **13**

1. *INTRODUCTION*

The M5C mirror system is located directly upstream of the NEXAFS/XPS endstation, on the soft x-ray 'M' branch. The purpose the M5C mirror system is to guide the soft x rays to the NEXAFS/XPS end station. The M5C optic is planar and uncooled. The optic is mounted to the base of the vacuum vessel and is manipulated using a hexapod, which gives six degrees of freedom. The optic is fitted with drain current take offs and a flexure based dithering mechanism to increase the vertical spot size at the end station.

The M5C optic may also be moved out of beam to allow the soft x rays from mirror M4D to reach the μNEXAFS end station, located further downstream.

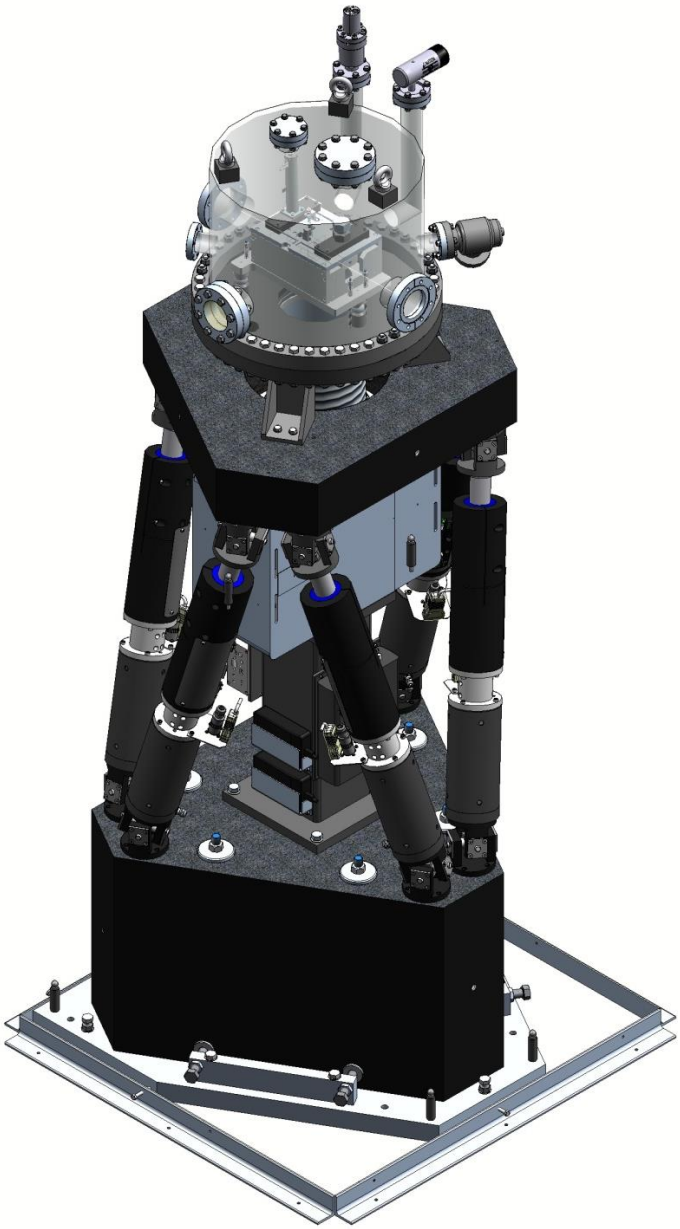

Figure 1. Mirror System M5C

1.1 AXIS

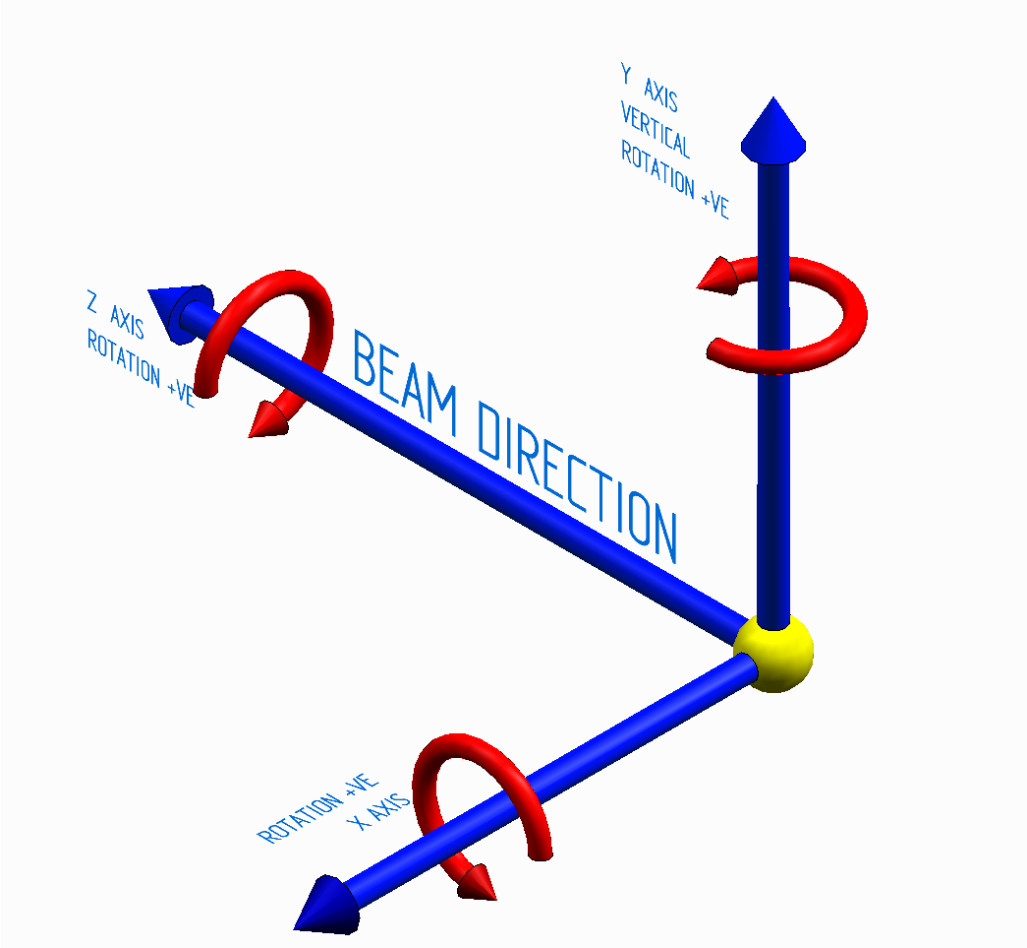

Figure 2. Beamline coordinate system

Inboard is defined as being in the negative x direction and outboard in the postive x direction.

The coordinate system employed complies with NSLS-II document:

Beamline Coordinate System Standards LT-C-XFD-STD-BL-COORD-001.

2. *SPECIFICATIONS*

2.1 MIRROR SYSTEM

Incoming Beam Height	1764 mm (at optic)
Operating Position	Vertically deflecting downwards
Manual Adjustments	± 10 mm in x and z (from grouted-in baseplate)
Optic location relative to centre of straight section (mm).	2546.7, 364, 60122 (x, y, z)

2.1.1 M5C Mirror Optic

Substrate material	Single crystal silicon
Substrate dimensions	120 mm L x 35 mm W x 30 mm D
Active Area (centred on substrate to within ± 0.5mm)	100 mm x 15 mm
Substrate Shape	Plane. Tangential radius > 20 km Sagittal radius > 3km
Grazing incidence angle	1.0°
Distance to source	∞ m
Distance to image	∞ m
Tangential slope error	<0.25 µrad RMS over active length
Sagittal slope error	<5 µrad RMS over active length on prepared substrate
Coating	Au 300 Å ± 10% thick 15 mm wide over Pt 100 Å ± 10% thick binder layer
Surface Roughness	<3 Å RMS
Surface Quality	0.5 scratches or points per cm^2 over 99% of active optical area

Cooling	Uncooled

2.2 MOTIONS

Motion	Parameter	Specification
Pitch (Ry)	Drive	Linear actuators, fitted with limit switches & encoder.
	Range	Nominal position ± 10 mrad
	Resolution	< 1µrad
	Repeatability	< 5 µrad
Roll (Rz)	Drive	Linear actuators, fitted with limit switches & encoder.
	Range	± 10 mrad
	Resolution	< 5 µrad
	Repeatability	< 10 µrad
Yaw (Rx)	Drive	Linear actuators, fitted with limit switches & encoder.
	Range	± 10 mrad
	Resolution	< 5 µrad
	Repeatability	< 10 µrad
Vertical (Ty)	Drive	Linear actuators, fitted with limit switches & encoder.
	Range	± 10 mm
	Resolution	< 1 µm
	Repeatability	< 5 µm

Lateral (Tx)	Drive	Linear actuators, fitted with limit switches & encoder.
	Range	± 20 mm
	Resolution	< 1 µm
	Repeatability	< 5 µm
Longitudinal (Tz)	Drive	Linear actuators, fitted with limit switches & encoder.
	Range	± 5 mm
	Resolution	< 2 µm
	Repeatability	< 10 µm

2.3 VACUUM SYSTEM

Maximum bakeout temperature – vessel and internal components	150-200 °C
Vacuum	UHV compatible (< 5 x10^{-10} mbar). Masses > 38 AMU shall have total pressure < 10^{-11} Torr (1.33 x 10^{-11} mbar)
Helium leak rate	< 1 x 10 $^{-10}$ mbar l/sec
Vacuum Pump	Gamma vacuum 300T ion pump located beneath the vessel
Vacuum gauges	One pirani gauge (MKS type 317)and one cold cathode gauge(MKS type 422) located on the mirror vessel
Right Angle Valve	VAT Valve type 54, DN40/CF70.

2.4 VACUUM VESSEL

The vacuum vessel for the M5C mirror system is cylindrical. The optic is mounted to the vessel, whose position is manipulated with the hexapod.

Purpose	Location	Size	Qty
Beam In	Beam inlet port at end 1	DN63/CF114	1

Beam Out	Beam outlet port at end 2	DN63/CF114	1
Ion Pump	Mounted on the base granite of the hexapod.	DN150/CF200	1
Roughing Port for RA valve	Outboard side of vessel	DN40/CF70	1
Viewport	Outboard side of vessel	DN63/CF114	1
Viewport	Incoming wall of vessel angled to look at substrate surface	DN40/CF70	1
Vacuum Gauges	Side of vessel	DN40/CF70	2
Spare	Top of vessel	DN63/CF114	1
Spare	Top of vessel	DN40/CF70	1
Mirror Loading	Baseplate	DN400/CF470	1
Feedthrough for dithering DPT (9 way d-type)	Baseplate	DN40/CF70	1
Feedthrough for optics drain currents	Baseplate	DN40/CF70	1

2.5 MIRROR CURRENT TAKEOFFS

The M5C mirror is fitted with drain current takeoffs to monitor the beam intensity. Two physical takeoffs are fitted to the optic stripe to allow the continuity of the electrical connection to be checked. The drain current will be measured using an I400.

2.6 DITHERING MECHANISM

The M5C mirror system is fitted with a piezo-driven flexure mechanism to dither the beam (increase the vertical spot size) at end station NEXAFS/XPS. The mirror needs to be dithered by approximately ±0.62 mrad to obtain a 5mm vertical stripe at the end station.

2.7 ELECTRICAL DATA

2.7.1 Linear Actuators (Hexapod legs)

Motor Type	McLennan Type 23HS309 stepper motor
Holding torque	87 Ncm
Step angle (full step drive)	1.8°/ or 200 steps/rev
Driving current	2 A
Gear box ratio	25:1
Thread pitch	2 mm
Resolution per step	0.4 µm
Maximum movement per actuator	± 50 mm
Connector (Motor and limits)	12 way trim trio (UTO)

2.7.2 Encoder Data

Readhead type	Renishaw Tonic T1000-05A
Readhead (interpolator) resolution	0.1 µm
Scale type	RGSZ20
Connector	15-Way sub D

2.7.3 Dithering Mechanism

Actuator type	Preloaded piezo stack driven flexure.
Range	±0.75 mrad

2.8 LIFTING POINTS

M5C mirror system weight: 500 kg approximately.

The mirror system is provided with three M16 lifting points in the base of the hexapod, in addition to three in the upper platform.

A lifting diagram for the system will be provided.

2.9 ALIGNMENT FEATURES

Fiducial mounts will be provided on the baseplate and on the upper platform of the hexapod. These will take the form of 0.25” reamed (H7) holes, suitable for 0.5” or 1.5” spheres.

3. FACTORY TESTING

Testing at FMB Oxford consists of Motion Testing, Vacuum Testing and Fiducialisation.

Full specifications and procedures covering all factory testing will be prepared in advance and these will be submitted to the customer prior to final design approval. Representatives from the customer are invited to witness these tests at FMB Oxford's works.

4. INSTALLATION AND UNIT ACCEPTANCE

The site acceptance testing, included in the installation option, will ensure that all components are carefully surveyed into position, all motors, actuators and sensors are functioning properly and the vacuum specifications are met. All motions will be tested and the correct functioning of all limit and datum switches checked. The complete set of detailed factory tests are not repeated on site.

There will be a full leak check of the installed vacuum sections. We expect that a turbo pump station, RGA rig, and He leak checker to be provided by the customer for our use while at the customer's site.

Final site acceptance will include:

- All factory test data, documentation and manuals
- Correct operation of all motions, limits and datum switches using FMB-O controls and cabling.
- Leak testing at the best achievable sensitivity after 24 hrs of pumping and prior to on site customer bakeout

5. *SCOPE OF SUPPLY*

- M5C optic and mirror system
- DPT dithering and controls
- I400 Current amplifier (optic drain current measurement)
- 300 l/s ion pump & pump controller (Gamma)
- Right angle valve (Vat valve)
- Cold cathode (series 422) and pirani (series 317) gauges and gauge controller (MKS 937B)
- Motion controls and specified in the motion controls functional specification.
- Field cables

Appendix D

FMB FDR documents and review reports

September 1, 2015

NIST SST Beamline Final Design Review Meeting

Room 156, Building 745, NSLS II, Brookhaven National Laboratory

Welcome by Dan Fischer from NIST in the absence of Andrew Broadbent. Attendance List generated

09:00 Beamline Overview

a) NIST will install 2 fast valves in the beamline a couple of metres upstream of the most upstream endstation to protect the beamline optics from an unforeseen vacuum failure
b) Secondary BS raytracing must be validated by calculation – currently planned for 2016 Q1
c) 14 bar at 30 minutes FAT is acceptable for internally-cooled mirrors, L1 and M1
d) For HP NEXAFS, VS7 will be removed at the time of installation and GV8 won't be installed and a simple spool piece will installed temporarily
e) [Scott Mowat: is there a pump, gauges on VS17?]
f) Design of VS27 still in progress – pump and RA valve are supplied, but no gauging
g) The supply of GV32 and GV33 is currently not in scope of supply
h) Correct endstation label: "NEXAFS/XPS ~~μNEXAFS~~"
i) Add cooled mask upstream of DCM in Tender Branch
j) Add label to Tender Branch Pink Beam Stop
k) Cryocooler moves ~1m downstream and flip over the support column for the cryolines
l) VS15 needs to be corrected, remove extraneous FS and add bellows

10:15 Project Plan

m) Chris Stebbins joined the meeting for this item
n) NIST will install 2 fast valves in the beamline a couple of metres upstream of the most upstream endstation to protect the beamline optics from an unforeseen vacuum failure
o) Goal to get BMM M1 installed during the early part of the September 2016 shutdown, otherwise it will have to wait until December shutdown

10:30 Mirror Optics

p) Reiterated agreed changes required on DCM – cooling lines, Si[311] crystal

12:00 Lunch

Andrew Broadbent joins meeting after lunch

13:00 High Heatload Components

q) What is the heatload of the new sources – 13.8kW/mrad^2 and 6.7kW/mrad^2 in 0.5 x 0.3 mrad aperture cf 4.1kW and 4.8kW => all checked OK
r) L1 mask, check power density of 13,800W/mrad^2 against 36 W/mm^2=> all OK

13:30 Diagnostics

s) This point skipped due to lack of time

14:20 Vacuum System

t) General comments, vacuum travellers to be filled during installation by NIST personnel, careful FIP binder, second position indicators to be added by BNL people after install
u) Alternatives to VAT Series 54 RA valves which can leak following bakeout
v) Action to define length of pump and gauge cables to determine how to buy the cable through NSLS II or backfill the NSLS II cable stock…
w) Fit burst discs to L1, M1 and L2 mirror systems in the FOE, M3, PGM and DCM on the experimental hall floor. Sizing calculation has been submitted and clarification on ASME-rated unit to be completed – complete with tags attached to items
x) Label front of controllers:- IPC:1, VGC:1, etc

14:35 Control Interfaces

y) Check on lateral positioning output signals from the DCM
z) Andrew to arrange session with Johnny Kirkland for hexapod interface
aa) Johnny to review the Functional Specification and discuss further with Doug Smith

15:00 EPS

bb) Define cryocooler digital interfaces (2 outputs, 1 input…)

15:15 Utilities

cc) Add nominal and minimal flow to each circuit on the controls FS

15:30 FAT and installation

dd) Standard tests for hexapods, screens, slits, cryocooler
ee) Optics to be accepted based upon vendor reports
ff) Acceptance on radiation elements via inspection
gg) Rigging is as per top level drawings and generally acceptable
hh) Survey is as previously agreed and is currently in progress
ii) Can consider an intermediate installation to minimize effort of final installation

16:00 Radiation Safety

jj) Need lead viewports on all elements outside the FOE
kk) Ray tracing must be imported into BNL drawing format, approved by BNL Radiation Specialist and uploaded into the vault
ll) On synchrotron raytrace examine the M branch and look at the most outboard source going through BTD1, BTD2, BTD3 and fixed mask, verify they are valid rays, and then ensure that the White Beam Stop does indeed block them.
mm) On synchrotron raytrace examine the L branch and look at the most inboard source going through BTD1, BTD2, BTD3 and fixed mask, verify they are valid rays, and then ensure that the White Beam Stop does indeed block them.

16:30 Action Item List

Reference	Action	Actionee
SST-1	Produce spool piece to replace HP NEXAFS endstation (not yet completed)	AF
SST-2	Correct model to include latest changes, and update labelling	AF
SST-3	Add labels to vacuum controllers	AF
SST-4	Advise alternative RA valves	AJB
SST-5	Confirm cryocooler EPS interfaces	AF
SST-6	Update raytracing to remove effect of FE fixed mask and reissue drawings	AF
SST-7	Provide approval for build of components, including radiation components	DF
SST-8	Update water circuit table for nominal and trip	AF

	limits	
SST-9	Define actual burst discs to be used	AF
SST-10	Deliver pressure test procedure at 14 bar for NSLS II waiver of delivered components	AF
SST-11	Test all further elements at 150psi x 1.5 = 225psi for 10 minutes	AF

Post Meeting Note:-

Add provision for gold evaporation on all soft x-ray gold mesh diagnostics.

What is the aperture required for the diagnostics in the dithered regions on the M branch beamline…

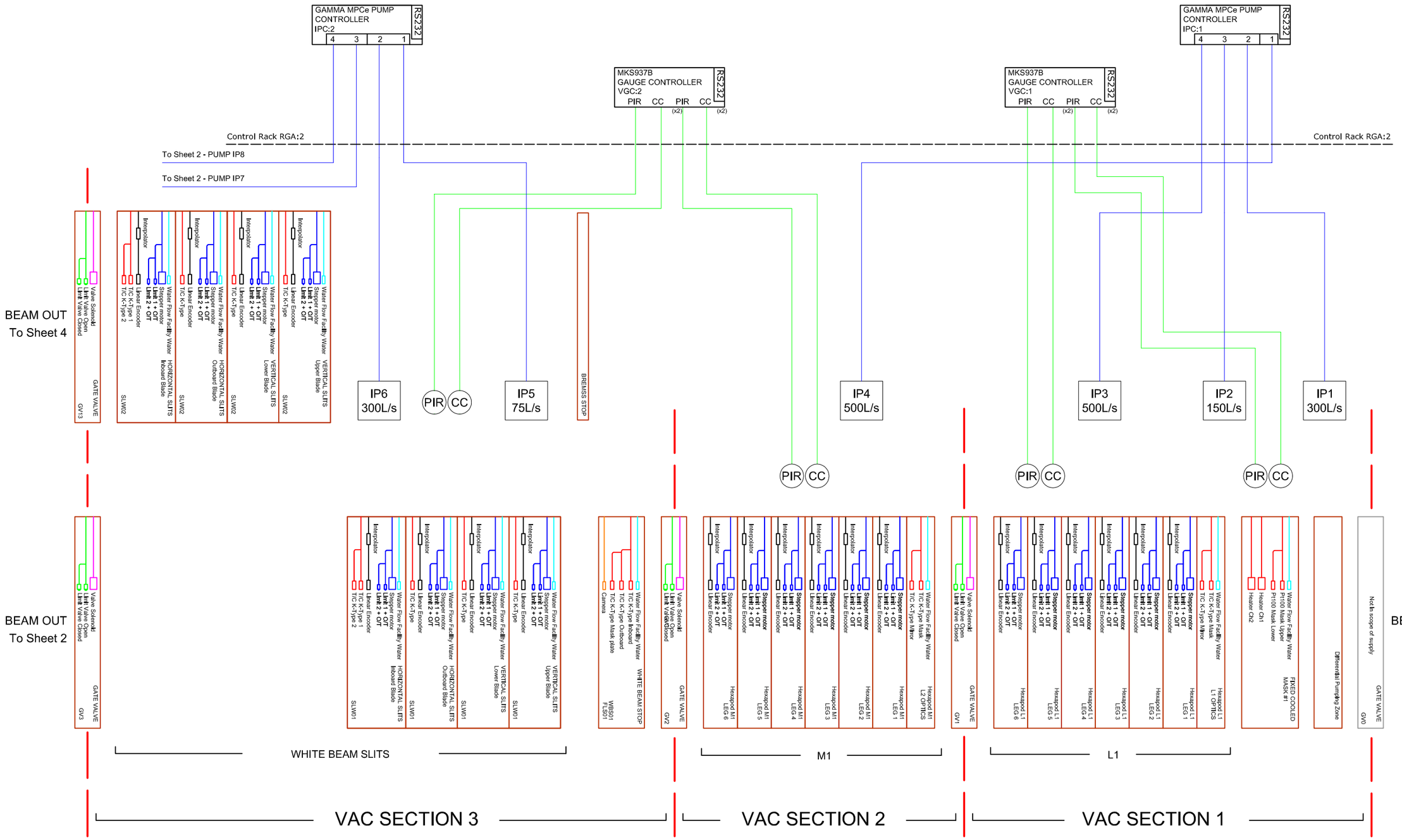

REV	DATE	DESCRIPTION/DMR No	DRN	CHKD
F	21/01/2015	PDR ISSUE	MKS	
G	07/07/2015	PRE FDR ISSUE	DJS	
H	13/08/2015	FDR ISSUE	DJS	

THIS DRAWING BELONGS TO FMB OXFORD LTD AND IS ISSUED ON CONDITION THAT IT IS NOT COPIED, REPRINTED OR DISCLOSED TO A THIRD PARTY WITHOUT PRIOR CONSENT IN WRITING FROM FMB OXFORD Ltd.

DRAWN D. Smith DATE 21/01/2015

CHECKED DATE

APPROVED DATE

FMB OXFORD LTD
UNIT 1 FERRY MILLS,
OSNEY MEAD, OXFORD, OX2 0ES.
ENGLAND

FMB Oxford

Title S3160 NIST SST BEAMLINE PID

Size A3 | Document Number CRP0469 | Rev H

Sheet 1 of 24

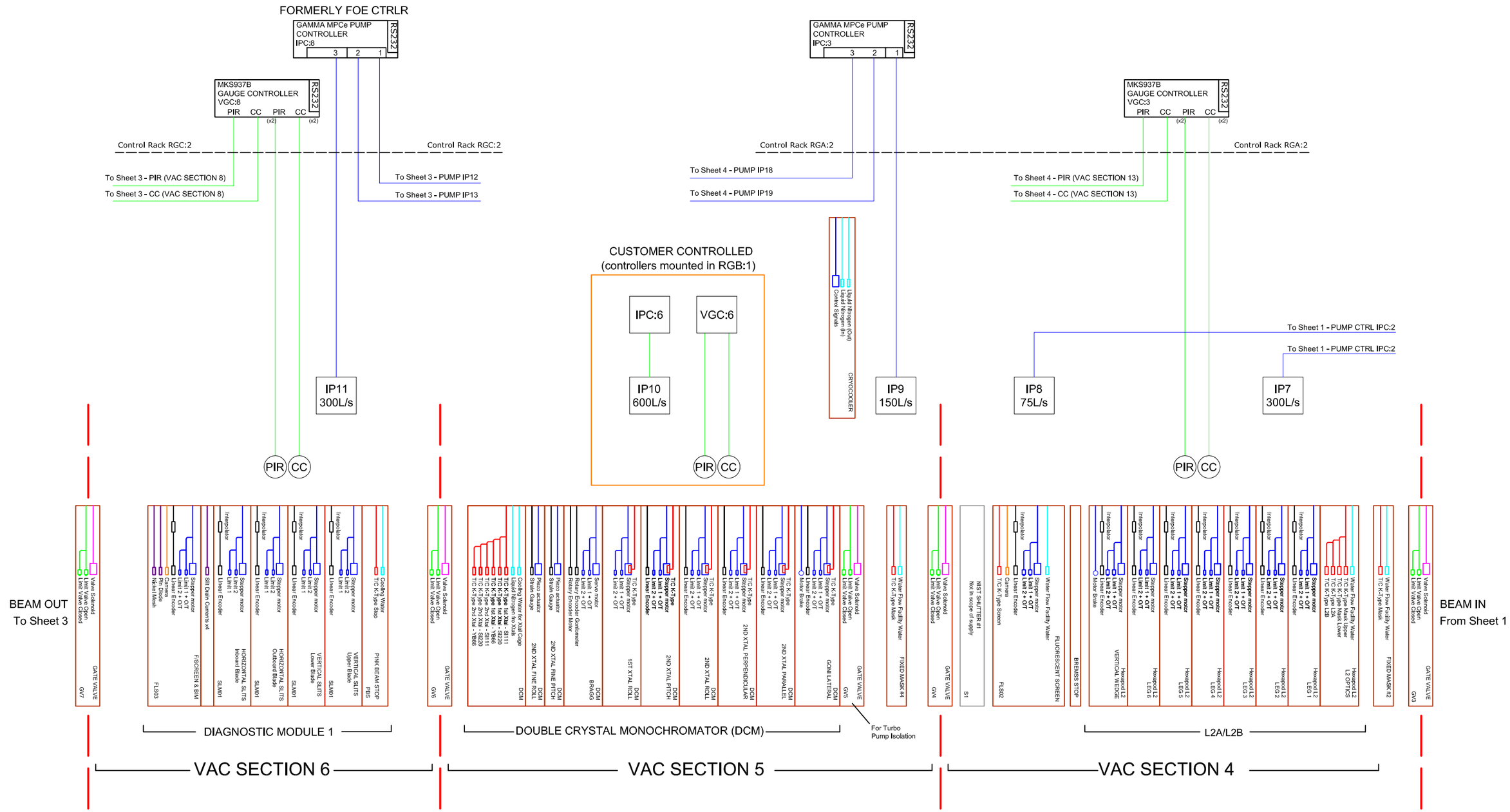

REV	DATE	DESCRIPTION/DMR No	DRN	CHKD
F	21/01/2015	PDR ISSUE	MKS	
G	07/07/2015	PRE FDR ISSUE	DJS	
H	13/08/2015	FDR ISSUE	DJS	

THIS DRAWING BELONGS TO FMB OXFORD LTD AND IS ISSUED ON CONDITION THAT IT IS NOT COPIED, REPRINTED OR DISCLOSED TO A THIRD PARTY WITHOUT PRIOR CONSENT IN WRITING FROM FMB OXFORD Ltd.

DRAWN D. Smith DATE 21/01/2015

CHECKED DATE

APPROVED DATE

FMB OXFORD LTD
UNIT 1 FERRY MILLS,
OSNEY MEAD, OXFORD, OX2 0ES.
ENGLAND

FMB Oxford

Title S3160 NIST SST BEAMLINE PID

Size A3 | Document Number CRP0469 | Rev H

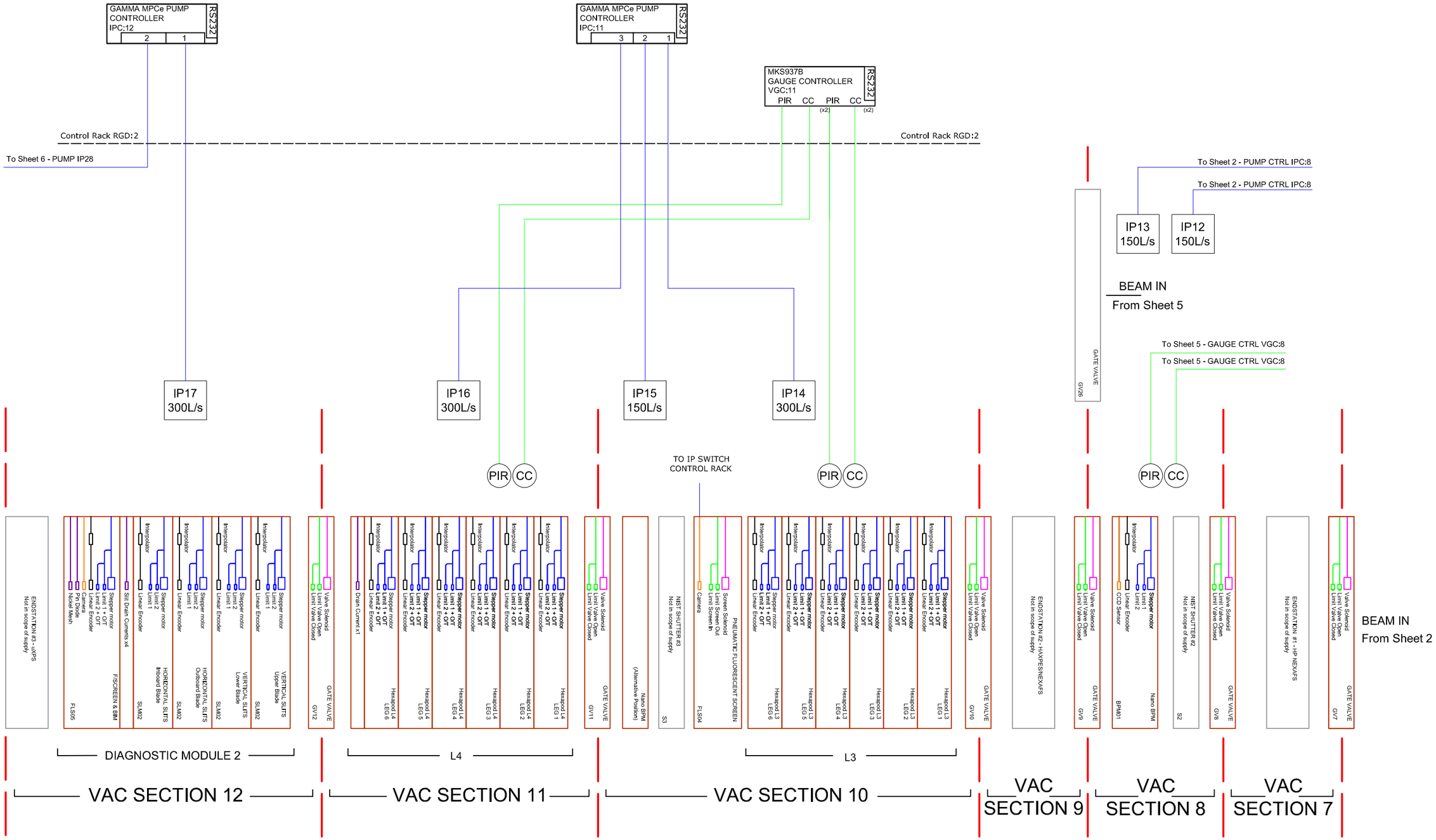

REV	DATE	DESCRIPTION/DMR No	DRN	CHKD
F	21/01/2015	PDR ISSUE	MKS	
G	07/07/2015	PRE FDR ISSUE	DJS	
H	13/08/2015	FDR ISSUE	DJS	

THIS DRAWING BELONGS TO FMB OXFORD LTD AND IS ISSUED ON CONDITION THAT IT IS NOT COPIED, REPRINTED OR DISCLOSED TO A THIRD PARTY WITHOUT PRIOR CONSENT IN WRITING FROM FMB OXFORD Ltd.

DRAWN D. Smith DATE 21/01/2015

CHECKED DATE

APPROVED DATE

FMB OXFORD LTD
UNIT 1 FERRY MILLS,
OSNEY MEAD, OXFORD, OX2 0ES.
ENGLAND

FMB Oxford

Title S3160 NIST SST BEAMLINE PID

Size A3 | Document Number CRP0469 | Rev H

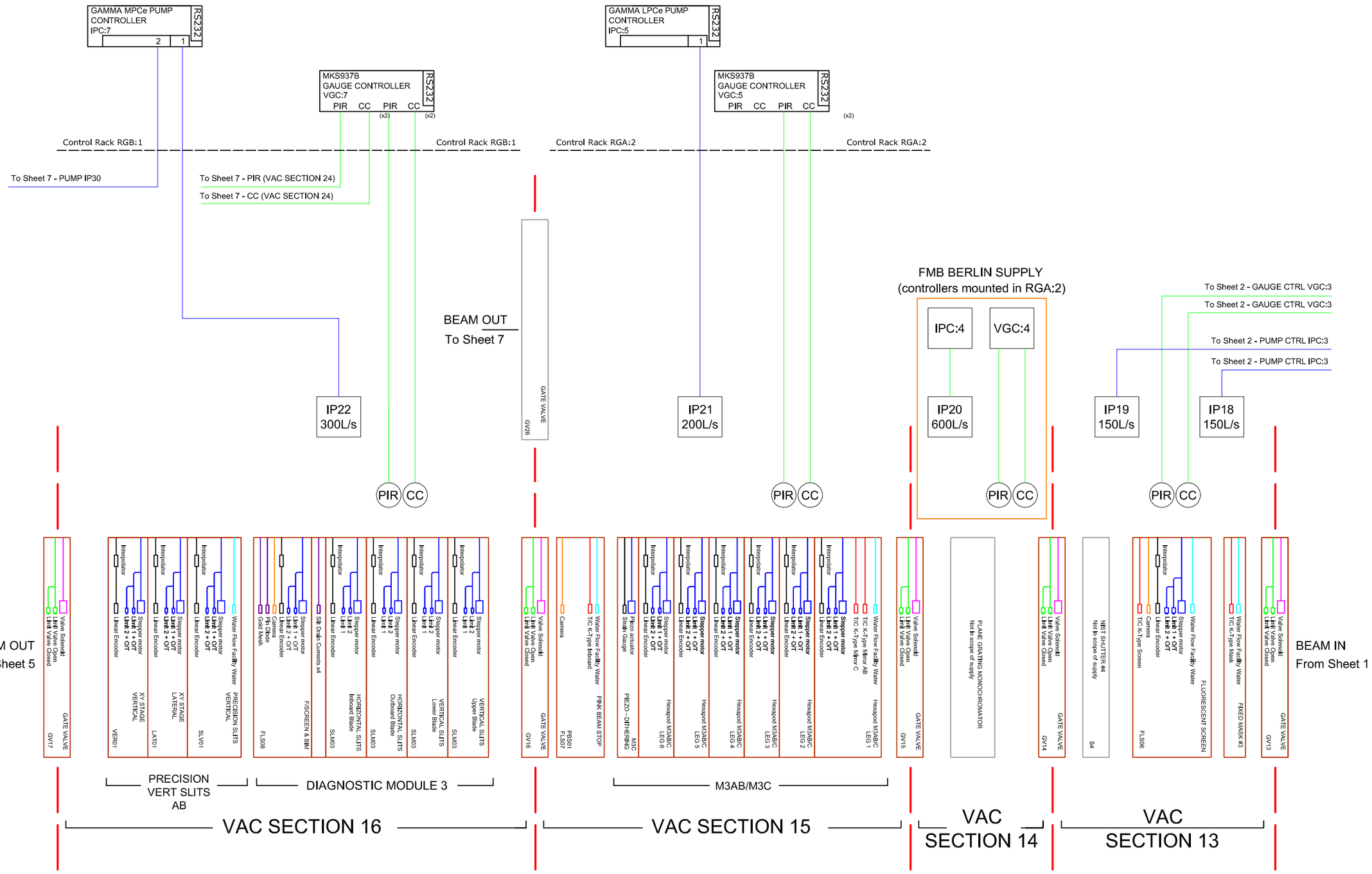

REV	DATE	DESCRIPTION/DMR No	DRN	CHKD
F	21/01/2015	PDR ISSUE	MKS	
G	07/07/2015	PRE FDR ISSUE	DJS	
H	13/08/2015	FDR ISSUE	DJS	

THIS DRAWING BELONGS TO FMB OXFORD LTD AND IS ISSUED ON CONDITION THAT IT IS NOT COPIED, REPRINTED OR DISCLOSED TO A THIRD PARTY WITHOUT PRIOR CONSENT IN WRITING FROM FMB OXFORD Ltd.

DRAWN: D. Smith DATE: 21/01/2015
CHECKED DATE
APPROVED DATE

FMB OXFORD LTD
UNIT 1 FERRY MILLS,
OSNEY MEAD, OXFORD, OX2 0ES.
ENGLAND

FMB Oxford

Title: S3160 NIST SST BEAMLINE PID

Size: A3 | Document Number: CRP0469 | Rev: H

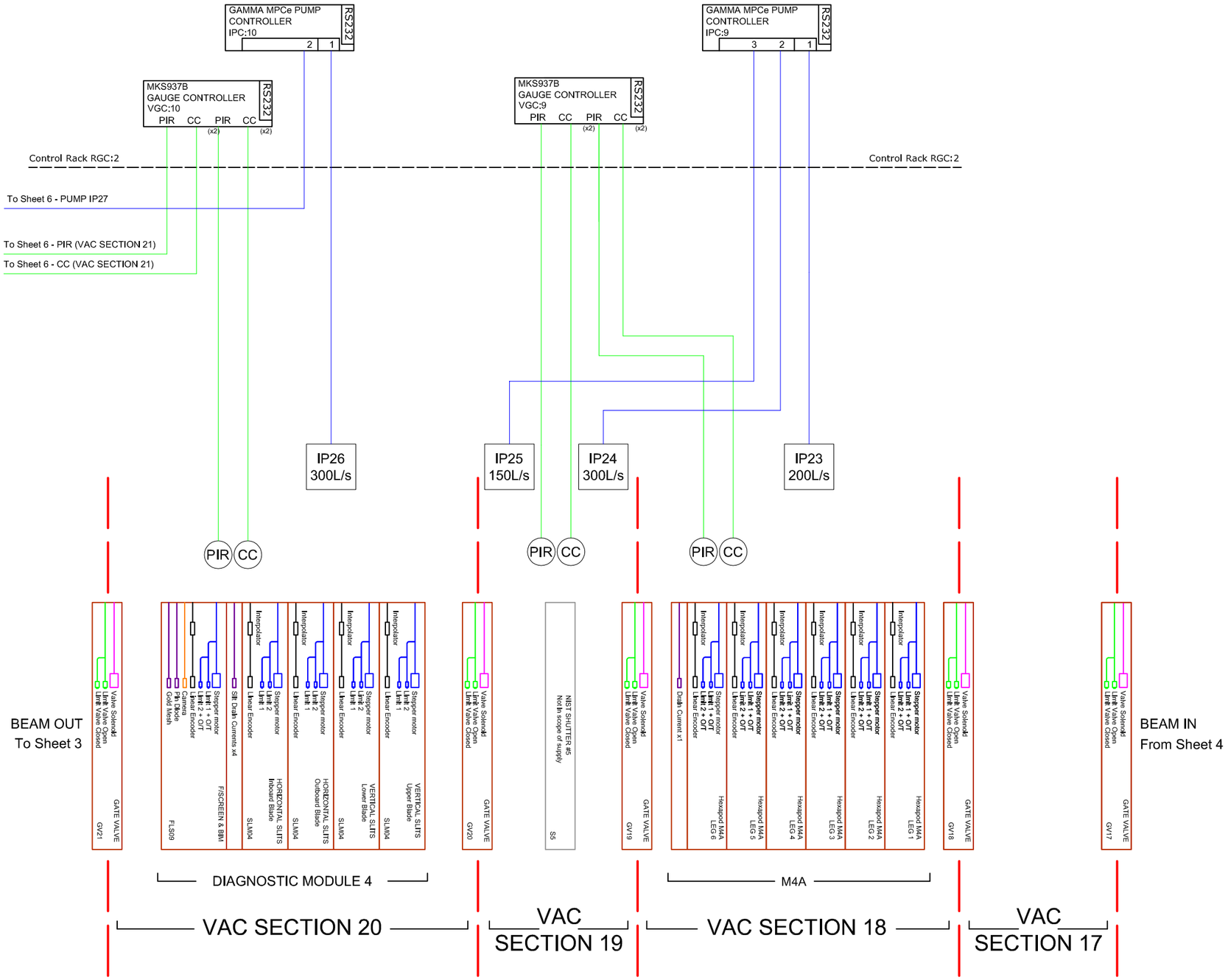

REV	DATE	DESCRIPTION/DMR No	DRN	CHKD
F	21/01/2015	PDR ISSUE	MKS	
G	07/07/2015	PRE FDR ISSUE	DJS	
H	13/08/2015	FDR ISSUE	DJS	

THIS DRAWING BELONGS TO FMB OXFORD LTD AND IS ISSUED ON CONDITION THAT IT IS NOT COPIED, REPRINTED OR DISCLOSED TO A THIRD PARTY WITHOUT PRIOR CONSENT IN WRITING FROM FMB OXFORD Ltd.

DRAWN D. Smith DATE 21/01/2015

CHECKED DATE

APPROVED DATE

FMB OXFORD LTD
UNIT 1 FERRY MILLS,
OSNEY MEAD, OXFORD, OX2 0ES.
ENGLAND

FMB Oxford

Title S3160 NIST SST BEAMLINE PID

Size A3 | Document Number CRP0469 | Rev H

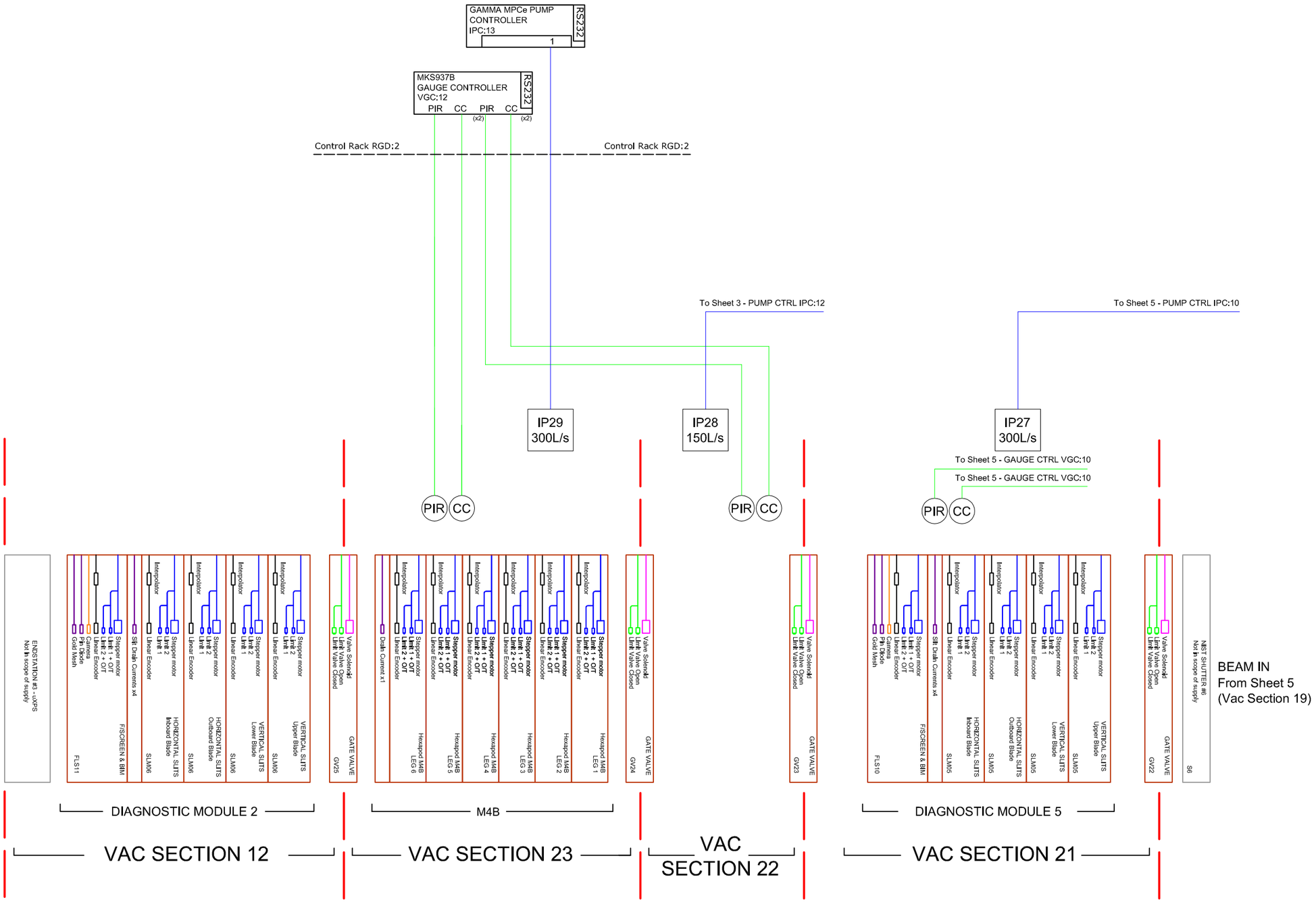

REV	DATE	DESCRIPTION/DMR No	DRN	CHKD
F	21/01/2015	PDR ISSUE	MKS	
G	07/07/2015	PRE FDR ISSUE	DJS	
H	13/08/2015	FDR ISSUE	DJS	

THIS DRAWING BELONGS TO FMB OXFORD LTD AND IS ISSUED ON CONDITION THAT IT IS NOT COPIED, REPRINTED OR DISCLOSED TO A THIRD PARTY WITHOUT PRIOR CONSENT IN WRITING FROM FMB OXFORD Ltd.

DRAWN D. Smith DATE 21/01/2015

CHECKED DATE

APPROVED DATE

FMB OXFORD LTD
UNIT 1 FERRY MILLS,
OSNEY MEAD, OXFORD, OX2 0ES.
ENGLAND

FMB Oxford

Title S3160 NIST SST BEAMLINE PID

Size A3 | Document Number CRP0469 | Rev H

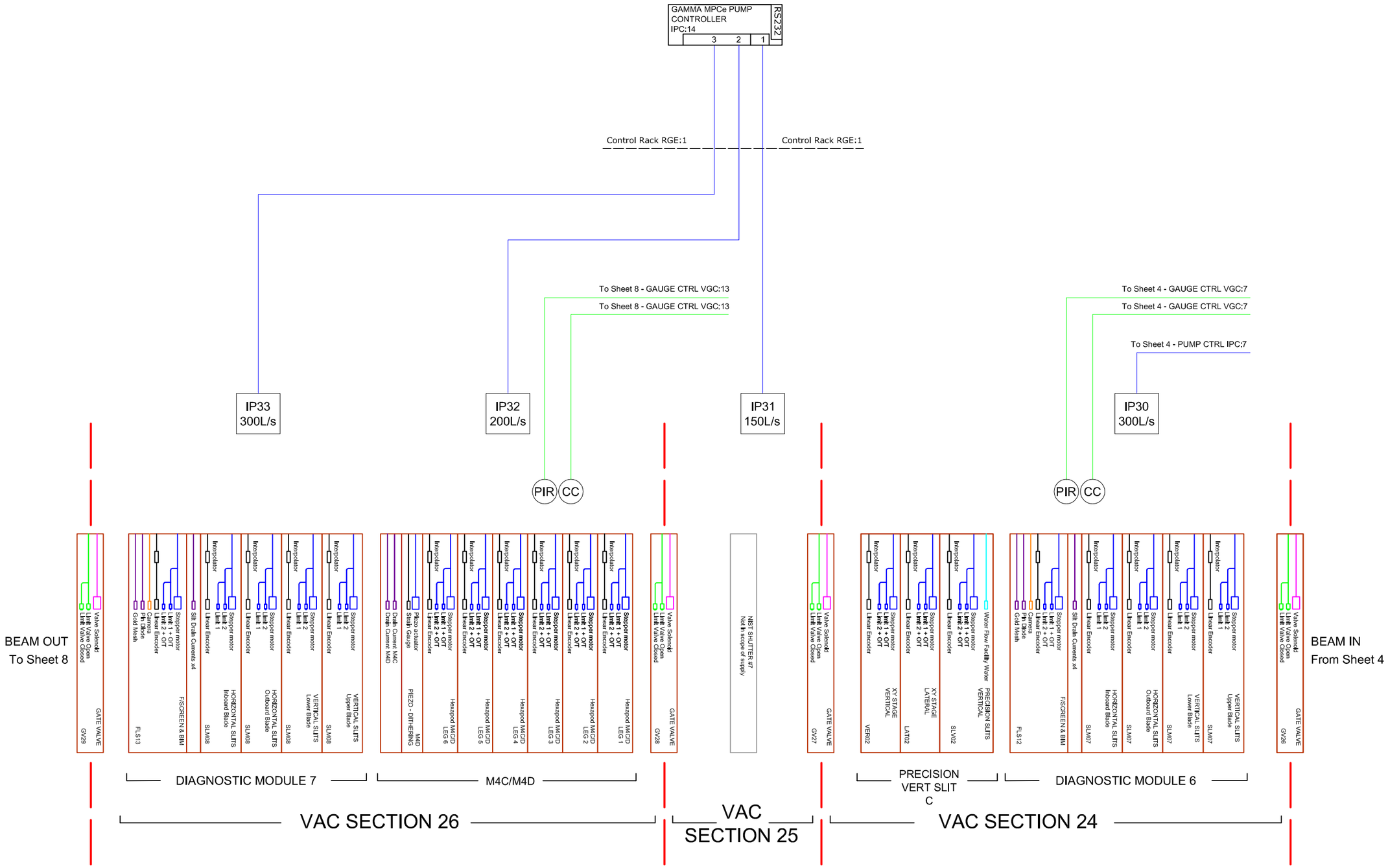

REV	DATE	DESCRIPTION/DMR No	DRN	CHKD
F	21/01/2015	PDR ISSUE	MKS	
G	07/07/2015	PRE PDR ISSUE	DJS	
H	13/08/2015	FDR ISSUE	DJS	

THIS DRAWING BELONGS TO FMB OXFORD LTD AND IS ISSUED ON CONDITION THAT IT IS NOT COPIED, REPRINTED OR DISCLOSED TO A THIRD PARTY WITHOUT PRIOR CONSENT IN WRITING FROM FMB OXFORD Ltd.

DRAWN D. Smith DATE 21/01/2015

CHECKED DATE

APPROVED DATE

FMB OXFORD LTD
UNIT 1 FERRY MILLS,
OSNEY MEAD, OXFORD, OX2 0ES.
ENGLAND

FMB Oxford

Title S3160 NIST SST BEAMLINE PID

Size A3 | Document Number CRP0469 | Rev H

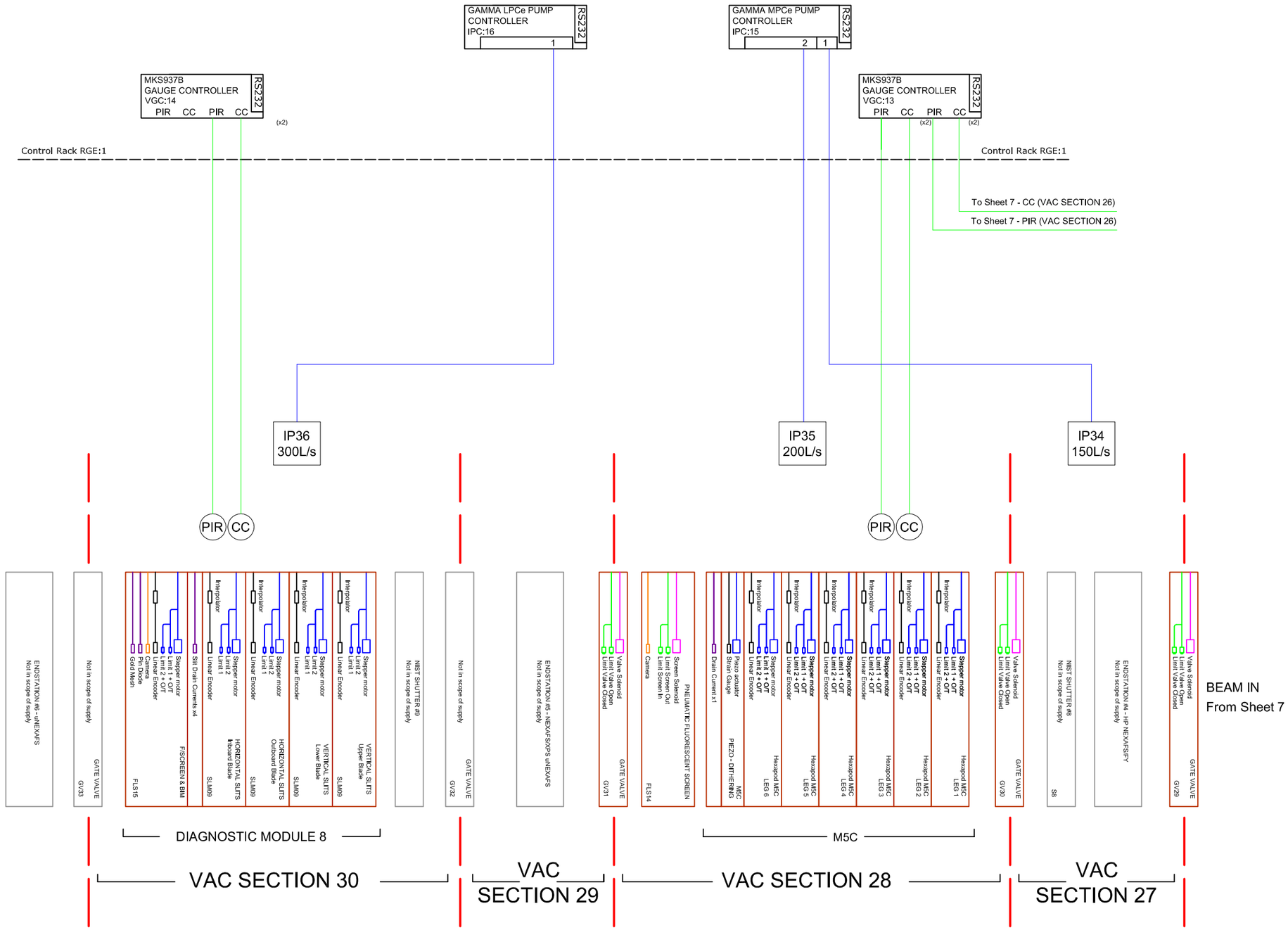

REV	DATE	DESCRIPTION/DMR No	DRN	CHKD
F	21/01/2015	PDR ISSUE	MKS	
G	07/07/2015	PRE PDR ISSUE	DJS	
H	13/08/2015	FDR ISSUE	DJS	

THIS DRAWING BELONGS TO FMB OXFORD LTD AND IS ISSUED ON CONDITION THAT IT IS NOT COPIED, REPRINTED OR DISCLOSED TO A THIRD PARTY WITHOUT PRIOR CONSENT IN WRITING FROM FMB OXFORD Ltd.

DRAWN D. Smith DATE 21/01/2015

CHECKED DATE

APPROVED DATE

FMB OXFORD LTD
UNIT 1 FERRY MILLS,
OSNEY MEAD, OXFORD, OX2 0ES.
ENGLAND

FMB Oxford

Title S3160 NIST SST BEAMLINE PID

Size A3 | Document Number CRP0469 | Rev H

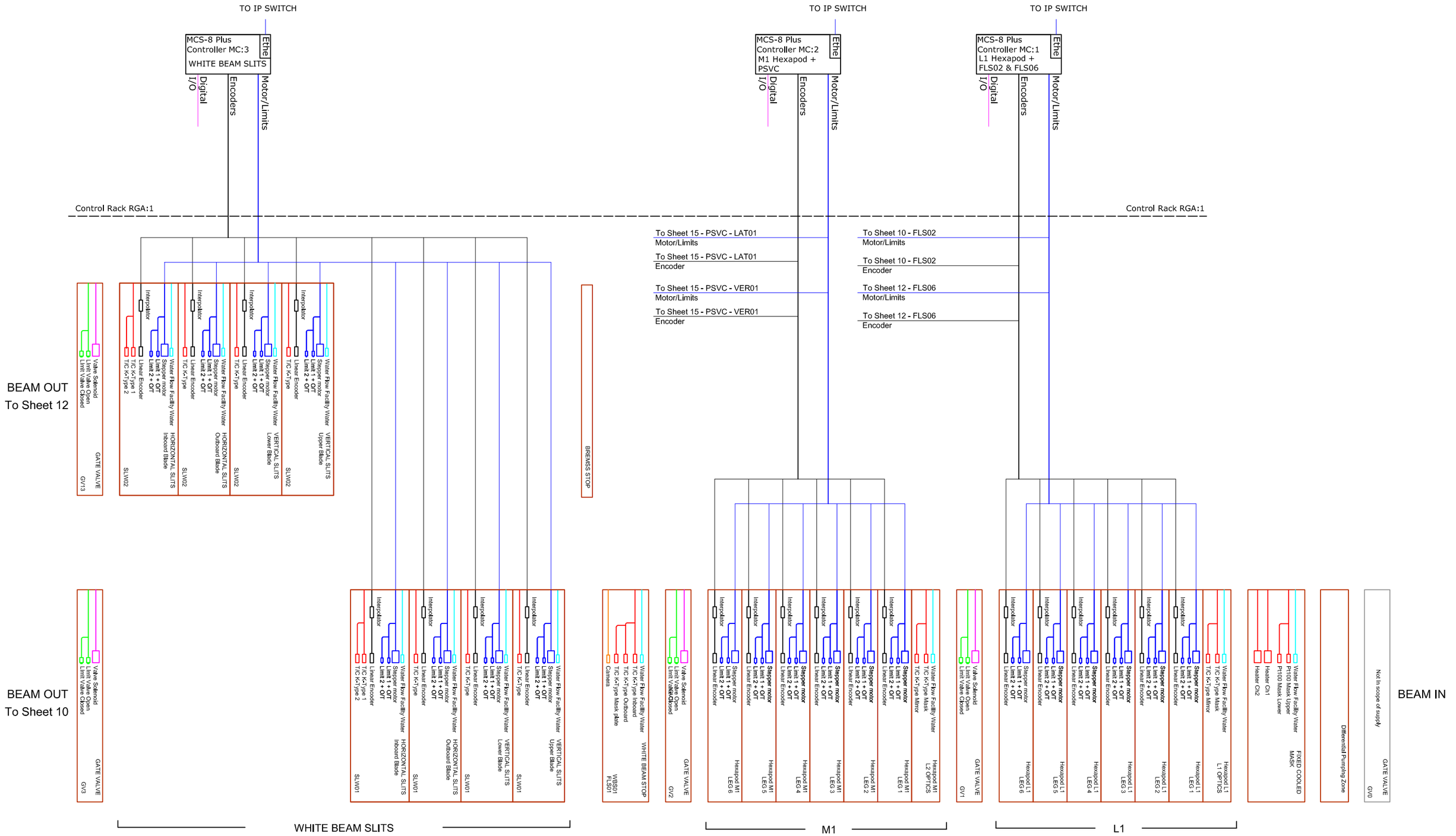

REV	DATE	DESCRIPTION/DMR No	DRN	CHKD
F	21/01/2015	PDR ISSUE	MKS	
G	07/07/2015	PRE FDR ISSUE	DJS	
H	13/08/2015	FDR ISSUE	DJS	

THIS DRAWING BELONGS TO FMB OXFORD LTD AND IS ISSUED ON CONDITION THAT IT IS NOT COPIED, REPRINTED OR DISCLOSED TO A THIRD PARTY WITHOUT PRIOR CONSENT IN WRITING FROM FMB OXFORD Ltd.

DRAWN: D. Smith — DATE: 21/01/2015
CHECKED — DATE
APPROVED — DATE

FMB OXFORD LTD
UNIT 1 FERRY MILLS,
OSNEY MEAD, OXFORD, OX2 0ES.
ENGLAND

FMB Oxford

Title: S3160 NIST SST BEAMLINE PID

Size: A3 — Document Number: CRP0469 — Rev: H

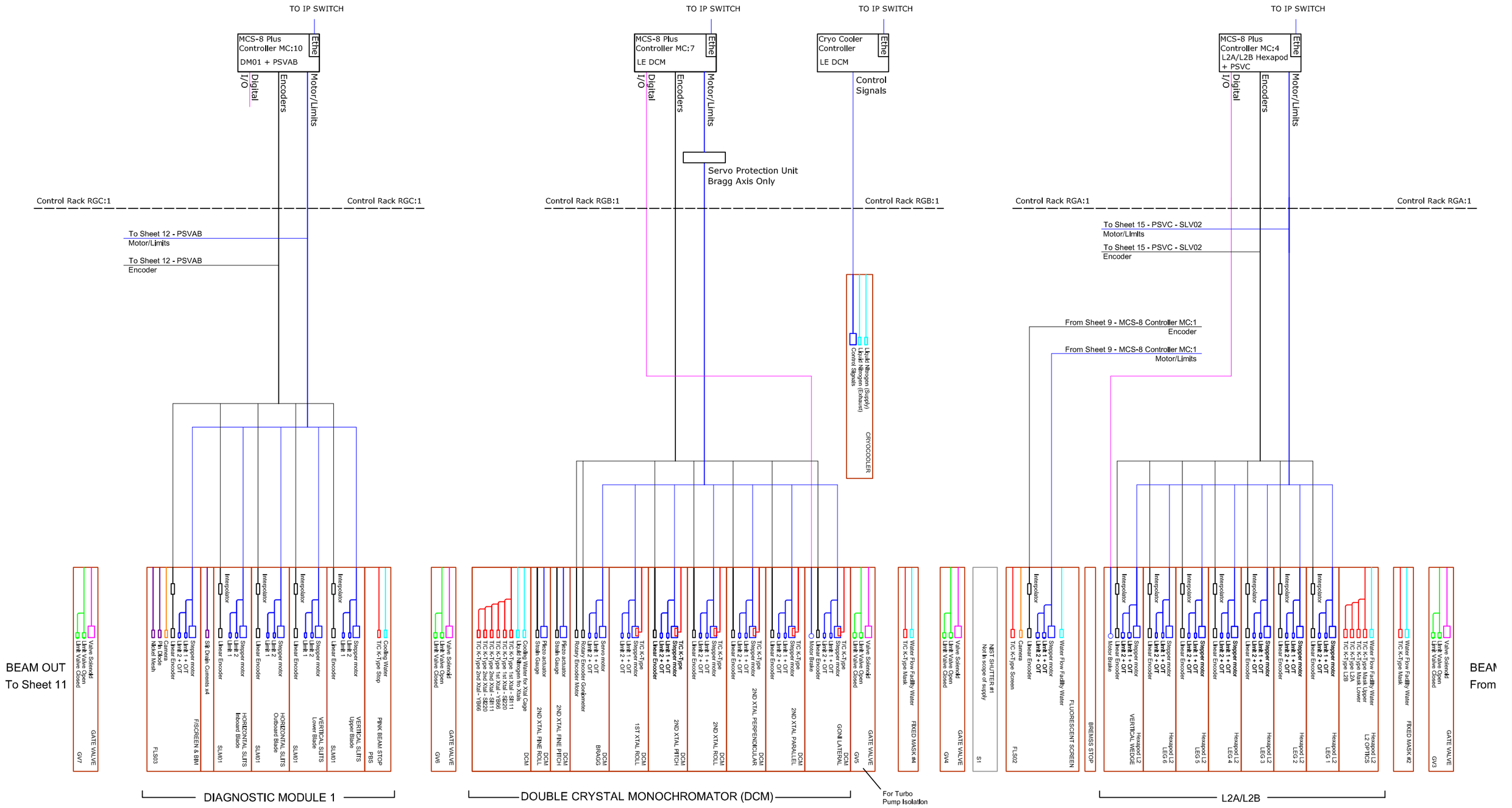

REV	DATE	DESCRIPTION/DMR No	DRN	CHKD
F	21/01/2015	PDR ISSUE	MKS	
G	07/07/2015	PRE FDR ISSUE	DJS	
H	13/08/2015	FDR ISSUE	DJS	

THIS DRAWING BELONGS TO FMB OXFORD LTD AND IS ISSUED ON CONDITION THAT IT IS NOT COPIED, REPRINTED OR DISCLOSED TO A THIRD PARTY WITHOUT PRIOR CONSENT IN WRITING FROM FMB OXFORD Ltd.

DRAWN D. Smith DATE 21/01/2015

CHECKED DATE

APPROVED DATE

FMB OXFORD LTD
UNIT 1 FERRY MILLS,
OSNEY MEAD, OXFORD, OX2 0ES.
ENGLAND

FMB Oxford

Title S3160 NIST SST BEAMLINE PID

Size A3 | Document Number CRP0469 | Rev H

Sheet 10 of 24

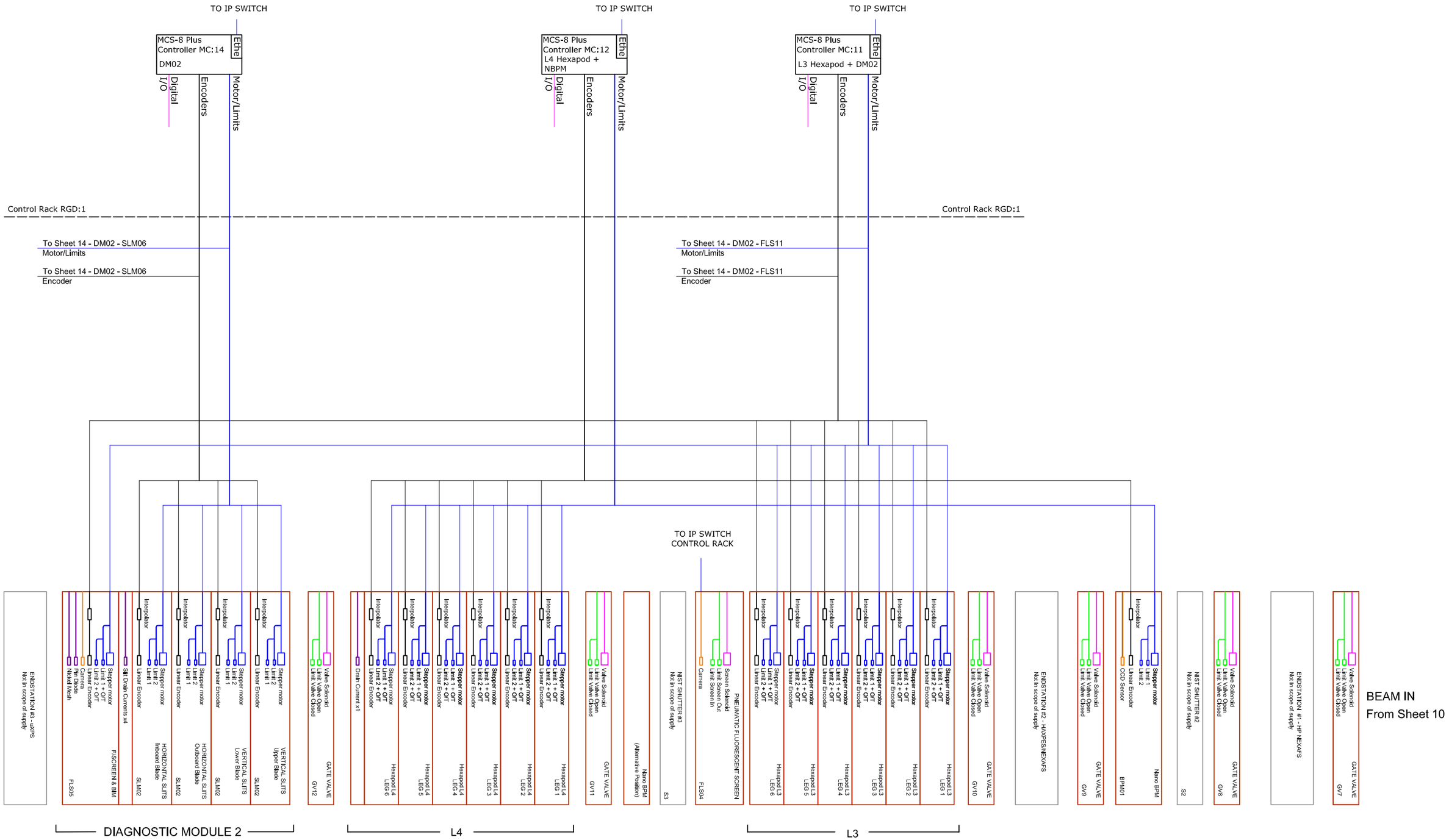

REV	DATE	DESCRIPTION/DMR No	DRN	CHKD
F	21/01/2015	PDR ISSUE	MKS	
G	07/07/2015	PRE FDR ISSUE	DJS	
H	13/08/2015	FDR ISSUE	DJS	

THIS DRAWING BELONGS TO FMB OXFORD LTD AND IS ISSUED ON CONDITION THAT IT IS NOT COPIED, REPRINTED OR DISCLOSED TO A THIRD PARTY WITHOUT PRIOR CONSENT IN WRITING FROM FMB OXFORD Ltd.

DRAWN D. Smith DATE 21/01/2015

CHECKED DATE

APPROVED DATE

FMB OXFORD LTD
UNIT 1 FERRY MILLS,
OSNEY MEAD, OXFORD, OX2 0ES.
ENGLAND

FMB Oxford

Title S3160 NIST SST BEAMLINE PID

Size A3 | Document Number CRP0469 | Rev H

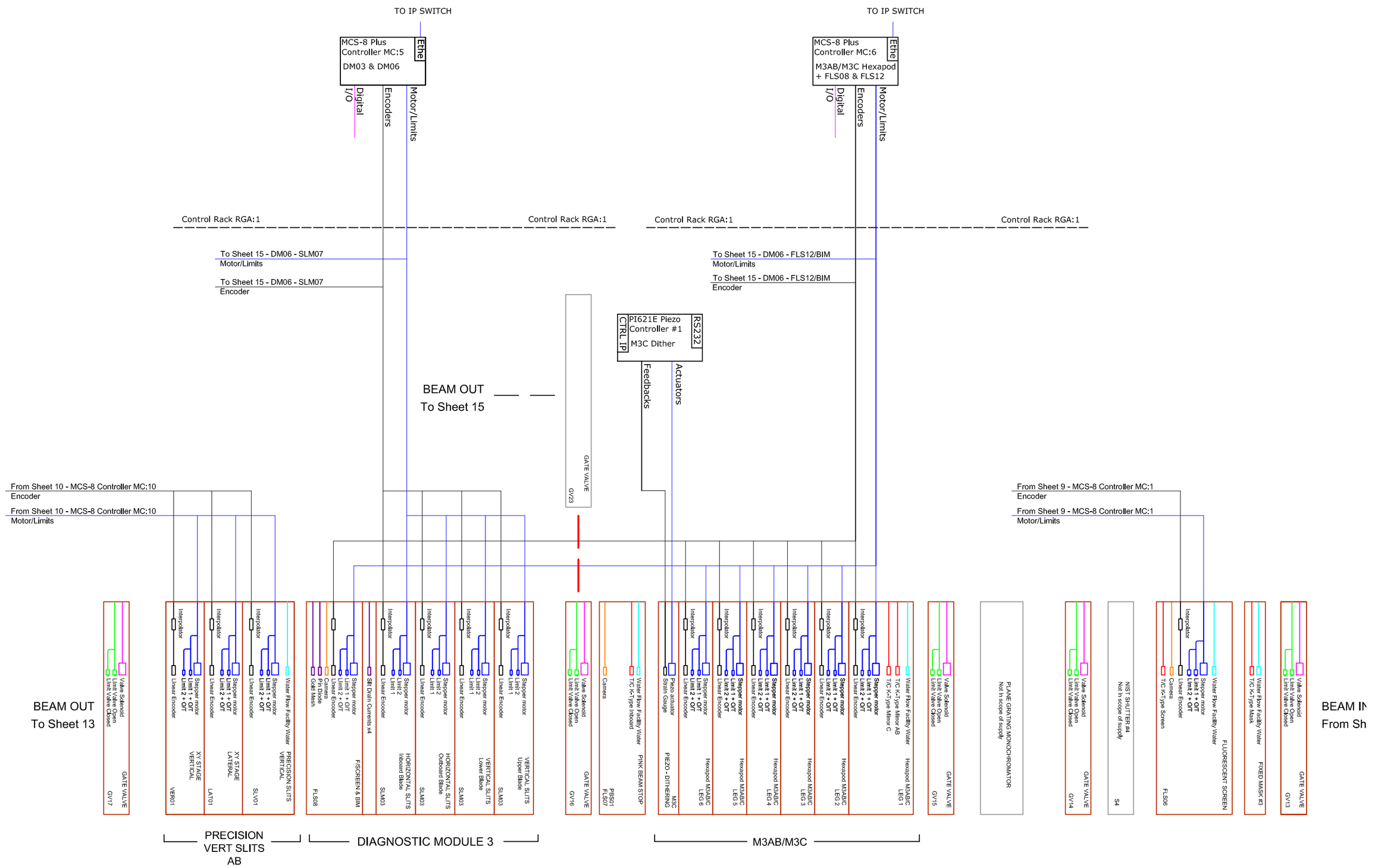

REV	DATE	DESCRIPTION/DMR No	DRN	CHKD
F	21/01/2015	PDR ISSUE	MKS	
G	07/07/2015	PRE FDR ISSUE	DJS	
H	13/08/2015	FDR ISSUE	DJS	

THIS DRAWING BELONGS TO FMB OXFORD LTD AND IS ISSUED ON CONDITION THAT IT IS NOT COPIED, REPRINTED OR DISCLOSED TO A THIRD PARTY WITHOUT PRIOR CONSENT IN WRITING FROM FMB OXFORD Ltd.

DRAWN: D. Smith DATE: 21/01/2015
CHECKED DATE
APPROVED DATE

FMB OXFORD LTD
UNIT 1 FERRY MILLS,
OSNEY MEAD, OXFORD, OX2 0ES.
ENGLAND

FMB Oxford

Title: S3160 NIST SST BEAMLINE PID

Size: A3 | Document Number: CRP0469 | Rev: H

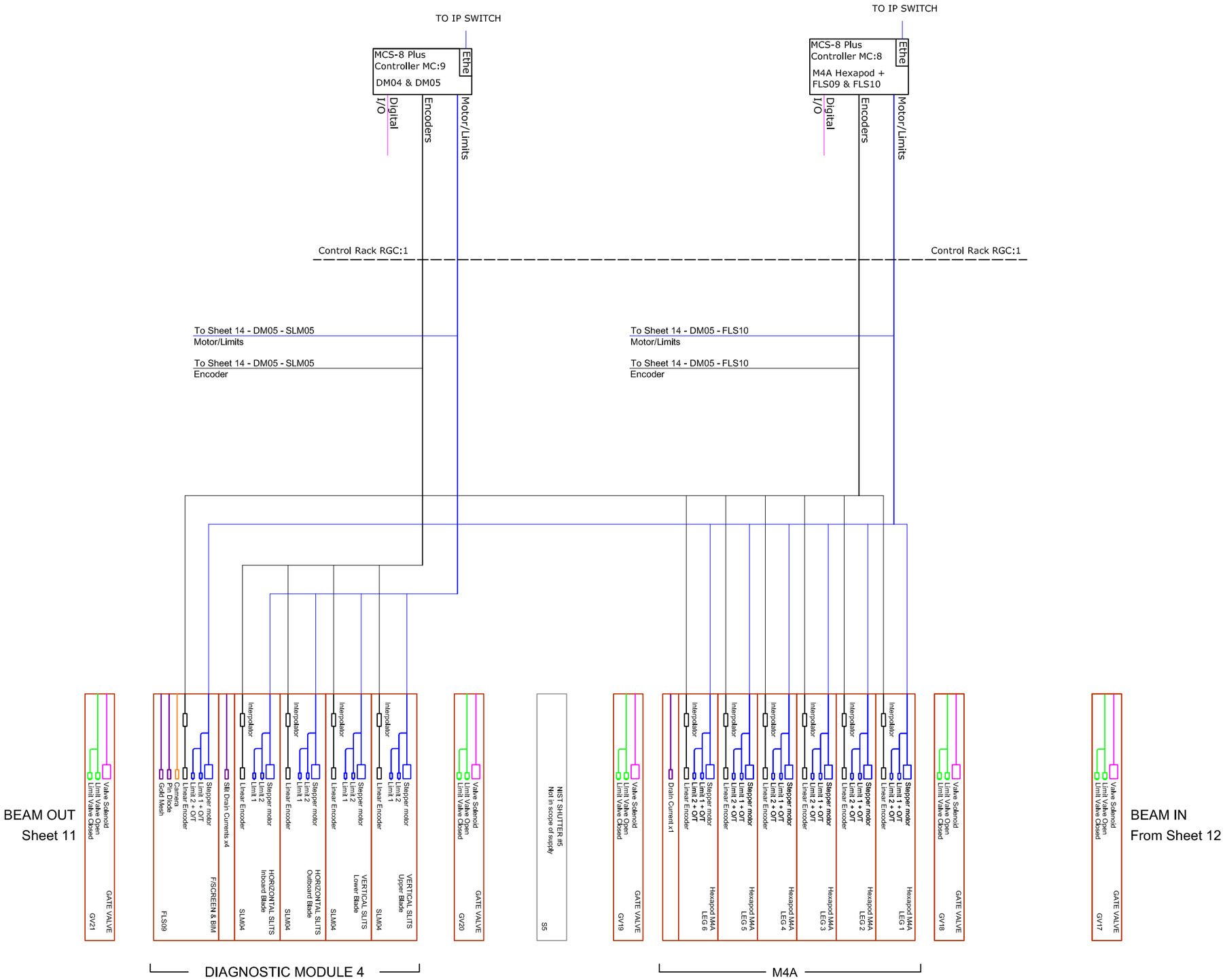

REV	DATE	DESCRIPTION/DMR No	DRN	CHKD
F	21/01/2015	PDR ISSUE	MKS	
G	07/07/2015	PRE FDR ISSUE	DJS	
H	13/08/2015	FDR ISSUE	DJS	

THIS DRAWING BELONGS TO FMB OXFORD LTD AND IS ISSUED ON CONDITION THAT IT IS NOT COPIED, REPRINTED OR DISCLOSED TO A THIRD PARTY WITHOUT PRIOR CONSENT IN WRITING FROM FMB OXFORD Ltd.

DRAWN: D. Smith DATE: 21/01/2015
CHECKED DATE
APPROVED DATE

FMB OXFORD LTD
UNIT 1 FERRY MILLS,
OSNEY MEAD, OXFORD, OX2 0ES.
ENGLAND

FMB Oxford

Title: S3160 NIST SST BEAMLINE PID

Size: A3 | Document Number: CRP0469 | Rev: H

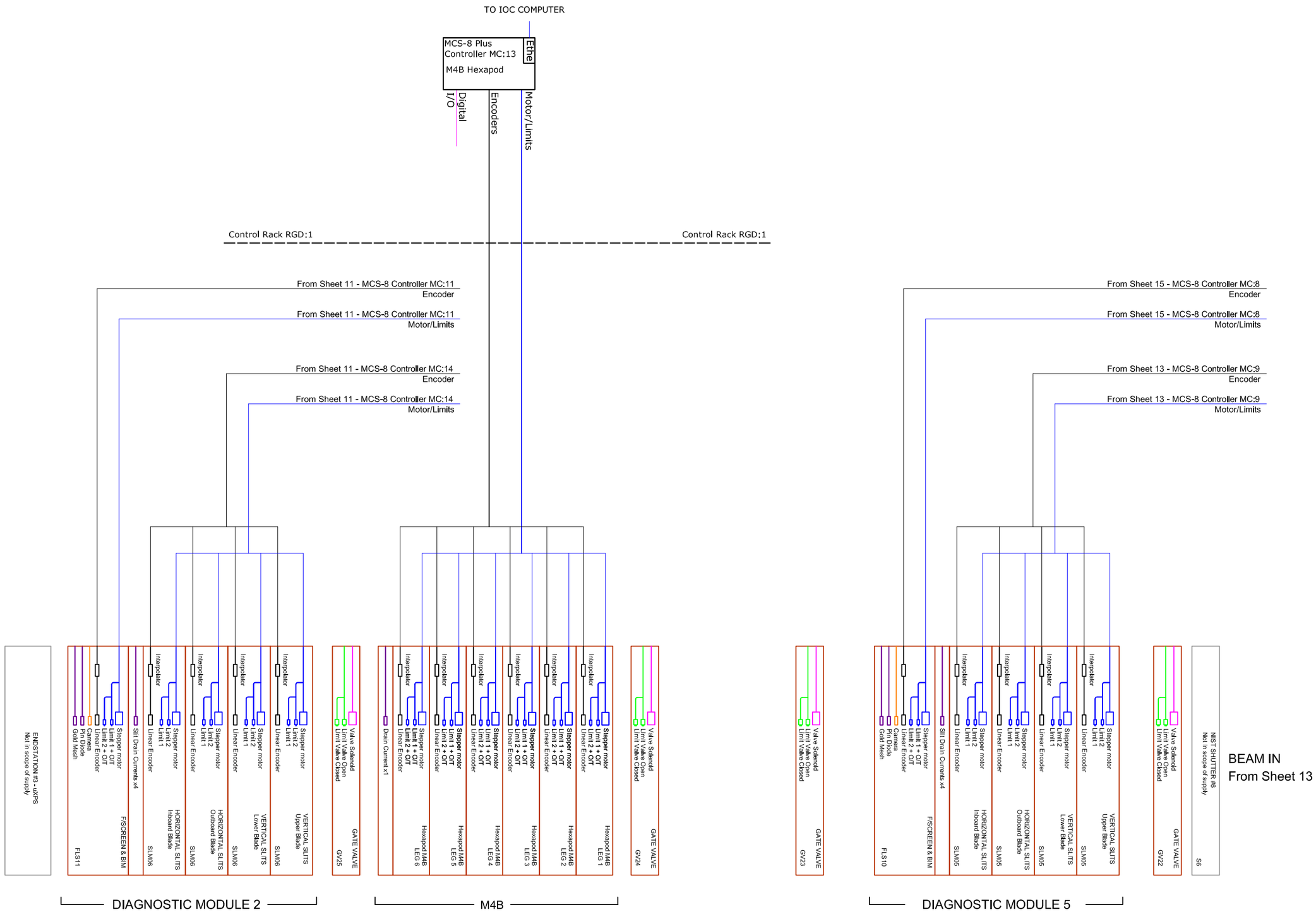

REV	DATE	DESCRIPTION/DMR No	DRN	CHKD
F	21/01/2015	PDR ISSUE	MKS	
G	07/07/2015	PRE FDR ISSUE	DJS	
H	13/08/2015	FDR ISSUE	DJS	

THIS DRAWING BELONGS TO FMB OXFORD LTD AND IS ISSUED ON CONDITION THAT IT IS NOT COPIED, REPRINTED OR DISCLOSED TO A THIRD PARTY WITHOUT PRIOR CONSENT IN WRITING FROM FMB OXFORD Ltd.

DRAWN D. Smith DATE 21/01/2015

CHECKED DATE

APPROVED DATE

FMB OXFORD LTD
UNIT 1 FERRY MILLS,
OSNEY MEAD, OXFORD, OX2 0ES.
ENGLAND

FMB Oxford

Title S3160 NIST SST BEAMLINE PID

Size A3 | Document Number CRP0469 | Rev H

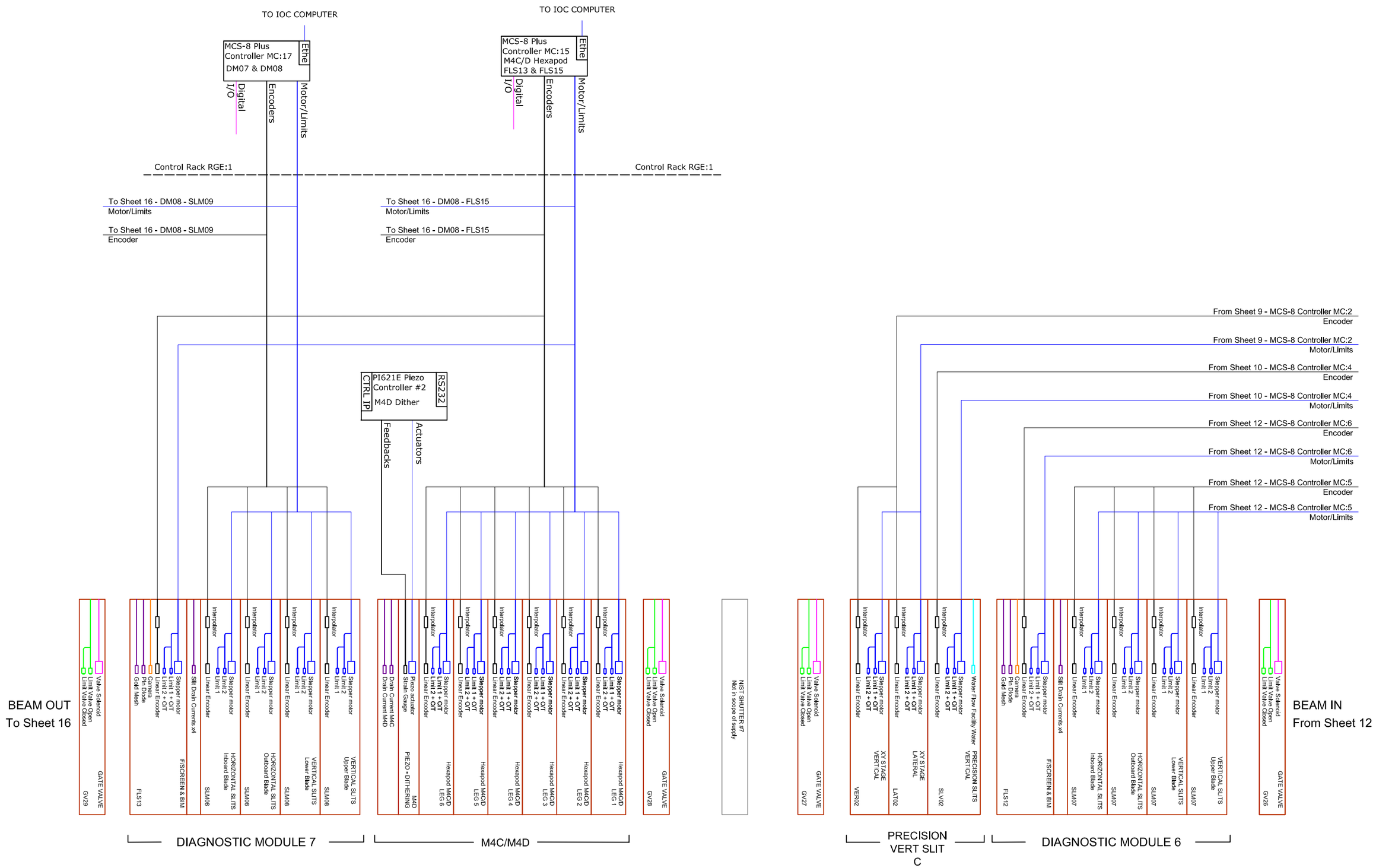

REV	DATE	DESCRIPTION/DMR No	DRN	CHKD
F	21/01/2015	PDR ISSUE	MKS	
G	07/07/2015	PRE FDR ISSUE	DJS	
H	13/08/2015	FDR ISSUE	DJS	

THIS DRAWING BELONGS TO FMB OXFORD LTD AND IS ISSUED ON CONDITION THAT IT IS NOT COPIED, REPRINTED OR DISCLOSED TO A THIRD PARTY WITHOUT PRIOR CONSENT IN WRITING FROM FMB OXFORD Ltd.

DRAWN S.SIEW DATE 21/01/2015

CHECKED DATE

APPROVED DATE

FMB OXFORD LTD
UNIT 1 FERRY MILLS,
OSNEY MEAD, OXFORD, OX2 0ES.
ENGLAND

FMB Oxford

Title S3160 NIST SST BEAMLINE PID

Size A3 | Document Number CRP0469 | Rev H

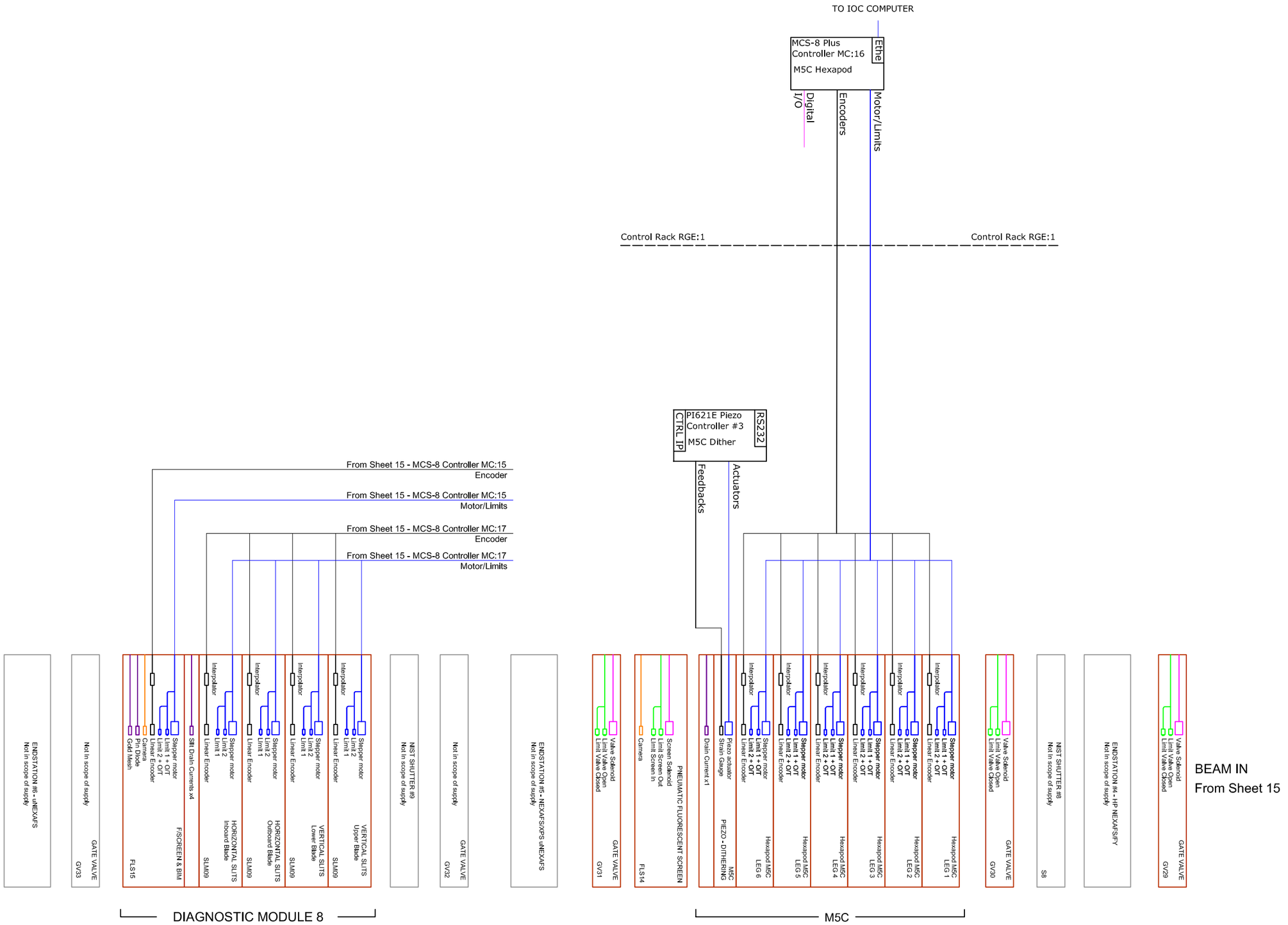

REV	DATE	DESCRIPTION/DMR No	DRN	CHKD
F	21/01/2015	PDR ISSUE	MKS	
G	07/07/2015	PRE FDR ISSUE	DJS	
H	13/08/2015	FDR ISSUE	DJS	

THIS DRAWING BELONGS TO FMB OXFORD LTD AND IS ISSUED ON CONDITION THAT IT IS NOT COPIED, REPRINTED OR DISCLOSED TO A THIRD PARTY WITHOUT PRIOR CONSENT IN WRITING FROM FMB OXFORD Ltd.

DRAWN: D. Smith DATE: 21/01/2015

CHECKED DATE

APPROVED DATE

FMB OXFORD LTD
UNIT 1 FERRY MILLS,
OSNEY MEAD, OXFORD, OX2 0ES.
ENGLAND

FMB Oxford

Title: S3160 NIST SST BEAMLINE PID

Size: A3 | Document Number: CRP0469 | Rev: H

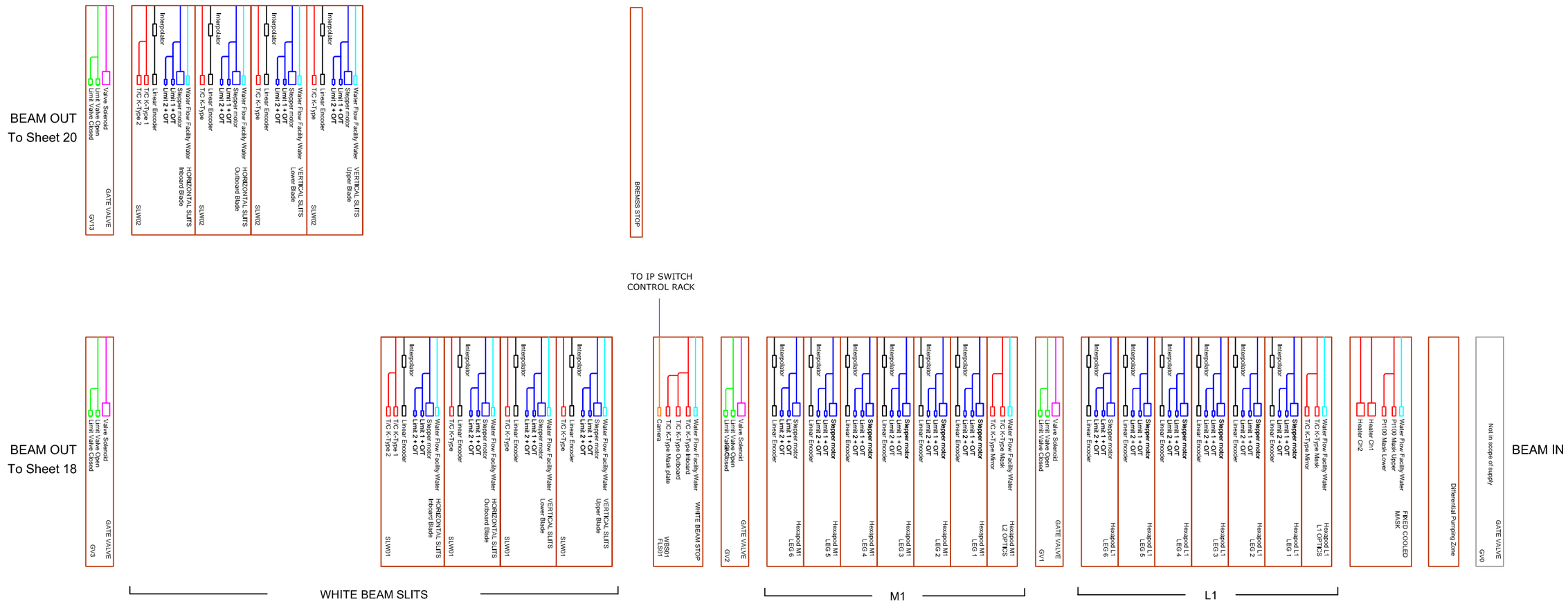

REV	DATE	DESCRIPTION/DMR No	DRN	CHKD
F	21/01/2015	PDR ISSUE	MKS	
G	07/07/2015	PRE FDR ISSUE	DJS	
H	13/08/2015	FDR ISSUE	DJS	

THIS DRAWING BELONGS TO FMB OXFORD LTD AND IS ISSUED ON CONDITION THAT IT IS NOT COPIED, REPRINTED OR DISCLOSED TO A THIRD PARTY WITHOUT PRIOR CONSENT IN WRITING FROM FMB OXFORD Ltd.

DRAWN: D. Smith — DATE: 21/01/2015

CHECKED — DATE

APPROVED — DATE

FMB OXFORD LTD
UNIT 1 FERRY MILLS,
OSNEY MEAD, OXFORD, OX2 0ES.
ENGLAND

FMB Oxford

Title: S3160 NIST SST BEAMLINE PID

Size: A3 — Document Number: CRP0469 — Rev: H

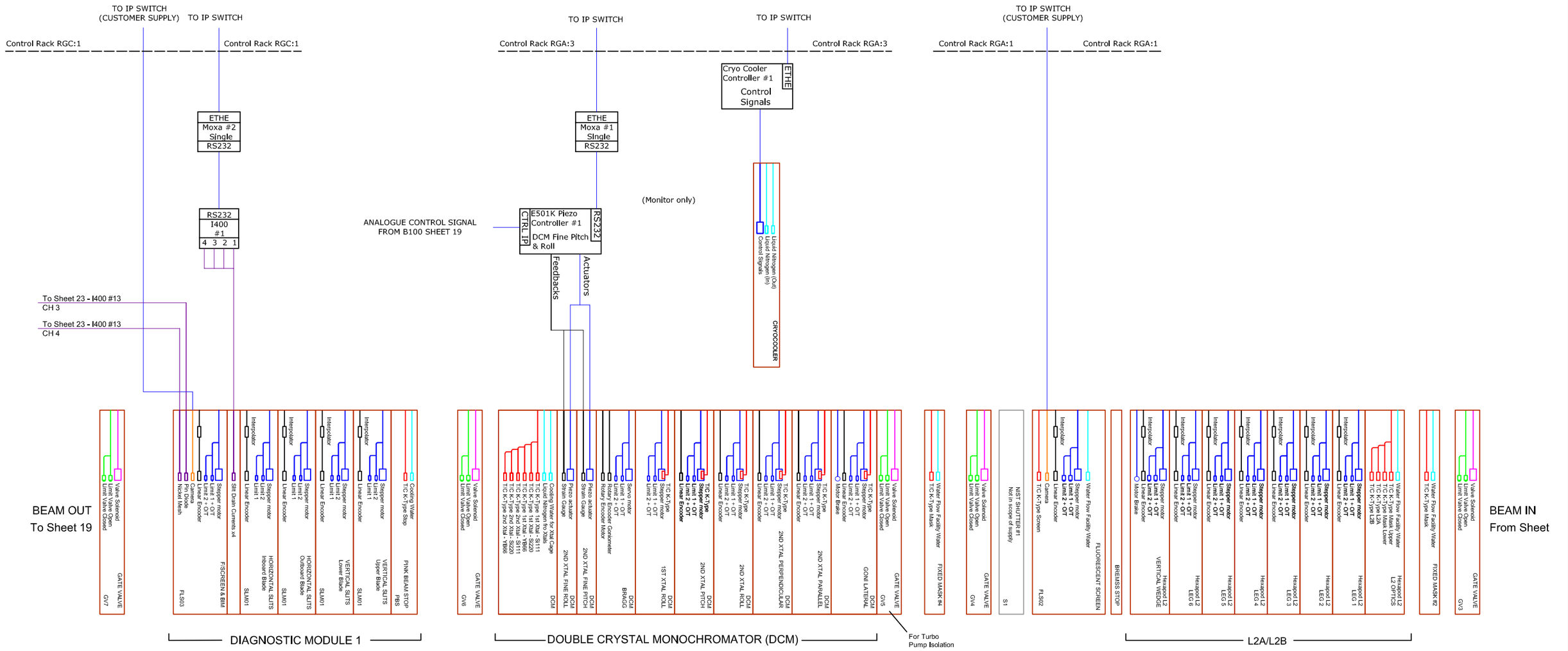

REV	DATE	DESCRIPTION/DMR No	DRN	CHKD
F	21/01/2015	PDR ISSUE	MKS	
G	07/07/2015	FDR FDR ISSUE	DJS	
H	13/08/2015	FDR ISSUE	DJS	

THIS DRAWING BELONGS TO FMB OXFORD LTD AND IS ISSUED ON CONDITION THAT IT IS NOT COPIED, REPRINTED OR DISCLOSED TO A THIRD PARTY WITHOUT PRIOR CONSENT IN WRITING FROM FMB OXFORD Ltd.

DRAWN D. Smith DATE 21/01/2015

CHECKED DATE

APPROVED DATE

FMB OXFORD LTD
UNIT 1 FERRY MILLS,
OSNEY MEAD, OXFORD, OX2 0ES.
ENGLAND

FMB Oxford

Title S3160 NIST SST BEAMLINE PID

Size A3 | Document Number CRP0469 | Rev H

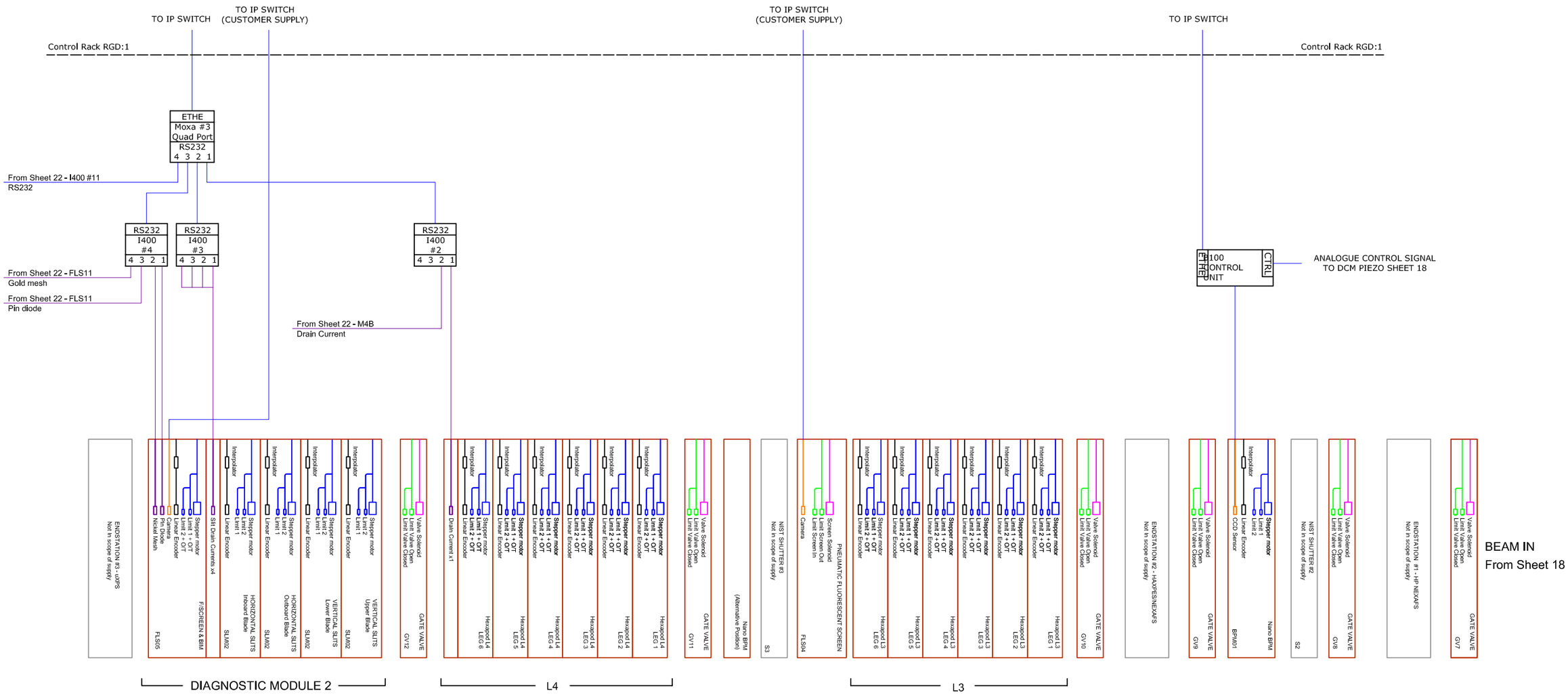

REV	DATE	DESCRIPTION/DMR No	DRN	CHKD
F	21/01/2015	PDR ISSUE	MKS	
G	07/07/2015	PRE FDR ISSUE	DJS	
H	13/08/2015	FDR ISSUE	DJS	

THIS DRAWING BELONGS TO FMB OXFORD LTD AND IS ISSUED ON CONDITION THAT IT IS NOT COPIED, REPRINTED OR DISCLOSED TO A THIRD PARTY WITHOUT PRIOR CONSENT IN WRITING FROM FMB OXFORD Ltd.

DRAWN: D. Smith DATE: 21/01/2015
CHECKED DATE
APPROVED DATE

FMB OXFORD LTD
UNIT 1 FERRY MILLS,
OSNEY MEAD, OXFORD, OX2 0ES.
ENGLAND

FMB Oxford

Title: S3160 NIST SST BEAMLINE PID

Size: A3 | Document Number: CRP0469 | Rev: H

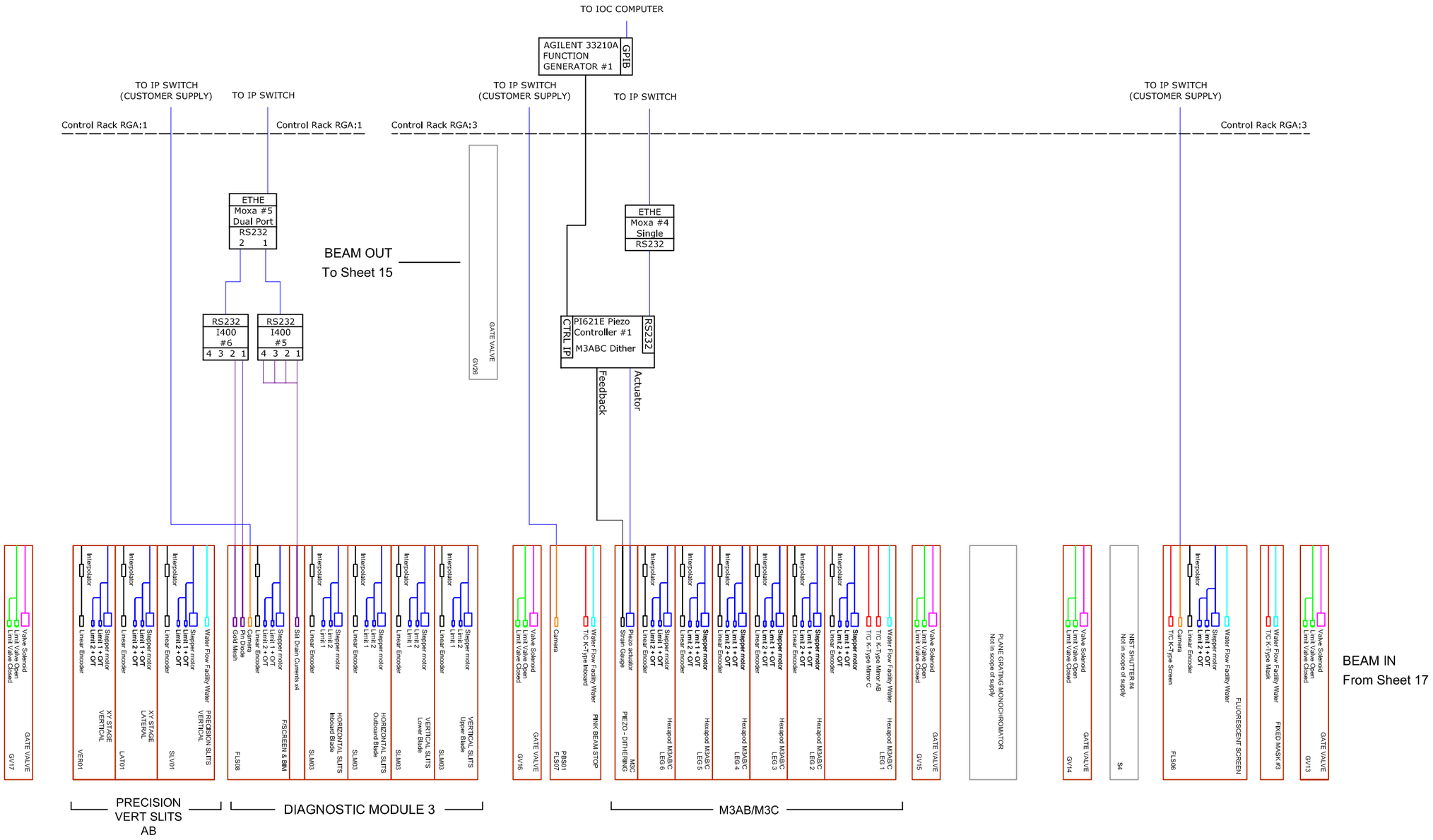

REV	DATE	DESCRIPTION/DMR No	DRN	CHKD
F	21/01/2015	PDR ISSUE	MKS	
G	07/07/2015	PRE FDR ISSUE	DJS	
H	13/08/2015	FDR ISSUE	DJS	

THIS DRAWING BELONGS TO FMB OXFORD LTD AND IS ISSUED ON CONDITION THAT IT IS NOT COPIED, REPRINTED OR DISCLOSED TO A THIRD PARTY WITHOUT PRIOR CONSENT IN WRITING FROM FMB OXFORD Ltd.

DRAWN: D. Smith DATE: 21/01/2015

CHECKED DATE

APPROVED DATE

FMB OXFORD LTD
UNIT 1 FERRY MILLS,
OSNEY MEAD, OXFORD, OX2 0ES.
ENGLAND

FMB Oxford

Title: S3160 NIST SST BEAMLINE PID

Size: A3 | Document Number: CRP0469 | Rev: H

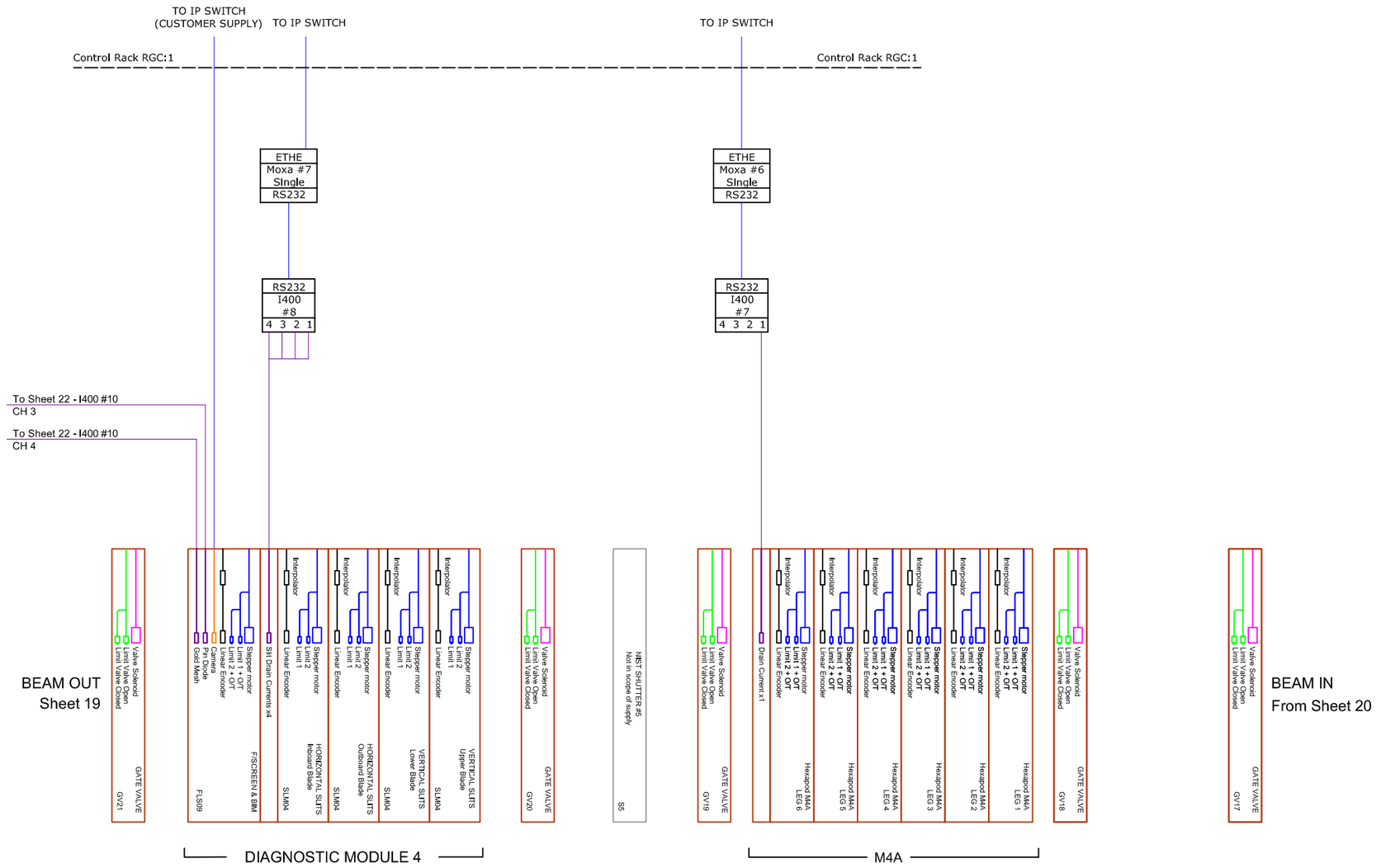

REV	DATE	DESCRIPTION/DMR No	DRN	CHKD
F	21/01/2015	PDR ISSUE	MKS	
G	07/07/2015	PRE FDR ISSUE	DJS	
H	13/08/2015	FDR ISSUE	DJS	

THIS DRAWING BELONGS TO FMB OXFORD LTD AND IS ISSUED ON CONDITION THAT IT IS NOT COPIED, REPRINTED OR DISCLOSED TO A THIRD PARTY WITHOUT PRIOR CONSENT IN WRITING FROM FMB OXFORD Ltd.

DRAWN: D. Smith DATE: 21/01/2015

CHECKED DATE

APPROVED DATE

FMB OXFORD LTD
UNIT 1 FERRY MILLS,
OSNEY MEAD, OXFORD, OX2 0ES.
ENGLAND

FMB Oxford

Title: S3160 NIST SST BEAMLINE PID

Size: A3 | Document Number: CRP0469 | Rev: H

Sheet 21 of 24

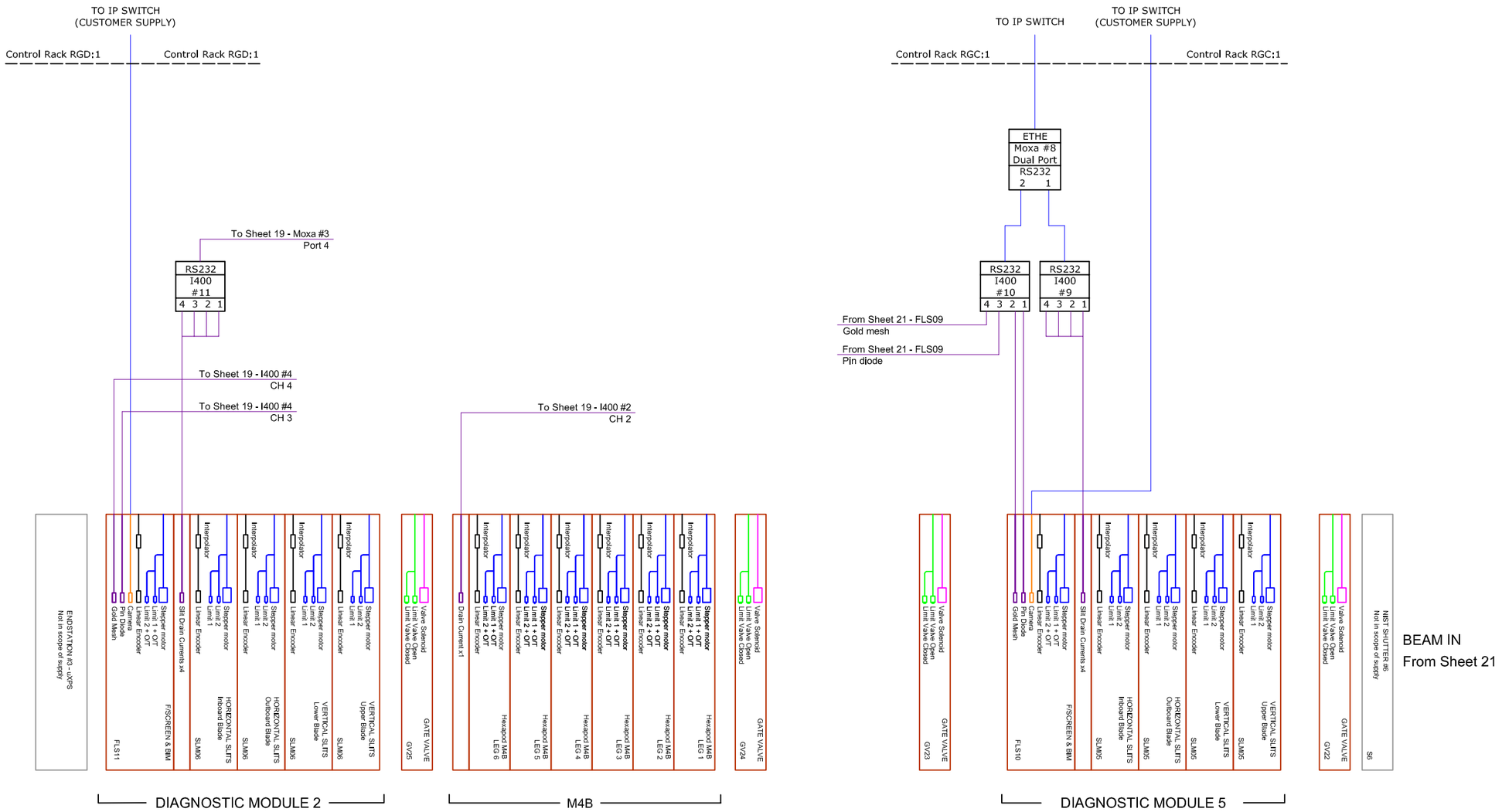

REV	DATE	DESCRIPTION/DMR No	DRN	CHKD
F	21/01/2015	PDR ISSUE	MKS	
G	07/07/2015	PRE FDR ISSUE	DJS	
H	13/08/2015	FDR ISSUE	DJS	

THIS DRAWING BELONGS TO FMB OXFORD LTD AND IS ISSUED ON CONDITION THAT IT IS NOT COPIED, REPRINTED OR DISCLOSED TO A THIRD PARTY WITHOUT PRIOR CONSENT IN WRITING FROM FMB OXFORD Ltd.

DRAWN D. Smith DATE 21/01/2015

CHECKED DATE

APPROVED DATE

FMB OXFORD LTD
UNIT 1 FERRY MILLS,
OSNEY MEAD, OXFORD, OX2 0ES.
ENGLAND

FMB Oxford

Title S3160 NIST SST BEAMLINE PID

Size A3 | Document Number CRP0469 | Rev H

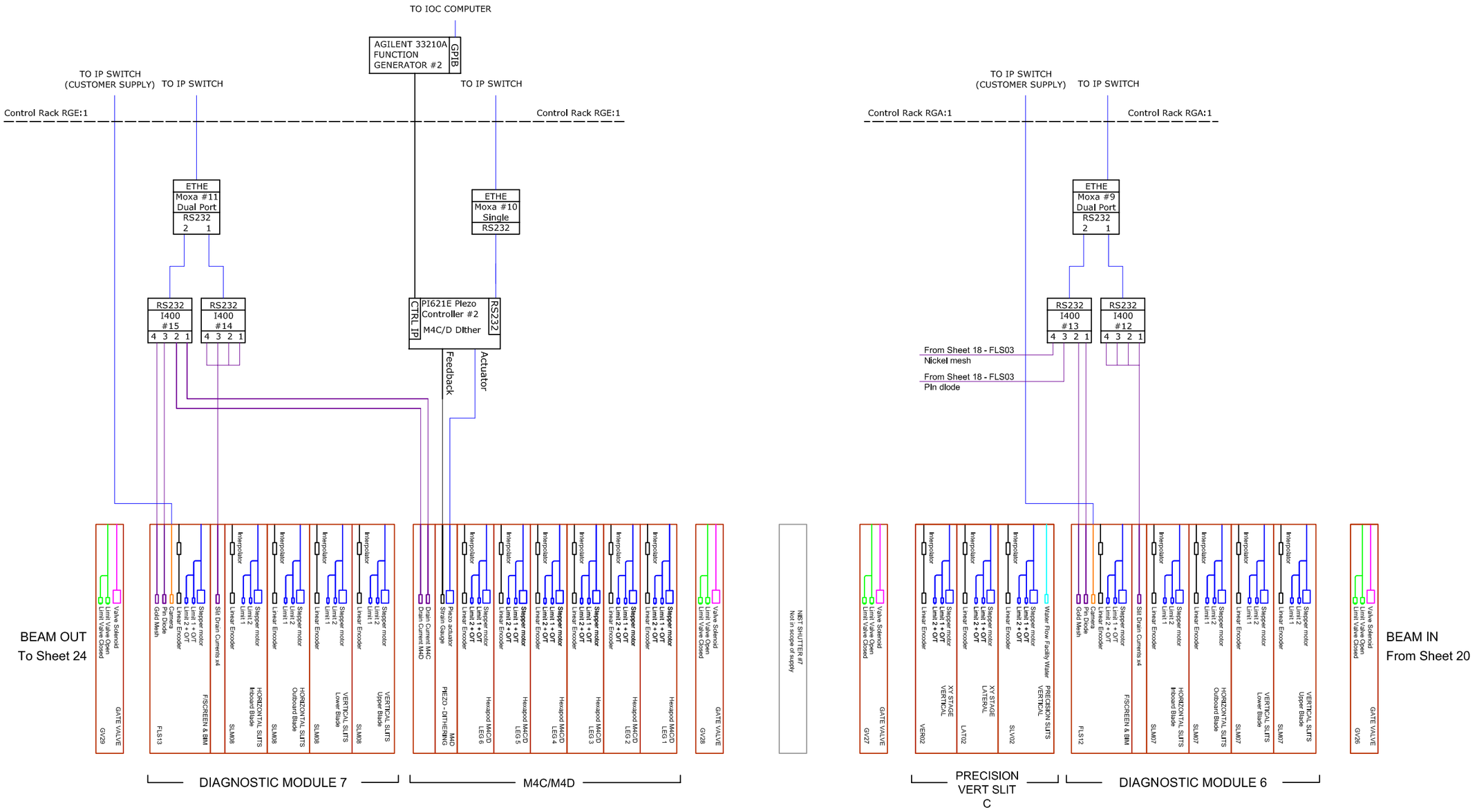

REV	DATE	DESCRIPTION/DMR No	DRN	CHKD
F	21/01/2015	PDR ISSUE	MKS	
G	07/07/2015	PRE FDR ISSUE	DJS	
H	13/08/2015	FDR ISSUE	DJS	

THIS DRAWING BELONGS TO FMB OXFORD LTD AND IS ISSUED ON CONDITION THAT IT IS NOT COPIED, REPRINTED OR DISCLOSED TO A THIRD PARTY WITHOUT PRIOR CONSENT IN WRITING FROM FMB OXFORD Ltd.

DRAWN D. Smith DATE 21/01/2015

CHECKED DATE

APPROVED DATE

FMB OXFORD LTD
UNIT 1 FERRY MILLS,
OSNEY MEAD, OXFORD, OX2 0ES.
ENGLAND

FMB Oxford

Title S3160 NIST SST BEAMLINE PID

Size A3 | Document Number CRP0469 | Rev H

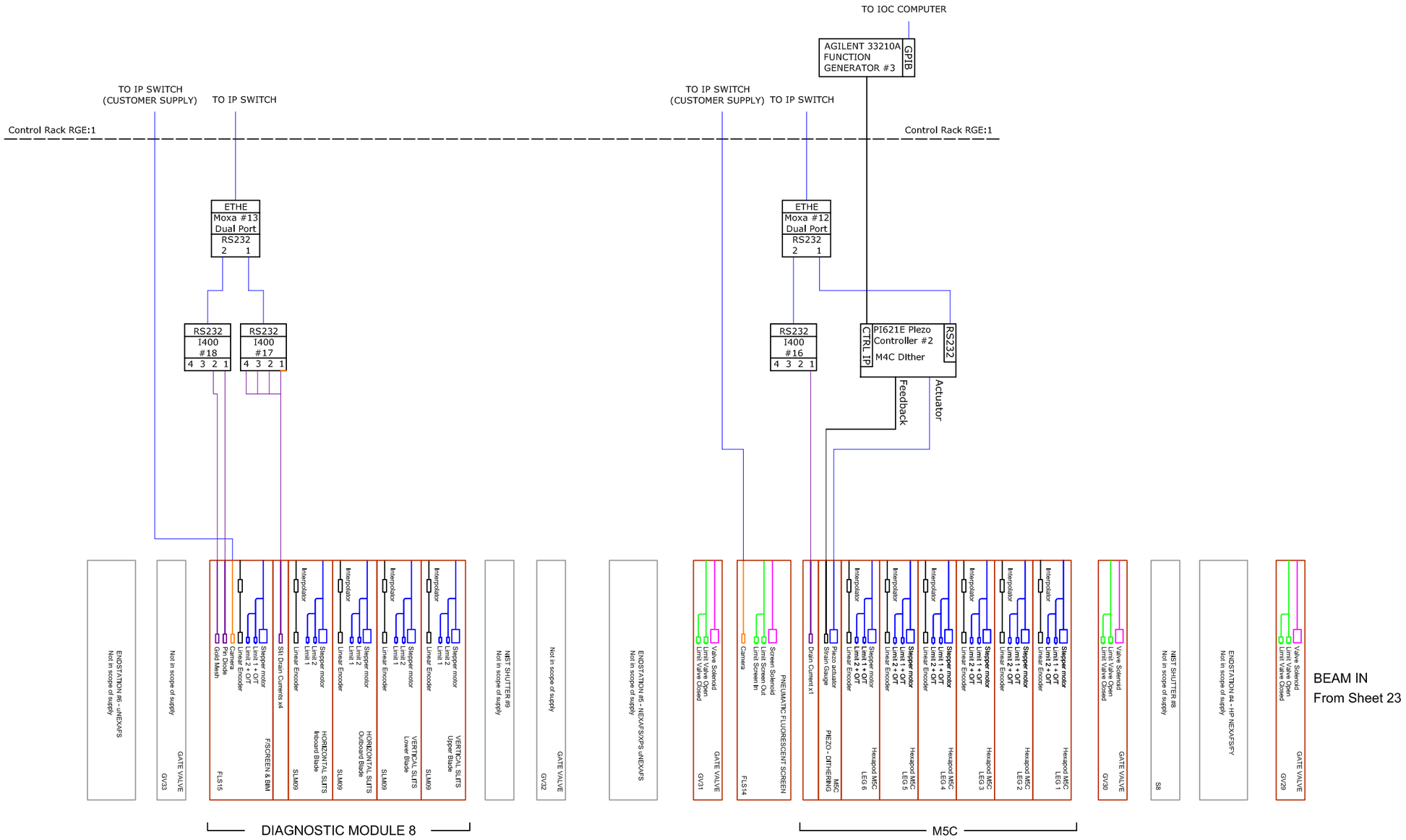

REV	DATE	DESCRIPTION/DMR No	DRN	CHKD
F	21/01/2015	PDR ISSUE	MKS	
G	07/07/2015	PRE FDR ISSUE	DJS	
H	13/08/2015	FDR ISSUE	DJS	

THIS DRAWING BELONGS TO FMB OXFORD LTD AND IS ISSUED ON CONDITION THAT IT IS NOT COPIED, REPRINTED OR DISCLOSED TO A THIRD PARTY WITHOUT PRIOR CONSENT IN WRITING FROM FMB OXFORD Ltd.

DRAWN D. Smith DATE 21/01/2015

CHECKED DATE

APPROVED DATE

FMB OXFORD LTD
UNIT 1 FERRY MILLS,
OSNEY MEAD, OXFORD, OX2 0ES.
ENGLAND

FMB Oxford

Title S3160 NIST SST BEAMLINE PID

Size A3 | Document Number CRP0469 | Rev H

Sheet 24 of 24

EXIT SLIT

FOR NIST-BEAMLINE @ NSLS-II

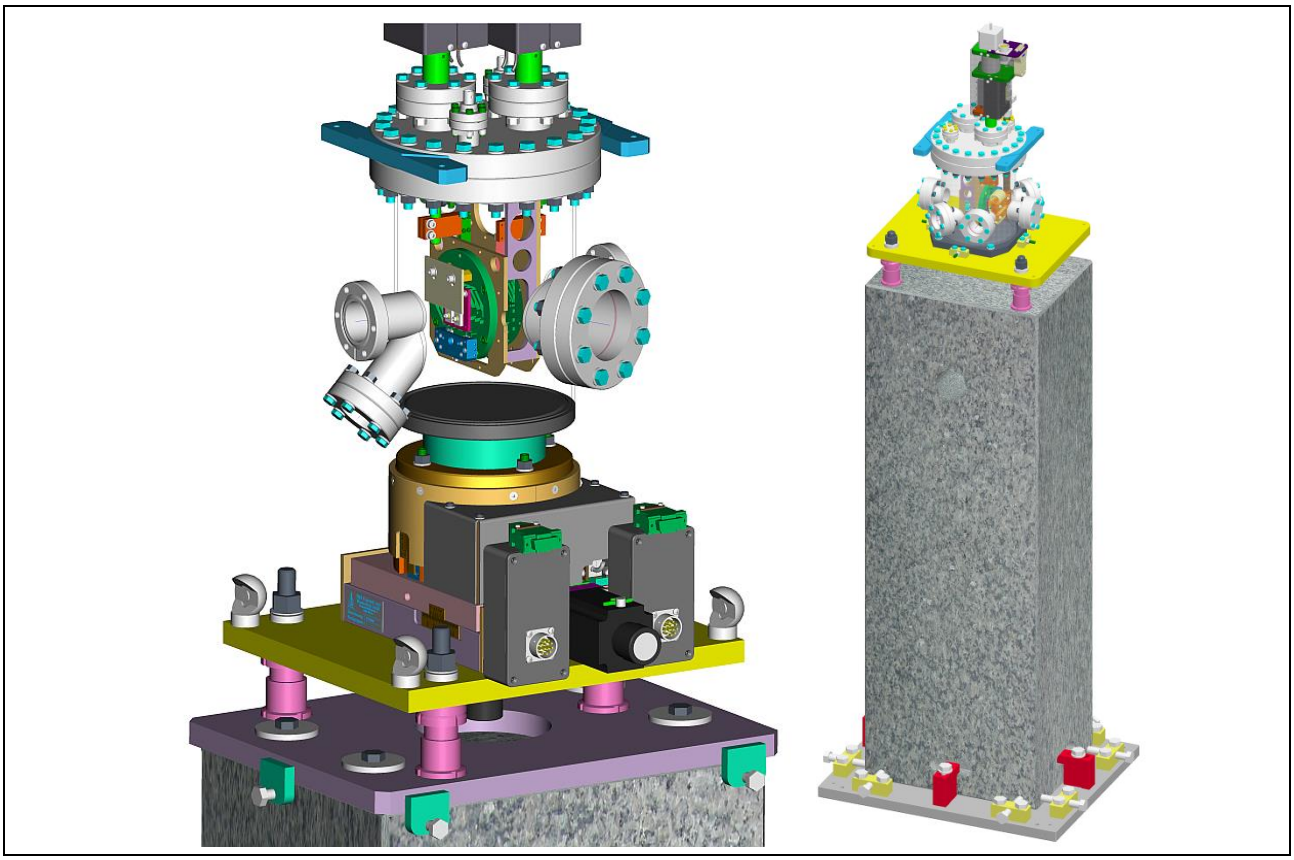

Project Number	***Project name***	***Author***
	Exit Slit for NIST-Beamline	Frieder MUELLER
	Customer	***Responsible contact***
	NIST	Dan FISHER

Issue	***Summary of change***	***Date***	***Approved***
01	Initial issue	29.04.2014	
02			
03			
04			

THIS DOCUMENT BELONGS TO FMB Feinwerk- und Meßtechnik GmbH AND IS ISSUED ON CONDITION THAT IT IS NOT COPIED, REPRINTED OR DISCLOSED EITHER WHOLLY OR IN PART TO A THIRD PARTY WITHOUT PRIOR CONSENT IN WRITING FROM FMB.

Table of Contents / Inhaltsverzeichnis *Page / Seite*

1 REFERRING DOCUMENTS 3

2 SYSTEM OVERVIEW 3

3 TECHNICAL SPECIFICATION 4

3.1 VACUUM CHAMBER 4

3.1.1 LIST OF PORTS AND FLANGE SIZES 4

3.2 PRECISION SLIT MECHANICS 5

3.3 SLIT BLADE GEOMETRY 6

3.4 PRECISION FEEDTHROUGH 6

3.5 EXIT SLIT SUPPORT 7

3.6 HORIZONTAL / VERTICAL STAGE 8

3.7 TECHNICAL DATA 9

3.8 VACUUM 10

4 INTERFACES 10

4.1 MECHANICAL INTERFACES 10

4.2 ELECTRICAL INTERFACE FOR DRAIN CURRENT MEASUREMENT 10

4.3 ELECTRICAL INTERFACE FOR STEPPER MOTOR 11

4.4 ELECTRICAL INTERFACE FOR TONIC-ENCODER INTERFACE (RENISHAW) 12

5 SCOPE OF SUPPLY 13

5.1 LIST OF COMPONENTS 13

5.2 FMB SCOPE OF SUPPLY 13

5.3 CUSTOMER SUPPLIED COMPONENTS / SERVICES 13

6 FACTORY TESTING 14

6.1 BAKEOUT AND VACUUM TESTING 14

6.2 HYDRAULIC TESTS 14

6.3 RESISTANCE/ISOLATION TESTS 14

6.4 MOTION TEST 14

6.5 METRICAL MEASUREMENT AND FIDUCIALIZATION 14

6.6 OPTICAL TEST 16

6.6.1 TEST PARAMETERS 16

7 DOCUMENTATION 17

THIS DOCUMENT BELONGS TO FMB Feinwerk- und Meßtechnik GmbH AND IS ISSUED ON CONDITION THAT IT IS NOT COPIED, REPRINTED OR DISCLOSED EITHER WHOLLY OR IN PART TO A THIRD PARTY WITHOUT PRIOR CONSENT IN WRITING FROM FMB.

1 REFERRING DOCUMENTS

Document	*Filename / Filedate*
Drawing-No.	…
Contract / Order-No.	…
FMB-B Project-No.	…

2 SYSTEM OVERVIEW

The exit slit unit contains a vertical defining slit mechanism mounted into a cylindrical vacuum chamber with a DN150CF top flange.

The precision slits mechanism is assembled on a NW150CF base flange. The slit blades of the shall be isolated in order to provide the possibility for drain current measurements.

The vacuum chamber shall be mounted on top of a granite column support, which allows to manually adjust the location of the slit in all 6 degrees of freedom.

Optionally a motorized X-Y-stage can be mounted between ganite support and vacuum chamber in order to allow a motorized horizontal and vertical motion.

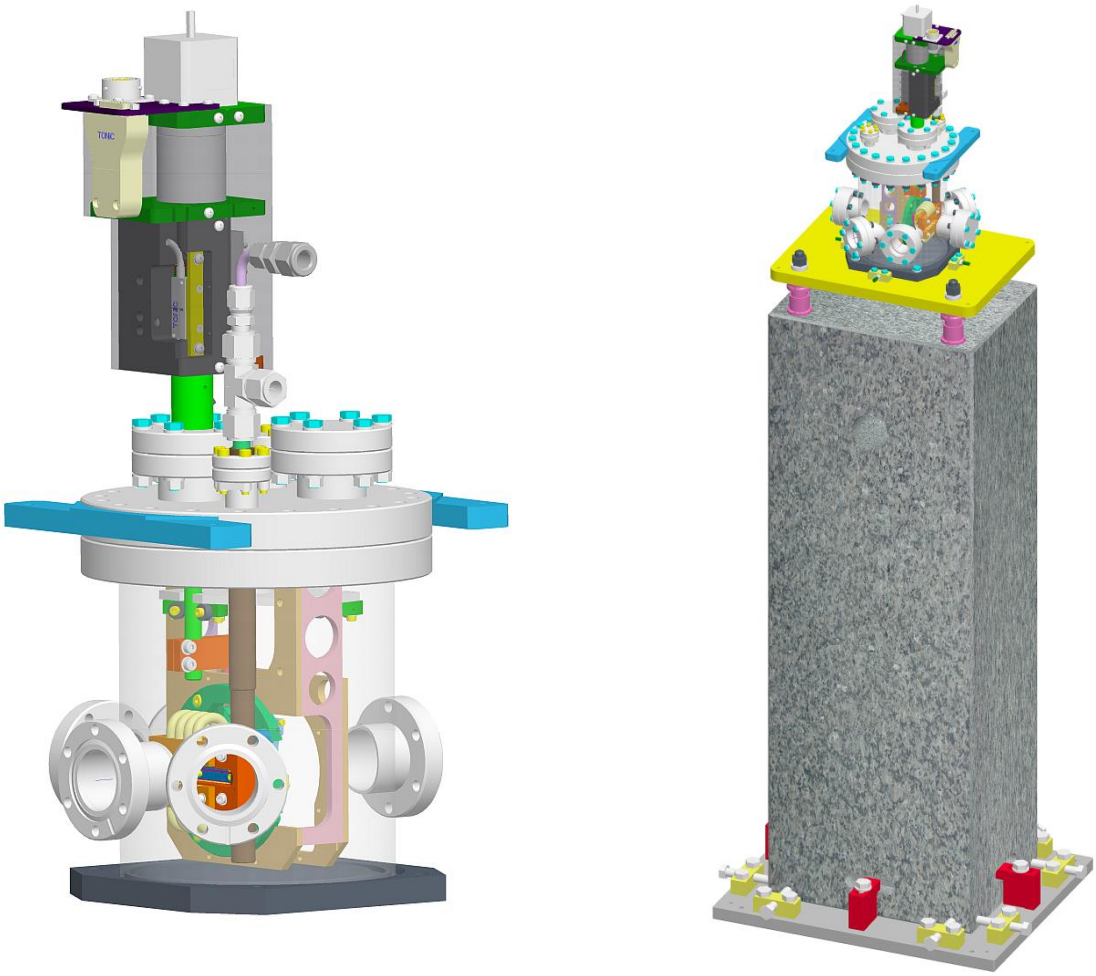

Figure 1: Example of an Exit slit (CSX-Beamline)

THIS DOCUMENT BELONGS TO FMB Feinwerk- und Meßtechnik GmbH AND IS ISSUED ON CONDITION THAT IT IS NOT COPIED, REPRINTED OR DISCLOSED EITHER WHOLLY OR IN PART TO A THIRD PARTY WITHOUT PRIOR CONSENT IN WRITING FROM FMB.

3 TECHNICAL SPECIFICATION

3.1 VACUUM CHAMBER

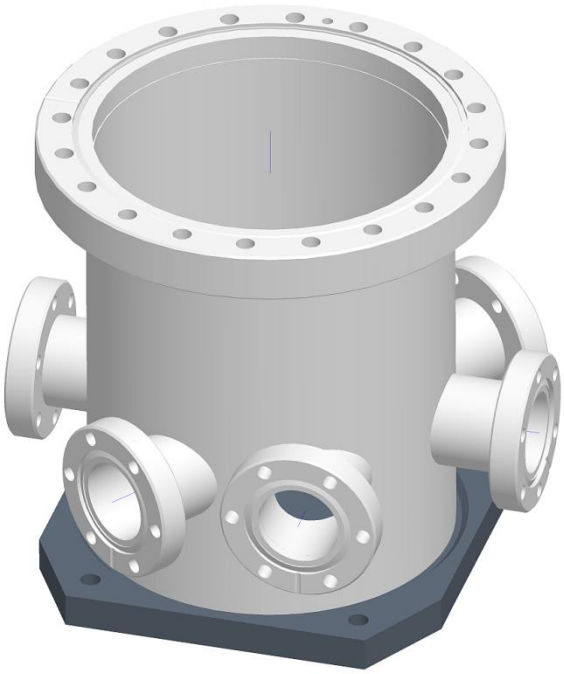

Figure 2: Exit slit vacuum chamber

The vacuum chamber has a DN150CF top flange for the h/v slit system. Beam-in and –out flanges are DN35CF.

One additional DN35CF-flange is equipped with a standard glass viewport for observation of the vertical defining slit gap and the fluorescence screen. Two other DN35CF-will be blanked off. They are to be used during the installation for surveying and alignment and will be later equipped by the customer with an angle valve and a vacuum gauge.

3.1.1 LIST OF PORTS AND FLANGE SIZES

Chamber part	***Port description***	***Type / nominal size***
Exit slit chamber	Beam entrance	DN35CF-F (in line)
	Beam exit	DN35CF-F (in line)
	Spare ports for surveying, vacuum gauge, angle valve	2x DN35CF (straddeled)
	Viewport	DN35CF (straddeled)
	Top flange for slit system	DN150CF

THIS DOCUMENT BELONGS TO FMB Feinwerk- und Meßtechnik GmbH AND IS ISSUED ON CONDITION THAT IT IS NOT COPIED, REPRINTED OR DISCLOSED EITHER WHOLLY OR IN PART TO A THIRD PARTY WITHOUT PRIOR CONSENT IN WRITING FROM FMB.

3.2 PRECISION SLIT MECHANICS

The main part of the precision slit mechanism is a solid body made of a Titanium-alloy which allows a play free and symmetrical motion of both slit blades. It is driven through a lever system by one linear vacuum feedthrough. The vacuum feedthrough is motorized, has one in-air linear encoder and high-precise limit switches. The connection between the linear feedthrough and the slit mechanism is made by a leaf spring. This allows a backlash and playfree action by pulling the slit wider but allows to protect the slit system from closing too far. An adjustable vacuum side hard stop allows to protect the slit blades from any damage.

The gear ratio of the flexible joint slit drive is optimized to be a nearly linear 1:1 movement between 0mm and 1mm slit gap. A 2:1 lever system works as reduction gearbox and allows the assembling of the linear feedthrough on top of the base flange as well as a drive with solely pulling force.

The slit system is mounted on a DN150CF base flange. The slit blades of the vertical defining slit shall be mounted electrically isolated on the drive mechanism. Both blades will be connected to a electrical BNC grounded shield vacuum feedthrough. It shall allow to measure the drain currents on the left and the right blade separately.

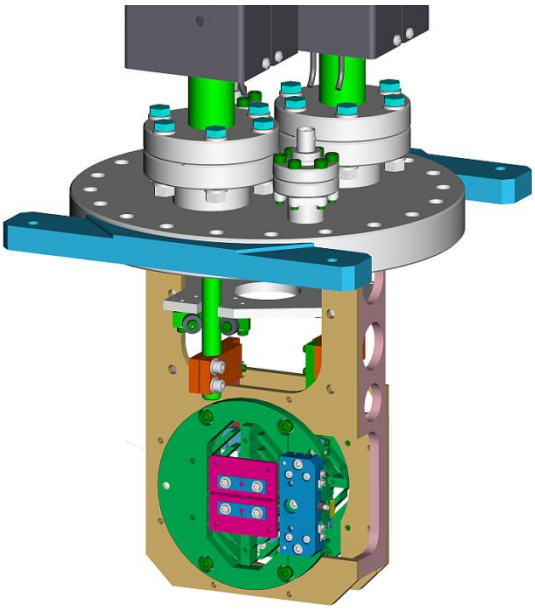

Figure 3: Precision slit slit system shown from the upstream side (Example picture with photo current measurement)

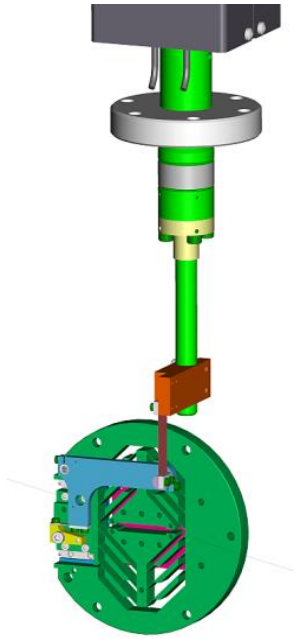

Figure 4: Precision slit drive and lever system shown from the downstream side.

THIS DOCUMENT BELONGS TO FMB Feinwerk- und Meßtechnik GmbH AND IS ISSUED ON CONDITION THAT IT IS NOT COPIED, REPRINTED OR DISCLOSED EITHER WHOLLY OR IN PART TO A THIRD PARTY WITHOUT PRIOR CONSENT IN WRITING FROM FMB.

3.3 SLIT BLADE GEOMETRY

The slit blades are made from Tungsten Alloy.

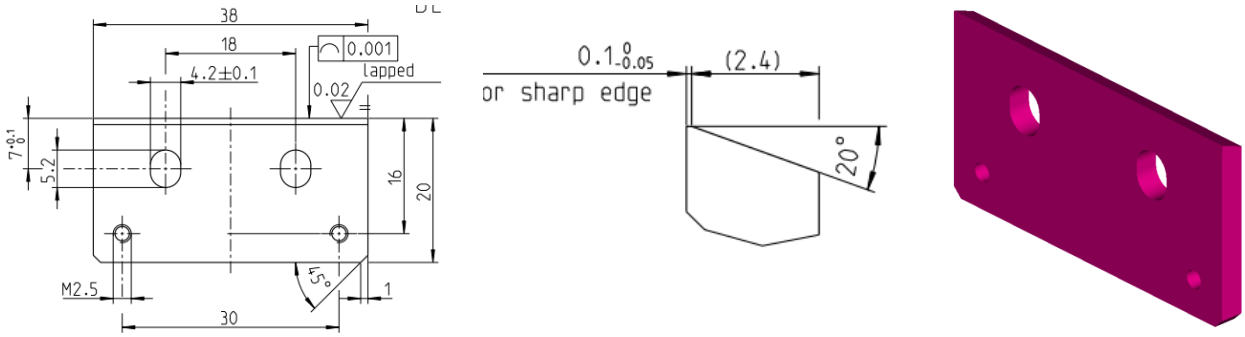

Figure 5: Geometrical dimensions of the slit blades and detail of the blade edge geometry

3.4 PRECISION FEEDTHROUGH

The precision feedthrough is a stepper motor driven linear feedthrough. It contains a harmonic drive geabox, a fine thread spindle drive, incremental linear encoder from RENISHAW and highly precise limit switches. The linear movement is compensated by a vacuum thight welded bellows system. The mounting flange size is DN35CF.

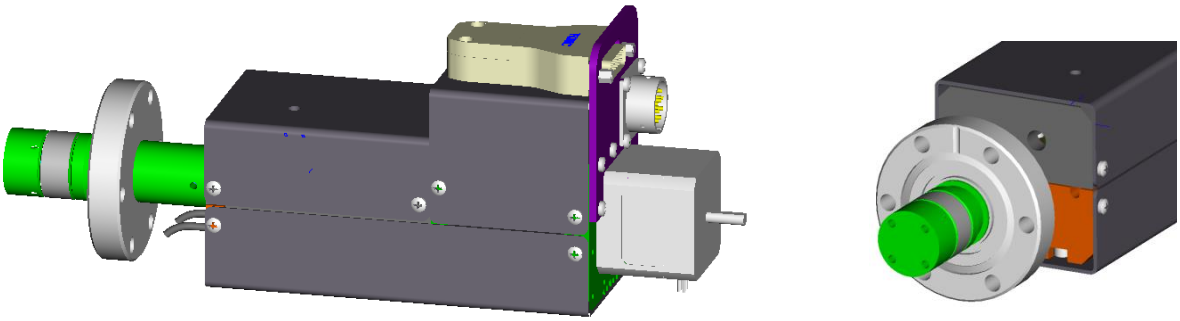

Figure 6: Motorized linear precision vacuum feedthrough

THIS DOCUMENT BELONGS TO FMB Feinwerk- und Meßtechnik GmbH AND IS ISSUED ON CONDITION THAT IT IS NOT COPIED, REPRINTED OR DISCLOSED EITHER WHOLLY OR IN PART TO A THIRD PARTY WITHOUT PRIOR CONSENT IN WRITING FROM FMB.

3.5 EXIT SLIT SUPPORT

Figure 7: Exit slit support with floor plate and granite column

The exit slit assembly is standing on its own support. To get the lowest possible thermal expansion and best possible vibration properties, the support will be made of a granite block. For the floor link FMB will deliver a steel plate which is to be glued to the concrete floor of the experimental hall.

This floor plate shall be adjusted horizontally and in the correct height before grouting with 3 thread bolts. When aligned, the gap between the bottom surface and the concrete floor shall be filled with epoxy resin. Finally the granite block is clamped with several clamps to the floor plate. The horizontal adjustment of the granite column can be done with side pushing bolts before it is fixed in position with the clamps.

On top of the granite column a steel plate reste on three height adjusters. The slit chamber will be bolted to that plate and can be fine adusted laterally and longitudinally on that plate with the help of side pushing bolts.

Counter nuts allow to fix the slit chamber in the adjusted position.

THIS DOCUMENT BELONGS TO FMB Feinwerk- und Meßtechnik GmbH AND IS ISSUED ON CONDITION THAT IT IS NOT COPIED, REPRINTED OR DISCLOSED EITHER WHOLLY OR IN PART TO A THIRD PARTY WITHOUT PRIOR CONSENT IN WRITING FROM FMB.

3.6 HORIZONTAL / VERTICAL STAGE

The stage can be offered optionally in case a motorized vertical and horizontal motion is needed.

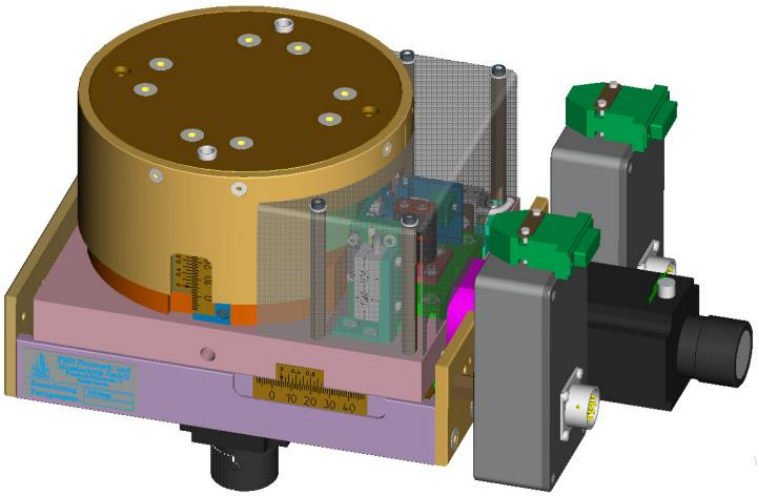

The horizontal / vertical stage provides a two axis motorized movement of the vacuum chamber mounted on top.

It is a proven design already used in a lot of synchrotron facilities together with FMB's X-blade beam position monitors.

Figure 8: horizontal/vertical stage with encoders

Parameter	***Dimension***
Vertical stroke	± 5 mm
Horizontal lateral stroke	± 5 mm
Resolution (stepper)	1.25 µm/halfstep
Resolution (encoder)	1 µm
Acurracy with encoder	±1 µm

THIS DOCUMENT BELONGS TO FMB Feinwerk- und Meßtechnik GmbH AND IS ISSUED ON CONDITION THAT IT IS NOT COPIED, REPRINTED OR DISCLOSED EITHER WHOLLY OR IN PART TO A THIRD PARTY WITHOUT PRIOR CONSENT IN WRITING FROM FMB.

3.7 TECHNICAL DATA

Parameter	***Specified Value***
Drive	Stepper motor 1.8° full step = 200steps/rev. Oriental PK244-01B
Holding torque	0.33Nm (stepper only without gearbox)
Step angle (full step drive)	1.8°/200 steps/rev
Driving current	0.85A/Phase (bipolar Series)
No. of ½ steps/revolution	400
Gear Ratio	1:50
Gearbox	Harmonic Drive PMG-11°-50-M-SP (solid wavegenerator 5H7)
Spindle	M8x1mm
Lever	2:1
	1 mm gap = 2 mm lever stroke = 2 spindle turns = 100 stepper turns = 20000 fullsteps 1 fullstep = 0.05 µm gap width 1 fullstep = 0.1 µm encoder count
Stroke (Slit gap)	0..2 mm symmetrically opening
Stepper resolution	0.2 µm / fullstep
Repeatability	≤ 1 µm (typical measurements are in the range between 0.5 µm and 1 µm)
Position measurement system	Renishaw incremental encoder TONiC T1001-05A Renishaw encoder interface TONiC Ti0200-E04A (0.1µm/4MHz/all References/Tri-State Alarm)
Encoder resolution	0.1 µm (@feedthrough stroke) 0.05 µm (@slit gap)
Limit switches	1 limit switch per limit, normally closed Metrol precision switch PT5S1CB
Blade material	Tungsten Alloy (Density 17.5)
Blade edge length	≥ 20 mm
Blade thickness	≥ 2.5 mm
Thickness at blade edge	≤ 0.1 mm
Blade rearside rake angle	10°
Edge straightness & roughness	≤ 1 µm
Slit gap parallelism	≤ 1 µm / 20 mm

THIS DOCUMENT BELONGS TO FMB Feinwerk- und Meßtechnik GmbH AND IS ISSUED ON CONDITION THAT IT IS NOT COPIED, REPRINTED OR DISCLOSED EITHER WHOLLY OR IN PART TO A THIRD PARTY WITHOUT PRIOR CONSENT IN WRITING FROM FMB.

3.8 VACUUM

The components are designed, manufactured, cleaned and tested to guarantee UHV conditions:

***Technical data*[*1)]**	
Helium leak rate:	≤ 2 x 10^{-10} mbar·l/s
Base pressure:	≤ 8 x 10^{-10} mbar
Baking temperature:	≤ 200 °C The precision feedhrough drive must not be baked!
[*1)] The given values are to be measured after baking without beam.	

4 INTERFACES

4.1 MECHANICAL INTERFACES

Interface	**Description**	**Type / nominal size**
Beam in	Fixed flange	DN35CF-F (in line)
Beam out	Fixed flange	DN35CF-F (in line)
Photo current measurement	2x BNC grounded shield	DN16CF / BNC
Surveying	fiducial holes for Hubbs sperical target mounts or similar	4 x ¼”H7 (6.35H7)
Floor	Floor plate to be grouted to the floor	See drawing 900-22-01-01

4.2 ELECTRICAL INTERFACE FOR DRAIN CURRENT MEASUREMENT

Connector-type: BNC grouded shield feedthrough welded into NW16CF flange

No	***Signal***		***Connector***
center pin	drain current		BNC grounded shield
shield	chamber ground		

THIS DOCUMENT BELONGS TO FMB Feinwerk- und Meßtechnik GmbH AND IS ISSUED ON CONDITION THAT IT IS NOT COPIED, REPRINTED OR DISCLOSED EITHER WHOLLY OR IN PART TO A THIRD PARTY WITHOUT PRIOR CONSENT IN WRITING FROM FMB.

4.3 ELECTRICAL INTERFACE FOR STEPPER MOTOR

Stepper motor type: see spec. above
Limit switches: normally closed type – switching against common ground
Connector: Souriau UTO 12-pin male

Machined contacts shall be used in all connectors. The contact size shall be Souriau #16. The contact wire connection size shall be appropriate for the wire size. Part numbers for the contacts currently in use are in the following table. Crimp connectors shall be used wherever possible.

Cable size (AWG/mm^2)	Pin contact	Socket contact
18/0.75 (motor cores)	RM16M23K	RC16M23K
22/0.25 (limit switch cores)	RM20M12K	RC20M12K

Letter	*No*	*Signal*	*Color*	
A	1		n/c	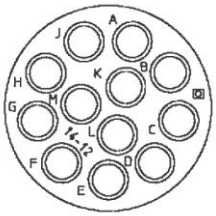 14-12
B	2	Phase A+		
C	3	Phase A-		
D	4	Phase B+		
E	5	Phase B-		
F	6		n/c	
G	7	CW (+) limit (NC)		
H	8	CCW (-) limit (NC)		
J	9		n/c	
K	10		n/c	
L	11	+24V limit switch supply		
M	12		n/c	

Limit and home switches operate with shared voltage supply or return (Pin K, L or M).

The rotation sense is defined by viewing from the rear of the motor towards the shaft. Clockwise running motor shaft means a positive movement (see also NSLS-2 Beamline Systems Instrumentation Interfacing Standard chapter 3.1).

A clockwise / positive running motor will close the slit gap.

THIS DOCUMENT BELONGS TO FMB Feinwerk- und Meßtechnik GmbH AND IS ISSUED ON CONDITION THAT IT IS NOT COPIED, REPRINTED OR DISCLOSED EITHER WHOLLY OR IN PART TO A THIRD PARTY WITHOUT PRIOR CONSENT IN WRITING FROM FMB.

4.4 ELECTRICAL INTERFACE FOR TONIC-ENCODER INTERFACE (RENISHAW)

No	*Signal for (+ cw) clockwise motor operation*	*Color*	**Connector: D-Sub 15-pin male**
1	X (Einstellung)		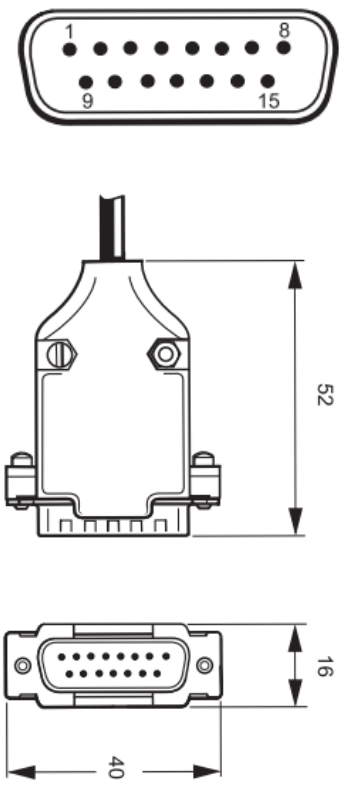
2	0V (U_B)		
3	Alarm		
4	Z- (Reference mark)		
5	B- (Incremental Signal)		
6	A- (Incremental Signal)		
7	+5V (U_B)		
8	+5V (Sense)		
9	0V (Sense)		
10	Q (Limit)	not applicable	
11	P (Limit)	not applicable	
12	Z+ (Reference mark)		
13	B+ (Incremental Signal)		
14	A+ (Incremental Signal)		
15	Inner shield	not connected	
Case	Outer shield	outer shield	

The encoder head counts +(positive) when it is moved in the direction towards the cable.
The encoder head counts +(positive) when the slit gap opens.

FMB-Berlin uses incremental Encoders from Renishaw (TONiC). Their pinout cannot be changed in the encoder connector, because the interpolation electronics is mounted inside the D-Sub connector. The PCB of the interpolator is soldered directly to the D-Sub connector. To translate the RENISHAW pinout to the NSLS-2 Encoder pinout (shown below) the field cable need to translate the pinout.

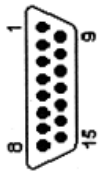

Pin	Encoder feedback
Pin 1	Ch A+
Pin 2	Ch A-
Pin 3	Ch B+
Pin 4	Ch B-
Pin 5	Ch C+
Pin 6	Ch C-
Pin 7	Encoder power (5 V)
Pin 8	Encoder power (0 V)
Pin 9	Commutation Input U/Stepper Direction +
Pin 10	Commutation Input V/Stepper Direction -
Pin 11	Commutation Input W/Stepper Pulse +
Pin 12	Commutation Input T/Stepper Pulse -
Pin 13	Resolver Excitation +
Pin 14	Encoder Power (5 V)
Pin 15	Resolver Excitation - / Encode power (0 V)

THIS DOCUMENT BELONGS TO FMB Feinwerk- und Meßtechnik GmbH AND IS ISSUED ON CONDITION THAT IT IS NOT COPIED, REPRINTED OR DISCLOSED EITHER WHOLLY OR IN PART TO A THIRD PARTY WITHOUT PRIOR CONSENT IN WRITING FROM FMB.

5 SCOPE OF SUPPLY

5.1 LIST OF COMPONENTS

Quantity	*Component*	*Supplier & Type*
1	Floor plate (to be grouted to the floor with epoxy)	FMB-B
1	Granite column support with lateral adjustment and 3 WASI height adjusters	FMB-B
1	Cylindrical vacuum chamber (see ports list)	FMB-B
1	Vertical defining precision slit on a base flange DN150CF	FMB-B
1	Water cooling finger with two cooling braids for cooling the slit blades	FMB-B
2	Tungsten carbide blades	FMB-B
1	Fluorescence screen to be mounted 1mm below the beam height	FMB-B

5.2 FMB SCOPE OF SUPPLY

- Delivery of the hardware listed in the component list
- Factory testing
- Delivery to site
- Documentation

5.3 CUSTOMER SUPPLIED COMPONENTS / SERVICES

Not included in FMB-B' s scope of supply are:

- Grouting of the floor plate
- On site installation and media connection
- Field cabling
- Motion control hardware
- Hot beam Commissioning

THIS DOCUMENT BELONGS TO FMB Feinwerk- und Meßtechnik GmbH AND IS ISSUED ON CONDITION THAT IT IS NOT COPIED, REPRINTED OR DISCLOSED EITHER WHOLLY OR IN PART TO A THIRD PARTY WITHOUT PRIOR CONSENT IN WRITING FROM FMB.

6 FACTORY TESTING

The components shall be tested at FMB before shipment. Full specifications and procedures shall be prepared in advance. These shall be submitted to the customer for information. Customer representatives may witness these tests at FMB's workshop.

6.1 BAKEOUT AND VACUUM TESTING

The component will be baked and vacuum tested at FMB prior to shipment. Smaller components will be tested together in one group. Vacuum testing shall include total pressure measurement and RGA scan.

6.2 HYDRAULIC TESTS

The cooling circuit will be tested for the following parameters:

- Water leak tightness (cooling water pressure drop over time)
- Water flow rate

6.3 RESISTANCE/ISOLATION TESTS

The resistance/isolation of electrical contacts for current measurements will be measured between the pin of the electrical feedthrough and the corresponding slit blade.

6.4 MOTION TEST

In the motion test each linear feedthrough shall be moved through the full stroke.
The following parameters shall be tested and recorded:

- Function of steppers and all limit switches
- Linear stroke/range
- Resolution
- Reference (home) position of the encoder with reference to the functional position e.g. blade edge on beam axis or zero gap

6.5 METRICAL MEASUREMENT AND FIDUCIALIZATION

The component is fitted with fiducials as mentioned in the interfaces chapter. The fiducials define the datum of the system and the active position of the component.

The offset distances between the beam axis / chamber center and the fiducial hole(s) are measured with a CMM and the coordinates (X, Y and Z) are reported.

THIS DOCUMENT BELONGS TO FMB Feinwerk- und Meßtechnik GmbH AND IS ISSUED ON CONDITION THAT IT IS NOT COPIED, REPRINTED OR DISCLOSED EITHER WHOLLY OR IN PART TO A THIRD PARTY WITHOUT PRIOR CONSENT IN WRITING FROM FMB.

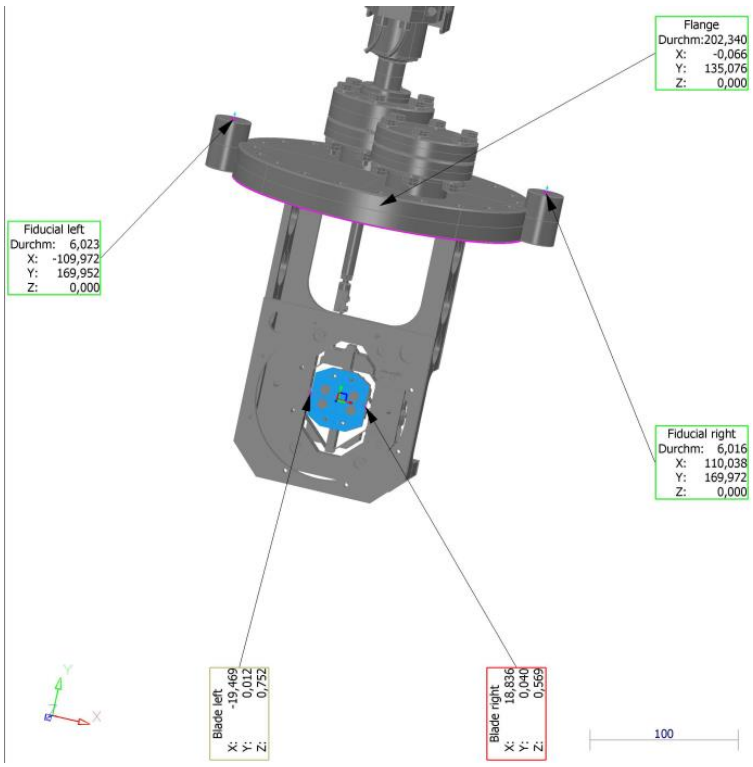

Figure 9: Example of a fiducialisation measurement report

THIS DOCUMENT BELONGS TO FMB Feinwerk- und Meßtechnik GmbH AND IS ISSUED ON CONDITION THAT IT IS NOT COPIED, REPRINTED OR DISCLOSED EITHER WHOLLY OR IN PART TO A THIRD PARTY WITHOUT PRIOR CONSENT IN WRITING FROM FMB.

6.6 OPTICAL TEST

The slit shall be testet for it's optical properties using a visible laser. The diffraction pattern projected by the laser to a screen shall be measured for different slit gaps.

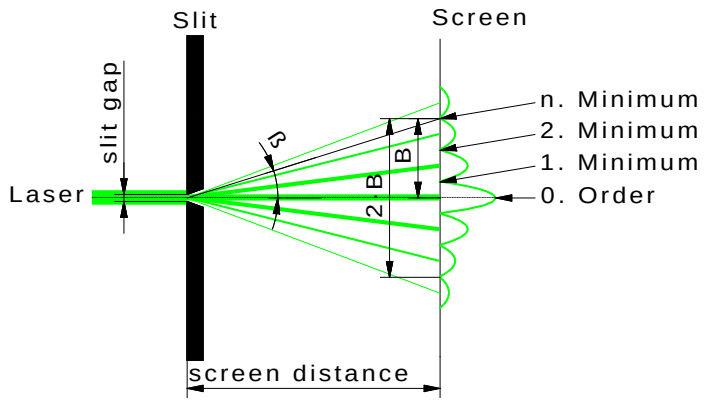

Figure 10: principle of measurement setup

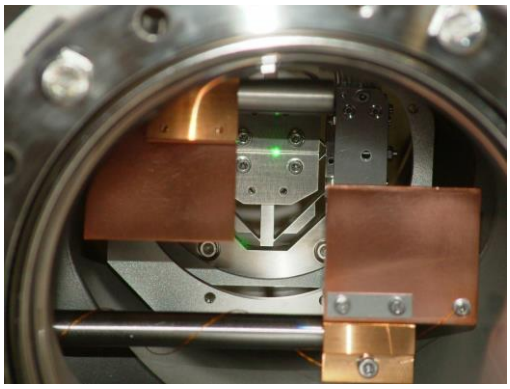

Figure 11: Laser spot on the precision slit blades

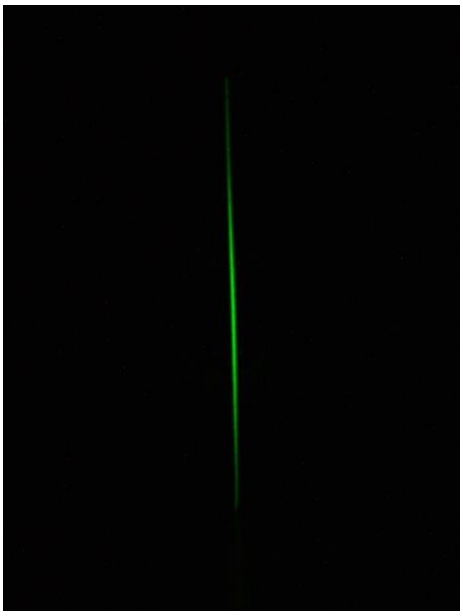

Figure 12: Example of a diffraction pattern @12.5µm slit gap

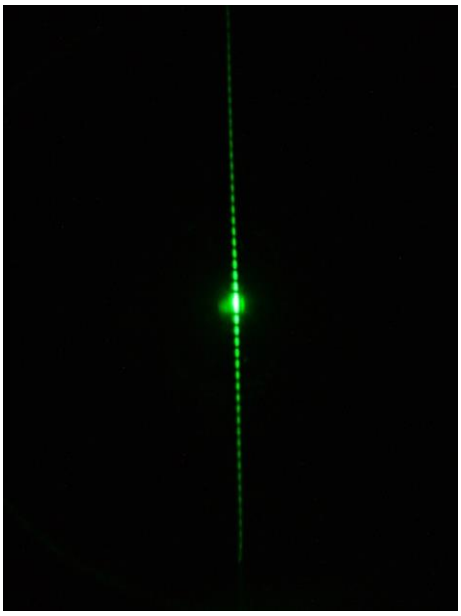

Figure 13: Example of a diffraction pattern @125µm slit gap

6.6.1 TEST PARAMETERS

Parameter	value
Distance slit to screen	2000mm
Wavelength green Diode-Laser	534.5nm

THIS DOCUMENT BELONGS TO FMB Feinwerk- und Meßtechnik GmbH AND IS ISSUED ON CONDITION THAT IT IS NOT COPIED, REPRINTED OR DISCLOSED EITHER WHOLLY OR IN PART TO A THIRD PARTY WITHOUT PRIOR CONSENT IN WRITING FROM FMB.

7 DOCUMENTATION

The component shall be designed, manufactured and tested to the agreed specification and drawings. All FMB documentation shall be written in English. Material certification will not be provided if not stated otherwise.

- General arrangement/assembly drawings of the systems shall be provided.
- Testing procedures and results shall be provided.

THIS DOCUMENT BELONGS TO FMB Feinwerk- und Meßtechnik GmbH AND IS ISSUED ON CONDITION THAT IT IS NOT COPIED, REPRINTED OR DISCLOSED EITHER WHOLLY OR IN PART TO A THIRD PARTY WITHOUT PRIOR CONSENT IN WRITING FROM FMB.

PLANE GRATING MONOCHROMATOR

FOR THE NIST BEAMLINE

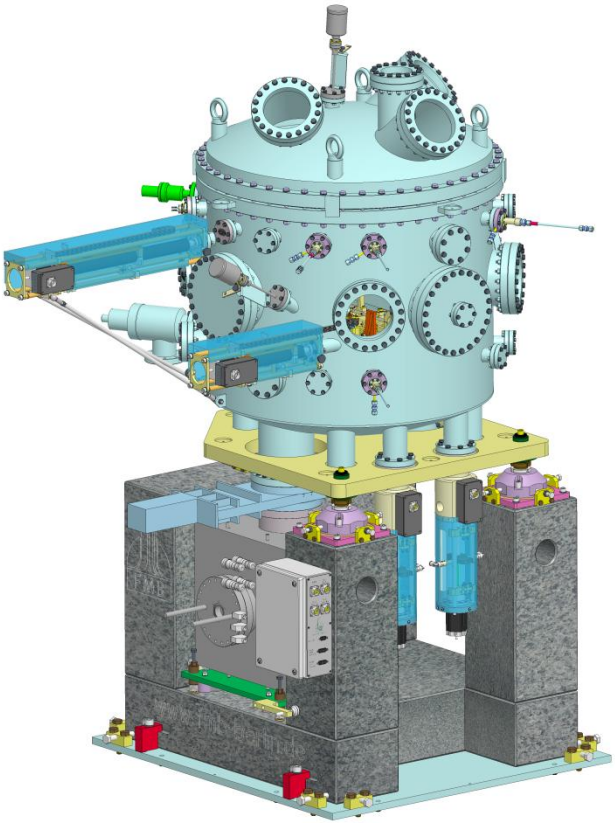

Project Number	***Project name***	***Author***
20080444	NIST PGM	Michael Roschka
	Customer	***Responsible contact***
	BNL	Daniel A. Fischer

Issue	***Summary of change***	***Date***	***Approved***
01	Initial issue for design review	31.03.2015	M. Roschka

THIS DOCUMENT BELONGS TO FMB Feinwerk- und Meßtechnik GmbH AND IS ISSUED ON CONDITION THAT IT IS NOT COPIED, REPRINTED OR DISCLOSED EITHER WHOLLY OR IN PART TO A THIRD PARTY WITHOUT PRIOR CONSENT IN WRITING FROM FMB.

Table of Contents / Inhaltsverzeichnis Page / Seite

1 REFERRING DOCUMENTS 3

2 SYSTEM OVERVIEW 3

2.1 LIST OF COMPONENTS 4

3 TECHNICAL SPECIFICATION 5

3.1 PHYSICAL PROPERTIES 5

3.2 MAIN DIMENSIONS 5

3.3 SUPPORT SYSTEM 5

3.4 PGM SETUP PARAMETERS 5

3.5 MECHANICAL PERFORMANCE 6

3.6 MIRROR AND GRATING PARAMETERS 7

3.7 ZERO ORDER MASK 7

3.8 DRIVE PARAMETERS 7

3.9 TEMPERATURE MEASUREMENT 8

3.10 WATER COOLING 8

3.11 VACUUM 9

4 INTERFACES 9

4.1 MECHANICAL INTERFACES 9

4.2 ELECTRICAL INTERFACES 10

4.2.1 ELECTRICAL INTERFACE FOR STEPPER MOTORS 11

4.2.2 ELECTRICAL INTERFACE FOR INCREMENTAL ENCODER (RENISHAW) 11

4.2.3 ELECTRICAL INTERFACE FOR SINUSOIDAL ENCODER (HEIDENHAIN) 12

4.2.4 ELECTRICAL INTERFACE FOR INTERLOCK 12

4.2.5 ELECTRICAL INTERFACE FOR THERMOCOUPLE 12

5 FACTORY TESTING 13

5.1 HYDRAULIC TESTS 13

5.2 ELECTRICAL TESTS 13

5.3 METRICAL MEASUREMENT AND FIDUCIALIZATION 13

5.4 MOTION TEST 14

5.5 BAKEOUT AND VACUUM TESTING 14

6 DOCUMENTATION 14

THIS DOCUMENT BELONGS TO FMB Feinwerk- und Meßtechnik GmbH AND IS ISSUED ON CONDITION THAT IT IS NOT COPIED, REPRINTED OR DISCLOSED EITHER WHOLLY OR IN PART TO A THIRD PARTY WITHOUT PRIOR CONSENT IN WRITING FROM FMB.

1 REFERRING DOCUMENTS

Document	*Filename / Filedate*
Customer technical specification	SB1341-08-RQ-0191
FMB technical description	TB-NIST-NSLS-VLSPGM-Rel1-080417
Updated specification of the optics	-
Purchase Order / Contract	SB134108SU0722

2 SYSTEM OVERVIEW

The function of the Plane Grating Monochromator (PGM) is to select and transmit radiation of the desired photon energy from an incident white synchrotron radiation beam. The principle set-up is pictured in figure 1:

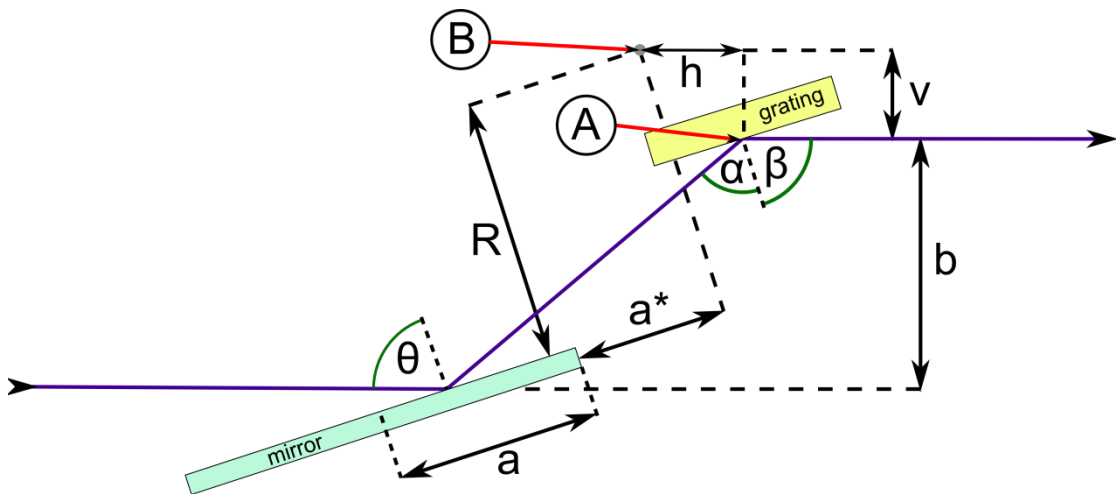

Figure 1: Principle set-up of a PGM

The incident white beam enters the monochromator (left-hand side) and hits the mirror with an angle θ. The reflected beam strikes the grating at point **A** with an angle of incidence α. The beam is diffracted and interference of the diffracted outgoing waves effects a spatial separation of waves with different wavelengths. One of these suchlike generated monochromatised beams escapes with a diffraction angle β. The angles θ, α, β are measured with respect to the optical elements surface normal. The monochromatic exit beam runs parallel to the incident white beam with a constant beam offset **b**. The energy will be selected by rotating the mirror and /or the grating and so by varying the angles θ, α, β. The axis of rotation for the grating is located in **A** on the grating surface. The axis of rotation for the mirror is located in **B** at some distance from the mirror. The position of **B** is specified by **v, h** with respect to **A**. **R** names the distance between **B** and the mirror surface, projected on an axis normal to the mirror surface. **a** is half the length of the mirror. **a*** is the distance between the mirror end side and an axis parallel to the mirror normal running through **B**, projected on an axis parallel to the mirror surface.

THIS DOCUMENT BELONGS TO FMB Feinwerk- und Meßtechnik GmbH AND IS ISSUED ON CONDITION THAT IT IS NOT COPIED, REPRINTED OR DISCLOSED EITHER WHOLLY OR IN PART TO A THIRD PARTY WITHOUT PRIOR CONSENT IN WRITING FROM FMB.

2.1 LIST OF COMPONENTS

Component		
PGM		
Quantity	***Sub- assembly/Subcomponent***	***Supplier***
1	Granite support	FMB
1	Vacuum chamber	FMB
1	Mirror / grating high precision mechanism	FMB
2	Motorized vertical working linear drives for mirror and grating pitch	FMB
2	Motorized horizontal lateral linear drive for grating exchange and mirror translation	FMB
2	Manual drives for mirror ROLL and grating alignment	FMB
1	Patch panel box for electrical connections	FMB
1	Optical element: Mirror	NSLS
4	Optical element: Gratings	NSLS
1	Ion getter pump with TSP	FMB
1	Angle valve	FMB
1	Rough vacuum gauge system	FMB
1	UHV vacuum gauge system	FMB

THIS DOCUMENT BELONGS TO FMB Feinwerk- und Meßtechnik GmbH AND IS ISSUED ON CONDITION THAT IT IS NOT COPIED, REPRINTED OR DISCLOSED EITHER WHOLLY OR IN PART TO A THIRD PARTY WITHOUT PRIOR CONSENT IN WRITING FROM FMB.

3 TECHNICAL SPECIFICATION

3.1 PHYSICAL PROPERTIES

Parameter description	*Data*
Energy range	50 eV up to 3000 eV
Distance to source	-

3.2 MAIN DIMENSIONS

Parameter description	*Data*
Height / direction of incoming beam	1400 mm / horizontal
Height / direction of out-going beam	1415 mm / horizontal
Support area (granite support)	960 x 880 (length x width) mm²
Operational area	1200 x 1700 (length x width) mm²
Height	2200 mm
Weight	approx. 2000 kg

3.3 SUPPORT SYSTEM

Description	*Parameter*	*Data*
Floor plate	thickness	20 kg
	weight	200 kg
Granite support	lateral bore diameter	70 mm
	weight	approx. 900 kg
3D adjustment foot	stroke lateral / vertical	± 15 mm, resolution 0,01 mm
	pitch, roll, yaw	± 2°, resolution 5 arcsec

3.4 PGM SETUP PARAMETERS

Description *(see figure 1)*	***Param.***	***Data***
Mirror axis horizontal offset	h	-0,005 mm (upstream grating axis)
Mirror axis vertical offset	v	7,625 mm
Mirrors plane distance	R	15,141 mm
Mirror mounting distance	a*	20 mm
Beam offset	b	15 mm
Mirror angular range	$\theta_{(range)}$	1° ..-11° with reference to incoming beam (and horizontal plane)
Grating angular range	$\beta_{(range)}$	1° .. -14° with reference to incoming beam (and horizontal plane)

THIS DOCUMENT BELONGS TO FMB Feinwerk- und Meßtechnik GmbH AND IS ISSUED ON CONDITION THAT IT IS NOT COPIED, REPRINTED OR DISCLOSED EITHER WHOLLY OR IN PART TO A THIRD PARTY WITHOUT PRIOR CONSENT IN WRITING FROM FMB.

3.5 MECHANICAL PERFORMANCE

Parameter description		*Data*
No. of available grating positions		4
Parallelism mirror axis / grating axis		≤ 5 arcsec
Grating pitch		
Limit switch positions		adapted to achieve grating angular range
Resolution		≤ 0.02 arcsec
Position accuracy		≤ 0.2 arcsec
Repeatability		≤ 0.2 arcsec
Grating lateral translation		
Range		about 222 mm
Resolution		≤ 1 µm
Repeatability	lateral	≤ ± 100 µm
	pitch / roll / yaw	≤ 0,2 / 0,2 / 1 arcsec
Mirror pitch		
Limit switch positions		adapted to achieve mirror angular range
Resolution		≤ 0.02 arcsec
Position accuracy		≤ 0.2 arcsec
Repeatability		≤ 0.2 arcsec
Mirror translation		
Range		60 mm
Resolution		≤ 1 µm
Manual grating alignment in vacuum		
Height range / Height resolution		± 1.0 mm / ≤ 1 µm
Angular range / Angular resolution		
Pitch		± 0,25° / ≤ 5 arcsec
Roll		± 0,25° / ≤ 5 arcsec
Yaw		± 0,25° / ≤ 5 arcsec
Manual mirror alignment in air		
Height range / Height resolution		± 1.0 mm / ≤ 1 µm
Angular range / Angular resolution		
Pitch		± 1° / ≤ 5 arcsec
Roll		± 1° / ≤ 5 arcsec
Manual mirror alignment in vacuum		
Angular range / Angular resolution		
Roll		± 3° / ≤ 5 arcsec

THIS DOCUMENT BELONGS TO FMB Feinwerk- und Meßtechnik GmbH AND IS ISSUED ON CONDITION THAT IT IS NOT COPIED, REPRINTED OR DISCLOSED EITHER WHOLLY OR IN PART TO A THIRD PARTY WITHOUT PRIOR CONSENT IN WRITING FROM FMB.

3.6 MIRROR AND GRATING PARAMETERS

Optical element	*Parameter*	*Data*
Mirror (intrinsic water cooled)	Outer dimensions	350 x 55 x 70 mm³ (lenght x width x height)
	Optical footprint	-
	Material / coating	silicon / -
	Slope error	0.2 arcsec meridional, 2 arcsec sagittal
	Roughness	-
Gratings: (4 gratings side cooled provided)	Outer dimensions	T-shape - 150 x 40 x 30(45) mm³ (lenght x height x wide)
	Optical footprint	-
	Material / coating	silicon
	Slope error:	0.2 arcsec meridional , 2 arcsec sagittal
	Roughness	-
	Side surface flatness	-

3.7 ZERO ORDER MASK

The PGM is equipped with a watercooled Zero Order Stop at the exit flange. The Zero Order Stop has not adjustable blades.

3.8 DRIVE PARAMETERS

Drive	*Component*	*Parameter*	*Value*
Grating and Mirror Pitch	Stepper motor	Full steps per revolution	200
	Spindle	Thread pitch	2 mm
	Gear box	Gear ratio	50:1
Horizontal grating transfer	Stepper motor	Full steps per revolution	200
	Spindle	Thread pitch	1,5 mm
	Motor coupling	Gear ratio	1:1

THIS DOCUMENT BELONGS TO FMB Feinwerk- und Meßtechnik GmbH AND IS ISSUED ON CONDITION THAT IT IS NOT COPIED, REPRINTED OR DISCLOSED EITHER WHOLLY OR IN PART TO A THIRD PARTY WITHOUT PRIOR CONSENT IN WRITING FROM FMB.

3.9 TEMPERATURE MEASUREMENT

Application	*Position*	*Type*
Mirror temperature	One for Mirror	Thermocouple type K, feedthrough flange DN 35 CF, miniature TC male connector
Grating temperature	One for each grating	Thermocouple type K, feedthrough flange DN 35 CF, miniature TC male connector

3.10 WATER COOLING

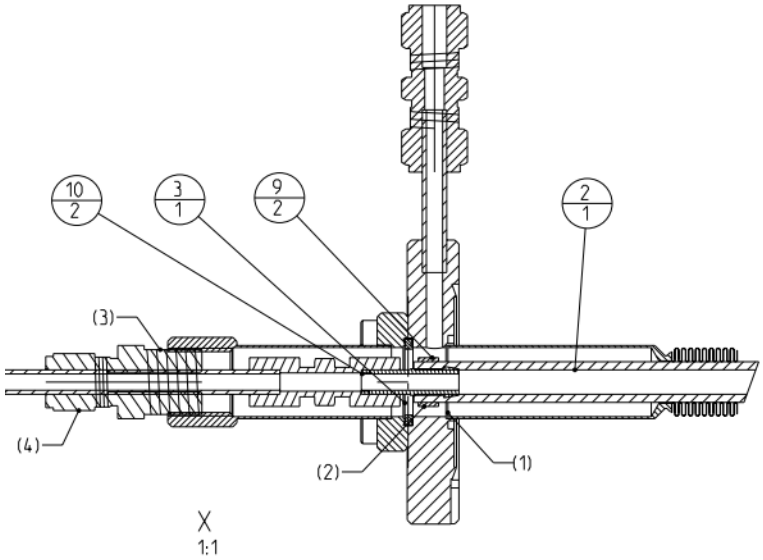

Figure 2: Air side connection of water cooling and guard vacuum at the vacuum feedthrough

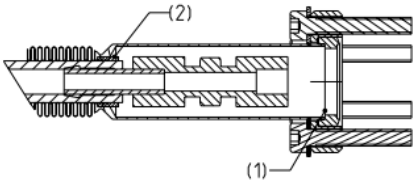

Figure 3: Vacuum side connection of water cooling and guard vacuum

Medium	demineralized water
Maximum allowed water pressure	6 bar
Maximum pressure drop	2 bar
Recommended water supply temperature	22°C
Recommended water flow rate	2 l/min
Smallest water cooling tube size	ø6x1

THIS DOCUMENT BELONGS TO FMB Feinwerk- und Meßtechnik GmbH AND IS ISSUED ON CONDITION THAT IT IS NOT COPIED, REPRINTED OR DISCLOSED EITHER WHOLLY OR IN PART TO A THIRD PARTY WITHOUT PRIOR CONSENT IN WRITING FROM FMB.

3.11 VACUUM

The components are designed, manufactured, cleaned and tested to guarantee UHV conditions:

Parameter	***Specified Value*** *1)*
Helium leak rate:	≤ 2 x 10^{-10} mbar·l/s
base pressure:	≤ 8 x 10^{-10} mbar
Baking temperature:	≤ 110 °C
*1) The given values are to be measured after baking and cooling without beam.	

All general design and manufacturing requirements for UHV components are standard at FMB.

The vacuum joints are metal sealed using CF gaskets made of OFHC copper. For water cooled components no direct water-to-vacuum joints are allowed. In vacuum water cooling connections are enclosed by guard vacuum bellows.
The internal and external surfaces of the vacuum vessels are glass ball blasted.

4 INTERFACES

4.1 MECHANICAL INTERFACES

Interface	***Description***	***Type / nominal size***
Floor mounting	Floor plate will be grouted directly on to the floor	Floor plate Drw.-No. 356-03-02 Distance to the foor is 10mm
Surveying	Holes and plane surfaces for surveying targets	4 x hole 6 H7 at upper chamber flange 6 x hole 6 H7 at each extension tower Drw.-No. 356-01-08-00
	Alignment pins	-
Water cooling	SWAGELOK connector for	2x Tube Ø 8x1 (mirror) 2x Tube Ø 6x1 (gratings
Guard vacuum	SWAGELOK connector for	4x Tube Ø 6x1 (gratings & mirror)
Beam in	Fixed flange	NW40CF
Beam out	Fixed flange	NW40CF
Ion getter pump	Fixed flange	NW150CF
Angle valve	Fixed flange	NW63CF
Rough vacuum gauge	Fixed flange	NW35CF, blanked off
UHV vacuum gauge	Fixed flange	NW35CF, blanked off

THIS DOCUMENT BELONGS TO FMB Feinwerk- und Meßtechnik GmbH AND IS ISSUED ON CONDITION THAT IT IS NOT COPIED, REPRINTED OR DISCLOSED EITHER WHOLLY OR IN PART TO A THIRD PARTY WITHOUT PRIOR CONSENT IN WRITING FROM FMB.

4.2 ELECTRICAL INTERFACES

Axis/Device name	Qty.	Unit	Description	Connector Type
Baking	1	Top lid heater	110V AC, 1513W,	CEE 7/7
Baking	1	Vessel heater	110V AC, 1921W,	CEE 7/7
Pitch drive	1/1	Stepper and limit switches	Oriental PK268-03B and 2x2 limit switch n/c	UTO 12-pin male
Grating / Mirror transfer	1/1	Stepper and limit switches	Oriental PK268-03B and 2x2 limit switch n/c	UTO 12-pin male
Pitch drive	1	Collision contact between grating and mirror pitch	contact opens at smallest allowed approximation	D-Sub 9 male
Grating / Mirror transfer	2/2	Decoupling contact	contact closed when grating transfer is in operation both contacts must be open before grating pitch operates	
Pitch drive	1/1	Multi-head incremental angular encoder	Heidenhain RON 905 -36000 MR4X00, 40IP00 UH-Vakuum	4 x D-Sub 15 female
Grating / Mirror transfer	1/1	Incremental linear Encoder	Renishaw - RGH24X15D00A	D-Sub 15pin male
Temperature	1	Mirror	Thermocouple type K	Miniature TC flat pin connector
Temperature	4	Gratings	Thermocouple type K	Miniature TC flat pin connector
Ion pump	1	with TSPC and 110V heater	GammaVacuum 600LX-DI-8P-SC-110-TSPC	
Rough vacuum gauge/ UHV gauge	1/1	Pirani gauge Cold Cathode Gauge	MKS317 MKS455	

THIS DOCUMENT BELONGS TO FMB Feinwerk- und Meßtechnik GmbH AND IS ISSUED ON CONDITION THAT IT IS NOT COPIED, REPRINTED OR DISCLOSED EITHER WHOLLY OR IN PART TO A THIRD PARTY WITHOUT PRIOR CONSENT IN WRITING FROM FMB.

4.2.1 ELECTRICAL INTERFACE FOR STEPPER MOTORS

Stepper motor type: See specification in 4.2

Limit switches: normally closed type – switching against common ground

Pin	*Signal for +cw (clockwise) motor operation*	*Connector*
A		Souriau UTO 12-pin male - or compatible 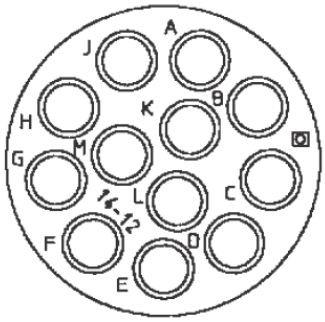
B	Phase A+	
C	Phase A-	
D	Phase B+	
E	Phase B-	
F		
G	Cw (+) limit (NC)	
H		
J	Ccw (-) limit (NC)	
K	Overtravel	
L		
M	Ground	

The rotation sense is defined by viewing from the rear of the motor towards the shaft.

4.2.2 ELECTRICAL INTERFACE FOR INCREMENTAL ENCODER (RENISHAW)

Encoder type: see spec. above

Pin	*Signal*	*Connector*
1	+5 V U_P	D-Sub 15-pin female 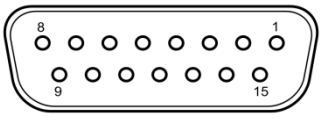
2	0 V U_N	
3	I_1 +	
4	I_1 -	
5		
6	I_2 +	
7	I_2 -	
8		
9	+5 V sensor	
10	I_0 +	
11	0 V sensor	
12	I_0 -	
13	Inner shield	
14, 15		
Case	Outer shield	

THIS DOCUMENT BELONGS TO FMB Feinwerk- und Meßtechnik GmbH AND IS ISSUED ON CONDITION THAT IT IS NOT COPIED, REPRINTED OR DISCLOSED EITHER WHOLLY OR IN PART TO A THIRD PARTY WITHOUT PRIOR CONSENT IN WRITING FROM FMB.

4.2.3 ELECTRICAL INTERFACE FOR SINUSOIDAL ENCODER (HEIDENHAIN)

Encoder type: see spec. above

Pin	*Signal*	*Connector*
1	+5 V U_P	D-Sub 15-pin female 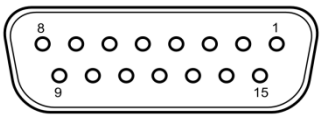
2	0 V U_N	
3	I_1 +	
4	I_1 -	
5		
6	I_2 +	
7	I_2 -	
8		
9	+5 V sensor	
10	I_0 +	
11	0 V sensor	
12	I_0 -	
13	Inner shield	
14, 15		
Case	Outer shield	

4.2.4 ELECTRICAL INTERFACE FOR INTERLOCK

Pin	*Signal*	*Connector*
1	Collision switch	D-Sub 9-pin male 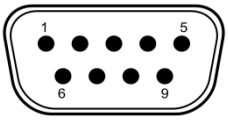
2	Decoupling grating	
3	Decoupling mirror	
4, 5		
6	Common ground	
7, 8, 9		
Case	Outer shield	

4.2.5 ELECTRICAL INTERFACE FOR THERMOCOUPLE

Pin	*Signal*	*Connector*
+	TC + type K (Chromel ®)	Miniature TC flat pin male 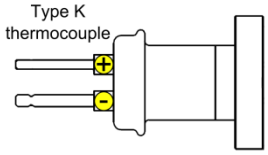
-	TC – type K (Alumel ®)	

THIS DOCUMENT BELONGS TO FMB Feinwerk- und Meßtechnik GmbH AND IS ISSUED ON CONDITION THAT IT IS NOT COPIED, REPRINTED OR DISCLOSED EITHER WHOLLY OR IN PART TO A THIRD PARTY WITHOUT PRIOR CONSENT IN WRITING FROM FMB.

5 FACTORY TESTING

The components shall be tested at FMB before shipment. Full specifications and procedures shall be prepared in advance. These shall be submitted to the customer for information. Customer representatives may witness these tests at FMB's workshop.

5.1 HYDRAULIC TESTS

The cooling circuit will be tested for the following parameters:

- Water leak tightness (cooling water pressure drop over time)
- Water flow rate

5.2 ELECTRICAL TESTS

Electrical tests of the component contain the following:

- Continuity check of all cable connections
- Isolation dielectric tests on cables and electrical components
- Functional check of limit switches, decoupling contacts and collision switch
- Functional check of encoders
- Functional check of motors
- Functional check of thermocouples

5.3 METRICAL MEASUREMENT AND FIDUCIALIZATION

The component is prepared for the adaption of fiducials as mentioned in 4.1.
The fiducials together with the FMB measuring protocol:
measurement-report-pgm-axes-chamber_02_07_2010.pdf
can be used to define the position of the optical elements axes and the beam entrance/exit flange.

THIS DOCUMENT BELONGS TO FMB Feinwerk- und Meßtechnik GmbH AND IS ISSUED ON CONDITION THAT IT IS NOT COPIED, REPRINTED OR DISCLOSED EITHER WHOLLY OR IN PART TO A THIRD PARTY WITHOUT PRIOR CONSENT IN WRITING FROM FMB.

5.4 MOTION TEST

In the motion test each linear feedthrough shall be moved through the full stroke.
The following parameters shall be tested and recorded:

- Function of steppermotors, encoders and limit switches
- Linear and angular range
- Reference (home) position of the encoders with reference to the beam axis
- Resolution, backlash, repeatability of horizontal and vertical drives

5.5 BAKEOUT AND VACUUM TESTING

The component will be baked and vacuum tested at FMB prior to shipment. Vacuum testing shall include total pressure measurement and RGA scan.

6 DOCUMENTATION

The component shall be designed, manufactured and tested to the agreed specification and drawings. All FMB documentation shall be written in English. Material certification will not be provided if not stated otherwise.The documentation includes:

- A user manual of the mechanism shall be written and supplied to the customer.
- General arrangement/assembly drawings of the systems shall be provided.
- Testing procedures and results shall be provided.

THIS DOCUMENT BELONGS TO FMB Feinwerk- und Meßtechnik GmbH AND IS ISSUED ON CONDITION THAT IT IS NOT COPIED, REPRINTED OR DISCLOSED EITHER WHOLLY OR IN PART TO A THIRD PARTY WITHOUT PRIOR CONSENT IN WRITING FROM FMB.

1. NIST SST DCM Burst Disk Sizing

Assumption: Burst Disc diameter must be sufficient to allow gaseous nitrogen to exit the vessel with a resulting pressure drop no greater than 0.5 bar/7.25 psi

$Q_n := 4.5 \cdot \frac{l}{min}$	$Q_n = 0.075 \ \frac{l}{s}$	Volume flow rate of liquid nitrogen into vessel
$\rho_n := 808 \cdot kg \cdot m^{-3}$		Density of liquid nitrogen
$m_n := \rho_n \cdot Q_n$	$m_n = 0.061 \ \frac{kg}{s}$	Mass flow rate of liquid nitrogen
$Q_{ng} := 646.46 \cdot Q_n$ $Q_{ng} = 102.733 \ \frac{ft^3}{min}$	$Q_{ng} = 48.485 \ \frac{l}{s}$	Assumption that all of the liquid expands in one second. Liquid nitrogen expands by 646.5 times when changing from liquid to gas at atmoshperic pressure.
$D_b := 40 \cdot mm$		Burst disc diameter (when burst) - DN40.
$A_d := \pi \cdot \frac{D_b^2}{4}$	$A_d = 1256.6 \ mm^2$	Burst disc area
$P_u := 1.5 \cdot bar$		Upstream pressure - absolute
$\Delta P := 0.5 \cdot bar$		Allowable pressure differential between vessel and atmosphere
$\rho_{ng} := 1.25 \cdot \frac{kg}{m^3}$		Gaseous nitrogen density
$C_f := 0.6$		Flow coefficient for gaseous nitrogen. Constant for Cv calculation
$Q_{bd} := C_f \cdot A_d \cdot \left(\frac{2 \cdot \Delta P}{\rho_{ng}}\right)^{0.5}$ $Q_{bd} = 451.869 \ \frac{ft^3}{min}$	$Q_{bd} = 213.258 \ \frac{l}{s}$	Volumetric flow rate through burst disc given pressure differential. See http://www.efunda.com/formulae/fluids/calc_orifice_flowmeter.cfm#calc

Need to check that the volumetric flow rate that the burst disk can handle (Qbd) is greater than the rate at which gaseous nitrogen is supplied (Qng).

Need to also confirm that the predicted flow rate that the burst disc can handle matches the manufacturers data sheet (below) - in this case 336 SCFM.

Created with PTC Mathcad Express. See www.mathcad.com for more information.

MDC
MDC VACUUM PRODUCTS

Roughing components

New

- Flanges and fittings
- Gate, inline and angle valves
- Roughing components
- Vacuum measurement
- Viewports and glass components
- Feedthroughs: electrical and optical
- Motion and manipulation
- Thin film deposition
- Chambers
- Custom engineering

UHV LP Burst Disk

Featuring

- ISO 4126-2 Certified
- Differential pressure relief range: 345 mbar – 483 mbar @ 25°C
- Leak tight to 1 x 10^{-9} mbar l/s of Helium
- 316 Stainless steel body and disk membrane
- Bakeable to 350°C
- Compact design with no moving parts
- Calculated flow rates:
  - 79 SCFM on DN16CF flange assembly
  - 336 SCFM on DN40CF flange assembly

As the burst disk has been designed to always rupture below the **pressure equipment directive** (PED) threshold of 0.5 barg (7.25 psig) at room temperature, it does not require CE marking.

Reserve your copy of our extensive vacuum components catalogue **on our website.**

www.mdcvacuum.co.uk

United Kingdom
MDC Vacuum Limited
Tel: +44 (0)1825 280 450
Fax: +44 (0)1825 280 440
sales@mdcvacuum.co.uk

France
MDC Vacuum Products Sarl
Tel: +33 (0)437 65 17 50
Fax: +33 (0)437 65 17 55
info@mdcvacuum.fr

Germany
MDC Vacuum Limited
Tel: +49 (0)2305 947 508
Fax: +49 (0)2305 947 510
sales@mdcvacuum.de

Holland
Evatec Process Systems BV
Tel: +31 343 595 470
Fax: +31 343 592 294
sales@mdcvacuum.nl

Italy
Kenosistec Srl
Tel: +39 02 9055200
Fax: +39 02 9052984
infocaburn@kenosistec.it

Russian Federation
MSH Technology Limited
Tel: +7 (495) 543 60 25
Fax: +7 (495) 722 12 90
shive@msht.ru

Created with PTC Mathcad Express. See www.mathcad.com for more information.

Low pressure relief system

UHV LP Burst Disk

New

Burst disks

MDC burst disks are designed as a safety device to protect vacuum systems against over-pressurisation during back-fill or from an accidental increase in pressure due to a system malfunction. UHV LP Burst disk burst disks feature all-metal stainless steel construction and are designed for use in UHV applications.

Application

Most vacuum vessels are designed and constructed with internal vacuum joints and welds that are rated for an external load of one atmosphere. They are not pressure vessels and as such should not be subjected to positive pressure loads. For this purpose MDC has developed a new line of UHV LP Burst disk burst disks to prevent the accidental pressurising of a vacuum vessel. MDC burst disks are offered with either DN16CF or DN40CF Del-Seal™ (CF style) metal seal flange connections. They can be fitted to any vacuum system where over pressurisation is a concern.

Improved design

Low pressure burst disks have been re-engineered to be ISO 4126-2 compliant. They are constructed with a frustum designed metal membrane which is capable of sustaining a vacuum load. As pressure inside a vacuum vessel reaches 483 mbar the disk membrane activates and fully opens, relieving the pressure in the system. The disk membrane is circular scored preventing fragmenting upon rupture and thus does not pose harm to local personnel or equipment. Once activated, the disk is not reusable and must be replaced to restore the vessel to an operational condition.

UHV LP Burst Disk

Minimum differential burst pressure data

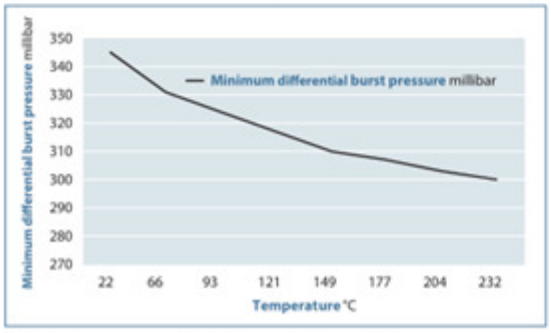

All dimensions are nominal in millimetres unless specified.

UHV LP Burst Disk

Features

- Diferential pressure relief range: 345 mbar – 483 mbar @ 25°C
- Leak tight to 1 x 10-9 mbar l/s of Helium
- 316 Stainless steel body and disk membrane
- Bakeable to 350°C
- Compact design with no moving parts
- Calculated flow rates:
  - 79 SCFM on DN16CF flange assembly
  - 336 SCFM on DN40CF flange assembly

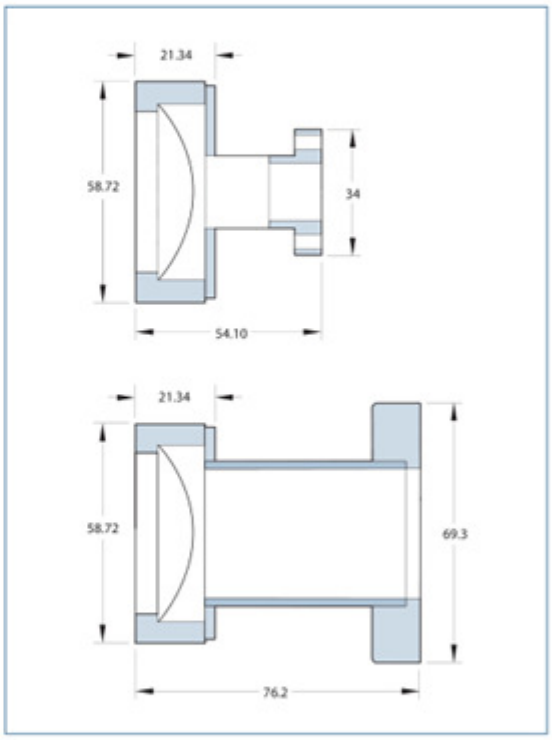

Description	Reference	Part number	£	€
Low pressure burst disk DN16CF	LP-BDA-133	**420035**	429	498

Description	Reference	Part number	£	€
Low pressure burst disk DN40CF	LP-BDA-275	**420036**	498	508

For further information on these or any other MDC product, contact your nearest sales office.

Telephone +44 (0)1825 280 450 **www.mdcvacuum.co.uk**

MDC

Created with PTC Mathcad Express. See www.mathcad.com for more information.

Reference Documents:

Reference Number	Date/ Issue	Title
SB1341-14-CN-0042	19/09/14	NIST Contract
	April 2014	NIST NSLS-II SST and BMM Beamline Backbones, Volume 2A, SST Technical Proposal
S3160	Nov 2014/REV 01	NIST SST BEAMLINE S3160 QUALITY PLAN
DOCM0110	June 2014	I400 4-Channel Digital Electrometer User Manual
-	Feb 2015, rev 03	Nano Beam Positioning Monitor User Manual
LT-C-XFD-STD-BL-COORD-001	May 2011	Beamline Coordinate System Standards
-	-	S3160 NIST SST Beamline Functional Specification
-	-	S3160 NIST SST Beamline Control and Software

FMB Oxford
Osney Mead
Oxford OX2 0ES
UK

Contact: Andrew Fairley
Telephone: +44 (0)1865 320 313
Fax: +44 (0)1865 320 301
E-mail: andrew.fairley@fmb-oxford.com

Change log:

Revision	Date	Summary of Change	Approval
1.0	23/03/15	First Issue	RG
2.0	17/08/15	Photodiode intensity monitor to place photodiode directly into beam. Scattering foil removed. NanoBPM removed from DM1. Additional diagnostic modules specified.	AJF
3.0			
4.0			
5.0			

TABLE OF CONTENTS **1**

1. *INTRODUCTION* **3**

1.1 AXIS 3

2. *SPECIFICATIONS* **4**

2.1 DIAGNOSTIC MODULE LOCATIONS 4

3. DIAGNOSTIC MODULE COMPONENTS **13**

3.1 4 BLADE IN-FLANGE SLITS 13

3.1.1 JAW SLITS PERFORMANCE PARAMETERS *14*

3.2 FLUORESCENT SCREEN 15

3.3 PINK BEAM STOP (DIAGNOSTIC MODULE 1 ONLY) 15

3.4 INTENSITY MONITORS 17

3.4.1 SOFT X-RAY MESH INTENSITY MONITOR (GOLD MESH) *17*

3.4.2 PHOTODIODE INTENSITY MONITOR *18*

3.4.3 Intensity Monitor/ Fluorescent Screen Actuator Motions *18*

3.4.4 Intensity Monitor Linear Actuator *18*

3.4.5 Intensity Monitor Encoder Data *19*

4. VACUUM SYSTEM **20**

4.1 VACUUM SPECIFICATION 20

4.2 VACUUM VESSEL PORTS 20

4.2.1 Diagnostic module 1 ..... *20*

4.2.2 Diagnostic module 2 ..... *21*

4.2.3 Diagnostic modules 3-8 ..... *21*

5. DIAGNOSTIC MODULE STAND **22**

5.1 LIFTING POINTS 22

5.2 ALIGNMENT FEATURES 22

6. INTERFACE PANEL **23**

6.1 DIAGNOSTIC MODULE 1 23

6.2 DIAGNOSTIC MODULE 2-8 23

7. FACTORY TESTING **24**

8. INSTALLATION AND UNIT ACCEPTANCE **25**

9. SCOPE OF SUPPLY **26**

9.1 SCOPE OF SUPPLY FOR CURRENT CONTRACT 26

9.2 SCOPE OF SUPPLY (CONTRACT ADDITIONS) 27

1. *INTRODUCTION*

The NIST SST beamline includes eight diagnostic modules. These include four-jaw uncooled slits for beam conditioning, in addition to diagnostics - fluorescent screen, intensity monitors (gold mesh and photodiode). The four jaw slits include isolated blades and feedthroughs to allow the measurement of drain currents. Diagnostic module 1 differs from the other diagnostic modules in that a pink beam stop is installed and that there is a port to allow the fitting of a NanoBPM.

1.1 AXIS

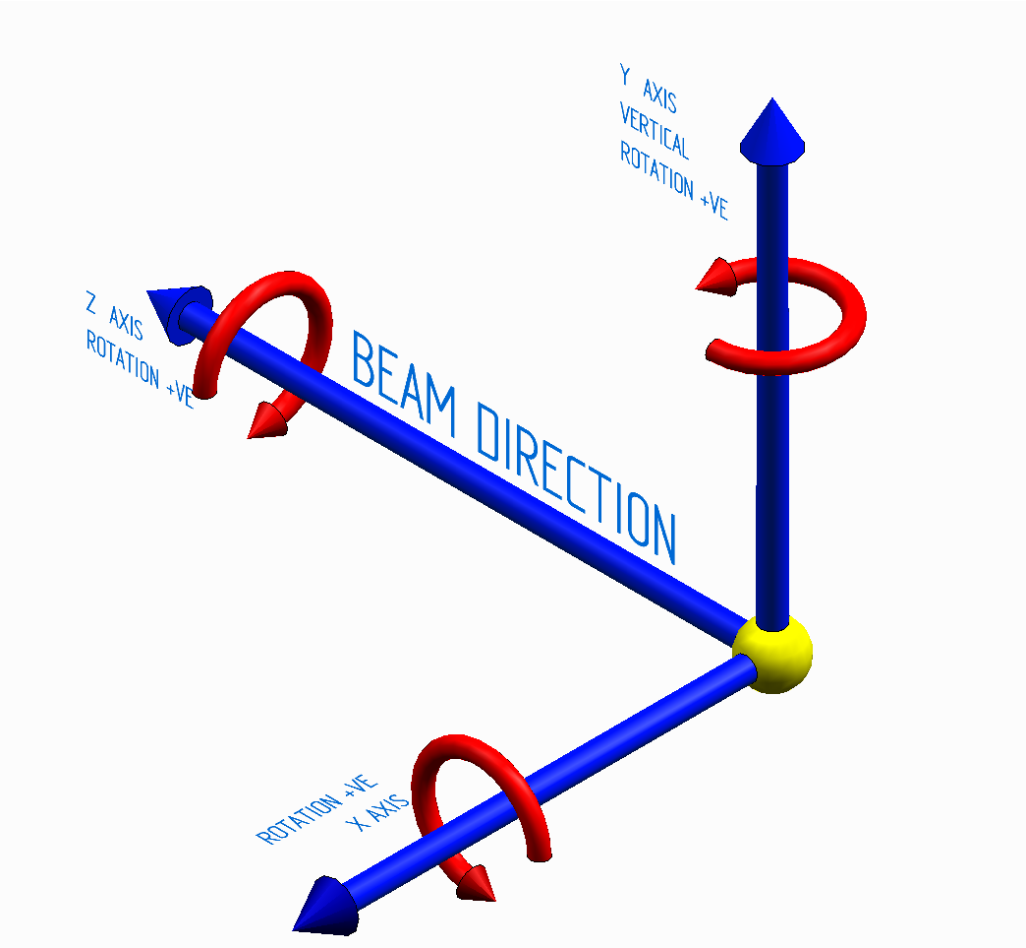

Figure 1. NSLS-II Coordinate System

The coordinate system employed complies with NSLS-II document:

Beamline Coordinate System Standards LT-C-XFD-STD-BL-COORD-001.

2. *SPECIFICATIONS*

2.1 DIAGNOSTIC MODULE LOCATIONS

The eight diagnostic modules are located as follows (see Figures 2 to 4):

1. DM1 - Downstream of the DCM in the tender 'L' beamline – between the DCM and the HP NEXAFS end station. Beam-in is located at 47614 mm and beam-out is located at 48370 mm from the centre of the straight section.

2. DM2 – Located downstream of the L4/M4B hexapod. This module is effectively two diagnostic modules with a common vessel and frame. It provides diagnostics for the soft and tender beams upstream of the µXPS end station. Beam-in is located at 67436 mm and beam-out is located at 67772 mm from the centre of the straight section (L branch).

3. DM3 – Located between mirror system M3AB/M3C and the precision vertical slit 'AB' on the soft x ray transfer branch. Beam-in is located at 45088 mm and beam-out is located at 45559 mm from the centre of the straight section.

4. DM4 - Downstream of the M4A mirror system in the HAXPES/NEXAFS branch of the 'M' soft x ray beamline. Beam-in is located at 57040 mm and beam-out is located at 57578 mm from the centre of the straight section.

5. DM5 - Downstream of the M4A mirror system in the µXPS branch of the 'M' soft beamline, allowing monitoring with optic in beam and out of beam (i.e. directly from the precision slit). Beam-in is located at 58395 mm and beam-out is located at 58866 mm from the centre of the straight section.

6. DM6 - Between mirror system M3AB/M3C and the precision vertical slit 'C' on the soft x ray beamline ('M' branch). Beam-in is located at 47492 mm and beam-out is located at 47960 mm from the centre of the straight section.

7. DM7 - Immediately downstream of the M4C/M4D mirror system. This enables monitoring of the beam with the optics in or out of beam. Beam-in is located at 53988 mm and beam-out is located at 54592 mm from the centre of the straight section.

8. DM8 – Located immediately upstream of the µNEXAFS end station. Beam-in is located at 63689 mm and beam-out is located at 64175 mm from the centre of the straight section.

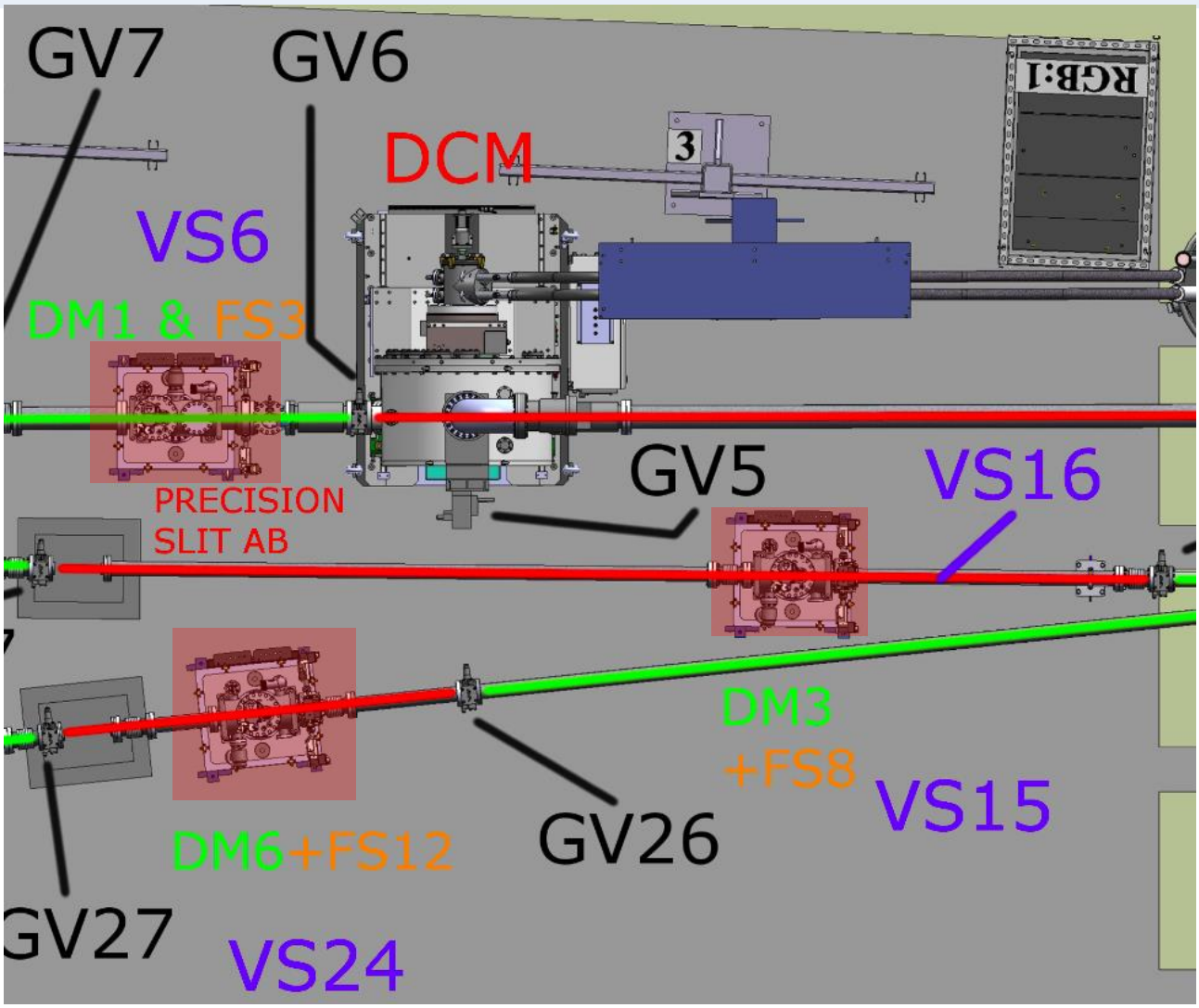

Figure 2. Location of Diagnostic modules DM1, DM3 and DM6.

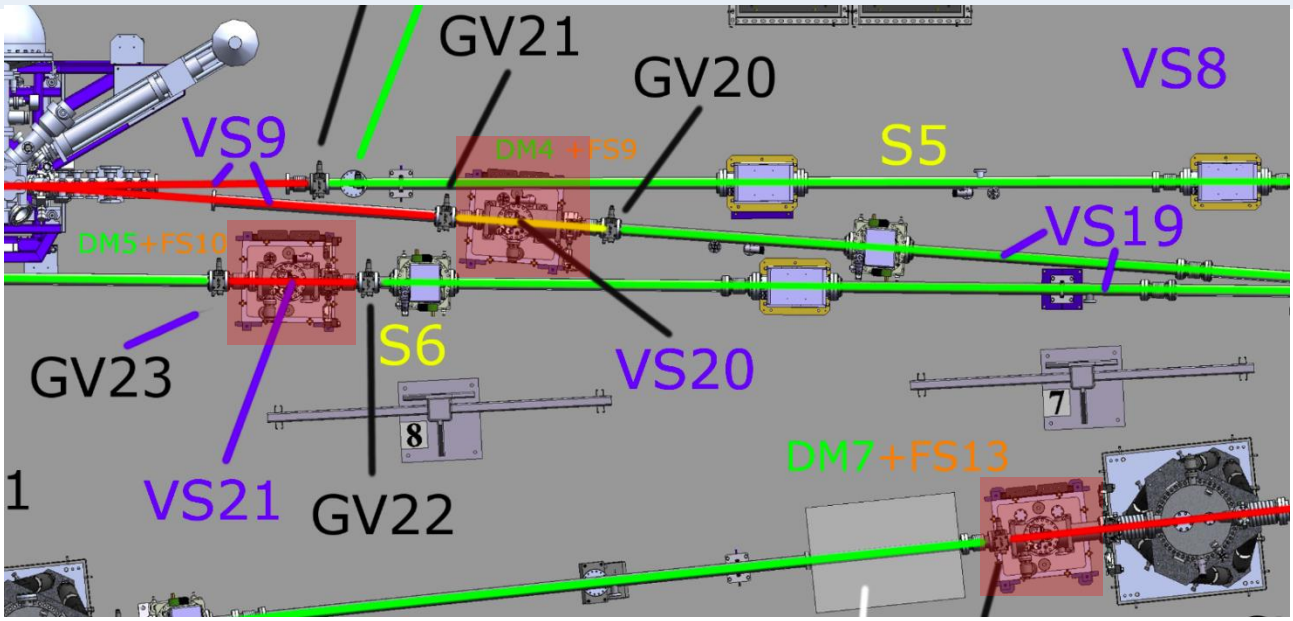

Figure 3. Location of diagnostic modules DM4, DM5 and DM7.

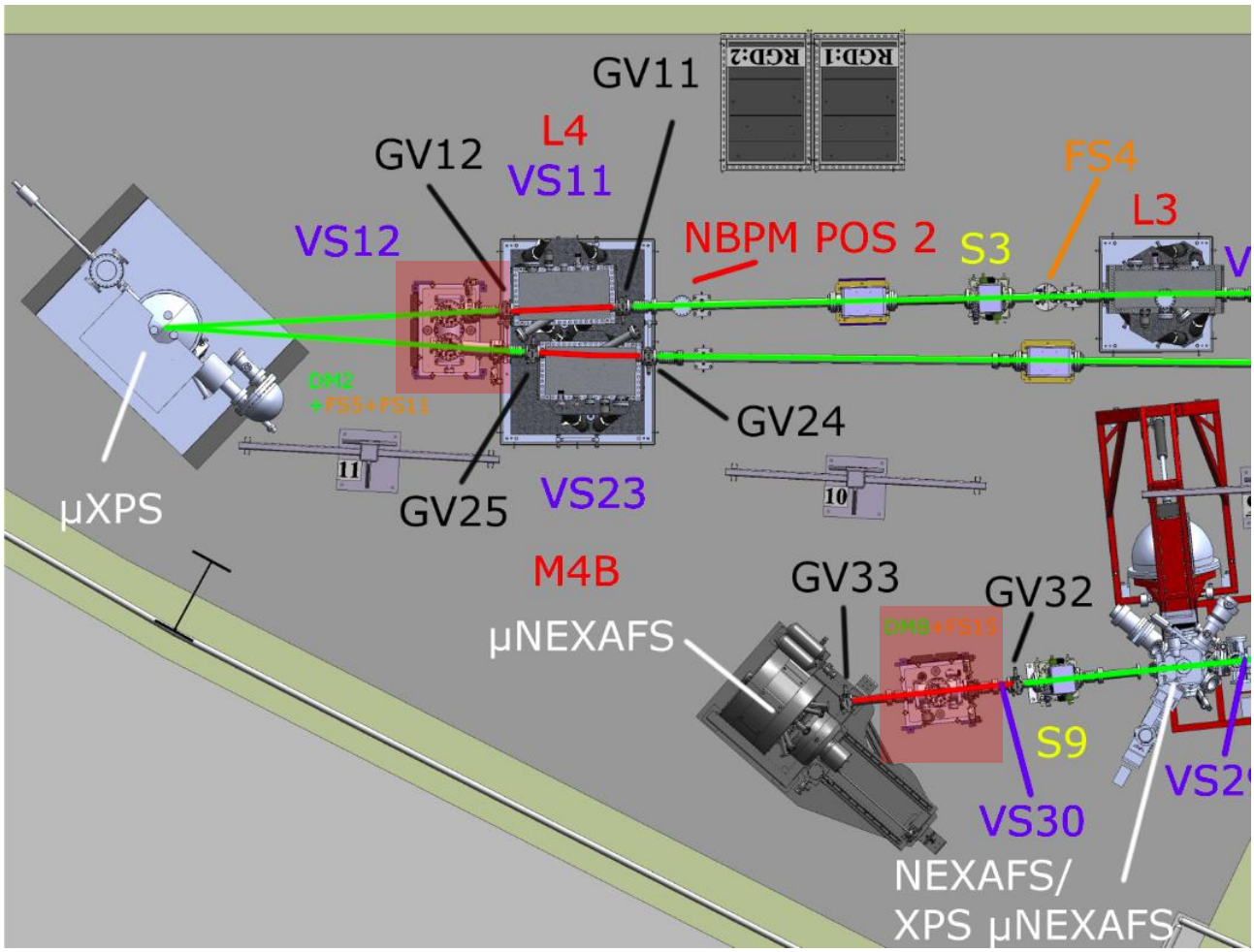

Figure 4. Location of diagnostic modules DM2 and DM8

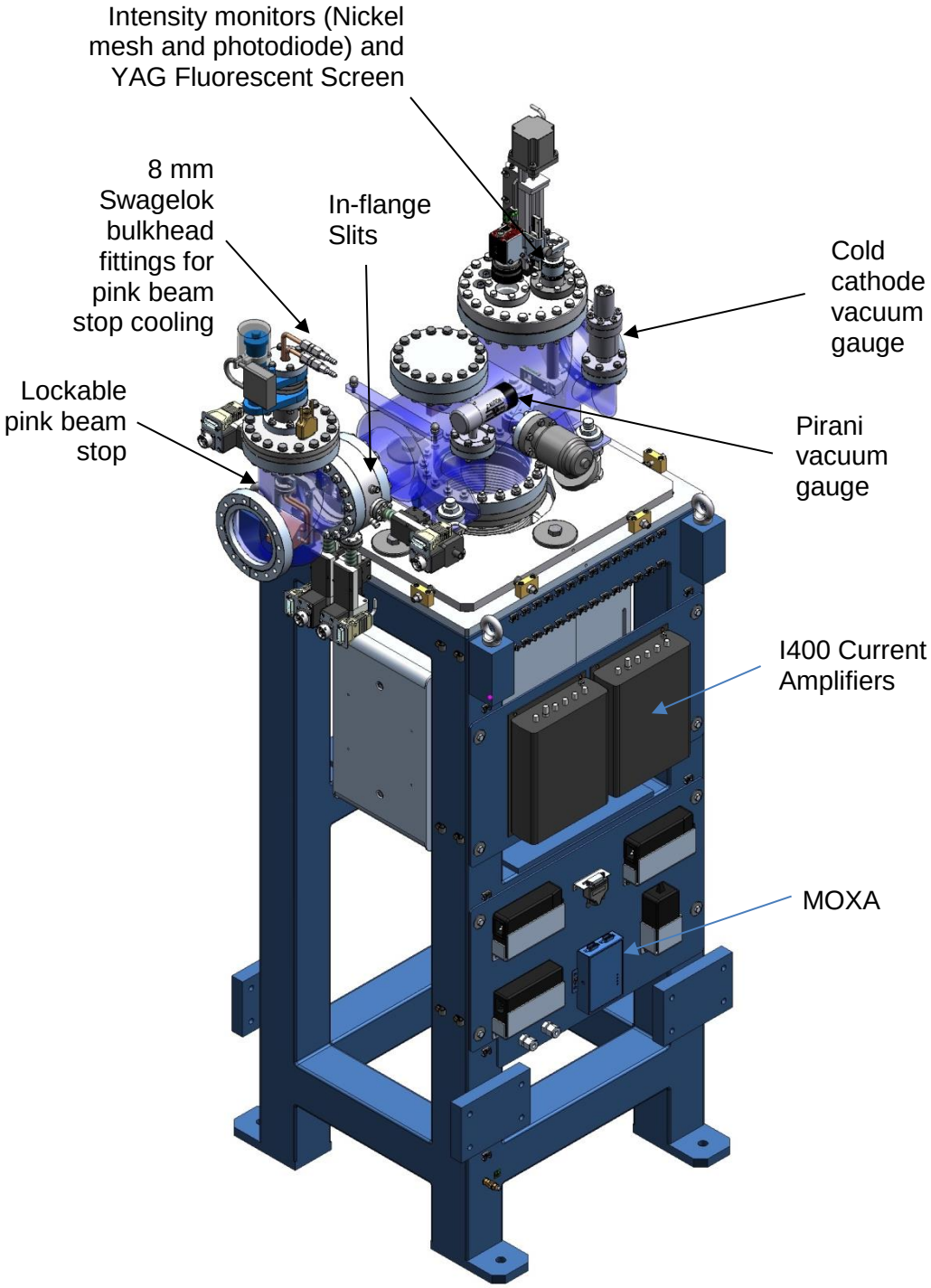

Figure 5. Diagnostic module 1

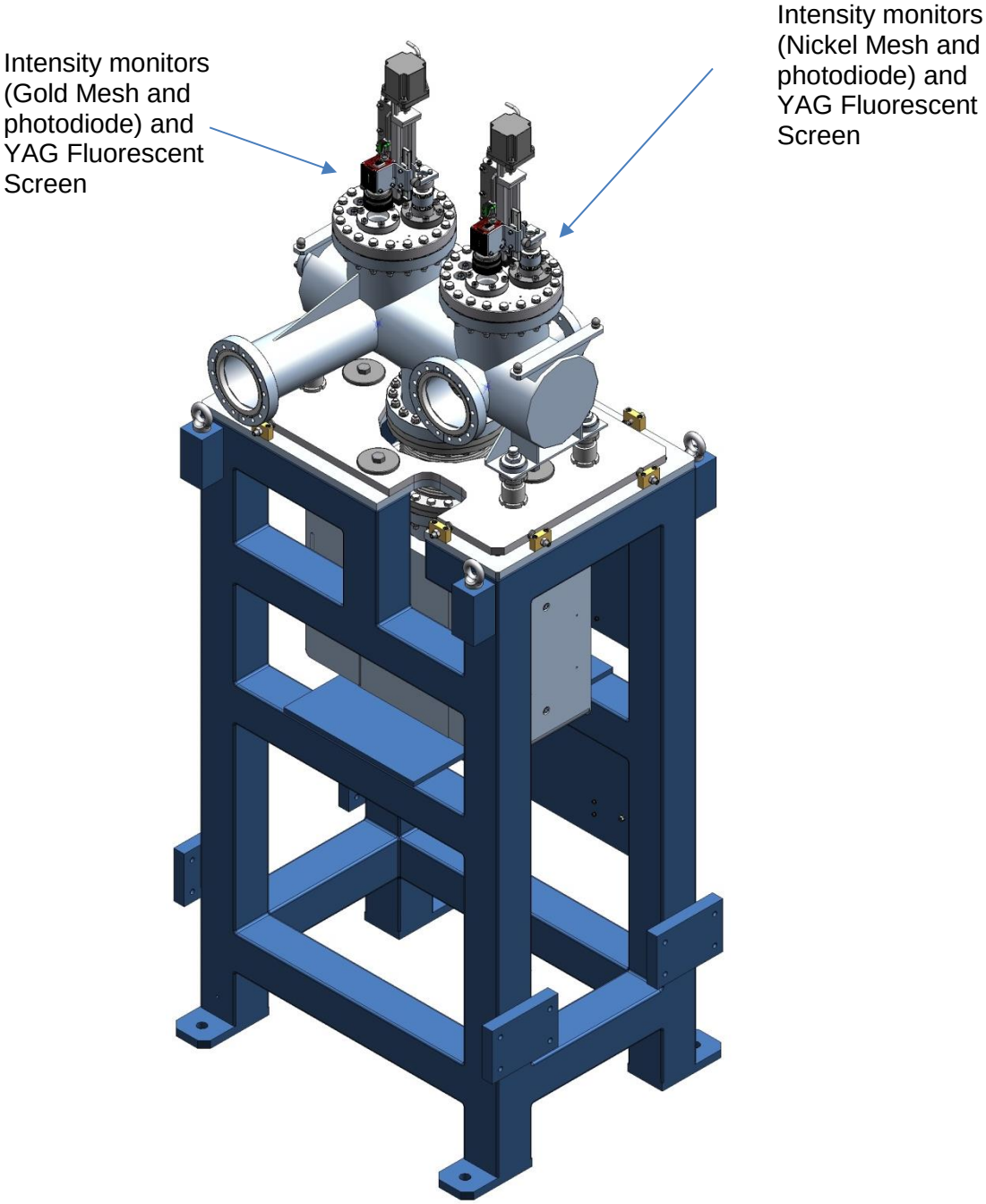

Figure 6. Diagnostic module 2

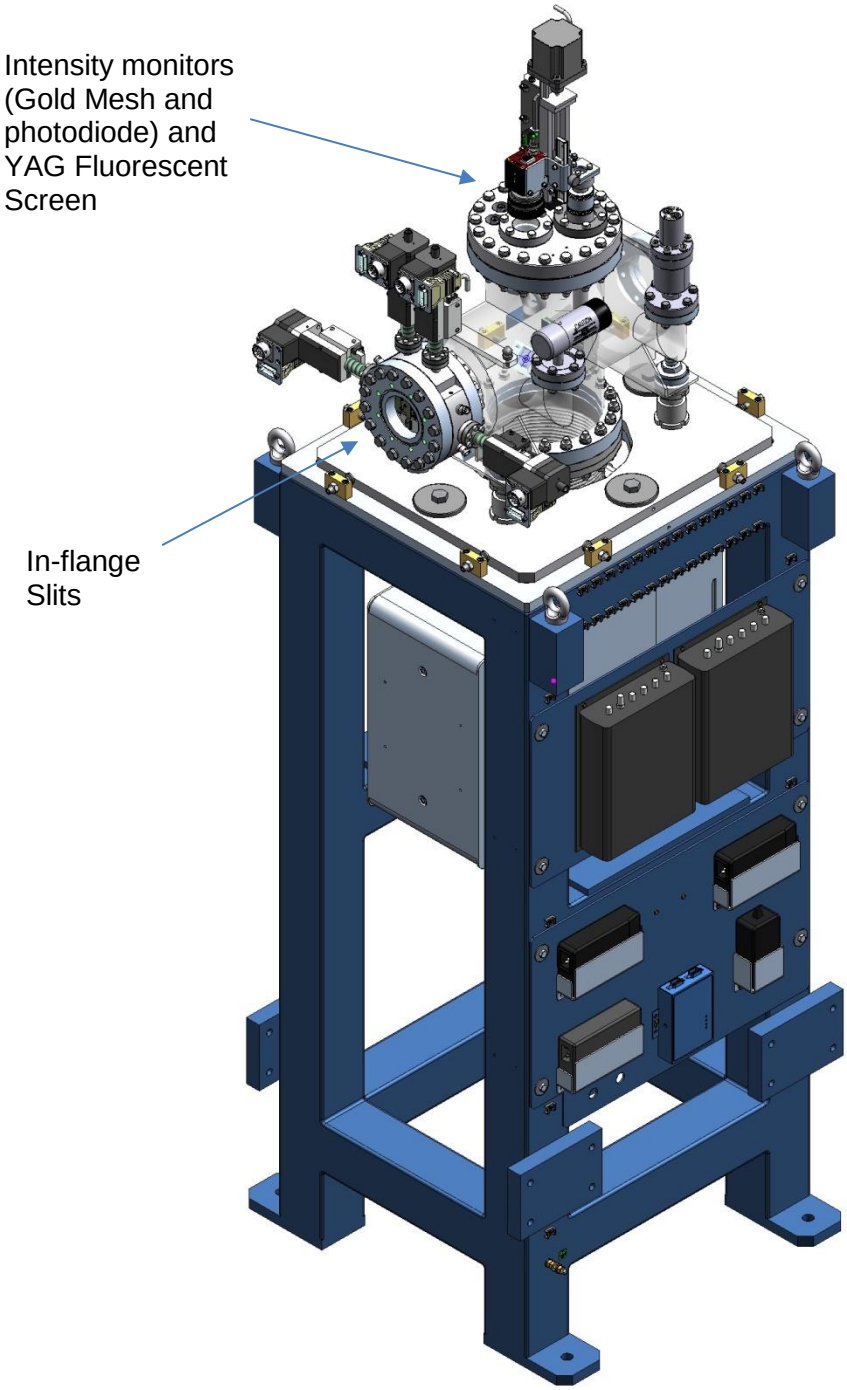

Figure 7. Diagnostic modules 3, 5 and 6

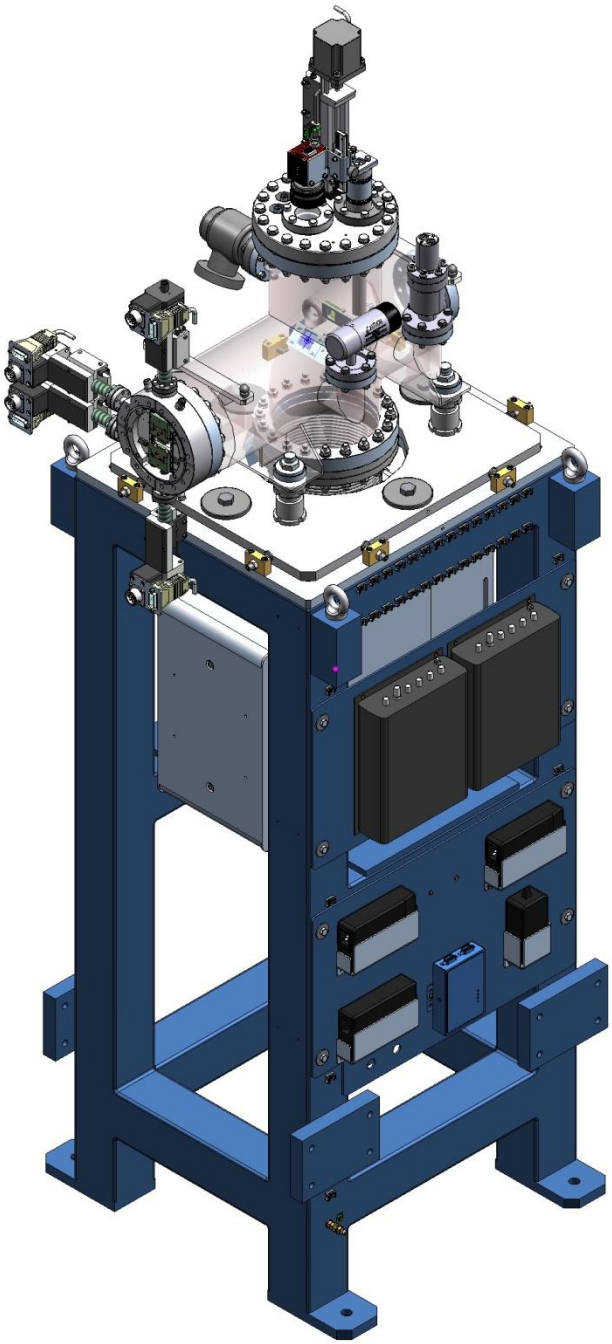

Figure 8. Diagnostic module 4

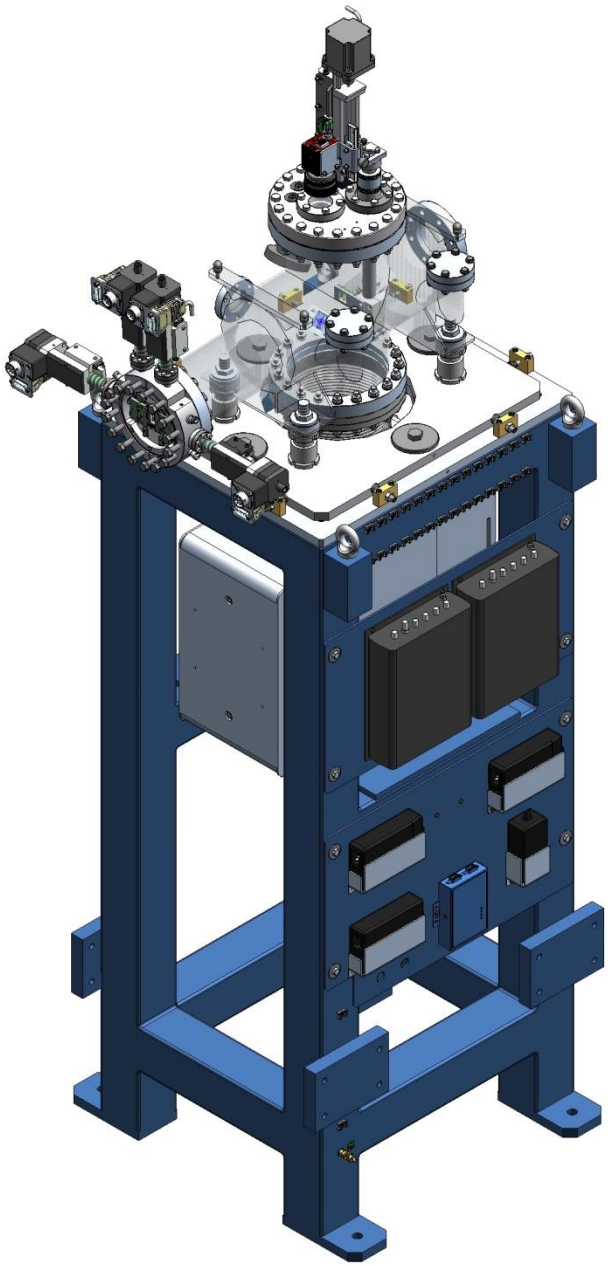

Figure 9. Diagnostic module 7

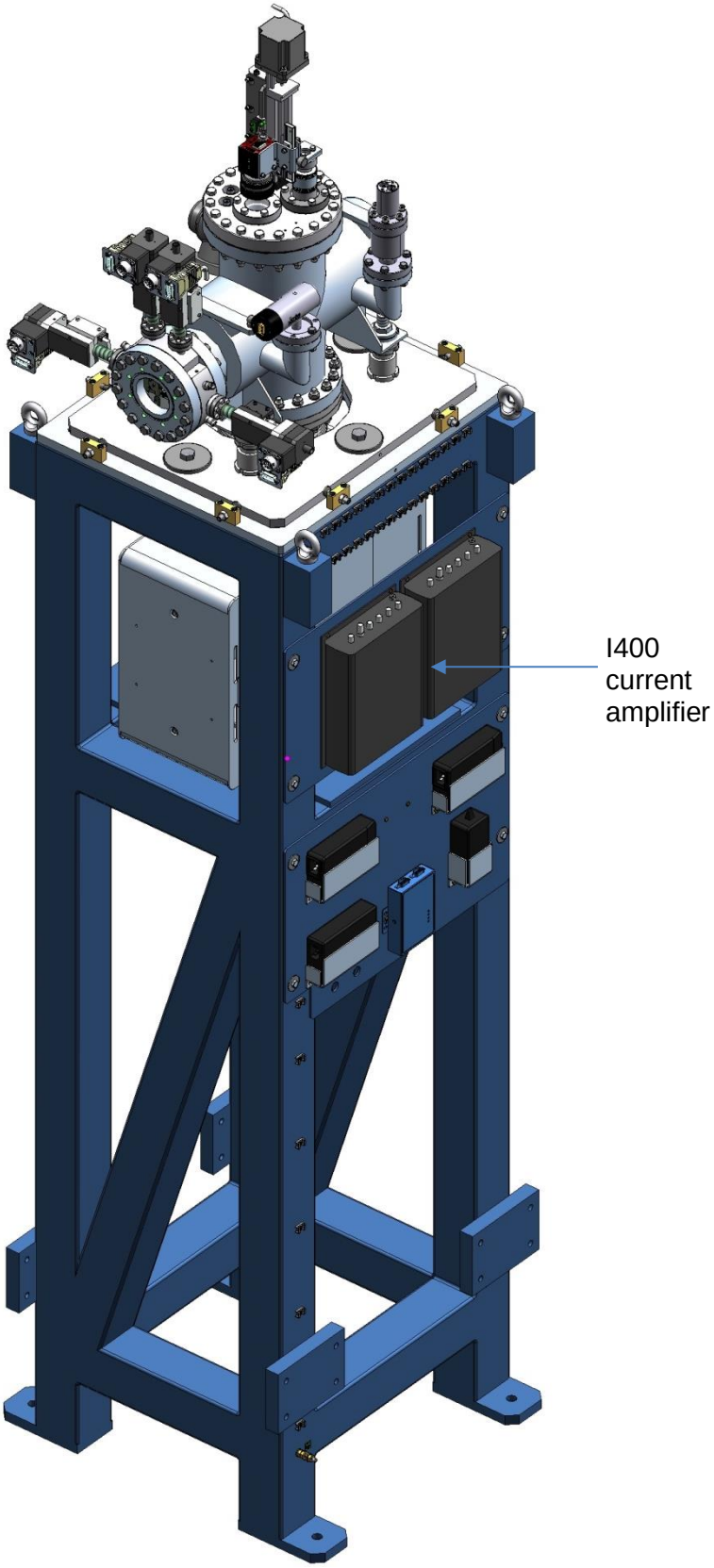

Figure 10. Diagnostic module 8

3. DIAGNOSTIC MODULE COMPONENTS

3.1 4 BLADE IN-FLANGE SLITS

The four blade in-flange slit unit consists of two blades to define the beam in the horizontal direction and two blades to define the beam in the vertical direction. The slits are able to close fully in horizontal and vertical directions. The slit blades move along in-vacuum guides to ensure that they remain parallel to each other.

The slit blades will be manufactured from tungsten. Each slit blade is moved by a stepper motor via a lead screw. An incremental linear optical encoder provides continuous feedback of the actual slit position. Limit switches are fitted at each end of the actuator travel. BNC feedthroughs are provided to allow measurement of the drain currents on each of the four blades.

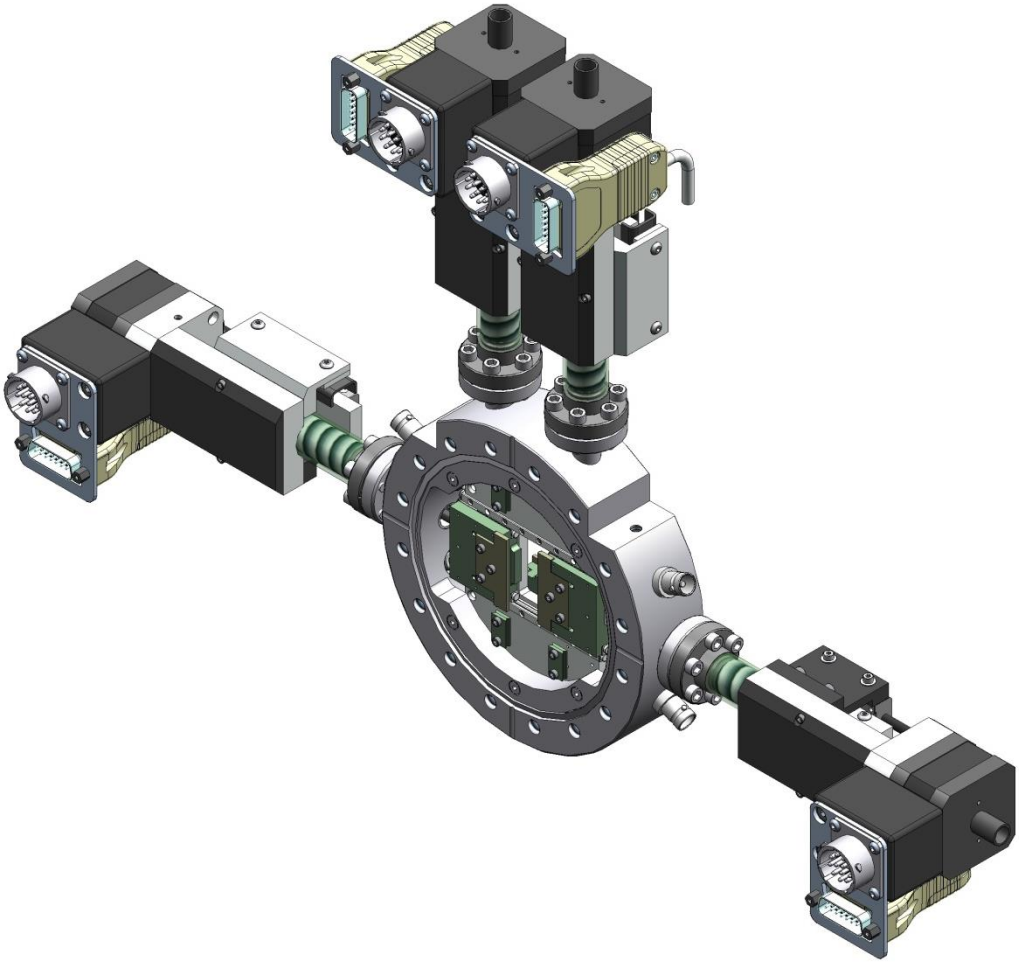

Figure 11. Four jaw in-flange slits with drain currents

3.1.1 JAW SLITS PERFORMANCE PARAMETERS

Slit Parameters

Maximum stroke available	15 mm
Maximum aperture	15 mm H x 15 mm V
Overlapping	Complete
Blade size	36 (W) mm x 20 mm (H) x 2 mm (T)
Blade Parallelism	10 μm
Blade defining edge radius	2 mm
Blade defining edge roughness	0.1 μm RMS
Blade defining edge straightness	< 5 μm
Resolution	< 0.5 μm
Repeatabillity	< 5 μm
Blade Material	Tungsten
End of travel limit switches	2, normally closed (one at each end of travel)
Mounting flange	DN100/CF150

Encoder details

Readhead type	Renishaw – Tonic T1000-05A
Interpolator type	Renishaw Ti0200E04A
Interpolator resolution	0.1 μm
Scale type	RGSZ20
Interpolator connector	15-Way sub D

Linear Actuator Parameters

Motor Type	Nanotec 2 phase, bi-polar, stepping linear actuator
Step angle (full step drive)	1.8° (200 steps/rev)
Driving current/Phase	1.4 A
Maximum velocity	20 mm/sec
Thread pitch	1 mm
Resolution per full step	5 µm
Maximum movement per actuator	20 mm
Maximum Overlap	5 mm
Maximum holding load (power off)	90 N
Motor connector	12 way Trim Trio

Limit switch parameters

Switch type	D2F Hinge lever
Max supply voltage	30 VDC
Max switching current	2A
Max temperature	65°C
Connector	12 way Trim Trio (with motor)

3.2 FLUORESCENT SCREEN

The fluorescent screen units located in the diagnostic modules use YAG crystals (Yttrium Aluminium Garnet) as the fluorescent material. The size of the crystal is 25 mm x 25 mm, with an aperture of 22 mm (H) x 15.5 mm (V).

The fluorescent screens used on the diagnostic modules are motorised and mounted on a DN150/CF200 conflat. The Prosilica GC1290 CCD camera is mounted on the same actuator thereby keeping the distance between screen and camera constant (see Figure 12).

3.3 PINK BEAM STOP (DIAGNOSTIC MODULE 1 ONLY)

A pink beam stop is located in Diagnostic module 1 and consists of a cooled copper block, which is fixed to a manually adjustable (lockable) vertical translation – see Figure 13. The height of the block is 40mm and the inclined face height 29 mm. The range of the vertical translation is 25 mm (± 12.5 about the nominal position, with the beam incident on the top of the block - see Figure 6). The face of the block which sees the beam is inclined at 45 degrees to the beam axis. The stop is fitted with a thermocouple.

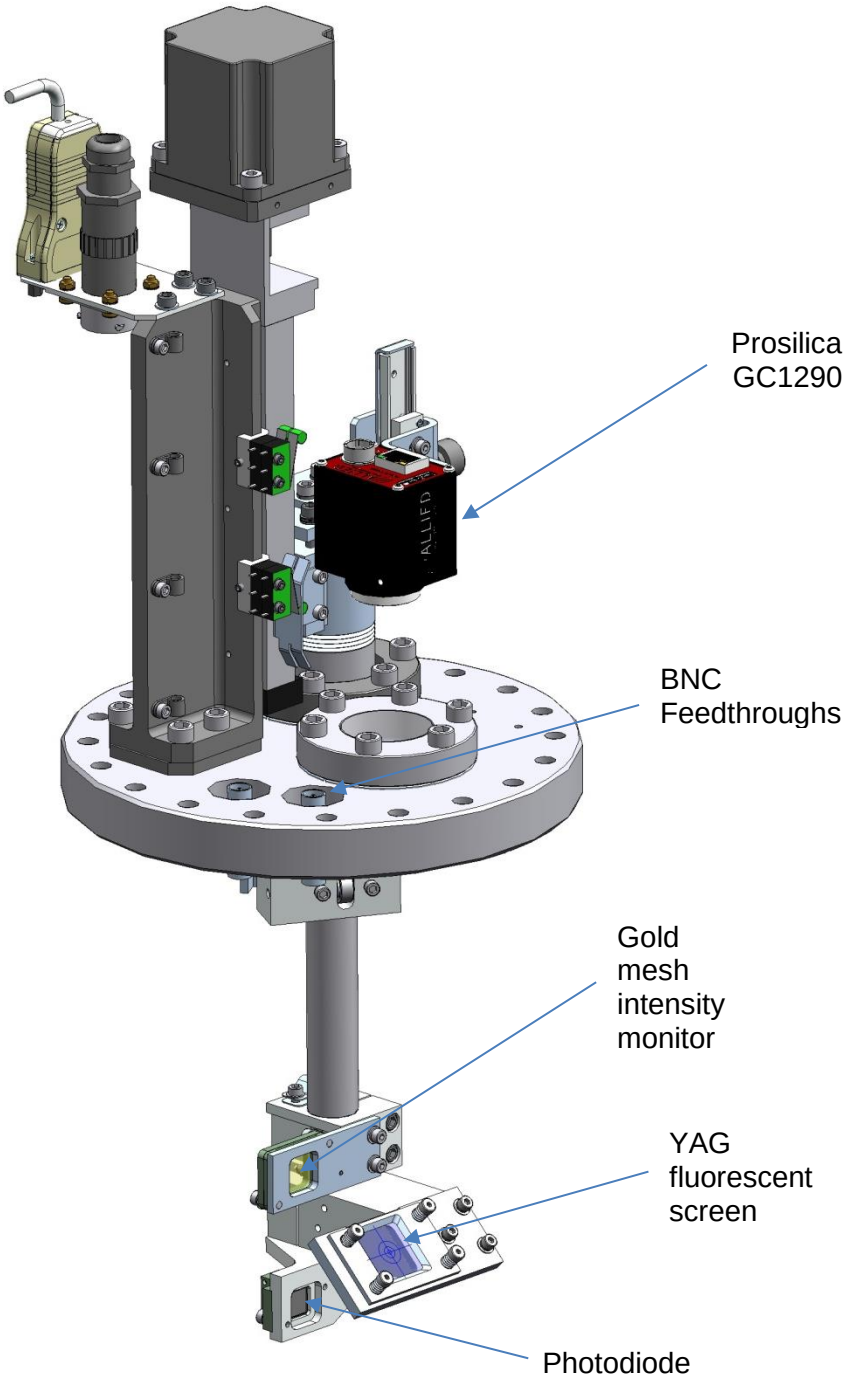

Figure 12. Fluorescent screen and intensity monitor actuator

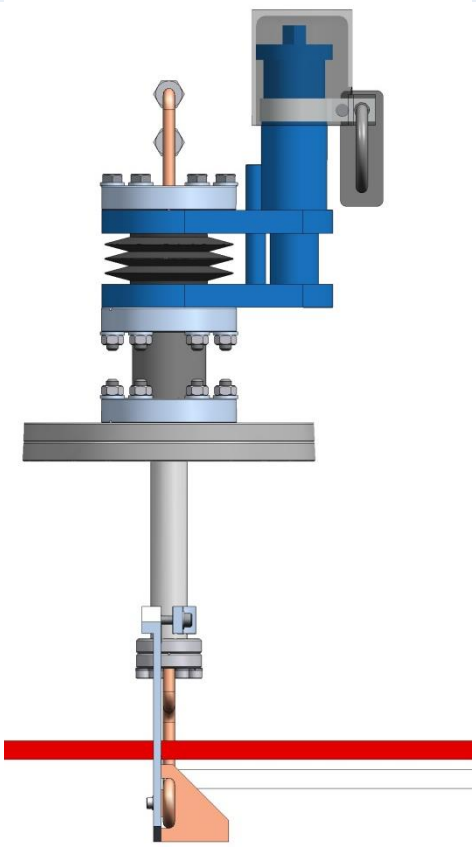

Figure 13. Cooled beam stop showing 'pink' and 'mono' beam at nominal position

3.4 INTENSITY MONITORS

The Gold/Nickel mesh intensity monitor and the photodiode intensity monitor are vertically stacked and mounted on the same stepper motor driven actuator.

3.4.1 SOFT X-RAY MESH INTENSITY MONITOR (GOLD MESH)

This diagnostic is used to measure the beam intensity by inserting an electrically isolated gold wire mesh into the beam and measuring the resultant photoionisation current using the I400 current amplifier. The photoionisation current is proportional to the beam intensity. Further details of the I400 are included in the supporting documents.

Gold Mesh Parameters

Size	16mm (H) x 12 mm (V)
Thickness	5 µm
Mesh pitch	100 lines per inch
Max transmission	Approx. 85%

Nickel Mesh Parameters (Diagnostic module 1 and diagnostic module 2 – L branch only)

Size	16mm (H) x 12 mm (V)
Thickness	5 µm
Mesh pitch	100 lines per inch
Max transmission	Approx. 85%

3.4.2 PHOTODIODE INTENSITY MONITOR

The photodiode intensity monitor consists of a mounted photodiode placed directly into the beam. The resultant output current from the photodiode is proportional to the beam intensity. This diagnostic interrupts the beam and therefore cannot be used for in-beam monitoring.

Photodiode parameters

Active Area	10 mm (H) x 10 (V) mm
Photodiode type	AXUV100G

3.4.3 Intensity Monitor/ Fluorescent Screen Actuator Motions

Linear actuator parameters

Motion	Parameter	Specification
Vertical (Y Direction)	Drive	Linear actuator, fitted with limit switches & encoder.
	Range	80 mm
	Repeatability	2 µm

3.4.4 Intensity Monitor Linear Actuator

Stepper motor and linear drive parameters

Motor Type	McLennan Type 23HSX-206, 2 phase, bi-polar stepper motor
Holding torque	98 Ncm
Step angle (full step drive)	1.8°/step or 200 steps/rev
Driving current	4.2 A
Thread pitch	2 mm
Resolution per half step	10 µm

3.4.5 Intensity Monitor Encoder Data

Stepper motor and linear drive parameters

Readhead type	Renishaw – Tonic T1001-05A
Readhead resolution	0.1 µm
Scale type	RGSZ20
Interpolator	Ti 0200 E 4 A
Connector	15-Way sub D

4. VACUUM SYSTEM

4.1 VACUUM SPECIFICATION

Maximum bakeout temperature – vessel and internal components	150-200 °C (110°C for diagnostic modules 2-6, limited by photodiode)
Vacuum	UHV compatible (< 5 x10^{-10} mbar).
Helium leak rate	< 1 x 10^{-10} mbar l/sec
Vacuum Pump	All of the diagnostic modules are equipped with Gamma Vacuum 300L ion pumps.
Vacuum gauges	One pirani gauge (MKS type 317) and one cold cathode gauge(MKS type 422) are located on the vacuum vessel of all modules except diagnostic module 7, where the gauges for the vacuum section are fitted to the adjacent mirror system.
Right Angle Valve	VAT Valve type 54, DN40/CF70.

4.2 VACUUM VESSEL PORTS

4.2.1 Diagnostic module 1

Purpose	Location	Size	Qty
Beam In	Beam inlet port	DN100/CF150	1
Beam Out (in flange slits)	Beam outlet port	DN100/CF150 R	1
Roughing Port for RA valve	Inboard side of vessel	DN40/CF70	1
Vacuum Gauges	Inboard Side of vessel	DN40/CF70	2
Fluorescent screen and intensity monitor actuator	Top of vessel	DN160/CF200 R	1
NanoBPM port	Top of vessel	DN100/CF150 R	1
Pink beam stop port	Top of vessel	DN100/CF150 R	1

Pump port	Bottom of vessel	DN160/CF200	1

4.2.2 Diagnostic module 2

Purpose	Location	Size	Qty
Beam In (soft and tender) : in-flange slits	Beam inlet port	DN100/CF150	2
Beam Out	Beam outlet port	DN63/CF114 R	2
Roughing Port for RA valve	Outboard side of vessel	DN40/CF70	1
Fluorescent screen and intensity monitor actuator	Top of vessel	DN160/CF200	2
Pump Port	Bottom of vessel	DN160/CF200	1

4.2.3 Diagnostic modules 3-8

Purpose	Location	Size	Qty
Beam In (in-flange slits)	Beam inlet port	DN100/CF150	1
Beam Out (in-flange slits)	Beam outlet port at end 2	DN63/CF114 R	1
Roughing Port for RA valve	Outboard side of vessel	DN40/CF70	1
Vacuum Gauges	Inboard side of vessel	DN40/CF70	2
Fluorescent screen and intensity monitor actuator	Top of vessel	DN160/CF200	1
Pump port	Bottom of vessel	DN160/CF200	1

5. DIAGNOSTIC MODULE STAND

The position of the diagnostic module components can be adjusted in x, y, and z relative to the support frame. There are two adjusters per side mounted on the frame, which can be used to adjust the lateral, longitudinal and angular (yaw) alignment of the vessel and components. In addition, the vessel is supported by adjustable feet (and spherical washers) which can be used to adjust the height, pitch and roll of the vessel.

Vessel Manual Adjustment (Lateral x & Longitudinal z)	±5 mm
Vessel Manual Adjustment (Vertical y)	±12.5 mm
Material	Mild Steel
Colour	RAL 5007 30% GLOSS

5.1 LIFTING POINTS

Diagnostic module 1 weight: 345 kg approximately.

Diagnostic module 2 weight: 410 kg approximately.

Diagnostic modules 3-7 weight: 330 kg approximately.

Diagnostic module 8 weight: 390 kg approximately

The diagnostic modules are provided with four M16 lifting points in the support frame.

Lifting diagrams for the diagnostic modules will be included in the top level assembly drawings.

5.2 ALIGNMENT FEATURES

Fiducial mounts will be provided on the vacuum vessel. These will take the form of 0.25” reamed (H7) holes, suitable for 0.5” or 1.5” spheres.

6. INTERFACE PANEL

6.1 DIAGNOSTIC MODULE 1

The interface panel for diagnostic module 1 includes:

1. Bulkhead swagelok union fittings (8 mm) to connect to the pink beam stop cooling lines.
2. 15 way d-type connection to the pink beam stop thermocouple.
3. Mounting for the MOXA and its power supply
4. Mounting for the camera power supply

6.2 DIAGNOSTIC MODULE 2-8

The interface panels for diagnostic modules 2-8 include:

1. Mounting for the I400 and its power supply
2. Mounting for the MOXA and its power supply
3. Mounting for the camera power supply

7. FACTORY TESTING

Testing at FMB Oxford consists of Motion Testing, Vacuum Testing and Alignment.

Full specifications and procedures covering all factory testing will be prepared in advance and these will be submitted to the customer prior to final design approval. Representatives from the customer are invited to witness these tests at FMB Oxford's works.

8. INSTALLATION AND UNIT ACCEPTANCE

The site acceptance testing, included in the installation option, will ensure that all components are carefully surveyed into position, all motors, actuators and sensors are functioning properly and the vacuum specifications are met. All motions will be tested and the correct functioning of all limit and datum switches checked. The complete set of detailed factory tests are not repeated on site.

There will be a full leak check of the installed vacuum sections. We expect that a turbo pump station, RGA rig, and He leak checker to be provided by the customer for our use while at the customer's site.

Final site acceptance will include:

- All factory test data, documentation and manuals
- Correct operation of all motions, limits and datum switches using FMB-O controls and cabling.
- Leak testing at the best achievable sensitivity after 24 hrs of pumping and prior to on site customer bakeout

9. SCOPE OF SUPPLY

9.1 SCOPE OF SUPPLY FOR CURRENT CONTRACT

- Diagnostic Module 1
  - Cooled pink beam stop
  - Nickel mesh intensity monitor
  - Photodiode intensity monitor
  - YAG Fluorescent screen
  - 300L Gamma Vacuum ion pump
  - Pirani vacuum gauge
  - Cold cathode vacuum gauge
  - Right angle valve
  - I400 Current amplifier (for intensity monitors only)
  - MOXA to connect the I400 output to the Ethernet
  - Prosilica GC1290 mono camera
- Diagnostic modules 3, 4, 5 and 6
  - Gold mesh intensity monitor
  - Photodiode intensity monitor
  - YAG Fluorescent Screen
  - 300L Gamma Vacuum ion pump
  - Pirani vacuum gauge
  - Cold cathode vacuum gauge
  - Right angle valve
  - I400 Current amplifier (for intensity monitors only)
  - MOXA to connect the I400 output to the Ethernet
  - Prosilica GC1290 mono camera
- Diagnostic module 7
  - Gold mesh intensity monitor
  - Photodiode intensity monitor

- YAG Fluorescent screen
- 300L Gamma Vacuum ion pump
- Right angle valve
- I400 Current amplifier (for intensity monitors only)
- MOXA to connect the I400 output to the Ethernet
- Prosilica GC1290 mono camera

9.2 SCOPE OF SUPPLY (CONTRACT ADDITIONS)

- Diagnostic Module 2
  - Gold mesh intensity monitor
  - Nickel mesh intensity monitor
  - Photodiode intensity monitor (2 off)
  - YAG Fluorescent screen (2 off)
  - 300L Gamma Vacuum ion pump
  - Right angle valve
  - I400 Current amplifier (for intensity monitors only)
  - MOXA to connect the I400 output to the Ethernet
  - Prosilica GC1290 mono camera (2 off)
- Diagnostic Module 8
  - Gold mesh intensity monitor
  - Photodiode intensity monitor
  - YAG Fluorescent screen
  - 300L Gamma Vacuum ion pump
  - Right angle valve
  - I400 Current amplifier (for intensity monitors only)
  - MOXA to connect the I400 output to the Ethernet
  - Prosilica GC1290 mono camera (2 off)

The contract additions also include:

- I400 current amplifiers to allow drain current measurements on the in-flange 4 jaw slits

S3160 BNL NSLS-II NIST SST BEAMLINE I/O LISTING

(This document should be treated as reference only, EPS PLC in NIST scope of supply)

FMB Oxford

Prepared by:	D. Smith
Revision:	C (FDR issue)
Date:	12-Aug-15

Notes:
Temperature and flow alarms must inhibit the beam
Flowmeters are not in the FMBO scope
Vacuum alarms inhibit opening of the relevant gate valves and inhibits the beam
The beam must be inhibited when gate valves are not open

Monitored Temperatures

Channel	Part	Type	Device	Fault condition
1	Fixed Mask #1	PT100	Temp sensor Fixed mask Upper	High temperature
2		PT100	Temp sensor Fixed mask Lower	High temperature
3	L1	K Type	Thermocouple Mask	High temperature
4		K Type	Thermocouple Mirror	High temperature
5	M1	K Type	Thermocouple Mask	High temperature
6		K Type	Thermocouple Mirror	High temperature
7	WBS01	K Type	Thermocouple Inboard	High temperature
8		K Type	Thermocouple Outboard	High temperature
9		K Type	Thermocouple Mask plate	High temperature
10	SLW01	K Type	Thermocouple Slit 1 - 1 Upper Blade	High temperature
11		K Type	Thermocouple Slit 1 - 2 Lower blade	High temperature
12		K Type	Thermocouple Slit 1 - 3 Outboard blade	High temperature
		K Type	Thermocouple Slit 1 - 4 Inboard blade (T/C1)	High temperature
13		K Type	Thermocouple Slit 1 - 4 Inboard blade (T/C2)	High temperature
14	SLW02	K Type	Thermocouple Slit 2 - 1 Upper Blade	High temperature
15		K Type	Thermocouple Slit 2 - 2 Lower blade	High temperature
		K Type	Thermocouple Slit 2 - 3 Outboard blade (T/C1)	High temperature
16		K Type	Thermocouple Slit 2 - 3 Outboard blade (T/C2)	High temperature
17		K Type	Thermocouple Slit 2 - 4 Inner blade	High temperature
18	Fixed Mask #2	K Type	Thermocouple Mask	High temperature
19	L2	K Type	Thermocouple Mask Upper	High temperature
20		K Type	Thermocouple Mask Lower	High temperature
21		K Type	Thermocouple L2A	High temperature
22		K Type	Thermocouple L2B	High temperature
23	FS2	K Type	Thermocouple Screen	High temperature
24	Fixed Mask #3	K Type	Thermocouple Mask	High temperature
25	Fixed Mask #4	K Type	Thermocouple Mask	High temperature
26	FS6	K Type	Thermocouple Screen	High temperature
27	DCM	K Type	Thermocouple 1st Crystal - Si111	High temperature
28		K Type	Thermocouple 1st Crystal - Si220	High temperature
29		K Type	Thermocouple 1st Crystal - YB66	High temperature
30		K Type	Thermocouple 2nd Crystal - Si111	High temperature
31		K Type	Thermocouple 2nd Crystal - Si220	High temperature
32		K Type	Thermocouple 2nd Crystal - YB66	High temperature
33	PGM	K Type	Thermocouple Mirror	High temperature
34		K Type	Thermocouple Grating	High temperature
35	M3AB/M3C	K Type	Thermocouple Mirror AB	High temperature
36		K Type	Thermocouple Mirror C	High temperature
37	PBS01	K Type	Thermocouple Inboard	High temperature

Note: Thermocouples on motors are not monitored by EPS. They are sometimes monitored during the commissioning phase and if a fault is suspected.
Note: Temperatures from the cryocooler are not monitored by the EPS but by the cryocooler controls. A fault will generate an alarm from the cryocooler.

Monitored inputs

Channel	Part	Type	Device		Signal description	Tag Name
1		Relay N/O	Cryo1		Cryocooler healthy	Cryo1
2		Relay N/O	CC01		Vacuum gauge controller #1A Cold Cathode	Vac 1a
3		Relay N/O	CC02		Vacuum gauge controller #1B Cold Cathode	Vac 1b
4		Relay N/O	CC03		Vacuum gauge controller #2A Cold Cathode	Vac 2
5		Relay N/O	CC04		Vacuum gauge controller #2B Cold Cathode	Vac 3
6		Relay N/O	CC05		Vacuum gauge controller #3A Cold Cathode	Vac 4
7		Relay N/O	CC06		Vacuum gauge controller #6 Cold Cathode	Vac 5
8		Relay N/O	CC07		Vacuum gauge controller #8A Cold Cathode	Vac 6
9		Relay N/O	CC08		Vacuum gauge controller #8B Cold Cathode	Vac 8
10		Relay N/O	CC09		Vacuum gauge controller #11A Cold Cathode	Vac 10
11		Relay N/O	CC10		Vacuum gauge controller #11B Cold Cathode	Vac 11
12		Relay N/O	CC11		Vacuum gauge controller #3B Cold Cathode	Vac 13
13		Relay N/O	CC12		Vacuum gauge controller #4A Cold Cathode	Vac 14
14		Relay N/O	CC13		Vacuum gauge controller #5A Cold Cathode	Vac 15
15		Relay N/O	CC14		Vacuum gauge controller #7A Cold Cathode	Vac 16
16		Relay N/O	CC15		Vacuum gauge controller #9A Cold Cathode	Vac 18
17		Relay N/O	CC16		Vacuum gauge controller #9B Cold Cathode	Vac 19
18		Relay N/O	CC17		Vacuum gauge controller #10A Cold Cathode	Vac 20
19		Relay N/O	CC18		Vacuum gauge controller #10B Cold Cathode	Vac 21
20		Relay N/O	CC19		Vacuum gauge controller #12A Cold Cathode	Vac 22
21		Relay N/O	CC20		Vacuum gauge controller #12B Cold Cathode	Vac 23

S3160 BNL NSLS-II NIST SST BEAMLINE I/O LISTING

(This document should be treated as reference only, EPS PLC in NIST scope of supply)

22		Relay N/O	CC21		Vacuum gauge controller #7B Cold Cathode	Vac 24
23		Relay N/O	CC22		Vacuum gauge controller #13A Cold Cathode	Vac 26
24		Relay N/O	CC23		Vacuum gauge controller #13B Cold Cathode	Vac 28
25		Relay N/O	CC24		Vacuum gauge controller #14A Cold Cathode	Vac 30
26	FM01/WBS01	Relay N/O	FLW01		Flowmeter Fixed mask & WBS	FM01/WBS
27	L1 / M1	Relay N/O	FLW02		Flowmeter L1 & M1	L1/M1
28	SLW01	Relay N/O	FLW03		Flowmeter SLW01	SLW01
29	SLW02	Relay N/O	FLW04		Flowmeter SLW02	SLW02
30	FM #2	Relay N/O	FLW05		Flowmeter Fixed mask	FM02
31	L2/FS02/FS06	Relay N/O	FLW06		Flowmeter L2/FS02/FS06	L2/FS02/FS06
32	FM03	Relay N/O	FLW07		Flowmeter Fixed mask	FM03
33	FM04	Relay N/O	FLW08		Flowmeter Fixed mask	FM04
34	DCM	Relay N/O	FLW09		Flowmeter DCM crystal cage	DCM
35	PGM	Relay N/O	FLW10		Flowmeter PGM Mirror	PGM1
36	PGM	Relay N/O	FLW11		Flowmeter PGM Grating	PGM2
37	PGM	Relay N/O	FLW12		Flowmeter PGM Mask	PGM3
38	DM1	Relay N/O	FLW13		Flowmeter WBS	WBS
39	M3ABC	Relay N/O	FLW14		Flowmeter M3 mirrors	M3
40	PBS01	Relay N/O	FLW15		Flowmeter PB stop	PBS
41	SLVAB	Relay N/O	FLW16		Flowmeter slit blades	SLVAB
42	SLVC	Relay N/O	FLW17		Flowmeter slit blades	SLVC
43	GV01	Switch N/O	GV01O		Limit switch, gate valve V1 open	Pos GV1
44		Switch N/O	GV01C		Limit switch, gate valve V1 closed	
45	GV02	Switch N/O	GV02O		Limit switch, gate valve V2 open	Pos GV2
46		Switch N/O	GV02C		Limit switch, gate valve V2 closed	
47	GV03	Switch N/O	GV03O		Limit switch, gate valve V3 open	Pos GV3
48		Switch N/O	GV03C		Limit switch, gate valve V3 closed	
49	GV04	Switch N/O	GV04O		Limit switch, gate valve V4 open	Pos GV4
50		Switch N/O	GV04C		Limit switch, gate valve V4 closed	
51	GV05	Switch N/O	GV05O		Limit switch, gate valve V5 open	Pos GV5
52		Switch N/O	GV05C		Limit switch, gate valve V5 closed	
53	GV06	Switch N/O	GV06O		Limit switch, gate valve V6 open	Pos GV6
54		Switch N/O	GV06C		Limit switch, gate valve V6 closed	
55	GV07	Switch N/O	GV07O		Limit switch, gate valve V7 open	Pos GV7
56		Switch N/O	GV07C		Limit switch, gate valve V7 closed	
57	GV08	Switch N/O	GV08O		Limit switch, gate valve V8 open	Pos GV8
58		Switch N/O	GV08C		Limit switch, gate valve V8 closed	
59	GV09	Switch N/O	GV09O		Limit switch, gate valve V9 open	Pos GV9
60		Switch N/O	GV09C		Limit switch, gate valve V9 closed	
61	GV10	Switch N/O	GV10O		Limit switch, gate valve V10 open	Pos GV10
62		Switch N/O	GV10C		Limit switch, gate valve V10 closed	
63	FLS04	Switch N/O	FLS04O		Limit switch, Fluorescent screen Out	Pos FLS04
64		Switch N/O	FLS04I		Limit switch, Fluorescent screen In	
65	GV11	Switch N/O	GV11O		Limit switch, gate valve V11 open	Pos GV11
66		Switch N/O	GV11C		Limit switch, gate valve V11 closed	
67	GV12	Switch N/O	GV12O		Limit switch, gate valve V12 open	Pos GV12
68		Switch N/O	GV12C		Limit switch, gate valve V12 closed	
69	GV13	Switch N/O	GV13O		Limit switch, gate valve V13 open	Pos GV13
70		Switch N/O	GV13C		Limit switch, gate valve V13 closed	
71	GV14	Switch N/O	GV14O		Limit switch, gate valve V14 open	Pos GV14
72		Switch N/O	GV14C		Limit switch, gate valve V14 closed	
73	GV15	Switch N/O	GV15O		Limit switch, gate valve V15 open	Pos GV15
74		Switch N/O	GV15C		Limit switch, gate valve V15 closed	
75	GV16	Switch N/O	GV16O		Limit switch, gate valve V16 open	Pos GV16
76		Switch N/O	GV16C		Limit switch, gate valve V16 closed	
77	GV17	Switch N/O	GV17O		Limit switch, gate valve V17 open	Pos GV17
78		Switch N/O	GV17C		Limit switch, gate valve V17 closed	
79	GV18	Switch N/O	GV18O		Limit switch, gate valve V18 open	Pos GV18
80		Switch N/O	GV18C		Limit switch, gate valve V18 closed	
81	GV19	Switch N/O	GV19O		Limit switch, gate valve V19 open	Pos GV19
82		Switch N/O	GV19C		Limit switch, gate valve V19 closed	
83	GV20	Switch N/O	GV20O		Limit switch, gate valve V20 open	Pos GV20
84		Switch N/O	GV20C		Limit switch, gate valve V20 closed	
85	GV21	Switch N/O	GV21O		Limit switch, gate valve V21 open	Pos GV21
86		Switch N/O	GV21C		Limit switch, gate valve V21 closed	
87	GV22	Switch N/O	GV22O		Limit switch, gate valve V22 open	Pos GV22
88		Switch N/O	GV22C		Limit switch, gate valve V22 closed	
89	GV23	Switch N/O	GV23O		Limit switch, gate valve V23 open	Pos GV23
90		Switch N/O	GV23C		Limit switch, gate valve V23 closed	
91	GV24	Switch N/O	GV24O		Limit switch, gate valve V24 open	Pos GV24
92		Switch N/O	GV24C		Limit switch, gate valve V24 closed	
93	GV25	Switch N/O	GV25O		Limit switch, gate valve V25 open	Pos GV25
94		Switch N/O	GV25C		Limit switch, gate valve V25 closed	

S3160 BNL NSLS-II NIST SST BEAMLINE I/O LISTING

(This document should be treated as reference only, EPS PLC in NIST scope of supply)

95	GV26	Switch N/O	GV26O		Limit switch, gate valve V26 open	Pos GV26
96		Switch N/O	GV26C		Limit switch, gate valve V26 closed	
97	GV27	Switch N/O	GV27O		Limit switch, gate valve V27 open	Pos GV27
98		Switch N/O	GV27C		Limit switch, gate valve V27 closed	
99	GV28	Switch N/O	GV28O		Limit switch, gate valve V28 open	Pos GV28
100		Switch N/O	GV28C		Limit switch, gate valve V28 closed	
101	GV29	Switch N/O	GV29O		Limit switch, gate valve V29 open	Pos GV29
102		Switch N/O	GV29C		Limit switch, gate valve V29 closed	
103	GV30	Switch N/O	GV30O		Limit switch, gate valve V30 open	Pos GV30
104		Switch N/O	GV30C		Limit switch, gate valve V30 closed	
105	FLS14	Switch N/O	FLS14O		Limit switch, Fluorescent screen Out	Pos FLS14
106		Switch N/O	FLS14I		Limit switch, Fluorescent screen In	
107	GV31	Switch N/O	GV31O		Limit switch, gate valve V31 open	Pos GV31
108		Switch N/O	GV31C		Limit switch, gate valve V31 closed	

Controlled Outputs

Channel		Output	Tag		Signal description	Tag Name
1		24Vdc	GV01		Allow Gate valve 1 to operate	Op GV1
2		24Vdc	GV02		Allow Gate valve 2 to operate	Op GV2
3		24Vdc	GV03		Allow Gate valve 3 to operate	Op GV3
4		24Vdc	GV04		Allow Gate valve 4 to operate	Op GV4
5		24Vdc	GV05		Allow Gate valve 5 to operate	Op GV5
6		24Vdc	GV06		Allow Gate valve 6 to operate	Op GV6
7		24Vdc	GV07		Allow Gate valve 7 to operate	Op GV7
8		24Vdc	GV08		Allow Gate valve 8 to operate	Op GV8
9		24Vdc	GV09		Allow Gate valve 9 to operate	Op GV9
10		24Vdc	GV10		Allow Gate valve 10 to operate	Op GV10
11		24Vdc	FLS04		Allow fluorescent screen to operate	Op FLS04
12		24Vdc	GV11		Allow Gate valve 11 to operate	Op GV11
13		24Vdc	GV12		Allow Gate valve 12 to operate	Op GV12
14		24Vdc	GV13		Allow Gate valve 13 to operate	Op GV13
15		24Vdc	GV14		Allow Gate valve 14 to operate	Op GV14
16		24Vdc	GV15		Allow Gate valve 15 to operate	Op GV15
17		24Vdc	GV16		Allow Gate valve 16 to operate	Op GV16
18		24Vdc	GV17		Allow Gate valve 17 to operate	Op GV17
19		24Vdc	GV18		Allow Gate valve 18 to operate	Op GV18
20		24Vdc	GV19		Allow Gate valve 19 to operate	Op GV19
21		24Vdc	GV20		Allow Gate valve 20 to operate	Op GV20
22		24Vdc	GV21		Allow Gate valve 21 to operate	Op GV21
23		24Vdc	GV22		Allow Gate valve 22 to operate	Op GV22
24		24Vdc	GV23		Allow Gate valve 23 to operate	Op GV23
25		24Vdc	GV24		Allow Gate valve 24 to operate	Op GV24
26		24Vdc	GV25		Allow Gate valve 25 to operate	Op GV25
27		24Vdc	GV26		Allow Gate valve 26 to operate	Op GV26
28		24Vdc	GV27		Allow Gate valve 27 to operate	Op GV27
29		24Vdc	GV28		Allow Gate valve 28 to operate	Op GV28
30		24Vdc	GV29		Allow Gate valve 29 to operate	Op GV29
31		24Vdc	GV30		Allow Gate valve 30 to operate	Op GV30
32		24Vdc	FLS14		Allow fluorescent screen to operate	Op FLS14
33		24Vdc	GV31		Allow Gate valve 31 to operate	Op GV31

Reference Documents:

Reference Number	Date/ Issue	Title
SB1341-14-CN-0042	19/09/14	NIST Contract
	April 2014	NIST NSLS-II SST and BMM Beamline Backbones, Volume 2A, SST Technical Proposal
S3160	Nov 2014/REV 01	NIST SST BEAMLINE S3160 QUALITY PLAN

FMB Oxford
Osney Mead
Oxford OX2 0ES
UK

Contact: Andrew Fairley
Telephone: +44 (0)1865 320 313
Fax: +44 (0)1865 320 301
E-mail: andrew.fairley@fmb-oxford.com

Change log:

Revision	Date	Summary of Change	Approval
1.0	06/01/15	First Issue	NJB
2.0	17/08/15	Platinum binder layer added for Gold coating. No binder layer permitted for Carbon coating.	AJF
3.0			
4.0			
5.0			
6.0			

TABLE OF CONTENTS **1**

1. *INTRODUCTION* **3**

1.1 AXIS 3

2. *SPECIFICATIONS* **5**

2.1 MIRROR SYSTEM 5

2.1.1 L3 Mirror Optic *5*

2.2 MOTIONS 6

2.3 VACUUM SYSTEM 7

2.4 VACUUM VESSEL 8

2.5 ELECTRICAL DATA 9

2.5.1 Linear Actuators (Hexapod legs) *9*

2.5.2 Encoder Data *9*

2.6 LIFTING POINTS 9

2.7 ALIGNMENT FEATURES 9

3. FACTORY TESTING **10**

4. INSTALLATION AND UNIT ACCEPTANCE **11**

5. *SCOPE OF SUPPLY* **12**

1. *INTRODUCTION*

The L3 mirror system is located upstream of the μXPS endstation (and mirror system L4). The purpose the L3 mirror system is to guide the tender x rays towards L4 and the end station. The L3 optic is planar and uncooled. The optic is mounted to the base of the vacuum vessel and is manipulated using a hexapod, which gives six degrees of freedom.

1.1 AXIS

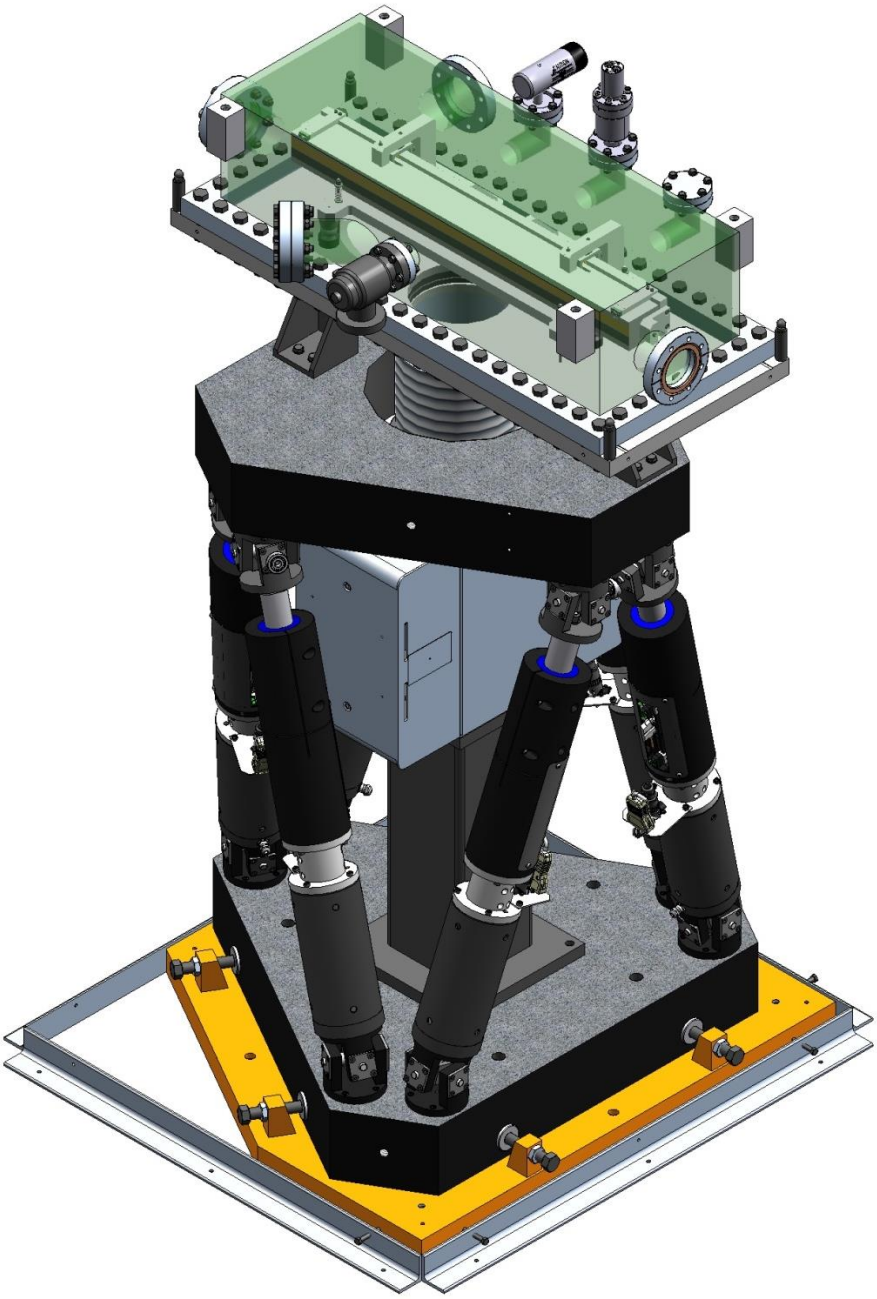

Figure 1. L3 mirror system

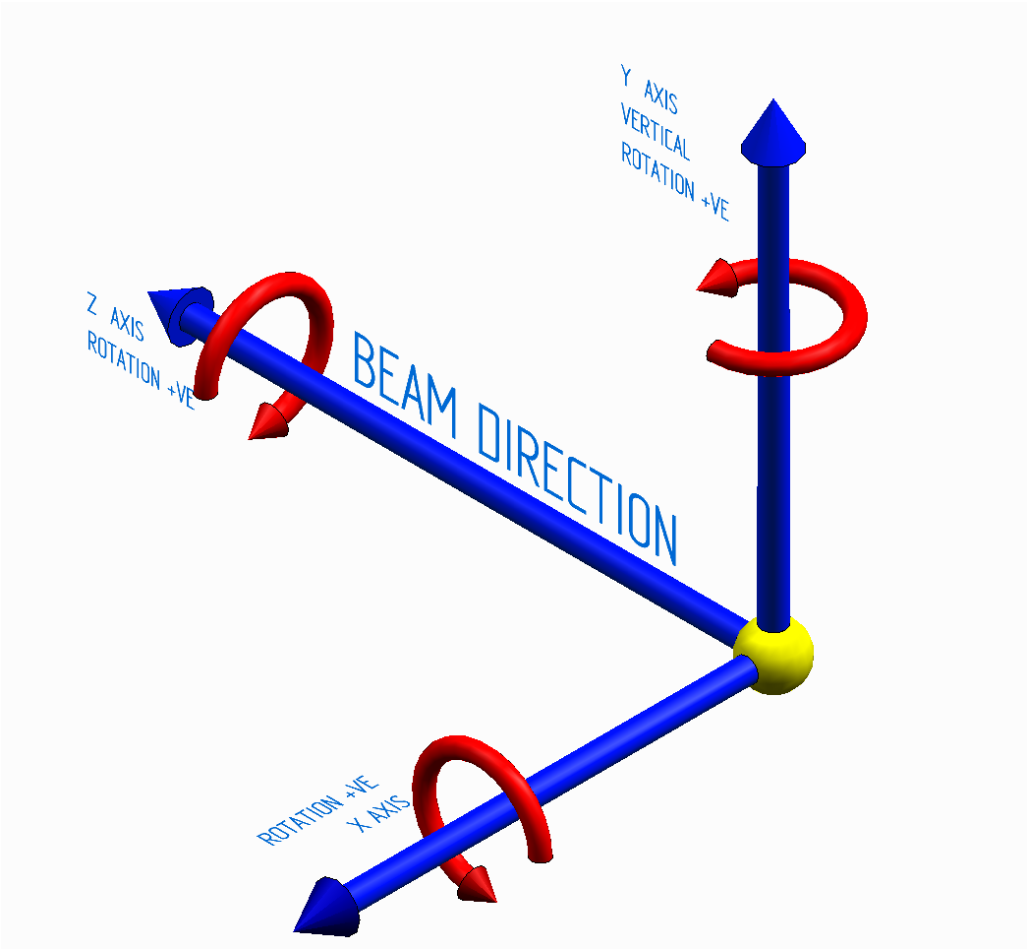

Figure 2. Beamline coordinate system

Inboard is defined as being in the negative x direction and outboard in the postive x direction.

The coordinate system employed complies with NSLS-II document:

Beamline Coordinate System Standards LT-C-XFD-STD-BL-COORD-001.

2. *SPECIFICATIONS*

2.1 MIRROR SYSTEM

Incoming Beam Height	1415 mm
Operating Position	Horizontally deflecting outboard
Manual Adjustments	± 10 mm in x and z (from grouted-in baseplate)
Optic location relative to centre of straight section (mm).	-40.33, 15, 62258 (x, y, z)

2.1.1 L3 Mirror Optic

Substrate material	Single crystal silicon
Substrate dimensions	670 mm L x 50 mm W x 60 mm D
Active Area (centred on substrate to within ± 0.5mm)	660 mm x 30 mm
Grazing incidence angle	0.61°
Substrate Shape	Planar, Tangential Radius ≥20 km, Sagittal Radius ≥3 km
Tangential slope error	<0.25 µrad RMS over active length
Sagittal slope error	<5 µrad RMS over active length on prepared substrate
Coating	Au 300 Å ± 10% thick, 21 mm wide over Pt 100 Å ± 10% thick binder layer C 300 Å ± 10% thick 21 mm wide. No binder layer permitted.
Surface Roughness	<3 Å RMS
Surface Quality	0.5 scratches or points per cm^2 over 99% of active optical area
Cooling	Uncooled

2.2 MOTIONS

Motion	Parameter	Specification
Pitch (Ry)	Drive	Linear actuators, fitted with limit switches & encoder.
	Range	Nominal position ± 10 mrad
	Resolution	< 1µrad
	Repeatability	< 5 µrad
Roll (Rz)	Drive	Linear actuators, fitted with limit switches & encoder.
	Range	± 10 mrad
	Resolution	< 5 µrad
	Repeatability	< 10 µrad
Yaw (Rx)	Drive	Linear actuators, fitted with limit switches & encoder.
	Range	± 10 mrad
	Resolution	< 5 µrad
	Repeatability	< 10 µrad
Vertical (Ty)	Drive	Linear actuators, fitted with limit switches & encoder.
	Range	± 20 mm
	Resolution	< 1 µm
	Repeatability	< 5 µm

Lateral (Tx)	Drive	Linear actuators, fitted with limit switches & encoder.
	Range	± 10 mm
	Resolution	< 1 µm
	Repeatability	< 5 µm
Longitudinal (Tz)	Drive	Linear actuators, fitted with limit switches & encoder.
	Range	± 5 mm
	Resolution	< 2 µm
	Repeatability	< 10 µm

2.3 VACUUM SYSTEM

Maximum bakeout temperature – vessel and internal components	150-200 °C
Vacuum	UHV compatible (< 5 x10^{-10} mbar). Masses > 38 AMU shall have total pressure < 10^{-11} Torr (1.33 x 10^{-11} mbar)
Helium leak rate	< 1 x 10^{-10} mbar l/sec
Vacuum Pump	Gamma vacuum 300T ion pump located beneath the vessel
Vacuum gauges	One pirani gauge (MKS type 317)and one cold cathode gauge(MKS type 422) located on the mirror vessel
Right Angle Valve	VAT Valve type 54, DN40/CF70.

2.4 VACUUM VESSEL

The vacuum vessel for the L3 mirror system is rectangular due to the length of the optic. The optic is mounted to the vessel, whose position is manipulated with the hexapod.

Purpose	Location	Size	Qty
Beam In	Beam inlet port at end 1	DN63/CF114	1
Beam Out	Beam outlet port at end 2	DN63/CF114R	1
Ion Pump	Mounted on the base granite of the hexapod.	DN150/CF200	1
Roughing Port for RA valve	Outboard side of vessel	DN40/CF70	1
Viewport	Outboard side of vessel	DN63/CF114	1
Viewport	Incoming wall of vessel angled to look at substrate surface	DN40/CF70	1
Vacuum Gauges	Side of vessel	DN40/CF70	2
Spare	Top of vessel	DN63/CF114	1
Spare	Top of vessel	DN40/CF70	1
Mirror Loading	Baseplate	Aluminium wire seal	1

2.5 ELECTRICAL DATA

2.5.1 Linear Actuators (Hexapod legs)

Motor Type	McLennan Type 23HS309 stepper motor
Holding torque	87 Ncm
Step angle (full step drive)	1.8°/ or 200 steps/rev
Driving current	2 A
Gear box ratio	25:1
Thread pitch	2 mm
Resolution per step	0.4 µm
Maximum movement per actuator	± 50 mm
Connector (Motor and limits)	12 way trim trio (UTO)

2.5.2 Encoder Data

Readhead type	Renishaw Tonic T1000-05A
Readhead (interpolator) resolution	0.1 µm
Scale type	RGSZ20
Connector	15-Way sub D

2.6 LIFTING POINTS

L3 mirror system weight: 500 kg approximately.

The mirror system is provided with three M16 lifting points in the base of the hexapod, in addition to three in the upper platform.

A lifting diagram for the system will be provided.

2.7 ALIGNMENT FEATURES

Fiducial mounts will be provided on the baseplate and on the upper platform of the hexapod. These will take the form of 0.25” reamed (H7) holes, suitable for 0.5” or 1.5” spheres.

3. FACTORY TESTING

Testing at FMB Oxford consists of Motion Testing, Vacuum Testing and Fiducialisation.

Full specifications and procedures covering all factory testing will be prepared in advance and these will be submitted to the customer prior to final design approval. Representatives from the customer are invited to witness these TESTS at FMB Oxford's works.

4. INSTALLATION AND UNIT ACCEPTANCE

The site acceptance testing, included in the installation option, will ensure that all components are carefully surveyed into position, all motors, actuators and sensors are functioning properly and the vacuum specifications are met. All motions will be tested and the correct functioning of all limit and datum switches checked. The complete set of detailed factory tests are not repeated on site.

There will be a full leak check of the installed vacuum sections. We expect that a turbo pump station, RGA rig, and He leak checker to be provided by the customer for our use while at the customer's site.

Final site acceptance will include:

- All factory test data, documentation and manuals
- Correct operation of all motions, limits and datum switches using FMB-O controls and cabling.
- Leak testing at the best achievable sensitivity after 24 hrs of pumping and prior to on site customer bakeout

5. *SCOPE OF SUPPLY*

- L3 optic and mirror system
- 300 l/s ion pump & pump controller (Gamma)
- Right angle valve (Vat valve)
- Cold cathode (series 422) and pirani (series 317) gauges and gauge controller (MKS 937B)
- Motion controls as specified in the controls functional specification
- Field cables

Reference Documents:

Reference Number	Date/ Issue	Title
SB1341-14-CN-0042	19/09/14	NIST Contract
	April 2014	NIST NSLS-II SST and BMM Beamline Backbones, Volume 2A, SST Technical Proposal
S3160	Nov 2014/REV 01	NIST SST BEAMLINE S3160 QUALITY PLAN

FMB Oxford
Osney Mead
Oxford OX2 0ES
UK

Contact: Andrew Fairley
Telephone: +44 (0)1865 320 313
Fax: +44 (0)1865 320 301
E-mail: andrew.fairley@fmb-oxford.com

Change log:

Revision	Date	Summary of Change	Approval
1.0	06/01/15	First Issue	NJB
2.0	17/08/15	IC-101 replaced by I400. Port for drain current feedthrough added. Tangential slope error amended. L4/M4B functional specs combined	AJF
3.0			
4.0			
5.0			
6.0			

TABLE OF CONTENTS **1**

1. *INTRODUCTION* **3**

1.1 AXIS 4

2. *SPECIFICATIONS* **5**

2.1 MIRROR SYSTEM L4/M4B 5

2.1.1 L4 Mirror Optic *5*

2.1.2 M4B Mirror Optic *6*

2.2 MOTIONS 7

2.3 VACUUM SYSTEM 8

2.4 VACUUM VESSELS 8

2.4.1 Vacuum Vessel L4 ..... *8*

2.4.2 Vacuum Vessel M4B *9*

2.5 MIRROR CURRENT TAKEOFFS 10

2.6 ELECTRICAL DATA 10

2.6.1 Linear Actuators (Hexapod legs) *10*

2.6.2 Encoder Data *10*

2.6.3 Electrical Interfacing *11*

2.7 LIFTING POINTS 11

2.8 ALIGNMENT FEATURES 11

3. FACTORY TESTING **12**

4. INSTALLATION AND UNIT ACCEPTANCE **13**

5. *SCOPE OF SUPPLY* **14**

1. *INTRODUCTION*

The L4/M4B mirror system is located directly upstream of the μXPS endstation. The purpose of both mirrors is to to focus the x rays at the μXPS end station. The M4B optic is ellipsoidal, uncooled and foucuses the soft x-rays from the transfer branch onto the end station. The L4 optic is also an uncooled, ellipsoidal optic which focuses the tender x-rays of the 'L branch' onto the end station. The optics are mounted to the bases of the vacuum vessels and are manipulated using a hexapod, which gives six degrees of freedom. The optics are fitted with drain current take offs.

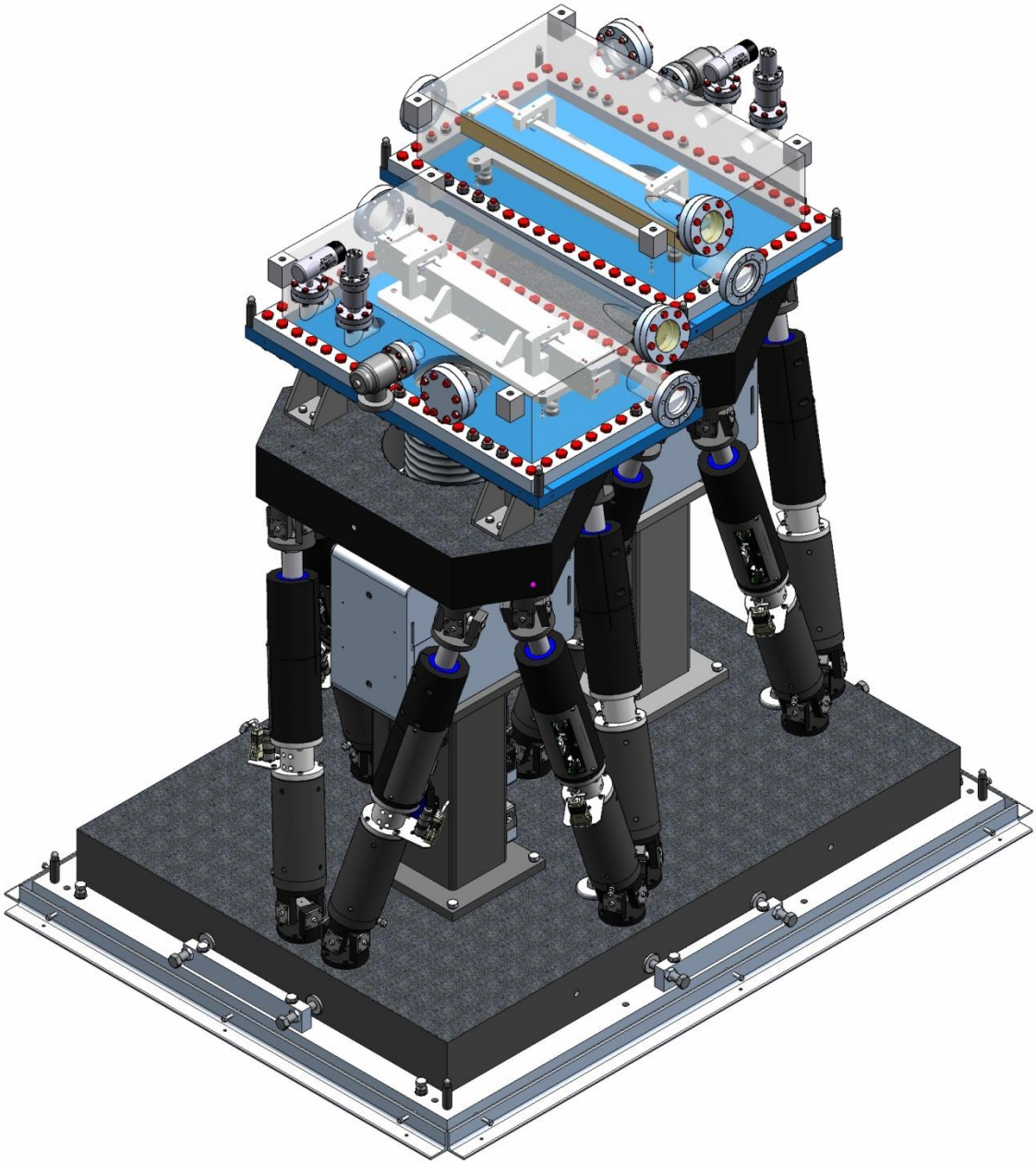

Figure 1. L4/M4B Mirror Sytem

1.1 AXIS

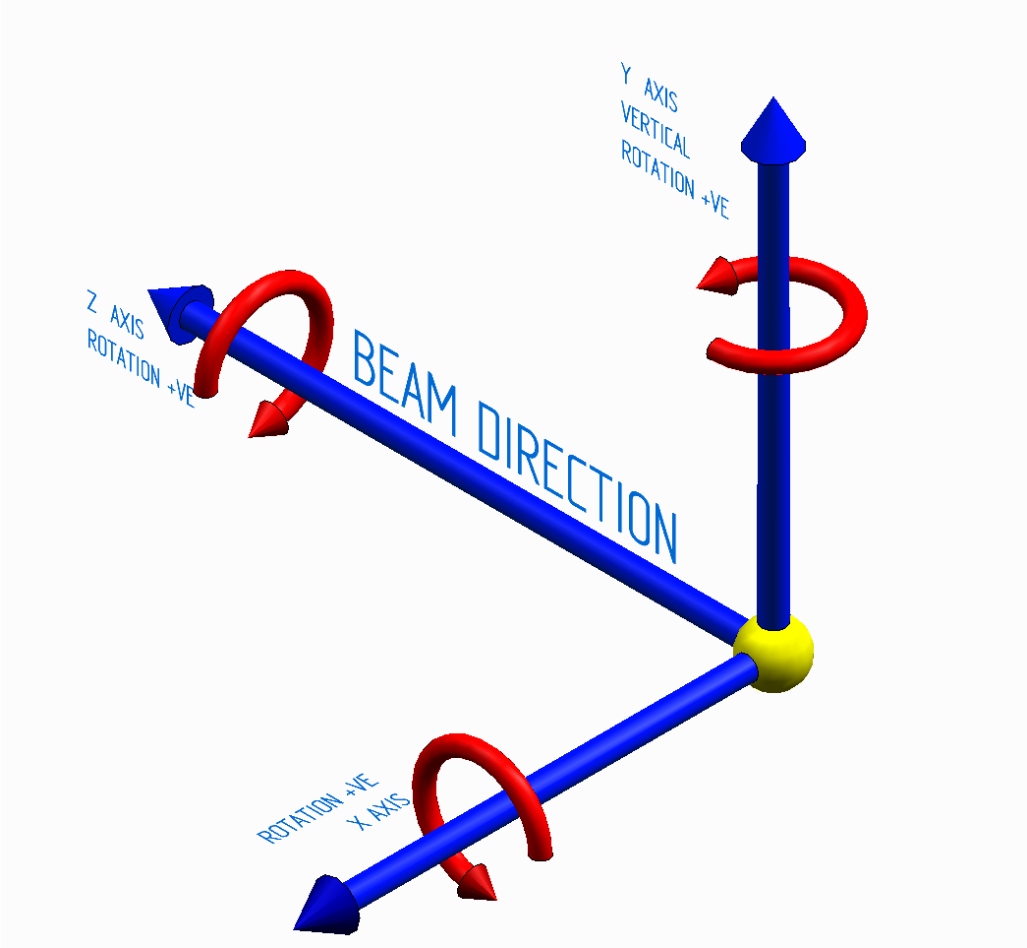

Figure 2. Beamline coordinate system

Inboard is defined as being in the negative x direction and outboard in the postive x direction.

The coordinate system employed complies with NSLS-II document:

Beamline Coordinate System Standards LT-C-XFD-STD-BL-COORD-001.

2. *SPECIFICATIONS*

2.1 MIRROR SYSTEM L4/M4B

Incoming Beam Height	1415 mm
Operating Position **(L4)**	Horizontally deflecting outboard, vertically and horizontally refocusing.
Operating Position **(M4B)**	Horizontally deflecting inboard, vertically and horizontally refocusing.
Manual Adjustments	± 10 mm in x and z (from grouted-in baseplate)
Optic location relative to centre of straight section (mm) – **(L4)**	66.59, 15, 66766 (x, y, z)
Optic location relative to centre of straight section (mm) – **M4B**	428.35, 15, 66570 (x, y, z)

2.1.1 L4 Mirror Optic

Substrate material	Fused silica
Substrate dimensions	600 mm L x 50 mm W x 60 mm D
Active Area (centred on substrate to within ± 0.5mm)	540 mm x 6 mm
Substrate Shape	Ellipsoidal. Major axis 35509.4 mm ± 1% Minor axis 152.8 mm ± 1%. Mirror pole X_0: 32509.7 mm (off axis) ± 1%. Mirror pole Y_0: 61.5 mm (off axis)
Grazing incidence angle	0.61°
Distance to source	68018.8 mm
Distance to image	3000.1 mm
Tangential slope error	<1.0 µrad RMS over active length

Sagittal slope error	<10 µrad RMS over active length on prepared substrate
Coating	Au 300 Å ± 10% thick 15 mm wide. No binder layer permitted.
Surface Roughness	<3 Å RMS
Surface Quality	0.5 scratches or points per cm^2 over 99% of active optical area
Cooling	Uncooled

2.1.2 M4B Mirror Optic

Substrate material	Fused silica
Substrate dimensions	600 mm L x 60 mm W x 60 mm D
Active Area (centred on substrate to within ± 0.5mm)	540 mm x 21 mm
Substrate Shape	Ellipsoidal. Major axis 10604.9 mm ± 1% Minor axis 231.9 mm ± 1%. Mirror pole $X_{0:}$ 7405.7 mm (off axis) ± 1%.
Grazing incidence angle	1.75°
Distance to source	18008.9 mm
Distance to image	3201 mm
Tangential slope error	<1.0 µrad RMS over active length
Sagittal slope error	<10 µrad RMS over active length on prepared substrate
Coating	Au 300 Å ± 10% thick 30 mm wide No binder layers are permitted.
Surface Roughness	<3 Å RMS
Surface Quality	0.5 scratches or points per cm^2 over 99% of active optical area

Cooling	Uncooled

2.2 MOTIONS

Motion	Parameter	Specification
Pitch (Ry)	Drive	Linear actuators, fitted with limit switches & encoder.
	Range	Nominal position ± 10 mrad
	Resolution	< 1µrad
	Repeatability	< 5 µrad
Roll (Rz)	Drive	Linear actuators, fitted with limit switches & encoder.
	Range	± 10 mrad
	Resolution	< 5 µrad
	Repeatability	< 10 µrad
Yaw (Rx)	Drive	Linear actuators, fitted with limit switches & encoder.
	Range	± 10 mrad
	Resolution	< 5 µrad
	Repeatability	< 10 µrad
Vertical (Ty)	Drive	Linear actuators, fitted with limit switches & encoder.
	Range	± 20 mm
	Resolution	< 1 µm
	Repeatability	< 5 µm

Lateral (Tx)	Drive	Linear actuators, fitted with limit switches & encoder.
	Range	± 10 mm
	Resolution	< 1 µm
	Repeatability	< 5 µm
Longitudinal (Tz)	Drive	Linear actuators, fitted with limit switches & encoder.
	Range	± 5 mm
	Resolution	< 2 µm
	Repeatability	< 10 µm

2.3 VACUUM SYSTEM

Maximum bakeout temperature – vessel and internal components	150-200 °C
Vacuum	UHV compatible (< 5 x10^{-10} mbar). Masses > 38 AMU shall have total pressure < 10^{-11} Torr (1.33 x 10^{-11} mbar)
Helium leak rate	< 1 x 10^{-10} mbar l/sec
Vacuum Pump	Gamma vacuum 300T ion pump located beneath the vessel
Vacuum gauges	One pirani gauge (MKS type 317)and one cold cathode gauge(MKS type 422) located on the mirror vessel
Right Angle Valve	VAT Valve type 54, DN40/CF70.

2.4 VACUUM VESSELS

The vacuum vessels for both mirror systems are rectangular due to the lengths of the optics. The optics are mounted to the vessel, whose position is manipulated with the hexapod.

2.4.1 Vacuum Vessel L4

Purpose	Location	Size	Qty

Beam In	Beam inlet port at end 1	DN63/CF114	1
Beam Out	Beam outlet port at end 2	DN63/CF114R	1
Ion Pump	Mounted on the base granite of the hexapod.	DN150/CF200	1
Roughing Port for RA valve	Outboard side of vessel	DN40/CF70	1
Viewport	Outboard side of vessel	DN63/CF114	1
Viewport	Incoming wall of vessel angled to look at substrate surface	DN40/CF70	1
Vacuum Gauges	Side of vessel	DN40/CF70	2
Spare	Top of vessel	DN63/CF114	1
Spare	Top of vessel	DN40/CF70	1
Mirror Loading	Baseplate	Aluminium wire seal	1
Optic drain current feedthrough (2x BNC)	Baseplate	DN40/CF70	1

2.4.2 Vacuum Vessel M4B

Purpose	**Location**	**Size**	**Qty**
Beam In	Beam inlet port at end 1	DN63/CF114	1
Beam Out	Beam outlet port at end 2	DN63/CF114	1
Ion Pump	Mounted on the base granite of the hexapod.	DN150/CF200	1
Roughing Port for RA valve	Outboard side of vessel	DN40/CF70	1
Viewport	Outboard side of vessel	DN63/CF114	1
Viewport	Incoming wall of vessel angled to look at	DN40/CF70	1

	substrate surface		
Vacuum Gauges	Side of vessel	DN40/CF70	2
Spare	Top of vessel	DN63/CF114	1
Spare	Top of vessel	DN40/CF70	1
Mirror Loading	Baseplate	Aluminium wire seal	1
Drain current feedthrough	Baseplate	DN40/CF70	1

2.5 MIRROR CURRENT TAKEOFFS

Both mirrors are fitted with drain current takeoffs to monitor the beam intensity. Two physical takeoffs are fitted to the optic stripe to allow the continuity of the electrical connection to be checked. The drain current will be measured using an I400.

2.6 ELECTRICAL DATA

2.6.1 Linear Actuators (Hexapod legs)

Motor Type	McLennan Type 23HS309 stepper motor
Holding torque	87 Ncm
Step angle (full step drive)	1.8°/ or 200 steps/rev
Driving current	2 A
Gear box ratio	25:1
Thread pitch	2 mm
Resolution per step	0.4 µm
Maximum movement per actuator	± 50 mm
Connector (Motor and limits)	12 way trim trio (UTO)

2.6.2 Encoder Data

Readhead type	Renishaw Tonic T1000-05A
Readhead (interpolator) resolution	0.1 µm
Scale type	RGSZ20
Connector	15-Way sub D

2.6.3 Electrical Interfacing

All in air motors, limits and encoders are connected locally to the relevant drive.

2.7 LIFTING POINTS

Combined weight of L4/M4B: 1800 kg approximately.

The mirror system is provided with four M16 lifting points in the base of the hexapod, in addition to three in the upper platform.

A lifting diagram for the system will be provided.

2.8 ALIGNMENT FEATURES

Fiducial mounts will be provided on the baseplate and on the upper platform of the hexapod. These will take the form of 0.25” reamed (H7) holes, suitable for 0.5” or 1.5” spheres.

3. FACTORY TESTING

Testing at FMB Oxford consists of Motion Testing, Vacuum Testing and Fiducialisation.

Full specifications and procedures covering all factory testing will be prepared in advance and these will be submitted to the customer prior to final design approval. Representatives from the customer are invited to witness these tests at FMB Oxford's works.

4. INSTALLATION AND UNIT ACCEPTANCE

The site acceptance testing, included in the installation option, will ensure that all components are carefully surveyed into position, all motors, actuators and sensors are functioning properly and the vacuum specifications are met. All motions will be tested and the correct functioning of all limit and datum switches checked. The complete set of detailed factory tests are not repeated on site.

There will be a full leak check of the installed vacuum sections. We expect that a turbo pump station, RGA rig, and He leak checker to be provided by the customer for our use while at the customer's site.

Final site acceptance will include:

- All factory test data, documentation and manuals
- Correct operation of all motions, limits and datum switches using FMB-O controls and cabling.
- Leak testing at the best achievable sensitivity after 24 hrs of pumping and prior to on site customer bakeout

5. *SCOPE OF SUPPLY*

- L4 and M4B optics and mirror system
- I400 Current amplifier (optic drain current measurement)
- MOXA
- 300 l/s ion pump & pump controller (Gamma) for each mirror vessel
- Right angle valve (Vat valve) – one per mirror vessel
- Cold cathode (series 422) and pirani (series 317) gauges and gauge controller (MKS 937B) – one of each for each mirror vessel
- Motion controls as specified in the controls functional specification.
- Field cables

S3160 NIST SST – MIRROR SYSTEM M3

Reference Documents:

Reference Number	Date/ Issue	Title
SB1341-14-CN-0042	19/09/14	NIST Contract
	April 2014	NIST NSLS-II SST and BMM Beamline Backbones, Volume 2A, SST Technical Proposal
S3160	Nov 2014/REV 01	NIST SST BEAMLINE S3160 QUALITY PLAN

FMB Oxford
Osney Mead
Oxford OX2 0ES
UK

Contact: Andrew Fairley
Telephone: +44 (0)1865 320 313
Fax: +44 (0)1865 320 301
E-mail: andrew.fairley@fmb-oxford.com

Change log:

Revision	Date	Summary of Change	Approval
1.0	06/01/15	First Issue	NJB
2.0	27/02/15	Tangential slope error amended. Port added in baseplate for DPT feedthrough. No binder layers permitted.	AJF
3.0			
4.0			
5.0			
6.0			

TABLE OF CONTENTS **1**

1. *INTRODUCTION* **3**

1.1 AXIS 3

2. *SPECIFICATIONS* **5**

2.1 MIRROR SYSTEM 5

2.1.1 M3AB Mirror Optic *5*

2.1.2 M3C Mirror Optic *6*

2.2 MOTIONS 8

2.3 VACUUM SYSTEM 9

2.4 VACUUM VESSEL 10

2.5 DITHERING MECHANISM 10

2.6 THERMAL STABILISATION CIRCUIT 11

2.7 ELECTRICAL DATA 11

2.7.1 Linear Actuators (Hexapod legs) *11*

2.7.2 Dithering Mechanism *11*

2.7.3 Encoder Data *11*

2.8 LIFTING POINTS 12

2.9 ALIGNMENT FEATURES 12

3. FACTORY TESTING **13**

4. INSTALLATION AND UNIT ACCEPTANCE **14**

5. *SCOPE OF SUPPLY* **15**

1. *INTRODUCTION*

The M3 mirror system is located downstream of the plane grating monochromator, on the soft x-ray 'M' branch. The purpose the M3 mirror system is to direct the soft x rays either to the 'M' branch or to the transfer branches of the beamline. For this reason, the mirror system is equipped with two optics, both of which are tangential ellipses. The optics focus the x-rays horizontally at precision vertical slits – either one located in the transfer branch (slit AB) or one located in the 'M' branch (slit C).

The M3 optics (M3AB and M3C) are both uncooled. The optics are mounted to the base of the vacuum vessel and are manipulated with a hexapod, which provides six degrees of freedom.

The optics are arranged side by side, so the hexapod platform translates horizontally to switch between mirror M3AB (which directs beam down the transfer line) and mirror M3C (which directs beam down the 'M' branch).

The M3C optic is fitted with a flexure based dithering mechanism to increase the horizontal spot size at the μNEXAFS end station. The beam from M3C travels to M4D and then on to the μNEXAFS end station, or it goes on to M4C to M5C and then onwards to the NEXAFS/XPS end station. In addition, the M3 optics are fitted with a thermal stabilisation circuit.

1.1 AXIS

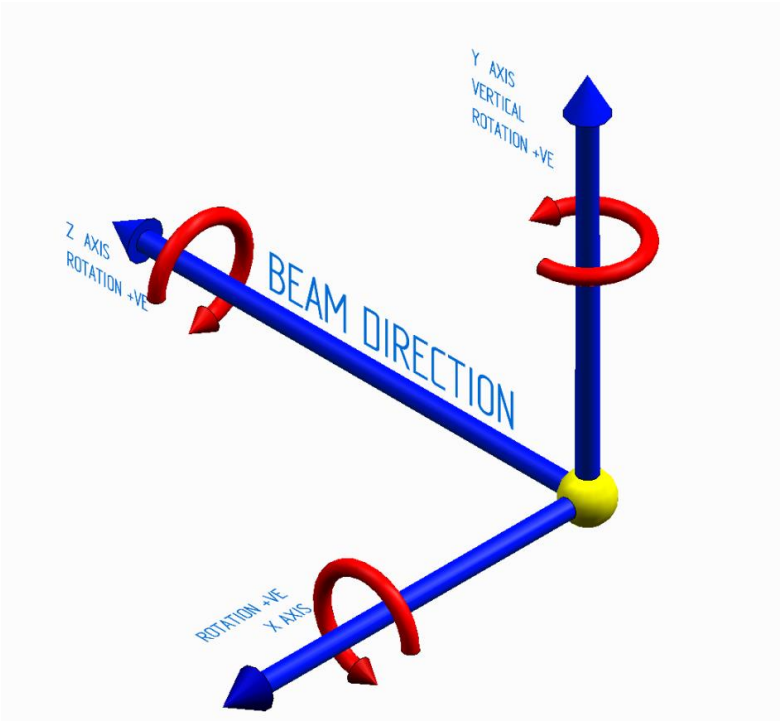

Figure 1. Beamline coordinate system

Inboard is defined as being in the negative x direction and outboard in the postive x direction.

The coordinate system employed complies with NSLS-II document:

Beamline Coordinate System Standards LT-C-XFD-STD-BL-COORD-001.

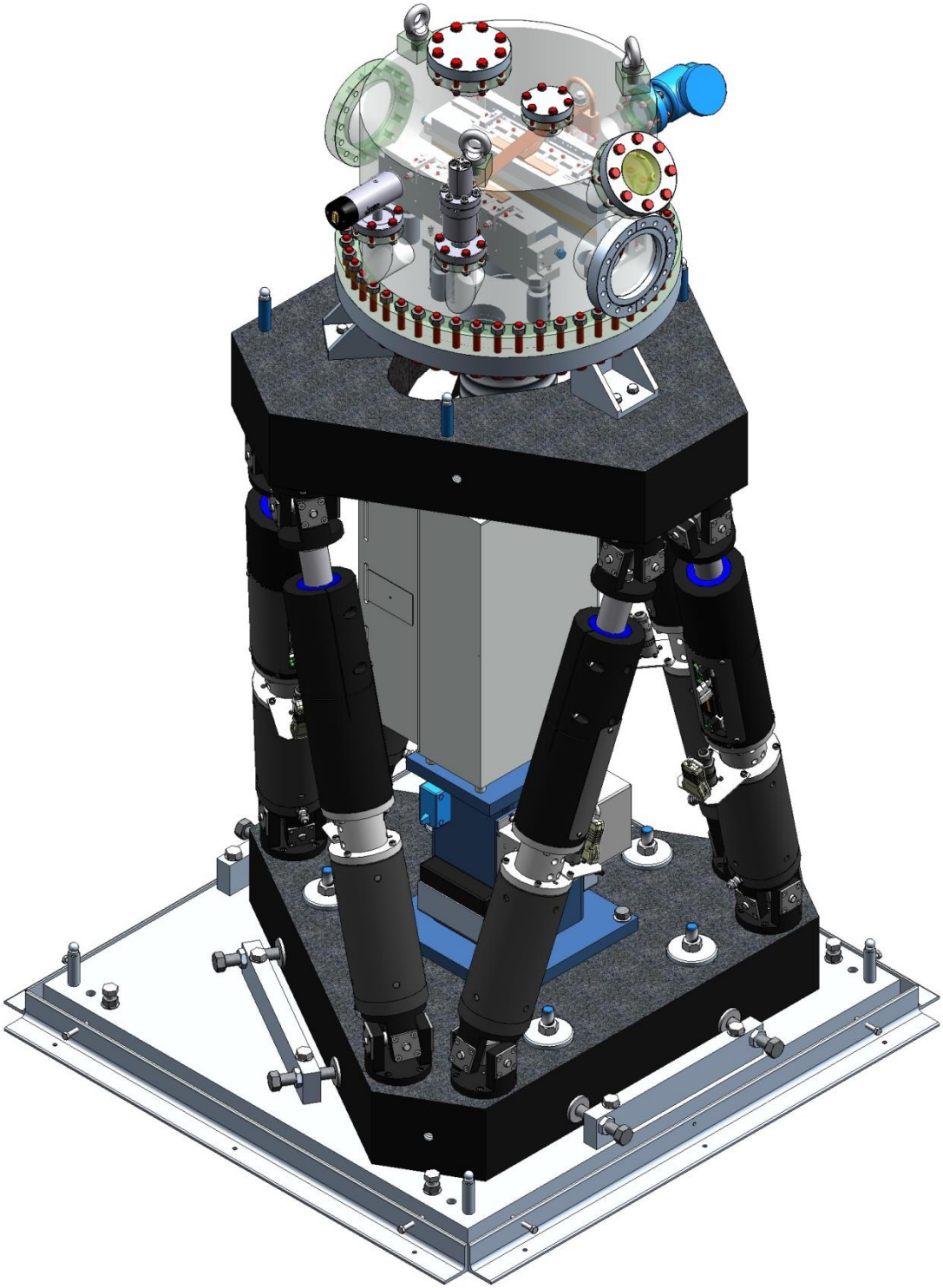

Figure 2. Mirror system M3AB/M3C

2. *SPECIFICATIONS*

2.1 MIRROR SYSTEM

Incoming Beam Height	1415 mm
Operating Position	Horizontally deflecting inboard, horizontally focusing (M3AB). Horizontally deflecting outboard, horizontally focusing (M3C).
Manual Adjustments	± 10 mm in x and z (from grouted-in baseplate)
Optic location relative to centre of straight section (mm)	666.7, 15, 42062 (x, y, z)

2.1.1 M3AB Mirror Optic

Substrate material	Fused silica
Substrate dimensions	280 mm L x 60 mm W x 40 mm D
Active Area (centred on substrate to within ± 0.5mm)	230 mm x 45 mm
Substrate Shape	Tangential Ellipse Major axis 23665.1 mm ± 1% Minor axis 497.5 mm ± 1% Mirror pole X_0: 17168.6 mm (off axis) ± 1%. *Sagittal Radius > 3km*
Grazing incidence angle	1.75° (deflecting beam inboard towards M4A & M4B)
Distance to source	40829.9 mm
Distance to image (precision vertical slit)	6500.3 mm
Tangential slope error	< 0.5 µrad RMS over active length
Sagittal slope error	< 10 µrad RMS over active length on prepared substrate

Coating	C 300 Ǻ ± 10% thick 13 mm wide Au 300 Ǻ ± 10% thick 13 mm wide Ni 300 Ǻ ± 10% thick 13 mm wide No binder layers are permitted.
Surface Roughness	<3 Å RMS
Surface Quality	0.5 scratches or points per cm^2 over 99% of active optical area
Cooling	Uncooled

2.1.2 M3C Mirror Optic

Substrate material	Fused silica
Substrate dimensions	310 mm L x 60 mm W x 40 mm D
Active Area (centred on substrate to within ± 0.5mm)	270 mm x 45 mm
Substrate Shape	Tangential Ellipse Major axis 23664.9 mm ± 1% Minor axis 426.4 ± 1% Mirror pole X_0 (off axis): 17167.8 mm ± 1%. *Sagittal Radius > 3km*
Grazing incidence angle	1.5° (deflecting outboard to M4C & M4D).
Distance to source	40829.9 mm
Distance to image (precision vertical slit)	6499.9 mm
Tangential slope error	<0.5 µrad RMS over active length
Sagittal slope error	< 10 µrad RMS over active length on prepared substrate

Coating	C 300 Á ± 10% thick 13 mm wide Au 300 Á ± 10% thick 13 mm wide Ni 300 Á ± 10% thick 13 mm wide No binder layers are permitted
Surface Roughness	<3 Å RMS
Surface Quality	0.5 scratches or points per cm^2 over 99% of active optical area
Cooling	Uncooled

2.2 MOTIONS

Motion	Parameter	Specification
Pitch (Ry)	Drive	Linear actuators, fitted with limit switches & encoder.
	Range	Nominal position ± 10 mrad
	Resolution	< 1µrad
	Repeatability	< 5 µrad
Roll (Rz)	Drive	Linear actuators, fitted with limit switches & encoder.
	Range	± 10 mrad
	Resolution	< 5 µrad
	Repeatability	< 10 µrad
Yaw (Rx)	Drive	Linear actuators, fitted with limit switches & encoder.
	Range	± 10 mrad
	Resolution	< 5 µrad
	Repeatability	< 10 µrad
Vertical (Ty)	Drive	Linear actuators, fitted with limit switches & encoder.
	Range	± 22 mm
	Resolution	< 1 µm
	Repeatability	< 5 µm

Lateral (Tx)	Drive	Linear actuators, fitted with limit switches & encoder.
	Range	± 30 mm
	Resolution	< 1 µm
	Repeatability	< 5 µm
Longitudinal (Tz)	Drive	Linear actuators, fitted with limit switches & encoder.
	Range	± 5 mm
	Resolution	< 2 µm
	Repeatability	< 10 µm

2.3 VACUUM SYSTEM

Maximum bakeout temperature – vessel and internal components	150-200 °C
Vacuum	UHV compatible (< 5 x10^{-10} mbar). Masses > 38 AMU shall have total pressure < 10^{-11} Torr (1.33 x 10^{-11} mbar)
Helium leak rate	< 1 x 10^{-10} mbar l/sec
Vacuum Pump	Gamma vacuum 500T ion pump located on a stand adjacent to the mirror system
Vacuum gauges	One pirani gauge (MKS type 317)and one cold cathode gauge(MKS type 422) located on the mirror vessel
Right Angle Valve	VAT Valve type 54, DN40/CF70.

2.4 VACUUM VESSEL

The vacuum vessel for the M3 mirror system is rectangular.

Purpose	Location	Size	Qty
Beam In	Beam inlet port at end 1	DN100/CF150	1
Beam Out	Beam outlet port at end 2	DN100/CF150	1
Ion Pump	Mounted on the base granite of the hexapod.	DN100/CF150	1
Roughing Port for RA valve	Inboard side of vessel	DN40/CF70	1
Viewport	Incoming wall of vessel angled to look at substrate surface	DN63/CF114	1
Vacuum Gauges	Outboard side of vessel	DN40/CF70	2
Spare	Top of vessel	DN63/CF114	1
Spare	Top of vessel	DN40/CF70	1
Port for mounting burst disc	Baseplate	DN40/CF70	1
DPT wiring feedthrough	Baseplate	DN63/CF114	1
Thermal stabilisation feedthrough	Baseplate	DN63/CF114	1
Mirror Loading	Baseplate	DN400/CF470	1

2.5 DITHERING MECHANISM

The M3C mirror system is fitted with a piezo-driven flexure mechanism to dither the beam (increase the horizontal spot size) at µNEXAFS end station. The mirror needs to be dithered by approximately ±0.22 mrad to obtain a 20 mm horizontal stripe at the end station.

The M3C optic is used in combination with either the M4D optic (to the µNEXAFS end station) or the M4C and M5C optics (to the NEXAFS/XPS end station).

2.6 THERMAL STABILISATION CIRCUIT

Both optics are fitted with a side clamped copper block, which is attached to a cooled copper piece via flexible copper braids. The copper block is cooled by water provided by a chiller. There are no in vacuum water joints.

2.7 ELECTRICAL DATA

2.7.1 Linear Actuators (Hexapod legs)

Motor Type	McLennan Type 23HS309 stepper motor
Holding torque	87 Ncm
Step angle (full step drive)	1.8°/ or 200 steps/rev
Driving current	2 A
Gear box ratio	25:1
Thread pitch	2 mm
Resolution per step	0.4 µm
Maximum movement per actuator	± 50 mm
Connector (Motor and limits)	12 way trim trio (UTO)

2.7.2 Dithering Mechanism

Actuator type	Preloaded piezo stack driven flexure.
Range	±0.25 mrad

2.7.3 Encoder Data

Readhead type	Renishaw Tonic T1000-05A
Readhead (interpolator) resolution	0.1 µm
Scale type	RGSZ20
Connector	15-Way sub D

2.8 LIFTING POINTS

M3 mirror system weight: 500 kg approximately.

The mirror system is provided with three M16 lifting points in the base of the hexapod, in addition to three in the upper platform.

A lifting diagram for the system will be provided.

2.9 ALIGNMENT FEATURES

Fiducial mounts will be provided on the baseplate and on the upper platform of the hexapod. These will take the form of 0.25” reamed (H7) holes, suitable for 0.5” or 1.5” spheres.

3. FACTORY TESTING

Testing at FMB Oxford consists of Motion Testing, Vacuum Testing and Fiducialisation.

Full specifications and procedures covering all factory testing will be prepared in advance and these will be submitted to the customer prior to final design approval. Representatives from the customer are invited to witness these tests at FMB Oxford's works.

4. INSTALLATION AND UNIT ACCEPTANCE

The site acceptance testing, included in the installation option, will ensure that all components are carefully surveyed into position, all motors, actuators and sensors are functioning properly and the vacuum specifications are met. All motions will be tested and the correct functioning of all limit and datum switches checked. The complete set of detailed factory tests are not repeated on site.

There will be a full leak check of the installed vacuum sections. We expect that a turbo pump station, RGA rig, and He leak checker to be provided by the customer for our use while at the customer's site.

Final site acceptance will include:

- All factory test data, documentation and manuals
- Correct operation of all motions, limits and datum switches using FMB-O controls and cabling.
- Leak testing at the best achievable sensitivity after 24 hrs of pumping and prior to on site customer bakeout

5. *SCOPE OF SUPPLY*

- M3AB and M3C optics and mirror system
- DPT dithering and controls for M3C.
- 500 l/s ion pump & pump controller (Gamma)
- Right angle valve (Vat valve)
- Cold cathode (series 422) and pirani (series 317) gauges and gauge controller (MKS 937B)
- Motion Controls as specified in the controls functional specification.
- Field cables

Reference Documents:

Reference Number	Date/ Issue	Title
SB1341-14-CN-0042	19/09/14	NIST Contract
	April 2014	NIST NSLS-II SST and BMM Beamline Backbones, Volume 2A, SST Technical Proposal
S3160	Nov 2014/REV 01	NIST SST BEAMLINE S3160 QUALITY PLAN

FMB Oxford
Osney Mead
Oxford OX2 0ES
UK

Contact: Andrew Fairley
Telephone: +44 (0)1865 320 313
Fax: +44 (0)1865 320 301
E-mail: andrew.fairley@fmb-oxford.com

Change log:

Revision	Date	Summary of Change	Approval
1.0	06/01/15	First Issue	NJB
2.0	17/08/15	Port added for drain current feedthrough. No binder layers are permitted.	AJF
3.0			
4.0			
5.0			
6.0			

TABLE OF CONTENTS **1**

1. *INTRODUCTION* **3**

1.1 AXIS 4

2. *SPECIFICATIONS* **5**

2.1 MIRROR SYSTEM 5

2.1.1 M4A Mirror Optic *5*

2.2 MOTIONS 6

2.3 VACUUM SYSTEM 7

2.4 VACUUM VESSEL 7

2.5 MIRROR CURRENT TAKEOFFS 8

2.6 ELECTRICAL DATA 9

2.6.1 Linear Actuators (Hexapod legs) *9*

2.6.2 Encoder Data *9*

2.7 LIFTING POINTS 9

2.8 ALIGNMENT FEATURES 9

3. FACTORY TESTING **10**

4. INSTALLATION AND UNIT ACCEPTANCE **11**

5. *SCOPE OF SUPPLY* **12**

1. *INTRODUCTION*

The M4A mirror system is located directly upstream of the HAXPES/NEXAFS endstation, on the soft x-ray transfer branch. The purpose the M4A mirror system is to focus the soft x rays at the HAXPES/NEXAFS end station. The M4A optic is ellipsoidal and uncooled. The optic is mounted to the base of the vacuum vessel and is manipulated using a hexapod, which gives six degrees of freedom. The optic is fitted with drain current take offs.

The M4A optic may also be moved out of beam to allow the soft x rays from optic M3AB to pass through to optic M4B, and from there be directed at end station μXPS.

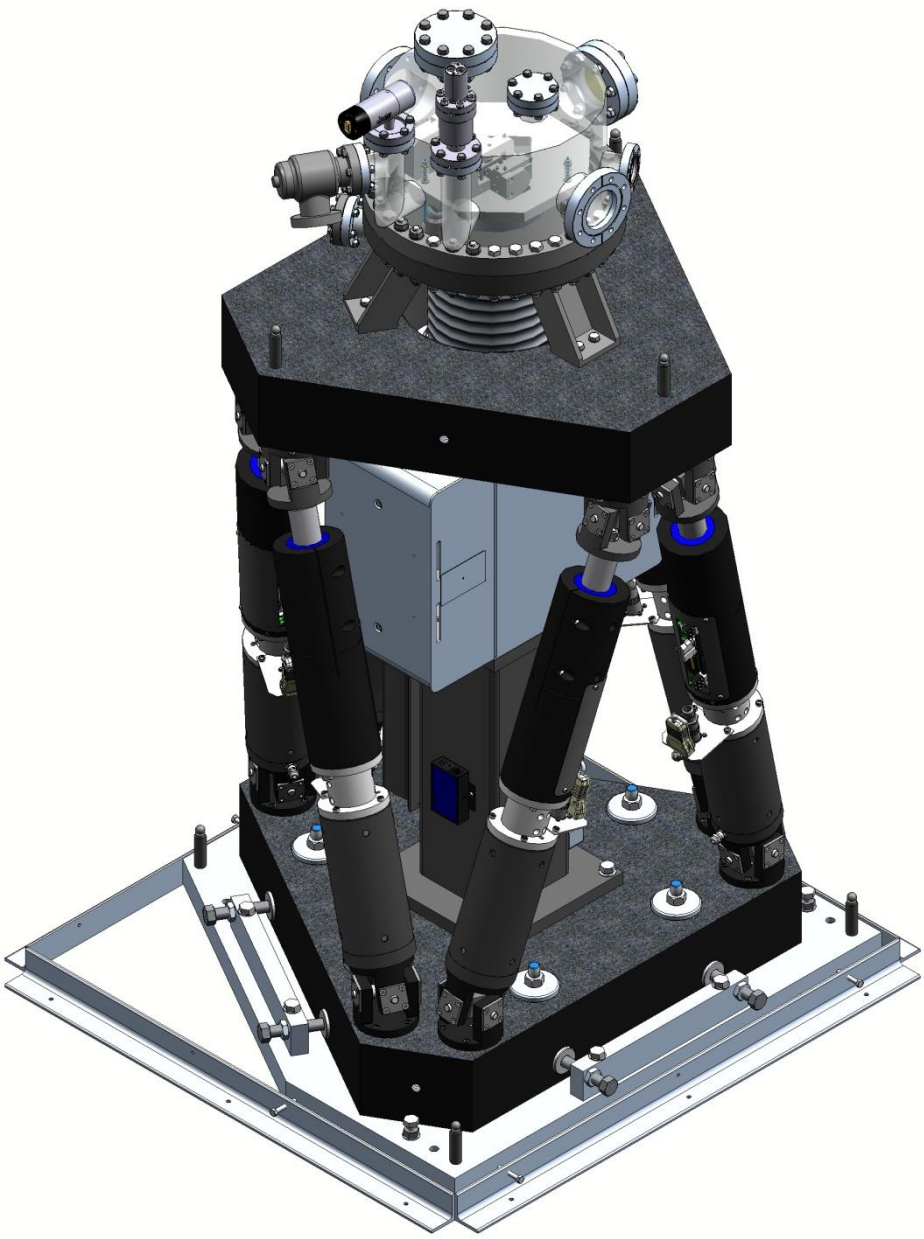

Figure 1. Mirror System M4A

1.1 AXIS

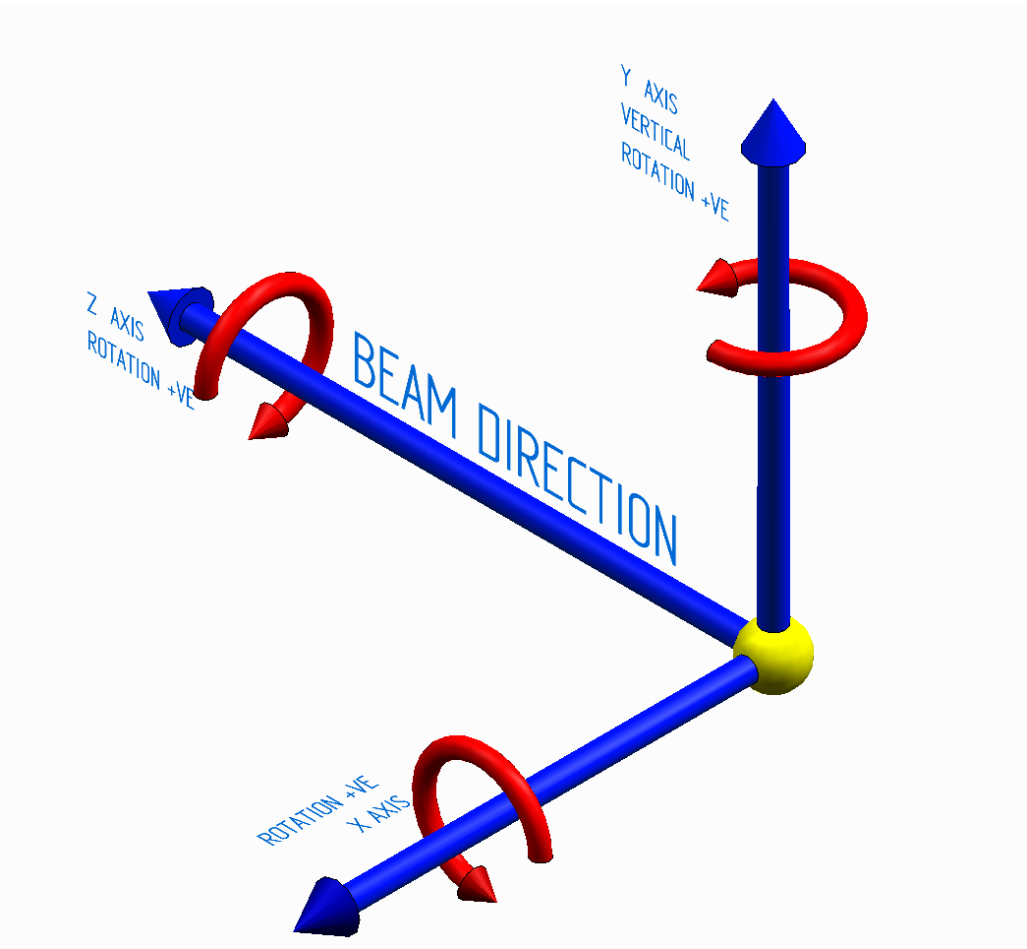

Figure 2. Beamline coordinate system

Inboard is defined as being in the negative x direction and outboard in the postive x direction.

The coordinate system employed complies with NSLS-II document:

Beamline Coordinate System Standards LT-C-XFD-STD-BL-COORD-001.

2. *SPECIFICATIONS*

2.1 MIRROR SYSTEM

Incoming Beam Height	1415 mm
Operating Position	Horizontally deflecting inboard, vertically and horizontally refocusing.
Manual Adjustments	± 10 mm in x and z (from grouted-in baseplate)
Optic location relative to centre of straight section (mm)	573.7, 15, 51628.8 (x, y, z)

2.1.1 M4A Mirror Optic

Substrate material	Fused Silica
Substrate dimensions	150 mm L x 25 mm W x 40 mm D
Active Area (centred on substrate to within ± 0.5mm)	110 mm x 10 mm
Substrate Shape	Ellipsoidal. Major axis 5903.8 ± 1% Minor axis 158.1 ± 1%. Mirror pole X_0 (off axis): 2837.9 mm ± 1%.
Grazing incidence angle	1.75°
Distance to source	3066.9 mm
Distance to image	8740.7 mm
Tangential slope error	<1.0 µrad RMS over active length
Sagittal slope error	<10 µrad RMS over active length on prepared substrate
Coating	Au 300 Å ± 10% thick 10 mm wide . No binder layers are permitted
Surface Roughness	<3 Å RMS

Surface Quality	0.5 scratches or points per cm^2 over 99% of active optical area
Cooling	Uncooled

2.2 MOTIONS

Motion	Parameter	Specification
Pitch (Ry)	Drive	Linear actuators, fitted with limit switches & encoder.
	Range	Nominal position ± 10 mrad
	Resolution	< 1µrad
	Repeatability	< 5 µrad
Roll (Rz)	Drive	Linear actuators, fitted with limit switches & encoder.
	Range	± 10 mrad
	Resolution	< 5 µrad
	Repeatability	< 10 µrad
Yaw (Rx)	Drive	Linear actuators, fitted with limit switches & encoder.
	Range	± 10 mrad
	Resolution	< 5 µrad
	Repeatability	< 10 µrad
Vertical (Ty)	Drive	Linear actuators, fitted with limit switches & encoder.
	Range	± 20 mm
	Resolution	< 1 µm
	Repeatability	< 5 µm

Lateral (Tx)	Drive	Linear actuators, fitted with limit switches & encoder.
	Range	± 10 mm
	Resolution	< 1 µm
	Repeatability	< 5 µm
Longitudinal (Tz)	Drive	Linear actuators, fitted with limit switches & encoder.
	Range	± 5 mm
	Resolution	< 2 µm
	Repeatability	< 10 µm

2.3 VACUUM SYSTEM

Maximum bakeout temperature – vessel and internal components	150-200 °C
Vacuum	UHV compatible (< 5 x10^{-10} mbar). Masses > 38 AMU shall have total pressure < 10^{-11} Torr (1.33 x 10^{-11} mbar)
Helium leak rate	< 1 x 10^{-10} mbar l/sec
Vacuum Pump	Gamma vacuum 300T ion pump located beneath the vessel
Vacuum gauges	One pirani gauge (MKS type 317)and one cold cathode gauge(MKS type 422) located on the mirror vessel
Right Angle Valve	VAT Valve type 54, DN40/CF70.

2.4 VACUUM VESSEL

The vacuum vessel for the M4A mirror system is cylindrical. The optic is mounted to the vessel, whose position is manipulated with the hexapod.

Purpose	Location	Size	Qty
Beam In	Beam inlet port at end 1	DN63/CF114	1

Beam Out	Beam outlet port at end 2	DN63/CF114	1
Ion Pump	Mounted on the base granite of the hexapod.	DN150/CF200	1
Roughing Port for RA valve	Outboard side of vessel	DN40/CF70	1
Viewport	Outboard side of vessel	DN63/CF114	1
Viewport	Incoming wall of vessel angled to look at substrate surface	DN40/CF70	1
Vacuum Gauges	Side of vessel	DN40/CF70	2
Spare	Top of vessel	DN63/CF114	1
Spare	Top of vessel	DN40/CF70	1
Mirror Loading	Baseplate	DN400/CF470	1
Drain current feedthrough (2 x BNC)	Baseplate	DN40/CF70	1

2.5 MIRROR CURRENT TAKEOFFS

The M4A mirror is fitted with drain current takeoffs to monitor the beam intensity. Two physical takeoffs are fitted to the optic stripe to allow the continuity of the electrical connection to be checked. The drain current will be measured using an I400.

2.6 ELECTRICAL DATA

2.6.1 Linear Actuators (Hexapod legs)

Motor Type	McLennan Type 23HS309 stepper motor
Holding torque	87 Ncm
Step angle (full step drive)	1.8°/ or 200 steps/rev
Driving current	2 A
Gear box ratio	25:1
Thread pitch	2 mm
Resolution per step	0.4 µm
Maximum movement per actuator	± 50 mm
Connector (Motor and limits)	12 way trim trio (UTO)

2.6.2 Encoder Data

Readhead type	Renishaw Tonic T1000-05A
Readhead (interpolator) resolution	0.1 µm
Scale type	RGSZ20
Connector	15-Way sub D

2.7 LIFTING POINTS

M4A mirror system weight: 500 kg approximately.

The mirror system is provided with three M16 lifting points in the base of the hexapod, in addition to three in the upper platform.

A lifting diagram for the system will be provided.

2.8 ALIGNMENT FEATURES

Fiducial mounts will be provided on the baseplate and on the upper platform of the hexapod. These will take the form of 0.25” reamed (H7) holes, suitable for 0.5” or 1.5” spheres.

3. FACTORY TESTING

Testing at FMB Oxford consists of Motion Testing, Vacuum Testing and Fiducialisation.

Full specifications and procedures covering all factory testing will be prepared in advance and these will be submitted to the customer prior to final design approval. Representatives from the customer are invited to witness these tests at FMB Oxford's works.

4. INSTALLATION AND UNIT ACCEPTANCE

The site acceptance testing, included in the installation option, will ensure that all components are carefully surveyed into position, all motors, actuators and sensors are functioning properly and the vacuum specifications are met. All motions will be tested and the correct functioning of all limit and datum switches checked. The complete set of detailed factory tests are not repeated on site.

There will be a full leak check of the installed vacuum sections. We expect that a turbo pump station, RGA rig, and He leak checker to be provided by the customer for our use while at the customer's site.

Final site acceptance will include:

- All factory test data, documentation and manuals
- Correct operation of all motions, limits and datum switches using FMB-O controls and cabling.
- Leak testing at the best achievable sensitivity after 24 hrs of pumping and prior to on site customer bakeout

5. *SCOPE OF SUPPLY*

- M4A optic and mirror system
- I400 Current amplifier (optic drain current measurement)
- MOXA
- 300 l/s ion pump & pump controller (Gamma)
- Right angle valve (Vat valve)
- Cold cathode (series 422) and pirani (series 317) gauges and gauge controller (MKS 937B)
- Motion controls as specified in the motion controls functional specification.
- Field cables

S3160 NIST SST – MIRROR SYSTEM M4C/M4D

Reference Documents:

Reference Number	Date/ Issue	Title
SB1341-14-CN-0042	19/09/14	NIST Contract
	April 2014	NIST NSLS-II SST and BMM Beamline Backbones, Volume 2A, SST Technical Proposal
S3160	Nov 2014/REV 01	NIST SST BEAMLINE S3160 QUALITY PLAN

FMB Oxford
Osney Mead
Oxford OX2 0ES
UK

Contact: Andrew Fairley
Telephone: +44 (0)1865 320 313
Fax: +44 (0)1865 320 301
E-mail: andrew.fairley@fmb-oxford.com

Change log:

Revision	Date	Summary of Change	Approval
1.0	06/01/15	First Issue	NJB
2.0	10/03/15	I200 replaced by I400. M4D binder layer removed. Ports added for feedthroughs. Tangential slope errors amended.Beam in and out ports size increased to DN100. Lateral range increased.	AJF
3.0	17/08/15	Ion pump size reduced.	AJF
4.0			
5.0			
6.0			

TABLE OF CONTENTS **1**

1. *INTRODUCTION* **3**

1.1 AXIS 4

2. *SPECIFICATIONS* **5**

2.1 MIRROR SYSTEM 5

2.1.1 M4C Mirror Optic *5*

2.1.2 M4D Mirror Optic *6*

2.2 MOTIONS 7

2.3 VACUUM SYSTEM 8

2.4 VACUUM VESSEL 8

2.5 MIRROR CURRENT TAKEOFFS 9

2.6 DITHERING MECHANISM 9

2.7 ELECTRICAL DATA 10

2.7.1 Linear Actuators (Hexapod legs) *10*

2.7.2 Encoder Data *10*

2.7.3 Dithering Mechanism *10*

2.8 LIFTING POINTS 10

2.9 ALIGNMENT FEATURES 11

3. FACTORY TESTING **12**

4. INSTALLATION AND UNIT ACCEPTANCE **13**

5. *SCOPE OF SUPPLY* **14**

1. *INTRODUCTION*

The M4 mirror system is located downstream of mirror system M3 and the precision vertical slit 'C', on the soft x-ray 'M' branch. The purpose of the M4 mirror system is to refocus and direct the soft x rays to the next (planar) mirror M5C (using optic M4C) and then on to the NEXAFS/XPS endstation or to guide and vertically dither the beam towards the last endstation on the 'M' branch (using optic M4D) - μNEXAFS.

The mirror system is equipped with two optics, an ellipsoid to refocus horizontally and vertically (M4C) and a plane optic (M4D) to provide vertical dithering (increased spot size).

The M4 optics (M4C and M4D) are both uncooled. Both optics are mounted to the vacuum vessel, which is manipulated with a hexapod.

The optics are arranged side by side, so the hexapod platform translates horizontally to switch between the optics.

The M4D optic is fitted with a flexure based dithering mechanism to increase the vertical spot size at the μNEXAFS end station. In addition, both optics are fitted with drain current takeoffs.

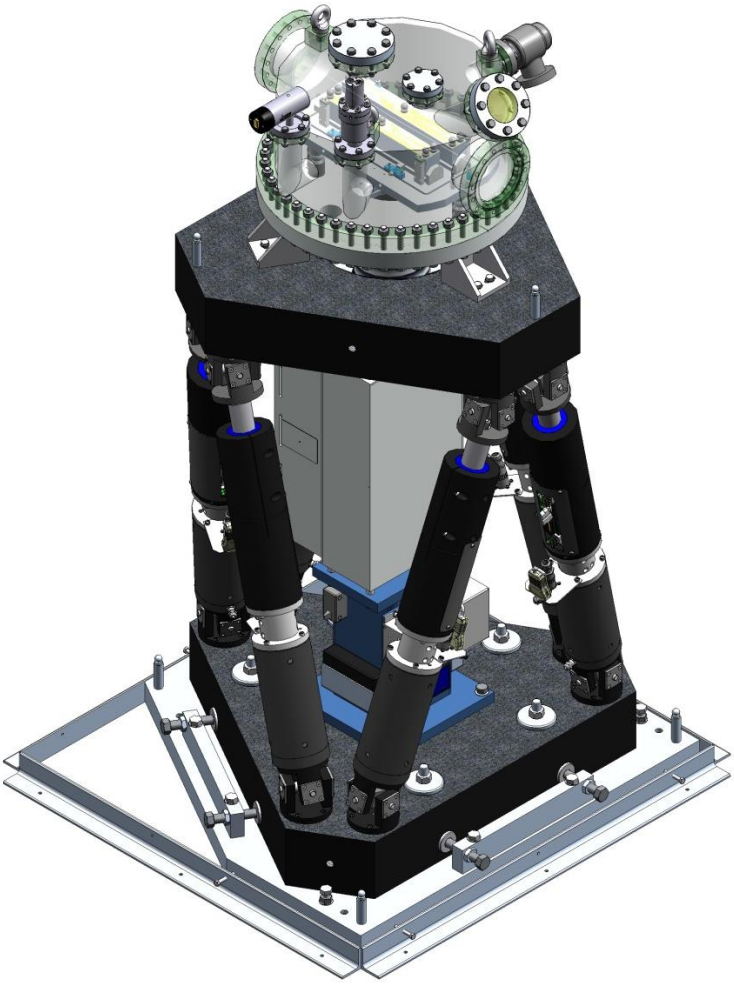

Figure 1. Mirror System M4C/D

1.1 AXIS

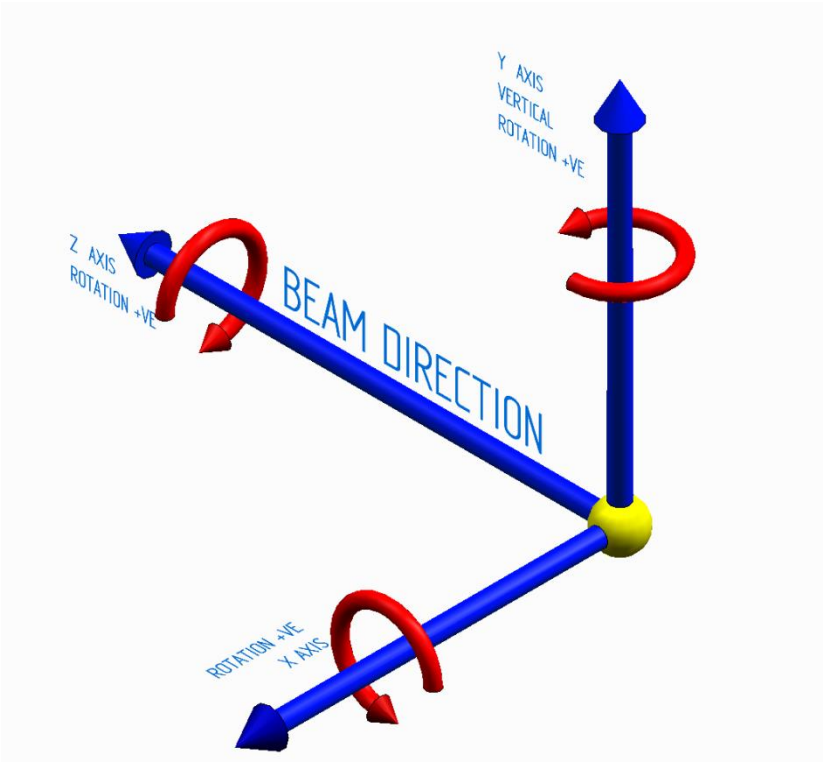

Figure 2. Beamline coordinate system

Inboard is defined as being in the negative x direction and outboard in the postive x direction.

The coordinate system employed complies with NSLS-II document:

Beamline Coordinate System Standards LT-C-XFD-STD-BL-COORD-001.

2. *SPECIFICATIONS*

2.1 MIRROR SYSTEM

Incoming Beam Height	1415 mm
Operating Position	Vertically deflecting upwards, horizontally and vertically refocusing (M4C). Vertically deflecting upwards (M4D).
Manual Adjustments	± 10 mm in x and z (from grouted-in baseplate)
Optic location relative to centre of straight section (mm).	1857.35, 15, 53500 (x, y, z)

2.1.1 M4C Mirror Optic

Substrate material	Fused Silica
Substrate dimensions	270 mm L x 35 mm W x 50 mm D
Active Area (centred on substrate to within ± 0.5mm)	230 mm x 15 mm
Substrate Shape	Ellipsoid Major axis 6835.9 mm ± 1% Minor axis 172.4 mm ± 1% Mirror pole X_0: 1836.6 mm (off axis) ± 1%. *Sagittal Radius > 3km*
Grazing incidence angle	1.5°
Distance to source	4999.9 mm
Distance to image	8672 mm
Tangential slope error	< 1.0 µrad RMS over active length
Sagittal slope error	< 10 µrad RMS over active length on prepared substrate
Coating	Au 300 Á ± 10% thick 15 mm wide No binder layers permitted

Surface Roughness	<3 Å RMS
Surface Quality	0.5 scratches or points per cm^2 over 99% of active optical area
Cooling	Uncooled

2.1.2 M4D Mirror Optic

Substrate material	Titania silicate low expansion glass
Substrate dimensions	250 mm L x 35 mm W x 50 mm D
Active Area (centred on substrate to within ± 0.5mm)	230 mm x 20 mm
Substrate Shape	Plane Tangential radius > 20 km Sagittal radius > 3km
Grazing incidence angle	1.5°
Distance to source	∞ m
Distance to image	∞ m
Tangential slope error	<0.25 µrad RMS over active length
Sagittal slope error	< 5 µrad RMS over active length
Coating	Au 300 Å ± 10% thick 15 mm wide over Pt 300 Å ± 10% binder layer
Surface Roughness	<3 Å RMS
Surface Quality	0.5 scratches or points per cm^2 over 99% of active optical area
Cooling	Uncooled

2.2 MOTIONS

Motion	Parameter	Specification
Pitch (Ry)	Drive	Linear actuators, fitted with limit switches & encoder.
	Range	Nominal position ± 10 mrad
	Resolution	< 1µrad
	Repeatability	< 5 µrad
Roll (Rz)	Drive	Linear actuators, fitted with limit switches & encoder.
	Range	± 10 mrad
	Resolution	< 5 µrad
	Repeatability	< 10 µrad
Yaw (Rx)	Drive	Linear actuators, fitted with limit switches & encoder.
	Range	± 10 mrad
	Resolution	< 5 µrad
	Repeatability	< 10 µrad
Vertical (Ty)	Drive	Linear actuators, fitted with limit switches & encoder.
	Range	± 10 mm
	Resolution	< 1 µm
	Repeatability	< 5 µm

Lateral (Tx)	Drive	Linear actuators, fitted with limit switches & encoder.
	Range	± 40 mm
	Resolution	< 1 µm
	Repeatability	< 5 µm
Longitudinal (Tz)	Drive	Linear actuators, fitted with limit switches & encoder.
	Range	± 5 mm
	Resolution	< 2 µm
	Repeatability	< 10 µm

2.3 VACUUM SYSTEM

Maximum bakeout temperature – vessel and internal components	150-200 °C
Vacuum	UHV compatible (< 5 x10^{-10} mbar). Masses > 38 AMU shall have total pressure < 10^{-11} Torr (1.33 x 10^{-11} mbar)
Helium leak rate	< 1 x 10 $^{-10}$ mbar l/sec
Vacuum Pump	Gamma vacuum 300T ion pump located beneath the vessel
Vacuum gauges	One pirani gauge (MKS type 317)and one cold cathode gauge(MKS type 422) located on the mirror vessel
Right Angle Valve	VAT Valve type 54, DN40/CF70.

2.4 VACUUM VESSEL

The vacuum vessel for the M4 mirror system is cylindrical.

Purpose	Location	Size	Qty
Beam In	Beam inlet port at end 1	DN100/CF150	1

Beam Out	Beam outlet port at end 2	DN100/CF150	1
Ion Pump	Mounted on the base granite of the hexapod.	DN100/CF150	1
Roughing Port for RA valve	Outboard side of vessel	DN40/CF70	1
Viewport	Incoming wall of vessel angled to look at substrate surface	DN63/CF114	1
Vacuum Gauges	Side of vessel	DN40/CF70	2
Spare	Top of vessel	DN63/CF114	1
Spare	Top of vessel	DN40/CF70	1
Mirror Loading	Baseplate	DN400/CF470	1
Double BNC feedthrough for optic drain currents	Baseplate	DN40/CF70	2
Feedthrough for dithering DPT (9 way d-type)	Baseplate	DN40/CF70	1

2.5 MIRROR CURRENT TAKEOFFS

The M4 optics are both fitted with drain current takeoffs to monitor the beam intensity. Two physical takeoffs are fitted to each optic stripe to allow the continuity of the electrical connection to be checked. The drain currents will be measured using an I400.

2.6 DITHERING MECHANISM

The M4D mirror system is fitted with a piezo-driven flexure mechanism to dither the beam (increase the vertical spot size) at the µNEXAFS end station. The mirror needs to be dithered by approximately ±0.43 mrad to obtain a 20 mm vertical stripe at the end station.

2.7 ELECTRICAL DATA

2.7.1 Linear Actuators (Hexapod legs)

Motor Type	McLennan Type 23HS309 stepper motor
Holding torque	87 Ncm
Step angle (full step drive)	1.8°/ or 200 steps/rev
Driving current	2 A
Gear box ratio	25:1
Thread pitch	2 mm
Resolution per step	0.4 µm
Maximum movement per actuator	± 50 mm
Connector (Motor and limits)	12 way trim trio (UTO)

2.7.2 Encoder Data

Readhead type	Renishaw Tonic T1000-05A
Readhead (interpolator) resolution	0.1 µm
Scale type	RGSZ20
Connector	15-Way sub D

2.7.3 Dithering Mechanism

Actuator type	Preloaded piezo stack driven flexure.
Range	±0.5 mrad

2.8 LIFTING POINTS

M4 mirror system weight: 500 kg approximately.

The mirror system is provided with three M16 lifting points in the base of the hexapod, in addition to three in the upper platform.

A lifting diagram for the system will be provided.

2.9 ALIGNMENT FEATURES

Fiducial mounts will be provided on the baseplate and on the upper platform of the hexapod. These will take the form of 0.25” reamed (H7) holes, suitable for 0.5” or 1.5” spheres.

3. FACTORY TESTING

Testing at FMB Oxford consists of Motion Testing, Vacuum Testing and Fiducialisation.

Full specifications and procedures covering all factory testing will be prepared in advance and these will be submitted to the customer prior to final design approval. Representatives from the customer are invited to witness these tests at FMB Oxford's works.

4. INSTALLATION AND UNIT ACCEPTANCE

The site acceptance testing, included in the installation option, will ensure that all components are carefully surveyed into position, all motors, actuators and sensors are functioning properly and the vacuum specifications are met. All motions will be tested and the correct functioning of all limit and datum switches checked. The complete set of detailed factory tests are not repeated on site.

There will be a full leak check of the installed vacuum sections. We expect that a turbo pump station, RGA rig, and He leak checker to be provided by the customer for our use while at the customer's site.

Final site acceptance will include:

- All factory test data, documentation and manuals
- Correct operation of all motions, limits and datum switches using FMB-O controls and cabling.
- Leak testing at the best achievable sensitivity after 24 hrs of pumping and prior to on site customer bakeout

5. *SCOPE OF SUPPLY*

- M4C and M4D optics and mirror system
- I400 Current amplifier (optic drain current measurement)
- DPT dithering and controls for M4D.
- 200 l/s ion pump & pump controller (Gamma)
- Right angle valve (Vat valve)
- Cold cathode (series 422) and pirani (series 317) gauges and gauge controller (MKS 937B)
- Motion controls as specified in the motion controls functional specification.
- Field cables

S3160 NIST SST – MIRROR SYSTEM M5C

Reference Documents:

Reference Number	Date/ Issue	Title
SB1341-14-CN-0042	19/09/14	NIST Contract
	April 2014	NIST NSLS-II SST and BMM Beamline Backbones, Volume 2A, SST Technical Proposal
S3160	Nov 2014/REV 01	NIST SST BEAMLINE S3160 QUALITY PLAN

FMB Oxford
Osney Mead
Oxford OX2 0ES
UK

Contact: Andrew Fairley
Telephone: +44 (0)1865 320 313
Fax: +44 (0)1865 320 301
E-mail: andrew.fairley@fmb-oxford.com

Change log:

Revision	Date	Summary of Change	Approval
1.0	06/01/15	First Issue	NJB
2.0	17/08/15	Ports added for dithering feedthrough and drain currents. Platinum binder layer added.	AJF
3.0			
4.0			
5.0			
6.0			

TABLE OF CONTENTS **1**

1. *INTRODUCTION* **3**

1.1 AXIS 4

2. *SPECIFICATIONS* **5**

2.1 MIRROR SYSTEM 5

2.1.1 M5C Mirror Optic *5*

2.2 MOTIONS 6

2.3 VACUUM SYSTEM 7

2.4 VACUUM VESSEL 7

2.5 MIRROR CURRENT TAKEOFFS 8

2.6 DITHERING MECHANISM 8

2.7 ELECTRICAL DATA 9

2.7.1 Linear Actuators (Hexapod legs) *9*

2.7.2 Encoder Data *9*

2.7.3 Dithering Mechanism *9*

2.8 LIFTING POINTS 9

2.9 ALIGNMENT FEATURES 10

3. FACTORY TESTING **11**

4. INSTALLATION AND UNIT ACCEPTANCE **12**

5. *SCOPE OF SUPPLY* **13**

1. *INTRODUCTION*

The M5C mirror system is located directly upstream of the NEXAFS/XPS endstation, on the soft x-ray 'M' branch. The purpose the M5C mirror system is to guide the soft x rays to the NEXAFS/XPS end station. The M5C optic is planar and uncooled. The optic is mounted to the base of the vacuum vessel and is manipulated using a hexapod, which gives six degrees of freedom. The optic is fitted with drain current take offs and a flexure based dithering mechanism to increase the vertical spot size at the end station.

The M5C optic may also be moved out of beam to allow the soft x rays from mirror M4D to reach the μNEXAFS end station, located further downstream.

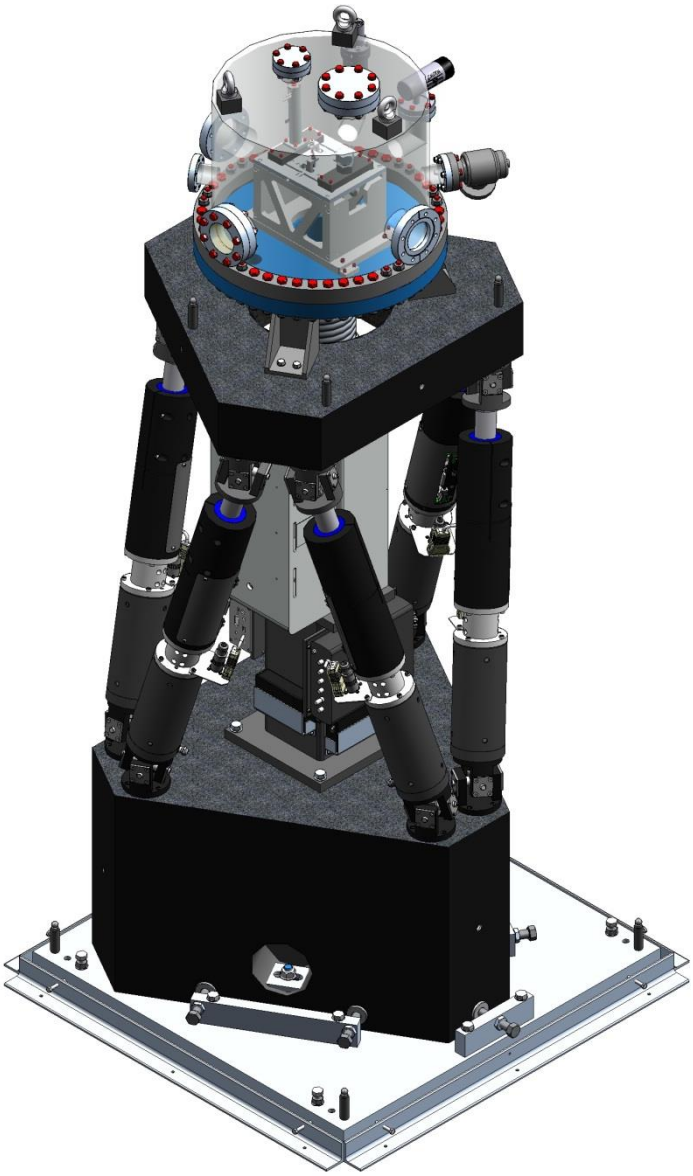

Figure 1. Mirror System M5C

1.1 AXIS

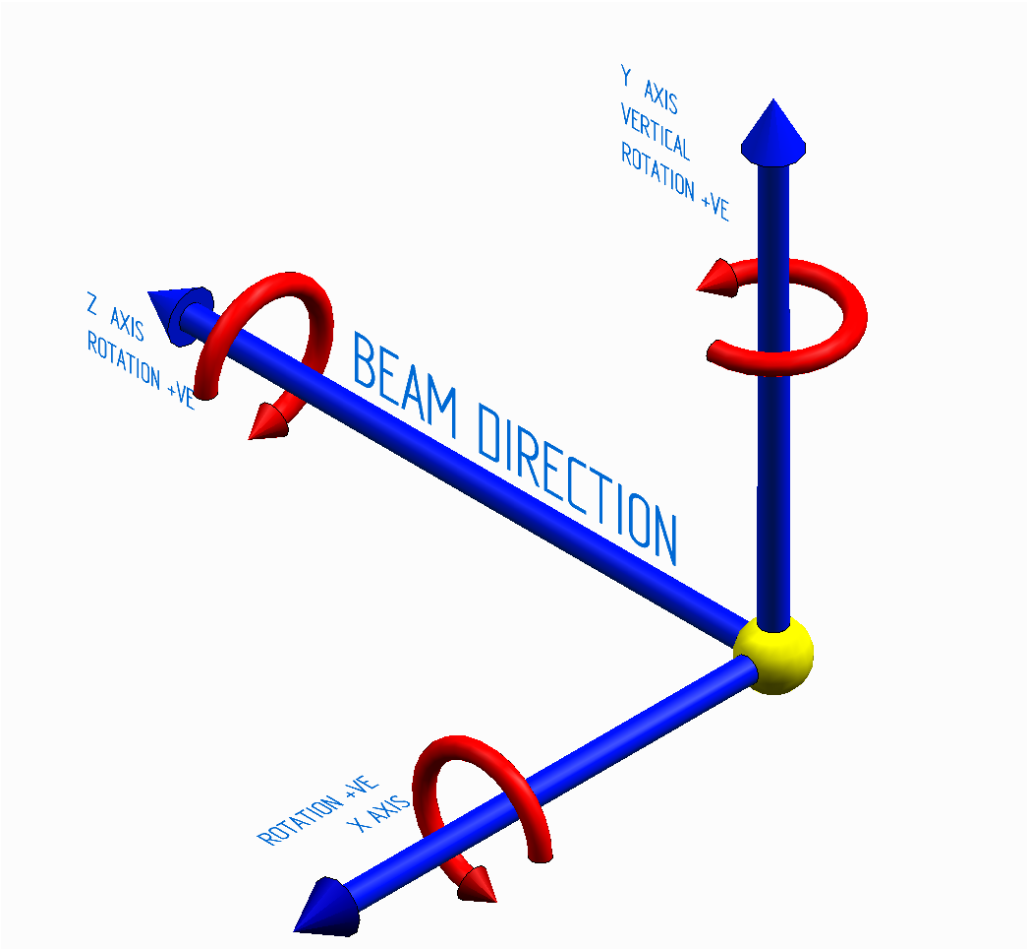

Figure 2. Beamline coordinate system

Inboard is defined as being in the negative x direction and outboard in the postive x direction.

The coordinate system employed complies with NSLS-II document:

Beamline Coordinate System Standards LT-C-XFD-STD-BL-COORD-001.

2. *SPECIFICATIONS*

2.1 MIRROR SYSTEM

Incoming Beam Height	1764 mm (at optic)
Operating Position	Vertically deflecting downwards
Manual Adjustments	± 10 mm in x and z (from grouted-in baseplate)
Optic location relative to centre of straight section (mm).	2546.7, 364, 60122 (x, y, z)

2.1.1 M5C Mirror Optic

Substrate material	Single crystal silicon
Substrate dimensions	120 mm L x 35 mm W x 30 mm D
Active Area (centred on substrate to within ± 0.5mm)	100 mm x 15 mm
Substrate Shape	Plane. Tangential radius > 20 km Sagittal radius > 3km
Grazing incidence angle	1.0°
Distance to source	∞ m
Distance to image	∞ m
Tangential slope error	<0.25 µrad RMS over active length
Sagittal slope error	<5 µrad RMS over active length on prepared substrate
Coating	Au 300 Å ± 10% thick 15 mm wide over Pt 100 Å ± 10% thick binder layer
Surface Roughness	<3 Å RMS
Surface Quality	0.5 scratches or points per cm^2 over 99% of active optical area

Cooling	Uncooled

2.2 MOTIONS

Motion	Parameter	Specification
Pitch (Ry)	Drive	Linear actuators, fitted with limit switches & encoder.
	Range	Nominal position ± 10 mrad
	Resolution	< 1µrad
	Repeatability	< 5 µrad
Roll (Rz)	Drive	Linear actuators, fitted with limit switches & encoder.
	Range	± 10 mrad
	Resolution	< 5 µrad
	Repeatability	< 10 µrad
Yaw (Rx)	Drive	Linear actuators, fitted with limit switches & encoder.
	Range	± 10 mrad
	Resolution	< 5 µrad
	Repeatability	< 10 µrad
Vertical (Ty)	Drive	Linear actuators, fitted with limit switches & encoder.
	Range	± 10 mm
	Resolution	< 1 µm
	Repeatability	< 5 µm

Lateral (Tx)	Drive	Linear actuators, fitted with limit switches & encoder.
	Range	± 20 mm
	Resolution	< 1 µm
	Repeatability	< 5 µm
Longitudinal (Tz)	Drive	Linear actuators, fitted with limit switches & encoder.
	Range	± 5 mm
	Resolution	< 2 µm
	Repeatability	< 10 µm

2.3 VACUUM SYSTEM

Maximum bakeout temperature – vessel and internal components	150-200 °C
Vacuum	UHV compatible (< 5 x10^{-10} mbar). Masses > 38 AMU shall have total pressure < 10^{-11} Torr (1.33 x 10^{-11} mbar)
Helium leak rate	< 1 x 10^{-10} mbar l/sec
Vacuum Pump	Gamma vacuum 300T ion pump located beneath the vessel
Vacuum gauges	One pirani gauge (MKS type 317)and one cold cathode gauge(MKS type 422) located on the mirror vessel
Right Angle Valve	VAT Valve type 54, DN40/CF70.

2.4 VACUUM VESSEL

The vacuum vessel for the M5C mirror system is cylindrical. The optic is mounted to the vessel, whose position is manipulated with the hexapod.

Purpose	Location	Size	Qty
Beam In	Beam inlet port at end 1	DN63/CF114	1

Beam Out	Beam outlet port at end 2	DN63/CF114	1
Ion Pump	Mounted on the base granite of the hexapod.	DN150/CF200	1
Roughing Port for RA valve	Outboard side of vessel	DN40/CF70	1
Viewport	Outboard side of vessel	DN63/CF114	1
Viewport	Incoming wall of vessel angled to look at substrate surface	DN40/CF70	1
Vacuum Gauges	Side of vessel	DN40/CF70	2
Spare	Top of vessel	DN63/CF114	1
Spare	Top of vessel	DN40/CF70	1
Mirror Loading	Baseplate	DN400/CF470	1
Feedthrough for dithering DPT (9 way d-type)	Baseplate	DN40/CF70	1
Feedthrough for optics drain currents	Baseplate	DN40/CF70	1

2.5 MIRROR CURRENT TAKEOFFS

The M5C mirror is fitted with drain current takeoffs to monitor the beam intensity. Two physical takeoffs are fitted to the optic stripe to allow the continuity of the electrical connection to be checked. The drain current will be measured using an I400.

2.6 DITHERING MECHANISM

The M5C mirror system is fitted with a piezo-driven flexure mechanism to dither the beam (increase the vertical spot size) at end station NEXAFS/XPS. The mirror needs to be dithered by approximately ±0.62 mrad to obtain a 5mm vertical stripe at the end station.

2.7 ELECTRICAL DATA

2.7.1 Linear Actuators (Hexapod legs)

Motor Type	McLennan Type 23HS309 stepper motor
Holding torque	87 Ncm
Step angle (full step drive)	1.8°/ or 200 steps/rev
Driving current	2 A
Gear box ratio	25:1
Thread pitch	2 mm
Resolution per step	0.4 µm
Maximum movement per actuator	± 50 mm
Connector (Motor and limits)	12 way trim trio (UTO)

2.7.2 Encoder Data

Readhead type	Renishaw Tonic T1000-05A
Readhead (interpolator) resolution	0.1 µm
Scale type	RGSZ20
Connector	15-Way sub D

2.7.3 Dithering Mechanism

Actuator type	Preloaded piezo stack driven flexure.
Range	±0.75 mrad

2.8 LIFTING POINTS

M5C mirror system weight: 500 kg approximately.

The mirror system is provided with three M16 lifting points in the base of the hexapod, in addition to three in the upper platform.

A lifting diagram for the system will be provided.

2.9 ALIGNMENT FEATURES

Fiducial mounts will be provided on the baseplate and on the upper platform of the hexapod. These will take the form of 0.25” reamed (H7) holes, suitable for 0.5” or 1.5” spheres.

3. FACTORY TESTING

Testing at FMB Oxford consists of Motion Testing, Vacuum Testing and Fiducialisation.

Full specifications and procedures covering all factory testing will be prepared in advance and these will be submitted to the customer prior to final design approval. Representatives from the customer are invited to witness these tests at FMB Oxford's works.

4. INSTALLATION AND UNIT ACCEPTANCE

The site acceptance testing, included in the installation option, will ensure that all components are carefully surveyed into position, all motors, actuators and sensors are functioning properly and the vacuum specifications are met. All motions will be tested and the correct functioning of all limit and datum switches checked. The complete set of detailed factory tests are not repeated on site.

There will be a full leak check of the installed vacuum sections. We expect that a turbo pump station, RGA rig, and He leak checker to be provided by the customer for our use while at the customer's site.

Final site acceptance will include:

- All factory test data, documentation and manuals
- Correct operation of all motions, limits and datum switches using FMB-O controls and cabling.
- Leak testing at the best achievable sensitivity after 24 hrs of pumping and prior to on site customer bakeout

5. *SCOPE OF SUPPLY*

- M5C optic and mirror system
- DPT dithering and controls
- I400 Current amplifier (optic drain current measurement)
- 300 l/s ion pump & pump controller (Gamma)
- Right angle valve (Vat valve)
- Cold cathode (series 422) and pirani (series 317) gauges and gauge controller (MKS 937B)
- Motion controls and specified in the motion controls functional specification.
- Field cables

Appendix E

Preliminary Bremsstrahlung and synchrotron ray-tracing for SST beamlines

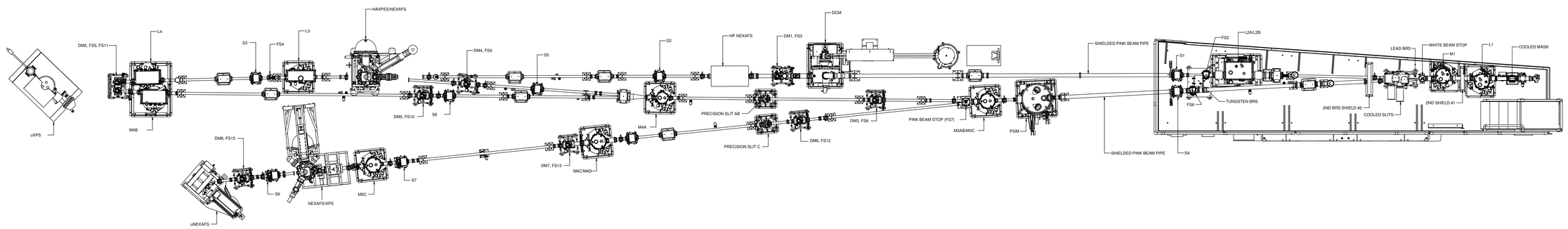

REV	DATE	DESCRIPTION/DMR No	DRN	CHKD
09	03/06/16	INCORPORATING LATEST BNL COMMENTS	AF	
08	10/05/16	INCORPORATING BNL COMMENTS	AF	
07	03/04/16	INCORPORATING SR-FE-IVU07-1001 REV B	AF	SM
06	25/09/15	MAX SYNCHROTRON FAN ADDED	AF	SM
05	22/06/15	SST FIRST SUBMISSION FOR FDR	AF	–

THIS DRAWING BELONGS TO FMB OXFORD LTD AND IS ISSUED ON CONDITION THAT IT IS NOT COPIED, REPRINTED OR DISCLOSED TO A THIRD PARTY WITHOUT PRIOR CONSENT IN WRITING FROM FMB OXFORD Ltd.

DRAWN: A FAIRLEY — DATE: 03/06/16

CHECKED — DATE:

APPROVED: A FAIRLEY — DATE: 03/06/16

FMB OXFORD LTD.,
UNIT 1 FERRY MILLS,
OSNEY MEAD, OXFORD, OX2 0ES.
ENGLAND

FMB Oxford

Title: NIST SST BEAMLINE RAYTRACE

Size: A3 — Document Number: AHB0531 — Rev: 08

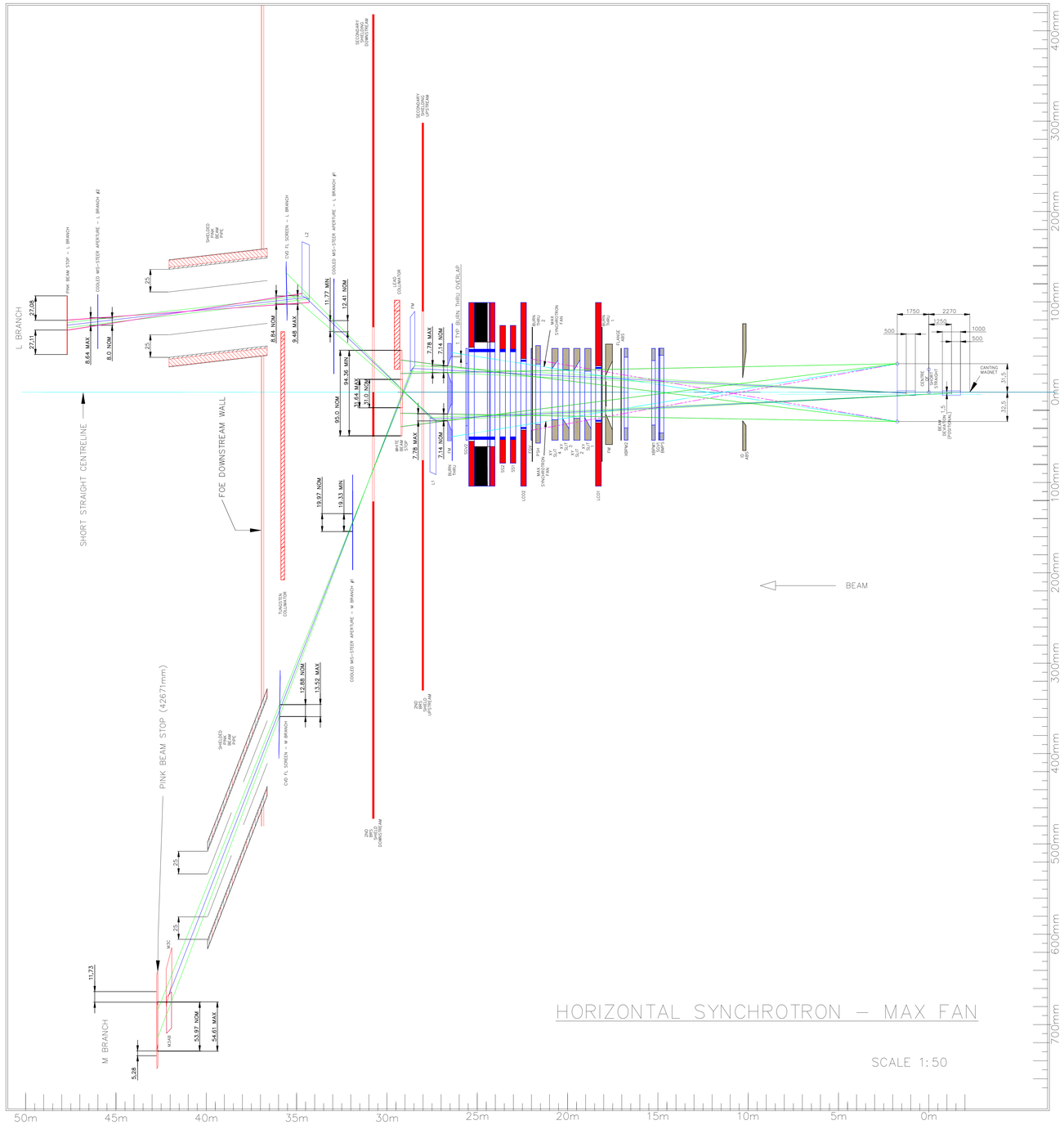

NOTES:
1. THIS DRAWING REFERENCES BNL DOCUMENT SR–FE–IVU07–1001 REV B

TABLE OF TOLERANCED DIMENSIONS (mm)

LINE	DESCRIPTION	NOMINAL	+/–	FABRICATION	+/–	POSITION	+/–	CLEARANCE	=	TOTAL
1	FIXED MASK – 'L' BRANCH (26563)	7.14 mm	+	0.20	+	0.44	+	–	=	7.78
2	FIXED MASK – 'M' BRANCH (26563)	7.14 mm	+	0.20	+	0.44	+	–	=	7.78
3	WHITE BEAM STOP APERTURE (29142)	31.0 mm	+	0.20	+	0.44	+	–	=	31.64
4	WHITE BEAM STOP EXTENT(29142)	95.0 mm	–	0.20	–	0.44	+	–	=	94.36
5	COOLED MIS–STEER APERTURE – L BRANCH #1	12.41 mm	–	0.20	–	0.44	+	–	=	11.77
6	CVD FL SCREEN – L BRANCH	8.84 mm	+	0.20	+	0.44	+	–	=	9.48
7	COOLED MIS–STEER APERTURE – L BRANCH #2	8.0 mm	+	0.20	+	0.44	+	–	=	8.64
8	COOLED MIS–STEER APERTURE – M BRANCH #1	19.97 mm	–	0.20	–	0.44	+	–	=	19.33
9	CVD FL SCREEN – M BRANCH	12.88 mm	+	0.20	+	0.44	+	–	=	13.52
10	PINK BEAM STOP – M BRANCH	53.97 mm	+	0.20	+	0.44	+	–	=	54.61

REV	DATE	DESCRIPTION/DMR No	DRN	CHKD
09	03/06/16	INCORPORATING LATEST BNL COMMENTS	AF	
08	10/05/16	INCORPORATING BNL COMMENTS	AF	
07	03/04/16	INCORPORATING SR–FE–IVU07–1001 REV B	AF	SM
06	25/09/15	MAX SYNCHROTRON FAN ADDED	AF	SM
05	22/06/15	SST FIRST SUBMISSION FOR FDR	AF	–

THIS DRAWING BELONGS TO FMB OXFORD LTD AND IS ISSUED ON CONDITION THAT IT IS NOT COPIED, REPRINTED OR DISCLOSED TO A THIRD PARTY WITHOUT PRIOR CONSENT IN WRITING FROM FMB OXFORD Ltd.

DRAWN: A FAIRLEY DATE: 03/06/16
CHECKED: DATE:
APPROVED: A FAIRLEY DATE: 03/06/16

FMB OXFORD LTD.,
UNIT 1 FERRY MILLS,
OSNEY MEAD, OXFORD, OX2 0ES.
ENGLAND

FMB Oxford

Title: NIST SST BEAMLINE RAYTRACE

Size: A3 | Document Number: AHB0531 | Rev: 08

TABLE OF TOLERANCED DIMENSIONS (mm)

LINE	DESCRIPTION	NOMINAL	+/−	FABRICATION	+/−	POSITION	+/−	CLEARANCE	=	TOTAL
1	FIXED MASK (26563)	4.76 mm	+	0.20	+	0.44	+	−	=	5.4
2	WHITE BEAM STOP (29142)	33.63 mm	−	0.20	−	0.44	+	−	=	32.99
3	PINK BEAM STOP (47677)	40 mm	−	0.20	−	0.44	+	−	=	39.36
4	COOLED APERTURE (35734)	11 mm	−	0.20	+	0.44	+	−	=	11.24

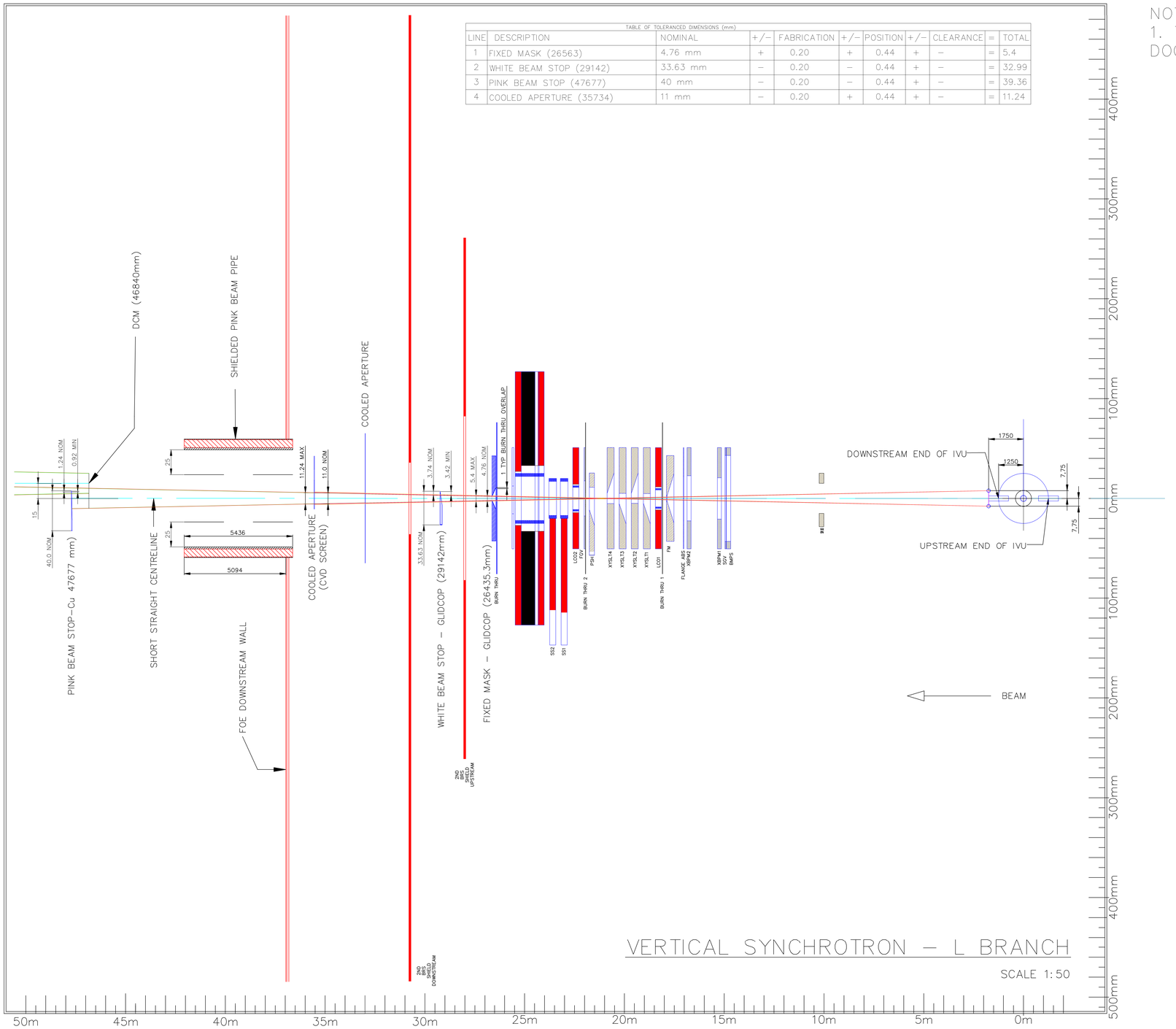

VERTICAL SYNCHROTRON – L BRANCH

SCALE 1:50

NOTES:
1. THIS DRAWING REFERENCES BNL DOCUMENT SR–FE–IVU07–1001 REV B

REV	DATE	DESCRIPTION/DMR No	DRN	CHKD
09	03/06/16	INCORPORATING LATEST BNL COMMENTS	AF	
08	10/05/16	INCORPORATING BNL COMMENTS	AF	
07	03/04/16	INCORPORATING SR–FE–IVU07–1001 REV B	AF	SM
06	25/09/15	MAX SYNCHROTRON FAN ADDED	AF	SM
05	22/06/15	SST FIRST SUBMISSION FOR FDR	AF	–

THIS DRAWING BELONGS TO FMB OXFORD LTD AND IS ISSUED ON CONDITION THAT IT IS NOT COPIED, REPRINTED OR DISCLOSED TO A THIRD PARTY WITHOUT PRIOR CONSENT IN WRITING FROM FMB OXFORD Ltd.

DRAWN: A FAIRLEY DATE: 03/06/16

CHECKED DATE

APPROVED: A FAIRLEY DATE: 03/06/16

FMB OXFORD LTD.,
UNIT 1 FERRY MILLS,
OSNEY MEAD, OXFORD, OX2 0ES.
ENGLAND

FMB Oxford

Title: NIST SST BEAMLINE RAYTRACE

Size: A3 | Document Number: AHB0531 | Rev: 08

Sheet 3 of 10

NOTES:
1. THIS DRAWING REFERENCES BNL DOCUMENT SR-FE-IVU07-1001 REV B

TABLE OF TOLERANCED DIMENSIONS (mm)

LINE	DESCRIPTION	NOMINAL	+/−	FABRICATION	+/−	POSITION	+/−	CLEARANCE	=	TOTAL
1	FIXED MASK (26563)	7.14 mm	+	0.20	+	0.44	+	–	=	7.78
2	WHITE BEAM STOP (29142)	33.63 mm	–	0.20	–	0.44	+	–	=	32.99
3	PINK BEAM STOP (47673)	60.0 mm	–	0.20	–	0.44	+	–	=	59.36
4	COOLED APERTURE (35936)	11.0 mm	–	0.20	+	0.44	+	–	=	11.24

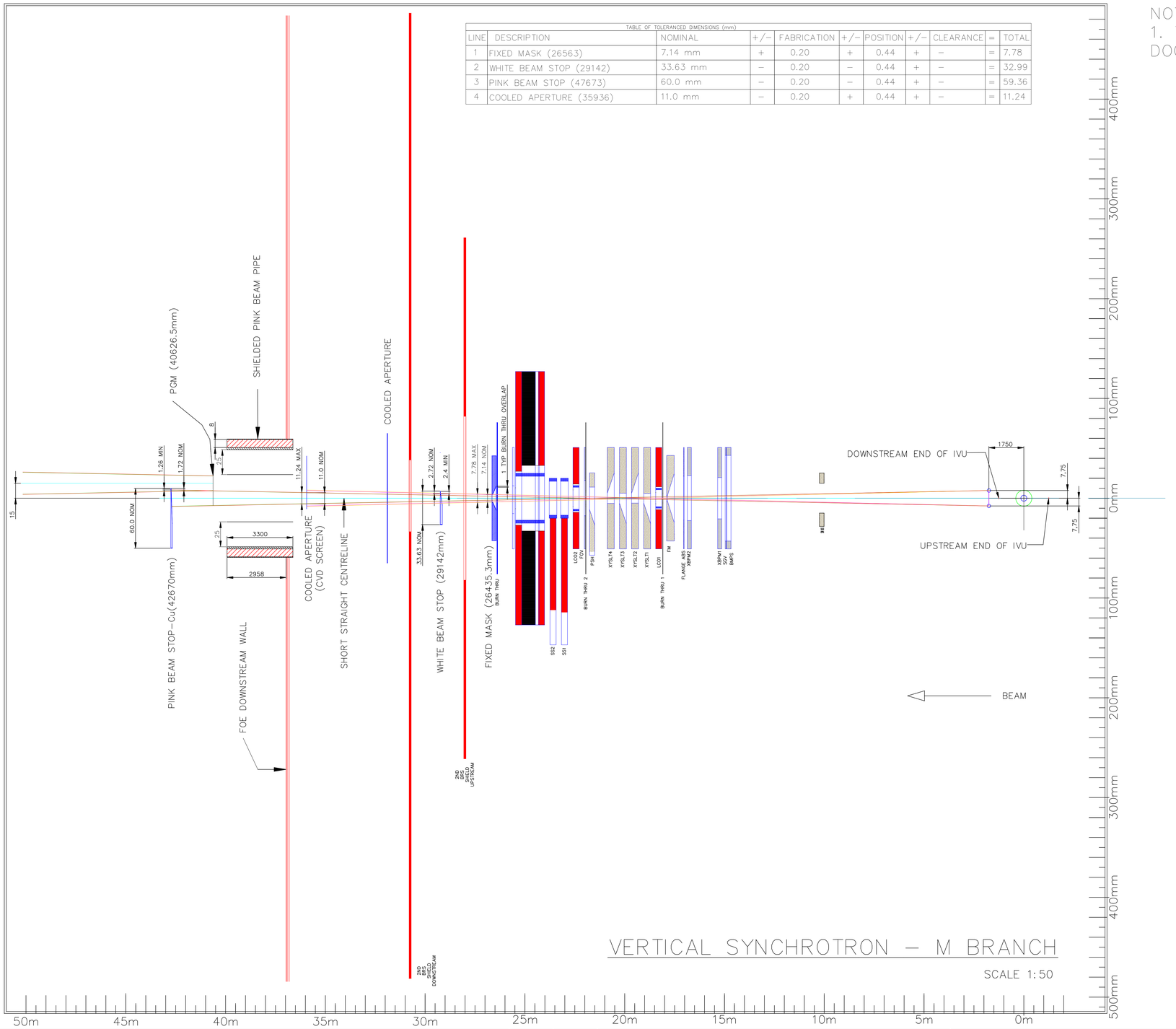

REV	DATE	DESCRIPTION/DMR No	DRN	CHKD
09	03/06/16	INCORPORATING LATEST BNL COMMENTS	AF	
08	10/05/16	INCORPORATING BNL COMMENTS	AF	
07	03/04/16	INCORPORATING SR-FE-IVU07-1001 REV B	AF	SM
06	25/09/15	MAX SYNCHROTRON FAN ADDED	AF	SM
05	22/06/15	SST FIRST SUBMISSION FOR FDR	AF	–

THIS DRAWING BELONGS TO FMB OXFORD LTD AND IS ISSUED ON CONDITION THAT IT IS NOT COPIED, REPRINTED OR DISCLOSED TO A THIRD PARTY WITHOUT PRIOR CONSENT IN WRITING FROM FMB OXFORD Ltd.

DRAWN: A FAIRLEY DATE: 03/06/16
CHECKED DATE:
APPROVED: A FAIRLEY DATE: 03/06/16

FMB OXFORD LTD.,
UNIT 1 FERRY MILLS,
OSNEY MEAD, OXFORD, OX2 0ES.
ENGLAND

FMB Oxford

Title: NIST SST BEAMLINE RAYTRACE

Size: A3 | Document Number: AHB0531 | Rev: 08

TABLE OF TOLERANCED DIMENSIONS (mm)										
LINE	DESCRIPTION	NOMINAL	+/−	FABRICATION	+/−	POSITION	+/−	CLEARANCE	=	TOTAL
1	LEAD COLLIMATOR (29288)	25.4 mm	+	0.20	+	0.44	+	−	=	26.04
2	TUNGSTEN COLLIMATOR (35666)	26 mm	−	0.20	−	0.44	+	−	=	25.36
3	TUNGSTEN COLLIMATOR (35666)	26 mm	−	0.20	−	1.24	+	−	=	24.56

NOTES:
1. THIS DRAWING REFERENCES BNL DOCUMENT SR−FE−IVU07−1001 REV B

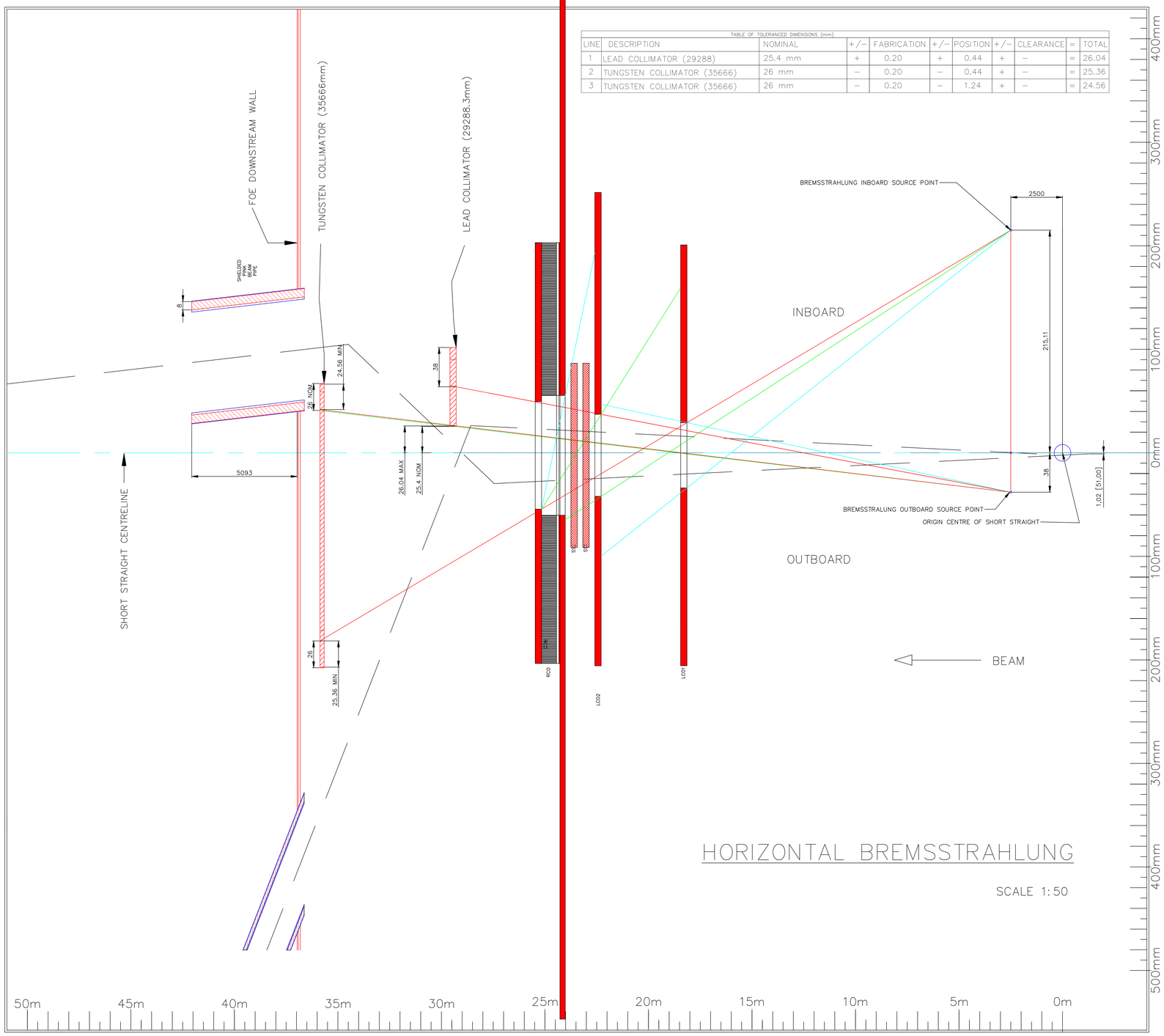

HORIZONTAL BREMSSTRAHLUNG

SCALE 1:50

VIEW ON 'A' – FRONT FACE OF FIRST BREMMSTRAHLUNG COLLIMATOR, IN AIR, LEAD LENGTH 300mm AT 29.288 m

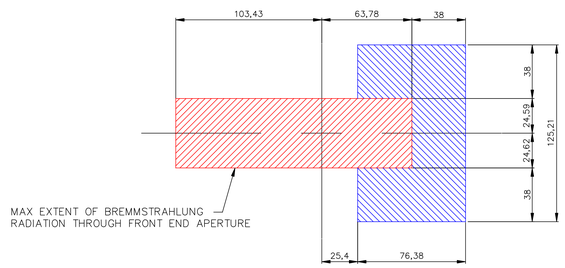

VIEW ON 'B' – FRONT FACE OF SECOND BREMMSTRAHLUNG COLLIMATOR, IN AIR, TUNGSTEN LENGTH 200mm AT 35.666 m

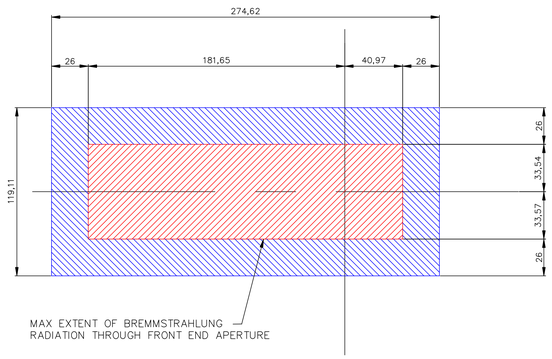

REV	DATE	DESCRIPTION/DMR No	DRN	CHKD
09	03/06/16	INCORPORATING LATEST BNL COMMENTS	AF	
08	10/05/16	INCORPORATING BNL COMMENTS	AF	
07	03/04/16	INCORPORATING SR−FE−IVU07−1001 REV B	AF	SM
06	25/09/15	MAX SYNCHROTRON FAN ADDED	AF	XX
05	22/06/15	SST FIRST SUBMISSION FOR FDR	AF	–

THIS DRAWING BELONGS TO FMB OXFORD LTD AND IS ISSUED ON CONDITION THAT IT IS NOT COPIED, REPRINTED OR DISCLOSED TO A THIRD PARTY WITHOUT PRIOR CONSENT IN WRITING FROM FMB OXFORD Ltd.

DRAWN: A FAIRLEY DATE: 03/06/16
CHECKED: DATE:
APPROVED: A FAIRLEY DATE: 03/06/16

FMB OXFORD LTD.,
UNIT 1 FERRY MILLS,
OSNEY MEAD, OXFORD, OX2 0ES.
ENGLAND

FMB Oxford

Title: NIST SST BEAMLINE RAYTRACE

Size: A3 | Document Number: AHB0531 | Rev: 08

TABLE OF TOLERANCED DIMENSIONS (mm)										
LINE	DESCRIPTION	NOMINAL	+/−	FABRICATION	+/−	POSITION	+/−	CLEARANCE	=	TOTAL
1	LEAD COLLIMATOR (29288)	125.22 mm	−	0.40	−	0.44	+	−	=	124.38
2	TUNGSTEN COLLIMATOR (35666)	119.11 mm	−	0.40	−	0.44	+	−	=	118.27

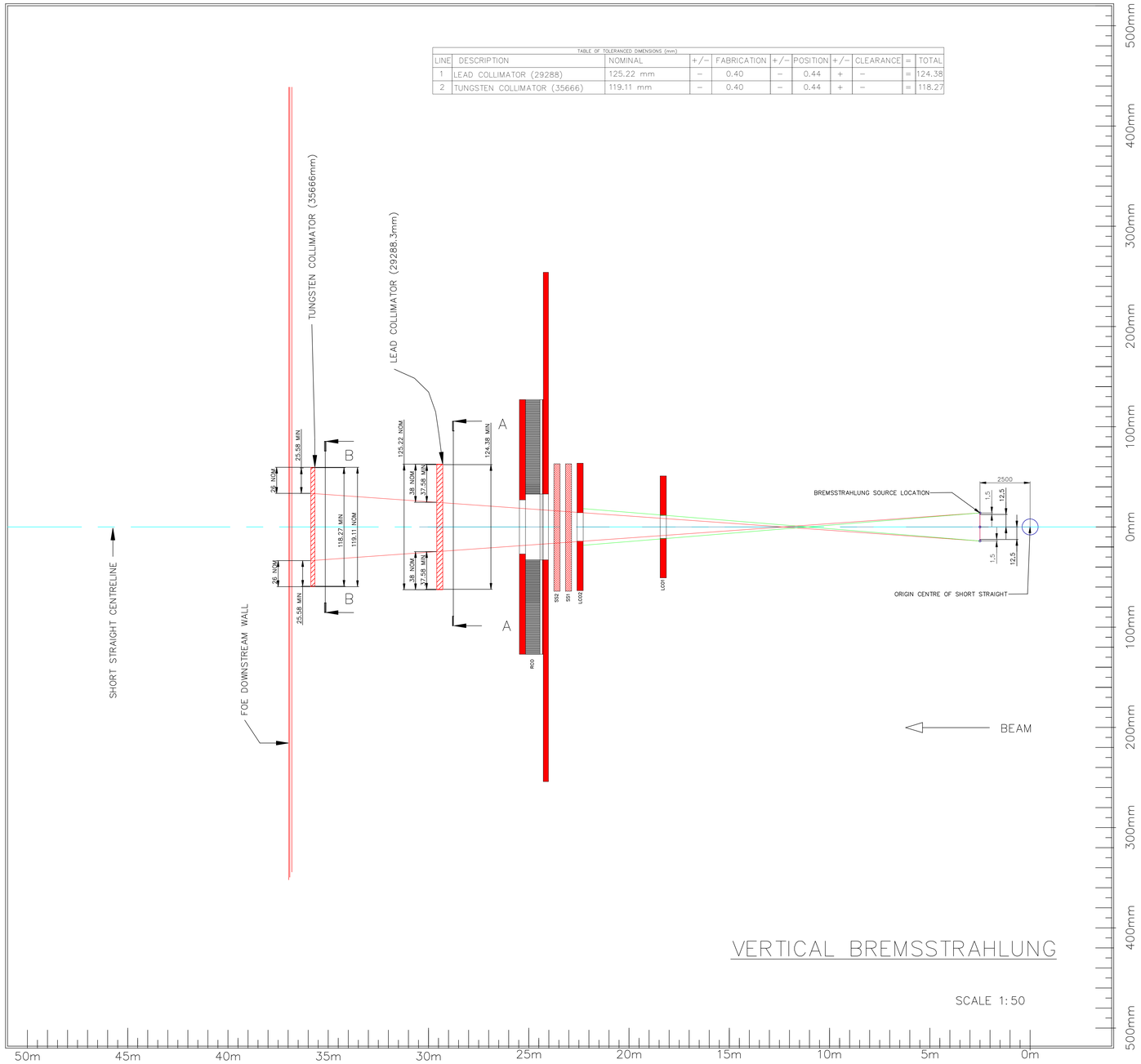

VERTICAL BREMSSTRAHLUNG

SCALE 1:50

NOTES:
1. THIS DRAWING REFERENCES BNL DOCUMENT SR-FE-IVU07-1001 REV B

REV	DATE	DESCRIPTION/DMR No	DRN	CHKD
09	03/06/16	INCORPORATING LATEST BNL COMMENTS	AF	
08	10/05/16	INCORPORATING BNL COMMENTS	AF	
07	03/04/16	INCORPORATING SR-FE-IVU07-1001 REV B	AF	SM
06	25/09/15	MAX SYNCHROTRON FAN ADDED	AF	SM
05	22/06/15	SST FIRST SUBMISSION FOR FDR	AF	–

THIS DRAWING BELONGS TO FMB OXFORD LTD AND IS ISSUED ON CONDITION THAT IT IS NOT COPIED, REPRINTED OR DISCLOSED TO A THIRD PARTY WITHOUT PRIOR CONSENT IN WRITING FROM FMB OXFORD Ltd.

DRAWN: A FAIRLEY — DATE: 03/06/16
CHECKED — DATE
APPROVED: A FAIRLEY — DATE: 03/06/16

FMB OXFORD LTD.,
UNIT 1 FERRY MILLS,
OSNEY MEAD, OXFORD, OX2 0ES.
ENGLAND

FMB Oxford

Title: NIST SST BEAMLINE RAYTRACE

Size: A3 — Document Number: AHB0531 — Rev: 08

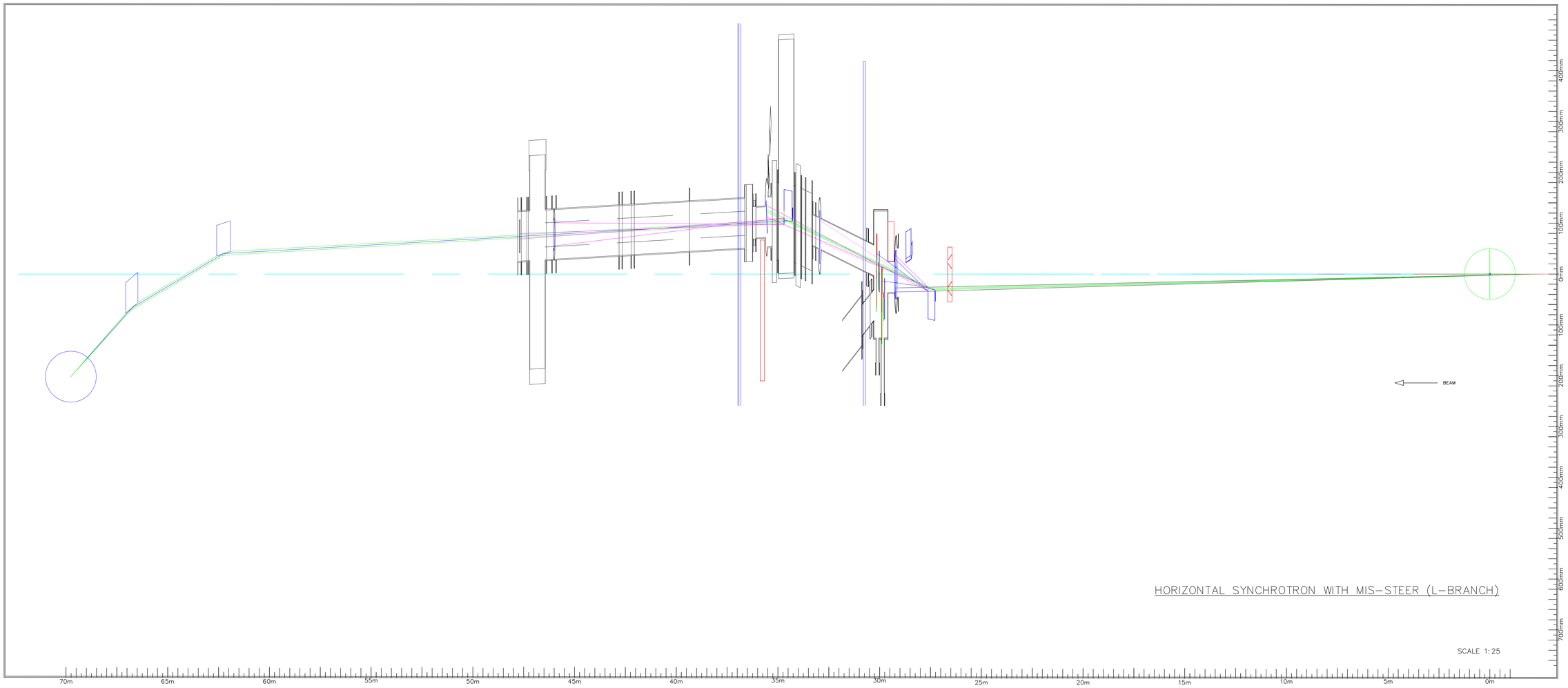

NOTES:
1. THIS DRAWING REFERENCES BNL DOCUMENT SR-FE-IVU07-1001 REV B

REV	DATE	DESCRIPTION/DMR No	DRN	CHKD
09	03/06/16	INCORPORATING LATEST BNL COMMENTS	AF	
08	10/05/16	INCORPORATING BNL COMMENTS	AF	
07	03/04/16	INCORPORATING SR-FE-IVU07-1001 REV B	AF	SM
06	25/09/15	MAX SYNCHROTRON FAN ADDED	AF	SM
05	22/06/15	SST FIRST SUBMISSION FOR FDR	AF	–

THIS DRAWING BELONGS TO FMB OXFORD LTD AND IS ISSUED ON CONDITION THAT IT IS NOT COPIED, REPRINTED OR DISCLOSED TO A THIRD PARTY WITHOUT PRIOR CONSENT IN WRITING FROM FMB OXFORD Ltd.

DRAWN A FAIRLEY DATE 03/06/16
CHECKED DATE
APPROVED A FAIRLEY DATE 03/06/16

FMB OXFORD LTD.,
UNIT 1 FERRY MILLS,
OSNEY MEAD, OXFORD, OX2 0ES.
ENGLAND

FMB Oxford

Title
NIST SST BEAMLINE RAYTRACE

Size A3 | Document Number AHB0531 | Rev 08

NOTES:
1. THIS DRAWING REFERENCES BNL DOCUMENT SR-FE-IVU07-1001 REV B

REV	DATE	DESCRIPTION/DMR No	DRN	CHKD
09	03/06/16	INCORPORATING LATEST BNL COMMENTS	AF	
08	10/05/16	INCORPORATING BNL COMMENTS	AF	
07	03/04/16	INCORPORATING SR-FE-IVU07-1001 REV B	AF	SM
06	25/09/15	MAX SYNCHROTRON FAN ADDED	AF	SM
05	22/06/15	SST FIRST SUBMISSION FOR FDR	AF	–

THIS DRAWING BELONGS TO FMB OXFORD LTD AND IS ISSUED ON CONDITION THAT IT IS NOT COPIED, REPRINTED OR DISCLOSED TO A THIRD PARTY WITHOUT PRIOR CONSENT IN WRITING FROM FMB OXFORD Ltd.

DRAWN: A FAIRLEY DATE: 03/06/16
CHECKED: DATE:
APPROVED: A FAIRLEY DATE: 03/06/16

FMB OXFORD LTD.,
UNIT 1 FERRY MILLS,
OSNEY MEAD, OXFORD, OX2 0ES.
ENGLAND

FMB Oxford

Title: NIST SST BEAMLINE RAYTRACE

Size: A3 | Document Number: AHB0531 | Rev: 08

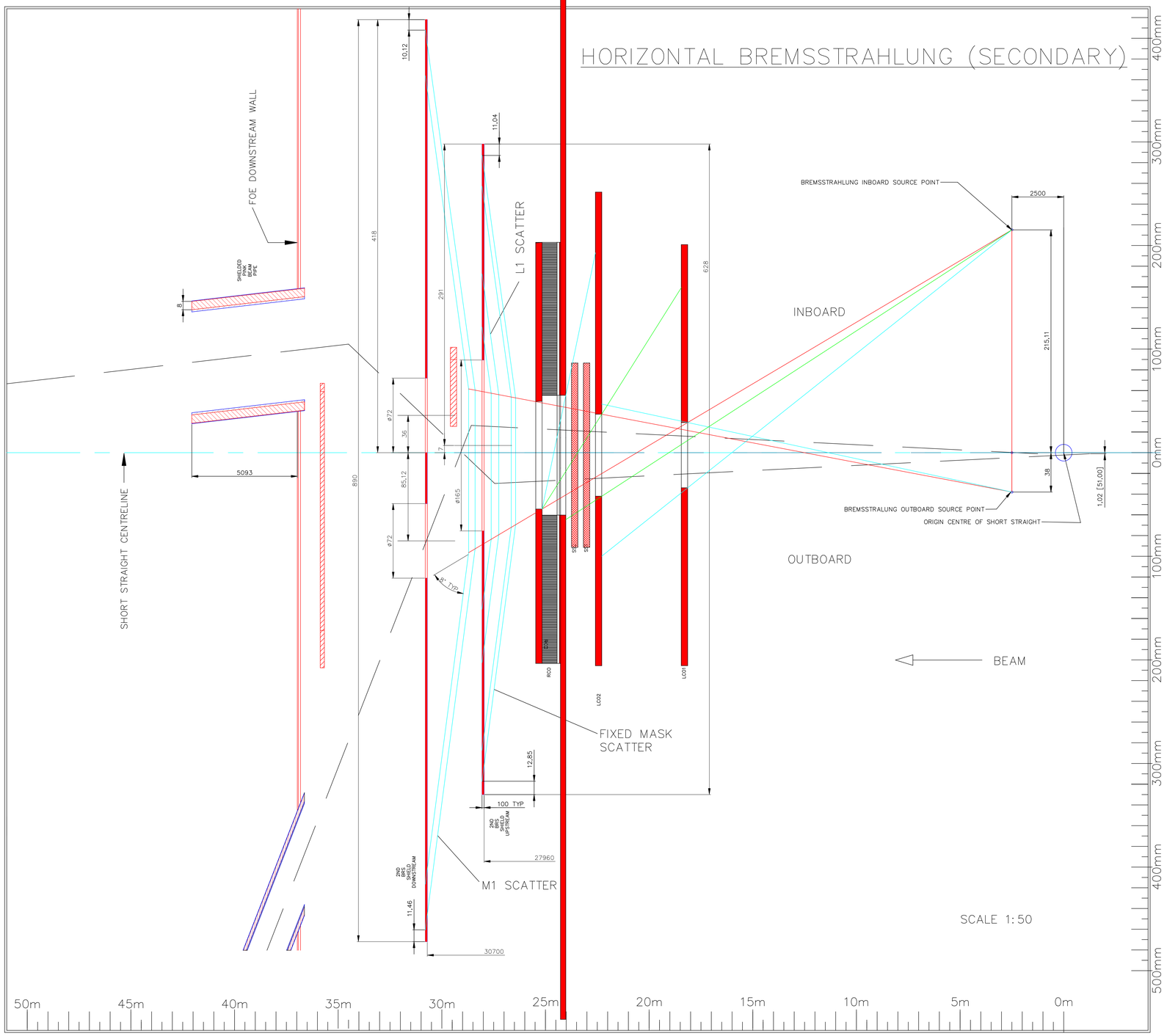

NOTES:
1. THIS DRAWING REFERENCES BNL DOCUMENT SR-FE-IVU07-1001 REV B

REV	DATE	DESCRIPTION/DMR No	DRN	CHKD
09	03/06/16	INCORPORATING LATEST BNL COMMENTS	AF	
08	10/05/16	INCORPORATING BNL COMMENTS	AF	
07	03/04/16	INCORPORATING SR-FE-IVU07-1001 REV B	AF	SM
06	25/09/15	MAX SYNCHROTRON FAN ADDED	AF	SM
05	22/06/15	SST FIRST SUBMISSION FOR FDR	AF	–

THIS DRAWING BELONGS TO FMB OXFORD LTD AND IS ISSUED ON CONDITION THAT IT IS NOT COPIED, REPRINTED OR DISCLOSED TO A THIRD PARTY WITHOUT PRIOR CONSENT IN WRITING FROM FMB OXFORD Ltd.

DRAWN: A FAIRLEY DATE: 03/06/16
CHECKED: DATE:
APPROVED: A FAIRLEY DATE: 03/06/16

FMB OXFORD LTD.,
UNIT 1 FERRY MILLS,
OSNEY MEAD, OXFORD, OX2 0ES.
ENGLAND

FMB Oxford

Title: NIST SST BEAMLINE RAYTRACE

Size: A3 | Document Number: AHB0531 | Rev: 08

Sheet 9 of 10

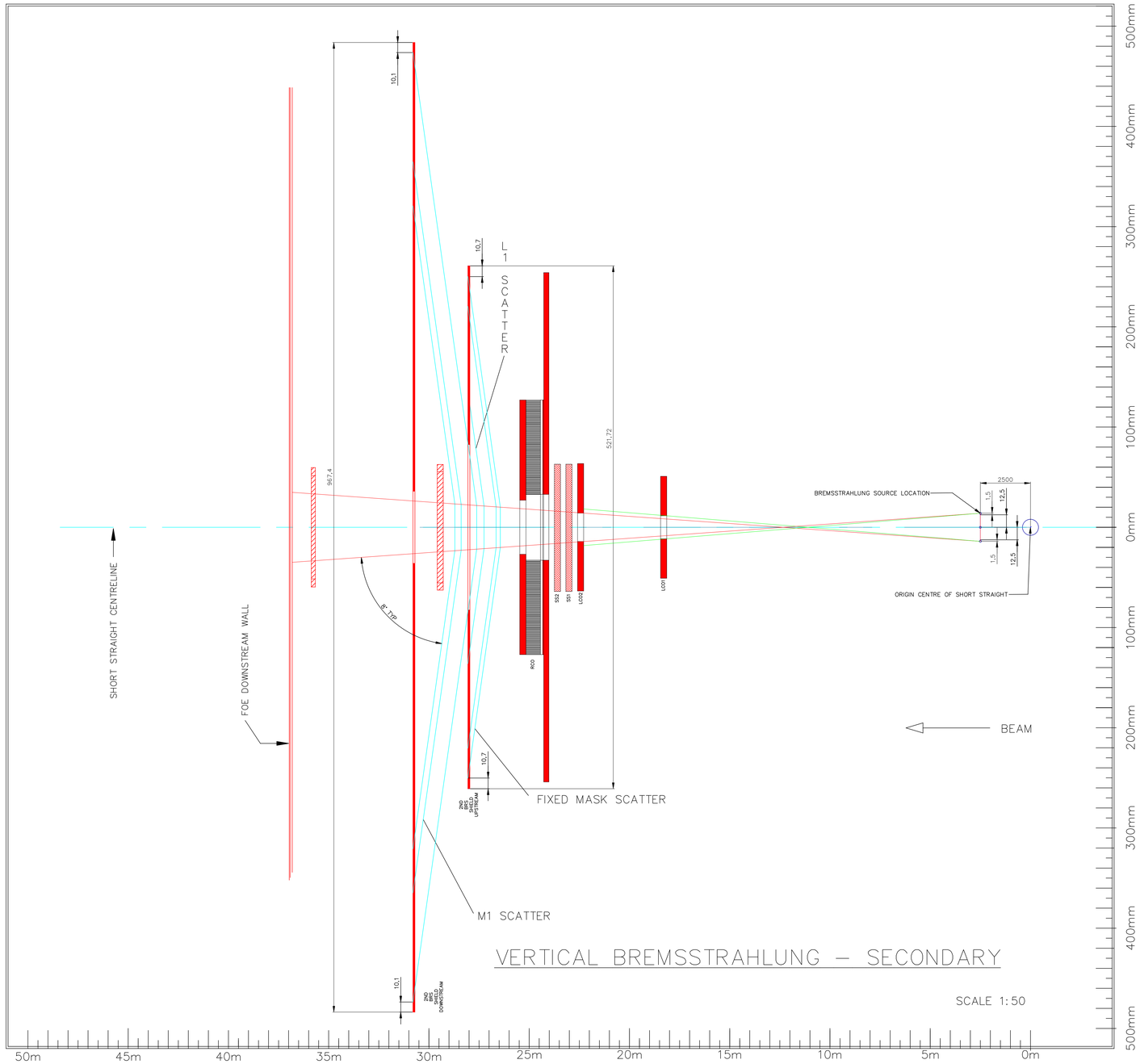

NOTES:
1. THIS DRAWING REFERENCES BNL DOCUMENT SR-FE-IVU07-1001 REV B

REV	DATE	DESCRIPTION/DMR No	DRN	CHKD
09	03/06/16	INCORPORATING LATEST BNL COMMENTS	AF	
08	10/05/16	INCORPORATING BNL COMMENTS	AF	
07	03/04/16	INCORPORATING SR-FE-IVU07-1001 REV B	AF	SM
06	25/09/15	MAX SYNCHROTRON FAN ADDED	AF	SM
05	22/06/15	SST FIRST SUBMISSION FOR FDR	AF	–

THIS DRAWING BELONGS TO FMB OXFORD LTD AND IS ISSUED ON CONDITION THAT IT IS NOT COPIED, REPRINTED OR DISCLOSED TO A THIRD PARTY WITHOUT PRIOR CONSENT IN WRITING FROM FMB OXFORD Ltd.

DRAWN: A FAIRLEY — DATE: 03/06/16
CHECKED — DATE:
APPROVED: A FAIRLEY — DATE: 03/06/16

FMB OXFORD LTD.,
UNIT 1 FERRY MILLS,
OSNEY MEAD, OXFORD, OX2 0ES.
ENGLAND

FMB Oxford

Title: NIST SST BEAMLINE RAYTRACE

Size: A3 — Document Number: AHB0531 — Rev: 08

Sheet 10 of 10

Appendix F

SST Beamline Development Proposal

NSLS-II Beamline Development Proposal

Type I ☐ Type II ☒

NIST Spectroscopy Beamline Suite: Soft and Tender X-ray Spectroscopy and Microscopy (100 eV to 7.5 keV canted sources) Three-Letter Acronym (SST-Spectroscopy Soft and Tender)	
Proposal Principal Team: Daniel Fischer *(Project Director and NIST Group Leader, dfischer@nist.gov)*, Joseph Woicik, and Bruce Ravel. (*NIST Synchrotron Methods Group located at NSLS, 631-344-5177)*	
Science and Technology Advisory Panel:	
Simon Bare, *Senior Principal Scientist* *UOP LLC, a Honeywell Company*	Joseph Lenhart, *Team Leader Polymers & Bio-Matls.* *Matls. & Manuf. Sci. Div., U.S. Army Res. Lab*
Raymond Browning, *President* *R. Browning Consultants Inc*	Laura Lewis, *Prof. & Chair* *Chemical Eng. Dept., North Eastern Univ.*
David Castner, *Prof., & Dir. NESAC/BI0* *Dept of Chem. Eng., U. of Wash., Seattle*	Pat Lysaght, *Senior Member Technical Staff* *SEMATECH*
Dean DeLongchamp, *Chemical Engineer* *Polymers Div., NIST*	Gary Mitchell, *Technical Leader in Surface Analysis* *The Dow Chemical Company*
Jan Genzer, *Prof. & Assoc. Head* *Chem. Eng. Dept., NCSU, Raleigh*	Chris Ober, *Prof. & Assoc. Dean of Engineering* *Materials Science Dept., Cornell Univ.*
Steve Hulbert, *Div. Head Experimental Systems* *NSLS*	Edward Principe, *President* *Synchrotron Research Inc.*
Eric Joseph, *Research Staff Member* *IBM T.J. Watson Research Center*	Ruben Reininger, *President* *Scientific Answers and Solutions Inc.*
Chi-Chang Kao, *Founding Director* *Joint Photon Sciences Institute (JPSI)*	Jose Rodriguez, *Group Leader, Catalysis* *Chemistry Dept., BNL*
Edward Kramer, *Prof.* *Chem. Eng. and Matls. Depts., UCSB*	Wen-Li Wu, *NIST Fellow* *Polymers Div., NIST*

NIST NSLS-II Spectroscopy Beamline Suite: Materials Measurement to Promote Innovation and Industrial Competiveness

Executive Summary: The National Institute of Standards and Technology (NIST) and the Department of Energy (DOE) have a 30 year ongoing partnership at the National Synchrotron Light Source (building to NSLS-II) developing advanced synchrotron measurement methods and delivering excellence in material science impacting important societal challenges in energy, health, environment, and national security improving our quality of life. This partnership promotes innovation and enhances US industrial competiveness for inorganic and organic semiconductors, photovoltaics, SAMs, biological and environmental materials, batteries, catalysts, fuel cells, polymers, superconductors, ferroelectrics, and ferromagnets. Located at the NSLS, the NIST Synchrotron Methods Group of nine operates a suite of three state-of-the-art spectroscopy beamlines (U7A, X24A, and X23A2) that span the entire absorption-edge energy range of the periodic table to establish structure function relationships in advanced materials. More than 200 industry and academic researchers each year use the NIST Beamline Suite to accelerate the development of new materials into devices and systems with advanced functionality for a broad spectrum of industries. Building upon this success, NIST proposes to establish an NSLS-II spectroscopy suite of three state-of-the-art high throughput beamlines (with X-ray Diffraction capability) described in two beamline development proposals; *Soft and Tender X-ray Spectroscopy and Microscopy (100 eV to 7.5 keV canted sources)* and *Hard X-ray Absorption Spectroscopy and Diffraction (4.5 keV to 40 keV three-pole wiggler source)*. Taken together, the NIST NSLS-II Spectroscopy Beamline Suite will be capable of measuring the electronic, chemical, and structural properties of almost any material, often at the nanoscale. NIST is committed to fully funding the construction of its proposed Spectroscopy Beamline Suite and to continuous world leading improvements in synchrotron measurement science and technology. Furthermore, NIST will build upon its NSLS based Synchrotron Methods Group to fully staff its stakeholder relationship in NSLS-II.

A. Science Case: Soft and Tender X-ray Spectroscopy and Microscopy (100 eV to 7.5 keV)

Synchrotron based X-ray Photoelectron Spectroscopy (XPS) and Near Edge X-ray Absorption Fine Structure (NEXAFS) spectroscopy are complementary techniques, probing occupied and unoccupied density of states respectively. The ability to perform both measurements on the same sample achieves a complete, non-destructive, depth selective measurement of electronic structure, chemistry, and bond orientation. *NIST proposes to build a pair of spectroscopy beamlines based on two canted undulator sources, one for soft x-rays (100 eV to 2.2 keV) and one for tender x-rays (1 keV to 7.5 keV).* The beamlines will have a total of 6 unique world class NEXAFS/XPS experimental stations (2 full field microscopes, 2 automated high-throughput, and 2 insitu high pressure); three will be served by the soft x-ray undulator and three by the tender x-ray undulator, thus a variety of soft and tender spectroscopy experiments can be accomplished simultaneously in this beamline complex. Two of the experimental stations (high-throughput XPS/NEXAFS and the XPS microscope) can utilize the soft and tender X-ray undulators (sequentially or even simultaneously) enabling a continuous selection of X-rays from 100 eV to 7.5 keV (at a common focal point) in a single experiment (unique capability, enhancing depth selectivity in XPS; i.e. in Hard X-ray Photoelectron Spectroscopy - HAXPES).

Enabled by the world class brightness of the proposed NIST NSLS-II canted undulator beamline pair, NIST is pioneering (at NSLS) two new and unique (large depth of field for practical materials) magnetic projection microscopes pushing the state-of-the-art in synchrotron XPS and NEXAFS spectroscopy full field imaging measurement science (details in appendix, page 13). (1) XPS microscope; combines nanometer scale spatial resolution with chemical and electronic state specificity and full three-dimensional mapping of the structure of nanomaterials and nanodevices at all points within their volume. (2) Large Area Imaging NEXAFS Microscope for high efficiency, highly parallel spectroscopic chemical and orientation maps of gradient samples, combinatorial arrays (e.g. 1000s of compositional samples at a time), and device arrays up to 4 cm^2 with simultaneous micron scale resolution.

The proposed *Soft and Tender X-ray Spectroscopy and Microscopy* beamline pair coupled with NIST's continuous development of automated high-throughput spectroscopy methods, world class high efficiency detectors, and unique NEXAFS and XPS microscopes will have a *large scale impact on the materials science of important societal challenges in energy, health, environment, and national security*. Some strategic science case examples follow. They illustrate how this proposed beamline pair will establish structure function relationships in advanced materials, often at the nanoscale, to accelerate the development of new materials into devices and systems with advanced functionality for promoting innovation and enhancing US industrial competitiveness.

1) Accelerating Organic Photovoltaics with Soft and Tender Spectroscopy and Microscopy
   Dean M. Delongchamp, NIST
2) Nanoscale Spectroscopy for Next Generation Semiconductor Microelectronics: CMOS and Beyond
   Pat Lysaght, SEMATECH

Additional Science Case Examples (3-13) appear in the appendix page 13:

3) Designing Biomaterials with High Through-Put Screening: Using the NIST NEXAFS Microscope
   David Castner (U. of Washington, Seattle)
4) Synchrotron Spectroscopy an Enabling Capability for the Defense and National Security Community
   Joseph Lenhart (WMRD, US Army Research Laboratory)
5) Nano to Microscale Spectroscopy for Environmentally Friendly Marine Anti-Fouling Coatings
   Edward Kramer (UCSB)
6) Spectroscopy and Microscopy for Advanced Hard and Soft Materials: Energy and Microelectronics
   Gary Mitchell (Dow)
7) Advanced Spectroscopy Promoting Breakthrough Catalysts for Energy Applications
   Simon Bare (UOP)

Accelerating Organic Photovoltaics with Soft and Tender Spectroscopy and Microscopy

Dean M. DeLongchamp (NIST)

Affordable, renewable power generation, a critical component of U.S. energy independence, has remained for many years perpetually on the threshold of technical and economic viability. The largest solar power development efforts have focused on incremental improvements of older technologies, and even with these efforts, photovoltaics still produce less than 0.05 % of our national electrical energy needs.[1] New solar energy technologies, such as organic photovoltaics (OPV), promise to break this paradigm by greatly reducing both the manufacturing costs and the capital required to increase production.[2] The active layers of an OPV module are formulated as liquid inks that can be applied to flexible surfaces using simple graphics arts printing techniques such as inkjet, spray, and screen printing, to create solar cell modules that can be spread over large areas as easily as unrolling a carpet. The commercialization of OPV technology has been slowed by two key technical challenges: enhancing the power conversion efficiency, and preventing aging-related performance loss. To address these challenges requires precise measurements of materials composition and molecular orientation with sub-100 nm spatial resolution.[3] These needs will be met by ***NIST's new soft and tender X-ray microscopes and beamlines*** described in this NSLS-II proposal, which promises to greatly accelerate the development of high-efficiency, long-lasting solar modules with the potential to build a new domestic solar cell manufacturing industry in the U.S. and transform our energy our energy production landscape in the coming decades.

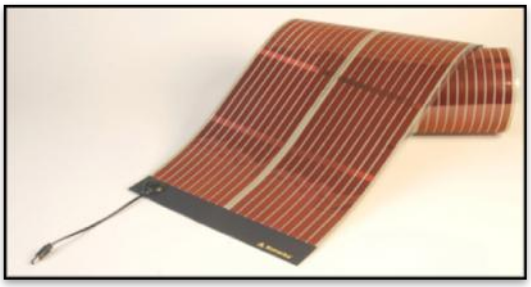

Konarka's Power Plastic© organic photovoltaics module. NIST has an active CRADA with Konarka (Lowell, MA).

The power conversion efficiency of bulk heterojunction (BHJ) OPV devices critically depends on the distribution of the polymer absorber and the fullerene electron acceptor (e.g., the blend morphology).[4] Synchrotron-based tools provide a critical means to probe the structure of the BHJ layer. For example, NIST recently applied Near-Edge X-ray Absorption Fine Structure (NEXAFS) spectroscopy to reveal that the vertical distribution of BHJ components follows segregation behavior similar to that of miscible polymer blends. The top (air) interface becomes rich in the polymer absorber, whereas the bottom interface depends on the substrate.[5] This effect greatly impacts charge carrier mobility measurement; transistors fabricated from BHJs can exhibit ambipolar or hole-only transport depending on the dielectric. These results were extended to practical photovoltaic devices by comparing BHJs cast upon hole transport layers that have similar work functions but different surface energies.[6] The molecular orientation of the absorber revealed by NEXAFS contributed to the development of accurate optical models for the practical devices. This work illustrates the importance of non-destructive interface measurements via ***high-throughput, automated NEXAFS*** to the acceleration of OPV technology development. High-throughput, automated NEXAFS acquisition on 100's of PV samples is required to rapidly build structure function relationships for intelligent PV materials design and processing.

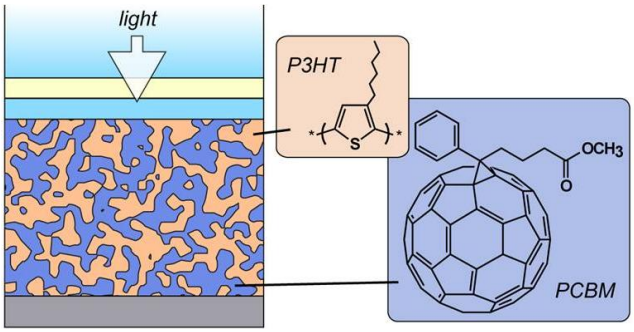

The BHJ active-layer morphology is critical to its power conversion efficiency.

[1] U.S. Energy Information Administration, Electric Power Monthly, May **2010.**
[2] "Organic and Dye-Sensitized Cell Photovoltaics: Materials, Applications, and Opportunites," *NanoMarkets*, **2010**.
[3] NIST Grand Challenges for Advanced Photovoltaic Technologies and Measurements Workshop, Denver, CO, **2010.**
[4] DOE SETP, National Solar Technology Roadmap Organic PV, **2007.**
[5] DS Germack et al., *Applied Physics Letters,* **2009,** 94, 233303.
[6] DS Germack et al., *Macromolecules*, **2010**, 43, (8), 3828-3836.

The ideal OPV system has a three-dimensional domain network structure with dimensions less than 100 nm. Small changes to the distributions of domain size and shape strongly impact OPV performance. Composition-sensitive microscopy methods with high spatial resolution are thus critical to the measurement and rapid optimization of OPV active layer structure. To this end, NIST recently demonstrated a new, full-field NEXAFS microscope (at NIST's U7A beamline) that is capable of measuring the three-dimensional compositional structure of OPV films. The images below show a BHJ film "by design" that has been purposefully structured by thermal annealing atop a chemically patterned template. The fullerene component is attracted to the high energy acid surface (yellow), whereas the polymer absorber is attracted to the lower energy alcohol surface (green). The powerful depth resolution of NEXAFS microscopy is revealed by comparing images collected at shallow and deep bias conditions. The loss of contrast at the shallow condition reveals that the surface is covered with a ~ 2 nm thick "skin" of the polymer. This information is required to understand and eventually control the three-dimensional domain structure of OPV active layers. Although compelling, the images shown below are proofs-of-concept with a ≈ 300 μm diameter stamp; the sub-micron resolutions of the proposed ***Larger Area Imaging NEXAFS Microscope*** and ***XPS (3D-Chemical) Microscope*** are required to approach lateral resolutions that are relevant to the frontiers of OPV technology. Whereas the XPS microscope will provide the most powerful measurement of domain structure, the NEXAFS microscope will be required to determine how variations in composition are correlated to variations in local orientation, which is critical to local photon absorption and nanoscale exciton / charge carrier transport processes.

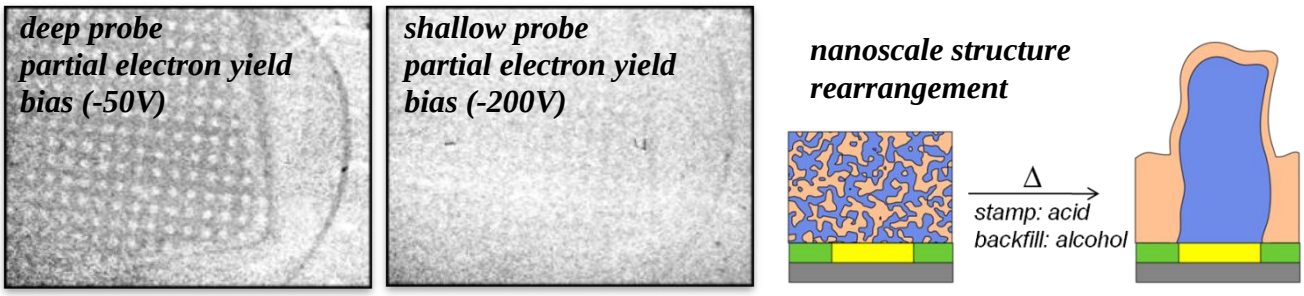

NIST's NEXAFS microscope(NSLS U7A) reveals the structure of an OPV film structured "by design" in collaboration with University of Washington (Ginger). Lighter areas are fullerene-rich; contrast is generated by split π resonance of fullerene.*

NEXAFS and XPS microscopy will also impact OPV technology development in the measurement of aging-related performance loss. High vertical and lateral resolutions are required to determine the precise locations of chemical degradation products. ***The unique 100 eV to 7.5 keV energy range of the NIST NSLS-II Spectroscopy Beamline Suite*** will provide unprecedented depth selectivity to measure the vertical distribution of degradation products near interfaces. Recent NEXAFS measurements(at NIST's U7A beamline) have shown the technique to be quite sensitive to oxygen incorporation in OPV materials. The polymer absorber is found to be chemically vulnerable at the point where a side chain is added to enhance solubility and aid processing. Oxygen π* and σ* resonance intensities increase commensurately, indicating a carboxyl-containing oxidation product. By nondestructively identifying the mechanisms of degradation, and their location within devices, these tools will greatly accelerate the development and deployment of robust, high-efficiency plastic solar cells.

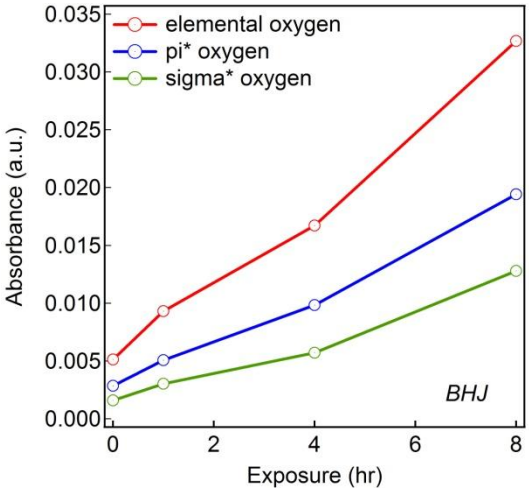

NEXAFS measurement of oxygen incorporation into an OPV active layer.

Nanoscale Spectroscopy for Next Generation Semiconductor Microelectronics: CMOS and Beyond

Pat Lysaght (SEMATECH)

SEMATECH is a non-profit consortium established more than 20 years ago to perform basic research in semiconductor manufacturing. In recent years, the consortium of leading semiconductor manufacturers has set global direction and bridged strategic R&D to manufacturing with a business model based on highly flexible collaboration and demonstrated internal information control. Today, SEMATECH continues accelerating the next technology revolution with nanoelectronics and emerging technology partners including federally funded research initiatives that directly enhance applications in information technology, communications, medicine, energy, and national security. To this end, SEMATECH has engaged in collaboration with the NIST Synchrotron Methods Group stationed at the NSLS and during the past 6 years has conducted state of the art research at each of NIST's three NSLS spectroscopy beamlines for materials screening and optimization research: X23A2, X24A, and U7A for EXAFS, high-energy XPS, and NEXAFS. Two current examples of DARPA funded SEMATECH programs include: i) Sub-threshold-slope Transistors for Electronics with Extremely-low Power (STEEP) and ii) Carbon Electronics for RF Applications (CERA).

The STEEP program goal is to develop a revolutionary transistor technology for logic circuits with extremely low power consumption while maintaining high performance for logic applications in areas such as unattended sensors with unlimited lifetimes or autonomous unmanned air vehicles navigated by vision systems. The key technical challenges of achieving steep-sub threshold-slopes over many decades of current; developing novel circuit designs accommodating asymmetric source-drain regions; demonstrating abrupt doping profiles at tunneling junctions; and integrating SiGe, Ge, or III-V compound semiconductors in transistor structures to facilitate the required tunneling currents – all require the most advanced analytical tools equipped with the highest spatial resolution available to assure success. ***SEMATECH is extremely excited anticipating process optimization results from samples studied via the new NIST NSLS-II soft and tender beamline pair for NEXAFS, high energy XPS, and chemical imaging.*** These new capabilities will uniquely impact the STEEP and other SEMATECH programs by enabling simultaneous nanoscale spatial resolution and depth selectivity (via variable kinetic energy high-energy XPS in the range of 100 eV to 7.5 keV) essentially operating as a rapid, ***non destructive 3D XPS microscope at the nanoscale***.

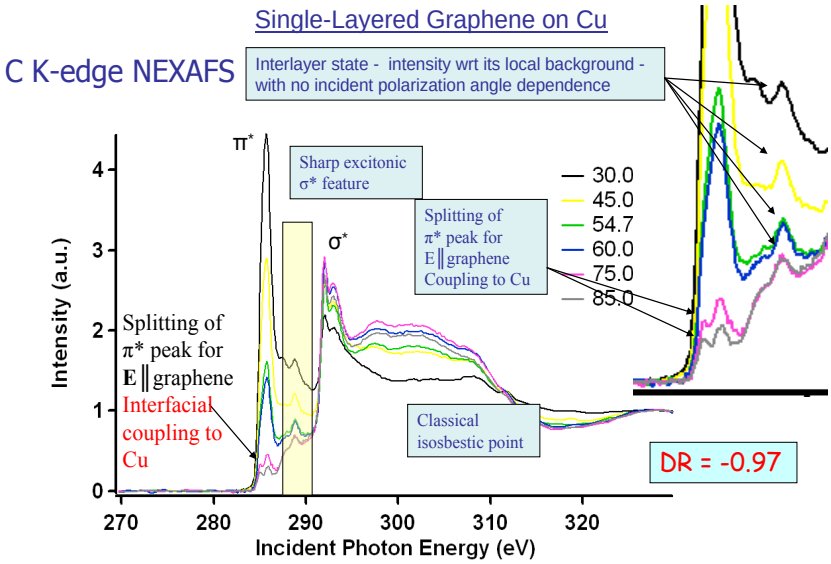

Figure 1. Polarization dependent NEXAFS spectra of single layer graphene on Cu foil which illustrates evidence of π splitting (at high polarization angles) and the interlayer state (inset).*

The CERA program targets development of wafer-scale graphene synthesis focused on enabling ultra-high-speed, low-power graphene-channel field-effect transistors through innovative approaches that enable revolutionary advances in materials science, epitaxial growth, transistor development, and RF circuit design. The research needed to achieve the goals of the CERA program is another area where NIST's proposed advanced synchrotron spectroscopy imaging techniques and advanced measurement instruments are pivotal to success. An example of the ***critical need for high-throughput low energy polarized NEXAFS*** as a probe for characterizing the electronic structure of graphene has recently been demonstrated in University of Buffalo-SEMATECH-NIST collaboration on NIST beamline U7A at the NSLS, which resulted in a publication on Cu/graphene substrate

hybridization [1]. Figure 1 illustrates the best resolved splitting (reported in the literature) of the π* absorption feature and indisputable evidence for the existence of an interlayer state that has been the subject of sharp debate for more than 20 years. These exciting results have stimulated the collaborative interest of theorists and modeling and simulation of the NEXAFS spectra is in progress.

In addition to the STEEP and CERA programs, all of the planar and non-planar CMOS logic and non-volatile memory device programs at SEMATECH are materials limited and critical challenges associated with continued scaling have ***demonstrated a clear and urgent need for both of NIST's proposed microscopes (nano and micro scales).***

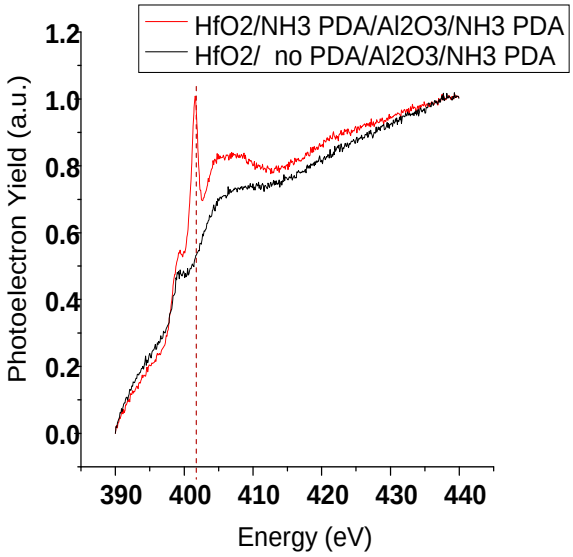

Figure 2. Surface sensitive N K edge absorption spectra shows that Al in-diffusion into HfO_2 (black curve) is limited when HfO_2 is preannealed in NH_3 ambient, evident by surface Al-N peak (red) [2].

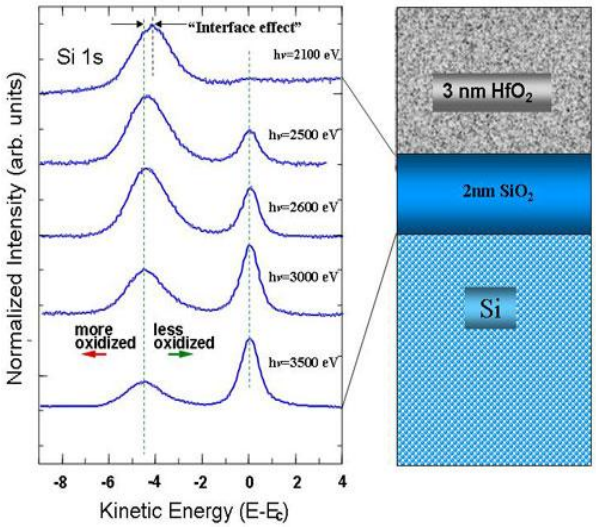

Figure 3. Si 1s spectra from 3nm HfO_2/ 2nm SiO_2 sample recorded with variable kinetic energy high-energy XPS (VKE-XPS) illustrates depth profiling and an interface effect near HfO_2/SiO_2 interface [3].

For example, there is a universal need to identify surface chemical states as a function of processing as achieved recent ***NEXAFS results from NIST beamline U7A*** (HfO_2/Al_2O_3, probing the outermost 1 nm of material as shown in fig. 2).

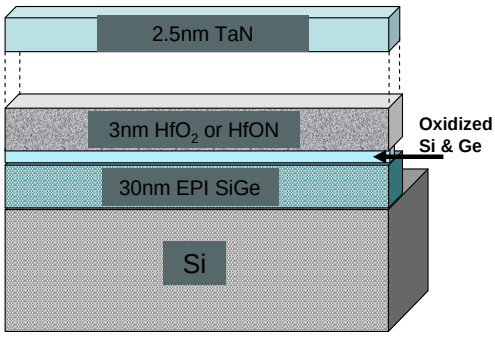

Figure 4. Material stack measured by high-energy XPS (a-d) on NIST beamline X24A at the NSLS. Acquisition of bulk sensitive (Si 2*p*, Ge 3*d*) and surface sensitive (Si 1*s*, Ge 2*p*) core lines allows the oxidation kinetics as a function of processing to be determined.

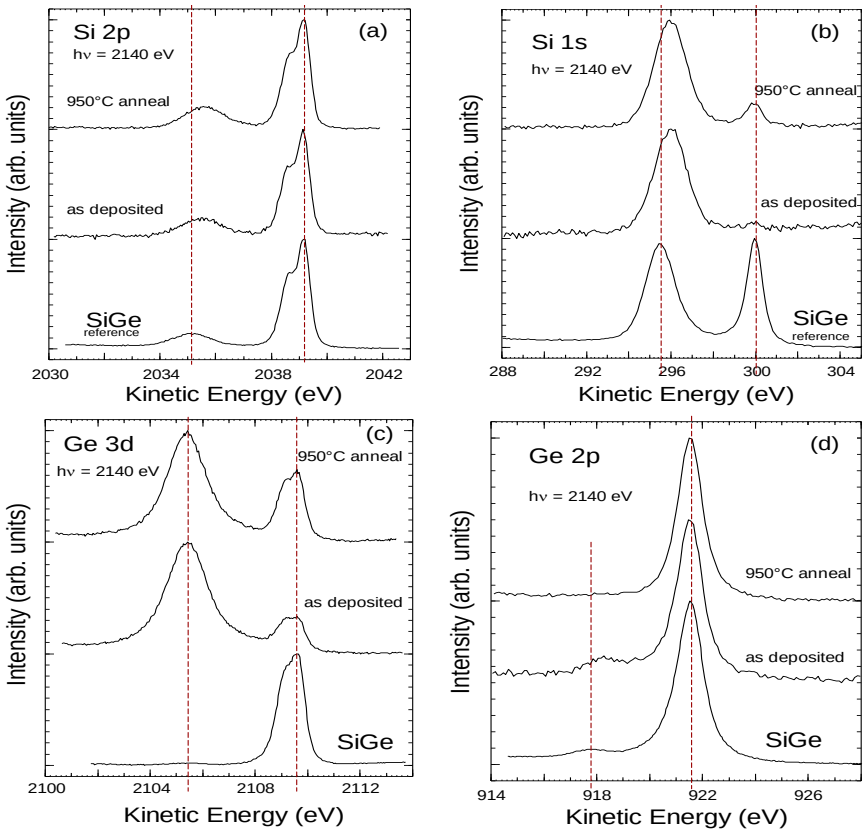

Also to determine the corresponding changes in binding energies of chemical constituents

of buried layers and interfaces as measured with ***tender XPS on NIST beamline X24A*** ($Hf0_2/SiO_2$, shown in fig. 3) and detecting variations in oxidation state of underlying engineered substrate elements (SiGe, shown in fig. 4), in order to ultimately explain the mechanisms that give rise to the limits of electrical performance. All these examples have a common need for spectroscopy of large numbers of samples generated by numerous materials and processing parameters, ***NIST's proposed NSLS-II soft and tender beamline pair and high-throughput NEXAFS/XPS stations answer this challenge***.

An example of the diverse and challenging device architectures and novel film systems verses power that are slated for manufacturing on a timeline according to *The International Technology Roadmap for Semiconductors 2009 edition* are given below.

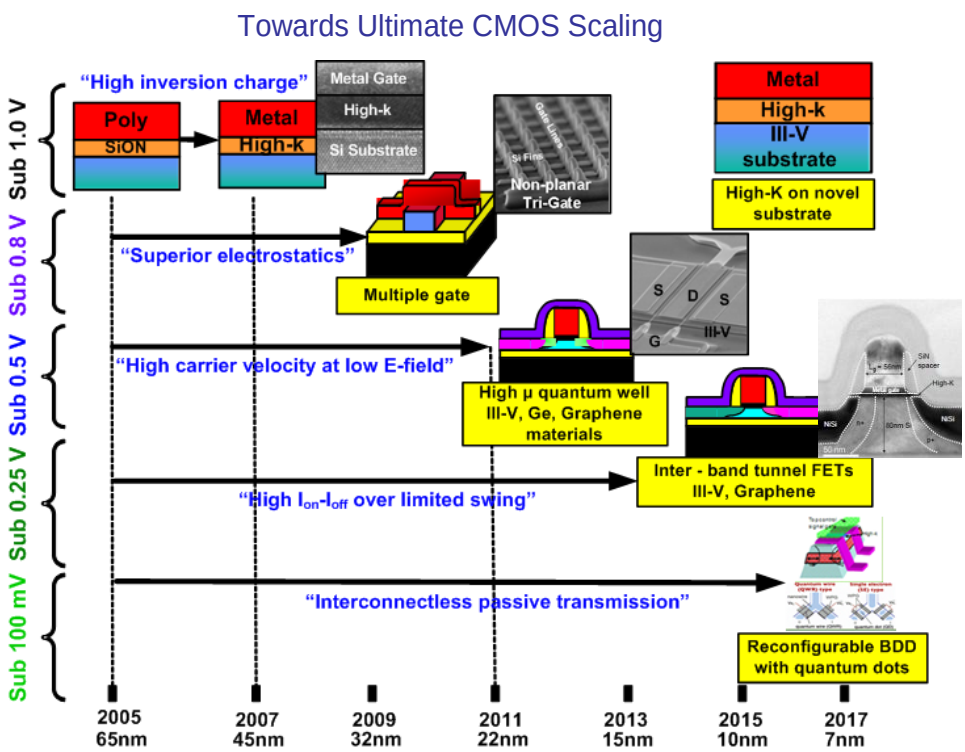

These architectures are currently being researched (many with no known solution). ***The proposed NIST XPS microscope with nano-scale spatial resolution is ideally suited to the timeline*** construction and materials (65 nm down to 7 nm resolution).

Continued collaborative access with NIST is critical to the success of SEMATECH as a pioneer of new technologies.

1. S. Banerjee, et al. J. Phys. Chem. Lett. 1, 1247–1253, (2010).
2. P. Lysaght, et al. International Journal of Materials Research (IJMR) June, (2009).
3. P. Lysaght, et al. J. Appl. Phys. 101, 024105 (2007).

B. Beamline Concept & Feasibility

NIST proposes to build a pair of spectroscopy beamlines served by two insertion devices canted at an angle of 2 mrad: a 2.5 m long APPLE II device for 100-2200 eV (soft x-rays) and a 1.5 m in-vacuum undulator covering the range 1.5-7.5 keV (tender x-rays). The newly developed full field XPS microscope requires a spot size of 10 microns over the full energy range of both beamlines and mandates to locate the insertion devices at a low beta straight section of NSLS-II. The undulator sources are imperative to deliver adequate brightness and flux for the microscopes, high resolution XPS, soft x-ray fluorescence yield NEXAFS and emission spectroscopy, and high-throughput (>10 times NSLS) electron yield NEXAFS.

The soft x-ray beamline is based on a variable line spacing plane grating monochromator (VLSPGM) capable of delivering a resolving power higher than $2x10^4$ over its full energy range (FMB Oxford, NIST contact awarded FY08). The tender x-ray beamline is based on an extended range (theta -3° to 85°) double crystal monochromator (LN_2 cooled DCM) equipped with YB66, Si(111) and (220) crystals to achieve medium and high resolution 333 reflection near normal (FMB Berlin, NIST contact awarded FY09). The expected flux in all experimental stations of the bemaline pair will be in the range 10^{12}-10^{13} photons/s with resolving powers between a few thousands and 10^4. A complete optical design including ray tracings, spot sizes and expected fluxes at each of the experimental stations will be available upon request.

The beamline pair will have 6 unique world class NEXAFS/XPS experimental stations as shown schematically below; red and blue denote which stations will recieve soft and/or tender x-rays, respectively. The automated high-throughput HAXPES/XPS/NEXAFS station and XPS/HAXPES microscope utilize both monochromatic soft and tender beams enabling a continuous selection of X-rays from 100 eV to 7.5 keV at a common focal point in a single experiment (unique capability, enhancing depth selectivity in XPS or HAXPES). Computer controlled mirrors and pass-through beams are used to rapidly switch soft and tender x-rays between the 6 stations to fully utilize and optimize all the available beamtime (an extension of NIST's NSLS U7A beamline operation among 4 endstations). The high energy limit (7.5 keV) was chosen so that the two beamlines could operate hutch-less (see CAD model below)

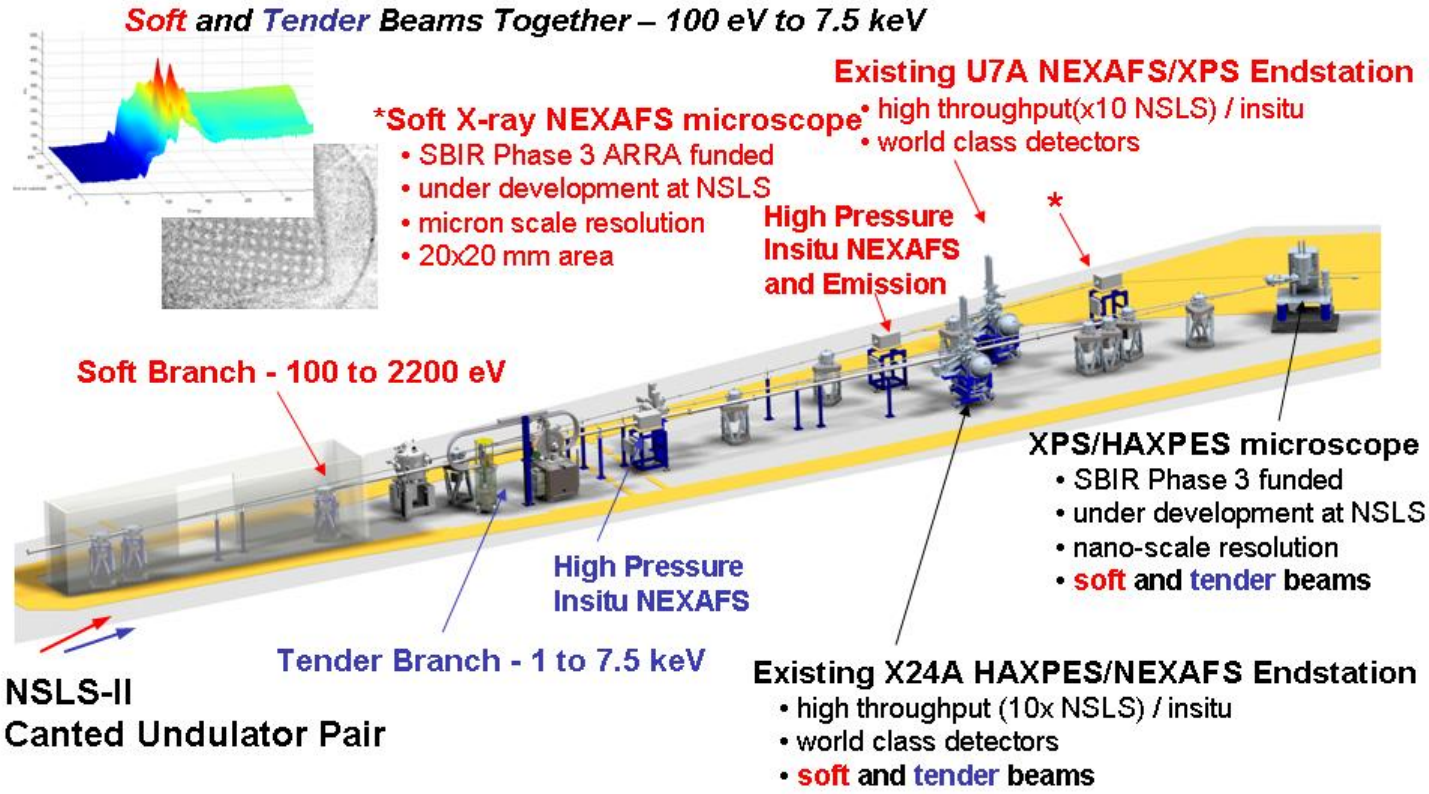

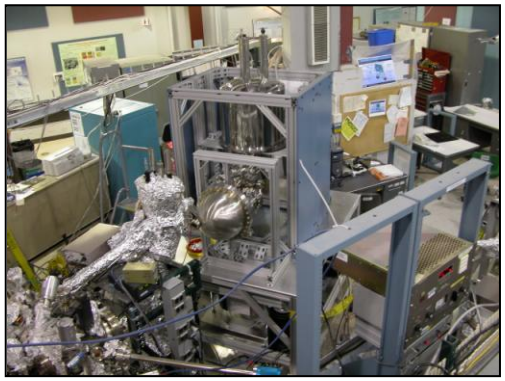

XPS Microscope Station (pictured at left, details in appendix, page 13) - This new XPS microscope is under development at NSLS (U4A). It is an SBIR Phase-III collaboration between NIST and *R. Browning Consultants*. To date, 4 Patents have been granted for this new microscope technology. At NSLS-II it will receive soft and/or tender beams via two KB mirror pairs that have a common focal spot of 13 µm. The new XPS microscope can be thought of as a super conducting magnetic projection lens x-ray photoemission electron microscope (XPEEM). The full field magnetic projection lens enables large depth of field nanoscale spatial and spectral XPS imaging over the full range of kinetic energy (100 eV to 7.5 keV) tuning the sensitivity from surface to bulk length scales ideally suited for photovoltaics and microelectronics. There are no high voltages; samples can be rough or insulating. Thus the XPS microscope, combines nanometer scale spatial resolution and depth selectivity with XPS chemical and electronic state specificity to enable full three-dimensional (3D) chemical mapping of the structure of nanomaterials and nanodevices at all points within their volume.

Existing X24 HAXPES/ NEXAFS Station (pictured at right) is the only hard x-ray photoelectron spectroscopy (HAXPES) facility in the United States and is in high demand for microelectronics interfacial characterization (e.g., SEMATECH). This automated high-throughput station has a load lock system capable of holding up to 100 samples at a time and a High Energy Scienta 4000 electron analyzer. Additionally, for NEXAFS it has large solid angle electron yield detector and a 7-element Ge ultra high resolution x-ray detector for soft and tender x-ray fluorescence yield. This HAXPES/XPS/NEXAFS station will be transferred to NSLS-II where it will receive soft and tender x-rays (100 eV to 7.5 keV) at a common focal point of less then 100 µm with intensity to enable at least a 10x gain in sample throughput over operation at NSLS X24A and improved X-ray energy resolution using near normal incidence Si(333) crystals.

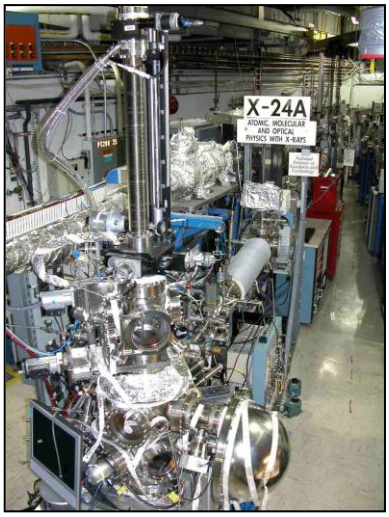

Existing U7A NEXAFS/XPS Station (pictured at left) is under 24/7 use for OPVs, nanomaterials, biomaterials, batteries, polymers and polymer interfaces (see science case examples). This automated high-throughput station has a load lock system capable of holding up to 100 samples at a time and a Scienta Wide Angle 4000 electron analyzer. For Electron Yield (EY) NEXAFS it has a large solid angle EY detector and a novel 36 channel detector array for measuring EY at all takeoff angles and at all angles of x-ray incidence simultaneously for high-throughput NEXAFS depth profiling of surface treatments in advanced materials. For Fluorescence Yield NEXAFS it has a 14-element ultra high resolution Si(Li) x-ray detector and a unique focusing graded multilayer mirror and proportional counter for ultra low background FY NEXAFS; e.g., reaction intermediates in catalysts. This NEXAFS/XPS station will be transferred to NSLS-II where it will receive soft x-rays (100-2200 eV) at a focal point of less then 100 µm with intensity to enable at least a 10x gain in sample throughput over operation at NSLS U7A. A dithering system will allow mm spot sizes when performing NEXAFS on radiation sensitive samples.

Large Area Imaging NEXAFS Microscope Station (pictured schematically at right, with details in appendix page 13) is a working prototype station at NIST's U7A beamline. It is a highly efficient 1 Tesla magnetic projection partial electron yield full field microscope imaging 13x18 mm at 50 µm spatial resolution with a large depth of field (rotatable sample see figure a right). The microscope has been used to image combinatorial arrays of SAMs, batteries, OPV and various designer surfaces (see science case examples). This automated high-throughput prototype NEXAFS imaging station has a load lock system capable of holding up to 10 samples at a time. An ARRA funded (FY09 NIST SBIR Phase III with *Synchrotron Research, Inc.*) superconducting magnet (8T) NEXAFS microscope for NSLS-II is under development, to be commissioned at NSLS U8B beamline. The new superconducting microscope will produce highly efficient, highly parallel spectroscopic chemical and orientation maps of gradient samples, combinatorial arrays (e.g. 1000s of compositional samples at a time), and device arrays up to 4 cm^2 with simultaneous micron scale resolution. This microscope end station will be transferred to NSLS-II and will receive soft x-rays (100-2200 eV) from a pair of dithered mirrors providing 4x4 cm high flux sample illumination.

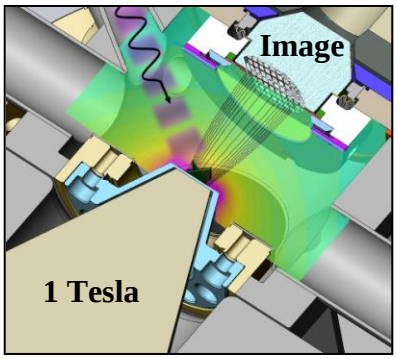

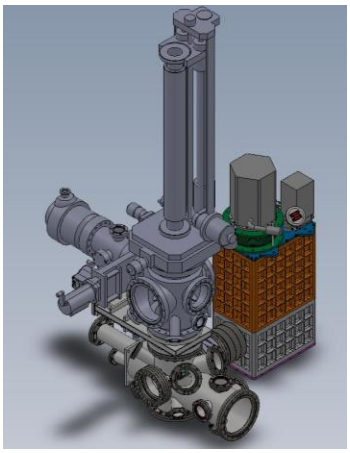

Existing U7A High Pressure Insitu Soft X-ray NEXAFS and Emission Station (pictured schematically at left) is a prototype station at NIST's U7A beamline. NIST is pioneering a 10 mm^2 area, 256 element, micro-calorimeter soft x-ray detector that will be capable of better the 1 eV resolution at 25 kHz count rate (details in appendix, page 13) for low background FY NEXAFS and soft x-ray energy dispersive emission spectroscopy. This automated high-throughput station has a load lock system capable of holding up to 100 samples at a time. High pressure capability will be achieved with windows and cells that are in routine use in soft x-ray microscopy. This station will be transferred to NSLS-II where it will receive unfocused soft x-rays (100-2200 eV) with spot size of 1 mm^2.

High Pressure Insitu Tender X-ray NEXAFS/XAS Station to be developed. The station will have FY and EY detectors, high pressure and instu operation to be achieved with standard windows and cells. Insitu catalytic studies of sulfide and chloride reaction intermediates will be routine in this station. At NSLS-II this end station will be located just down stream of the tender monochromator where it will receive unfocused tender x-rays (1-7.5 keV) with a spot size of 1 mm^2.

C. Required Technical Advances (if any)

No beamline technical advances are required to achieve the level of performance in this proposal. The soft and tender beamline optical design is complete, including the common focal point at two experimental stations for continuous 100 eV to 7.5 keV operations. The two new NIST full field microscopes (NEXAFS and XPS) are fully funded, developing quickly and will be ready for the start of NSLS-II.

D. User Community and Demands

XPS and NEXAFS spectroscopies have a large and growing user base as evidenced by the development of state of the art spectroscopy (and microscopy) insertion device beamlines at 3'rd generation synchrotrons throughout the world. In particular, here at NSLS (building to NSLS-II) NIST's existing spectroscopy beamlines (soft U7A, tender X24A, and hard X23A2) have oversubscribed general user programs. All the NIST *Participating Research Team* (PRT) beamtime is fully utilized for NIST scientific collaborations (fundamental and applied materials science) and advanced measurement method development (detectors, high-throughput automation, and microscopy). ***The breadth, diversity, and demands of NIST's user community that consists of 25 Industrial, 25 Academic, and 14 National Laboratory Scientific Groups (complete list in appendix page 13) are highlighted in the proposal selected Science Case examples.***

The anticipated strong user demand for NIST's proposed *Soft and Tender X-ray Spectroscopy and Microscopy (100 eV to 7.5 keV) canted undulator beamline pair* is based in part on the existing NSLS user base established at U7A (16 years) and X24A (6 years) for NEXAFS and XPS/HAXPES respectively and documented user needs from various recent workshops. NSLS and NSLS-II conducted a series of workshops in early 2008 as part of the process of gathering community input to form the strategic scientific plans for beamline development at the two facilities. NIST's NSLS-II beamline plans for spectroscopy and microscopy where endorsed and promoted in three of the resulting white papers (representing about 150 scientists) ; *Chemical and Energy Sciences, Soft and Biomolecular Materials, and Hard Condensed Matter and Materials Physics.* NIST chaired an *International Workshop for New Opportunities in Hard X-ray Photoelectron Spectroscopy: HAXPES 2009* (sponsored by NIST, NSLS, NSLS-II, and BNL Condensed Matter Physics). This three-day workshop brought

together approximately 100 scientists from 14 countries to discuss progress and future prospects for this rapidly developing field of research and included sessions devoted to industrial use of HAXPES. Currently, NIST's NSLS X24A beamline is the only United States HAXPES facility; the workshop made a compelling strategic case for NIST's investment in a state of the art undulator NSLS-II beamline for HAXPES and microscopy. In particular, for industrial applications (*real samples from the real world*) such as layered structures this is exemplified in the SEMATECH Science Case (page 5) by Pat Lysaght *Nanoscale Spectroscopy for Next Generation Semiconductor Microelectronics: CMOS and Beyond* (tuning the length scale of XPS).

Brookhaven National Laboratory hosts the Joint Photon Science Institute (JPSI), which brings together Industry, National Laboratories, and Universities to catalyze innovation using synchrotron radiation at NSLS-II. NIST is a founding member of JPSI and Dr. Chi-Chang Kao is the Director (and a member of this proposal's Science and Technology Advisory Panel). Over the past year, JPSI has held *NSLS/NSLS-II New Opportunity Workshops in Microelectronics, Batteries, and Photovoltaics.* Each of these workshops has brought together technology and academic leaders (total of 150) who see NIST's proposed NSLS-II spectroscopy beamlines as an important key to solving some of the Nation's most challenging problems (see attached JPSI letter of endorsement from Dr. Chi-Chang Kao in the appendix, page 13).

XPS (or ESCA) is a fully established and widely used surface chemical analytical technique with in house XPS laboratory instruments at most major university, national, and industrial laboratories. Commercial XPS microscopes (5 micron resolution) are also often included; e.g. NIST Gaithersburg has two. These laboratories represent substantial capital and staff investment, speaking strongly to the importance and impact of XPS in the general scientific material science community. This large and well-developed laboratory based XPS user group is a nearly untapped community that will be brought to NSLS-II (although NIST has made a good start e.g. SEMATECH, Dow, GE, UOP, Sandia and BNL). In this beamline proposal, NIST's synchrotron based XPS offers the existing lab based community unique depth selectivity (continuous selection of X-rays from 100 eV to 7.5 keV in a single experiment), automated high-throughput sample handling, and nanoscale XPS microscopy. Our XPS user base has enthusiastically endorsed NIST's NSLS-II XPS plans embodied in this proposal (see the individual Science Case examples).

E. Proposal Team Expertise and Experience *(not included in page count)*

The Proposal Principal Team Daniel Fischer (project director), Joseph Woicik, and Bruce Ravel are members of NIST's Synchrotron Methods Group of 9 staff (all located at the NSLS fulltime, Fischer is the group leader) that currently run 3 NIST PRT Spectroscopy Beamlines (U7A, X24A, X23A2) and 2 NIST *Measurement and Instrument Development Team* (MIDT) Beamlines for each of the NIST' NSLS-II microscope development projects. These NIST staff members represent a permanent and growing investment by NIST in developing and operating beamlines at NSLS-II (Type-II beamline development). Fischer, Woicik, and Ravel are senior members of the technical staff and are all highly regarded scientists within the NIST institution. The Proposal Principal Team has significant and highly successful direct beamline experience building, developing, maintaining, and managing spectroscopy user facilities, continuously improving measurement capabilities, and producing excellent science spanning nearly three decades. They are all highly respected members of the synchrotron community and are valued NIST ambassadors to the DOE at the NSLS (and NSLS-II). The team often represents the user community on the NSLS User Executive Committee and numerous NSLS and DOE advisory teams and review panels. *A one page brief bio of each Principal Proposal Team member appears in the appendix (see page 13).*

F. Suggestions for BAT Membership *(not included in page count)*

Science and Technology Advisory Panel: all listed on page 1 *(not included in page count)* have agreed to serve

G. Funding and Management *(not included in page count)*

NIST NSLS-II Soft and Tender Beamline Total Capital Investment to Date: $10 million
(Details outlined below)

Existing U7A fully automated world-class soft x-ray spectroscopy station	$2,000K
Existing X24A fully automated world-class tender x-ray spectroscopy station	$1,500K
Large Area Imaging NEXAFS Microscope station (ARRA FY09 funding, NIST SBIR Pahse III)	$2,500K
XPS Microscope station (SBIR Phase III ongoing funding)	$1,500K
Existing U7A High Pressure Insitu Soft X-ray NEXAFS and Emission Station (NIST developed 256-element transition edge detector)	$1,500K
Varied Lined Spacing Plane Grating Monochromator (FMB Oxford contact awarded FY08)	$500K
Tender Double Crystal Monochromator, LN_2 cooled ((FMB Berlin contact awarded FY09)	$500K

NIST NSLS and NSLS-II Funding and Staffing Overview: NIST is committed to fully funding the construction of its proposed Spectroscopy Beamline Suite and to continuous world leading improvements in synchrotron measurement science and technology. NIST will build upon its NSLS based Synchrotron Methods Group to fully staff our stakeholder relationship in NSLS-II to develop the proposed NSLS-II Spectroscopy Beamline Suite.

NIST NSLS-II Beamline Development Approach Overview: (1) Finish optical design and specification of all mirrors. (2) Develop a detailed beamline conceptual design including cost and schedule. (3) Develop a beamline organizational and management system. (4) Develop a full Beamline Project Execution Plan in coordination with NSLS-II management and staff.

NIST Transition Plan to NSLS-II Overview: (1) Maintain NIST's leading role in synchrotron materials measurement science together with our partners as fully committed long time stakeholders at the NSLS moving to an operational NSLS-II. (2) As soon as possible, begin assembling and commissioning on the floor of NSLS-II a new NIST Spectroscopy Beamline Suite teaming with expert contractors to leverage our NIST group at NSLS. (3) Strategically move NIST's NSLS state-of-the-art endstations to their new NIST NSLS-II beamlines, thereby minimizing down time.

Appendix

Part A Science Case continued: *Science Case examples highlighting materials science in important societal challenges in energy, health, environment, and national security.*

Designing Biomaterials with High Through-put Screening: Using the NIST NEXAFS Microscope
David Castner (U. of Washington, Seattle). 14

Synchrotron Spectroscopy an Enabling Capability for the Defense and National Security Community
Joseph Lenhart (WMRD, US Army Research Laboratory) 16

Nano to Microscale Spectroscopy for Environmentally Friendly Marine Anti-fouling Coatings
Edward Kramer (UCSB) 18

Spectroscopy and Microscopy for Advanced Hard and Soft Materials: Energy and Microelectronics
Gary Mitchell (Dow) 20

Advanced Spectroscopy Promoting Breakthrough Catalysts for Energy Applications
Simon Bare (UOP) 23

Materials Research for Next Generation Lithium Batteries Using Soft and Tender X-ray Spectroscopy and Microscopy - *Xiao-Qing Yang and Kyung-Wan Nam (Battery Research Group, BNL Chemistry)* 25

Hard X-ray Photoelectron Spectroscopy (HAXPES) and Near Edge X-ray Absorption Fine Structure (NEXAFS) of Phase Change Materials for Next-Generation Non-Volatile Memory Applications - *Eric Joseph and Jean Jordan-Sweet (IBM)* 27

Fundamental Spectroscopy Studies of the Active Sites of Metal/Oxide Catalysts: Water-gas Shift Reaction on Au-CeO_2 and Cu-CeO_2 Systems - *Jose A. Rodriguez (Chemistry Department, BNL)*. . . . 30

Optimizing Novel Materials for Energy Applications: Electronic Structure of Doped Oxides Using Hard X-ray Photoelectron Spectroscopy (HAXPES) - *Abdul Rumaiz (NSLS, BNL)* 31

Correlating the Geometric and Electronic Structure of Nanomaterials: Finite Size Effects for Tailoring Materials Properties - *Sarbajit Banerjee (SUNY Buffalo)* 33

NEXAFS Imaging of Propagating Waves of Self-Assembly in Organosilane Monolayers
Jan Genzer (NC State U., Raleigh). 37

Part B Beamline Concept & Feasibility continued:

XPS Microscope development project details 40
Large Area Imaging NEXAFS Microscope development project details 42
Micro-calorimeter high resolution soft x-ray detector - soft x-ray emission and NEXAFS spectroscopy 44

Part D User Community and Deamnds:

NIST's User Community: 25 Industrial, 25 Academic, and 14 National Laboratory Scientific Groups. 46
JPSI letter of endorsement from Dr. Chi-Chang Kao. 47

Part E Proposal Team Expertise and Experience continued:

One page bio for each Proposal Principal Team member including selected publication references
Daniel A. Fischer. 48
Joseph C. Woicik. 49
Bruce Ravel. 50

Designing Biomaterials with High Through-put Screening: Using the NIST NEXAFS Microscope

David Castner (U. of Washington, Seattle)

Interactions between solid surfaces and the biological environment play an important role in many areas of medicine [1]. Examples include biocompatibility of implants, biomolecule separations, bacterial-induced corrosion and biosensors. When biomaterials such as implants are exposed to biological media their surfaces will rapidly be covered by a monolayer of adsorbed proteins [2] followed by attachment of cells (neutrophiles, macrophages, etc.). Since the nature of the surface can strongly influence the structure and orientation of the adsorbed protein layer, which in turn can affect the subsequent cellular interactions, understanding the structure of surfaces and the nature of adsorbed protein films are key links in understanding interfacial biology. Similarly, for biosensors, the effectiveness and activity of the sensor depends on the orientation and conformation of the surface bound biomolecule. Specifically, DNA, carbohydrate and protein modified surfaces have all received considerable attention in the fields of bio- and nanotechnology due to their importance in the development of biosensors and biomaterials. The development of surfaces with bound DNA, proteins or carbohydrates of known orientation hold the possibility to improve biosensor microarray development, as well as biomaterials that induce normal healing. Microarrays generally involve large areas of micron size spots (see Figure 1 for schematic of typical microarray spot dimensions.) Until recently it has been difficult to get direct chemical information from the actual micron size spot, and large area modifications and analysis have been used to determine the chemistry. NEXAFS is a key technique to provide information about order and orientation within these modified surfaces. Some recent preliminary studies have used NEXAFS (and the capabilities at NIST's beamline U7A at the NSLS) to directly examine the detailed structure and orientation of surface-bound peptides [3-5] and proteins [5,6]. NEXAFS can be used to study increasingly more complex biomolecules (from short chain amino acids to more complex proteins).

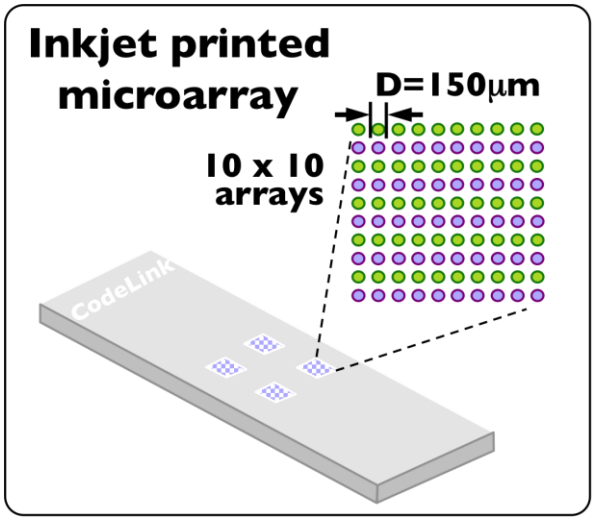

Figure 1: Schematic of DNA micro-array

The NIST NEXAFS Microscope allows for unprecedented high throughput screening of samples for biomedical applications. We rapidly evaluated different self-assembled monolayer (SAM) preparation methods by imaging arrays of 45 samples with a surface area of 1 mm^2 each (see Figure 2). The spectral information extracted out of just three image stacks taken within three hours was equivalent to the amount of data typically collected during five days of NEXAFS beam time. ***Using the full 20 x 20 mm field of view of the new NIST NEXAFS Microscope makes it possible to simultaneously run up to 400 samples***. This novel, highly parallel data acquisition approach will benefit biomedical

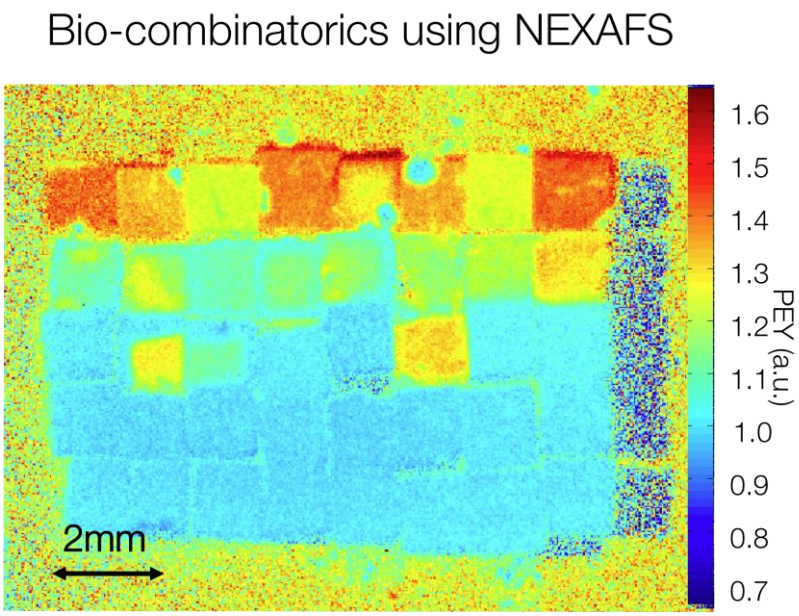

Figure 2: NIST NEXAFS Microscope image of SAM sample array. The contrast is based on signal in the 284.5-285.6 eV X-ray energy band related to aromatic π* resonances. Azobenzene-terminatedself assembled monolayers on gold based on different binding units and backfill strategies were screened for azobenzene surface density.

research tremendously since it allows to test a wide range of preparative conditions and replicates without the need for prohibitively extended beam times. Also, the small scale reduces the amount of biological material needed for sample preparation, a valuable savings for samples where µg quantities of a particular DNA sequence or protein can cost hundreds of dollars.

For nanomedical applications the control of protein orientation is key because the ensemble sizes get extremely small and "every protein counts". For miniaturization advances to be realized in the nanomedicine field that are comparable to the advances seen in the semiconductor industry, major efforts are needed to optimize protein uniformity within extremely small feature sizes. Techniques such as imaging surface plasmon resonance, IR, Raman and fluorescence microscopy have been used to probe protein arrays. However, analysis tools to probe the spatial distribution of protein orientation and structure within individual spots on a microarray surface have not yet been developed. ***The availability of structure and chemistry sensitive imaging techniques is required to enable development of this next generation of biomedical arrays. The advances in NEXAFS and XPS based microscopic end-stations recently designed and implemented by the NIST Synchrotron Methods group hold great promise in this context.***

NEXAFS imaging allows macroscopic sample areas to be imaged with very high spectral quality, low X-ray exposure, virtually unlimited depth of focus and a spatial resolution of 50 µm. This make the technique ideally suited for biological samples. NEXAFS imaging performed at NIST's beamline U7A allowed us to create protein density and orientation maps of inkjet-printed bovine serum albumin (BSA) and RNAse B arrays (Figure3).

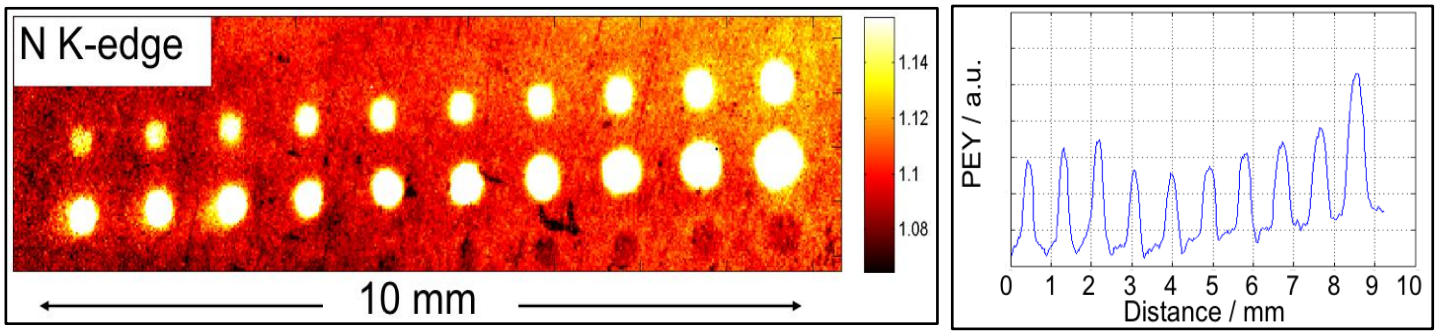

Figure 3: Left: Nitrogen K-edge image from NIST NEXAFS Microscope of a protein array printed onto a self-assembled monolayer. RNAse (top row) and BSA (bottom row) are specifically bound via glycan linkers. Each pixel in the image contains a NEXAFS spectrum allowing orientation and chemical analysis. Right: Line analysis for the row of BSA spots. The intensity of the nitrogen signal varies with the protein surface density.

The *NIST XPS Microscope* (as designed for the NSLS-II) will have interesting applications towards the analysis of nanoparticles with biomedical coatings. Most specifically the depth selectivity (via variable photon energy from 100 eV to 7.5 keV) will be a significant advantage for analyzing the different layers of the nanoparticles. Current XPS techniques of angle resolved analysis to analyze layered materials are not applicable to nanoparticles. Thus, currently questions remain as to effectiveness of chemical modifications of the nanoparticle as well as where the chemical modifications are occurring (surface, sub-surface, bulk, etc.). NIST's non-destructive depth analysis method that does not require a flat sample would add significant to this research.

1. D. G. Castner and B. D. Ratner, Surface Science, 2002, 500 (1-3) , p 28.
2. T. A Horbett, "Proteins at Interfaces – An Overview, in Proteins At Interfaces. 1995, ACS: Washington. P 1.
3. T. Weidner, J.S. Apte, L.J. Gamble and D.G. Castner, *Langmuir*, 2010, 25 (5) p 3433.
4. T. Weidner, N.T. Samuel, K. McCrea, L.J. Gamble, R.S. Ward, D.G. Castner, Biointerphases, 2010, 9 p 5.
5. J. E. Baio, T. Weidner, N. T. Samuel, K. McCrea, L. Baugh, P. S. Stayton D. G. Castner JVST B, accepted.
6. L. Baugh, T. Weidner, P.-C. T. Nguyen, J. Baio, L. J. Gamble, D. G. Castner, P. S. Langmuir, in press, doi: 10.1021/nn1004638.

Synchrotron Spectroscopy an Enabling Capability for the Defense and National Security Community

Joseph L. Lenhart (WMRD, US Army Research Laboratory)

Current military drivers to reduce size, weight, power consumption, and cost; while still increasing performance; necessitate multi-functional materials with increased complexity.[1] Novel measurement techniques, with the capability to investigate the chemistry, structure, and properties in the bulk, at the surface at interfaces, and over various length-scales, with improved sensitivity, selectivity, spatial resolution, and through-put, are critical enablers of current and future national security missions. The Weapons and Materials Research Directorate (WMRD) at the US Army Research Laboratory executes fundamental and applied research programs involving polymer systems for military applications. Polymer based materials and devices are pervasive in the national security community with applications ranging from vehicles and armor to combat casualty care and first responder capabilities. ***The following pages highlight two national security related research programs within WMRD, where the NIST proposed beamlines at the NSLSII can provide enabling measurement capabilities.***

Chemical and Biological Defense: Chemical and biological warfare and terrorism represents a substantial threat to both military personnel and civilians.[2] The Department of Defense currently protects its assets (tanks, vehicles, aircraft, etc) from chemical contamination by using CARCs (Chemical Agent Resistant Coatings).[3] Future CARCs will be complicated polymeric systems that are deliberately engineered to degrade and prevent the permeability of a broad spectrum of chemical, biochemical, and environmental threats. Figure below shows a schematic of a future CARC. A polymer matrix provides the mechanical base. Pigments, as well as, micro and nano scale fillers will be added to control material properties. Active chemical receptors will be engineered to segregate to the film surface, both detecting and degrading a threat. Electronic circuitry will be integrated into the film to provide additional functionality.

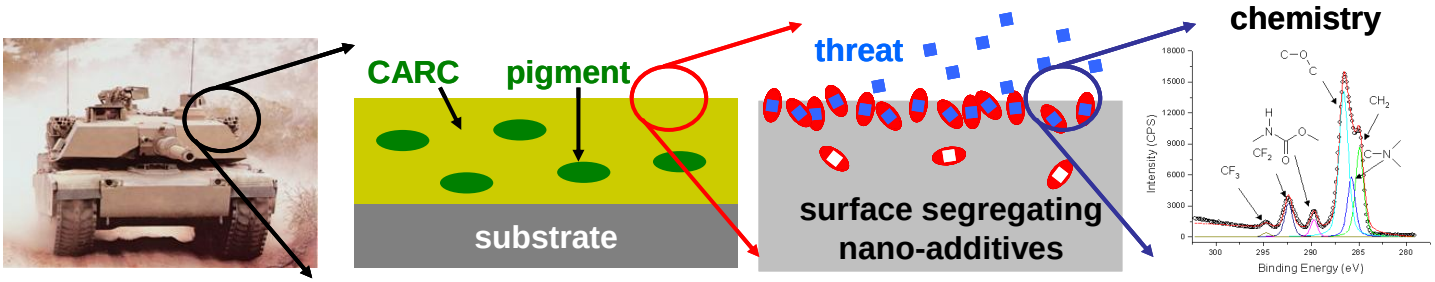

The CARC surface represents an intelligently designed array of materials where various length-scales are critical: the macroscopic surface chemistry of the polymeric resin (mm or larger); the integrated electronics and pigment additives (10's of microns); the nano-fillers (10's nano-meters); the catalytic nano-additives that degrade the threat (10's nano-meters); the filler-resin interface (nano-meters); and the specific receptor sites for agent detection (angstroms). ***The NIST beamline at NSLSII can facilitate future CARC development in the following manner:*** 1) higher brightness and state of the art detector technology will provide improved peak resolution to extract the chemical details in these complicated formultations; 2) higher through put capability on the current U7A and X24A beamlines along with NEXAFS microscopy will provide rapid, combinatorial screening capability for optimizing the complex formulations; 3) the energy range from 100 to 7500 eV enables investigation of core level transitions for C, N, O, F, P, S, Cl, K, and Ca, all of which are important for the various materials, threats, and countermeasures that will be exploited in future CARC coatings; 4) the NEXAFS microscopy with micron resolution and XPS microscopy with nm scale resolution will allow chemical mapping of the surface over critical length scales enabling detailed investigation of threat adsorption, mobility, and degradation mechanisms on the CARC surface; 5) Variable Kinetic Energy XPS coupled with microscopy will enable investigation of compositional gradients at the film surface as a function of depth, which is critical for CARC effectiveness, since certain additives are engineered to segregate to the film surface.

Armor Systems: Light weight body and vehicle armor systems are critical for protecting soldiers, while enabling stealth and maneuverability. Figure below shows a model armor package composed of a metal or ceramic plate (top) adhered to a fiber reinforced polymer composite backing (bottom). The armor was shot by a high velocity projectile. Light green coloring highlights the damage zones. Similar to CARCs, future armor packages will be complicated materials systems with critical length scales ranging from angstroms to microns. The ceramic plates will have grain sizes from microns to tens of nanometers, and nano-scale grain boundaries that control energy absorption. The fiber reinforced polymer will have micron scale fibers with nano-fiber interlayer mats to control crack propagation. The micron scale fibers will have nano-roughened surfaces and atomistically engineered chemical coatings to enhance damping behavior and interfacial friction during fiber pull-out. The polymer resin will be engineered to optimize strength and energy dissipation, while containing nano-additives to further improve high strain rate toughness. Interfaces in these armor systems are critical for controlling functional properties.[4] ***However, no current techniques offer the chemical sensitivity or spatial resolution necessary to fully investigate these interfacial regions. In particular, the microscopy techniques developed at the proposed NIST beamline at NSLSII, will provide this measurement capability.*** For example, the microscopy techniques will enable characterization of the nano-scale chemical heterogeneities on fiber coatings, and the nano-scale interfacial regions at a polymer-substrate interface, both of which are postulated to control composite performance.

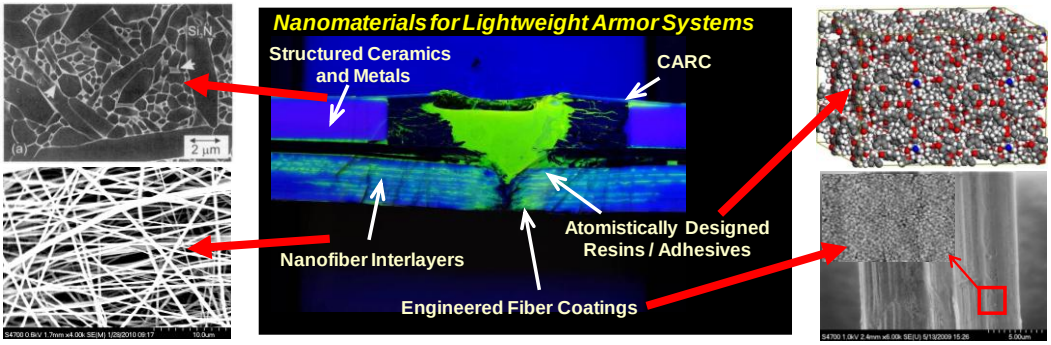

The discussions above present two programs where interfacial phenomena dominate the system level response. ***The advanced interfacial characterization equipment that will be developed for the NIST beamlines at NSLSII will provide the throughput, chemical sensitivity, and spatial resolution to intelligently design and optimize the critical interfacial regions in these systems. While the examples presented are defense related, advancement of these materials (facilitated by the NSLSII) will have a much broader societal impact.*** For example, variations of CARC coatings are being explored as antimicrobial / antibacterial paints and coatings for construction materials, transportation facilities, clothing, and hospitals.[5] They could be particularly beneficial for medical facilities in poverty stricken regions of the world, where the extensive cleanliness practices of today's modern hospitals are not affordable. The principles of high strength, light weight, and high toughness armor systems will be readily transferable to automobiles and commercial transportation enhancing the safety and fuel efficiency in this broad economic sectors.[4]

1. B. K. Fink, "Performance Metrics for Composite Integral Armor," *J. Thermoplastic Comp. Mater.*, **13**, 417, (2000).
2. Greenfield R. A., et. al., "Microbiological, Biological, and Chemical Weapons of Warfare and Terrorism," *Amer. J. Med. Sci.*, **323**, 326 (2002); Eubanks L. M., et. al., "Technological Advancements for the Detection of and Protection Against Biological and Chemical Warfare Agents," *Chem. Soc. Rev.*, **36**, 458 (2007).
3. K. R. Stone, D. A. Tolle, "Life Cycle Assessment of Chemical Agent Resistant Coatings" *Int. J. LCA*, **3**, 3 (1998); http://www.ppg.com/corporate/governmentsolutions/militarydefense/MilitaryCoatings/Pages/topcoats.aspx
4. P. J. Hogg, "Composites in Armor," *Science*, **314**, 1100 (2006); R. E. Jensen, S. H. McKnight, "Inorganic-Organic Fiber Sizings for Enhanced Energy Absorption in Glass Fiber Reinforced Composites Intended for Structural Applications," *Comp. Sci. Technol.*, **66**, 509 (2006).
5. L. Chen, et. al., "Multifunctional Electrospun Fabrics via Layer-by-Layer Electrostatic Assembly for Chemical and Biological Protection," *Chem. Mater.*, **22**, 1429 (2010).

POC: Dr. Joseph L. Lenhart; WMRD, US Army Research Laboratory, 4600 Deer Creek Loop, Aberdeen Proving Ground, MD 21005-5069; 410-306-1940; joseph.lenhart1@us.army.mil

Nano to Microscale Spectroscopy for Environmentally Friendly Marine Anti-fouling Coatings

Edward Kramer (UCSB)

Figure 1 *Fouling on ship in Gulf of Alaska – photo courtesy A. Hexemer.*

The fouling of ship hulls and other man-made marine structures causes high operational and maintenance costs to industry (~ $3 billion/yr) and increased carbon emissions (~20 million tons) across the world.[7] An example of extreme fouling is shown in Figure 1. Traditional antifouling paints have relied upon the inclusion of biocides, most of which are now considered to be environmentally undesirable. In recent years, research has focused on the development of environmentally benign fouling-release coatings, especially low modulus, low surface energy silicone elastomers.[8] Although these materials readily release most macrofouling organisms, they do not deter settlement or colonization, i.e., they are not "antifouling". Therefore, a considerable research effort is now focused on examining the potential of a range of antifouling surface designs that reduce the initial attachment of organisms.[9,10] In the biomedical field, success in preventing biofouling has been achieved at the hydrophilic end of the wettability spectrum, for example, through the use of poly(ethylene glycol) (PEG) materials.[11] When PEG polymers are grafted to a surface, a close association exists between water molecules and PEG arising from hydrogen bonding. Such formation of a hydration layer has been shown to hinder the nonspecific adsorption of proteins[12] and has the potential to deter the adhesion of cells or microorganisms.[13]

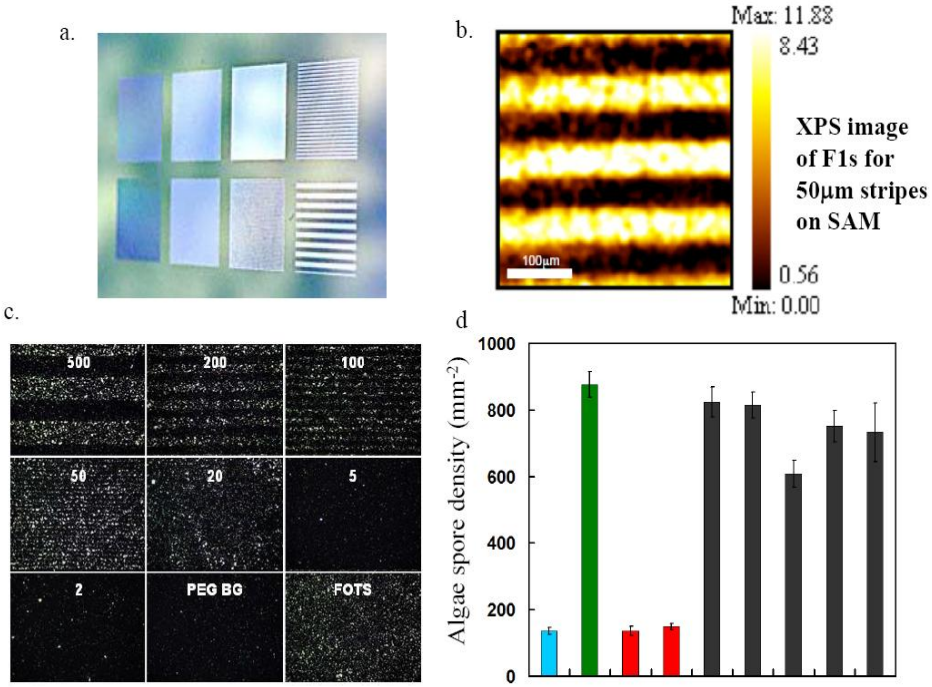

Figure 2 a.) *Stripe patterns of perfluoroalkyl and PEG self-assembled monolayers on Si. b.) XPS image of photoelectrons from the F1s core level – the spatial resolution for this commercial instrument is ~ 5 µm. c.) Fluorescence optical microscopy images of Ulva spores on stripe patterns of various width (µm). d.) Ulva spore settlement on SAM patterns – note when the stripes are 5 µm or narrower, the settlement is greatly reduced.*[17]

Several studies on the settlement of marine algae have indicated a preference for hydrophobic compared to hydrophilic

---

[7] Townsin, R. L. *Biofouling* 2003, *19* (supplement), 9.
[8] Brady, R. F.; Singer, I. L. *Biofouling* 2000, *15*, 73.
[9] Krishnan, S.; Wang, N.; Ober, C. K.; Finlay, J. A.; Callow, M. E.; Callow, J. A.; Hexemer, A.; Kramer, E. J.; Sohn, K. E.; Fischer, D. A. *Biomacromolecules* 2006, *7*, 1449.
[10] Genzer, J.; Efimenko, K. *Biofouling* 2006, *22*, 339.
[11] Senaratne, W.; Andruzzi, L.; Ober, C. K. *Biomacromolecules* 2005, *6*, 2427.
[12] Harder, P, Grunze, M.; Dahint, R.; Whitesides, G. M.; Laibinis, P. E. *J. Phys. Chem. B* 1998, 102, 426.
[13] Andruzzi, L.; Senaratne, W.; Hexemer, A.; Sheets, E. D.; Ilic, B.; Holowka, D.; Kramer, E. J.; Baird, B.; Ober, C. K. *Langmuir* 2005, *21*, 2495.

surfaces.[14,15] However, the strength of attachment of settled zoospores is typically stronger to hydrophilic compared to hydrophobic surfaces.[16] These differences in settlement and adhesion behavior have inspired the development of "ambiguous" surfaces, which present both hydrophilic and hydrophobic domains to settling (attaching) cells and organisms. In recent years, a number of novel coatings in which the surface layers phase-segregate to produce a mosaic of hydrophilic and hydrophobic domains have shown promise as foul-release coatings.[17,18] In the amphiphilic networks formed from hyperbranched fluoropolymer and linear poly(ethylene glycol), the dimensions of the surface-segregated components inferred from AFM images are in the micrometer range,[11] while the amphiphilic block copolymers of Krishnan et al.[12] may present a surface that is heterogeneous on a much finer length scale. The optimum design of "ambiguous" segregated surfaces requires information regarding the scale at which settling cells detect hydrophobic or hydrophilic domains. This has been explored through the use of patterned model surfaces, showing that when the hydrophobic/hydrophilic pattern was on a sufficiently small scale, algae cells do not settle (Figure 2).[19]

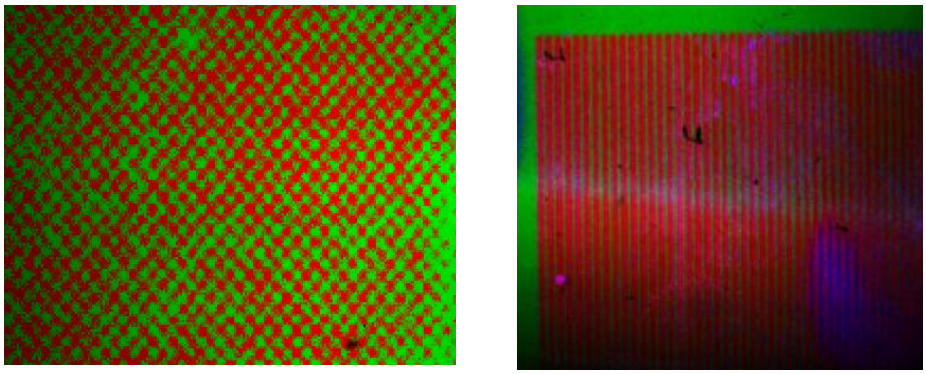

NIST recently demonstrated a new, full-field NEXAFS microscope (at NIST's U7A beamline) that is capable of measuring the patterened surfaces of figure 2. The images to the left are made using Principal Component Analysis of a NEXAFS image stack, green is FOTS and red is PEG SAMs with 100 micron features. ***These NEXAFS prototype large area full field images highlight the chemical bond sensitivity and selectivity of this new imaging method. At NSLS-II NIST will be extending this important capability to the micron scale.*** Patterned surfaces, with pattern dimensions comparable to those of cells and below, continue to be of interest in the study of cell-surface interaction in other contexts as well, for high-throughput screening, for example.[14] A major unmet challenge however, especially for non-regular coatings, is to characterize the composition distribution over the ambiguous surface. ***This is where the NIST SST NSLS-II Beamline Suite will have a major impact. Chemists and material scientists developing these coatings and patterned surfaces will have the capability to use NEXAFS in a way never before possible to microscopically image concentrations and orientations of organic groups down to length scales (~ 1 μm) never before possible. Depth profiling will be possible by using a unique, semicircular 33 electron detector array as well as by varying the negative bias grid voltage on the detectors. The soft and tender XPS microscopy capability of this Beamline Suite will likewise provide spatial resolution parallel to the surface to ~10 nm while state of the art XPS systems now struggle to achieve 5 μm resolution. Better still, the possibility for tuning the incident X-ray energy over the range from 100 eV to 7.5 keV will lead to a combination of depth resolution and depth penetration never before possible. Finally NEXAFS and XPS are almost completely complementary spectroscopies so having this combination of beamlines side by side will enable rapid and complete analysis of these chemically non-uniform surfaces.***

[14] Ista, L. K.; Callow, M. E.; Finlay, J. A.; Coleman, S. E.; Nolasco, A. C.; Simons, R. H.; Callow, J. A.; Lopez, G. P. *Appl. Environ. Microbiol.* 2004, *70*, 4151.
[15] Statz, A.; Finlay, J.; Dalsin, J.; Callow, M.; Callow, J. A.; Messersmith, P. B.. *Biofouling* 2006, *22*, 391.
[16] Finlay, J. A.; Callow, M. E.; Ista, L. K.; Lopez, G. P.; Callow, J. A. *Integr. Comp. Biol.* 2002, *42*, 1116.
[17] Gudipati, C. S.; Finlay, J. A.; Callow, J. A.; Callow, M. E.; Wooley, K. L. *Langmuir* 2005, *21*, 3044.
[18] Krishnan, S.; Ayothi, R.; Hexemer, A.; Finlay, J. A.; Sohn, K. E.; Perry, R.; Ober, C. K.; Kramer, E. J.; Callow, M. E.; Callow, J. A.; Fischer, D. A. *Langmuir* 2006, *22*, 5075.
[19] Finley, J.A., Krishnan, S.; Callow, M.E.; Callow, J.A.; Dong, R.; Asgill, N.; Wong, K.; Kramer, E.J.; Ober, C.K. *Langmuir*, 2008, *24*, 503.

Spectroscopy and Microscopy for Advanced Hard and Soft Materials: Energy and Microelectronics

Gary Mitchell (Dow Chemical Company)

The Dow Chemical Company is a chemical and advanced materials manufacturer. It connects chemistry and innovation with the principles of sustainability to help address many of the world's most challenging problems such as the need for clean water, renewable energy generation and conservation, and increasing agricultural productivity. Dow's diversified industry-leading portfolio of specialty chemical, advanced materials, agrosciences and plastics businesses delivers a broad range of technology-based products and solutions to customers in approximately 160 countries and in high growth sectors such as electronics, water, energy, coatings and agriculture. Dow R&D has been one of the top industrial users of synchrotron technology over the last 15 years.

The Dow Chemical Company has partnered with NIST to characterize advanced materials using x-ray spectroscopy techniques at the NSLS for over 14 years. Dow and NIST collaborated to build a materials science end station at U7A that has been continually updated by NIST and now provides a powerful arsenal of unique tools for characterization of both soft and hard materials with soft x-rays. We are eagerly looking forward to utilizing the NIST expanded capabilities that will be provided by the new NIST beamlines at NSLS-II and the new instruments that are being developed now for placement at NSLS-II. We are particularly excited about the new microscope capabilities being developed, but will still need access to the strictly spectroscopic probes as well.

Microscopy

In fabricating integrated circuits, photolithography technology is continually being advanced to keep up with the diminishing dimensions needed to make smaller, lower power consumption and faster electronics. Dow has active R&D programs in this area and has an ongoing need for analytical methods that can resolve features at ever decreasing size scales and provide chemical details necessary for progress. For instance, we have used scanning photoemission micro-spectroscopy (SPEM) for analyzing features in circuits made with Photo-BCB (CYCLOTENE™ 4024 or 4026 Advanced Electronics Resins) which are photosensitive polymers developed by The Dow Chemical Company for use in micro-electronics applications [[20]]. One important issue to understand is how fully the polymer is removed from the surface in unexposed areas during developing. The material left in unexposed areas after developing has been called "scum" and procedures to "descum" these areas by plasma cleaning have been developed, but it is difficult to determine the quality of the descumming in a precise sense, due to the spatial limitation of the laboratory based XPS measurements. (Electron microscopy only helps here when scum is many molecule layers thick.) Using the SPEM we were able to image patterned surfaces and from microprobe spectra, calculate the relative

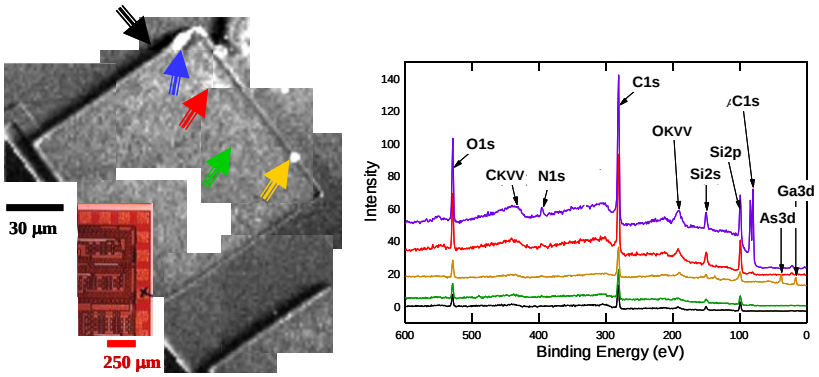

Figure 2. *A montage of SPEM images which together provide an image of most of a large gold solder pad located near the edge of the die. At bottom left is a visible light microscope image of the die. The x marks the gold solder pad imaged by SPEM. The differently colored arrows indicate where the microprobe XPS spectra in the graph at right were obtained.*

[20]. E. Rutter jr., E. Moyer, R. Harris, D. Frye, V. St. Jeor, and F. Oaks, Proceedings of First International Conference on Multichip Modules (ISHM & IEPS), Denver Co, (1992) 394.

surface coverage of contaminants and thus determine the quality of descumming procedures (Figure 1) [21]. However the SPEM measurements are limited by electrical surface charging [2]. ***The new technology being developed by NIST will allow the use of charge compensation methods that are already well developed for lab based instruments to compensate charging and provide good quality data even for insulator surfaces. Photoemission electron microscopy (PEEM) also suffers from charging issues that prevents its use for surfaces of insulators and many materials questions that have been solved with PEEM, such as mono or few layer wetting-dewetting phenomena [22] will be applicable to insulator surfaces using the NIST XPS microscope.***

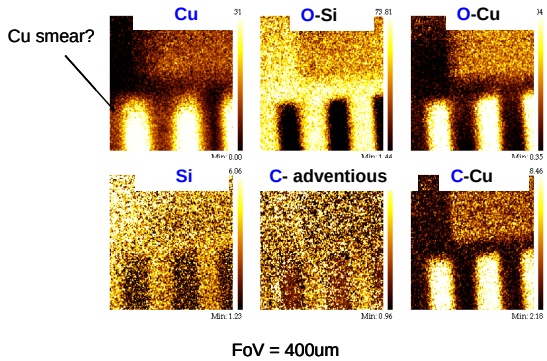

Figure 3. XPS images of a Si based IC with Cu connectors. The quantified images are generated by collecting a hyperspectral image and deconvolving into elemental images.

A critical issue to Dow's program in advanced electronic materials is to determine the quality of surfaces of integrated circuits after undergoing planarization using chemical mechanical polishing (CMP) to understand smearing of phases. This is a breakthrough technology that has been developed in the last few years and has revolutionized IC manufacturer. By using CMP in between layers of an IC, many more layers are now possible on a single device, increasing the allowed complexity. This is one of the key enablers for the dual and larger microprocessors, for instance. The spectral images reproduced in Figure 2 were measured on our lab based XPS system with 30 μm spatial resolution. ***The spatial resolution of the NIST XPS microscope will be applicable to many more situations with transistor dimensions smaller than 100 nm and by varying the excitation energy one will be able to quantitatively measure thicknesses.***

Spectroscopy

An important area of research at Dow involves developing new catalyst systems and enhancing existing ones to manufacture products more efficiently and with fewer byproducts to minimize waste. These catalysts systems are often heterogeneous, meaning they consist of a solid catalyst interacting with a fluid phase reactant stream. The solid catalyst usually is some active metal species supported on a ceramic carrier that provides a high surface area to increase contact with the gas or liquid reactants and products. In order to understand the microscopic details of the reactions that take place on a catalyst we have partnered with NIST to use the unique Multi-Layer-Mirror (MLM) facility at U7A to analyze catalyst being developed. ***With MLM one can detect very low levels of carbon or nitrogen based intermediates adsorbed on a catalyst with reactant gases present using fluorescence yield near edge x-ray absorption [23].*** Usually the presence of reactant gases and the high level of oxygen in the support would obscure the signal coming from the low level of adsorbed intermediates on the catalyst. The MLM is tuned to the C (or N) fluorescence only, thus providing sufficient signal to detect the adsorbed species [24]. The MLM was used to study an experimental catalyst being developed to make propylene oxide by a direct pathway from oxygen and ethylene without need for chlorinated intermediates [3]. Propylene oxide is one of the highest volume chemicals made in the world and is used in the production of plastics, surfactants and non-toxic antifreeze, so that limiting byproducts and maximizing the efficiency of conversion is important to the world environment and economy. Using the MLM instrument, one can observe

---

21. Gary E. Mitchell, Dan Scheck, Dave D. Hawn, Greg F. Meyers, Ralf Graupner, George Meigs, Ivaylo Koprinarov, ALS Compendium of User Abstracts 2000.

22. David Tulumello, Glyn Cooper, Ivo Koprinarov, and Adam P. Hitchcock, Edward G. Rightor, Gary E. Mitchell, Steve Rozeveld, Greg F. Meyers, and Ted M. Stokich, J. Phys. Chem. B 2005, 109, 6343.

23. S. Sambasivan, D. A. Fischer, A. Kuperman, B. M. DeKoven, Adv. Mater. 2000, 12, 1809.

24. D. A. Fischer, S. Sambasivan, A. Kuperman, Y. Platonov, J. L. Wood, Rev. Sci. Instrum. 2002, 73, 1469.

the chemical state of adsorbed propylene inside the cavities of a zeolite (which was the porous, high surface area ceramic support in this case) and assess the degree of perturbation to the double bond which is related to the ease of reaction with the oxygen to form the product propylene oxide. ***This MLM technology will be even more powerful on NSLS-II with the higher intensity available there.***

Other areas where the NIST spectroscopic probes proposed in this beamline proposal will be key to breakthroughs in understanding materials and driving progress include characterizing surfaces and thin films for photovoltaic devices, advanced battery materials such as high performance cathodes, separators and anodes, improved reverse osmosis membranes, functional coatings and buried interfaces in complex materials. NIST's proposal highlight's the use of variable excitation energy XPS one can non-destructively profile the chemistry as a function of depth up to about 25 nm at 7.5 keV [[25]]. This technology has been shown to be useful in understanding and optimizing the phase structure of thin film solar cells [25] and with charge compensation, it will be very useful to understand films on insulating polymeric materials.

Reverse osmosis membranes have shown improvements in their properties (resistance to fouling, enhanced salt rejection or flux) by coating the surface of the discrimination layer with various chemistries [[26,27],[28],[29]]. The surfaces of RO membranes, especially, of the FT30 type with polyamide discrimination layer are very rough [28] and thus depth profiling by angle resolved XPS or sputter depth profiling XPS give inaccurate results.
In order to analyze the chemistry and depth of coatings, NIST's variable excitation XPS will be more accurate. Nanoscale imaging capability will allow the determination of lateral uniformity as well. The in-situ NEXAFS capabilities at U7A have already been shown to be useful for analysis of Li ion batteries [[30]]. Dow has recently announced that it is investing in a new plant to make Li ion batteries for use in electric automobiles [[31]]. In-situ characterization of batteries using the NIST beamlines is expected to provide very useful information about chemical and structural changes occurring during charging and discharging. The important issues to resolve with these sorts of batteries involve the loss of capacity with cycling and increasing the power to weight ratio. The loss of capacity may be related to chemical structure changes that occur in the cathode during charge-up. The metals in the cathode and anode, as well as C based species in the electrolyte are all possible to analyze by L-edge or K edge x-ray absorption spectroscopy with soft or tender x-rays. The L-edge spectroscopy of transition metals which make up the cathode intercalation compounds is particularly sensitive to the valence electronic structure [[32],[33]]. By measuring the chemical structure in-situ at different charge states and after varied amounts of cycling we hope to understand and improve capacity reduction caused by cycling.

---

[25]. H. Mönig, Ch.-H. Fischer, R. Caballero, C.A. Kaufmann, N. Allsop, M. Gorgoi, R. Klenk, H.-W. Schock, S. Lehmann, M.C. Lux-Steiner, I. Lauermann, Acta Materialia 57 (2009) 3645.

[26]. John Cadotte, US Patent # 4039440 (1977).

[27]. Hao Jua, Alyson C. Sagle, Benny D. Freeman,, James I. Mardel, Anita J. Hill, Journal of Membrane Science 358 (2010) 131.

[28]. Viatcheslav Freger, Jack Gilron, Sofia Belfer, J. Membr. Sci. 209 (2002) 283.
[29]. D.S. Wavhal, E.R. Fisher, Langmuir 19 (2003) 79.

[30]. C.F. Petersburg, R.C. Daniel, C. Jaye, D.A. Fischer and F.M. Alamgir, Journal of Synchrotron Radiation 16, (2009), 610.

[31]. http://www.mlive.com/business/mid-michigan/index.ssf/2009/04/dow_chemical_battery_venture_w.html.

[32]. J. G. Chen B. Frühberger, and M. L. Colaianni, J. Vac. Sci. Technol. A 14(1999) 1668.

[33]. Shirakawa J, Nakayama M, Wakihara M, et al., J. Phy. Chem. B, 110 (2006) 17743.

Advanced Spectroscopy Promoting Breakthrough Catalysts for Energy Applications

Simon R. Bare (UOP LLC, a Honeywell Company)

UOP LLC, headquartered in Des Plaines, IL, USA, is a leading international supplier and licensor of process technology, catalysts, adsorbents, process plants and consulting services to the petroleum refining, petrochemical, and gas processing industries. UOP is a wholly-owned subsidiary of Honeywell International, Inc. and is part of Honeywell's Specialty Materials strategic business group. UOP has been using synchrotron radiation primarily to probe the structure of its catalysts and adsorbents since the early 1980's and was a charter member of the original Matrix PRT at the NSLS in the mid-1980's. UOP is currently a member of MR-CAT at the APS and a member of the SCC at the NSLS and has collaborated with NIST at the NSLS for many years. ***This collaboration is essential; we anticipate full utilization of the world-class capabilities of SST.***

UOP fully supports the development and construction of the SST beamline suite by NIST. The capabilities envisioned for this suite of beamlines are unparalleled, and will provide new insights into catalyst structure and function leading to development and implementation of new breakthrough catalyst systems. In this section, due to space limitations, only a single catalyst system is discussed: zeolitic catalysts. However, this example shows how the complementarity of the techniques proposed at SST will beautifully combine to provide a complete picture of the characterization of this important class of catalyst.

The use of zeolites and molecular sieves in catalysis and adsorbent technology is ubiquitous[34]. The annual market is estimated to exceed 1.8 million tons worldwide, and have applications ranging from petroleum refining to use in detergents to nuclear waste cleanup. There is an ever increasing discovery of new compositions and structural topologies. Basically zeolites and molecular sieves are solids with pores of the size of molecular dimensions. One traditional class of these materials is known as aluminosilicates, and is comprised of infinitely extending 3D four-connected framework of AlO_4 and SiO_4 tetrahedra. The substitution of aluminum (+3 cation) into the silicate (+4 cation) framework leads to the presence of Brønsted acid sites. It is this acidity which leads to an important application of these materials: as a solid acid catalyst. The exact location, and acid strength, and subsequent activity of these acid sites in the often complex zeolite framework is of ongoing research. Moreover, in the commercialization of a zeolite the material may undergo numerous post-synthesis treatments to stabilize and modify the activity. Each of these treatments will affect the activity of the zeolite, and potentially change the morphology and location and distribution of the aluminum. These treatments include calcination, steaming, acid washing, and surface modification. There are a plethora of catalyst characterization techniques that can be used to characterize catalysts, each with particular strengths and weaknesses. ***The suite of characterization capabilities at SST will open up a new regime for zeolite characterization from micro to nano length scales***.

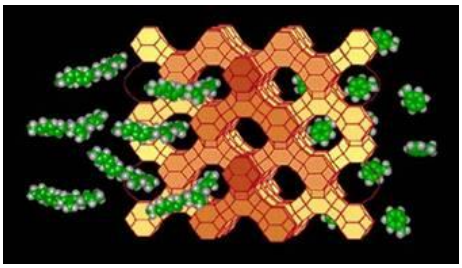

For example, pore mouth catalysis has long-been debated in the literature[35]. This has huge implication for the processing of heavy petroleum feeds where the molecules may be too large to enter the pores, or for processing feeds of mixed molecular weight where one reactant may diffuse into the zeolite and another may not. The key question here is the location of the acid sites in the zeolite crystal and whether there is a gradient of aluminum in the zeolite. This is even more relevant as new synthesis methodologies are developed to produce nano-size zeolite particles. XPS has been the technique of choice for determining the Si/Al ratio in a zeolite, but due to the high mean free path of photoelectrons using a laboratory XPS instrument the signal originates from the outer 4-10 nm - thus not truly surface sensitive. ***The variable kinetic energy XPS (VKE-XPS) beamline pair (100 eV to 7.5 keV) proposed in SST will allow, for the first time, non-destructive depth profiling from the outer surface***

[34] Zeolites in Industrial Separation and Catalysis, Wiley-VCH, Weinheim, Germany, 2010. S Kulprathipanja, Ed.

[35] P.C. Mihindou-Koumba et al., J. Catal. 255 (2008) 324; J.A. Martens et al., Angew Chem. Int. Ed. 107 (1995) 2726; W. Souverijns et al., J. Catal. 174 (1988) 177.

layer to deep into the bulk of zeolites. Thus, this critically important information will be obtained as a function of the calcination temperature/time, steaming temperature/time, etc. for a wide array of zeolite topologies. ***An intriguing extension of this is to determine this information from individual zeolite crystals by making use of the NIST's proposed XPS microscope and variable VKE.*** Outer surface molecular diffusional barriers have recently been identified in zeolite intergrowths, but the supporting XPS data were collected using a laboratory instrument drastically limiting the information content as the Si/Al ratio were obtained destructively used sputter depth profiloing. Figure 1 shows the SEM, AFM and XPS-derived Si/Al ratio as a function of sputter depth of a single MFI zeolite crystal[36].

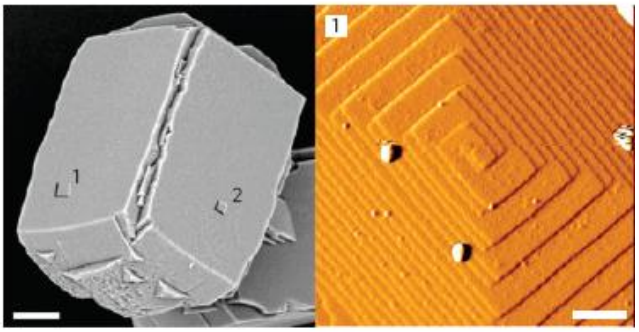

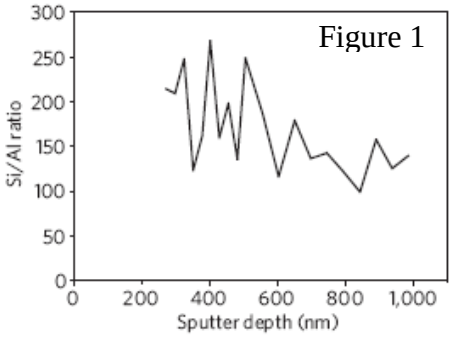

As zeolites are used in hydrocarbon processing they often deactivate with time on stream. Identifying the cause of the deactivation is often not straightforward. For example Figure 2 shows the bright field TEM image of a carbonaceous residue on a spent zeolite together with the carbon K-edge EELS spectrum (below) from the film showing the carbon to be primarily amorphous. It was believed that the buildup of this carbon led to the deactivation. ***At NIST' proposed SST using the capabilities of the in situ carbon NEXAFS, coupled with the VKE-XPS we will be able to study the structure of the carbon in the initial stages of the reaction - something that cannot be studies in the TEM.*** Carbon NEXAFS is ideal tool for studying these deposits: it has high sensitivity, the total amount of C can be quantified, the type of carbon can be identified, surface and bulk signals obtained, and this work will be coupled with in situ studies.

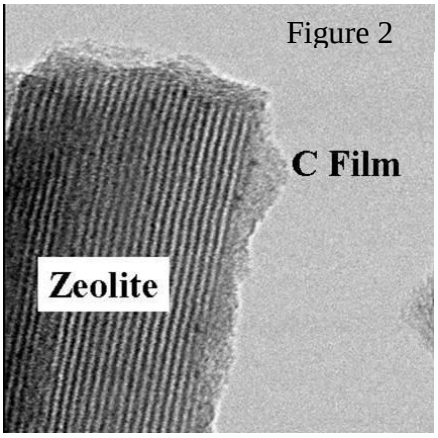

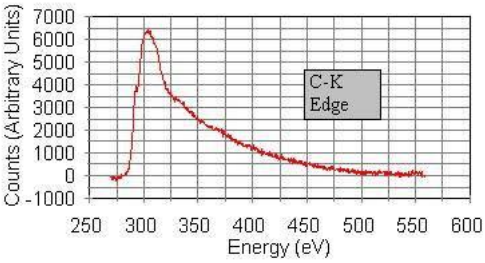

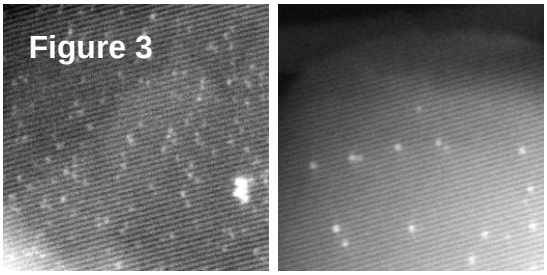

Metals are often added to zeolites to provide bifunctional activity: the acid catalysis from the zeolite and the metal-catalysis from the added metal. For example, Figure 3 shows TEM images of Pt clusters inside a Y-zeolite. Here the growth of the clusters from 1 nm (left) to 2nm (right) from fresh to spent catalyst is clearly observed. The TEM can only show the size and shape of these Pt nanoclusters but reveals nothing about their catalytic activity. ***The full suite of tools at SST will be used to provide catalytic activity in an unprecedented manner. The electronic structure of the Pt nanoparticles will be probed using the XPS microscope at nanometer length scales; using the adsorption of probe molecules (e.g. CO) carbon NEXAFS will provide information on the cluster size and shape and potentially location (internal or external to the zeolite); and the VKE-PE will provide non-destructive information on the depth distribution. Each will be conducted as a function of processing of the particular catalyst.***

[36] L. Karwacki et al., Nature Mater. 8 (2009) 959.

Materials Research for Next Generation Lithium Batteries Using Soft and Tender X-ray Spectroscopy and Microscopy

Xiao-Qing Yang and Kyung-Wan Nam (Battery research group, BNL chemistry)

Batteries are the key elements of clean energy technologies for hybrid & electric vehicles (HEV & EV), smart grid to utilize the green energy sources such as wind and solar electric energies. The in-depth understanding of the changes in electronic and crystal structures of the electrode materials during charge-discharge cycling or under abuse conditions will provide the important information for developing new materials with higher energy and power densities, longer life and better safety characteristics. In this regard, the BNL battery research group has been carrying out DOE funded projects (Vehicle Technologies (VT) program, office of Energy Efficiency and Renewable Energy (EERE)) which focus on developing new diagnostic tools during charge-discharge cycling or under abuse conditions using synchrotron based hard and soft X-ray techniques. The primary objectives of these projects are to determine the contributions of electrode materials changes, interfacial phenomena, and electrolyte decomposition to cell capacity, power decline, and safety. To this end, the ***BNL battery group has engaged in collaboration with the NIST Synchrotron Methods Group stationed at the NSLS and has conducted state of the art battery research using NIST's soft X-ray spectroscopy for more than 10 years. Soft X-ray absorption spectroscopy (XAS) at NIST beamline U7A has been unique diagnostic tools for our battery research.*** For example, soft X-ray absorption spectroscopy (XAS) at NIST U7A beamline has been used to distinguish the structural differences between surface and bulk of cathode materials such as $LiCoO_2$, $LiNi_{0.5}Mn_{0.5}O_2$, and $LiNi_{1/3}Co_{1/3}Mn_{1/3}O_2$ at certain states of charge-discharge using both electron yield (EY) and fluorescence yield (FY) detectors in both O-K and transition metal (Mn, Fe, Co and Ni) L-II, III edges.[1,2] (Fig. 1) These results provided valuable information for the development of new battery materials with high capacity and the improvement in capacity of the materials being used currently. ***Furthermore, These results demonstrate that the NIST's proposed NEXAFS/XPS beamlines are crucial and essential diagnostic tools for characterizing advanced battery materials***.

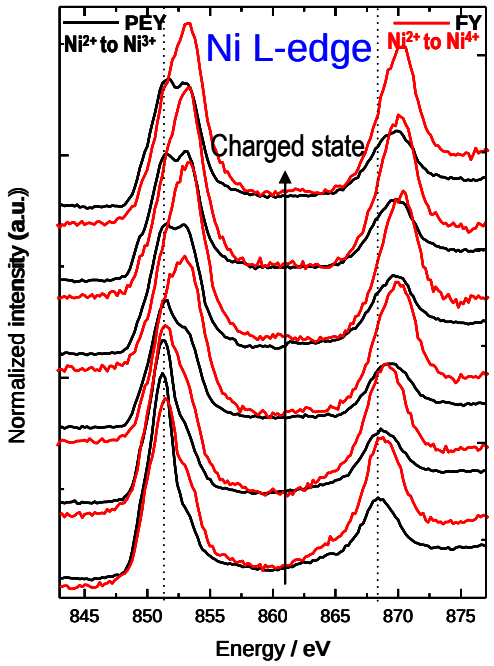

Figure 1. Ni L-edge NEXAFS spectra for LiNi1/3Co1/3Mn1/3O2 material during charge showing different electronic structure changes between bulk and surface.

Reversible conversion nano-materials are new type of lithium battery materials which shows much higher specific capacity with 260% over today's state-of-the-art $LiCoO_2$ positive electrode material. Unlike the intercalation cathode materials like $LiCoO_2$, reversible conversion process results in the full reduction of the transition metal cation to its elemental (i.e., metallic) state during the discharge. (Scheme at right) However, although promising from a number of fundamental energy perspectives, the conversion materials still face cycle life challenges and overpotentials in the voltage profile which decrease charge/discharge efficiency. In order to overcome above challenges, it is crucial to understand conversion/reconversion reaction pathways, and chemical/ compositional perturbations induced during the charge-discharge cycles. In this regard, we have done NEXAFS microscope studies on a combinatorial array of FeOF nanocomposite electrodes with different state of charge-discharge at NIST U7A beamline. (Figure 2) The preliminary results are quite exciting and encouraging. As

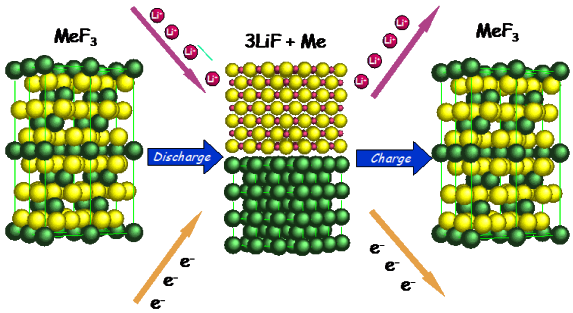

Schematic diagrams of conversion reactions used for energy storage materials.

sown in Fig. 2, we have clearly observed the reversible oxygen composition changes during the first discharge-charge cycle suggesting that the fluorine (F) is being extracted from and re-inserted to the FeOF nanocomposite materials during the conversion and reconversion reactions. In addition, NEXAFS image results provide spatial profiles about oxygen concentrations within each electrode. Regardless of the state of charge, relatively higher oxygen concentrations are observed especially at the edges of the rectangular shaped electrodes indicating the conversion reaction begins first at the edge sides.

Another critical question to be answered to the success of the conversion reaction approach is the elucidation on the formation of a locally stoichiometric, highly chemically-heterogeneous metal particle- Li salt nanocomposite on the order of 1-5nm during charge-discharge. The proposed NIST XPS microscope with nano scale spatial resolution will be ideal tool to characterize the nano-scale interface formed during conversion reaction. ***Therefore, combination of NIST's proposed NEXAFS and XPS image microscopes with nano and micro scales will have enormous impact on the development of new advanced next-generation battery materials which are driven by displacement and conversion reactions.***

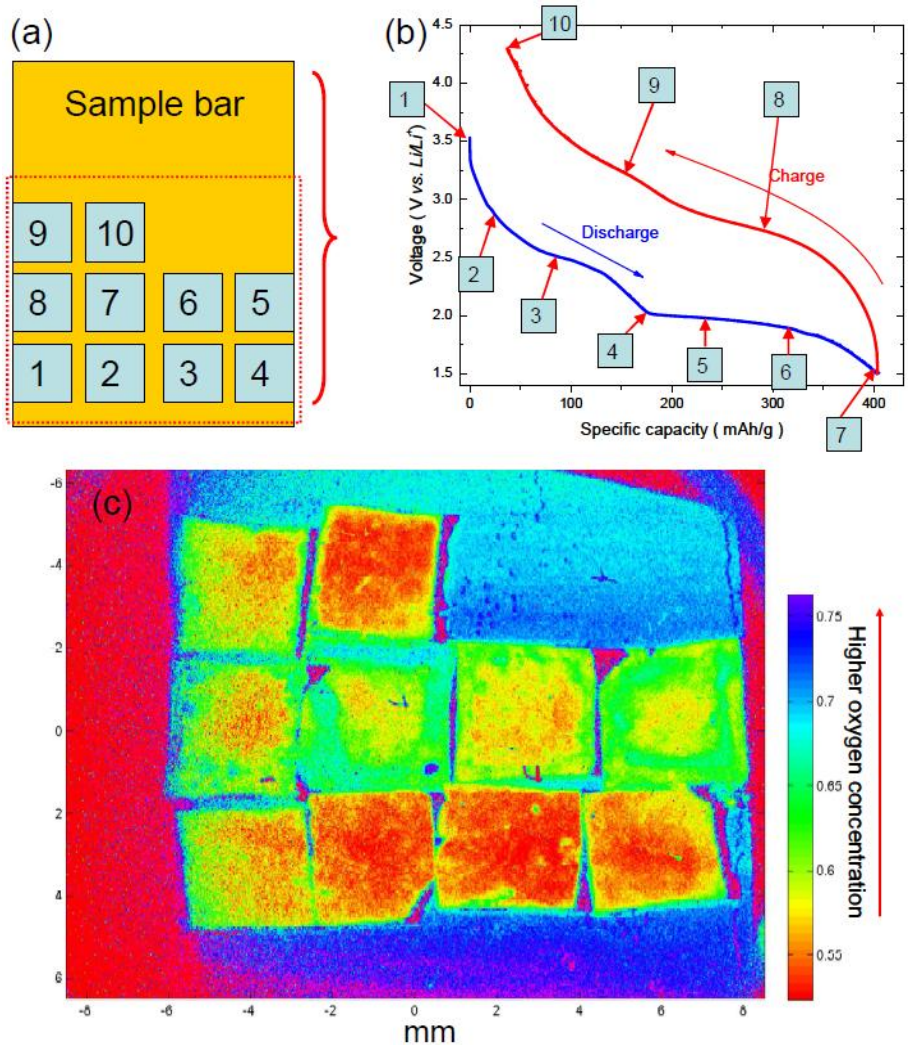

Figure 2. NEXAFS microscope image results for combinatorial array of FeOF nanocomposite electrodes with different state of charge-discharge. (a) sample description; (b) charge-discharge curves of FeOF nanocomposite electrode; (c) oxygen K-edge NEXAFS mapping results.

References

1. *Won-Sub Yoon et al*., J. Electrochem. Soc., 151, A246 (2004).
2. *Won-Sub Yoon et al*., J. Am. Chem. Soc., 127, 17479 (2005).

Hard X-ray Photoelectron Spectroscopy (HAXPES) and Near Edge X-ray Absorption Fine Structure (NEXAFS) of Phase Change Materials for Next-Generation Non-Volatile Memory Applications

Eric A. Joseph and Jean Jordan-Sweet (IBM T.J. Watson Research Center)

Chalcogenide glass materials have recently garnered significant interest for solid-state, non-volatile phase-change memory (PCM) applications due to their potential for scalability beyond that of conventional DRAM and Flash memory technologies [1]. Additionally, such materials may serve in storage class memory (SCM) devices which would substantially reduce the number of devices, physical space, and power requirements necessary for Exascale Computing, enabling an energy efficient, green technology [2].

	2020 Storage Bandwidth Requirement		Disk	PCM SCM
Compute-centric	1.7 PB/s	Devices	5.6M disks	1.7M modules
		Space	26,292 sq.ft.	300 sq.ft.
		Power	25 MW	173 KW
Data-centric	8.4 Giga-SIO/s	Devices	21M disks	35,000 modules
		Space	98,568 sq.ft.	12 sq.ft.
		Power	93 MW	4 KW

Figure 1: Projected PCM Impact to Exascale Computing for compute-centric (Petabytes per second) and data-centric (Giga–start input outputs per second) applications [2].

Chalcogenide phase-change memory is based on the orders-of-magnitude change in resistivity these materials exhibit during rapid crystallization and re-amorphization. However, such device applications require specific crystallization properties to ensure that their crystallization temperature (Tx) is sufficiently above standard CMOS device operation ranges (~80ºC), but also well below the melting point for thermal stability. Consequently, a thorough understanding of the phase-change material system and the role by which the material stoichiometry and local bonding environment affect the crystallization properties are important elements to optimizing the technology. As an example, one method of adjusting material properties is to dope the chalcogenide. Doping favorably modifies crystallization speed, crystallization temperature, and thermal stability. However, the chemical role of the dopant is not always understood, and in many cases it may lead to adverse effects.

IBM began collaborating with NIST in 2008 conducting state of the art, synchrotron research on chalcogenide material systems using the current NIST suite of spectroscopy beamlines at NSLS. The goal of the research was to provide a greater understanding of the local bonding environment of the material system and determine the specific location and bonding nature of the dopant atoms. An example of previous work is the high-energy XAFS measurements of nitrogen doped $Ge_2Sb_2Te_5$ completed on NIST beamline X23A2. By studying the Ge K edge, this work found that nitrogen doping preferentially forms stable Ge-N bonds. This result suggests that nitrogen doping does not lead to substitution of N into the FCC lattice, nor does it lead to distortion of the FCC lattice, but rather the N dopant instead resides on the grain boundary, where stability and structural nature of Ge-N and Ge-N-Ge bonding refines the grain [3].

It is eagerly anticipated that the electronic structure and local bonding geometry of the lighter "Z" dopant will be determined directly using Near Edge X-ray Absorption Fine Structure Spectroscopy (NEXAFS) and high energy XPS at the new NIST NSLS-II soft and tender beamline. Under current conditions at NSLS, it was not possible to acquire such data from this sample (at NIST beamline U7A) due to the low level

concentration of the dopant. ***The significantly higher brightness of the NIST NSLS-II Soft and Tender beamline and its advanced detector capabilities should allow such NEXAFS measurements of low level, low "Z" dopants. In addition, the beamline's expanded energy range (100eV to 7.5 keV) and enhanced nanometer scale spatial resolution thanks to its ensemble of microscopes will enable chemical mapping of samples which have undergone various (re)crystallization treatments.***

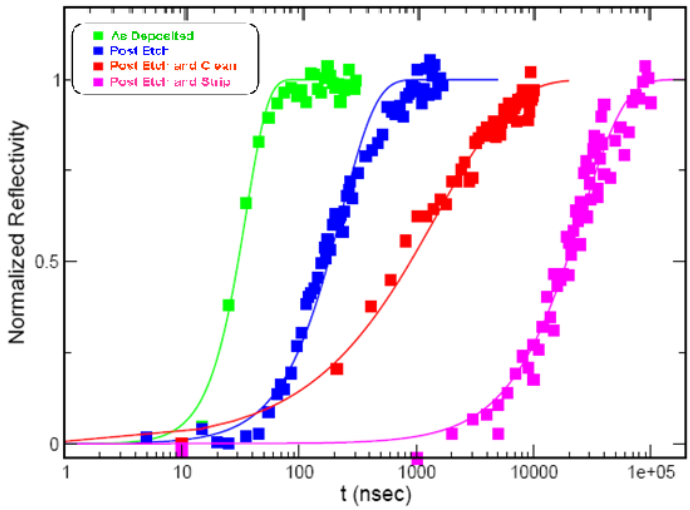

Figure 2: Normalized time resolved laser reflectivity measurements for as-deposited, plasma etched, plasma etched and cleaned and plasma etched and stripped nitrogen doped GeSbTe samples.

In addition to dopant specific studies, the effects of processing on the material crystallization properties are also of interest since it is known that there is an etch-induced material modification layer resulting from patterning [4]. Processing of chalcogenides significantly reduces their crystallization properties. Time resolved laser reflectivity data is shown in Figure 2, demonstrating a three order of magnitude shift in crystallization time upon exposure to the plasma etch and strip processes. To elucidate the nature of this material modification, a combination of depth profiled XPS, time resolved XRD, and XAS would be ideal. Results of previous depth profiled XPS data shown in Figure 3 obtained on a Physical Electronics Quantum 2000 ESCA Microprobe using a monochromatic Al K_α source reveal selective antimony removal and nitrogen dopant loss at depths up to 12nm. However, *such depth profiling measurements are extremely destructive in nature* due to the use of 1.0 keV Ar+ ion sputtering which can *cause significant disruption to the material itself.* In reality, the etch process likely created the non-uniform concentration of antimony and nitrogen that are measured for the amorphous control sample.

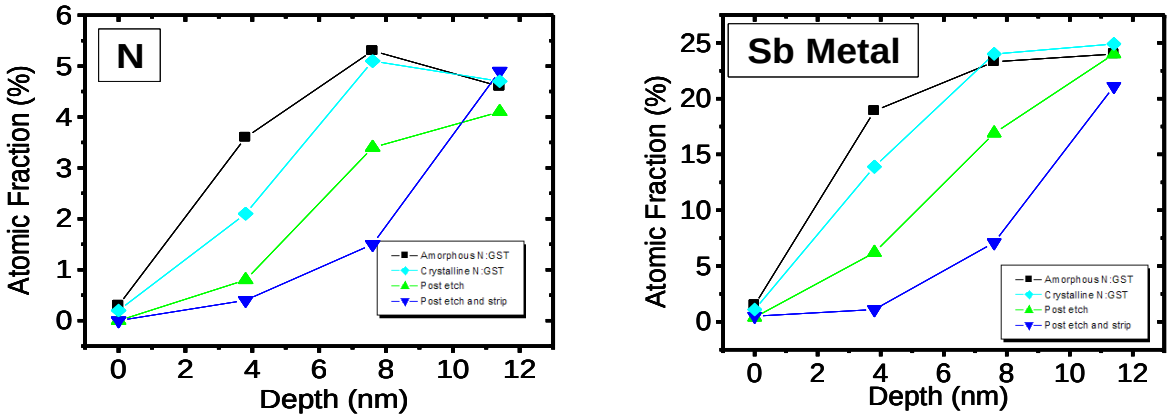

Figure 3: Depth profiled XPS measurements for N and Sb elements of N-GST films. Post-etch data follows etching in an Ar/CHF3/Cl2 chemistry. Post etch and strip follows the same etch with an additional dry strip [2].

As a big step towards alleviating this issue, variable kinetic energy XPS (VKE-XPS or HAXPES) obtained by varying the *incident photon energy* in a high resolution, high energy XPS measurement, a capability planned for the NIST NSLS-II Soft and Tender beamline, will provide non-destructive, depth profiling measurements simply by tuning the kinetic energy of the materials' core lines and exploiting the intrinsic, energy dependent, surface sensitivity of photoemission. This advancement should enable higher resolution, *non-destructive* and *unambiguous* depth profiling measurements for materials systems such as these. ***Coupled with the new nanometer scale spatial resolution planned for the VKE-XPS endstation, these advanced capabilities will effectively enable a 3D chemical imaging XPS microscope unique to NSLS-II.***

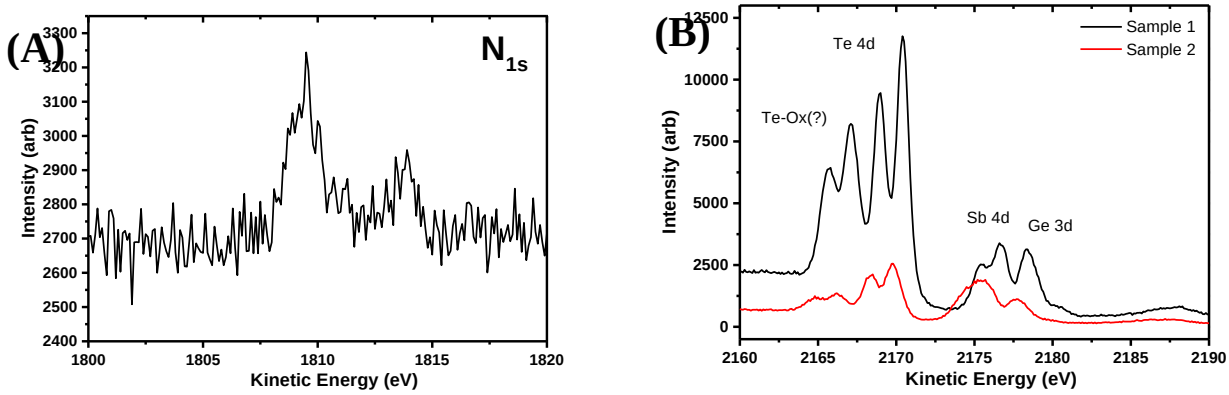

Figure 4: Synchrotron based XPS measurements of (A) nitrogen and (B) Ge, Sb, and Te core levels in N doped GST films measured with a photon energy of 2.1keV at NIST beamline X24A at the NSLS.

Already under development by the NIST team at NSLS, VKE-XPS (or HAXPES) data from NIST beamline X24 are shown in Figure 4. The data show the improved capability over a laboratory source to achieve high resolution XPS measurements for the N1s core level in N-doped GST (Figure 3a) and the often elusive lower binding energy (BE=30-40eV) GST peaks such as Te4d, Sb4d, and Ge3d core levels (Figure 3b). ***The benefit from higher flux VKE-XPS measurements available at NSLS-II will improve the signal to noise ratio of these data while providing the necessary depth and spatial resolution to generate an effective 3D chemical map.***

[1] Y.C. Chen, C.T. Rettner, S. Raoux *et al.*, IEDM Tech. Dig., p. S30P3, 2006.
[2] R.F. Freitas and W.W. Wilcke, IBM J Res & Dev Vol 92 No 4/5 p.439 2008
[3] J. S. Washington, Ph.D. Dissertation, NC State University, May 2010
[4] E. A. Joseph, T. D. Happ, S.-H. Chen, S. Raoux, et al., Symp. VLSI-Technology Systems and Applications, 2008. pg 142-143, 2008

Fundamental spectroscopy studies of the active sites of metal/oxide catalysts: Water-gas shift reaction on Au-CeO_2 and Cu-CeO_2 systems

Jose A. Rodriguez, Chemistry Department, Brookhaven National Laboratory

The concept of the "active site" in catalysis has been used since its introduction in the 1920s by Taylor and Langmuir. However, despite considerable scientific effort over many years, our knowledge of what exactly the active sites are and how they really work is in most cases very primitive. It is necessary to identify the active site and fully characterize its electronic, structural and temporal properties, and their dependence on temperature. ***What we propose here is a unique effort that will take advantage of the capabilities of NIST's Soft and Tender beamline for surface and materials characterization.***

With the onset of the hydrogen economy and future global energy challenges, the ability to produce molecular H_2 from a sustainable source has been pushed to the forefront of chemical research.[37] The water gas shift (WGS, $CO + H_2O \rightarrow H_2 + CO_2$) in particular has come to the fore of catalytic reactions that can answer this problem, in particular with the ability to undertake this process with the use of relatively abundant resources (CO and H_2O). New ceria (Au, Cu or Pt on CeO_2) based nanocatalysts are very promising candidates for high activity, lower temperature WGS systems.[38,39] These metal/oxide catalysts exhibit a substantially higher activity than the traditional Cu/ZnO WGS catalysts. The design and optimization of the ceria-based WGS catalysts is hindered by controversy about basic questions regarding the nature of the active sites and the reaction mechanism. It has been proposed with some controversy that the predominant intermediate species for this reaction is either a *formate* ($HCOO^-$) or a *carbonate* (CO_3^{2-}) and most recently theoretical calculations suggest the possibility of a *carboxyl* ($HOCO^-$) intermediate:

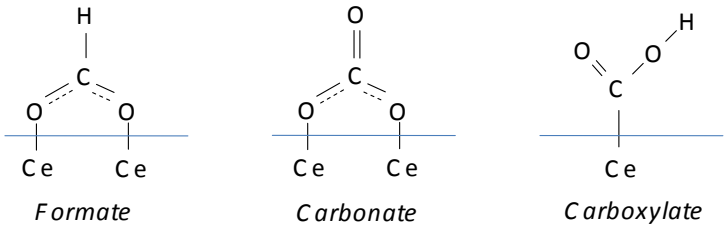

Using the new capabilities of NIST's NSLS-II beamline, one will be able to study the kinetics of decomposition of *formate* and *carbonate* on different metal oxide surfaces and compare it with the overall rate for the formation of H_2 and CO_2 during the WGS reaction. This will point to the key intermediate as a function of surface composition. It has been observed that the *formate* and the *carbonate* have similar C 1s XPS signatures. ***Since the NIST NSLS-II beamline will allow the combination of photoemission and*** *NEXAFS* studies, it will be possible to distinguish the formation of *formate* or *carbonate* intermediates as a consequence of the reaction of CO and OH in the early stages of the WGS.[40] The characteristics of the beamline will make it an excellent tool for identifying active sites and for studying their behavior.

[20] J.J. Spivey, Catal Today 100 (2005) 171.
[21] Q. Fu, H. Saltsburg and M. Flytzani-Stephanopoulos, Science, 301 (2003) 935.
[39] J.A. Rodriguez, S. Ma, P. Liu, J. Hrbek, J. Evans, and M. Perez, Science, 318 (2007) 1757.
[40] S.D. Senanayake, D.R. Mullins, J. Phys. Chem. C 112 (2008) 9744.

Optimizing Novel Materials for Energy Applications:
Electronic Structure of Doped Oxides Using Hard X-ray Photoelectron Spectroscopy (HAXPES)

Abdul Rumaiz (BNL)

The finite nature of fossil fuels has created a greater need for an alternate and stable energy source. A significant portion of this effort has been directed towards solar energy and hydrogen generation. In both these areas there is a greater need for novel materials which can be tailored for higher efficiencies. Transitional metal oxides, especially titanium dioxide (TiO_2) and zinc oxide (ZnO), are being aggressively studied as viable photovoltaics and photocatalysts for the electrochemical splitting of water [1,2].

TiO_2 was found to be capable of splitting water molecules into oxygen and hydrogen gases in 1972 by Fujishima and Honda [3]. However, owing to its relatively large band gap (3.0 and 3.2 eV for rutile and anatase, respectively), photovoltaic application of this photocatalyst is limited to the ultra-violet portion of the electromagnetic spectrum. The quantum conversion efficiency of TiO_2 can be enhanced if its band gap is made to absorb in the visible range. To achieve this there have been several efforts to dope the oxide and therefore introduce new energy levels into the band gap [4] allowing it to absorb light in the visible region. The substitutional doping of TiO_2 with transition metals [4] and with anion impurities [5] have often enhanced its photocatalytic performance. However, transition metal dopants often create localized deep *d* states in the TiO_2 band gap that are generally responsible for reducing charge-carrier lifetime due to an increased recombination rate thereby decreasing efficiency.

Among all dopants tested, nitrogen is consistently recognized as one of the most effective dopants, both theoretically and experimentally. The electronic structure study of N doped TiO_2 by Asahi [5] based on the density of states (DOS) calculations reveal that substitutionally doping TiO_2 with N creates localized N_{2p} states just above the valance-band edge. This results in a mild reduction in the band gap (~0.2 eV) and red shifts the optical absorption edge by about 100 nm beyond the UV region. The key element in understanding these materials is in fully understanding their electronic structure.

Figure 1 shows the band gap calculated from diffused reflectance measurements as a function of N doping in TiO_2 synthesized by reactive pulsed laser deposition [6]. Other works have shown evidence for band gap reductions from samples synthesized by different techniques [7, 8]. However, the reasons for the observed band-gap change still remain debated. Asahi et al [5] proposed a narrowing of the TiO_2 band gap due to the hybridization of O and N *2p* states in the valence band. This can be attributed to the natural extension of the valence-band maximum to lower binding energy, since the N *2p* level has lower binding energy relative to O *2p*. More recent studies, however, have proposed that the dopant N *2p* orbital forms a localized state just above the valence-band maximum of O *2p*.

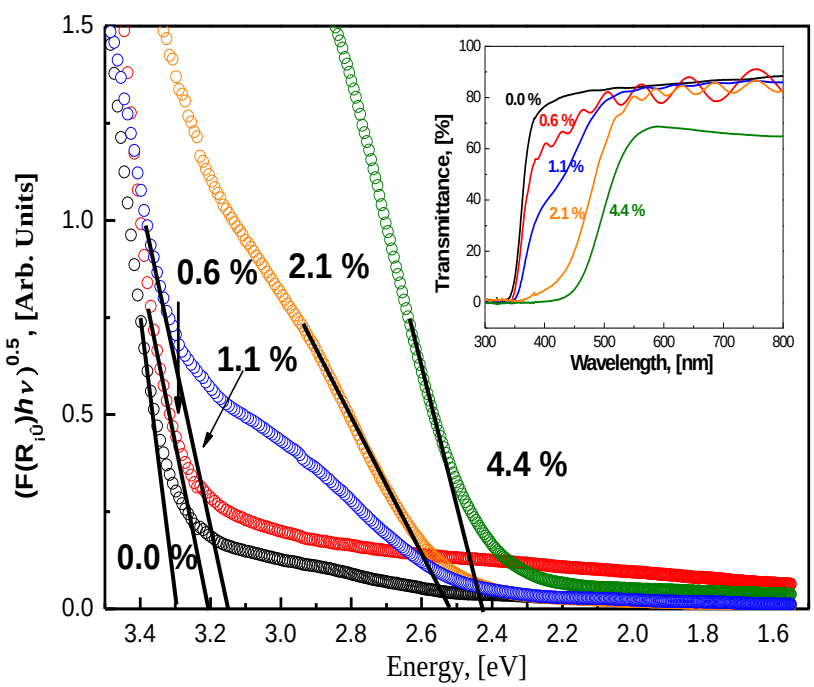

Figure 1: Band gap approximation using transformed Kubelka Monk function. Insert is the corresponding optical transmittance spectra for all samples.

HAXPES measurement performed on NIST beamline X24A at the NSLS gave unambiguous determination of the electronic structure of N doped TiO_2 [9]. Comparing bulk sensitive, valence-band HAXPES measurements (recorded with photon energy hν = 2140 eV) with ab-initio calculations revealed the role of oxygen vacancies in the doped oxide structure (Figure 2). It was shown that near a N substituted atom it was energetically favorable for an oxygen vacancy to form. The excess electrons, due to the oxygen vacancies, occupy the Ti *3d* states near the Fermi level, as seen in Figure 2. Although the valence band structure shows tailing to lower energies due to the incorporation of less tightly bound N *2p* which is hybridized with O *2p* causing a reduction in band gap, the shift is not large enough to account for the measured change in band gap from reflectivity data (Figure 1). It therefore is concluded that the combination of N impurity and O vacancy is responsible for the UV-vis absorption response in the visible region.

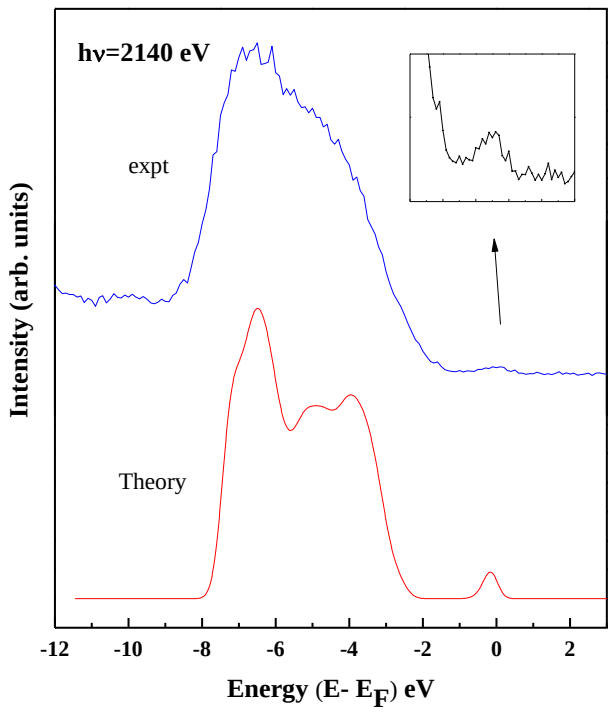

Figure 2: Valence band of N doped TiO_2

This measurement shows the power of HAXPES in studying bulk electronic structure, and, in particular, the changes in electronic structure upon bulk doping owing to the reduced surface sensitivity of higher kinetic energy photoelectrons in a HAXPES experiment. Conventional, low photon-energy, surface-sensitive measurements employ Ar^+ etch to clean the surface. This method leads to preferential etching of oxygen and the natural formation of oxygen vacancies. Thus it becomes impossible to resolve the origin of the vacancies in a low energy photoemission experiment. Our work has showed that oxygen vacancy creation is due to N doping (charge compensation) and is present within the bulk of the sample.

Significant future studies of the change in the electronic structure of transition-metal oxides with dopant incorporation and the advance of theoretical simulations of electronic structure should follow from the development of the NIST soft and tender beamline for hard x-ray photoelectron spectroscopy (HAXPES). This beamline will offer higher photon energies (up to 7.5 keV) with better experimental resolution than currently available at X24A. In particular, as demonstrated, HAXPES allows the study of bulk electronic structure from samples introduced from air without surface treatment which may perturb both their atomic and electronic structures.

Reference:

1. A.L. Linsebigler, G. Lu, and J.T. Yates Jr, Chem. Rev. **95**, 735 (1995).
2. B. O'Regan and M. Gratzel. Nature **353** 737, (1991)
3. Fujishima A, Honda K, Nature **1972**, *238*, 37
4. S.I. Shah, W. Li, C.-P. Huang, O. Jung and C. Ni. PNAS **99** 2, 6482. (2002)
5. R. Asahi, T. Morikawa, T. Ohwaki, K. Aoki, and Y. Taga, Science, **293**, 269 (2001).
6. H.Y. Lin, A.K. Rumaiz, M. Schulz, C. P. Huang and S.I. Shah, J. Appl Phys (in print)
7. A. Nambu, J. Graciani, J.A. Rodriguez, Q. Wu, E. Fujita and J.F. Sanz, J. Chem. Phys., **125**, 094706 (2006).
8. K. Kobayakawa, Y. Murakami and Y. Sato, J. Photochem. Photobio. A: Chem. **170**, 177 (2005).
9. A.K. Rumaiz, J.C. Woicik, E. Cockayne, H.Y. Lin, G.H. Hassnain and S.I Shah, Appl. Phys. Lett., **95**, 262111 (2009).

Correlating the Geometric and Electronic Structure of Nanomaterials:
Finite Size Effects for Tailoring Materials Properties

Sarbajit Banerjee (Department of Chemistry, SUNY Buffalo)

I. Graphene: Probing Electronic Structure to Inform Device Design

Graphene, a one-atom thick, two-dimensional (2D) electronic material constituted from a single layer of carbon atoms tightly packed within a honeycomb lattice, has few parallels in condensed matter physics. It has captured the attention of scientists and engineers because of its unique electronic structure and the resulting possibilities for novel device concepts and technological paradigms originating from its massive carrier mobilities, size-tunable band gaps, and room-temperature quantum transport phenomena (Geim, A. K. and Novoselov, K. S., *Nat. Mater. 6* (3), 183-191, 2007).

As major breakthroughs are achieved in the scalable fabrication of graphene, fundamental studies of graphene interfaces are entering the realm of possibility. Specifically, being a one-atom thick layer, it is to be expected that interfacial phenomena will strongly impact its electronic structure and carrier transport. ***The proposed NIST NSLS-II combined XPS/NEXAFS and imaging capabilities would meet an urgent need* to develop localized and global probes that can be used to *simultaneously probe valence- and conduction-band structures as well as the Fermi level with high spatial resolution* as a function of different perturbations applied at graphene interfaces.**

The University at Buffalo, SUNY team has been investigating the conduction band structure of graphene in collaboration with the NIST Synchrotron Methods Group and the Front-End Process Division at SEMATECH. Our preliminary polarized ***NEXAFS spectroscopy and imaging*** studies of graphene prepared by chemical vapor deposition and solution exfoliation routes have yielded a wealth of information regarding the substrate hybridization, surface chemistry, and local corrugation of graphene.

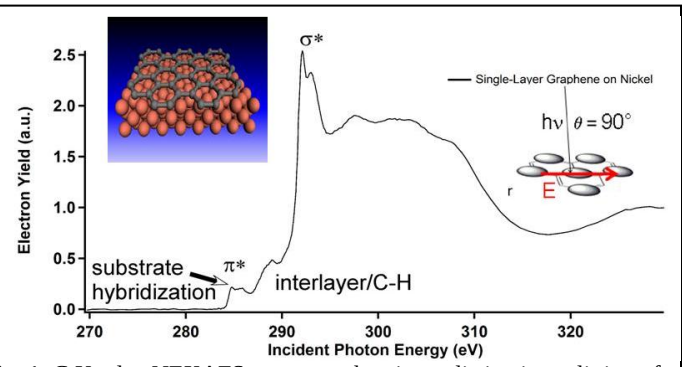

Fig. 1. C K-edge NEXAFS spectrum showing a distinctive splitting of the π* resonance due to the hybridization of the graphene sheet to the underlying Ni substrate. We have also demonstrated the presence of interlayer states for few-layered graphene. Polarized NEXAFS experiments also serve as an excellent probe of the rippling of graphene sheets.

Our findings include: (**a**) Evidence for strong hybridization of graphene π* states to the d_{z2} orbitals of underlying Ni and Cu substrates (Fig. 1) (Lee, V., et al., *J. Phys. Chem. Lett. 1*, 1247-1253, 2010.); (**b**) graphene grown on Cu shows a high degree of substrate alignment but significant rippling is introduced during transfer to SiO_2/Si substrates; (**c**) the π* structure of chemically derived graphene is substantially restored upon the reduction of exfoliated graphene oxide (Lee, V., et al., *Chem. Mater. 29*, 3905-3916, 2009); and (**d**) a comparative NEXAFS evaluation of the efficacy of different reducing agents in defunctionalization and restoration of the conjugated graphene π* network has been performed and has informed the development of solution-chemistry routes for the preparation of large-area graphene (currently being commercialized for indium tin oxide (ITO) replacement and for graphene-based acrylics for aircraft windows by UB in collaboration with Graphene Devices Limited). The chemically derived graphene technologies based on solution processes for exfoliating and defunctionalizing graphene oxide are of tremendous importance for the large-scale fabrication of graphene for use in nanocomposites with potential applications in armor or electromagnetic interference shielding. In addition, fundamental studies of high-quality graphene prepared by CVD are instructive in identifying electronic interactions at key graphene interfaces such as will be found in the next generation of electrical interconnects and high electron mobility transistors.

Currently, there is a significant gap in our understanding of how the valence and conduction band states of graphene are modified by perturbations such as the *formation of metal, dielectric, semiconductor, and molecular interfaces*. ***Being simultaneously able to perform XPS and NEXAFS measurements*** of the same

sample region will enable the development of a comprehensive picture of how the valence and conduction band structures are altered such as upon deposition of an overcoating thin dielectric layer or by hybridization to an underlying substrate. For example, an angle-resolved comprehensive XPS and NEXAFS study of graphene grown on different transition metals will be performed and in conjunction with density functional theory (DFT) modeling of graphene/metal interfaces will help in the derivation of a map of the relative strength and directionality of graphene/metal bonding.

The potential to modify the electronic structure of graphene via the pi-stacking of extended aromatic molecules represents a particularly tantalizing possibility that will also be explored by the same combination of XPS, NEXAFS, and DFT modeling. XPS chemical shifts of the adsorbed molecules in conjunction with NEXAFS evidence for hybridization to graphene will enable the development of chemical routes to modulating the electronic structure of graphene with significant potential impact in organic electronics.

The increased corrugation and rippling of graphene—related to coupling with the underlying substrate or membrane bending introduced during a transfer process—deleteriously impacts the mobilities of charge carriers. It has been predicted that electrons propagating through graphene are scattered by corrugations and ripples in the graphene sheet through a potential approximately proportional to the square of the local curvature. Polarized NEXAFS measurements are incredibly sensitive to the rippling of graphene. ***The proposed unprecedented spatial resolution of NIST's NEXAFS imaging will allow the acquisition of high spectral resolution NEXAFS data accurately pinpointing the location of graphene asperities (Patridge, et al., in preparation, 2010).***

For chemically derived graphene, the NEXAFS imaging capabilities will allow unprecedented chemical mapping of the location of functional groups. Combined XPS and NEXAFS studies will enable the conclusive identification of graphene functional groups retained after defunctionalization with various reducing agents, thus resolving a longstanding controversy over the nature and relative concentrations of different graphene surface functional groups and their NEXAFS spectral signatures.

II. Nanostructured Vanadium Oxides: Correlating Geometric and Electronic Structure to Massive Electronic Instabilities

Metal—insulator transitions in strongly correlated materials, induced by varying either temperature or dopant concentration, remain a topic of enduring interest in solid-state chemistry and condensed matter physics owing to their fundamental importance in answering longstanding questions regarding correlation effects and the possible generalizability of the underlying mechanisms to explain a wide range of quantum transport and spin phenomena including superconductivity (Qazilbash, M. M., et al., *Science 318*, 1750-1753, 2007; Imada, M., et al., *Rev. Mod. Phys. 70*, 1039-1263, 1998). Furthermore, the underlying operating principles for a diverse array of technological applications ranging from switching elements and thermochromic coatings to Mott field-effect transistors and infrared modulators essentially involve the thermal or voltage-driven induction of an insulator—metal transition.

In this context, the University at Buffalo, SUNY team has been collaborating with the NIST Synchrotron Methods group to explore correlation effects and electronic instabilities that arise from scaling vanadium oxides to the nanometer-size regime. Vanadium oxides have a rich and complex phase diagram originating from the facile accessibility of different vanadium oxidation states and the various structural distortions adopted to accommodate non-stoichiometry and point defects (Chernova, N. A., et al., *J. Mater. Chem. 19* (2526-2552), 2009).

Understanding the influence of finite size on the phase stabilities will not only contribute to fundamental understanding of the remarkable phase transition behavior, but significantly, our preliminary results (Fig. 2) indicate that scaling materials to nanoscale dimensions also offers the tantalizing possibility of enabling the observation of novel single-domain phenomena that are otherwise obscured in bulk samples.

In the absence of single-crystal diffraction data or detailed atomistic simulations, very little is known about subtle changes in the electronic (*V—O rehybridization, extent of charge disproportionation*) and geometric structure (*lattice expansion/contraction, defect density, surface reconstruction*) of vanadium oxides induced as a result of scaling to the nanometer-sized regime. Subtle changes in geometric and electronic structure are likely implicated in the strong modifications to the metal—insulator phase transition temperatures and hysteresis widths observed for the archetypical phase transition material VO_2 as well as novel $M_xV_2O_5$ nanostructures upon scaling to finite size and substitutional/intercalative doping. ***The proposed NIST NSLS-II beamlines will significantly impact the fields of solid-state chemistry and condensed matter physics of nanoscale correlated materials by enabling simultaneous measurements of geometric and electronic structure*** using V $L_{III,}L_{II}$ and O K-edge NEXAFS measurements using soft X-rays and V K-edge measurements using tender X-rays for the same sample across the metal—insulator transition temperature. The XANES features will provide valuable insight into solid-state dispersion effects and enable the mapping of the delocalized conduction band states derived from *p* orbitals, whereas the EXAFS features will allow development of detailed atomistic understanding of the vanadium coordination environment. Additionally, XPS measurements as a function of temperature will allow the formal valence distribution of different vanadium sites to be measured across the metal—insulator phase transition.

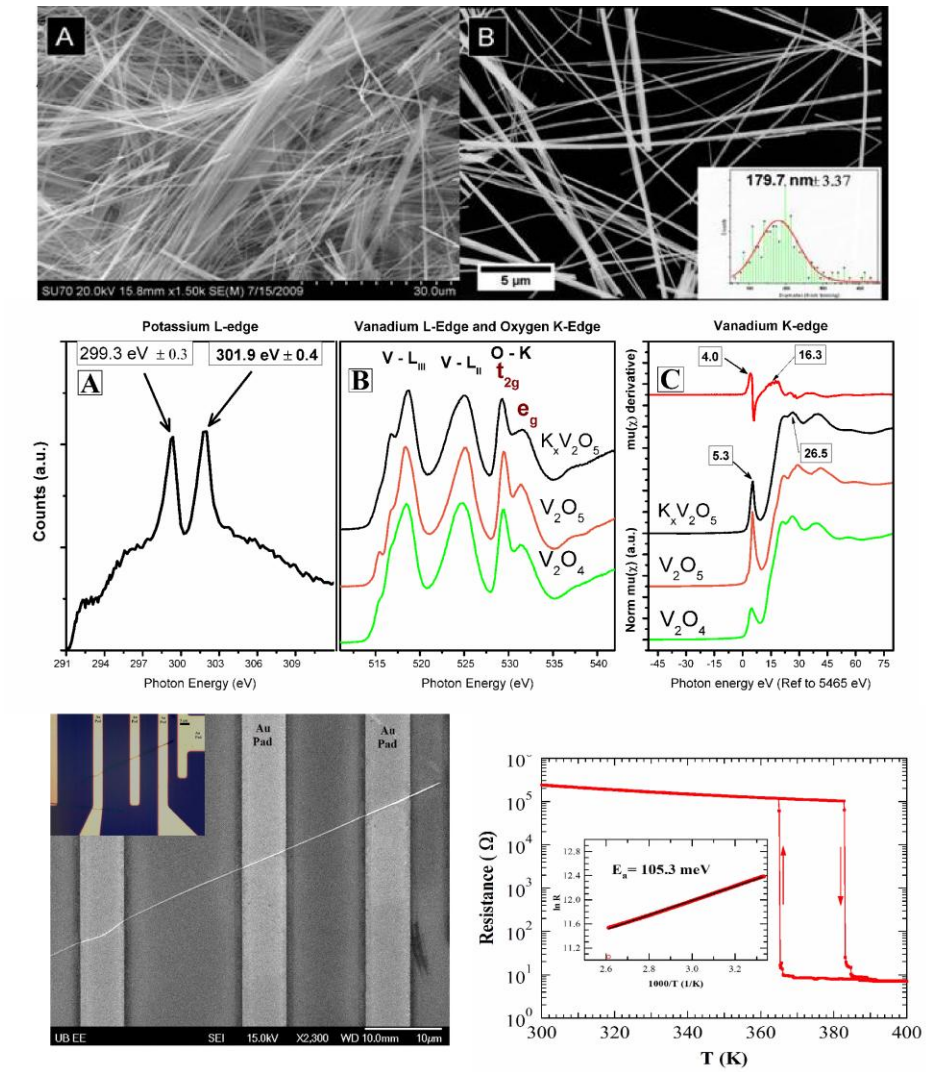

Fig. 2. Top panel: A) Scanning electron microscopy image of δ-KV_4O_{10} nanowires; B) Transmission electron microscopy image of δ-KV_4O_{10} nanowires. Middle panel: A) Potassium L-edge, B) V L-edge and O K-edge, and C) V K-edge X-ray absorption spectra acquired for the δ-$K_xV_2O_5$ nanowires. Lower panel: (left) a single nanowire aligned within a device and (right) resistance of the single nanwire measured as a function of temperature indicating a four-orders of magnitude metal—insulator phase transition.

Notably, we have developed a solvothermal synthetic protocol for the facile and high-yield synthesis of doped and undoped VO_2 and various $M_xV_2O_5$ phases where *M* = Na, K, Cu, and Zn. The VO_2 nanostructures show a pronounced depression and large hysteresis for the metal—insulator phase transition upon scaling to nanometer-sized dimensions or doping with tungsten. As for the non-stoichiometric $M_xV_2O_5$ bronzes, we have observed a hitherto undiscovered four orders of magnitude near-room-temperature metal—insulator phase

transition in nanostructures of a novel δ-KV_4O_{10} phase with remarkable stochastic switching between the phases near the phase transition temperature (Patridge, C. J. et al., *Nano Lett.*, in press, 2009). This material thus represents a rare new addition to the pantheon of materials exhibiting pronounced metal—insulator transitions in proximity to room-temperature.

Some of our published findings on the electronic structure of vanadium oxides indicate (**a**) the d_{xy} origin of the conduction band of V_2O_5 deduced using angle-resolved NEXAFS measurements of highly oriented V_2O_5 nanowires (Velazquez, J. M. et al. *J. Phys. Chem. C 113*, 7639-7645, 2009.); (**b**) massive hysteresis in electronic structure concurrent with changes in geometric structure for VO_2 nanowires (Whittaker, L., et al. *J. Am. Chem. Soc. 131*, 8884–8894, 2009), and (**c**) evidence for room-temperature charge disproportionation and reduction of specific vanadium sites from V^{5+} to V^{4+} upon the intercalation of alkali or transition metal ions in $Cu_xV_2O_5$ and δ-KV_4O_{10} bronze nanostructures (Patridge, C. J. et al., *Nano Lett.*, in press, 2009**;** Patridge, C. J., et al. *Inorg. Chem.* (48), 3145-3152, 2009**).** Figure 2 shows some potassium L-edge, vanadium L-edge, oxygen K-edge, and vanadium K-edge data acquired at the NIST beamlines U7A and X23A2 of the NSLS for δ-KV_4O_{10} nanowires along with electrical transport data showing pronounced metal—insulator phase transitions.

The proposed soft/tender NIST beamlines at NSLS-II will have a pronounced impact on our understanding of changes in electronic and geometric structure that accompany scaling to finite size and will help explain the strong alterations to metal—insulator phase transition temperatures and hystereses observed for vanadium oxide nanostructures. Specifically

(i) ***The combination of soft- and tender-X-ray beamlines will allow*** simultaneous acquisition of both XANES and EXAFS data at the *V L-edge, O K-edge, and V K-edge* and possibly also at K- or L-edges of dopant or intercalant atoms. This will enable both the geometric and electronic structure of VO_2 and $M_xV_2O_5$ nanostructures to be simultaneously studied.

(ii) Combined XPS and NEXAFS measurements across the phase transition will allow the development of a comprehensive picture of the electronic structure.

(iii) ***The high-throughput microscopes will allow simultaneous acquisition of XANES, EXAFS and XPS data*** at various edges such as shown in Fig. 2 in a single experiment and will thus enable structure—function correlations to be developed for nanowires with varying stoichiometry, dimensions, and morphology.

For example, it will be possible to explore the electronic structure of nanostructured vanadium oxides across the metal—insulator transition using 1s → 2p transitions (probing relatively more delocalized states) via NEXAFS spectroscopy at the O K-edge and XANES measurements at the V K-edge. Furthermore, NEXAFS data acquired at V $L_{III,II}$-edges corresponding to transitions from 2p→3d states will be valuable in understanding the conduction band features involved in transport and optoelectronic material properties.

Perhaps even more informative than the XANES features will be the oscillations observed >40 eV above the absorption edge, the EXAFS. EXAFS oscillations will be best-fitted to obtain values of nearest neighbor and next-nearest neighbor distances (out to about 5 Å from the excited atom), the coordination number, and the disorder in the distances for each coordination shell. Clearly, this will yield a wealth of local structural information and enable subtle changes in lattice parameters to be detected. Further, XPS measurements as a function of temperature will allow the formal valences of different vanadium sites to be mapped across the metal—insulator phase transitions for VO_2 and $M_xV_2O_5$ and will shed light into the critical V^{4+}/V^{5+} ratio required to trigger instabilities at the Fermi level that give rise to pronounced metal—insulator phase transitions.

Detailed structure—function correlations established in these experiments will pave the way for the design of vanadium oxide nanostructures with optimal dimensions, morphology, and composition that exhibit tunable metal—insulator phase transitions at specific temperatures with well-defined magnitudes.

NEXAFS Imaging of Propagating Waves of Self-Assembly in Organosilane Monolayers

Jan Genzer, NC State University

Impetus. Wave-fronts associated with reaction-diffusion and self-assembly processes are ubiquitous in the natural world. For instance, propagating fronts arise in crystallization and diverse other thermodynamic ordering processes. In biology, propagating fronts influence cell movement and division, as well as in the competitive social interactions and population dynamics of animals at much larger scales see Figure 1 below. While it is often claimed that self-sustaining or *autocatalytic* front propagation is well-described by mean-field 'reaction-diffusion' or 'phase field' ordering models, recent simulations and theoretical arguments show that *fluctuation effects* in lower spatial dimensions can lead to appreciable deviations from the classical mean-field theory of this type of front propagation. While these observations have significant implications for diverse types of ordering fronts that occur under confinement conditions in biological or materials-processing contexts, not much is known about the molecular aspects of this process. In collaboration with NIST, our groups has recently carried out preliminary experiments aimed at providing some missing links to the picture using a model system based on directional self-assembly of organosilane (OS) molecules on surfaces. Specifically, we reported that these OS adlayers organize from the substrate edge as *propagating wave-fronts* having well-defined velocities and shapes.[41] While these initial experiments offered valuable insights that may be applicable to any autocatalytic front propagation process, much more work needs to be done in order to gain detailed understanding of the assembly and dynamics of OS precursors deposited from vapor phase in a directional manner onto flat solid silica substrates.

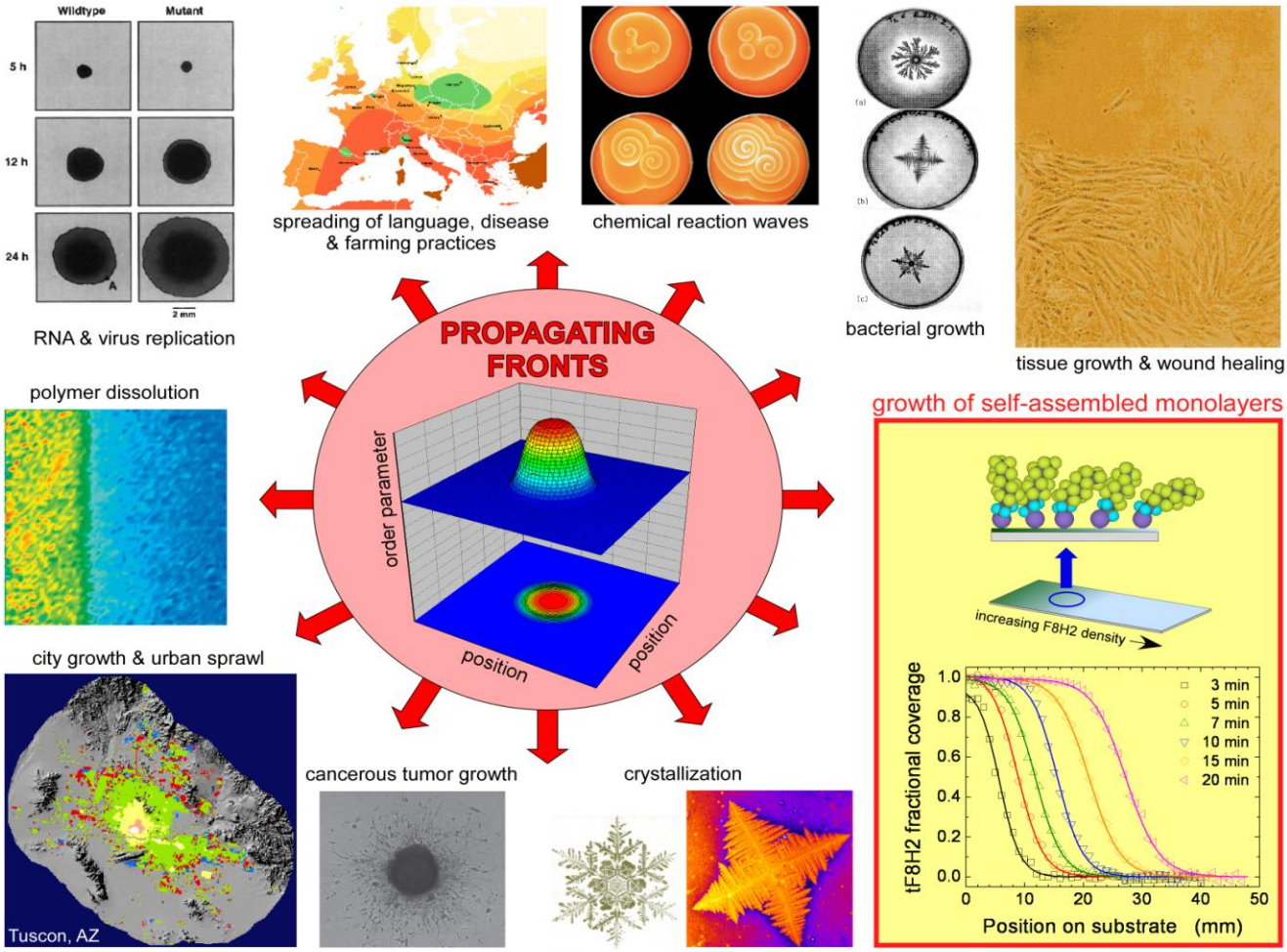

Figure 1. Examples of propagating fronts. See http://www.engr.ncsu.edu/news/news_articles/waveprop.html

[41] J.F. Douglas, K. Efimenko, D.A. Fischer, F.R. Phelan, J. Genzer, Propagating waves of self-assembly in organosilane monolayers", *PNAS*, **104**, 10324 (2007).

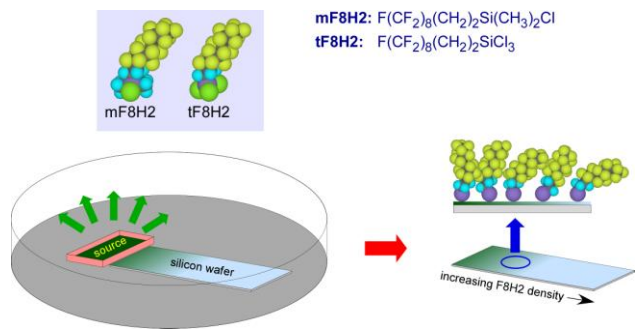

Figure 2. Schematic illustration of surface energy gradient formation in SAM layers. The average angular orientation of the molecules directly tracks the OS concentration and thus the normalized local concentration is identified with an order parameter for SAM ordering.

Approach. We utilize a method of creating self-assembled monolayers (SAMs) using OS molecular gradients[42,43], proposed by Chaudhury and Whitesides (*cf.* **Figure 2**).[44] Rather than employing a solution as a carrier for the depositing SAM molecules, Chaudhury and Whitesides simply placed a drop of high vapor pressure OS at the edge of a silica-covered substrate and enclosed the entire system in a Petri dish container to avoid convection effects. As the OS molecules traverse through the atmosphere above the substrate, the molecules 'rain down' and self-assembled spontaneously on the substrate. The *symmetry breaking* associated with placing the source of diffusing material to the side of the wafer leads to the initial formation of a concentration gradient of the OS molecules on the substrate that provides a direction to the self-assembly process. The geometry of the container modulates the nature of this gradient and the type of organization that occurs.[45] With increasing time, further OS molecules are deposited on the surface and the position of the maximum in the gradient in the molecular concentration and SAM ordering (*i.e.*, the interface between the assembled and non-assembled regions on the substrate) progresses across the substrate. Upon landing and molecular reorganization, the OS molecules react with the surface-bound -OH groups; the gradient is fixed into position by removing the OS source. We have recently argued that this kind of molecular self-assembly provides an example of a generic autocatalytic organizational process.[41] We provided indirect but sound experimental evidence from scaling experimentally-measured diffusion profiles and comparing them to predictions of computer simulations modeling autocatalytic fronts in confined spaces. Importantly, our work suggested that when the aforementioned deposition process is carried out under confinement (Petri dish container) it exhibits autocatalytic nature. We contrasted this behavior to the case where the deposition under "no confinement" (inverted 2-liter beaker) produced concentration profiles of surface-bound OS that can be very reasonably described using a classical Fickian diffusion model.

We plan to study the effect confinement on wave-front development due to in-plane constraints present on the substrate. The diffusing fronts will be formed using semifluorinated OS molecules both in the confined and unconfined geometries. The concentration of the deposited OS molecules in the wave-fronts will be monitored with ***NIST's Large Area Imaging NEXAFS Microscope***, a new experimental technique recently developed at the NIST's NSLS Beamline U7A. The ***NEXAFS Microscope*** represents a much improved combi-NEXAFS;[46] it takes snapshots of Auger electrons as a function of the photon energy across substrates of $\approx 12 \times 18$ mm^2. The collection time is fast, it takes about 8 minutes to collect NEXAFS image spectra with sufficiently high counts. This is important in order to minimize any damage to the samples due to x-rays (semifluorinated OS are particularly sensitive to these effects.[47]). By combining images from neighboring areas at various angles θ, the

---

42 J. Genzer, "Molecular gradients: Formation and applications in soft condensed matter science," in Encyclopedia of Materials Science, (K.H.J. Buschow, R.W. Cahn, M.C. Flemings, B. Ilschner, E.J. Kramer, S. Mahajan, eds., (Elsevier, Oxford, 2002).

43 J. Genzer, R.R. Bhat, T. Wu, K. Efimenko, "Molecular gradient nanoassemblies," Encyclopedia of Nanoscience & Nanotechnology, (H. S. Nalwa, ed.), American Scientific Publishers, Vol. 5, pp. 663-676 (2003).

44 M.K. Chaudhury, G.M. Whitesides, "How to make water run uphill," *Science* **256**, 1539 (1992).

45 J. Genzer, K. Efimenko, D.A. Fischer, "Formation mechanisms and properties of semifluorinated molecular gradients on silica surfaces," *Langmuir* **22**, 8532 (2006).

46 J. Genzer**,** D. A. Fischer and K. Efimenko, "Combinatorial near-edge x-ray absorption fine structure: Simultaneous determination of molecular orientation and bond concentration on chemically heterogeneous surfaces", *Applied Physics Letters* **82**, 266 (2003).

47 B. Jäger, et al., "X-ray and low energy electron induced damage in alkanethiolate monolayers on Au-substrates", *Phys. Chem.* **202**, 263 (1997); M. Wirde, et al., "Modification of self-assembled monolayers of alkanethiols on gold by ionizing radiation",

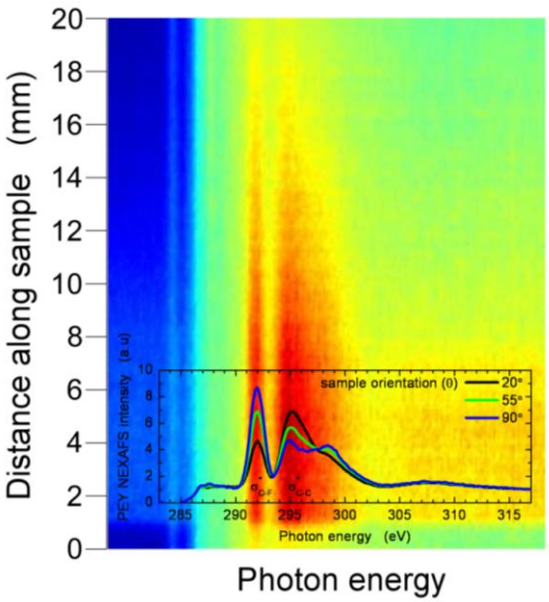

Figure 3. Electron yield intensity in imaging NEXAFS collected along tF8H2 gradient (distance 2 cm) at θ=50°. The red stripes correspond to the $1s \rightarrow \sigma^*_{C\text{-}F}$ and $1s \rightarrow \sigma^*_{C\text{-}C}$ transitions in tF8H2; their decreasing intensity across the sample is due to the presence of the decreasing concentration of tF8H2. For clarity, we superimpose typically NEXAFS spectra collected from homogeneous tF8H2 SAMs collected at three different angles θ.

compositional and orientation map can be obtained from the entire specimen. In **Figure 3** we plot an example of a compositional map collected from a tF8H2 gradient as a function of the position on the sample (ordinate). Note the position-dependent decrease in the intensity at 292 and 296 eV, corresponding to the $1s \rightarrow \sigma^*_{C\text{-}F}$ and $1s \rightarrow \sigma^*_{C\text{-}C}$ transitions. The current lateral resolution of the technique is ≈80 μm; this is sufficiently good for measuring the concentration of OS molecules in narrow wells on the substrate. The newly proposed ***NEXAFS Microscope*** instrument for NIST' that will be part of NIST's SST beams at NSLS II will promise further enhancement of the capabilities of this unique instrument. With a scanning area of 20 x 20 mm^2 and lateral resolution at 1 μm, we may even be able to visualize the concentration fluctuations at the wave-front directly with this exceptional analytical probe. There is no doubt that new important information about self-assembly processes (including, lateral distribution, chemical composition and molecular orientation) will be gathered that will enable much needed information about ubiquitous molecular assembly on surfaces.

Potential impact. Many molecular processes as well as the population dynamics of humans and other organisms can be described in terms of fundamental 'entities' undergoing random local displacement events. These exhibit regular motion at large scales and associated pattern formation as the participating entities collectively move from some unstable situation to a relatively stable state of greater energetic or competitive 'advantage'. These pattern formation processes are ubiquitous in the natural world and largely govern successive waves of evolutionary development. **Figure 1** depicts a few such examples. Since the spreading of autocatalytic waves is a pervasive phenomenon, modeling and analogies conceived to describe them can be applied to other everyday 'invasive' phenomena, *e.g.*, the introduction of foreign plant species into new environments, triggering waves of invasive growth in the countryside, the growth of urban sprawl, frontal polymerization, corrosion of metallic films, polymer dissolution, and many others (*cf.* **Figure 1**). Fluctuation effects tend to make these fronts increasingly incoherent (diffuse) in time, and thus are expected to greatly impact the *interactions between* frontal patterns under conditions where species (or different types of ordering) are competing for supremacy. Indeed, the *interaction* of two counter-propagating autocatalytic wave-fronts is one of the key areas we plan to study in this work. To that end, ***NEXAFS Microscope*** at the NSLS II will be a key instrument we plan to utilize in our work.

Nucl. Instr. Meth. Phys. Res. B **131**, 245 (1997); M. Zharnikov, et al., "Modification of alkanethiolate monolayers on Au-substrates by low energy electron irradiation: Alkyl chains and the S-Au interface", *Phys. Chem. Chem. Phys.* **1**, 3163 (1999).

The NIST Full Field XPS Magnetic Projection Microscope (XPS-MPM):
Chemical and structural imaging at 1nm using a new class of microscope

Raymond Browning (R. Browning Consultants) and Daniel Fischer (NIST)

Our objective is to create a new chemical measurement microscope and NIST user facility at NSLS II to advance the development of functional nano-materials such as organic photo-voltaics, and novel catalytic systems for energy conversion and storage, and nanoelectronics (CMOS and beyond). The target spatial resolution will be **1nm** for nondestructive, **in-situ**, 3 dimensional (**3D**) chemical and structural imaging.

Our approach is to continue development of the new class of X-ray photoelectron microscope that R. Browning Consultants has invented under NIST SBIR contracts (currently 3 US patents awarded, and four applications). This new class of photoelectron microscope (US Pat. 7,718,961) has several major developments in electron optical design that distinguish it from previous microscopes, including: a cyclotron orbit radius filter (US Pat. 7,608,838), a magnetic field terminating electron spectrometer (US Pat. 7,569,861), and an integrated magnetic shield and projection lens (Patent applied for). These, and other developments, will lead to a first in class facility.

The development of the new microscope, a full field imaging X-ray Photoelectron Spectroscopy Magnetic Projection Microscope (XPS-MPM), will be in stages leading to a 1nm imaging tool and General User Facility at the state-of-art NIST beamlines at NSLS-II.

NSLS-II high brightness undulator beamlines will be critical for this microscope, opening the door for a wide range of applications. A key beamline element is sufficient brightness over a wide tunable range of energies. The imaging technology can be developed such that chemical, electronic, and structurally specific signals can be simultaneously extracted from the multiple photoemission core levels. The proposed NIST NSLS-II Soft and Tender beamlines with its continuous selection of X-rays from 100 eV to 7.5 keV gives access to these core levels, and with sufficient flux to provide 1nm resolution, with nondestructive 3D chemical imaging by varying the kinetic energy of the photoelectron. The unique XPS-MPM optics also has a wide field of view, a large depth of focus, and thus will be suitable for many real world industrial samples including ambient pressure catalysis studies. The NIST XPS-MPN at NSLS-II is expected to enable advances in virtually all materials (polymeric, inorganic, and biologic) and devices for myriad applications.

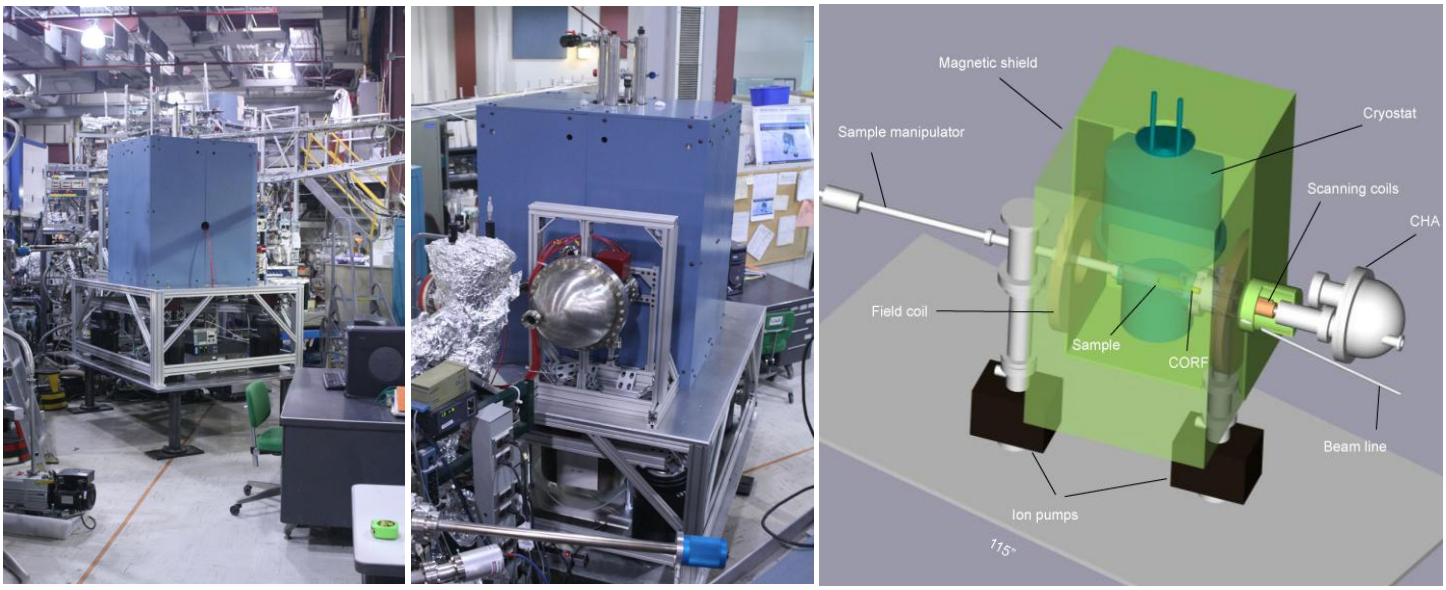

Full field NIST XPS magnetic projection microscope under development by R. Browning Consultants funded under NIST Small Business Innovation Research grants at NSLS beamline U4A

US Patents: `Inventor: R.Browning`
`7,569,861 'Electron Spectrometer' August 4, 2009`
`7,608,838 'Electron Optical Component' October 27, 2009`
`7,718,961 'Photoelectron Microscope' May 18, 2010`

The XPS-MPM can be compared to photoelectron emission microscopy (PEEM) to illustrate the power of the technique. The table below gives an overview of the major advantages given by the magnetic projection lens of the XPS-MPM over the high voltage electrostatic immersion lens of PEEM. These advantages, can be summarized by the XPS-MPM having applications over a wide range of sample types of direct relevance to industry.

	PEEM **2D** chemical and magnetic imaging on flat conducting surfaces **Surface Science** Method based on high voltage electrostatic immersion lens with the sample as part of the lens, best resolution for very low energy photoelectrons and very flat surfaces	**NIST XPS-MPM** **3D+** chemical, chemical phase, and structural imaging on many surfaces, **General Industrial User** Method based on magnetic projection lens, resolution relatively independent of sample type, and photoelectron energy
Ultimate Resolution	**3-5nm.** Good theoretical and test piece resolution - down to 3nm on latest instruments. 50nm more common in practice	**1-5nm.** UPS and XPS ultimate resolutions below 10nm expected on most samples
Depth of Field	**Small.** Small depth of field. Flat surfaces if chemical contrast is required. Topography is a strong contrast mechanism that degrades resolution	**Very Large.** Large depth of field. 1-2mm, Topographic contrast due to shadowing and projection angle effects, does not degrade resolution
Sample Types	**Conducting.** Conducting surfaces are required for high resolution, the sample is part of the extraction optics	**Multiple** surface types, rough non-conducting
Imaging types	**Elemental, Chemical, Magnetic**	**Elemental, Chemical, Phase Analysis, Structural**
Field of View	**1-100µ**	**1µ – 2mm**
Depth of signal	**2 dimensions <1nm** very surface sensitive	**3 dimensions, 1-10nm** tunable with photon energy and surface angle. Non-destructive depth profiling
Time resolved	**2ps** with streak camera	**20ps** from beam line NSLS II
Availability	**Commercial suppliers**	**An UNIQUE microscope** Commercial XPS microscopes are 5-50µ resolution and lack quantitative image analysis capabilities
Applications	**Many well understood applications:** Very nice work on magnetic materials, time resolved domain movements	**Many novel applications:** Post CMOS nanoelectronics, organic photo-voltaics, organic semiconductors, **3D** functional material structures, in-situ processing of catalysts
Ambient pressure	**No.** Not feasible because of high voltage breakdown	**Yes. New method with no differential pumping**

Four-Dimensional Hyperspectral Chemical Imaging Based Upon Large Area Near-Edge X-Ray Absorption Fine Structure (NEXAFS) Contrast Using State-of-Art Synchrotron Sources at NSLSII

E. Principe and P. Sobol (Synchrotron Research, Inc.) & D. Fischer (NIST)

The Large Area Rapid Imaging Analytical Tool (LARIAT) NEXAFS end station together with the NSLS II synchrotron source and advanced data mining enables critical pathways in the design of nanochemical systems. The LARIAT (NIST SBIR funding) is one key to unlock understanding of nanochemistry based upon directed self-assembly and novel panoscopic patterning methods; the foundation of future advanced materials applied to biology, photonics and electronics.

NEXAFS is an established synchrotron-based "near-surface" characterization method uniquely able to provide quantitative information on the nature of chemical bonding (e.g., bond type, bond angle, bond length), molecular concentration and orientation of molecular systems① like self-assembled monolayers (SAMS). Such information is critical to understanding the behavior of new material systems and our ability to control molecular patterns in three dimensions. To that end the NSLS II provides a high brightness tunable energy source (significantly improving data acquisition rates) and an undulator providing polarization control of the electric light vector (expanding the range of information). Reaching the full potential of the new generation NSLS II light source also requires a new generation of analytical end stations compatible with high throughput and efficient data analysis. The LARIAT MKII matches the potential of the NSLS II source with a second generation full field imaging NEXAFS spectrometer designed for automated parallel acquisition of hyperspectral chemical image datacubes. The term "hyperspectral chemical imaging"② refers to collection of a set of chemical images as a contiguous function of energy, where each image is the result of excitation at a spectrum energy point. Electron energy filtering through the spectrometer discriminates Z-depth information. The X-Y lateral dimensions and Z-depth information combined with the energy spectrum form a four-dimensional datacube. The data may be summed to create high S/N images or spectra can be extracted from any image point as a function of energy. A large area parallel imaging approach to NEXAFS promotes a new paradigm in design of experiment and combinatorial analysis. While the full field imaging aspect promotes experiments based upon arrays, the spectrometer is also designed for higher throughput to take advantage of the higher brightness of the NSLSII. In about the same amount of acquisition time spent on NSLS I using the LARIAT MKI, the LARIAT MKII on NSLS II will yield a nearly 700X increase in areal information. This improvement is derived from a factor of 1.7 increase in imaging area (400mm^2) while simultaneously improving the areal resolution by a factor of up to 400. Collectively these factors further scientific development and enable more efficient use of the synchrotron facilities; science progresses faster at lower cost.

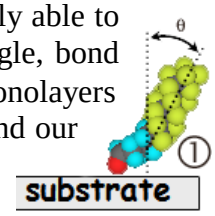

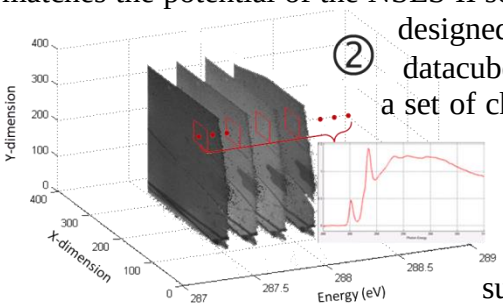

The LARIAT MKII NEXAFS spectrometer produces rapid full field chemical images using a simple elegant design and basic physics principles. Deflection optics scan the synchrotron source beam rapidly across an area up to 20X20mm while the energy is tuned across an absorption edge (e.g., K or L). Resonance at the edge region stimulates a highly sensitive bond dependent yield of electrons across the surface of the specimen, the essence of the NEXAFS process, which the LARIAT detects in parallel. Using an axial magnetic field coupled with a parallel imaging detector the LARIAT detects secondary electrons while preserving their spatial position on the sample. A high strength axial magnetic field ($\vec{B}_0$) immersing the sample couples to a lower magnetic field at the detector plane ($\vec{B}_Z$). Diverging magnetic flux lines ($\vec{B}$) couple the fields between the two coils as shown ③. A voltage V_g applied to electrostatic elements form a high pass energy filter for electrons with axial energy, E_a, below V_g. The stimulated electrons emanating from all angles and areas of the sample are forced to follow helical paths around the magnetic flux lines shown in ③. In the schematic the path appears as a sinusoidal curve with increasing amplitude, but it is actually an expanding helix in three dimensions. This helix is formally the electron

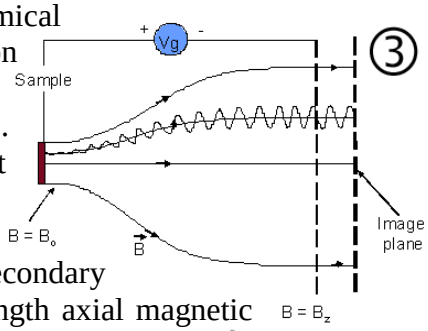

cyclotron radius (ECR) and for a electron with transverse energy E_T; $ECR_{max} \propto \sqrt{E_T} \div \vec{B}$. It is the ECR at the sample that to first order determines the lateral resolution of the spectrometer. A larger magnetic field at the sample produces a smaller ECR and hence higher lateral resolution at a given electron energy. The coupled fields allow the electrons to form a coherent image on the detector, which is comprised of a micro channel plate (MCP), a phosphor conversion layer bonded to a fiber optic (FO) bundle taper ④, and a 16 mega pixel CCD camera operating at 1MHz (not shown). As the electron energy and intensity distributions are related to the chemistry on the sample surface; chemical information is represented in the image.

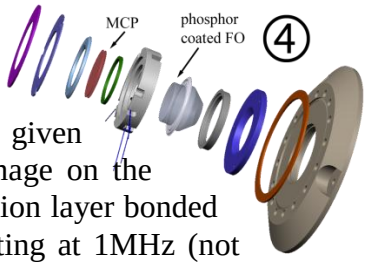

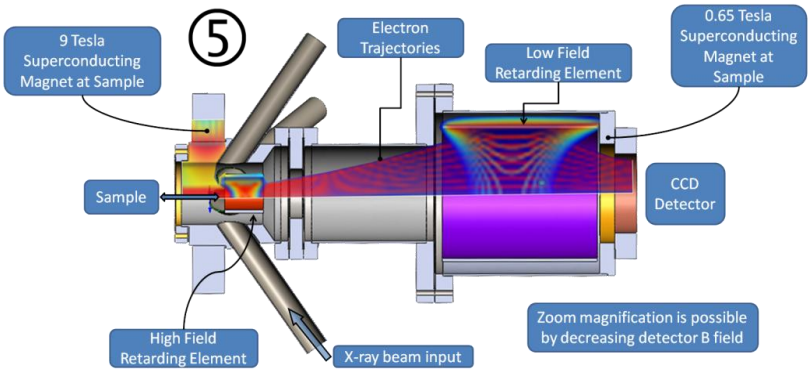

The LARIAT MKII ⑤ employs superconducting magnets with a field at the sample of 9 Tesla and 0.65 Tesla at the detector. Two electrostatic elements, a High Field and a Low Field retarding element, screen both axial energy and angular emission to permit depth and energy dependent filtering. System resolution, throughput and energy-depth discrimination has been improved significantly for LARIAT MKII on NSLS II.

The first application example of the LARIAT confirms successful patterning of single stranded DNA by distinguishing two types of nitrogen chemistry through chemical imaging ⑥ (D. Castner, NESAC/BIO, Univ. of Wash.). The green in the image on the right represents the Adenine π^* bond of DNA patterned against the nitrogen chemistry of the substrate, shown in red. The analysis not only confirms the successful patterning but discriminates between subtle differences in the two sets of spectra depicted on the left. Another significant aspect of this application example is the integration of the multivariate analysis package AXSIA. This export restricted analytical software developed at Sandia National Laboratory dramatically improves S/N, here reducing a 300 count image stack to one super image. AXSIA employs a proprietary principal component analysis algorithm to mine large spectral data sets for small but relevant spectral variations. AXSIA's continued expansion into diverse scientific disciplines reflects the trend toward hyperspectral and multispectral analytical methods. Optimal scientific methods require cutting edge hardware and software and the LARIAT incorporates custom data acquisition and a sophisticated data reduction tool suite in a complete analytical system.

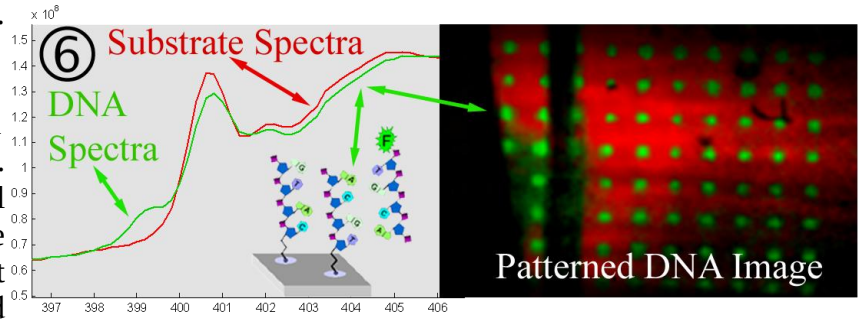

A second example relates to organic photo voltaic patterning via SAMs templates. NEXAFS chemically distinguishes between the electron acceptor (PCBM) and light absorber (P3HT) chemistries and the LARIAT produces chemical data at varying depth to reveal 3D photovoltaic structural information (D. Delongchamp, NIST/MSEL) ⑦. The "shallow" chemical image coded in beige shows the surface to consist exclusively of P3HT. The "deep" chemical image coded in blue and beige shows the pattern of PCBM (blue) below the surface in the P3HT matrix. Examined collectively the 3D structural is a pattern consisting of PCBM successfully patterned on the SAMs template and covered with a skin of P3HT.

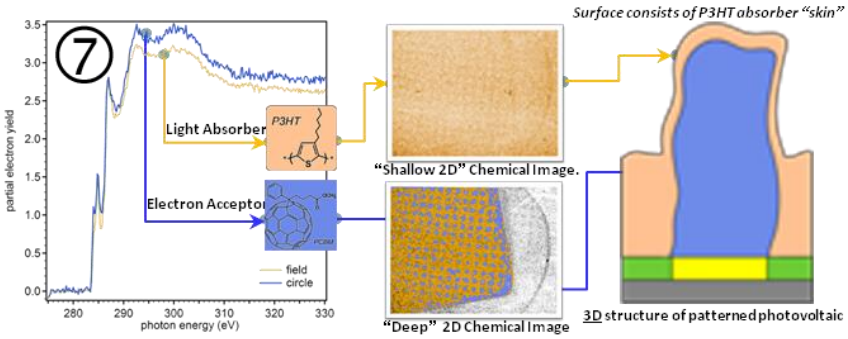

Micro-calorimeter High-resolution Soft X-ray Detector: Soft x-ray Emission and NEXAFS Spectroscopy

Randy Doriese and Daniel Fischer (NIST)

High-resolution x-ray fluorescence (XRF) spectroscopy, like x-ray photoelectron spectroscopy (XPS), is sensitive to occupied electronic states. A principle difference from XPS, however, is that XRF can probe buried layers from which photoelectrons cannot escape. Such a technique is thus crucial for studying organic photovoltaics, where layer-interface chemistry determines device properties. The few instruments in the world that can perform high-resolution XRF spectroscopy rely on highly inefficient grating spectrometers. Acquisition of useful spectra can take hours or days, even with an undulator beamline, so many classes of experiments, such as spatial scans of nonuniform samples, and observations of time-evolving reactions, are all but ruled out.

The NIST-Boulder Quantum Sensors Project has been collaborating with NIST-Synchrotron Methods Group based at the NSLS since late 2007 to develop a novel x-ray-fluorescence spectrometer that has no wavelength-dispersive element, and is instead based on a array of 256 superconducting transition-edge microcalorimeters. ***When installed at NIST's SST NSLS-II beamline, this instrument will provide spectrometry capabilities – a combination of X-ray energy resolution and measurement speed – that exist nowhere else in the world.***

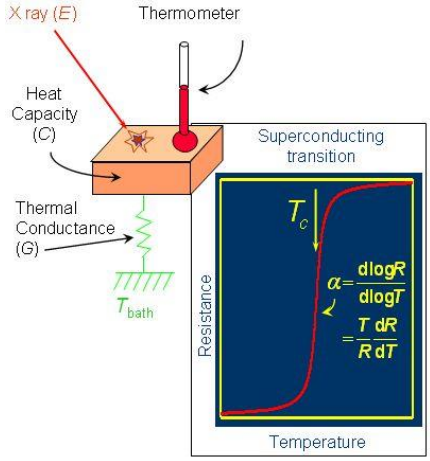

Fig. 1 (Left): TES microcalorimeter. The sharp superconducting transition and low noise due to low-temperature (100 mK) operation allow energy resolution approaching that of grating spectrometers, but with much higher photon efficiency.

A transition-edge-sensor (TES) microcalorimeter is a superconducting thin film that is voltage-biased into its superconducting-to-normal-metal transition. The film is weakly connected to a thermal bath. An x-ray photon striking the film raises its temperature and thus its electrical resistance. The resulting pulsed decrease in electrical current, measured via a SQUID ammeter, has pulse height proportional to the photon energy. Fig. 1 shows a cartoon of a TES.

TESs can be tiled into two-dimensional arrays of hundreds to thousands of pixels. The resulting detector array combines the collecting efficiency of a CCD camera with energy resolution approaching that of a dispersive (crystal or grating) spectrometer. TESs have achieved energy resolution (FWHM) of 22 eV at 100 keV and 1.8 eV at 6 keV. ***In the sub-keV soft-x-ray range, resolution of 0.5 eV in a properly optimized TES should be possible.***

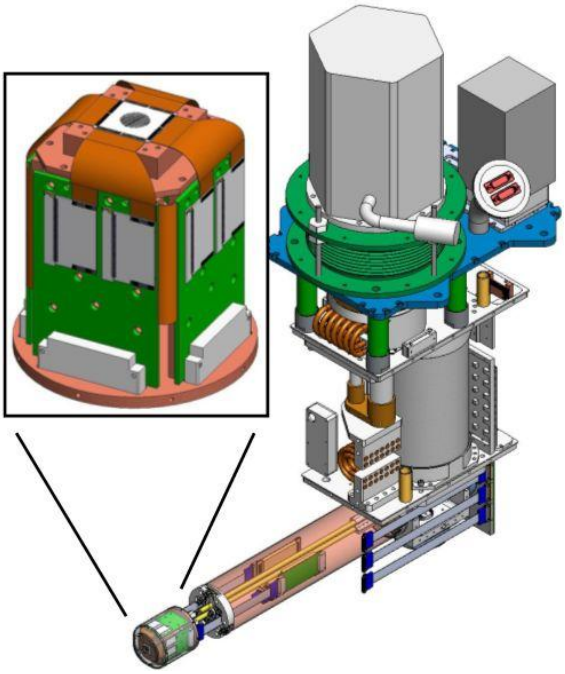

Fig. 2 (right): CAD rendering of the microcalorimeter spectrometer with its vacuum and cryogenic-shield shells removed. The cryogenics consist of a NIST-designed FAA/GGG (50 mK/ 1K) adiabatic demagnetization refrigerator, backed by a Cryomech pulse-tube cryocooler (3 K) in a High Precision Devices cryostat. There will be IR-blocking windows at the 50 mK, 3 K, and 60 K stages with total transmission of about 0.1-1% at 275 eV. The inset shows the 50 mK detector snout. The detector array is on top, and time-division-SQUID-multiplexer chips are arrayed around the sides of the cube.

Our first prototype spectrometer, under development for the NSLS U7A beamline, is optimized for K-alpha fluorescence of carbon and other low-Z elements. ***The design specifications are as follows: 256 pixels, each of size 200 um square, and each capable of receiving up to 100***

x-ray counts per second with energy resolution of 1 eV (FWHM); thus, the total instrument will have collecting area of 10 mm^2 and count rate of 25 kHz. Fig. 2 shows a CAD rendering of the full instrument.

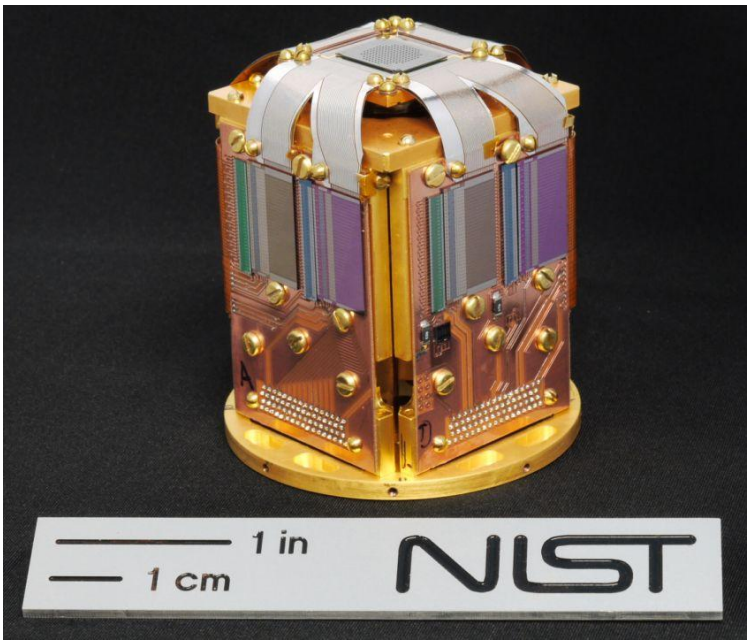

Fig. 3 (left and below): **Photograph of the fully-populated detector snout, which will receive first-light photons from a tube source at NIST-Boulder in June, 2010.**

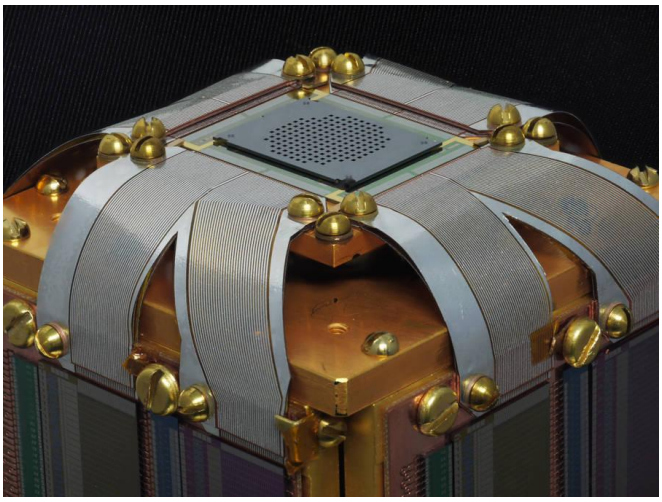

At U7A, the spectrometer will be stationed in an upstream sample chamber, which will allow the instrument to be deployed for testing, but also to be removed easily from the beamline without impacting the rest of the end stations. This will provide the ideal R&D environment. A CAD rendering of the full system installed into the sample chamber is shown in Fig. 4. This chamber was installed at U7A in May, 2010. Delivery of the instrument is slated for early 2011. We anticipate that by the NSLS / NSLS-II change-over, the microcalorimeter spectrometer will have transitioned from an R&D-grade instrument to a full science instrument that will provide unique spectrometry capabilities to the NSLS-II.

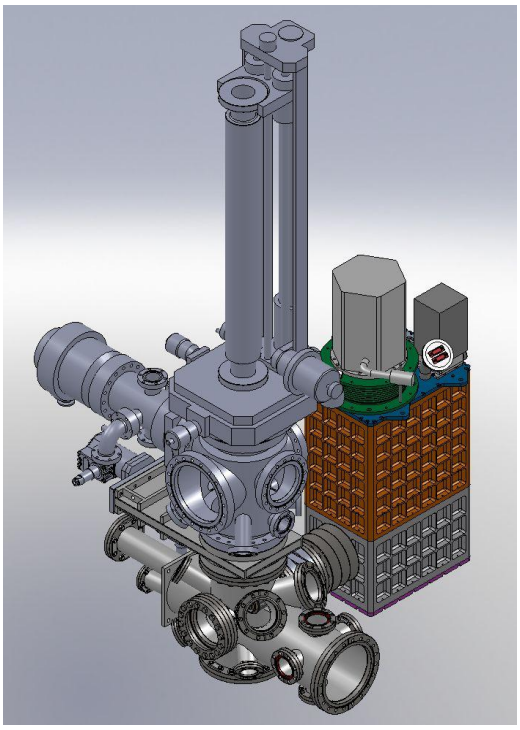

Fig. 4: CAD rendering of the complete microcalorimeter spectrometer installed in its sample chamber.

NIST's User Community:
25 Academic, 25 Industrial, and 14 National Laboratory Scientific Groups

Academia	Industry	National Laboratories
ASU	Advanced Materials	Army Research Laboratory
Albany Nano Tech	Aerodyne	BNL, Battery Group
Berkley	Afton Chemical	BNL, Catalysis Group
Clarkson University	Air Products	BNL, Center for Functional Nanomateials
Cornell	Corning	BNL, Instrumentation Div.
Georgia Tech	Detector Technology	BNL, NSLS Detector Group
Harvard Univ.	Dow Chemical Company	BNL, Superconductivity Group
Hunter College	General Electric	Naval Research Laboratory
Michigan Molecular Institute	H.C. Stark	NIST, Chemical Sciences and Technology Lab.
MIT	IBM	NIST, Electronics and Electrical Engineering Lab.
NCSU, Raleigh	IMEC	NIST, Functional Properties Group
Northeastern Univ.	Int. Radiation Detectors	NIST, Nanomechanical Properties Group
Northwestern Univ.	Konarka	NIST, Polymers Div.
Penn State	Merck	Sandia
Princeton	Motorola	
Stanford Univ.	Ovonic Synthetic Materials	
SUNY Albany	Parc	
SUNY Buffalo	Plextronics	
SUNY Stony Brook	Princeton Gamma Tech	
U. of Delaware	R. Browning Consultants	
U. of Kentucky	SEMATECH	
U. of Penn.	Synchrotron Research, Inc.	
U. of Wash. Seattle	UOP	
UCSB	Xerox	
Yale	X-Lubes	

JOINT PHOTON SCIENCES INSTITUTE

STONY BROOK UNIVERSITY
CHEMISTRY BLDG, ROOM 405
STONY BROOK, NY 11794-3400
631-632-8196
JPSI@SUNYSB.EDU

June 21, 2010

Ladies and Gentlemen:

The Joint Photon Sciences Institute (JPSI) was established at Brookhaven National Laboratory (BNL) and Stony Brook University (SBU) in the fall of 2008. The mission of JPSI is to exploit the properties of advanced photon sources to address the nation's most critical scientific and technical problems. In particular, JPSI will explore the opportunities offered by the unprecedented brightness of the National Synchrotron Light Source II (NSLS-II).

Specifically, JPSI will create an innovative environment where researchers from universities, industries, and government laboratories can work together to identify major scientific and technological opportunities, create device solutions using the most advanced research tools, and catalyze discovery to deployment. The key element of JPSI's strategy is to leverage the presence of thousands of researchers from the more than 400 companies, universities, and government laboratories that carry out research at the NSLS today and will continue to do so at NSLS-II. In addition, JPSI has formed a strategic alliance with the National Institute of Standards and Technology to promote the usage of synchrotrons by industry.

So far, JPSI has focused its program on four themes: microelectronics, energy storage, extreme environments, and solar energy. In each area, leaders from universities, government laboratories and industries were invited to a focused workshop where major technology challenges and capabilities of advanced research tools were presented, new scientific opportunities identified, and collaborative teams formed. These activities have led to major funding from New York State in energy storage, beamline upgrades at the NSLS for microelectronics research, and a new beamline proposal at the NSLS and NSLS-II for advanced lithography. In parallel, JPSI has launched basic research programs in coherent diffraction imaging and nano-diffraction.

As the Directors of JPSI, we are writing in support of the NIST Spectroscopy Beamline Suite: Soft and Tender X-ray Spectroscopy and Microscopy (100 eV to 7.5 keV canted sources), and Hard X-ray Absorption Spectroscopy and Diffraction (4.5 keV to 40 keV three-pole wiggler source) beamline proposal. The proposed beamline is part of the suite of scientific capabilities identified in the four major workshops. It is the intention of JPSI to engage NSLS-II in a partnership agreement to develop these capabilities and to share the stewardship of these beamlines. The aim is to maximize their impact by engaging the intellectual expertise within JPSI and its research partners in these techniques, and to continue to expand these successful research programs at the NSLS today and NSLS-II tomorrow.

Sincerely yours,

Chi-Chang Kao, Director John B. Parise, Co-Director

BROOKHAVEN NATIONAL LABORATORY

STONY BROOK STATE UNIVERSITY OF NEW YORK

Daniel A. Fischer

Education: 1984 Physics Ph.D. SUNY, Stony Brook

Professional Employment:

Group Leader (2003-present) Synchrotron Methods, Physicist (1991-present):
Ceramics Division, Material Science and Engineering Laboratory,
National Institute of Standards and Technology

Physicist: Exxon Research and Engineering Co., 1984-1991.

Post Doctoral Research Associate: City University of New York, 1984.

Awards:

- *2005 Arthur S. Flemming Award (Scientific Category)*, for pioneering work in developing a critical facility for soft X-ray absorption spectroscopy that has enabled key scientific and technological advances in cutting-edge technology and for groundbreaking work on self-assembled nanoparticles, nanotubes, biomaterials, and high-temperature superconductors.
- *2004 Department of Commerce Gold Medal, Individual Award*, for pioneering development of a unique national measurement facility for soft x-ray absorption spectroscopy enabling breakthrough materials advances.
- *1998 Department of Commerce Bronze Medal, Group Award*, for leadership and scientific achievement in the development, implementation, and application of advanced x-ray techniques for materials science.
- *1994 Department of Commerce Bronze Medal, Individual Award*, for the development of ultra-soft x-ray techniques to measure molecular structure at surfaces and buried interfaces.

Selected Recent Service to the Scientific Community:
2005-2008: Chair and Vice Chair National Synchrotron Light Source User Executive Committee
2006: NSLS User meeting Chair (over 400 attendees, 3 days, 9 workshops)
2006-present: Editorial Board Member- Review of Scientific Instruments
1998-present: Chair NSLS Vacuum Ultraviolet Proposal Study Panel
2007-present: Member NSLS to NSLS II Beamline Transition Working Group

Over 250 Journal Publications
(Below some selected publications; *Journal Covers and +NSLS Science Highlights)

***+** "Enhanced Photovoltaic Properties of Potassium-Adsorbed Titania Nanotubes", C Richter, C Jaye, D Fischer, L Lewis, R Willey, L Menon, J. Mater. Chem., 19, 2963–2967 (2009).

+ "Influence of Dielectric Surface Chemistry on the Microstructure and Carrier Mobility of an n-Type Organic Semiconductor,P Dhagat, H Haverinen", J Klein, Y Jung, D Fischer, D Delongchamp, G Jabbour, Adv. Func. Mater., 19, 2365-2372 (2009).

+ "Enhancement of Engine Oil Wear and Friction Control Performance Through Titanium Additive Chemistry", J Guevremont, G Guinther, D Szemenyei, M Devlin, T Jao, C Jaye, J Woicik, D Fischer, Tribol. Trans., 51(3), 324-331 (2008). *(Selected for Editor's Choice Award)*

* "Multilayer mirror fluorescence detection system for photon-in photon-out in-situ carbon K-edge NEXAFS", D Fischer, S Sambasivan, A Kuperman, Y Platonov , J Wood , Synch.. Rad. News, 15, 16-20 (2002).

Name: Joseph C. Woicik

Education/Training:

Institution and Location	Degree	Year	Field of Study
Stanford University, Stanford CA	Ph.D. and M.S.	1989	Applied Physics
Stanford University, Stanford CA	M.S.	1989	Applied Physics
Cornell University, Ithaca NY	B.S.	1983	Applied Physics

Research and Professional Experience:

National Institute of Standards and Technology

Senior Physicist	1999-present
Physicist	1991-1999
National Research Council Post Doctoral Fellow	1989-1991

Professional Activities:

Spokesperson, beamline X2A2 NSLS
Local contact, beamline X24A NSLS
Staff member, APS Sector 33, 2002-2004
Chair, International Workshop for New Opportunities in Hard X-ray Photoelectron Spectroscopy: HAXPES 2009, Brookhaven National Laboratory, 5/20/09 – 5/22/09.
Chair, Advanced Photon Source Spectroscopy Review Panel, 2003-2005

Recent Awards:

Department of Commerce Bronze Metal 1998

Selected Publications:

1. Performance of a 4-element Si drift detector for x-ray absorption fine-structure spectroscopy: Resolution, maximum count rate, dead-time correction, and incorporation into the Athena data analysis software, J.C. Woicik, B. Ravel, D.A. Fischer, and W.J. Newburgh, *J. Synch. Rad.* **17**, 409 (2010).
2*****. Oxygen vacancies in N doped anatase TiO_2: Experiment and first-principles calculations, A.K. Rumaiz, J.C. Woicik, E. Cockayne, H.Y. Lin, G.H. Jaffari, and S.I. Shah, *Appl. Phys. Lett.* **95**, 262111 (2009).
3******.A ferroelectric oxide made directly on silicon, M.P. Warusawithana, C. Cen, C.R. Sleasman, J.C. Woicik, Y. Li, L.F. Kourkoutis, J.A. Klug, H. Li, P. Ryan, L.-P. Wang, M. Bedzyk, D.A. Muller, L.-Q. Chen, J. Levy, and D.G. Schlom, *Science* **324**, 367 (2009).
4*****. Phase identification of self-forming Cu-Mn based diffusion barriers on p-SiOC:H and SiO2 dielectrics using x-ray absorption fine structure, J.M. Ablett, J.C. Woicik, Zs. Tokei, S. List, and E. Dimasi, *Appl. Phys. Lett.* **94**, 042112 (2009).
5. Strain-induced change in local structure and its effect on the ferromagnetic properties of $La_{0.5}Sr_{0.5}CoO_3$ thin films, C.K. Xie, J.I. Budnick, W.A. Hines, B.O. Wells, and J.C. Woicik, *Appl. Phys. Lett.* **93**, 182507 (2008).
6. Ferroelectric distortion in $SrTiO_3$ thin films on Si(001) by x-ray absorption fine structure spectroscopy: Experiment and first-principles calculations, J.C. Woicik, E.L. Shirley, C.S. Hellberg, K.E. Andersen, S. Sambasivan, D.A. Fischer, B.D. Chapman, E.A. Stern, P. Ryan, D.L. Ederer, and H. Li, *Phys. Rev. B* **75**, *Rapid Communications*, 140103 (2007).
7. Site-specific valence x-ray photoelectron spectroscopy, J.C. Woicik, *Synchrotron Radiation News* **17**, 48 (2004).
8*****. Hybridization and bond-orbital components in site-specific x-ray photoelectron spectra of rutile TiO_2, J.C. Woicik, E.J. Nelson, L. Kronik, M. Jain, J.R. Chelikowsky, D. Heskett, L.E. Berman, and G.S. Herman, *Phys. Rev. Lett.* **89**, 077401 (2002).
9. Direct measurement of valence-charge asymmetry by x-ray standing waves, J.C. Woicik, E.J. Nelson, and P. Pianetta, *Phys. Rev. Lett.* **84**, 773 (2000).
10*****.Bond-length distortions in strained-semiconductor alloys, J.C. Woicik, J.G. Pellegrino, B. Steiner, K.E. Miyano, S.G. Bompadre, L.B. Sorensen, T.-L. Lee, and S. Khalid, *Phys. Rev. Lett.* **79**, 5026 (1997).
11. Diffraction anomalous fine structure: A new x-ray structural technique, H. Stragier, J.O. Cross, J.J. Rehr, Larry B. Sorensen, C.E. Bouldin, and J.C. Woicik, *Phys. Rev. Lett.* **23**, 3064 (1992).
12. Studies of Si - Ge interfaces with Surface EXAFS and photoemission, J.C. Woicik and P. Pianetta, in Synchrotron Radiation Research: Advances in Surface and Interface Science: Issues and Technology, Ed. R.Z. Bachrach, 1992 Plenum Press, New York.

*** NSLS/BNL Highlight**
**** APS/ANL Highlight**

Name: Bruce Ravel

Education/Training:

Institution and Location	Degree	Year	Field of Study
University of Washington	Ph.D	1997	Physics
Wesleyan University	B.A.	1989	Physics (*magna cum laude*)

Research and Professional Experience:

National Institute of Standards and Technology	
Scientist, Synchrotron Measurement Group	Nov. 2007-present
National Research Council Postdoctoral Fellow	1997-1999
Argonne National Laboratory	
Physicist, Biology Division	2005-2007
Naval Research Laboratory	
Physicist, Chemistry Division	2001-2005
Centre Nationale de la Recherche Scientifique	
Visiting scientist	2000-2001

Professional Activities:

- Beamline experience
  - Local contact, beamline X23A2 2007-present
  - Staff member, APS Sector 10, 2005-2007
  - Spokesperson, beamlines X11A, X11B, X23B, 2003-2005
- Committees
  - Executive committee member, International X-ray Absorption Society, 2005-present
  - Chair, NSLS User Executive Committee, 2009-2010
- XAS software and education
  - Organizer/instructor XAS Schools: NSLS (2003-2005, 2008, 2009), APS (2006-2009), SLS (2007,2009), Thai Synchrotron (2009,2010), University of Alberta (2005), Polish Academy of Science (2006), University of Ghent (2010)
  - Co-author of the IFEFFIT package, a widely used package for XAS data analysis, 2001-present
  - Contributing author of FEFF8, a widely used XAS theory program
- Review Panels
  - Proposal Review Panel, National Synchrotron Light Source, 2007-present
  - Proposal Review Panel, Advanced Photon Source, 2006-present
  - Proposal Review Panel, Canadian Light Source, 2006-present

Selected Publications:

1. *ATHENA, ARTEMIS, HEPHAESTUS: data analysis for X-ray absorption spectroscopy using IFEFFIT*, B. Ravel and M. Newville, *J. Synchrotron Rad.* **12**, pp. 537-541 (2005), doi:10.1107/S0909049505012719
   At 706 citations, this is the most frequently cited article from The Journal of Synchrotron Radiation.
2. *Real Space Multiple Scattering Calculation and Interpretation of X-Ray Absorption Near Edge Structure*, A.L. Ankudinov, B. Ravel, J.J. Rehr, and S. Conradson, *Phys. Rev* **B58**, #12, pp. 7565-7576, (1998), doi: 10.1103/PhysRevB.58.7565
3. *Simultaneous XAFS measurements of multiple samples*, B. Ravel, C. Scorzato, D.P. Siddons, S.D. Kelly, S.R Bare, J. Sycnhrotron Radiat., **17** (2010) 380-385, doi:10.1107/S0909049510006230
4. *Performance of a four-element Si drift detector for X-ray absorption fine-structure spectroscopy: resolution, maximum count rate, and dead-time correction with incorporation into the ATHENA data analysis software*, J.C. Woicik, B. Ravel, D.A. Fischer, W.J. Newburgh, J. Sycnhrotron Radiat., **17** (2010) 409-413, doi:10.1107/S0909049510009064
5. *The structure of ion beam amorphised zirconolite studied by grazing angle X-ray absorption spectroscopy*, D.P. Reid, M.C. Stennett, B. Ravel, J.C. Woicik, N. Peng, E.R. Maddrell and N.C. Hyatt, Nuclear Instruments and Methods in Physics Research B **268**:11-12, (2010) 1847-18521, doi:10.1016/j.nimb.2010.02.026
6. Condensed Matter Astrophysics: A Prescription for Determining the Species-specific Composition and Quantity of Interstellar Dust Using X-rays, J.C. Lee, J. Xiang, B. Ravel, J. Kortright K. Flanagan, The Astrophysical Journal 702:2 (2009) 970, doi: 10.1088/0004-637X/702/2/970
7. *Protein Oxidation Implicated as the Primary Determinant of Bacterial Radioresistance* M. J. Daly, E. K. Gaidamakova, V. Y. Matrosova, A. Vasilenko, M. Zhai, R. D. Leapman, B. Lai, B. Ravel, S.-M. W. Li, K. M. Kemner, J. K. Fredrickson *PLOS Biology* **5**:4, (2007), doi:10.1371/journal.pbio.0050092